

AD-A160 550

①

# Relaxations in Complex Systems

K.L. Ngai and G.B. Wright  
Editors



*Naval Research Laboratory  
Washington, DC 20375-5000*



DTIC FILE COPY

*Office of Naval Research  
Arlington, VA 22217*

DTIC  
ELECTE  
OCT 22 1985  
S A E D

Approved for public release; distribution unlimited.

85 10 22 001

# **RELAXATIONS IN COMPLEX SYSTEMS**

# RELAXATIONS IN COMPLEX SYSTEMS

*Editors:*

K.L. Ngai  
*Naval Research Laboratory*

and

G.B. Wright  
*Office of Naval Research*

Accession For	
NTIS GRA&I	<input checked="" type="checkbox"/>
NTIC TAB	<input type="checkbox"/>
Unannounced	<input type="checkbox"/>
Justification	
\$15.50	
NTIS	
Distribution/	
Availability Codes	
Dist	Avail and/or Special
A-1	21



## PREFACE

Relaxation plays an important role in many branches of science, technology and engineering. Connections can be made between relaxation phenomena that occur in biophysics, physics, chemistry, materials science, rheology, metallurgy, glass sciences, polymer physics and engineering, fiber optics, and electronics. It is of primary concern in basic physics, such as statistical mechanics of irreversible processes and spin glasses, as well as in very practical applications such as injection molding of polymeric systems, composite materials for aviation, aging of glasses, very large scale integration of small devices in electronics, nuclear waste management, etc. The wide variety of areas in which relaxation enters into consideration demonstrates its interdisciplinary nature.

There is presently an exciting opportunity for development of the physics of relaxation in complex systems. The basic ideas of early days still have a strong influence on the thinking in various disciplines. Since the physics involved in these early ideas (for example, distribution of relaxation times) is not very deep and predictions offered are meager, relaxations in complex systems have been left on phenomenological level. Condensed matter physicists, who are in a good position to advance the physics of relaxations in complex systems, in the past decades have either avoided or neglected this subject. The situation is made worse by the dispersion of workers into different specialized areas of relaxation phenomena in their efforts to gain an improved understanding. The trend has been to focus one's attention on a certain class of materials or a specific relaxation phenomenon. Common features of the problems in different areas are ignored. This fragmentation of research efforts has made progress even more difficult and the search for the causes of the underlying commonality in relaxation in complex systems more obscure. The common thread for these diverse systems is the time dependence or relaxation which can be expressed as

$$R(t) \sim \exp - (t/\tau_p)^{1-n}, \quad 0 \leq n < 1.$$

In our own work we have come to believe in the importance of a *second* "universal" relation, namely,  $\tau_p$  and  $n$  in the expression above are in turn related to a microscopic relaxation time  $\tau_0$  via the relation:

$$\tau_p \sim \tau_0^{1/(1-n)}.$$

Recognizing this commonality in the behavior of relaxation over a broad spectrum of disciplines, and the desirability of discussing it in a broader community, we organized a workshop on "Relaxations in Disordered Systems" with the help of Prof. T.K. Lee at Virginia Polytechnic Institute and State University, Blacksburg, Virginia, in July, 1983. The invited experts were from disciplines as various as mathematical physics, condensed matter physics, chemistry, thermodynamics, glass science, metallurgy, rheology, polymer science and engineering. In spite of different and sometimes even divergent viewpoints of the participants, they share the common conviction that the physics of relaxation is central to their individual pursuits. In this workshop some success was apparent in getting these diverse groups of scientists, who normally have no rapport with each other, to discuss the issues in the physics of relaxations in complex systems.

We thought it desirable to ask these experts to write articles on the subjects of their interest, assemble them in a single volume, easily accessible to the broader community. The resulting book presents a survey and review of relaxation phenomena in many research fields. Both theoretical and experimental aspects were equally emphasized. The reader of this volume can obtain in one place a good idea of the typical research problems in relaxation phenomena. We have imposed no length limit to any article in this volume to enable the contributor to write in any style he wants with a common purpose of conveying to the readers the state of the art in his research area. All contributions were written in 1984, and received by the editors in the period April-August, 1984.

The Blackburg Workshop could not have taken place without the support of Profs. T.K. Lee, Robert E. Marshak and many staff members of the Physics Department of Virginia Polytechnic Institute and State University, and the generous financial support of the Office of Naval Research, and General Electric Corporate Research and Development Center. We especially acknowledge Mrs. Carol Frendewey of VPI for her excellent job as Workshop Secretary. We are grateful to Mrs. Pauline T. Iaconangelo and Mr. G.R. Fong for their help in preparing this book. One of us (KLN) sincerely thanks the management of the Naval Research Laboratory and Drs. G.M. Borsuk, B.D. McCombe (now at New York State University at Buffalo), A.I. Schindler, and S. Teitler for encouragement.

Finally, the success of this book is ultimately determined by the contributions contained therein. To those of you who invested a great deal of effort in preparing these excellent papers, we are truly grateful.

October 1984

K.L. Ngai  
G.B. Wright

## LIST OF PARTICIPANTS

J.J. Aklonis  
Loker Hydrocarbon Research Institute  
Department of Chemistry  
University of Southern California  
Los Angeles, CA 90089-1661

C.A. Angell  
Department of Chemistry  
Purdue University  
West Lafayette, Indiana 47907

J.T. Bendler  
Polymer Physics and Engineering Branch  
General Electric Corporate R & D  
Schenectady, NY 12301

S.P. Bowen  
Department of Physics  
Virginia Polytechnic Inst.  
and State University  
Blacksburg, VA 24061

S.T. Chui  
Bartol Research Foundation of  
The Franklin Institute  
University of Delaware  
Newark, DE 19716

E.A. DiMarzio  
National Bureau of Standards  
Washington, DC 20234

D. Emin  
Sandia National Labs  
Solid State Theory Division  
Albuquerque, NM 81781

R. Fisch  
Department of Physics  
Washington University  
Saint Louis, MO 63130

M. Goldstein  
Division of Natural and  
Mathematical Sciences  
Yeshiva University  
New York, NY 10033

G.S. Grest  
Exxon Corporation  
P.O. Box 45  
Linden, NJ 07036

I.M. Hodge  
BF Goodrich R & D Center  
Brecksville, OH 44141

C.Y. Huang  
Los Alamos National Laboratory  
Los Alamos, NM 87545

G.P. Johari  
Department of Metallurgy and Materials Science  
McMaster University,  
Hamilton, Ont. L8S 4L7  
Canada

A. Kriman  
Department of Physics  
Princeton University  
Princeton, NJ 08544

T.K. Lee  
Department of Physics  
Virginia Polytechnic Inst.  
and State University  
Blacksburg, VA 24061

S. Matsuoka  
AT&T Bell Laboratories  
Murray Hill, NJ 07974

K.L. Ngai  
Naval Research Laboratory  
Washington, DC 20375-5000

R.G. Palmer  
Department of Physics  
Duke University  
Durham, NC 27706

G.D. Patterson  
AT&T Bell Laboratories  
Murray Hill, NJ 07974

D.J. Plazek  
Department of Metallurgical and  
Materials Engineering  
University of Pittsburgh  
Pittsburgh, PA 15261

W.M. Prest, Jr.  
Xerox Corporation  
Webster Research Center  
Webster, NY 14580

A.K. Rajagopal  
Department of Physics and Astronomy  
Louisiana State University  
Baton Rouge, LA 70803

T.V. Ramakrishnan  
Department of Physics  
Indian Inst. Science  
Bangalore 560012, India

R.W. Rendell  
Naval Research Laboratory  
Washington, DC 20375-5000

W.M. Risen, Jr.  
Department of Chemistry  
Brown University  
Providence, RI 02912

M.F. Shlesinger  
Physics Division  
Office of Naval Research  
800 North Quincy Street  
Arlington, VA 22217

D.L. Stein  
Department of Physics  
Princeton University  
Princeton, NJ 08540

U. Strom  
Naval Research Laboratory  
Washington, DC 20375-5000

A.I. Taub  
General Electric Corporate R&D  
Schenectady, NY 12301

P.L. Taylor  
Department of Physics  
Case Western Reserve University  
Cleveland, OH 44106

S. Teitler  
Naval Research Laboratory  
Washington, DC 20375-5000

V. Vulovic  
Department of Physics  
Princeton University  
Princeton, NJ 08544

T.C. Ward  
Department of Chemistry  
Virginia Polytechnic Inst.  
and State University  
Blacksburg, VA 24061

C.D. Williams  
Department of Physics  
Virginia Polytechnic Inst.  
and State University  
Blacksburg, VA 24061

F.W. Wiegel  
Dept. Appl. Phys.  
Twente Tech. University  
7500AE Enschede, Holland

S.Y. Wu  
Department of Physics  
University of Louisville  
Louisville, KY

A.F. Yee  
General Electric Corporate R&D  
Schenectady, NY 12345

## CONTENTS:

Preface	v
List of Participants	vii
<b>Viscous Liquids and Glasses</b>	
C.A. Angell, Strong and Fragile Liquids	3
Martin Goldstein, The Signature of the Glass Transition	13
G.P. Johari, Phenomenological Aspects of Glass Transition and Molecular Motions in Glasses	17
Edmund A. Di Marzio, The Nature of the Glass Transition	43
David Ng and J.J. Aklonis, Multiple Ordering Parameter Models of the Glass Transition and Approaches to Equilibrium	53
Ian M. Hodge, The Effects of Physical Aging on Enthalpy Relaxation in Polymers—A Phenomenological Approach	65
<b>Relaxations in Polymers</b>	
Donald J. Plazek, The Creep Behavior of Amorphous Polymers	83
G.D. Patterson, Light Scattering Spectroscopy of Pure Fluids Near the Glass Transition	111
Philip L. Taylor, Relaxation in Crystalline Polymers	121
Gregory B. McKenna, Measurement of the Torque and Normal Force in Torsion in the Study of the Thermoviscoelastic Properties of Polymer Glasses	129
K.L. Ngai and A.F. Yee, Nonlinear Viscoelastic Behavior of Glassy Polymers	145
<b>Metallic Glasses</b>	
A.I. Taub, Comparison of Flow and Structural Relaxation in Amorphous Alloys with Physical Aging in Amorphous Polymers	167
<b>Spin Glasses</b>	
C.Y. Huang, Recent Experimental Advances in Spin Glasses	177
<b>Electrical Relaxations in Ionic Conductors</b>	
C.A. Angell, Relaxation by "Fast" Ions in Viscous Liquids and Glasses	203
Steven G. Greenbaum and John J. Fontanella, NMR, Electrical Relaxation, and High Pressure Electrical Conductivity in Ion Conducting Polymers	211
H. Jain and K.L. Ngai, Electrical Relaxations in Oxide Glasses	221
U. Strom, Elementary Excitations in Glasses	229
<b>Theory and Models</b>	
Siu-Tat Chui, First Principles Microscopic Understanding of Glasses and Glass Transitions	247
R.G. Palmer and D.L. Stein, Broken Ergodicity in Glass	253
John T. Bendler and Michael F. Shlesinger, Fractal Time Defect Diffusion and the Williams-Watts Model of Dielectric Relaxation	261
A.K. Rajagopal and K.L. Ngai, Models of Temporal Stretched Exponential Relaxation in Condensed Matter Systems	275
A.K. Rajagopal and F.W. Wiegell, Nonexponential Decay in Relaxation Phenomena and the Spectral Characteristics of the Heat Bath	303
R.W. Rendell and K.L. Ngai, A Fundamental Relation Between Microscopic and Macroscopic Relaxation Times: Evidence in Relaxation Data	309

# **VISCOUS LIQUIDS AND GLASSES**



## STRONG AND FRAGILE LIQUIDS

C. A. Angell  
Department of Chemistry  
Purdue University  
West Lafayette, Indiana 47907

### Abstract

Characteristic variations of the fundamental structural relaxation time with temperature, over 18 orders of magnitude in  $\tau_g$ , are reviewed for the case of a simply constituted glass-forming liquid, and made the basis for comparative examination of a wide variety of liquids for which viscosities  $\eta$  are available. On scaling temperatures by the value for which  $\eta$  has a common high value of  $10^{13}$  poise, a broad pattern with a common high temperature limit is obtained. The extremes in the pattern are designated "strong" and "fragile," the liquids at each extreme showing common characteristics in the temperature dependence and non-exponentiality of relaxation which can be related to structure. Chemical manipulations of the structure, by bond breaking, coordination number-changing, etc. can convert "strong" liquids into intermediate liquids, intermediate into fragile, etc. Correlations of configurational thermodynamic properties with "fragility" exist, with alcohols as frequent exceptions.

### Introduction

The purpose of these comments is to describe some general characteristics, over wide temperature and viscosity ranges, of liquids whose behavior will lead us to classify them, according to both thermodynamic and transport criteria, as "strong" at one extreme and as "fragile" at the other. Our survey will cover a broad range of behavior extending from the glass transition at the long relaxation time limit to the inverse quasi-lattice vibration frequency at the short time limit.

The classification is as follows. Liquids in the "strong" class exhibit very small changes in their heat capacity on accessing the liquid state at the glass transition temperature due to a stability in the short and intermediate range order and change their relaxation times with temperature between the long and short time limits in an almost Arrhenius fashion, exhibiting only a single relaxation time in the whole range. "Fragile" liquids, on the other hand, have structures which degrade rapidly on

increase of temperature above the glass transition as manifested by a very large change in heat capacity at the glass transition, while their average relaxation time changes between the long and short time limits in a complex fashion, exhibiting both high and low temperature Arrhenius ranges with an intermediate region of highly non-Arrhenius character. The relaxation time spectrum is also a complex function of temperature, certain relationships between the spectrum and the temperature dependence of the average value (to be discussed below) being observed.

By way of other preliminary observations we might note that several liquids which fall into the "strong" liquid category are well known in technology as progenitors of glass-forming systems of a wide range of possible compositions. Foremost among these is liquid  $\text{SiO}_2$ , which spawns the broad class of silicate glasses pre-eminent in both technology and nature. Most molecular liquids congregate near the other extreme. Interestingly enough, we also find there the ionic liquids based on heavy metal fluorides which, in their vitreous forms, are currently attracting much interest as possible improvements on  $\text{SiO}_2$  glass currently used in low loss fiber optical communications.

### The Average Relaxation Time and Its Temperature Dependence

To set up the basis for this classification we will focus attention on the average relaxation time with which the liquid structure returns to equilibrium following some small perturbation. This characteristic is known for many liquids at medium relaxation times through ultrasonic relaxation studies and at longer times through time-dependent fiber elongation or beam bending experiments. Relatively little is known in the high temperature short relaxation time region where such information can only be accessed by light scattering techniques, or microwave dielectric relaxation measurements in such cases where the dielectric and structural relaxation times are closely related. For a few cases, however, the high frequency studies have recently been carried out and we will use the

findings of one of these to provide an overview of the behavior pattern which is classified as that of a "fragile" liquid.

The case of a simple glass-forming ionic liquid containing only  $K^+$ ,  $Ca^{++}$ , and  $NO_3^-$  ions has received much attention from experimentalists over the past decade because of its convenient temperature range of liquid behavior (60–400°C) and ease of vitrification (1). In a recent paper (2) the similarity of its behavior to that of supercooled argon studied on the same time scale, was demonstrated. Figure 1 shows, for the most-studied composition, the behavior of the longitudinal relaxation time,  $\tau_L$ , and, over wider ranges, the (average) shear relaxation time  $\tau_S$  obtained from the shear viscosity and the high frequency (glass-like) shear modulus according to the Maxwell relation

$$\eta = G_{\infty} \tau_S \quad (1)$$

The necessary viscosity data are obtained (3) at low temperatures by beam bending techniques (3), at intermediate temperatures by spindle Brookfield viscometry (3), and at high temperature by capillary viscometry (4). The value of  $G_{\infty}$  has been best determined by hypersonic measurements (5) which fix the temperature dependence of the modulus more accurately than is possible with ultrasonics (6). The high temperature shear relaxation times are indistinguishable from the longitudinal relaxation times obtained (7,8) from the half width of the Brillouin scattering spectra in the vicinity of maximum band width (which corresponds to the condition  $\omega_B \tau_L = 1$ ).

Figure 1 shows that for long relaxation times going into the glass transition, the temperature dependence is Arrhenius in form with a very high activation energy (approximately 150 kcal per mole (2)), at intermediate temperatures a highly non-Arrhenius behavior is encountered, while at high temperatures a return to Arrhenius behavior occurs with an intercept at  $1/T = 0$  of  $\tau = 10^{-13.5}$  sec (8). The latter corresponds well with the average period of vibration of the liquid quasi-lattice which may be assessed from far IR studies of the glassy state, of which a characteristic spectrum is shown in the insert to Figure 1. This is, of course, an entirely reasonable and probably fairly general result.

If the latter fixes the short time limit for the relaxation time we must ask what determines the long time limit if it exists, and the temperature at which it is reached. A partial answer to this question is available from the thermodynamic studies on stoichiometric compounds, according to the argument of Kauzmann (9). Kauzmann pointed out that in those cases where the entropy of fusion of a liquid, and the heat capacities of the crystalline and liquid states (including supercooled states) was available, it was found quite generally that the difference in total entropy between supercooled liquid and crystalline states was tending to vanish at a temperature not too far below that

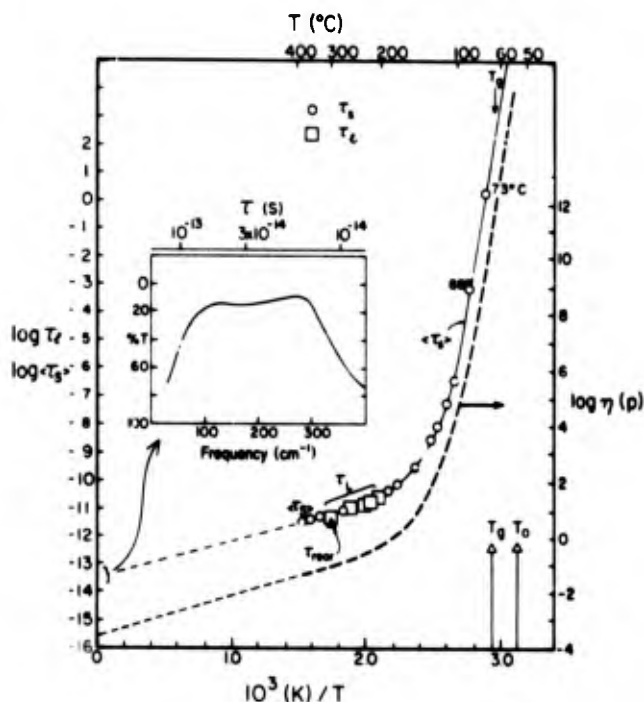


Figure 1. Longitudinal and shear relaxation times for the glass-forming ionic liquid  $K^+-Ca^{++}-NO_3^-$  ( $K^+:Ca^{++} = 3:2$ ), showing high and low temperature Arrhenius regions. The dashed line shows the corresponding behavior of the shear viscosity. The solid triangle is an approximate value of the nitrate anion reorientation time obtained from Raman line width measurements.

Insert: Far infrared spectrum of a thin film of the glassy solid showing quasi-lattice vibrational mode spectrum.

of the observed glass transition. This is illustrated for the cases of several molecular and ionic liquids in Figure 2.

The implication was that either the supercooled liquid must transform to an internally equilibrated glassy state at some very long relaxation time (possibly infinite in principle, though not necessarily so) or crystallize in the temperature range  $T_g$  to  $(T_g - 50^\circ)$ . Of these, Kauzmann preferred the latter, and the final answer is not yet in. For Kauzmann's solution, the long time limit on  $\tau_S$  is given by the condition  $\tau_S = \tau_n$ , where the latter is the inverse of the nucleation rate (per volume unit sufficient for structural relaxation to occur). In at least two cases (10,11), it seems from available evidence that this condition could never be met before the condition  $S_{liquid} - S_{crystal} = 0$  is reached.

#### The Overall Pattern for Liquids

In Figure 1 we have included a dashed curve and a second scale illustrating the variation of the shear viscosity with temperature for the

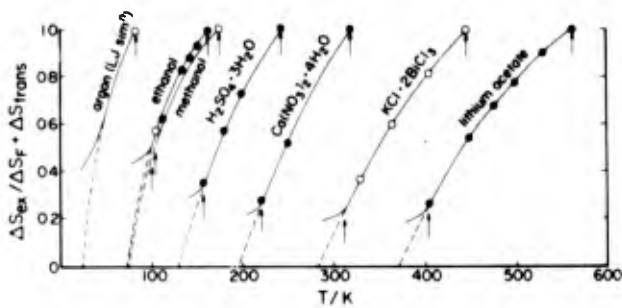


Figure 2. Variation of the excess entropy of the liquid over that of the most stable ordered solid. The diagram indicates that sum of the entropy of fusion and the entropy of any solid state transition occurring between  $T_g$  and the melting point, tends to vanish only a short interval of temperature below  $T_g$  (Kauzmann paradox). The approaching crisis becomes more obvious the higher the temperature of the glass transition and the more "fragile" the liquid under consideration.

same  $\text{Ca}^{++}\text{-K}^+\text{-NO}_3$  liquid for which the relaxation times have been discussed in order to show how little the temperature dependence of the term  $G_\infty$  in Eq. (1) affects the general form of the

relaxational behavior. With this in mind we can hope to obtain a broader picture of the relaxation time vs. temperature behavior of liquids by plotting the more generally available shear viscosity as a function of reduced reciprocal temperature using the temperature of the glass transition, defined for the present purpose as the temperature at which  $\eta = 10^{13}$  poise, as a normalizing parameter. At this temperature, Figure 1 implies  $\tau$  will be about  $10^4$  sec. The pattern of behavior which results is shown in Figure 3 to which we will give much attention. It might be expected that the common point at the high temperature limit would be subject to less variation amongst the different liquids in the case of a reduced viscosity plot than in the case of the more fundamental relaxation time plot, since those liquids with high lattice vibration frequencies (hence short limiting relaxation times) will in general also have large values of  $G_\infty$ , the two tending to cancel in the viscosity representation according to Eq. (1). Figure 3 provides the first full temperature range representation of this type of  $T_g$ -reduced Arrhenius viscosity plots of which partial and less provocative examples have appeared before (12).

Figure 3 shows a tendency of the inorganic tetrahedrally coordinated network liquids of relatively open network structure [ $\text{SiO}_2$ (13,14,)

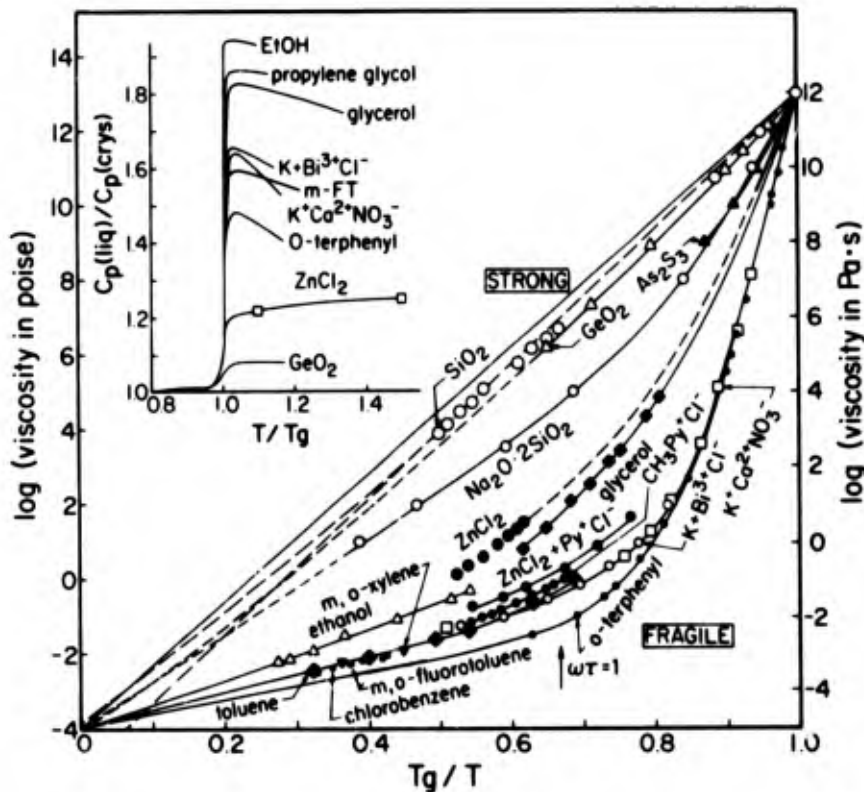


Figure 3.  $T_g$ -scaled Arrhenius plots for viscosities of glass-forming liquids of various types. "Strong" liquids fall at the top of the pattern, "fragile" liquids (see text) fall at the bottom.  $T_g$  is defined as the temperature at which the viscosity reaches  $10^{13}$  poise (see Table 1). Insert: Liquid-to-crystal heat capacity ratio through the glass transition temperature, showing correlation of  $\Delta C_p$  with "fragility." Alcohols, which are intermediate in viscosity behavior, are exceptions.

Table 1

Values of  $T_g$  ( $T_g = T_{\eta = 10^{13}p}$ ) used for Figure 1.

System	$T_g$
SiO <sub>2</sub>	1446
GeO <sub>2</sub>	818
Na <sub>2</sub> O·2SiO <sub>2</sub>	713
As <sub>2</sub> S <sub>3</sub>	454
ZnCl <sub>2</sub>	370.5
glycerol	180
ethanol	94
69ZnCl <sub>2</sub> ·31Py <sup>+</sup> Cl <sup>-</sup>	275
CH <sub>3</sub> Py <sup>+</sup> Cl <sup>-</sup>	225
K <sup>+</sup> Ca <sup>2+</sup> NO <sub>3</sub> <sup>-</sup> (K:Ca = 3:2)	332
K <sup>+</sup> Bi <sup>3+</sup> Cl <sup>-</sup> (K:Bi = 1:2)	306
toluene	110
chlorobenzene	123
m-fluorotoluene	117
o-fluorotoluene	115
o-xylene	123
o-terphenyl	240

GeO<sub>2</sub> (14)] to cluster on the upper side of the viscosity curves. At this extreme, the "strong" liquid extreme, the viscosity is seen to vary between the low and high temperature fixed points in an almost Arrhenius fashion. The case of BeF<sub>2</sub> is discussed separately.

In the intermediate region we find a collection of chemically dissimilar liquid types behaving in a similar manner. Firstly, there is the single component inorganic substance ZnCl<sub>2</sub> (17) which is known to be a tetrahedrally coordinated network-type liquid (18,19) but one in which the Zn-Cl-Zn angles are so bent that the structure is also well described as a close packed array of chloride ions with Zn<sup>2+</sup> ions filling the tetrahedral holes (18). Secondly there are the cases of strong network liquids whose structures have been degraded by addition of modifying components which chemically break the bridge bonds (20). Thirdly, there are the multilaterally hydrogen bonded liquids containing two or more alcohol groups per molecule (21), and fourthly, there are covalently bonded non-network liquids like As<sub>2</sub>S<sub>3</sub> (22). These substances are all characterized by systematically curvilinear Arrhenius plots whose curvature can be described over the whole temperature range by the three parameter Vogel-Tamman-Fulcher equation

$$\eta = A \exp [B/(T-T_0)] \quad (2)$$

(in which A, B and T<sub>0</sub> are constants) with little change in parameters over the 13 orders of magnitude of observable relaxation time

change (20,21).

Just as the "strong" network liquids can be converted into intermediate cases by chemically breaking a fraction of the bridging bonds, so can the intermediate case ZnCl<sub>2</sub> be converted into a "fragile" liquid by chemically breaking Zn-Cl bridging bonds, e.g. by adding 30% of a basic ionic chloride such as KCl, or pyridinium chloride (17,23) see also Fig. 4. In each case what is being accomplished is the removal of restrictions on the configurational states which the system can adopt. The question of liquid topology and fragility is examined more closely in a final section.

The "fragile" liquids, grouped at the bottom of the Figure 3 family, form the largest class, and indeed this would seem to be the "normal" liquid behavior. We find in this group simple unpolymerized ionic liquids like the K<sup>+</sup>-Ca<sup>++</sup>-NO<sub>3</sub><sup>-</sup> mixture of Figure 1, the depolymerized chlorozincates and other ionic chloride glass-forming mixtures (24) and phenyl ring-based van der Waals liquids like toluene (25) and ortho-terphenyl (26). In fact, available data for the latter place it at the outer limit of the "fragile class," (except perhaps for water which is so exceptional (27) that it eludes classification by the present criteria.) There are, unfortunately relatively few data for glass-forming van der Waals liquids of this type over wide viscosity ranges, though data at low viscosities for a number of familiar cases such as chlorobenzene and the xylenes can be added now that their glass transition temperatures can be determined using emulsion techniques (28). They tend to group in the narrow region between the fragile ionic liquids and o-terphenyl, hence to provide a rational basis for extrapolating each of the latter to the high temperature limit. Data on the metal-metalloid system PdCuSi are available in the viscosity region 10<sup>11</sup>-10<sup>15</sup> poise (29). They fall between o-terphenyl and glycerol implying quasi-fragile character.

Before we leave this section we should make reference to two cases, one a "strong" and one a "fragile" liquid, which seem exceptional to this pattern. Both are liquid fluorides. They have been omitted from Figure 3 which is already congested, and are shown instead in Figure 4. The anomalous strong liquid is BeF<sub>2</sub>, whose viscosity is strictly Arrhenius over 13 orders of magnitude in viscosity (30) (as expected from its well-defined tetrahedral network structure), but which does not extrapolate to the common intercept. Rather it slopes more steeply, cutting across the Na<sub>2</sub>O·2SiO<sub>2</sub> plot at T<sub>g</sub>/T = 0.55, a behavior presumably to be associated with its peculiar, continuously increasing heat capacity behavior (see Figure 4). The anomalous fragile liquid is actually a group of heavy metal fluorides containing ZrF<sub>4</sub> which behave just as expected at high T<sub>g</sub>/T (31), but in the fluid region deviate in the opposite sense from BeF<sub>2</sub> in that they become too weakly dependent on temperature. This is perhaps due

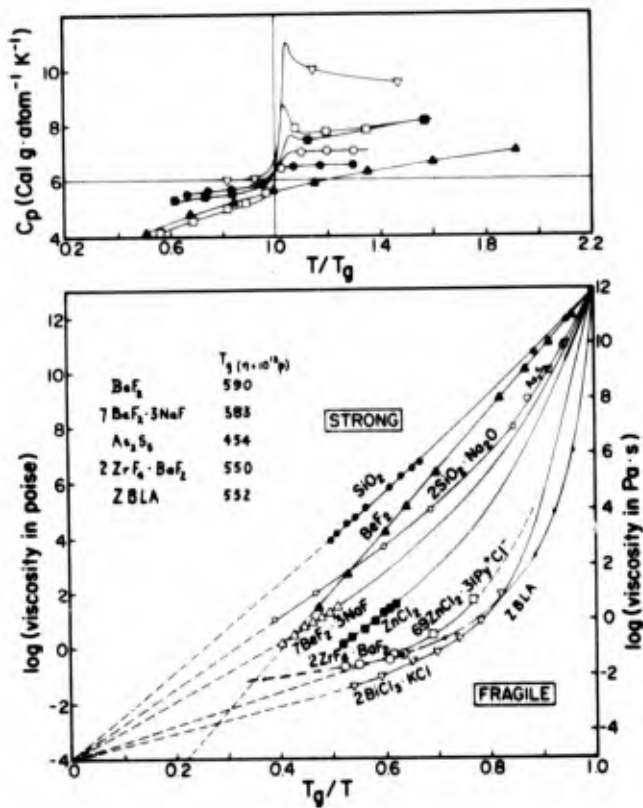


Figure 4. Effect of addition of bridge-bond breaking additives on "strength" of network liquids (a)  $\Delta C_p$  at  $T_g$  (b) temperature dependence of viscosity, ( $T_g$ -reduced scale). Part (b) also displays anomalous behavior of heavy metal fluoride melts at higher temperatures, and of  $\text{BeF}_2$  over the whole observed range. The latter (too-steep reduced Arrhenius slope) can be associated with steadily increasing value of  $C_p$  in the liquid range. [ZBLA  $\equiv$   $57\text{ZrF}_4 \cdot 36\text{BaF}_2 \cdot 3\text{LaF}_3 \cdot 4\text{AlF}_3$  (61)].

to a tendency to generate non-cohesive molecular sub-units, consistent with the high vapor pressure of  $\text{ZrF}_4$ .

#### The Structural Relaxation Function

Associated with the above pattern of viscosity (or average shear relaxation time behavior) is apparently a pattern of behavior for the detailed relaxation kinetics.

For the strong liquids it seems that the equilibrium state following some perturbation, is approached exponentially,  $\phi(t) = e^{-t/\tau}$ , over almost the whole temperature range available for study. For liquid  $\text{GeO}_2$ , for instance, volume relaxation studies by Napolitano et al. (32) imply that the bulk viscosity relaxes with a single relaxation time at and above the temperature  $545^\circ\text{C}$  at which  $\eta = 10^{13}\text{p}$ , since a rapid broadening in the relaxation time distribution was only setting in at considerably lower temperatures,  $T < 519^\circ\text{C}$ . A small departure from Arrhenius behavior in the viscosity was just commencing in the range  $10^{11}$ - $10^{14}$  poise.

The same sort of behavior was found for the disrupted silica network (intermediate) cases, though the nonexponentiality commenced further from  $T_g$  in association with the loss of Arrhenius behavior (30). On the other hand, it has long been known from time domain creep studies (31, 32) ( $\equiv$  very low frequency measurements) near, and particularly below,  $T_g$  that structural relaxation is non-exponential. Typically, glass rheologists have (for decades) described the observed behavior using the currently popular fractional exponential function

$$\phi(t) = e^{-[(t/\tau)^\beta]} \quad (3)$$

where  $\beta$  is typically 0.3-0.5.

In the temperature range above its melting point a single relaxation time behavior was found for  $\text{ZnCl}_2$  (intermediate strength liquid) by Gruber and Litovitz in the ultrasonic range (33) and this finding has recently been extended into the hypersonic frequency (high temperature) range by Knappe (34). Near  $T_g$ , however, the single relaxation time has been lost, according to volume relaxation time measurements by Goldstein and Nakoneczny (35), though it is still relatively close to exponential. In this regime the apparent activation energy (35) is also much larger, as implied by Figure 3 data near  $T_g/T = 1$ . Thus the pattern for intermediate strength liquids of inorganic character is one of exponential relaxation over much of the accessible liquid range, with departures becoming increasingly evident as the (normal) transformation range is approached.

For the polyalcohols, which overlap  $\text{ZnCl}_2$  in Figure 2, a different behavior is found, and this is probably to be associated with their distinctive thermodynamic properties to be discussed below. In these cases, typified by glycerol, non-exponential relaxation behavior is always found (36-39), the simplest description of which may be made using the relaxation function Eq. (3) in which  $0 < \beta < 1$  varies almost continuously between 0.8 and 0.5 as temperature falls from the highest temperatures of measurement to  $T_g$  (36-39). For the more fluid (lower  $T_g$ ) cases where data are available over a wider temperature range (e.g. ethanol) it seems a single relaxation time may be required at the highest temperatures though the data interpretation is not unambiguous.

For the fragile liquids, on the other hand, a definite pattern seems to have emerged and may be correlated with the characteristic changes in temperature dependence of the average relaxation time. Referring to Figure 1, the work of Torell (3,7,8,24) has shown that at least for the ionic examples of fragile liquids (which are the most straightforward to study because of the absence of internal modes which can otherwise couple with the structurally relaxing modes and complicate the phenomenology) the high temperature Arrhenius region is associated with simple exponential relaxation, which is then lost in the same temperature range

$T = 1.5-2.0 T_g$  where the Arrhenius temperature dependence is lost. After a region of rapid change in both the apparent activation energy, and the fractional exponent  $\beta$  [Eq. (3)], Arrhenius behavior is regained in association with the stabilization of  $\beta$  at some value in the range 0.3-0.5 depending on the particular substance.

A connection between departure from Arrhenius behavior and exponential relaxation was interpreted by Tweer et al. (40) in terms of the characteristic distance  $r_0$  over which coupling between elements of the structure could occur. It is also the expectation of the current quantum mechanical coupling model of Ngai (41,42). An investigation of the occurrence or otherwise of these phenomena in computer simulated systems (which are classical systems) should help resolve the origin of these effects.

#### Thermodynamic Properties and Changes at the Glass Transition

The liquids we have classed as fragile systematically exhibit large changes in heat capacity at  $T_g$ . In those cases where the liquids are constituted of relatively heavy ions, the heat capacity change,  $\Delta C_p$ , seems (24) to be consistently of the order of 3.5-4.0 cal g<sup>-1</sup>K<sup>-1</sup> [or 0.6  $C_p$  (glass) per g atom where the glass  $C_p$  is already classical at  $T_g$ ]. The strong liquids on the other hand, exhibit systematically small changes in heat capacity at their glass transitions. These trends are displayed in the insert to Figure 3, (Figure 4 for BeF<sub>2</sub>). As noted by this author some time ago (23) the magnitude of  $\Delta C_p$  increases when we make chemical changes which, by bond-breaking, convert strong liquids into intermediate liquids, or intermediate liquids into fragile liquids. This is best seen in a separate plot Figure 4 documenting the two cases, SiO<sub>2</sub> (strong) + Na<sub>2</sub>O·2SiO<sub>2</sub> (intermediate), BeF<sub>2</sub> (strong) + 3LiF·7BeF<sub>2</sub> (intermediate) and ZnCl<sub>2</sub> (intermediate) + pyridium chlorozincate (fragile).

These correlations are fully consistent with the theory for relaxation processes developed by Adam and Gibbs (43) in which the relaxation time is exponentially related to the inverse of the total configurational entropy,  $S_c$ . The latter depends for its magnitude on the value of  $\Delta C_p$  integrated over the temperature range  $T_K$  (see Figure 2) to  $T$ . In fact, a hyperbolic relation between  $\Delta C_p$  and  $T$ ,

$$\Delta C_p = D/T \quad (3)$$

which is the simplest general description of the observed behavior, is all that is needed (23) to convert the Adam-Gibbs equation

$$\tau = A_\tau \exp(C/TS_c) \quad (4)$$

into the VTF equation [Eq. (2)], in which  $T_0 \equiv T_K$ , and the constant  $B$  is now seen to contain  $T_0$  itself,  $B = DT_0$ . This equation describes the viscosity of intermediate liquids

like polyalcohols very well (44). It also describes that of fragile liquids well in the range (1.2-1.7)  $T_g$  though in these cases yields  $T_0$  values which are higher than determined from thermodynamic data and in some cases, e.g., o-terphenyl (45), even exceed  $T_g$ —which is of course unphysical and serves to predict the return to Arrhenius behavior which occurs at lower temperatures.

The alcohols as a class are exceptional to the pattern we have described. In Figure 3 the viscosity temperature dependence of glycerol and ethanol would lead to the expectation of small values of  $\Delta C_p$ , as for ZnCl<sub>2</sub>, whereas the relative  $\Delta C_p$  values are exceptionally high, see Figure 3 inset. Since the non-Arrhenius temperature dependence itself is correctly accounted for by the entropy model in these cases (21) (i.e.  $\Delta C_p$  plays its expected role, and  $T_0 = T_K$ ) and since the non-exponential relaxation observed in these cases (36) is also more characteristic of liquids with large entropy effects in the temperature dependence, it seems probable that the source of the anomalous behavior should lie in the non-thermodynamic factor  $C$  in Eq. (4). This is determined by the height of the energy barrier which must be surmounted during the cooperative rearrangement (43). This would imply that the isothermal (constant  $S_c$ ) relaxation or viscosity would have an exceptionally large temperature dependence. Such measurements, which have been made for metallic (45) and oxide (46) glasses, have not yet been made for the polyalcohols as far as this author is aware. Should the isostructural relaxation in fact prove unexceptional, then an anomalous configurational heat capacity will be indicated, associated presumably with the peculiarities of the hydrogen bond. It is noteworthy in this connection that the configurational expansion coefficient for alcohols is not abnormally large. (This has the very practical result that the variation of the relaxation time with increasing pressure is particularly small

$$\frac{dT_g}{dp} = \frac{dT}{dp} = 0.005 \text{ K kbar}^{-1} \quad (5)$$

making 1:1 CH<sub>3</sub>OH + CH<sub>3</sub>CH<sub>2</sub>OH the medium of choice as an ultrahigh pressure transmitting fluid, serving to 100 kbar at R.T.) For the general case, that of the fragile liquids, it seems that  $\Delta\alpha$  and  $T_g$  are related by (47)

$$T_g \Delta\alpha = 0.112 \pm 0.02 \quad (6)$$

The Kauzmann paradox, i.e. the approach to the supercooled liquid-crystal entropy crossover, Figure 2, is more dramatic the larger the  $\Delta C_p$ . Except for the alcohols all the liquids for which the problem is illustrated in Figure 2 fall into the "fragile" classification. For strong liquids the problem does not exist, as is shown in Figure 5 where the case of GeO<sub>2</sub> (48) is contrasted with that of H<sub>2</sub>SO<sub>4</sub>·3H<sub>2</sub>O, (12(b), 49) seen earlier in Figure 2. In the latter

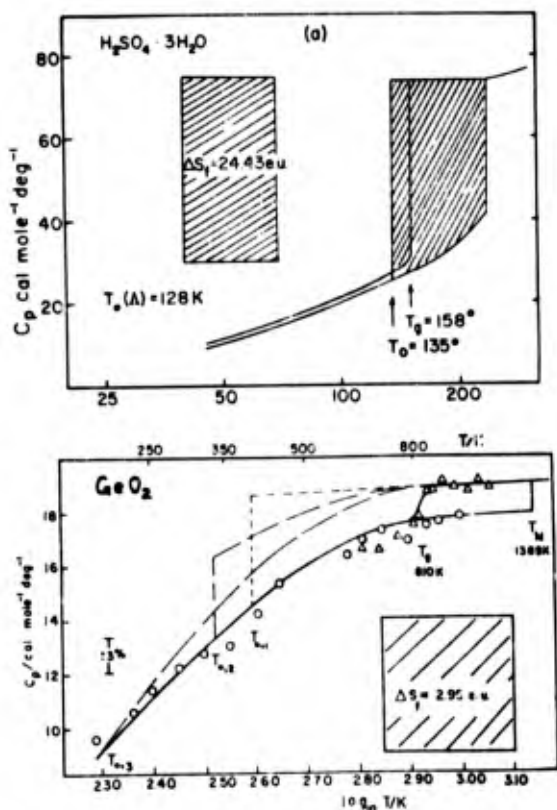


Figure 5. Comparison of the rate at which the total entropy of supercooling liquid approaches that of the corresponding crystal (at  $T_0$ ) for a moderately "fragile" liquid ( $\text{H}_2\text{SO}_4 \cdot 3\text{H}_2\text{O}$ ) and a "strong" liquid ( $\text{GeO}_2$ ). In the latter case a  $T_0$  value cannot be properly assigned because of the variety of ways the entropy excess at  $T_g$  can be imagined to disappear during hypothetical metastable equilibrium cooling processes. Precise data for  $\text{H}_2\text{SO}_4 \cdot 3\text{H}_2\text{O}$  are from J. E. Kunzler and W. F. Giaque, *J. Am. Chem. Soc.* 74, 797 (1952). The data for  $\text{GeO}_2$  are from ref. 12(b). The value of  $T_0(\lambda)$  noted in Figure 1 comes from an Eq. (2) fit of precise equivalent electrical conductivity data.

case there is little choice in the possible sub- $T_g$  extrapolation of  $C_p$  before the excess entropy is exhausted whereas for  $\text{GeO}_2$  many can be chosen which are consistent with the data.

All the foregoing thermodynamic characteristics and the concomitant relaxation behavior presumably find their origin in the characteristic changes in the liquid structure. Relatively little is known about such changes but some broad features may be discerned, and we consider these in the next section.

#### Structural Relationships

The structural requirement for "strong" liquid behavior is, clearly, that the size and charge or bonding relationship between particles be such that at normal pressures each particle has a single accessible small coordination number

and that this is achieved within a three dimensionally extensive network. The consequence of these relationships is that both the short (nearest neighbor) and the intermediate (second nearest neighbor) order is well specified, and therefore resistant to thermal degradation. The degeneracy associated with thermal excitation or rupture of a bond is relatively small in such materials so the configurational heat capacity is very small (49),  $C_p(\text{liq})/C_p(\text{glass}) \approx 1$  and  $\Delta C_p$  at  $T_g$  may be small or undetectable as a "transition" in the case of  $\text{BeF}_2$  (50).

Flow in such a material is rather solid-like in nature proceeding through a sort of defect migration mechanism as indicated by simulation studies of liquid  $\text{SiO}_2$  (51) and  $\text{BeF}_2$  (52). Brawer (52,53) in particular has emphasized the importance of the five-coordinated network center as a defect.

That the strong liquid behavior is associated with small coordination number network stability can be shown in principle by changing the pressure in such a way as to force alternative coordination numbers to become competitive. Increases in diffusivity and fluidity with increasing pressure have been known from simulation studies on  $\text{SiO}_2$  (51) and experiments on  $\text{GeO}_2$  (54) for some time, although it has not been clear whether the characteristics distinguishing strong from fragile liquids in Figure 3 were being changed. Current computer studies on  $\text{SiO}_2$  (55) show that the temperature dependence of diffusivity in liquid  $\text{SiO}_2$  is changed dramatically by increases in pressure, in the direction appropriate to more "fragile" behavior. Laboratory experiments to establish this relationship should be feasible for both  $\text{BeF}_2$  and  $\text{ZnCl}_2$ .

The effect on "strength" of reducing intermediate range order stability by chemical bond breaking, shown by Figures 3 and 4 is so clear as to need no further comment. At the distillate composition (see Figure 3) the fraction of bridges broken is such that two dimensional sheets may form [as in  $\text{Li}_4\text{Si}_2\text{O}_{10}$  or the common micas in which 1/4 of the Si are replaced by Al to give  $(\text{AlSi}_3\text{O}_{10})^{5-}$  sheets] and this structure is preserved in the glass (56). It is perhaps not too surprising that the reduced viscosity behavior is similar to that of liquid  $\text{As}_2\text{S}_3$  whose "raft-like" structure has been discussed by several authors recently (57-59).

The reason that  $\text{ZnCl}_2$  is intermediate in character is presumably because the radius ratio of  $\text{Zn}^{2+}$  and  $\text{Cl}^-$  is less favorable to four coordination and directionality of the Zn-Cl tetrahedral bonding is insufficient to compensate. The result is a network less open in character, closer 5th ligands, and easier coordination exchanges. It would be interesting to study the dependence of "strength" characteristics with composition in mixed bridge systems such as  $\text{ZnCl}_2\text{-ZnBr}_2$  and  $\text{GeS}_2\text{-GeSe}_2$ .

Finally in the salt mixtures, even when some

specificity in intermediate range order in the form of chain catenation remains (as in chlorozincate and fluorozirconate liquids) the full  $14 \text{ J g. atom}^{-1} \text{K}^{-1}$  of configurational heat capacity can be excited, and typical "fragile" behavior is found. The configurational degeneracy is then comparable with that for van der Waals liquids, and a common pattern with minor variations is found. Factors distinguishing liquids like o-terphenyl and the fluorotoluenes from toluene chlorobenzene, etc., remain to be decided.

#### Concluding Remarks

The relationships developed here have useful aspects but are very incomplete at this time. Many data on covalently bound semi-conducting glasses, (the chalcogenides glasses) exist, and have not yet been incorporated. Many studies, and in particular those at high pressure, remain to be carried out. Additional relevant studies will be discussed elsewhere (60).

#### Acknowledgments

Helpful discussions with Dr. L. M. Torell and Dr. C. T. Moynihan, and the assistance of Artemis Arzimanoglou with some of the data reduction, are gratefully acknowledged. The research has benefited from the support of the National Science Foundation under Solid State Chemistry Grant No. DMR 8007053A2.

#### References

- (1) A. Dietzel and H. J. Poegel, Proceedings of the Third International Glass Congress, Venice, Italy, 1953, p. 219.
- (2) R. Weiler, R. Bose, and P. B. Macedo, *J. Chem. Phys.* **53**, 1258 (1970).
- (3) C. A. Angell and L. M. Torell, *J. Chem. Phys.* **78**, 937 (1983).
- (4) E. Rhodes, W. E. Smith and A. R. Ubbelohde, *Trans. Faraday Soc.* **63**, 1943 (1967).
- (5) L. M. Torell and R. Arronsen, *J. Chem. Phys.* **78**, 1121 (1983).
- (6) G. M. Glover and A. J. Matheson, *Trans. Faraday Soc.* **67**, 1960 (1971).
- (7) L. M. Torell, *J. Chem. Phys.* **76**, 3467 (1982).
- (8) L. M. Torell Lecture Notes in Physics, Springer **172**, 92 (1982).
- (9) W. Kauzmann, *Chem. Revs.* **43**, 219 (1948).
- (10) D. R. MacFarlane, Ph.D. Thesis, Purdue University, 1982.
- (11) D. R. Uhlmann, *Glasstech. Ber.* **56**, 822 (1983).
- (12) (a) W. T. Laughlin and D. R. Uhlmann, *J. Phys. Chem.* **76**, 2317 (1972).  
(b) C. A. Angell and J. C. Tucker in "Physical Chemistry of Process Metallurgy: the 1973 Richardson Conference," ed. Jeffes and Tait, Inst. Min. Met. Publ. 1974, p. 207.  
(c) C. A. Angell and W. Sichina, *Ann. N.Y. Acad. Sci.* **279**, (Proc. Workshop on the Glass Transition and the Nature of the Glassy State) (1976), p. 53.
- (d) The author had earlier [*J. Phys. Chem.* **70**, 2793 (1966)] shown striking correlations of transport properties for different liquids when normalized by  $T_0$  of Eq. (2).
- (13) R. Bruckner, *J. Non-Cryst. Sol.* **6**, 177 (1971).
- (14) E. H. Fontana and W. H. Plummer, *Phys. Chem. Glasses* **7**, 139 (1966).
- (15) C. R. Kurkjian and R. W. Douglas, *Phys. Chem. Glasses* **1**, 19 (1960).
- (16) C. T. Moynihan and S. Cantor, *J. Chem. Phys.* **48**, 115 (1968).
- (17) A. J. Eastale and C. A. Angell, *J. Chem. Phys.* **56**, 4231 (1972).
- (18) F. L. Galeener, J. G. Mikkelsen, Jr., A. G. Wright, *J. Non-Cryst. Sol.* **42**, 23 (1980).
- (19) C. A. Angell and J. Wong, *J. Chem. Phys.* **53**, 2053 (1970).
- (20) (a) J. P. Poole, *Verres et Refractaires* **2**, 222 (1948).  
(b) G. S. Meiling and D. R. Uhlmann, *Phys. Chem. Glasses* **8**, 62 (1967).
- (21) C. A. Angell and D. L. Smith, *J. Phys. Chem.* **86**, 3845 (1982).
- (22) S. V. Nemilov, *Soviet Phys. Sol. State* **6**, 1075 (1964).
- (23) (a) C. A. Angell and J. C. Tucker, *Ann. N.Y. Acad. Sci.* **279**, 53 (1976).  
(b) J. Wong, C. A. Angell, "Glass Structure by Spec.," Dekker, N.Y., 1976, Chap. 1.
- (24) L. M. Torell, D. C. Ziegler and C. A. Angell, *J. Chem. Phys.* (submitted).
- (25) A. J. Barlow, J. Lamb, and A. J. Matheson, *Proc. Roy. Soc.* **A292**, 322 (1965).
- (26) R. Weiler, R. Bose and P. B. Macedo, *J. Chem. Phys.* **53**, 1258 (1970).
- (27) C. A. Angell, *Ann. Revs. Phys. Chem.* **34**, 593 (1983).
- (28) D. R. MacFarlane and C. A. Angell, *J. Phys. Chem.* **86**, 1927 (1982). For such cases  $4 \text{ K}$  has been subtracted from the quoted scanning calorimetry  $T_g$  to obtain a value appropriate for the condition  $\eta = 10^{13}$  poise.
- (29) S. S. Tsao and F. Spaepen, "Modeling the Structure and Properties of Amorphous Materials," ed. V. Vitele, TMS-AIME Symposia Proceedings, 1983.
- (30) (a) S. V. Nemilov, *Fiz. Tverd. Tela* **6**, 1375 (1964).  
(b) C. T. Moynihan and S. Cantor, *J. Chem. Phys.* **48**, 115 (1968).
- (31) (a) Moynihan et al., First International Congress on Halide and other Non-oxide Glasses, Cambridge, 1981.  
(b) H. Hu and J. D. Mackenzie, *J. Non-Cryst. Solids* **54**, 241 (1983).
- (32) A. Napolitano and P. B. Macedo, *J. Res. Natu. Bur. Stand.* **72A**, 425 (1968).
- (33) G. J. Gruber and T. A. Litovitz, *J. Chem. Phys.* **40**, 13 (1964).
- (34) G. Knape, *J. Chem. Phys.* (to be published).
- (35) M. Goldstein and M. Nakonecznyi, *Phys. Chem. Glasses* **6**,
- (36) T. E. McDuffie and T. A. Litovitz, *J. Chem. Phys.* **37**, 1699 (1962).
- (37) C. Demoulin, C. J. Montrose and N. Ostrowsky, *Phys. Rev. A* **9**, 1740 (1974).



- (38) T. A. Litovitz and D. Sette, *J. Chem. Phys.* 21, 17 (1953).
- (39) D. C. Champeney and F. O. Kaddour, *Mol. Phys.* (1984) (to be published).
- (40) H. Tweer, J. H. Simmons and P. B. Macedo, *J. Chem. Phys.* 54, 1952 (1971).
- (41) K. L. Ngai, *Comments on Solid State Physics* 9, 127 (1979); 9, 141 (1980).
- (42) K. L. Ngai, *Solid State Ionics* 5, 27 (1981).
- (43) G. Adam and J. H. Gibbs, *J. Chem. Phys.* 43, 139 (1965).
- (44) C. A. Angell and D. L. Smith, *J. Phys. Chem.* 86, 3845 (1982).
- (45) S. S. Tsao and F. Spaepen, "Amorphous Materials: Modelling of Structure and Properties," ed. V. Vittek, *Met. Soc. AIME*, 1983, p. 323; *Proc. 4th Int. Conf. on Rapidly Quenched Metals*, Sendai, 1981, p. 463.
- (46) O. V. Mazurin, Yu. K. Startsen, and S. V. Stoljar, *J. Non-Cryst. Solids* 52, 105 (1982).
- (47) R. Simha and R. R. Boyer, *J. Chem. Phys.* 37, 1003 (1962).
- (48) J. C. Tucker, Ph.D. Thesis, Purdue University 1974.
- (49) J. E. Kunzler and W. F. Giauque, *J. Am. Chem. Soc.* 74, 797 (1952).
- (50) C. A. Angell and K. J. Rao, *J. Chem. Phys.* 57, 470 (1972).
- (51) L. V. Woodcock, C. A. Angell and P. A. Cheeseman, *J. Chem. Phys.* 65, 1565 (1976).
- (52) S. A. Brawer and M. J. Weber, *J. Non-Cryst. Solids* 38&39, 9 (1980).
- (53) S. A. Brawer, *J. Chem. Phys.* 75, 3516 (1981).
- (54) S. K. Sharma, D. Virgo and I. Kuchiro, *J. Non-Cryst. Solids* 33, 235 (1979).
- (55) C. A. Angell and S. Tamaddon (unpublished work).
- (56) M. Imaoka, H. Hasegawa and I. Yasui, *Phys. Chem. Glasses* 24, 72 (1983).
- (57) A. J. Leadbetter and A. J. Apling, *J. Non-Cryst. Solids* 15, 250 (1974).
- (58) L. E. Busse, *Phys. Rev. B* 29(6), 3639 (1984).
- (59) J. C. Phillips, *J. Non-Cryst. Solids* 43, 37 (1983); 44, 17 (1981).
- (60) C. A. Angell and A. Arzimanoglou (to be published).
- (61) C. T. Moynihan, D. L. Gavin, K.-H. Chung, A. J. Bruce, M. G. Drexhage and O. H. El-Bayoumi, *Glasstech. Ber.* 56K, 862 (1983).

## THE SIGNATURE OF THE GLASS TRANSITION

Martin Goldstein  
Division of Natural and Mathematical Sciences  
Yeshiva University  
New York, New York 10033

When a macroscopic sample of a liquid (other than helium) is cooled without crystallizing, the viscosity increases rapidly until at some temperature  $T_g$  it becomes so large it is no longer feasible to measure it. When x-ray diffraction shows the sample to have the characteristic structures of an amorphous liquid, we know the liquid must have undergone a glass transition. There is no ambiguity here.

But there are other systems and other processes which mimic in one way or another the behavior of cooled but uncrystallized liquids. When is the term "glass transition" appropriate and when is it not? Are some of us using the term too broadly, to cover cases which really have very little in common with the physical reality of the "true" glass transition? Or are others of us using the term too narrowly, and shutting our eyes to possible insights that could come from systems we prefer not to recognize?

As I am a "strict" constructionist", preferring a narrow definition of the glass transition, I will begin with a warning against taking my ideas too seriously. I am defending the sort of thinking that probably led some of the first scientists who studied critical phenomena in gases to fail to see that studies of phase separation in alloys or magnetic could transitions have any relevance to their field.

Let us consider some specific examples of transition phenomena to which the term "glass transition" has been, or could be, applied.

When amorphous metals were first prepared by extremely fast quenching, there was some dispute about whether they were true glasses or microcrystalline materials. Diffraction methods confirmed their amorphousness but there is always the possibility of explaining the patterns obtained as arising from very, very small crystals. The question was definitively resolved by Chen and Turnbull (1), who reheated the amorphous metals

carefully, and found the characteristic specific heat behavior of the glass transition region. Ever since, amorphous metals have undergone glass transitions, and no one objects.

Let us briefly state what the "characteristic specific heat behavior" is. The glass transition as it occurs in liquids being cooled is first of all a kinetic phenomenon. The rapid fall of specific heat is a rate-sensitive rather than an equilibrium effect. This is easily shown by all sorts of hysteresis effects, but more specifically, by the fact that slower cooling rates produce the falling specific heat at a lower temperature. The explanation of this behavior is quite straightforward, and goes back to F. Simon (2). At higher temperatures the liquid is in a (metastable) equilibrium state. At  $T_g$ , molecular mobility is so slowed down that the usual molecular measurements that keep the liquid structure in equilibrium do not take place on the experimental time scale, and degrees of freedom of the system appear to be lost. Is this the signature of the glass transition? A little thought will show that behavior resembling this will be observed when the rate of any physical or chemical process that shifts its equilibrium with temperature slows down to the point of unobservability. Not every such kinetic freezing-out process can properly be called a glass transition. One observes the freezing out of degrees of freedom contributing to the specific heat when sound waves of varying frequency are sent through a gas. There is a critical frequency too high for equilibration of vibrational degrees of freedom in the gas molecules and one observes a "transition" in the dependence of sound velocity on frequency (3), but I am not comfortable with the idea of a gaseous glass.

Many polymer physicists and physical chemists have confused matters by describing some of the relaxational transitions, observed below  $T_g$  in polymers by such techniques as dielectric and mechanical relaxation and nmr (4), as additional sub- $T_g$  "glass transitions". These transitions are certainly associated with

the kinetic freezing-out of degrees of freedom, but their status as "glass transitions" is dubious.

When then are the defining characteristics of a "true" glass transition? Let us look again at the indubitable case of a cooling liquid.

We find a number of characteristics of liquid behavior, which on the one hand do not seem to be specific to certain chemical categories of liquids but are general, but on the other hand are not invariably observed in every single case.

1. A high apparent activation energy for molecular mobility at  $T_g$  (arbitrarily defined as the temperature where the molecular relaxation time is of the order of an hour).

2. A temperature dependent activation energy for an appreciable range above  $T_g$ ; a good empirical description of the dependence of relaxation time  $\tau$  on temperature is an equation given originally by Vogel, equation (5)

$$\tau = \tau_0 \exp E/R(T-T_0)$$

with  $E$ ,  $T_0$  and  $\tau_0$  adjustable parameters.

3. Characteristic non-linear relaxational behavior for such thermodynamic properties as  $V$  (studied by dilatometry) and  $H$  (studied by DTA or DSC) in the region around  $T_g$ , including a rate-dependent fall in thermal expansion or specific heat on cooling through  $T_g$ .

4. A second kinetic transition occurring (for measuring frequencies of 1 KHz) at a temperature about 3/4 of  $T_g$ , with a broad spectrum of retardation times and a low and temperature independent activation energy. This transition is termed the "B" transition, and has been observed in about 3/4 of polymeric, molecular, and fused-salt glasses, but not clearly in metallic glasses (6).

5. Specific heat and other anomalies at temperatures 1K and below, explainable in terms of tunneling effects in 2-level systems (7,8).

6. Last and not least, the tendency of the liquid entropy to fall so much more rapidly than that of the crystal, that if its course continued a short range below  $T_g$  (where human time-scales prevent us from measuring it), the entropy of liquid and crystal phases would become equal - the Kauzmann paradox (9).

Now I have already conceded that not all liquids undergoing their glass transitions show each and every one of the above criteria. While  $\beta$ -relaxations for example occur in the majority of glasses, there is no one chemical type of which every individual member

undergoes a transition. In addition, as noted, the metallic glasses as a class have not so far been shown to undergo such a transition.

Angell has put forward at this conference the concept of "strong" vs. "weak" liquids (10). The strong liquids which include that quintessential glass-former fused quartz, show large activation energies but temperature-independent ones, for a considerable range above  $T_g$ . Such liquids also show barely detectable changes in specific heat at  $T_g$ , and since a detectable difference between glass and liquid is required for the Kauzmann paradox to reveal itself, they may fail to have this feature as well.

Can we require some specified fraction of the 6 criteria given above, say any 4 of them, as a distinguishing condition? This Chinese restaurant menu system seems arbitrary and unsatisfying.

Let me suggest an alternative: suppose we make the distinction not substance by substance, but phenomenon by phenomenon. Let us for example consider the spin glasses, and ask, not if each and every spin glass shows each and every one of the above criteria, but rather, for each of the criteria in turn, whether it is shown by the majority of spin glasses. Let us do the same with the "glassy plastic crystals" discovered by Suga and associates, (11) and similarly for any phenomenon claimed to be a glass-like transition.

The results of such a test are interesting. The spin glasses do not pass it, but the plastic crystals do.

Plastic crystals are crystalline substances beyond any doubt. In the phase stable just below the melting point they show rotational disorder, with orientational molecular rearrangements taking place by transitions over potential barriers. At lower temperatures they undergo a first-order transition to a non-rotationally disordered phase. Rapid cooling of the rotationally disordered phase will lead to supercooling of this phase and a kinetic freezing out of the orientational rearrangements. There is a specific heat drop and hysteresis of the enthalpy. The rate of rotational hopping obeys a Vogel equation.  $\beta$ -relaxations have been observed. There is a Kauzmann paradox of the excess entropy of the rotationally disordered phase (11). There is recent evidence that they show the low temperature specific heat anomalies of two-level systems (12).

The conclusion is that if we could understand the transition behavior in the plastic crystal transition we would also understand the glass transition itself. As the problem of orientational disorder in a crystal

is a more tractable problem than the problem of the liquid state itself, this offers considerable hope for a solution to the problem of the glass transition. Theories, anyone?

#### References

1. H.S. Chen and D. Turnbull, J. Chem. Phys. 48, 2560 (1968).
2. F. Simon, Ann. Physik. 68, 278 (1922).
3. K.F. Herzfeld and T.A. Litovitz, Absorption and Dispersion of Ultrasonic Waves, (Academic Press, New York, 1959).
4. N.G. McCrum, B.E. Read, and G. Williams, Anelastic and Dielectric Effects in Polymer Solids, John Wiley, New York 1967.
5. H. Vogel, Phys.Z. 22, 645 (1921).
6. G.P. Johari and M. Goldstein, J. Chem. Phys. 53, 2372 (1970); 55, 4245 (1971).
7. G.P. Phillips, J. Low Temp. Phys. 7, 51 (1972).
8. P.W. Anderson, B.J. Halperin and C.M. Varma, Phil. Mag. 25, 1 (1971).
9. W. Kauzmann, Chem. Revs. 43, 219 (1948).
10. C.A. Angell, These Proceedings.
11. H. Suga and S. Seki, J. Non-Cryst. Solids, 16 171 (1974).
12. D. Moy, J.N. Dobbs and A.C. Anderson, Phys. Rev. B29, 2160 (1984).

## PHENOMENOLOGICAL ASPECTS OF GLASS TRANSITION AND MOLECULAR MOTIONS IN GLASSES

G. P. Johari  
Department of Metallurgy and Materials Science,  
McMaster University, Hamilton, Ont. L8S 4L7, Canada

This article is a review of our current experimental and theoretical understanding of the thermodynamic and kinetic aspects of molecular motions that lead to the formation of a glass and of those that occur in the glassy state. The limitations of our theoretical approaches have been critically assessed, mainly in the light of similarities of glass transitions observed in orientationally-disordered and liquid crystals with those in isotropic liquids. In almost its entirety, this article is taken from one which appeared in "Plastic deformation of amorphous and semicrystalline materials", Les Houches Lectures 1982, (Les Editions de Physique, France, 1982), p. 109.

### Metastable Amorphous Solids and Glasses

A glass can first be described as a special case amongst metastable amorphous solids, quite distinct from others, and then second as a liquid which takes an inconveniently long time to flow. The behaviour of such metastable solids depends upon the mechanism of the disorder itself, and while the ultimate source of randomness in the distribution of positions and/or orientations of atoms or molecules in most cases is thermal, and the state is defined as being metastable with respect to some ground state of ordered structure, the metastability can be produced in several ways. For example, the excess free energy over the ordered arrangement of a crystal, which is necessary to form a metastable amorphous solid, can be frozen into a stable phase by sudden changes of a thermodynamic intensive variable such as temperature or pressure, as in a glass, or as chemical potential, as in desiccated gels. In some amorphized solids it can be "pumped in" by the process involved. The structure of a crystal can be destroyed to produce a noncrystalline solid by (a) the high shearing stresses produced during grinding, (b) electron, neutron or  $\alpha$ -particle irradiation, (c) oxidation at a low temperature and (d) by application of a high pressure at a low temperature. Certain liquids change their composition and produce a gel which in turn can be heated to form a different type of amorphous solid. Vapours when slowly deposited on a cold substrate also produce

thin noncrystalline films, with structures that depend in some cases upon the temperature of the substrate. It is noteworthy that although each of the amorphous solids is obtained by adding free energy to a stable state, and that in some cases a thermodynamic path between the various amorphous states exists via this stable phase, there is no direct thermodynamic path between them. The various amorphous solids of the same material are generally not directly interconvertible.

But it is also important to realize that the various amorphous solid forms of the same material have different physical properties. This means that, although the molecular arrangement in all of them lacks a long range order of positions, differences in their short range order are quite considerable. One such difference is found from an analysis which, based on the argument that, on supercooling, a liquid cannot lose more than its entropy of fusion, suggests a paradox, namely that the structural state of supercooled water cannot approach the structural state of amorphous solid water without violating the third law of thermodynamics (1,2). Differences in the density of an amorphous material obtained by various methods have been found also in germanium (3), and such observations must raise the possibility of the existence of a type of polymorphism in the amorphous state. This, of course, is less easily characterizable than the polymorphism of crystals.

## Glass Formation

It is common knowledge that materials in the glassy state inherit their structure from the liquid from which they are formed by cooling sufficiently below their freezing point, and this is held to be part of the definition of the glassy state. But it is less commonly known that compression of certain materials, as for example of glycerol or selenium, above their freezing pressure can also lead to the formation of a glass. The classical explanation for the formation of a glass is that when a liquid is cooled, or compressed, its fluidity ( $= \text{viscosity}^{-1}$ ) decreases and at a certain temperature below, or pressure above, the freezing point it reduces to a sufficiently low value such that the liquid does not flow in the duration (generally  $10^3$ s or 20 min) of an experiment. At this temperature the liquid is said to have become a glass, and the glass formation is regarded as a kinetic process.

Several thermodynamic changes occur at this temperature. Although the first derivatives of the free energy of the liquid with respect to temperature and pressure, namely, the enthalpy  $H$ , entropy  $S$ , and volume  $V$ , do not change at this temperature, the second derivatives, namely, the heat capacity  $C_p$ , expansivity  $\alpha$ , and compressibility  $\beta$ , rapidly decrease to a magnitude comparable to that in the corresponding completely ordered crystalline state. Thus a glass at its formation temperature maintains the energy, the volume and the structure of the liquid, but the changes in the energy and volume with temperature and pressure in it are similar in magnitude to those of the crystalline solid. The nature of the observed changes in the thermodynamic properties thus make it seem that the liquid has undergone a second-order thermodynamic transition, though the cause of the change is the cessation of the molecular, or atomic mobility, on the time scale of  $10^3$ s. The relative change in the expansivity at glass transition is usually greater in magnitude than the change in the heat capacity. This is due to the fact that expansivity is determined only by the anharmonic components of the low frequency modes of atomic motions, while the heat capacity is determined by both the harmonic component, approximately according to the Debye-Einstein theory, and the anharmonic component, according to the Grunelsen constant.

It is now widely recognized that the occurrence of a glass transition is an almost universal property of the matter in the isotropic liquid state. Glasses are formed by pure or mixed substances of quite diverse molecular structures and of varying strengths of molecular interactions in them. For example, the ionic salts, with their strong electrostatic interactions, organic polymers,

$\text{SiO}_2$ ,  $\text{As}_2\text{S}_3$ , and selenium with covalent bonds, alcohols with hydrogen bonds, mixtures of pyridine with other rigid molecules with possible charge transfer interactions and simple organic liquids such as decalin with weak Van der Waals interactions and mixtures of metals all supercool to form a glass. For our discussion, therefore, a distinction based upon their structural features, resulting from variations in the strength and directionality of interactions, is not worth maintaining. In view of the aforementioned features, several commonly accepted attributes of glasses should now be abandoned. These are: the structural isotropy, optical transparency, brittleness and poor electrical conductivity. Glasses made from nematic, cholesteric and smectic liquids are anisotropic, and those made from mixtures of metals are quite opaque for visible light, have a strength approaching the ultimate attainable and are excellent conductors of electricity. It also now needs to be recognized that no particular feature of inter- or intramolecular bonding is necessarily required for the formation of a glass, although the ease with which crystallization can be prevented seems to depend to some degree on the molecular complexity.

## The Nature of the Glassy State

The glassy state of a material is thermodynamically unstable for two reasons, (i) the excess free energy of the supercooled, or "superpressed" liquid over the crystalline solid and (ii) the free energy barriers which resist changes in the position of the molecules and make the state metastable with respect to an already metastable but internally equilibrated state of the supercooled liquid. Thus a glass is thermodynamically unstable in a sense which differs from that in which the metastable supercooled liquid is unstable and other amorphous states are unstable. This instability causes the state of a glass to ultimately move into a series of states which are continuous with the states of the metastable supercooled liquid above  $T_g$ .

In the glass transition range an extensive thermodynamic variable such as  $V$ ,  $S$  or  $H$  of a material varies with temperature in a manner illustrated in Fig. 1. The curve corresponding to the equilibrium liquid is labelled  $AG_0$ . According to the rate of cooling employed, the material departs from its equilibrium behaviour at, say a point  $G$ , at its glass transition temperature,  $T_g$ , and proceeds along  $GG_1$ . However, the material can be cooled at a higher rate, so that it departs from an equilibrium at  $T > T_g$  at a point  $F'$  and proceeds along  $F'F'_1$ , or cooled at a lower rate so that it departs at a  $T < T_g$  at a point  $F$  and proceeds along  $FF_1$ . The

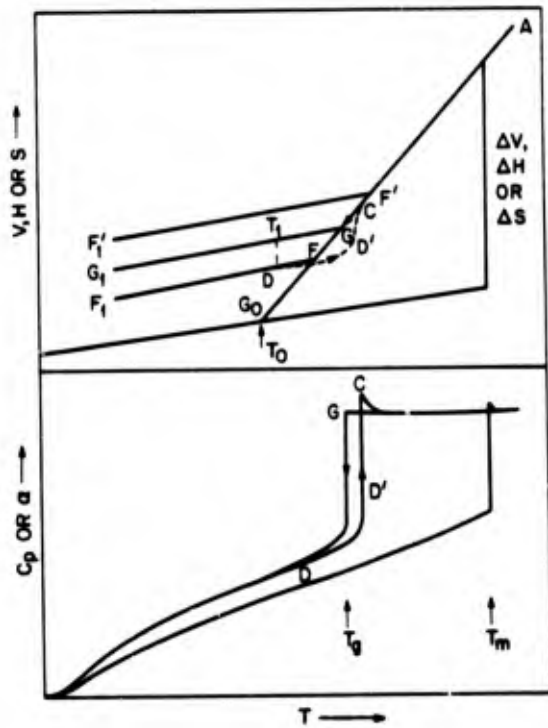


Fig. 1: The variation of thermodynamic properties of a liquid and a glass with temperature and with time.

configurational state of the glass at any point on these three lines will correspond to one of the configurational states of the equilibrium liquid at point G, F' or F, respectively. If the temperature of the glass is held constant at  $T_1$ , the value of the property in question will move along a vertical line towards the value of the equilibrium liquid at a rate which depends mainly on  $T_1$ . If the glass is now heated at a certain rate the properties will not retrace the original path but follow a curve DD'C which would lie below the equilibrium line AGO. Thus even when the cooling and the heating rates are the same, and the thermodynamic variables decrease monotonically on cooling, on reheating they tend to fall below the cooling curve as the transition temperature is approached, and increase more rapidly at a higher temperature in the transition region as if to "catch up" with the properties of the equilibrium liquid. The heat capacity and thermal expansion show a hump at the highest temperature as a simple consequence of the relaxation during the course of heating.

By using ideas drawn from statistical mechanics, Simon (4), gave a qualitative explanation for the glass formation and the zero point entropy of a glass. He suggested that, as a liquid is cooled through its transformation temperature, the molecular

motions which are necessary to affect the appropriate change in configurations are increasingly inhibited and finally become practically impossible in the duration of one's experiment. Thus an order parameter  $z$ , whose variation with temperature describes the energy added to or taken from the liquid on account of changes in potential energy due to changing configurations, is frozen in at this temperature. Part of the heat capacity corresponding to changes in potential energy is thus eliminated; the configurational contribution to any other property similarly disappears and the liquid ceases to be in a true (metastable) thermodynamic equilibrium. If one waits longer the structure irreversibly moves to its equilibrium state of lower volume with a different value of  $z$ , with evolution of heat. This draws attention to the possibility of variation in the structure of glasses which have been obtained by cooling at different rates.

Several analyses of the glass transition have been made from relationships (5) between the changes in  $C_p$ ,  $V$ ,  $\alpha$  and  $\beta$  at  $T_g$ . By extending the ideas of Simon and the theoretical treatments of Ehrenfest (6) and Prigogine and Defay (7), Davies and Jones (8) have shown that at equilibrium at  $T_g$  the Gibbs' free energy with respect to  $z$  is minimum and,

$$\Delta\beta/\Delta\alpha = TV\Delta\alpha/\Delta C_p, \text{ or } \Delta\beta\Delta C_p/TV\Delta\alpha^2 = 1$$

If more than one order parameter is required, the Prigogine-Defay ratio,  $\Delta\beta\Delta C_p/TV\Delta\alpha^2 > 1$ . The measured ratio is generally  $> 1$ , therefore more than one parameter is needed to describe the state of a glass.

The basic supposition of Simon's picture that the configuration of a glass remains frozen-in between OK and  $T_g$  - is difficult to investigate directly by x-ray or other methods, but indirect methods of investigation of molecular motions in a glass, utilized many years after Simon's suggestion, indicate that the configurational state of a glass may not remain unchanged between  $T_g$  and OK, for certain degrees of molecular freedom remain available at temperatures well below  $T_g$ . This, of course, also makes it difficult to assign a single parameter  $z$  to a glass.

#### Nature of Disorder in Some Unusual Glasses

It has recently been observed that changes in the thermodynamic properties and dielectric relaxation in a manner phenomenologically similar to the glass transition also occur when orientationally disordered, or plastic, crystals (8,9) and the mesomorphic states of liquid crystals (10-12) are supercooled below their transformation temperatures to an ordered crystal. Although disordered, the glass-like or glassy states in such cases have certain characteristics of the completely

ordered crystalline state, that is their structures have a long range order for molecular positions or for molecular orientations. In orientationally disordered, or plastic crystals, the situation is reminiscent of spin glasses, wherein the centre of mass of the molecule has a translational invariance but the orientations of molecules are random. The transformation temperature from a disordered to a completely ordered structure of the crystal is analogous to the freezing point of a liquid. In the case of mesomorphic states of certain liquids, the long rigid molecules cannot pack together without inducing correlations in their relative orientations, and although their molecules do not lie on a regular lattice, the situation is akin to magnetic ordering wherein the structure of the glass obtained by supercooling the liquid crystal has long range order for molecular orientations. Cyclohexanol is an example of the first type of glass (13) and the nematic phase of *o*-hydroxy-*p*-methoxybenzylidene *p*-butylaniline (10, 11) of the second type of glass.

It is also noteworthy that the glass-like transition in an orientationally disordered crystal occurs at about the same temperature as the glass transition in the liquid phase of the same substance. For example, glass transition in liquid cyclohexene and the

glass-like transition in its orientationally disordered crystalline state both occur at 81K (8,14) and both the glass transition in liquid ethanol and glass-like transition in its disordered crystal occur at about 97K (15). In such cases it is possible to determine the contribution to heat capacity that arises entirely from positional disorder in their glassy state. The change in the heat capacity of ethanol ( $\sim 40 \text{ JK}^{-1} \text{ mole}^{-1}$ ) is 50% higher for a glass than ( $\sim 28 \text{ JK}^{-1} \text{ mole}^{-1}$ ) for the glass-like transition of its orientationally disordered crystal.

All three types of disorder, namely, (i) orientational and positional, as in ordinary glasses, (ii) positional, as in glassy liquid crystals, and (iii) orientational, as in glassy crystals, are observed in an ice clathrate, whose crystal structure is shown in Fig. 2. Its lattice is formed by water molecules hydrogen bonded in a framework of closest packing of polyhedral cage-like structures, which are occupied by molecules of a suitable size known as guests. The centre of mass of the guest molecules does not lie at the centre of symmetry of the cage they occupy, and they are randomly oriented. Thus there is no long-range order for either their positions or their orientations. Certain guest molecules inside the clathrate cages become ferroelectrically ordered at low

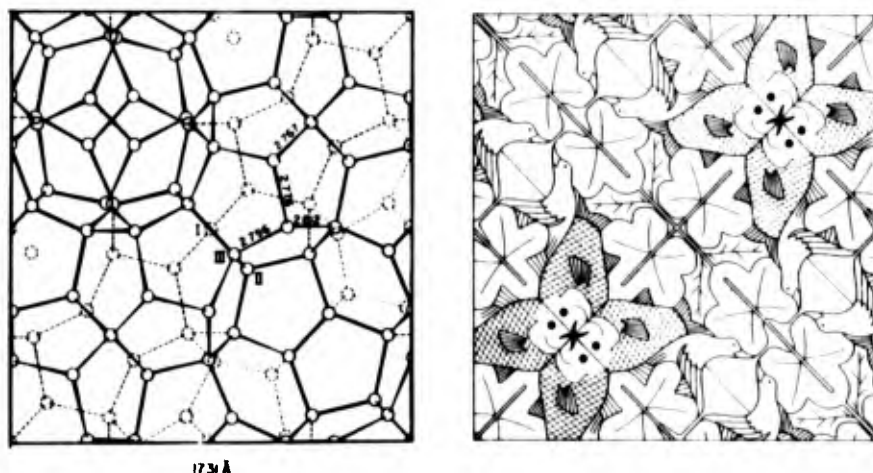


Fig. 2: The crystal structure of ice clathrate of type II in space group  $Fd\bar{3}m$ . The unit cell is marked by the border and is redrawn from Johari (J. Chem. Phys. 74, 1326 (1981)), and its size  $a$  is given. Circles represent oxygen atoms. The arrangement of hydrogen atoms is disordered, but they lie close to an oxygen atom along the line joining the two oxygen atoms. Molecules that occupy the cages are not shown. To the right is a drawing wherein most of the symmetry of the clathrate crystal is retained. The unit cell (drawing) can be produced by rotation, translation inversion (rotation by  $180^\circ$ ) and/or reflection of a structural unit (motif), cube (square), whose edge (side) is equal to  $\frac{1}{2}(a/\sin 45^\circ)$ . The unit (motif) lies with its corner at the center of the unit cell (drawing) and whose edge (side) coincides with either of the two diagonals. The change from a three- to a two-dimensional representation reduces the dimensions of the unit cell in the drawing to  $\frac{1}{2}a/\sin 45^\circ$ , such as to contain only four complete motifs. The space groups of drawing is  $pmm$  (No. 6 on p. 61 in International Tables for x-ray crystallography, Kynoch Press, Birmingham, 1965) but in a square system, instead of rectangular given in the International Tables. The drawing is in Escher's style.



temperatures. At such temperatures there is a long-range order for the orientations of the guest molecules but no long-range order for their positions. Water molecules that form the framework of cage-like structures have no long-range order of their orientations, but their centre of mass is translationally invariant. The structure also bears a certain resemblance to a glass for the reason that it has a relatively large unit cell (a glass has an infinitely large unit cell, and a crystal a very small unit cell).

#### An Entropy Paradox

The explanation given by Simon (4) for the behaviour of a liquid near  $T_g$ , while essentially correct, raises an important question regarding the thermodynamic state of the equilibrium supercooled liquid at temperatures below  $T_g$ . In principle, but not in practice, it is possible to follow the equilibrium liquid below  $T_g$  along  $AG_0$  in Fig. 1, by waiting for a long time, to a temperature where the liquid may have the same entropy, enthalpy and volume as the corresponding ordered crystalline state. If so what order parameter or structure can be envisaged for a liquid whose entropy is equal to that of the crystal? Kauzmann (16) pointed out that the situation becomes paradoxical, for an extrapolation of  $S$ ,  $H$  and  $V$  of the liquid towards absolute zero along  $AG_0$  suggests that the supercooled liquid could reach an entropy lower than the crystal. By considering the variation with temperature in the structure of the liquid below  $T_g$ , which was suggested by the model of Mott and Gurney (17), Kauzmann deduced that the probability of relaxation of a liquid into a crystalline state becomes much higher than the probability of relaxation into an amorphous state of lower energy. The liquid state, therefore, cannot be maintained below a certain temperature, because crystallization would occur first and the situation becomes metaphysical rather than physical. Any attempt to resolve the paradox is operationally meaningless. But it seems necessary to resolve it, for the behaviour is associated with the cause of the rapid fall of entropy with temperature near  $T_g$ . Several theories (18), have attempted to do so by arguing that the molecular shapes of certain atactic vinyl polymers cannot pack in a regular array when in their lowest energy configuration and their crystalline forms do not exist. Thus a disordered state near  $G_0$  is possible. Kauzmann's view is however supported by the observation of rapid crystallization of glycerol at  $T < T_g$  (19) and by the presence of crystal-like short range order in vitreous silica observed from refined x-ray studies (20, 21), but the question regarding a thermodynamic transition remains in this poorly understood problem of phase transition.

#### Glass Transition in a Stable Phase?

The glass formation as a rule occurs at temperatures where the liquid, or the plastic crystalline phase, is metastable with respect to a completely ordered crystalline state, and this is part of the reason for the entropy paradox. But one of our most abundant orientationally disordered crystals, hexagonal ice, seems to be an exception to this rule, for it shows a decrease in the heat capacity and a relaxation of enthalpy in the temperature range 90-110K for  $H_2O$  ice (22) and 110-123K for  $D_2O$  ice (23), in a manner similar to that observed at the glass transition. Yet ice does not undergo a disorder  $\rightarrow$  order transformation above 100K. The dielectric relaxation time for the two ices in their respective temperature range is  $10^3$ - $10^4$ s (24) which, being comparable to the time scale of a thermodynamic experiment, suggests that the dielectric and enthalpy relaxations involve similar types of physical processes. Near 100K, ice has relaxational characteristics similar to those seen in liquids near  $T_g$  (25), which means that molecular configurations in ice at this temperature may differ in energy by an amount comparable to  $kT$ , but a disorder  $\rightarrow$  order transformation does not occur. The decrease in the heat capacity at the glass-like transition temperature of ice is  $0.12 \text{ JK}^{-1} \text{ mole}^{-1}$  (22), which is too small to allow a detailed analysis of the enthalpy relaxation, but it is clear that the paradoxical situation pointed out by Kauzmann cannot exist for ice, for it has no corresponding ordered state above  $T_g$ . Thus hexagonal ice appears to be a material in which a glass-like transition occurs in a stable phase.

This brings us to a further point of interest, which is that, contrary to the generally held view, and based upon our practical experience on the glass transition phenomenon, it seems that there is no thermodynamic reason for a glass transition to occur in the supercooled metastable state of a liquid or of a crystal. In an analysis of the relationship between the relaxation rate, temperature, and pressure, it has been inferred that the melting curve of glycerol would cross the glass transition curve in a temperature pressure plane at negative 25 kbar, and that below this pressure the glass transition in glycerol would occur above its melting point (26). Such a high negative pressure is certainly well above the tensile strength of glycerol and is not attainable. The argument, however, does suggest that for substances in which the entropy of fusion is small or the volume of fusion is large, it may be possible to achieve a pressure, temperature condition at which the glass transition would occur in a stable phase above the freezing point of the liquid. Thus while a resolution of Kauzmann's paradox is experimentally impossible because of the near-infinite time

needed to reach an equilibrium state below  $T_g$ , it is possible to find conditions in which the paradox cannot exist. Negative pressures of  $\sim 1$  kbar can at present be produced and glass transition of certain liquids under such pressures can be studied.

### Phenomenological Theories of Glass Transition

In view of the variety of molecular interactions in the liquids which are known to form glasses, one is faced with the choice of either rejecting the various *ad hoc* structural theories and developing a phenomenological theory of glass formation, or developing a different theory for each type of glass. Since glass transition is a phenomenon of almost universal occurrence, several theories assign to it a thermodynamic character, but it is generally agreed that the progressively rapid increase in the viscosity, or decrease in the molecular mobility, on cooling is a correct explanation for the experimentally observed glass transition (27). It seems that this view is also subject to revision, for plastic crystals do not show a Newtonian flow and it is difficult to assign to a mesomorphic liquid a certain viscosity the increase in which on cooling causes the liquid ultimately to behave as a glass. Nevertheless, the basically relaxational characteristic of the glass transition in isotropic liquids implies a shear modulus  $G$  for a liquid, a relaxation time  $\tau$ , and a shear viscosity  $\eta (= \tau G)$ , properties which can be studied from acoustic or other measurements. Therefore, the theory

of glass transition is closely related to the theory of viscosity. The problem is that we do not, as yet, have a theory of viscosity of liquids, based on principles of molecular dynamics. The present theories for the viscous flow of liquids which form glasses are, therefore, necessarily crude depending more upon physical intuition than mathematical or physical rigour. But in general all theories of glass formation attempt in some way to explain a temperature dependence of viscosity near  $T_g$  according to an empirical equation proposed independently by Vogel (28), Fulcher (29) and Tamman and Hesse (30),

$$\ln \eta = \ln \eta_0 + [B/(T - T_0)] \quad (1)$$

Here  $B$ ,  $\eta_0$  and  $T_0$  are experimentally determined parameters.  $T_0$  represents an experimentally inaccessible state point of infinite viscosity, which can be obtained by extrapolation. If  $T_0 = 0K$ , Eq. (1) becomes an Arrhenius equation but no variation of  $\eta_0$  or  $B$  with  $T$  in an Arrhenius equation can give Eq. (1). Considerable significance has been attached to this quantity for one *infers* it to be the point representing a singularity (31) (as, for example, the Curie-Weiss temperature) in the behaviour of the equilibrium liquid.

Several measurements of  $\eta$  (32,33) at temperatures close to  $T_g$  indicate an approach towards  $T_0 = 0K$ . But it is not certain whether it is an artifact of an experimental method or whether it indicates

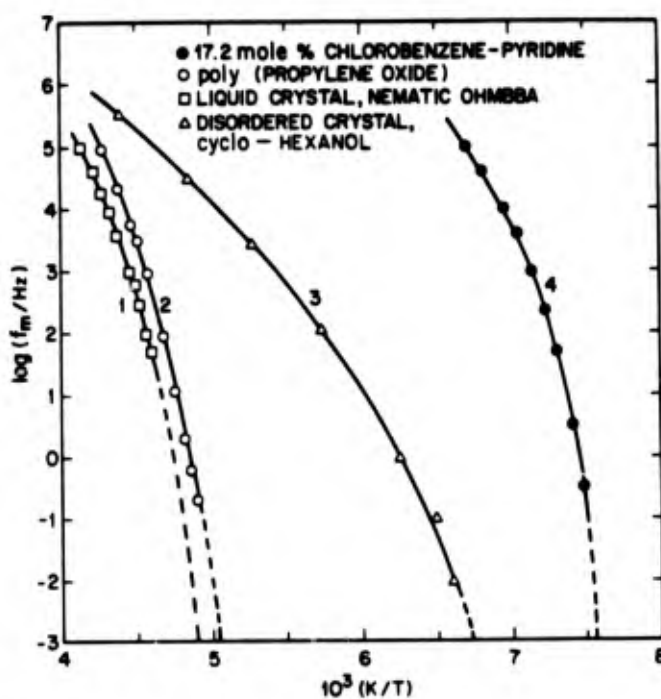


Fig.3: The approach toward  $T_g$  of the dielectric relaxation rates of several types of substances. The temperature at which the curves intersect the baseline is  $T_g$ . The source of data are: 1(11),2(35) 3(78) and 4(36).

the dominance of another process (such as of hydrogen bond breaking and reforming in alcohols). However, it should be remembered that the magnitude of  $T_0$  for the same material may vary according to the accuracy of the data or the length of extrapolation used in obtaining it, but the fact that in most cases  $T_0 > 0K$  is significant, for the viscosity (34), and relaxation times measured from dielectric (Fig. 3 (35,36)) enthalpy, volume, shear or nmr experiments, and the molecular diffusion rates, all admit to a variation with temperature according to the Vogel-Fulcher-Tamman equation,

$$\tau_{\text{dielectric}}, \tau_{\text{shear}}, \tau_{\text{volume}}, D^{-1}, \eta = A \exp [B/(T - T_0)] \quad (2)$$

and therefore to a common physical mechanism. The temperature at which the glass transition occurs is defined as one at which  $\eta = 10^{13}P$  or  $\tau = 10^3s$ , and the theories for it are based upon our conceptual models of the free volume and entropy. These can be grouped as follows:

### The Free Volume Theories

The concept that some sort of extra or free volume in a liquid is responsible for its transport property has been employed in several statistical thermodynamical theories of the liquid state (37-41), as it has generally been considered that, through the cooperation of several degrees of freedom, the random accumulation of free volume, as a result of its redistribution in a liquid, forms a void or a hole of molecular diameter. Molecular transport occurs when a molecule moves into this void. The probability of formation of voids decreases with the macroscopic volume and at low temperatures when the total volume is small, this probability becomes small and the inability of the molecules to diffuse causes the glass transition. Thus the motions of molecules below  $T_g$  are no longer translational within a free volume, but rather vibrational as in a crystal. The heat capacity and expansivity at  $T_g$  therefore decrease to values similar to those of the crystal. Fox and Flory (42) were first to consider the glass transition in polymers as being due to a decrease in the free volume to some small value. But the development of a theory based on this concept began after Doiittle (43, 44) showed that the viscosity of hydrocarbons at  $T \gg T_g$  can be represented by an empirical equation,

$$\eta = A \exp (bv_0/v_f) \quad (3)$$

where A and b are empirical constants,  $v_0$  is the Van der Waal's volume of the molecule at 0K and  $v_f$  is the free volume given by,  $v_f = v - v_0$ , where v is the average volume per molecule in the liquid. Williams, Landel and Ferry (45) have also shown that the viscosity and dielectric and shear relaxation times of

amorphous polymers can be given by an empirical but "Universally" applicable equation,

$$\log a_T = \log \frac{\tau(T)}{\tau(T_g)} \approx \log \frac{\eta(T)}{\eta(T_g)} = \frac{-C_1^g(T - T_g)}{C_2^g + (T - T_g)} \quad (4)$$

where  $C_1^g$  and  $C_2^g$  are "Universal" constants for polymers. If the fractional free volume  $f(=v_f/v_0)$  increases above  $T_g$  according to,

$$f(T) = f(T_g) + \alpha_f(T - T_g) \quad (5)$$

where  $\alpha_f$  has the dimensions of thermal expansion coefficient, Eqs. (3) and (5) can be combined to obtain Eq. (4), and the empirical constants can be written as,

$$C_1^g = b/2.303f(T_g), \quad C_2^g = f(T_g)/\alpha_f.$$

$$\alpha_f = 480 \text{ MK}^{-1} \quad \text{and} \quad f(T_g) = 0.025$$

These values in Eq. (4) imply that glass transition in polymers occurs at a temperature when the free volume is equal to 2.5% of the molecular volume.

The formulation of the approximate molecular theories of glass transition is based on the Stokes-Einstein relation, that the self diffusion coefficient, D, of nearly spherical molecules is inversely related to the viscosity, by,

$$D = (kT/3\pi a_0 \eta) \quad (6)$$

where k is the Boltzmann constant and  $a_0$  is the diameter of the sphere corresponding to the volume of the molecule. Bueche (46) has given a theory for the glass transition in polymers by assuming that movement of a segment of a chain is possible only when the local fractional free volume exceeds a certain value. From considerations of random fluctuations in local free volume, he showed that Eq. (2) can be obtained at low temperatures, but at high temperatures the relaxation rates vary according to an Arrhenius equation. Thus Bueche's theory for glass transition in polymers seems consistent with the experimental data.

A theory of molecular transport based on a model of molecules or atoms as hard spheres was given by Cohen and Turnbull (47) almost concurrently with the other developments of similar types (48). Their treatment is based upon the following three assumptions:

- (1) on a molecular scale, an average local volume  $v$  is associated with each atom or molecule and the excess of  $v$  over a certain critical value  $v_c$  (of molecular volume) is the free volume,

$$v_f (=v - v_c).$$

- (ii) the free volume is continuously redistributed with time and no local free energy is required for the redistribution; thus its distribution is entirely random, and,
- (iii) molecular transport occurs by the movement of atoms or molecules into a void of approximately atomic or molecular size which is formed as a result of the redistribution of the free volume.

Although diffusion in Eq. (6) implies that, when a molecule moves, its surrounding molecules forming the 'cage' move simultaneously, Cohen and Turnbull assumed the cage to be stationary so that a translational jump of the molecule across the void within its cage is possible. Now the probability that  $n$  increments of free volume of the average size  $v_f$  would accumulate is directly proportional to  $\sim(1/e)^n$  where  $n = v_c/v_f$ , or to  $\exp[-\gamma v_c/v_f]$ . Thus the diffusion coefficient,

$$D = D_0 \exp[-\gamma v_c/v_f] \quad (7)$$

where  $D_0$  is proportional to the molecular diameter and the gas kinetic velocity and  $\gamma$  is a constant with a value between 0.5 and 1. This is similar to Eq. (3) if  $D$  is inversely proportional to  $n$ . The difference between the two equations is that in Eq. (7), the  $v_f$  is introduced at a certain temperature  $T_0$ , ( $v_f = 0$  at  $T = T_0$ ) while in Eq. (3),  $v_f$  is introduced at 0K ( $v_f = 0$  at  $T = 0$ ). That is the total volume  $v = v_0 + \Delta v_c + v_f$ , where  $\Delta v_c (=v(T_0) - v_0)$  can be thought of as that excess volume, which, in contrast to  $v_f$ , requires a local free energy for distribution. The shift factor  $\Delta v_c$  seems justified on the basis of Lennard-Jones pair potential function of a molecule inside a "cage" as a function of the cage radius. For small cage radius, at  $T < T_0$ , a large energy would be required for the redistribution of  $v_f$ , while for a sufficiently large radius, corresponding to the nearly linear region of the potential energy curve, the free volume is redistributed with no energy change. Thus if  $\alpha$  is the average expansivity and  $\bar{v}_m$  the average molecular volume in the temperature range  $T_0$  and  $T$ ,

$$v_f \approx \alpha \bar{v}_m (T - T_0) \text{ at } T \geq T_0. \quad (8)$$

and,

$$v_f = 0 \text{ at } T < T_0$$

Combining Eqs. (6), (7) and (8) gives the Vogel-Flucher-Tamman equation, and  $\gamma v_c$  of Eq. (7) is numerically close to  $v_0$  in the Doolittle equation (3).

## The Entropy Theory

Gibbs (49) has asserted that a thermodynamic consideration for glass transition is necessary, by saying in effect that the mere explanation of a phenomenon being a rate process does not explain the phenomenon; it merely shifts the point of emphasis. It is intuitively obvious that molecular relaxation rates must have an explanation in the ground state and the lower-lying excited states of a system and, therefore, must admit to a thermodynamic origin. This has been ignored in the concept of the free volume theory.

Gibbs and DiMarzio (50) have developed a thermodynamic theory of glass transition which is applicable to specifically polymer molecules. In polymer molecules, single carbon-carbon bond allows rotational freedom, but there are potential barriers that resist the rotation. Above  $T_g$ , enough thermal energy is available, the barriers are crossed frequently, and each polymer molecule has available to it a distinct number of possible spatial conformations. Associated with each of the spatial conformations, there are a set of vibrational states for the whole molecule corresponding to the bond stretching, or libration, within the potential well but these states do not interact with the external translational and rotational states of the molecule. The rotation about any one bond of a molecule depends on the state of the neighbouring bonds of the same molecule and on the distances and interactions between the non-bonded groups. Thus they introduced the need for cooperative interaction between the restrictions to the rotation about the C-C bonds by indicating that characterization of the hindrance, or restriction, to the rotation about any individual bond may not in general be independent of the conformation of the rest of the molecule. Therefore, it is necessary to consider the energy of conformation of each molecule as a whole. There are several minima in the potential as rotation about the  $2\pi$  angle associated with a C-C bond occurs but Gibbs and DiMarzio assumed that all minima except the lowest have approximately the same depth. The polymer chains are flexible and since their conformational state changes with time, they have a high entropy. The statistical thermodynamics of such states in a polymer liquid is described by the quasi-lattice model of Meyer (51), Flory (52) and Huggins (53), which was also used by Gibbs and DiMarzio. The special usefulness of the model here is that approximations in it have a less serious consequence for polymers than for simple molecules, for one can justifiably treat less rigorously the external rotational and translational degrees of freedom of molecules than one can the intramolecular or internal degrees of freedom. The mathematical formulation of the partition function is given in an article by Gibbs (49), but qualitatively

it follows that, on cooling, the polymer chain would assume a conformation for which each rotational coordinate occupies the minima of lowest energy. Thus the flexibility of the chain of molecules, or their ability to choose among many different configurations decreases with temperature. This decrease causes a corresponding decrease in the number of ways in which molecules can be packed together on a lattice. The number of ways of packing, which is directly related to the entropy, rapidly decreases with temperature such that at a finite temperature it becomes unity and the configurational entropy becomes zero. The theory therefore suggests a thermodynamic phase transformation of Ehrenfest type at a temperature,  $T_2$ , at which the configurational entropy is zero. This temperature is represented by point  $G_0$  in Fig. 1. Since the glass transition is a kinetic rather than thermodynamic process, caused by the progressively increasing viscosity or some other kinetic property, Gibbs and DiMarzio proposed that the difficulty in packing together of the polymer molecule, or the increase in the stiffening of the chain, is reflected in the difficulty of producing a configurational change and hence an increasing viscosity. The thermodynamic and kinetic behaviour are thus interrelated. The suggestion is that the kinetic behaviour observed at  $T_g$  is in a sense a reflection of the second order thermodynamic transition one would observe at  $T_2$  if the metastable liquid in the equilibrium state could be studied below  $T_g$ . The plausibility of this unique suggestion, of course, cannot be experimentally tested, but the value of  $T_2$  can be obtained by extrapolation. In a plot of heat capacity against logarithmic temperature,  $T_2$  is the temperature at which the area enclosed by this curve, and by the curve of heat capacity of the crystal is exactly equal to the entropy of fusion of the liquid. The value of  $T_2$  thus obtained is usually 15-20% lower than the calorimetric  $T_g$ . The theory, therefore, seems to resolve the entropy paradox, by suggesting that at a point  $G_0$  in Fig. 1. the liquid settles down into its ground state(s) of amorphous packing and appears to have undergone a second order thermodynamic transition. The dearth of available configurations at temperatures far above  $T_2$  causes the glass transition and thus a kinetic phenomenon intervenes in the approach of a liquid towards its second order thermodynamic transition; the singularity at  $T_2$  is the basis of glass transition.

Adam and Gibbs (54) have extended these ideas by finding a minimum size of molecular group capable of rearranging at a given temperature. They showed that this size, hence the rearrangement probability, is a function of configurational entropy,  $S_{conf} = (S(T) - S(T_2))$  according to,

$$W(T) = A \exp(-C/TS_{conf})$$

and

$$\tau = \tau_0 \exp(-C/TS_{conf}) \quad (9)$$

where  $C$  is a constant.

Since,  $S_{conf} = \int_{T_2}^T \Delta C_p d \ln T$ , and  $\Delta C_p = C_p(\text{liquid}) - C_p(\text{crystal}) \propto T^{-1}$ , Eq. (9) can be written in the form of the Vogel-Fulcher-Tamman equation (2), with  $T_2 = T_0$ .

#### Extension of the Free Volume Theory

The treatment of glass transition within the concepts of free volume has been carried further (55,56) to include the decrease in entropy on cooling and here support has been sought from experiments of a quite different nature. In recent years studies of molecular dynamics of hard spheres (57) have suggested the existence for a relatively long time of cellular or cage structures in dense liquids. Cohen and Grest assert that this justifies the assumption that in liquids the movement of each molecule is restricted to within its cell, or cage, which is defined by its nearest neighbours. Kirkwood (58) had envisaged the existence of such cells in liquids and by assuming that all cells are identical, had defined a communal entropy,  $S_c$ , which arises from the diffusion of molecules throughout the entire volume of the liquid. This is given by

$$F = \int f_1 - TS_c, \quad (10)$$

where  $F$  is the free energy and  $f_1$  is the free energy of the atom or molecule moving within its own cell in the mean potential of its neighbours. (This is implicit in delocalizing of the atoms as we go from a crystal to a disordered fluid. In a crystal each lattice cell contains no more than one atom; in the limit of an ideal gas the number of atoms in any small test volume fluctuates over a Poisson distribution, and in the in-between range of density  $S_c$  is some function of the volume.) In the extended treatment all postulates regarding the free volume remain the same as in the original Cohen-Turnbull's description (47). The local free energy  $f_1$  of a cell depends only upon its volume  $v_1$ ,  $f = f(v)$  and Eq. (10) becomes

$$F = N \int P(v)[f(v) + kT \ln P(v)] dv - TS_c \quad (11)$$

where additional entropy term  $P(v)$  is the probability that a cell has a volume  $v$ . Cohen and Grest consider that the local free-energy-function  $f(v)$  represents two conditions (i) the negative of the work needed to remove the molecule from the interior of a cage of volume  $v$ ,  $f_0(v)$  and (ii) the work to expand the cage to the volume  $v$  from its average value,  $f_1(v)$ . The contribution from (i) is assumed to vary with cage volume in the same manner as the intermolecular pair

potential with pair separation, but that from (11) is complicated, for it depends upon the state of neighbour of the particular cage. The total local free energy  $f(v) = f_0(v) + f_1(v)$  is, however, an approximately quadratic function of  $v$ , when the cage volume is less than a certain critical volume,  $v_c$ , but has an additional linear term when  $v \geq v_c$ . Thus when  $v < v_c$  the cells are solid-like and when  $v > v_c$  they are liquid-like. Only liquid-like cells have a free volume,  $v_f = v - v_c$ . Part of the local free energy depends only upon the average  $v_f$  and remains unchanged by any redistribution of  $v_f$  among the liquid-like cells. Such an exchange occurs only within the liquid-like cells which are nearest neighbours and which have a sufficiently large (but temperature-dependent) number of other liquid-like cells as neighbours. During the exchanges, the volumes of any neighbouring solid-like cells are unaffected. Thus a minimum size of the cluster is defined within which an exchange in free volume without restrictions by the neighbouring solid-like cells can occur. This notion leads directly to the introduction of percolation theory, which is used to describe the generation of communal entropy. When the fraction of liquid-like cells is above a critical value, there is an infinite connected liquid-like cluster and the material is liquid. But when it is below this value, only finite liquid-like clusters are present and a glass phase exists.

A discussion of the entire derivation is beyond our scope but in essence atoms diffuse when a cell volume of  $v_m$  or greater occurs as a result of redistribution of the free volume within a cluster. For diffusion to occur, the total free volume within a cluster of size  $v$  must be greater than  $v_m$ . Such a cluster is a liquid cluster and each molecule or atom in it moves through the entire cluster. The configurational space of each molecule is available to any other within the cluster and this generates the communal entropy,  $S_c$ , which only enters the free energy as  $TS_c$ . Thus the size of the liquid cluster  $v > v_m/v_f$  where  $v_f$  is the average free volume. Clusters of this size are frozen-in at temperatures below  $T_g$ .

The theory is capable of describing the changes in the thermodynamic variables usually associated with the freezing out of diffusion near  $T_g$ , but it also predicts a first order phase transformation (with latent heat and a discontinuity of macroscopic volume) at a temperature  $T_p$ , which is not very far below  $T_g$ , from a liquid to glass phase, i.e. from a state of an infinite connected cluster of liquid-like cells to the state of finite clusters. The viscosity of the liquid according to the theory does not follow the Vogel-Flucher-Tamman equation, rather it predicts a temperature  $T^0$ , which is

substantially above  $T_g$  and at which the  $\log \eta$  increases approximately as  $T^{-1/2}$ , according to the equation,

$$\log_{10} \eta = A + 2B/(T - T^0) + [(T - T^0)^2 + \text{constant} \times T]^{1/2}$$

The prediction is that near  $T^0$ , there is a gradual change in the behaviour of viscosity with temperature, but there is no single temperature (except OK) at which  $\eta \rightarrow \infty$ .

### A Critique, Other Views and Conclusions

The strength of the two types of theories lies in their qualitatively correct explanations of glass transition using the equilibrium thermodynamic properties. One is based on the model of hard spheres, or the inert gas type of glasses, and the second applies only to flexible macromolecules, or polymers. Neither can be expected to explain the behaviour of a wide variety of supercooled liquids near  $T_g$ , but, while some of the incompatibility of the free volume theories with the observed pressure dependence of viscosity has been removed by allowing  $v_0$  to depend both upon  $T$  and  $P$  (59), several objections (of a fundamental nature) to accepting this theory remain. As Anderson (31) has pointed out, one is the physically implausible assumption of a constant value of expansivity from  $T = T_0$  (where  $v_f = 0$ ) to  $T > T_g$ , and the second is of a constant  $\Delta v_c$  between absolute zero and  $T_0$ , which is necessary in order to avoid a conflict with Van der Waal's equation (which requires  $T_0 = OK$ ). I think the fact that the expansivity is not constant within any range of  $T$  is implied in Doolittle's (44) analysis, but apparently has been ignored by Cohen and Turnbull (47). His preference for the variation of  $\eta$  with free volume by Eq. (3) was based on his finding that viscosity could not be fitted to the Andrade or Arrhenius equations. If, as Cohen and Turnbull assume, the expansivity remained constant with  $T$ , Eq. (3) would be equivalent to the Andrade or Arrhenius equations. It is difficult to see how the introduction of a temperature-dependent expansivity in Eq. (8) could be reconciled with the documented success of Doolittle's Eq. (3).

Furthermore, the free volume theory is strictly a theory for self diffusion. The diffusion coefficient,  $D$ , in Eq. (7) is related to  $\eta$  by Eq. (6). But I think the assumptions inherent in the two equations make them mutually exclusive, not complementary. In the derivation of Eq. (6) it is assumed that the cage surrounding the molecule moves with the molecule, but in that of Eq. (7) the cage remains stationary so that the translational jump across a void within its cage is possible. It seems that the

consequences of some of these approximations become apparent in Cohen and Grest's (55, 56) calculations of the effect of annealing on the position of the heat capacity anomaly in a temperature plane. The theory shows, contrary to the experiments (Fig. 1), that annealing of a glass shifts the temperature of its heat capacity anomaly downwards and that the lower the annealing temperature, the larger the shift.

Neither of the theories explains the distribution of dielectric or volume relaxation times or the retarded elastic deformation characteristic of liquids near  $T_g$ . They also do not provide a satisfactory explanation of the state of a liquid below  $T_g$  along the path  $GG_0$  (Fig. 1). In the extended free volume theory, the arrival at a percolation threshold with decreasing volume on cooling below  $T_g$  is suggested to cause a first order transition to an amorphous ground state of fixed configuration (55), and the entropy paradox thus seems to have been resolved. But it is possible to supercool through a first order transition and be led into a more complicated situation (in which the equilibrium liquid is metastable with respect to the amorphous ground state as well as to the ordered crystalline state), without resolving the paradox. The entropy theory suggests that the configurational state of a liquid is frozen-in at  $T < T_g$  and there is no further decrease in the configurational entropy from  $T_g$  to OK. The presence of secondary relaxations and configurational degrees of freedom in a glass indicate that this suggestion is oversimplified, therefore, making a resolution of the entropy paradox difficult. Furthermore, the weakness of the entropy theory in resolving this paradox is inherent in Flory-Huggins (52,53) approximations of a lattice model and Gujarati and Goldstein (60) have suggested that the explanation of the paradox is an artifact of the model.

There is also a difficulty in understanding how the communal entropy of Kirkwood's equation and of Cohen and Grest's theory can be generated in orientationally disordered crystals, where the molecules are confined to the sites of a periodic lattice. As mentioned here earlier, these crystals show a loss of entropy and a decrease in the relaxation rate on cooling in the same way as ordinary liquids; and in some cases the loss is more in the glass-like state than in the glassy state of the same substance. One would therefore consider that the similarity of the entropy loss in "true" glasses to that in the orientationally disordered glass-like states of crystals is evidence for the important role of factors other than communal entropy in the glass transition.

A theory of glass transition should not merely be a theory of self diffusion related to viscosity by Einstein-Stokes' or some other

empirical relation. It should also explain, as Goldstein (61) has emphasized, how the external stress biases a local molecular rearrangement, and how this rearrangement produces an irreversible macroscopic deformation of a liquid. Goldstein himself provides a tentative explanation by considering a potential energy barrier picture for viscous flow in which the configurational state of a liquid can be specified as being in any one of the minima in a  $(3N + 1)$  dimensional potential energy surface for an  $N$  particle system. The state point of the liquid may be considered to drift in a random walk fashion among the many possible minima of varying depths. (This feature alone distinguishes a liquid from an ordered crystal.) The deep minima are less numerous and are separated by larger potential barriers. Thus a temperature dependent activation energy is associated generally with a decreasing configurational entropy. At a low temperature, therefore, a glass, like a crystal, is at or near a potential energy minima. The clarity and physical insight of Goldstein's description is difficult to improve upon, and his picture leads to an understanding of how an initial reversible strain becomes irrecoverable after a period of time in terms of the erasure, through a series of local rearrangements, of the memory of the original potential energy surface and the concomitant generation of a thermodynamically equivalent new surface. The picture, whose thermodynamic formulation has been possible (61), thus incorporates the essentially cooperative character of the relaxation process with a consequence that retarded elastic deformation is a phenomenon associated with viscous flow, and the relaxation process involved in shear has a distribution of relaxation times. The cooperative character here means that molecular motions cannot be treated in terms of a smoothed out quasicontinuum, or in terms of binary encounters, but rather as a gradual dying-out of the encounters with distance in a certain local region. It also suggests the possibility of some molecular motions at  $T < T_g$  of the same type that are involved in the viscous flow.

There are several other suggestions that focus attention on an extra volume as "holes" or "defects" of uniform size, randomly distributed in a liquid. Molecular relaxation occurs when a defect diffuses to a molecular site. The original treatment of the defect diffusion due to Glarum (62) has been extended by Phillips *et al.* (63) to explain the viscoelastic behaviour and the extended treatment predicts a viscosity according to the Vogel-Fulcher-Tamman equation. Another sophisticated treatment of the "hole model" has been given by Nose (64). However, there is a difficulty in reconciling these and the other free volume type treatments as a description of an occasionally found glass transition, which occurs with a negative

change in expansivity (65). There is a further difficulty, for, in their simplest form, such models are two-state, one-order-parameter descriptions and do not agree with the observation that Prigogine-Defay ratio generally exceeds unity. The entropy theory has two parameters: (i) the fraction of the flexible bonds motions about which contribute to  $C_p$  and (ii) the number of holes which contribute to  $\alpha$  and  $\beta$ . If both parameters freeze at  $T_g$  then the Prigogine-Defay ratio is  $>1$ . Taken together these findings seem to give strong reasons for preferring an entropy or energy as a basis for discussion of glass transition.

#### Molecular Mobility in Glasses - Secondary Relaxations

It is important to realize at this point that not all molecular mobility ceases to occur in a glass at temperatures below  $T_g$ . In addition to the librational, rotational, and stretching vibrations of atoms or molecules, there are small scale atomic or molecular rearrangements that continue to occur in glasses to temperatures of several Kelvins. (These should not be confused with the molecular motions associated with the irreversible change in the physical properties on annealing of a glass (66) or to those involved in tunneling between the configurations corresponding to the asymmetric double-well potentials (67).) The evidence for these is generally from dielectric and mechanical relaxation (68) and from nuclear magnetic resonance (69) studies which reveal them as secondary relaxations. Their average time scale is usually several orders of magnitude lower than the time scale of the motions responsible for the main relaxation, or viscous flow. The latter, though imperceptibly, also of course continues to occur in glasses.

Until some years ago, explanations for these types of molecular motions were based on ad hoc hypotheses, one for each substance, or for a class of substances. They were attributed to an internal degree of freedom of the molecule which fortuitously remained active even when the molecule as a whole was frozen in place in a glassy matrix, although it was also known that the same degrees of freedom were inactive when the molecule was in its fully ordered crystalline state. In amorphous polymers, the presence of such relaxations are often explained by the hindered rotation of the molecular group attached to the main chain, when the rotation about the C-C bond of the chain itself is imperceptibly slow below  $T_g$ . Relaxations of a similar type when observed in polymers without a side group, as in poly (vinyl chloride), have been explained by the possibility of a special type (crank-shaft) of motion of the main polymer chain (70). But poly (propylene oxide) also shows such a

relaxation below  $T_g$  (35) for which this explanation is not valid. In silicate glasses, wherein the assumed network structure is inconsistent with the existence of individual molecules, two types of explanations have been offered: relaxation of the network itself involving hindered motions about silicon-oxygen bonds, or diffusion of mobile species from site to site within a rigid network (71).

It is now considered that the presence of some molecular mobility is an intrinsic property of the amorphous packing and does not require the aforementioned ad hoc explanations. Convincing evidence for it is the presence of secondary relaxations in glasses obtained from rigid-molecular substances (72, 73). The prediction that this would be the case for glasses of all types was made by Goldstein (61), and was one of the consequences of the considerations implicit in his energy barrier picture for glass transition.

In this picture, one envisages a situation where a macroscopic sample of a liquid has been cooled into a rigid condition even though certain local regions in it have potential minima still accessible to them at low temperatures. Argon (74) was led to a similar conjecture on the basis of a description of delayed elasticity and viscous flow in organic glasses, but this possibility was originally suggested by Orowan (75), whose ideas were also used in the development of the potential energy barrier picture. The consideration of this picture has become even more interesting, for Haylor and Goldstein (73) have found that the probability distribution of the average relaxation times for these molecular motions is such that in rigid molecular glasses not one but several relaxation peaks appear between 10K and  $T_g$ .

#### Dielectric and Mechanical Relaxations

In a glass, the molecular motions of an unspecified nature are, of course, occurring all the time in the absence of an external stress; the external stress, by biasing them, reveals their existence, although they can be studied in the absence of a stress by other means. In most experiments the stress applied is either the electric field as in a dielectric measurement, or a mechanical stress, as in a mechanical measurement, and use is made of the fact that the polarization or strain response of a glass to a sinusoidal field of a suitable frequency lags behind the applied electric field, or the mechanical stress. This phase lag results from the time necessary for molecular rearrangement, and is analogous to the time lag observed in the step-function experiments. If  $\epsilon'$  and  $\epsilon''$  are the real and imaginary components of the complex dielectric permittivity and  $J'$  and  $J''$  that of complex shear compliance, the loss



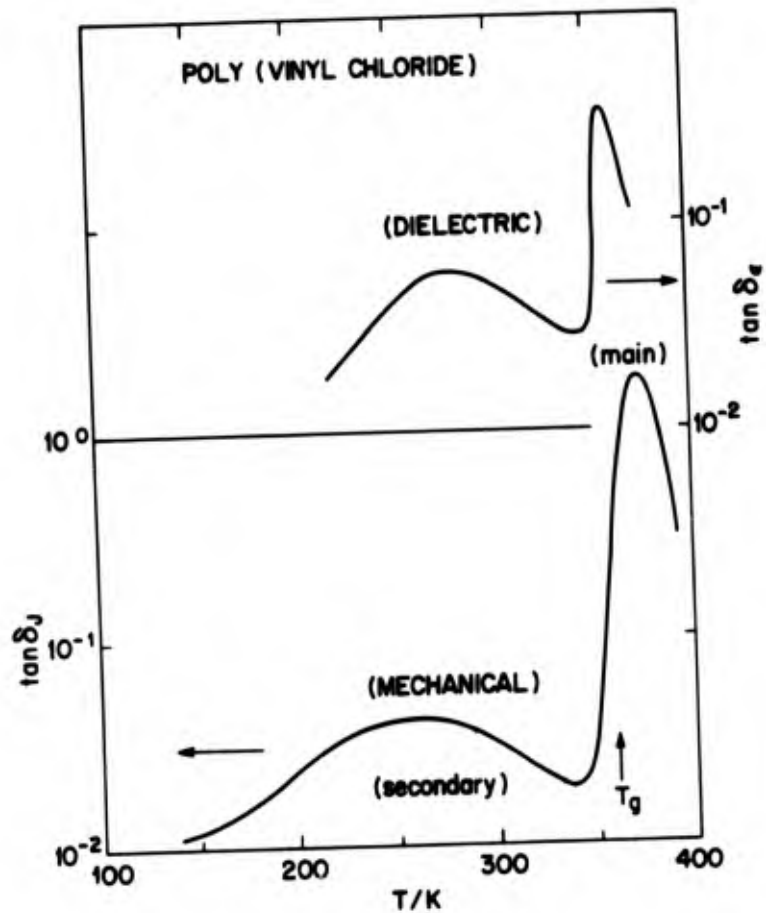


Fig. 4: The dielectric(76) and mechanical(77) loss factor at 100 Hz of polyvinyl chloride plotted against temperature. The two peaks represent the main and secondary relaxations.  $T_g$  is the glass transition temperature.

tangent  $\tan \delta_e = (c''/c')$ , and  $\tan \delta_j = (J''/J')$ , and, in most cases, the angular frequency  $\omega_m$  at which  $\tan \delta_e$  or  $\tan \delta_j$  is maximum is equal to the average relaxation rate of the molecular motions involved. In a mechanical relaxation it is more convenient to measure  $\tan \delta_j$  at a fixed frequency as a function of temperature. Since the rate of molecular relaxation given by  $\omega_m$  decreases with temperature according to an Arrhenius equation, the average relaxation rate is equal to the frequency of measurement at a temperature  $T_m$  where  $\tan \delta_j$  or  $\tan \delta_e$  is maximum. The variation of  $\tan \delta_j$  with  $T$  for the case of single relaxation time is given by,

$$\tan \delta_j = \frac{(J_s - J_\infty) \omega / \omega_m}{(J_s J_\infty)^{1/2} (1 + (\omega / \omega_m)^2)}$$

and

$$\omega_m = \omega_0 \exp(-E/RT)$$

where  $J_s$  and  $J_\infty$  are the limiting low and high frequency values of the shear compliance, which are analogous to  $c_s$  and  $c_\infty$  of the dielectric response. Measurement of

$\tan \delta_e$  at a fixed frequency as a function of temperature is just as convenient as its measurement with frequency at a fixed temperature, but the two measurements, as we now know (73,11) do not give the same value of  $\omega_m$  at the same temperature.

Most mechanical measurements are made at frequencies of a few Hz and the value of  $\omega_m$  or  $T_m$  obtained often agrees with the corresponding extrapolated value from dielectric (68) and nmr studies (69), although the shape of the  $\tan \delta$ -temperature plots in the mechanical and dielectric measurements differs. Examples of these types of measurements (76,77) for poly (vinyl chloride) are given in Fig. 4.

Though mechanical measurements on rigid molecular glasses have not so far been carried out, their dielectric studies show an essential similarity in the relaxation characteristics with amorphous polymers. Furthermore, the secondary relaxations in the glass-like states of orientationally disordered crystals (9,78) and in glasses obtained from liquid crystals (11,12) are remarkably similar to those in amorphous polymers. This suggests that the processes

involved in the secondary relaxation admit to the same physical mechanism, despite the differences in the complexity of molecules or state of their aggregation in the amorphous solid.

### Thermodynamic Changes

If certain localized configurational states in the otherwise rigid matrix of a glass were to exist, as the relaxation data indicate, then the thermodynamic properties of a glass would have contributions from two sources: first, the lattice vibrations and second, the configurational states. Simha and others (79) have shown that the latter contribution to the expansivity of polymers is substantial and Goldstein (80) and Johari (81,82) found that such configurational states also make a significant contribution to the heat capacity and entropy of a glass.

The analysis which led to this conclusion was done in terms of the excess entropy,  $S_{exc}$ , which is the difference between the calorimetric entropy of the disordered phase and of the corresponding crystalline phase, viz., the residual (zero-point) entropy of the two phases has been subtracted from the entropy itself. The  $S_{exc}$  is evaluated from the difference between the area of their respective ( $C_p/T$ ) against temperature plots. The value of  $S_{exc}$  increases with temperature in a manner seen in Fig. 5 which is remarkably similar among the various types of disordered solids,

despite the differences in the states of their molecular aggregation. As the temperature is raised, there is a slow increase in  $S_{exc}$  followed by an apparent tendency towards a constant value and then a progressively higher increase beginning at a temperature of  $0.8 T_g$ , or lower. A discussion in quantitative terms of this increase in  $S_{exc}$  has been difficult because it is not yet possible to formulate the potential energy surface of a disordered matrix, with small potential energy minima, which may account for the secondary relaxations observed below  $T_g$ . There are further complications because the configurational and vibrational partition functions of a condensed state are not quite independent of each other, as the configurational states of lower energy also have a higher frequency of vibrations. It has been possible, however, to discuss in the most general terms what physical changes the observed increase of  $S_{exc}$  with temperature indicates.

For two phases of a material having the same anharmonic vibrational contributions and configurational entropy, the plot of  $S_{exc}$  against temperature would resemble the Debye heat capacity curve; that is, with increasing temperature it would have an initial rise followed by an approach towards an asymptotic value at a characteristic temperature given by,  $\theta = (hv/k)$  per degree of freedom, of the frequencies that differ between the two phases. This would be the case also if the contribution to  $S_{exc}$  in both phases were

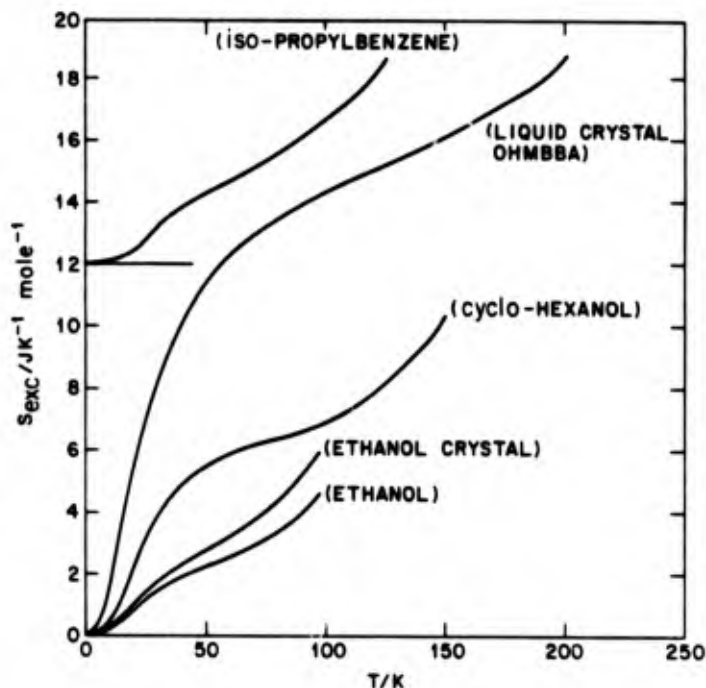


Fig. 5: The excess entropy of several types of glasses plotted against temperature(82). The curves are terminated at  $T_g$ .  $S_{exc} = 0$  at 0 K for all glasses.

entirely vibrational in origin and the vibrations were harmonic. If this simplification is accepted then the progressively higher increase in  $S_{exc}$  with temperature is due largely to the configurational changes involving small-scale molecular rearrangement and/or internal molecular degrees of freedom. A small contribution to  $S_{exc}$  from the difference between the anharmonic effects in the disordered and the ordered form is also anticipated, but whether this contribution would raise or lower the  $S_{exc}$  is not known. The contribution from anharmonic effects depends upon the changes in the force constant, and in the density of states of the low-frequency lattice modes with temperature and volume, and neither of these changes are known for either the disordered or the crystalline form. We might expect that the magnitude of such changes in an orientationally disordered crystal and its ordered form would be similar and therefore, the anharmonic effects would make a much smaller contribution to the  $S_{exc}$  of a disordered crystal below  $T_g$  than to that of a glass. The fact that the two classes of solids have a similar increase in  $S_{exc}$  beginning at about 20-80° below their respective  $T_g$ s, suggests that the configurational contribution must be significant in glasses. But the convincing evidence for it comes from measurements of the isopropyl benzene glass wherein a decrease in the excess heat capacity occurs near a temperature (83) at which the extrapolated rate of the secondary relaxation is  $\sim 10^{-4}$ s (72).

The thermodynamic parameters of several types of glasses and disordered solids have been given earlier (82). These are useful for a further discussion of the configurational state of a glass. More data of similar type for several organic and inorganic glasses, ortho-terphenyl, selenium, poly (vinyl chloride) and other polymers have been given by Goldstein (84) and Goldstein and Gujarati (85).

Several points of interest can be deduced from these parameters. One is related to the residual entropy of a disordered solid. It is generally assumed that a glass is in one of the configurational states associated with a certain potential minimum of the liquid at a temperature  $T_g$ . Thus the residual entropy of the glass corresponds to the configurational entropy of the liquid at  $T_g$ . The analysis (80-85) shows that  $\Delta S(T_g)$  is considerably higher than  $\Delta S(OK)$ . The fraction of the entropy difference at  $T_g$  and OK ranges from 0.2 to 0.7 for a variety of disordered solids, i.e. 20-70% decrease in the entropy of these materials occurs on cooling from  $T_g$  to OK. It is apparent that a significant fraction of the configurational heat capacity above  $T_g$ , comes from small-scale configurational changes that also occur in the disordered solid, and

therefore the thermodynamic properties of a disordered solid are not determined solely by the vibrations of a rigid lattice in which every atom is bound to a fixed site.

The vibrational contribution to the excess entropy is of some significance in the discussion of the glass transition. As discussed here earlier, Kauzmann (16) pointed out that, if the curves of entropy, volume and enthalpy of the liquid phase were extrapolated toward absolute zero, the liquid phase would have, paradoxically, a smaller entropy and volume than the crystal at absolute zero. The point raised by Kauzmann, and its further consideration by Gibbs and DiMarzio, are based on the assumption that the vibrational  $C_p$  of the liquid is equal to that of the crystal. In the treatment of Gibbs and DiMarzio (50), the excess configurational entropy of an internally equilibrated liquid may become zero at a certain temperature, but it is difficult to envisage why the excess vibrational entropy should also be tending to zero at this temperature. Rather, it is anticipated that the entropy of the "liquid phase", having a near-zero configurational contribution at  $T_2$ , would be higher than that of the crystal by an amount related to the difference between their Debye temperatures. This difference in the vibrational entropy would decrease to zero, in most cases, at OK. Unfortunately, the Debye temperature has not been determined as a function of annealing, or fictive temperature, of the glass, but it is reasonable to expect that the excess vibrational entropy of the glass, which is substantial according to Fig. 5 (82), would not greatly decrease on annealing to an internally equilibrated state of a liquid. This view conflicts with the prediction of the second-order thermodynamic transition of Ehrenfest type in the experimentally inaccessible range of temperature below  $T_g$ .

#### Kinetics of Molecular Motion

The average rate of the secondary relaxation in glasses, seen in Fig. 6 (11,35,36,78) varies with temperature, according to the Arrhenius equation with an activation energy between 18 - 40 kJ mole<sup>-1</sup> for different materials. Since this value is much lower than the "activation energy" for the rate of the main relaxation or of the viscous flow near  $T_g$ , it follows that at a certain temperature above  $T_g$ , where the liquid is less viscous, the rates of the main and secondary relaxations should be equal. Therefore, the two curves of the rates of the respective molecular processes in a  $T^{-1}$  plane should merge above  $T_g$ . This conclusion was in fact reached from results on rigid molecular glasses (72), an example of which is shown in Fig. 7 (36). Experimental difficulties have prevented the observation of the merger of the two curves and, therefore, the viscosity or the molecular diffusion rate of the liquid at which this is inferred to

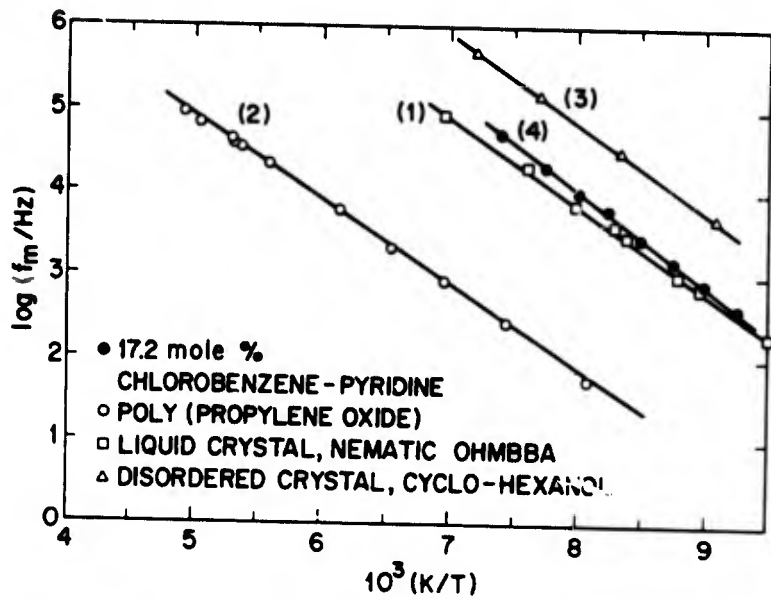


Fig. 6. The Arrhenius plot of the dielectric relaxation rates in several types of glasses. The source of data are: 1(11), 2(35), 3(78), 4(36).

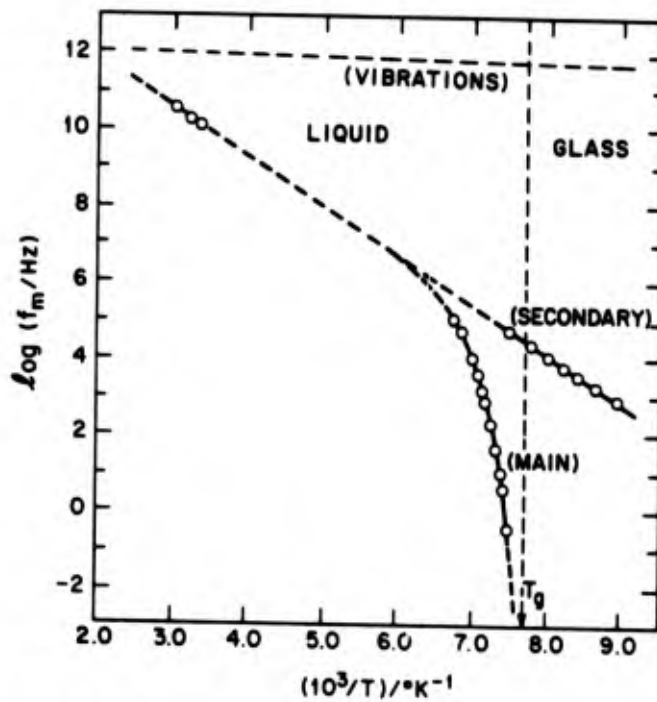


Fig. 7. The different types of molecular motions in a liquid and a glass(36). The data are for 17.2 mole% chlorobenzene-cis-decalin solution. In addition to the vibrational modes, there are two types of molecular processes, known as secondary and main relaxations.  $T_g$  is the glass transition temperature.

occur is not known. But the situation can be qualitatively understood in terms of the potential energy barrier picture of glass transition (61, 9). In this view, the configurational state of a glass is trapped in one deep minimum in a multidimensional potential energy surface. This deep minimum, which is associated with a configuration representing the barriers for the main relaxation, has in it multiple "local" minima of varying depths separated by potential barriers smaller than those that separate the deep minima. The main configuration can be graphically represented as a deep well in the configurational space with a "rough and corrugated" bottom rather than a round one. The configurational changes involving the deep minima determine the rate of the main relaxation. An interpretation of the results according to this view means that, as a glass is heated from OK, the lower energy barriers become surmountable to its configurational point, while the deep minima in which a given configurational state is trapped remain largely unaltered. If this continued to occur on heating then at a certain temperature above  $T_g$ , there would no longer be a distinction between the respective minima involved in the molecular rearrangements that give rise to the main and secondary relaxations. This temperature would be the one at which the processes apparently merge. Above this temperature the configurational points are likely to involve the many minima separated by small potential energy barriers and changes between these states would be observed only as what appears to be the secondary relaxation.

The kinetics of these molecular motions has two more distinct features. One is that they apparently involve a wide distribution of relaxation times (9, 12). The half width of their relaxation spectrum is 4-6 decades of frequency - in contrast to 1.14 decades, which is characteristic of a Debye-type single relaxation time - and it increases further on cooling. No distribution function has been able to account for the width of the spectrum and it has generally been considered that the spectrum represents a sum of several single relaxation processes, each being Debye-type. The second feature is that the total polarization associated with the secondary relaxation rapidly decreases with temperature (9,86). While this obviously indicates a gradual decrease on cooling in the number of molecular groups that contribute to the polarization, it also suggests that the excess entropy of a glass arising from these molecular motions should decrease with temperature, as discussed earlier.

#### Relation with the Equilibrium Liquid

The inference that the rate of the secondary relaxation in a glass becomes equal to the rate of the main relaxation at a temperature above  $T_g$ , raises the question

whether the secondary relaxation and the molecular motions responsible for it continue to occur at  $T > T_g$  or whether its existence is associated with the thermodynamically non-equilibrium and, as in some cases mechanically strained, state of a glass. In effect, we are asking, will the secondary relaxation in a glass persist if it is allowed enough time to become an equilibrium liquid? To answer this question measurements have been made at temperatures above the calorimetric  $T_g$  and these have shown the presence of secondary relaxations in several molecular glasses (36). Similar results have been found also in the rubber region (above  $T_g$ ) of poly (ethyl methacrylate) (87,88). Thus the molecular motions seen in a glass are a property of the equilibrium liquid state above  $T_g$ . Calculations of the dipole moment from the magnitude of polarization suggest that nearly 20-50% of the total polarization at  $T > T_g$  is due to the secondary relaxations (9). This percentage is comparable with the magnitude deduced from an entropy analysis (82), suggesting that nearly 30-70% of the configurational heat capacity or entropy of the liquid arises from molecular motions involved in the secondary relaxation.

These results have an immediate consequence for our understanding of disorder in liquids, for it seems to be required that secondary relaxations have their origin in the configurational states of the liquid which remain essentially unaltered during the glass formation. If one accepts the existence of the two types of molecular motions in the liquid, a theory of glass formation should account for: (i) the bifurcation of the curve of the relaxation rate at  $T > T_g$  in a manner seen in Fig. 7, (ii) the progressive separation on cooling of the main from the secondary relaxation and (iii) the rapid increase in the magnitude of the main and a decrease in that of the secondary relaxation at  $T \leq T_g$ . The existence of two relaxation regions in a liquid and glass merely reflects the difference between the average time scales of the molecular motions involved.

#### Relation with the Non-equilibrium in Glasses

One of the characteristics of the glassy state is that its thermodynamic properties change on annealing or on changing its fictive temperature, thus the lower the fictive temperature of a glass, the lower its residual (zero point) entropy. But annealing seems also to cause a decrease in the number of molecules which contribute to secondary relaxations (72). This conclusion was based upon the finding that the height of the secondary relaxation peak decreased on annealing. This conclusion has been subject to doubt, for mechanical measurements on several polymers (89) seem to show that annealing has no effect on the secondary relaxations, but causes the high temperature

"tail" of the broad spectrum of the main relaxation to shift to a lower temperature, thus carrying with it a fraction of its contribution to  $\tan\delta$  at temperatures where a secondary relaxation is observed.

Haddad and Goldstein (90) have given a new turn to this problem by suggesting that the analysis of the results of annealing is considerably more complicated by the presence of a frequency-independent background dielectric, or mechanical, loss on which the secondary relaxation peak is superposed. This loss, being an order of magnitude (or more) higher in the amorphous solid than in the corresponding crystal, also has a  $T^n$  dependence, and the decrease in the height of the secondary relaxation peak on annealing may be partially due to a decrease in the background loss itself. Though they did find evidence for a decrease in the magnitude of the secondary relaxation in two cases, the resolution of this problem is not difficult. During the course of isothermal annealing, if  $\tan\delta$  in the spectrum decreases more at low than at high frequencies, the decrease in the height of the secondary relaxation peak is due predominantly to a shift toward lower frequencies of the main relaxation. If  $\tan\delta$  decreases by nearly the same amount at all frequencies, the observed effect is due predominantly to a decrease in the background loss. But if  $\tan\delta$  decreases more at higher than at lower frequencies, or the decrease itself is maximum at some frequency, the effect is due predominantly to a decrease in the number of molecules contributing to the secondary relaxation. Using these as criteria, dielectric measurements made on a rigid-molecular glass, on polymers (35) and on nematic (11) and cholesteric (12) glasses and mechanical measurements on a chalcogenide ( $As_2Se_{18}$ ) show direct evidence for the decrease in the magnitude of the secondary relaxation on isothermal annealing. Thus the irreversible thermodynamic changes on annealing, or a decrease of fictive temperature, of a glass decreases the number of molecules involved in its secondary relaxation. The excess entropy of the quenched glass over an annealed one (80,84) must arise partially from this effect.

The above discussion leads to a different type of question, namely, is there an equilibrium magnitude of the secondary relaxation at a certain temperature at a point along the line  $AG_0$  in Fig. 1? The answer is that there must be, for it has been shown earlier that the magnitude of the secondary relaxation has a certain fixed value in the equilibrium liquid above  $T_g$ . But, if so, would there be a secondary relaxation at the hypothetical temperature  $T_0$  or  $T_2$  at point  $G_0$  in Fig. 1? It seems a definite physical possibility that the magnitude of the secondary relaxation would be very small, if any, at this temperature. There is no experiment to test this assumption directly,

but, on the other hand, no existing result contradicts it. Some idea as to whether this could be the case may be gained from measurement of the effect of volume on the magnitude of the secondary relaxation and extrapolating to a volume corresponding to the point  $G_0$  in Fig. 1.

#### Possible Molecular Origin

It is generally agreed that both the main and secondary relaxation processes should involve major rearrangements in the position and/or orientation of several molecules in a certain local region and that these motions probably involve a distribution in the heights of energy barriers. But a distribution in the heights of potential energy barriers resisting the molecular jumps, though responsible for the presence of some molecular mobility in a glass, would not produce two separate maxima. Instead, it would suggest a spreading out of the dielectric or mechanical relaxation spectrum over a wide frequency range. It would seem necessary to assume a form of density of states vs energy relationship, different from that inferred from thermodynamics, if secondary and main relaxations are to be thought of as two different processes.

It is conceivable, after Williams and others (91,92) suggestion, that molecular dipoles may exist in a variety of different environments, and may be partially relaxed by local motions in their particular environments; and this local motion may appear as a high-frequency, or secondary relaxation. The rest of the  $\mu^2$  that is not relaxed by local motions may relax slowly by the grosser process of the co-operative micro-Brownian motion of the environment itself, and this may appear as main relaxation. With increasing temperature the rate of micro-Brownian motion increases much more rapidly than that of local motions, and therefore at  $T > T_g$  the curves of the two relaxations (Fig. 7) merge. Thus the correlation function for a dipolar reorientation involves both the main and secondary relaxations. Reid and Evans (93) have considered a similar picture but have extended it by showing that the main, and secondary relaxations, and the absorption at infrared frequencies are continuous and represent the evolution with time of a single ergodic process whose long time behaviour is given by the main relaxation. While this is a reasonable picture of dielectric relaxation of a polar molecule interacting with a smoothed out quasi continuum, it fails to account for the very broad spectrum of relaxation times, the non-Arrhenius behaviour of Eq. (1), and in particular, the variation in the magnitude of the two relaxations with temperature.

A second possibility is that a glass is structurally non-uniform and that a number of statistically distributed regions of low density, in which a molecule or molecules can

sit with non-equivalent probabilities in many possible orientation sites, exist in its structure. The secondary relaxation may then be envisaged as arising from hindered rotation of some molecules in these local regions, which are encaged by a larger region wherein the requirement for a concerted, or a cooperative, motion has made relatively immobile the arrangement of the majority of molecules. The motion of the molecules in the local regions is analogous with the motion of guest molecules in a clathrate structure (94, 95), where the orientations of the molecules forming the cage lattice are relatively fixed. With this analogy in mind it is easy to envisage how nearly all the characteristics of secondary relaxation can be anticipated.

At any point inside a cage of ill-defined geometry the electrostatic field  $\underline{E}$  determines the distribution of barrier heights through contributions of the form  $\mu \cdot \underline{E}$ . Thus the presence of a broad distribution of electrostatic fields and field directions imposed by the molecules surrounding a given local region would lead to a highly variable perturbation of the potential energy function that describes the short range interaction between the molecule at any of the several points in the local region and its fixed neighbours. As no symmetry of the field is imposed inside the local region by the surrounding "rigid" molecular matrix, the orientation of the molecule in question would become distinguishable from an isotropic reorientation, and thus the secondary relaxation would depart from a single relaxation time. Furthermore, the potential energy contours in the different local regions would be far from identical, thus further causing a wide distribution of the relaxation times. The asymmetry of the loss spectrum is, therefore, mainly attributable to the effect of  $\underline{E}$  from the surrounding molecules in lowering the barrier to rotation of the molecules within the local regions. (For example,  $\underline{E}$  would tend to lower the barrier between two orientations most favoured by the field direction and to raise the barrier between those less favoured. The net effect is that the absorption is more at low frequencies than at high and the loss spectrum becomes asymmetric.)

It also follows that the magnitude of the secondary relaxation would increase with temperature, and the loss spectrum would become narrow, for the orientations favoured by the electrostatic field become less populous as  $kT$  increases. Furthermore, the number of such "islands of mobility" would increase with temperature because of a concurrent decrease in the size of the "cooperatively" rearranging regions. The increase in the magnitude would occur at the expense of the contribution due to the main relaxation. This of course has been observed in several molecular glasses (9) and in polymers (87,88).

The number of such local regions in a glass, where molecules can admit different orientations, would, under isothermal conditions, decrease with the molecular volume and therefore with the fictive temperature of the glass. The magnitude of the secondary relaxation would then be lower for an annealed glass than for one obtained by fast cooling, as discussed earlier.

At a  $T > T_g$ , the total dipolar reorientation would be hindered by the potential energy barriers that are different from those involved in the cooperative rearrangements. At very high temperatures, therefore, the secondary relaxation would be similar to that seen in liquids and in orientationally disordered crystals at the microwave frequencies. This is shown in Fig. 7, where the dashed line indicates a possible extension of the rates of the main relaxation process. It is evident that the rate of the secondary relaxation in the glassy state extrapolates linearly to very close to the values of the relaxation rates at room temperature and above, with an Arrhenius energy at  $24.4 \text{ kJ mole}^{-1}$ . Although the extrapolation may not be entirely unambiguous, it is significant that the secondary relaxation has about the same Arrhenius energy as the relaxation process seen in liquids at a viscosity of several centipoises.

One may conjecture, therefore, that in liquids, both the cooperative and hindered types of molecular rearrangements occur at  $T \geq T_g$ . The relative contribution of the main and secondary relaxation processes to the transport property varies with the temperature. As the liquid approaches  $T_g$ , there is an increasing proportion of cooperative molecular process in the rate-temperature plane. This can be considered the main relaxation. The glass transition occurs at the cessation of this relaxation on the time scale of one's measurement. The secondary relaxation, which is due to the hindered rearrangement of the molecules, continues to exist through the complete temperature range of the liquid and the glass.

#### Molecular Motions and Structure of a Glass

It is obviously necessary that the existence of molecular motions associated with the secondary relaxations should be treated as a part of the theory of liquids or at least should be taken into account in considering the models for the microstructure of a glass. The most familiar models involve dense random packing (96,97), microcrystals (98), dislocations (99-102), mixed clusters of competing polymorphs (103,104), disclinations (105) and mixtures of disclinations and dislocations (106). These different possibilities, however, are not mutually exclusive. But, within the general features associated with amorphous packing, the

molecular mobility may be interpreted in two ways. The first is to suggest that the short-range structural states resulting from density fluctuations in the liquid at  $T_g$  are frozen in the glass. Thus a glass has two types of molecular environments (36): (i) where the structure is relatively loose and molecules can undergo hindered rotations (regions referred to as "islands of mobility"), and (ii) where the structure is closely packed and cooperative rearrangement responsible for the main relaxation occurs. In this view a fraction of the total number of molecules contribute to the secondary relaxation.

The second interpretation has all molecules in a glass in essentially equivalent environments of its dense packed structure, but each molecule capable of moving by a small angle in a relatively short time, followed by a large angle movement over a very long time, the former being responsible for the mobility in the glass and the latter for its main relaxation or viscous flow. The small angle jump is a necessary prior step to the long angle jump. In this view all molecules contribute to the secondary relaxation.

The main difference between the two interpretations is that the first assumes a non-ergodic behaviour of the relaxational states in the structure of a glass, the second assumes an ergodic behaviour in that all molecules go through all their relaxational states as a function of time. There is a basic objective to the latter assumption for an amorphous solid (31), but there are other objections to accepting the second interpretation, which are based on experiments. For example, according to this interpretation the annealing of a glass should decrease the rate of secondary relaxation in the same manner (but to a lesser extent) as it does the rate of main relaxation. This has not been found. Furthermore, it does not explain why the probability distribution of relaxation times is centred about at least two average values, and why nematic, cholesteric and smectic glasses containing rod-like molecules show a relative magnitude of the secondary relaxation much smaller than that found in the isotropic glasses (11,12).

It seems therefore that the pursuit of the amorphous cluster models is more promising for the structure of a glass. The basic units of the structure may be polyhedra, or highly ordered regions such as microcrystals, connected by loose interstitial packing (graphically referred to as "glue" or "connective tissue"), where molecular motions are possible even when the polyhedra are fixed in place (107). Since thin films of nematic, cholesteric and smectic glasses are anisotropic, it may be argued that the polyhedra in the structure are not microcrystals or crystal nuclei arrested in

various stages of their growth, for a random arrangement of such polyhedra of the amorphous cluster model would produce a macroscopically isotropic, not anisotropic, structure.

### Conclusions

During the ten years following the suggestion that the existence of molecular motions is an intrinsic property of the glassy state and has to do with the amorphous packing rather than with the molecular shapes, size or degrees of freedom, a considerable amount of experimental evidence has been obtained to determine the characteristics of these motions. But the understanding of the molecular process itself is crude and merely intuitive. The explanations for it in terms of the structure of a glass, or the energy states in a multidimensional configuration space are restatements of the problem and may seem tautologous, without a predictive value.

In an apparent tradition following Tamman (108), who likened the increase in viscosity with the phenomenon in clays of the rigid jamming together of the platelike particles when the interstitial water separating them falls to a critical proportion, and Simon (4), who considered an order parameter for their molecular description, most scientists have given to glasses some sort of structural or geometric description (96,97,100,102,109-12) involving microcrystallites, vitrons, amorphons, etc. Amongst them, Hoare (113), following Bernal's description (96), has generated icosahedral models which might be regarded as basic units in the structure of a glass. Such structures exist because it is possible to place only 12 spheres around a fixed one, and yet be able to move each of the 12 spheres on a tangential surface. When the spheres are arranged as regularly as possible they form a regular icosahedron, which has the remarkable property of possessing six symmetry axes each having a five fold rotation. Such an axis is incompatible with a group of translations and therefore is not crystallographic. Thus it is not possible to build a crystal by adding more spheres to the unit of 13. Hoare (113) has generated such structures containing 115 atoms interacting with a Lennard-Jones potential. The implication is that the basic units in the structure of a glass can also be well-packed polyhedra of high symmetries connected together by loosely packed interstitial regions in which molecular motion is still possible. This can also be an explanation for the almost universal intrinsic mobility of a glass.

Several other questions, however, remain unanswered. If the mobility in a glass at  $T < T_g$  indicates the availability of certain configurational states in some local regions outside the clusters, how can the variation with  $kT$  of such states in a composite of clusters can be quantitatively explained. We



do not as yet know if there is a distribution in the size of such clusters or if there is a fixed number of clusters at each temperature below  $T_g$ . The structural theories of glass must take into account such changes with temperature.

#### FURTHER COMMENTS

Since the time of the Workshop on Relaxation Effects in Disordered Systems, when these lectures were given, several developments in the experimental studies and theoretical concepts of the glassy state have occurred. Those within the context of the preceding text are briefly outlined in the following. Others may be found in the articles of the various authors.

Mishima, Calvert and Whalley(114) have recently obtained an amorphous solid water by application of a high pressure to an ice crystal, which irreversibly destroyed its crystallinity. This amorphous solid has a density substantially higher than that of the vapour-deposited amorphous solid water or supercooled glassy water. This seems to further suggest the existence of polymorphism in the amorphous state of water. MacFarlane and Angell(115) have now concluded that no change in the heat capacity prior to crystallization occurs on heating the amorphous solid water they obtained from vapor phase deposition. Thus the vapor-deposited amorphous solid water shows no glass transition temperature. This has put into question the correctness of several experiments by others who have found a glass transition temperature in the heat capacity measurements on heating the solid. It is difficult to judge the significance of MacFarlane and Angell's(115) recent results, for they did not ascertain that an amorphous solid state of water was formed in their vapor deposition experiments. It seems that the paradox regarding the inability of the structural state of the supercooled water in approaching the structural state of vapor-deposited amorphous solid water without violating the third law of thermodynamics has remained unresolved, thus pointing to the existence of polymorphism in the amorphous state of solid water. This seems even more likely now after the discovery by Mishima, Calvert and Whalley (114) of yet another well characterizable phase of the amorphous solid, whose properties do not extrapolate to the properties of liquid water in a simple manner.

Mayers(116) experiments further show that the x-ray diffraction pattern of the glassy water obtained by depositing fine liquid droplets on a substrate substantially differs from the x-ray diffraction pattern of the vapor-deposited amorphous solid water, but agrees with that of the jet-cooled glassy water he had made earlier by cooling in a cryomedium(117). He seems to have thus confirmed the difference in the structures of the two amorphous solids.

From the differential thermal analysis of the various vapor-deposited amorphous forms of solid water, Mayer and Pletzer(J. Chem. Phys. 80, 2939 (1984) have clearly shown the occurrence of polymorphism in the amorphous state, as was suggested here.

It is possible to conceive a molecularly or atomically disordered arrangement like that of a glass in a glasslike state of an orientationally disordered crystal. In such crystals, the centre of mass of the molecule does not exactly lie at a lattice site. Thus one may consider a molecule as an assemblage non-symmetrically distributed about a lattice site. The assemblage may be represented by several unequal-sized spheres, each of which is able to acquire any of the several positions relative to the other but all remaining within the assemblage near the lattice site. This mutual orientations of the separate sphere would be equivalent to a positional disorder of the spheres. Its pictorial representation is relatively simple. For example, a cyclohexanol molecule can be thought of as an assembly of two spheres, one representing the O-H group and the second obtained by rotating the  $C_6H_{11}$  group about a certain axis. All possible arrangements of the two spheres within the constraints of the covalent bond near a lattice site can now be pictured. This process when repeated at all lattice sites would generate a structure in which the arrangement of neither of the two spheres has a long range order. The orientational disorder can thus be envisaged as a positional disorder.

It is also noteworthy that glass transition in the nematic, cholesteric and smectic liquid crystals has a certain resemblance to the glass transition in metallic alloys and in the computer simulated experiments on aggregates of hard spheres, where the choice of spheres precludes the possibility of an orientational disorder and where the configurational restrictions that lead to the formation of a glass involve only the positions of the atoms or molecules.

It seems to us that Gibbs-DiMarzio's treatment(49, 50) of glass transition of a polymer chain is a special case of molecular interactions in which atoms can occupy all possible sites around each other, but constrained in distances and mutual positions by a suitable interatomic potential. In their treatment of a polymer chain, the interactions acquire a highly directional character of tetrahedral bonding and of a fixed distance between the atoms. The difficulty of reconciling the theory and the Kauzmann's paradox with the existence of the entropy associated with secondary relaxations still remains.

From the existence of a secondary relaxation peak in the dynamic shear measurements of  $KNO_3 \cdot Ca(NO_3)_2$  glass, we have found(118) that certain modes of ionic motions may be mechanically active but dielectrically inactive.

It may therefore seem necessary to study both the dielectric and mechanical relaxations before concluding on the absence of secondary relaxations in certain glasses. The dynamic shear studies also show the general occurrence of secondary relaxations in glasses(119), which have been interpreted in terms of the existence of microshear domains(119,120), similar to the concept of the islands of mobility, in the structure of a glass.

In recent studies of physical ageing on the kinetic properties of a glass by dynamic shear measurements, we have found(121) that the height of the secondary relaxation peak in a chalcogenide glass,  $As_2Se_{18}$ , is decreased by more than half of its original value after isothermal physical ageing for 28 days. We have also noted that Struik's data on polymers(122) can be explained only if the height of the secondary relaxation peak itself decreased on physical ageing. This is contrary to the conclusion by Struik(122) that physical ageing does not affect secondary relaxations.

From both dielectric and mechanical measurements, it now seems certain that densification of a glass on physical ageing affects its properties quite differently than densification on cooling or compression.

Our failure in confirming the applicability of time-temperature superposition for the real and imaginary parts of the shear modulus,  $G'$  and  $G''$ , of polymers(while "good" master curves of  $G'$  and  $G''$  can be obtained by such superposition, a master curve of  $(G''/G')$  can not. We have also argued that the applicability of time-temperature superposition would in principle violate Curie's Law of inverse dependence of modulus with temperature) has led us to suggest that the effect of physical ageing and the memory effect observed in polymers can also be explained in terms of changes in the structure of a glass of the localized high-volume, high-entropy states, which contribute to its secondary relaxations (123).

On the basis of temperature dependence of the amplitude of secondary relaxation and its dependence on physical ageing, we have pointed out(124) that the explanation of secondary relaxations in amorphous polymers in terms of the motion of the side group is inconsistent with the observed decrease in the amplitude of relaxations with decreasing temperature.

Montroull and Bendler(125) have shown that the dielectric loss data of the secondary relaxation in a rigid molecular glass and in a glass-like state of an orientationally disordered crystal can be fitted to Williams-Watt-Kohlrausch's function, and it is already known that the main relaxation can also be fitted to the same function but with very different parameters. This raises an interesting situation, namely, that of the occurrence in time of a bimodal probability of a macroscopic dipolar relaxation process of the same functional

form, but different in the shape parameters and characteristic times. From their theory, it seems important to understand how raising the temperature of a glass brings closer in their characteristic times the probability of the occurrence of the secondary and main relaxation processes such that the two processes apparently merge at a temperature far above  $T_g$ .

#### References

- (1) M.R. Chowdury, J.C. Dore and J.T. Wenzel, *J. Noncryst. Solids*, **53**, 747 (1982).
- (2) G.P. Johari, *Phil. Mag.* **35**, 1077 (1977).
- (3) K. Tamura, J. Fukushima, H. Endo, S. Minomara, O. Shimomura, and K. Asami, *The Physics of Liquid Metals*, edited S. Takeuchi (Taylor and Francis, London, 1972) p. 295.
- (4) F.E. Simon, *Ergebn. exakt. Naturwiss.* **9**, 244 (1930).
- (5) R.O. Davies and G.O. Jones, *Adv. Phys.* **2**, 370 (1953).
- (6) P. Ehrenfest, *Leiden Comm. Suppl.* 726 (1933).
- (7) I. Prigogine and R. Defay, *Chemical Thermodynamics*, (Longmans Green, N.Y. 1954) chap. 19.
- (8) H. Suga and S. Seki, *J. Noncryst. Solids* **16**, 171 (1974).
- (9) G.P. Johari, *Ann. N.Y. Acad. Sci.* **279**, 117 (1976).
- (10) M. Sora and S. Seki, *Molec. Crystals. Liq. Crystals.* **23**, 299 (1973).
- (11) G.P. Johari, *Phil. Mag.* **46**, 549 (1982).
- (12) G.P. Johari, J.W. Goodby and G.E. Johnson, *Nature*, **297**, 315 (1982); *J. Chem. Phys.* **77**, 5165 (1982).
- (13) K. Adachi, H. Suga and S. Seki, *Bull. Chem. Soc. Japan*, **41**, 1073 (1968).
- (14) Haida, H. Suga and S. Seki, *Bull. Chem. Soc. Japan*, **50**, 802 (1977).
- (15) S. Haida, H. Suga and S. Seki, *J. Chem. Thermodynamics*, **9**, 1133 (1977).
- (16) W. Kauzmann, *Chem. Rev.* **43**, 219 (1948).
- (17) N.F. Mott and R.W. Gurney, *Trans. Faraday Soc.* **36**, 364 (1939).

- (18) J.H. Gibbs, *J. Chem. Phys.* 25, 185 (1956); E.A. DiMarzio, *Ann. N.Y. Acad. Sci.* 371, 1 (1981).
- (19) A.G. Oblad and R.F. Newton, *J. Am. Chem. Soc.* 59, 2495 (1937).
- (20) J.H. Konnert and J. Karle, *Science* 179, 177, (1972).
- (21) A.H. Narten, *J. Chem. Phys.* 56, 1905 (1972).
- (22) O. Haida, T. Matsuo, H. Suga and S. Seki, *J. Chem. Thermodynamics*, 6, 815 (1974).
- (23) O. Haida, H. Suga and S. Seki, *Proc. Japan Acad. Sci.* 49, 191 (1973).
- (24) G.P. Johari and S.J. Jones, *J. Chem. Phys.* 62, 4213 (1975).
- (25) G.P. Johari and S.J. Jones, *Proc. Roy. Soc. (London)* A349, 467 (1976).
- (26) G.P. Johari and E. Whalley, *Faraday Symp. Chem. Soc.* 6, 23 (1972).
- (27) G. Tamman, *Der Glaszustand* (L. Voss, Leipzig, 1935).
- (28) H. Vogel, *Physik*, Z. 22, 645 (1921).
- (29) G.S. Fulcher, *J. Am. Ceram. Soc.* 77, 3701 (1925).
- (30) G. Tamman and W. Hesse, *Z. Anorg. Allgem. Chem.* 156, 245 (1926).
- (31) P.W. Anderson, in *Mal Condense Materie*, Edited R. Balian, R. Maynard and G. Toulouse, Les Houches 1978, Session XXXI (North Holland, 1979) p. 171.
- (32) A.C. Ling and J.E. Willard, *J. Phys. Chem.* 72, 1918, 3349 (1968).
- (33) P.B. Macedo and A. Napolitano, *J. Chem. Phys.* 49, 1887 (1968).
- (34) D.J. Plazek and J.H. Magill, *J. Chem. Phys.* 45, 3038 (1966); 46, 3757 (1967).
- (35) G.P. Johari, *J. Chem. Phys.* 77, 4619 (1982); to be published.
- (36) G.P. Johari, *J. Chem. Phys.* 58, 1766 (1973).
- (37) J. Frenkel, *Trans. Faraday Soc.*, 33 58 (1937); *Theory of Liquids*, (Clarendon Press, Oxford, 1946) pp. 93.
- (38) J.E. Lennard-Jones and A.F. Devonshire, *Proc. Roy. Soc. (Lond)* A169, 317 (1939); A170, 464 (1939).
- (39) H. Eyring, *J. Chem. Phys.* 4, 283 (1936).
- (40) S. Glasstone, K.J. Laidler and H. Eyring, *The Theory of Rate Processes* (McGraw Hill, 1941).
- (41) R. Fowler and E.A. Guggenheim, *Statistical Thermodynamics* (Cambridge University Press, 1956).
- (42) T.G. Fox and P.J. Flory, *J. Appl. Phys.* 21, 581 (1950); *J. Phys. Chem.* 55, 221 (1951); *J. Polymer Sci.* 14, 315 (1954).
- (43) A.K. Doolittle, *J. Appl. Phys.* 22, 1471 (1951); *ibid*, 23, 236 (1952).
- (44) A.K. Doolittle and D.B. Doolittle, *J. Appl. Phys.* 28, 901 (1957).
- (45) M.L. Williams, R.F. Landel and J.D. Ferry, *J. Am. Chem. Soc.* 77, 3701 (1955).
- (46) F. Beuche, *J. Chem. Phys.* 21, 1850 (1953); *ibid*, 24, 418 (1956); *ibid* 30, 748 (1959).
- (47) M.H. Cohen and D. Turnbull, *J. Chem. Phys.* 31, 1164 (1959); D. Turnbull and M.H. Cohen, *ibid*, 34, 120 (1961); *ibid*, 52, 3038 (1970).
- (48) S. Kumar, *Phys. Chem. Glasses* 4, 106 (1963).
- (49) J.H. Gibbs, "Nature of Glass Transition and the Vitreous State", in *Modern Aspects of the Vitreous State*, J.D. Mackenzie Ed. (Butterworths, 1960), Vol. I, pp. 152-187.
- (50) J.H. Gibbs and E.A. DiMarzio, *J. Chem. Phys.* 28, 373 (1958).
- (51) K.H. Meyer, *Z. Phys. Chem.* B44, 383 (1939).
- (52) P.J. Flory, *J. Chem. Phys.* 10, 51 (1942); *Proc. Roy. Soc. (Lond)*, A234, 60 (1956).
- (53) M.L. Huggins, *J. Phys. Chem.* 46, 151 (1942); *Ann. N.Y. Acad. Sci.*, 41, 1 (1942); *J. Am. Chem. Soc.* 64, 1712 (1942).
- (54) G. Adam and J.H. Gibbs, *J. Chem. Phys.* 43, 139 (1965).
- (55) M.H. Cohen and G.S. Grest, *Phys. Rev.* B20, 1077 (1979); *Ann. N.Y. Acad. Sci.* 371, 199 (1981).
- (56) G.S. Grest and M.H. Cohen, *ibid*, 21, 4113 (1980).
- (57) A. Rahman, M.J. Mandell and J.P. McTague, *J. Chem. Phys.* 64, 1594 (1976).
- (58) J.G. Kirkwood, *J. Chem. Phys.* 18, 380 (1950).

- (59) A.J. Matheson, *J. Chem. Phys.* **44**, 695 (1966).
- (60) P.D. Gujarati and M. Goldstein, *J. Chem. Phys.* **74**, 2596 (1981).
- (61) M. Goldstein, *J. Chem. Phys.* **51**, 3728 (1969); *ibid* **67**, 2246 (1977).
- (62) S.H. Glarum, *J. Chem. Phys.* **33**, 639 (1960).
- (63) M.C. Phillips, A.J. Barlow and J. Lamb, *Proc. Roy. Soc. (London)* **A329**, 193 (1972).
- (64) T. Nose, *Poly. Journal*, **2**, 124, 427, 437, 445 (1971); *ibid* **4**, 217 (1973).
- (65) E. Williams and C.A. Angell, *J. Poly. Sci., Poly. Lett.* **11**, 383 (1979).
- (66) J.J. Aklonis and A.J. Kovacs, *Contemp. Topics Polym. Sci.* **3**, 267 (1979); M.A. Marcus, *Acta Metallurg.* **27**, 879 (1979).
- (67) P.W. Anderson, B.I. Halperin and C.M. Varma, *Phil. Mag.* **25** 1 (1972); W.A. Phillips, *J. Low Temp. Phys.* **7**, 351 (1972).
- (68) N.G. McCrum, B.E. Read and G. Williams, *Anelastic and Dielectric Effects in Polymeric Solids* (Wiley, N.Y. 1967).
- (69) D.W. McCall, *Natl. Bur. Std. (U.S.) Special Publ.* **301**, 475 (1969).
- (70) T.F. Shatzky, Meeting of Am. Chem. Soc. Div. Polymer Chem., Atlantic City, September, *Polymer Preprints* **6**, 646 (1965).
- (71) I.L. Hopkins and C.R. Kurkjian, in *Physical Acoustics*, edited by W.P. Mason (Academic Press, N.Y. 1965), Vol. II, Part B. p. 91.
- (72) G.P. Johari and M. Goldstein, *J. Chem. Phys.* **53**, 2372 (1970); *ibid*, **55**, 4245 (1971).
- (73) L. Haylor and M. Goldstein, *J. Chem. Phys.* **66**, 4736 (1977).
- (74) A.S. Argon, *J. Appl. Phys.* **39**, 4080 (1968).
- (75) E. Orowan "Creep in Metallic and Non-Metallic Materials", *Proceedings of the First National Congress of Applied Mechanics* (American Society of Chemical Engineers, New York, 1952), pp. 453-472.
- (76) Y. Ishida, *J. Polymer Sci.* **A2-7**, 1835 (1969).
- (77) E.W. Anderson, H.E. Bair, G.E. Johnson, T.K. Kwei, F.J. Padden, Jr., and D. Williams, *Adv. Chem. Series*, **176** (Am. Chem. Soc. 1979), 418.
- (78) K. Adachi, H. Suga, S. Seki, S. Kubota, S. Yamaguchi, O. Yano and Y. Wada, *Molec. Cryst. Liq. Cryst.* **18**, 345 (1972).
- (79) R. Simha, J.M. Roe and V.S. Nanda, *J. Appl. Phys.* **43**, 4312 (1972).
- (80) M. Goldstein, *Ann. N.Y. Acad. Sci.* **279**, 68 (1976).
- (81) G.P. Johari, *Ann. N.Y. Acad. Sci.* **279**, 102 (1976).
- (82) G.P. Johari, *Phil. Mag.* **41**, 41 (1980).
- (83) H. Suga and S. Seki, *Bull. Chem. Soc. Japan.* **46**, 3020 (1973).
- (84) M. Goldstein, *J. Chem. Phys.* **64**, 4767 (1976).
- (85) M. Goldstein and P.D. Gujarati, *J. Chem. Phys.* **84**, 859 (1980).
- (86) G.P. Johari and C.P. Smyth, *J. Chem. Phys.* **56**, 4411 (1972).
- (87) G. Williams and D.A. Edwards, *Trans. Faraday Soc.* **62**, 1329 (1966).
- (88) G. Williams, *ibid*, **62**, 2091 (1966).
- (89) L.C.E. Struik, *Ann. N.Y. Acad. Sci.* **279**, 78 (1976); *Physical Aging in Amorphous Polymers and Other Materials*, (Elsevier, 1978) pp. 22-25.
- (90) J.M. Haddad and M. Goldstein, *J. Noncryst. Solids*, **30**, 1 (1978).
- (91) G. Williams and D.C. Watts, *Trans. Faraday Soc.* **67**, 1971, 2793 (1971).
- (92) G. Williams, *Farady Symp. Chem. Soc.* **6**, 45 (1972); *Adv. Poly Sci.* **33**, 59 (1979).
- (93) C.J. Reid and M.W. Evans, *J. Chem. Soc. Faraday II*, **75**, 1218 (1979).
- (94) J.S. Dryden, *Trans. Faraday Soc.* **49**, 1333 (1953).
- (95) D.W. Davidson, *Canad. J. Chem.* **49**, 1224 (1971).
- (96) J.D. Bernal, *Nature*, **185**, 68 (1960); *Proc. Roy. Soc. Lond.* **A280**, 299 (1964); "The Geometry of the Structure of Liquids" in *Liquids: Structure, Properties and Solid Interactions*. T.J. Hughel, Ed. (Elsevier, 1965) pp. 25.
- (97) J.L. Finney, *Nature* **226**, 309 (1977).

- (98) D. Turnbull and D.E. Polk, J. Noncryst. Solids 8-10, 19 (1972).
- (99) J.J. Gilman, J. Appl. Phys. 44, 675 (1973).
- (100) M.F. Ashby and J. Logan, Scripta Metallurg. 7, 513 (1973).
- (101) J.C.M. Li, in Frontiers of Science, Ed. L.E. Murr and C. Stein (Marcell Decker, N.Y. 1976), p. 527.
- (102) S.F. Edwards and M. Warner, Phil. Mag. 40A, 527 (1979).
- (103) C.H.L. Goodman, Nature 257, 370 (1975).
- (104) R. Wang and M.D. Metz, Nature 260, 35 (1976).
- (105) N. Rivier, Phil. Mag. 40A, 859 (1979).
- (106) R.C. Morris, J. Appl. Phys. 50, 3250 (1979).
- (107) M. Goldstein, J. Phy. Paris Colloq. C2, C2-3 (1975).
- (108) G. Tamman, Der Glasszustand, Section IV (Leopald Voss, Leipzig, 1933) p. 12.
- (109) E.A. Parai-Kosic, Glastechn. Ber. 32, 450 (1959).
- (110) B. Echstein *ibid*, 36, 323 (1963).
- (111) R. Hoseman, Z. Phys. 128, 465 (1950).
- (112) E. McLaughlin and A.R. Ubbelohde, Trans. Faraday Soc. 54, 1804 (1958).
- (113) M. Hoare, Ann. N.Y. Acad. Sci. 279 186 (1976); and references therein.
- (114) S. Mishima, L. D. Calvert and E. Whalley, Nature(in press) 1984.
- (115) D. R. MacFarlane and C. A. Angell, J. Phys. Chem. 88,759(1984).
- (116) E. Meyer (private communication) in press(1984).
- (117) E. Mayer and P. Bruggeller, Nature, 298, 715(1982).
- (118) C. Mai, S. Etienne, J. Perez and G. P. Johari, submitted for publication, (1984).
- (119) J. Perez and P. F. Gobin, Rev. Phys. Appl. 12, 819(1976).
- (120) J. Perez, J. Y. Cavaille, S. Etienne, F. Fouquet and F. Guyot, Ann. Phys., Fr., 8, 417(1983).
- (121) S. Etienne, J. Y. Cavaille, J. Perez and G. P. Johari, submitted for publication(1984).
- (122) L. C. E. Struik, Ann. N.Y. Acad. Sci. 279, 78(1976).(fig.8).
- (123) J. Y. Cavaille, S. Etienne, J. Perez and G. P. Johari, to be submitted for publication(1984).
- (124) G. P. Johari, J. Chem. Phys. 77, 4624-5(1982).
- (125) E. W. Montroll and J. T. Bendler, J. Stat. Phys. 34, 129(1984).

## The Nature of the Glass Transition

Edmund A. Di Marzio  
National Bureau of Standards  
Washington, DC 20234

### Abstract

Reasons are given for the need to study the equilibrium properties of glasses. It is shown that some materials have the amorphous phase as their lowest temperature equilibrium phase. The ubiquitous nature of the glass transition is explained by postulating that glassification occurs when the configurational entropy decreases to a critically small value. This postulate is shown to lead to correct predictions for glass transitions in polymeric systems where the lattice model can be used to calculate the partition function. The fluctuation-dissipation theorem is used to explain the observed parallelism in the behavior of thermodynamic and dissipative variables near the glass transition. Order parameters and collective variables are discussed and defined and application to glasses is made. A constraint on the simultaneous application of the William-Watts formula to both dielectric and mechanical relaxation is described.

### (I) Equilibrium Considerations

The first thing we wish to establish is that it is meaningful to inquire into the equilibrium properties of glasses. Ordinarily, it would suffice to state that any collection of molecules has equilibrium properties and that it is legitimate to ask what these properties may be. Indeed, for most scientists this statement carries validity. However, there is a group of scientists studying glasses who view that glassy behavior consists precisely in the nonequilibrium aspects of the materials. Or to say it in another way, deviations from equilibrium are "the subject matter" in the study of glasses. At most, the approach of the material towards equilibrium is of interest. For this group we give four reasons to study the equilibrium properties of those collections of molecules that we happen to call glasses.

#### (IA) Necessity for an Equilibrium Theory of Glasses

(1) The Crystal Phase is not Ubiquitous. In a previous paper<sup>1</sup> we divide all material into two classes. Class I is crystallizable material

and Class II is noncrystallizable material. We showed that Class II was not null.

Class IIA consists of many different kinds of molecules each of which can take on many shapes. Atactic polymer molecules constitute an example within this class that are not crystallizable.

Class IIB consists of many kinds of molecules each of which can take on only one shape. Such systems are the subject of tiling theory<sup>2</sup>. Penrose has a system of several (the minimum being two) kinds of 2-dimensional molecules that can completely cover a surface without any repetition of pattern<sup>3</sup>. A recent paper<sup>4</sup> generalizes nonperiodic tilings to 3-dimensions.

Class IIC consists of one kind of molecule that can take on many shapes. Many polymer and biopolymer molecules are of this type. We can perform a gedanken experiment which shows that in principle at least, this class contains noncrystallizable systems. Let us imagine ourselves to be master chemists and then create a polymer molecule so that each shape has the same energy as any other shape. The equilibrium state of a system of such molecules will be an amorphous phase with each shape occurring, even at a temperature of absolute zero. This then is our first example. A second, more realistic, example occurs when we allow one of the many possible shapes to be the lowest energy shape and let all other shapes be of the same higher energy. We choose this lowest energy shape to be one which cannot pack in regular array in a space filling manner (we shall prove later that such shapes exist). At high temperatures each of the shapes occurs with roughly equal probability. As we lower the temperature more and more molecules fall into their lowest energy shape. As we approach absolute zero all the molecules want to go into their lowest energy shape. However, because this cannot happen only two other options remain. (1) Molecules can always be aligned in regular spatial array if we are willing to place them far apart from each other. However, being master chemists we have made our molecules with strong intermolecular interaction

energies so that the molecules must pack tightly in space. This leaves only option (2) A certain fraction of the molecules fall into their lowest energy shape but the remainder are free to sample continuously their vast number of higher energy shapes. Such an equilibrium state is obviously not a crystal.

To complete the proof we must now show that certain polymer shapes cannot pack together densely in regular array (i.e., cannot crystallize when all of the molecules have the same shape). Let us pick as the lowest energy shape one of the many shapes that has linear dimensions on the order of  $r^{1/2}$  where  $r$  is the molecular weight. For simplicity it is useful to imagine polymer chains on a lattice but a lattice is not necessary to the argument. Imagine also that the shape we have chosen is roughly spherical in shape, being one of the many such random-walk shapes available to a polymer molecule. Now because of close packing the distance between adjacent molecule centers is  $r^{1/3}$ . However, the size of the molecules is  $r^{1/2}$ . Thus, there is a large overlap and extensive mutual interpenetration of neighboring molecules. The number of molecules,  $N$ , contained in a sphere of radius  $R = r^{1/2}$  is equal to the total number of sites within the sphere ( $r^{3/2}$ ) divided by the number sites occupied by one molecule ( $r$ )

$$N = r^{1/2} \quad (1)$$

Now let us make an estimate of the number of interferences in two chains whose center of masses must of necessity be a distance  $r^{1/3}$  apart. For large  $r$  we can let each of the molecules occupy the same sphere of radius  $r^{1/2}$ . In the following arguments we allow the segments of each of the two chains to doubly occupy lattice sites. The shapes of the individual chains, however, are chosen so that there is no double occupancy of lattice sites by segments within the same molecule. The probability of a given site chosen at random within the sphere being doubly occupied is  $1/r$  and since there are  $r^{3/2}$  such sites the expected number of doubly occupied sites between the pair of molecules is  $r^{1/2}$ . Since the number of other chains within the volume is  $(r^{1/2} - 1)$  we have  $(r^{1/2} - 1)r^{1/2} = r$  as the expected number of chains in its neighborhood. This is good physics. If a volume is almost filled by segments and we place into that volume a polymer of  $r$  segments we expect virtually all of the  $r$  segments to suffer interference. We have then,

$$\langle N_d \rangle = r \quad (2)$$

where  $N_d$  is the number of double occupations. Let us now estimate the probability,  $p$ , that a chain of fixed a priori chosen shape will not suffer interference from the other  $(r^{1/2} - 1)$  chains occupying the same volume. Let us first do the case of interference between two chains.

The probability that a given segment of the first chain does not overlap any segment of the second chain is  $(1 - 1/\sqrt{r})$ , and the probability that none of the  $r$  segments of the first chain do not overlap segments of the second chain is

$$(1 - 1/\sqrt{r})^r = \exp(-\sqrt{r}) \quad (3)$$

The probability,  $p$ , that the one chain shows no overlap with every segment of the other  $(r^{1/2} - 1) = r^{1/2}$  chains is

$$p = (\exp(-\sqrt{r}))^{\sqrt{r}} = \exp(-r) \quad (4)$$

which is a very small number. The numbers we have calculated are expectation values and there is a small but finite chance that a particular chain whose shape is picked at random may have no interferences. Indeed we have argued that this probability  $p$  is given by Eq. (4). However, in order for there to always be an equilibrium crystalline state every possible shape must be able to pack in regular array. But this possibility is clearly in contradiction to both Eqs. (4) and (2). These equations show that the vast majority of molecular shapes allowed to a polymer molecule are shapes that cannot pack in regular array in a space filling manner without double occupancy of lattice sites.

Real polymer molecules have a range of energies associated with their various shapes rather than just two as assumed above. As long as the lower energy shapes are of the kind that do not pack we know that the low temperature equilibrium state will be noncrystalline. This constitutes the third example within Class IIC.

Class IID consists of systems composed of one kind of molecule, one kind of shape. We have just finished proving that the vast majority of the enormous number of polymer shapes cannot close pack on a lattice. That is to say, we proved the existence of Class IID in order to prove the existence of Class IIC. But we now wish to show that even when the molecule does not have an open structure and is compact we still may not have a crystalline phase. The open structured polymer molecules we have been considering have a Hausdorff dimension<sup>5</sup> of  $D = \ln(N)/\ln(r) = 2$ . Normal globular proteins are compact structures and have a Hausdorff dimension of 3. It is for such molecules that the crystal phase is common and almost universal. However, we wish to show that even for this case there exist molecules that cannot crystallize.

Hoare<sup>6</sup> has discussed the problem of densely packing molecules that locally at least abhor local regular arrangement. A prototype of this kind of molecule is a pentagon which does not pack nicely because of the nonexistence of five fold crystal symmetry. Higher-order regular polygons, with numbers of sides that are not multiples of 2 or 3, retain this amorphous nature and do not pack well locally. Such

objects (and their analogues in dimensions other than 2) are called amorphons or vitrons<sup>7</sup>. Monte Carlo calculations on such objects always result in amorphous liquids<sup>6</sup>. Though suggestive these calculations do not constitute a proof of the existence of a low energy noncrystalline structure of systems composed of amorphons (molecular dynamics calculations on these materials would give added weight to the conclusion but seem to have not yet been performed). One must be open to the possibility that small clusters of amorphons (say three pentagons) can pack in regular array. The question then is whether there is a strain induced by the attempt to pack the clusters in regular array and whether this strain is sufficiently strong to distort the cluster to the point of breaking the crystal symmetry. Although there is evidence that in Class IID we have low temperature amorphous systems, we must admit that for this class and this class alone, we have no proof. The other three classes, however, have provided us with ample examples.

Finally, we should at least mention that the geometry of amorphous solids whose atoms are covalently connected in a nonperiodic three dimensional network has been studied extensively. A useful reference is Zallen<sup>8</sup>.

(2) Equilibrium Theory is a Necessary Foundation for Nonequilibrium Theory. The second reason for an equilibrium theory of glasses is that equilibrium considerations provide a necessary foundation for all the kinetic theories. As an example, consider the fluctuation dissipation theorem which relates the dissipative measures of material behavior to the spontaneous deviations of the material from equilibrium<sup>9</sup>. A description of these deviations is possible only within the context of equilibrium statistical mechanics.

(3) Equilibrium Theory Necessary to Resolve Kauzmann's Paradox. The third reason for an equilibrium theory of glasses has to do with a resolution of Kauzmann's paradox<sup>10</sup>. If one examines the experimental entropy or volume curves one sees that as the temperature is lowered these quantities stop their precipitous descent at the glass temperature and level off to appropriate values. Let us suppose that the reason for the leveling off is that kinetic considerations have come into play. Then one can estimate the equilibrium properties simply by extrapolating the high temperature behavior through the glass transition. However, when this is done it is found that inadmissible values of volume and entropy result (negative entropies and volumes smaller than crystal volumes). This is the paradox. It appears as if "kinetic sluggishness always intervenes to save the thermodynamic day." Kauzmann's observation actually provides strong evidence that there is a fundamental connection between kinetic and thermodynamic quantities. To resolve the paradox we must develop an equilibrium

theory and use it to correctly predict the high temperature properties of the amorphous phase (above the glass temperature). Only then can we with confidence "extrapolate" beyond the glass temperature. We simply calculate the values of entropy and volume for temperatures less than the glass temperature. This operation defines the word extrapolate. We see below that the paradox is indeed resolved by the thermodynamic theory.

(4) Agreement with Many Experimental Observations. In addition to the above a priori reasons for studying the thermodynamics of glass-forming materials, there is also an a posteriori one. The thermodynamic theory has, in fact, explained many experimental results. See below.

(IB)  $S_0 = 0$  is the Rosetta Stone of the Hieroglyphics of Glass Formation

Long ago (not quite as long ago as the unearthing of the Rosetta Stone or the creation of hieroglyphics) the lattice model was used to calculate the equilibrium properties of bulk polymers<sup>11</sup>. Entropy,  $S$ , and volume,  $V$ , were computed and found to agree with experimental observations. The equations displayed a second order transition in the Ehrenfest sense. This transition occurs where the configurational entropy,  $S_c$ , equals zero, and serves to define a transition temperature  $T_2(P)$ .

$$S_c(T,P) = 0 \quad (5)$$

Kauzmann's paradox is immediately resolved because there is a break in the slopes of  $V(T)$  and  $S(T)$  at the thermodynamic transition temperature  $T_2$ .  $T_2$  is a lower bound to the glass temperature  $T_g$  ( $T_2 < T_g$ ). The large increase in viscosity which occurs as we cool is simply understood to be a consequence of the drastic reduction in the number of available configurations as we approach  $T_g$  from above. It is more difficult for the system to move from one allowed configuration to another as they become more and more separated in phase space. This fact serves to explain why "kinetics always intervenes to save the thermodynamic day" in the Kauzmann construction.

(IC) Test of the  $S_0 = 0$  Hypothesis with Experiment

In order to compare theory with experiment we identify the observed  $T_g$  with  $T_2$  and choose experimental data obtained with cooling and heating rates of degrees per hour or minute rather than faster rates. It is not necessary to identify  $T_g$  with  $T_2$ ; it is sufficient to allow the difference  $T_g - T_2$  to be a constant. It is not necessary to insist that  $S_0 = 0$ ; it is sufficient only that  $S_0$  approach a critical small value. The comparison with experiment has been adequately summarized in reference 1. Here we simply enumerate the comparisons in



order to display the wide region of applicability and to comment on the thermodynamic character of the comparison. It is to be emphasized that in all cases the agreement of theory with experiment is good.

1. The glass temperature  $T_g$  is correctly predicted as a function of molecular weight for homopolymers<sup>11,12</sup>. It is shown in agreement with experiment that the  $T_g$  of a polydisperse system varies as the number average molecular weight. This is a thermodynamic result. If glassification were primarily a kinetic phenomenon one might have expected that viscosity average molecular weight was the proper variable.
2.  $T_g$  vs. plasticizer content curves are correctly predicted. To first order the main determinant of glass temperature depression is mole fraction of diluent<sup>13</sup>. This result is analogous to melting point depression by mole fraction of impurity. It also is the kind of result that is expected from a thermodynamic theory. Glass temperature depression is also a function of stiffness and size of the plasticizer when the plasticizer molecules are large<sup>13</sup>.
3.  $T_g$  of a copolymer as a function of copolymer composition both for addition and condensation copolymers is adequately predicted. The formula is the same as that for blends<sup>1</sup>.
4.  $T_g$  as a function of pressure is calculated<sup>14</sup>. Available experimental evidence is meager because of the difficulty of the experiments, but the available results are consistent with the theory.
5. The glass temperature of a rubber is predicted as a function of stretch ratio and as a function of cross-link density<sup>15</sup>. The two formulas have two very interesting features. First, only thermodynamic quantities enter into the equations. Second, they are parameter free universal equations applicable to all cross-linked polymers. These equations provide a critical test of the thermodynamic views of glassification. Available data agree with the predictions, but critical experiments have not yet been done.
6. The specific heat discontinuity at the glass transition, has been predicted to an accuracy of 15% without any parameters<sup>16</sup>.

An important aspect of the predictions is that of the 6 sets of predictions 4 of them are no-parameter fits! In set 1, the  $T_g$  of the infinite molecular weight sample is required, and in set 4 the size of a cell is a parameter. Another important aspect of the comparison with experiment is that one does not want the agreement with experiment to be too good! The reason for this is that kinetic effects in glasses

are important and we must therefore allow that kinetics have sensible effects on our measurements.

#### (ID) Critique of a Correct Equilibrium Theory of Glasses

(1) Experimental Data for Glasses is Predicted Correctly. It is a necessary but not sufficient condition for the validity of a theory that all predictions must be quantitatively and qualitatively correct. Section IC is an admirable step in this direction in that we have attempted to compare the theory to all manner of experiments. It is most important that the theory not fail even once. One fully documented failure is enough to discredit an entire theory and require its revision. In addition to the requirement of agreement with experiment there are four other conditions which are necessary for a theory of glasses to be valid. We now discuss these.

(2) If the Theory Makes Predictions for Materials Other Than Glasses, They Too Must Be Correct; even if we do not happen to be interested in those results. Here we have a happy circumstance. The same lattice model that predicts the equilibrium properties of glasses so nicely also predicts correctly the equilibrium properties of liquid crystals! We have a logical synergism. The correctness of the prediction for liquid crystals argues for the correctness of the prediction for glasses and conversely. The lattice model shows that the root cause behavior of the two classes of materials is the same. In each case the difficulty that the chains have in packing against one another in space leads to the transition. The case of liquid crystals is understood more easily. Imagine rigid rods oriented randomly in a solvent. As we withdraw the solvent the chains have difficulty packing against each other in a random fashion. If we withdraw even more solvent from the solution we reach a concentration for which the rigid rods can no longer pack at random and must align themselves along some common axis. This then, explains the transition from isotropic liquid to nematic liquid crystal. The reader can obtain an appreciation for the packing problem in 2-dimensions by placing pencils on a table. The same packing difficulties occur when an amorphous polymer liquid is cooled. The chains being semiflexible stiffen as we cool. Also, the volume shrinks. These two factors (but mostly the stiffening) make it difficult for the chains to pack. If the chains have the option of straightening as they stiffen then they can either form liquid crystals or crystals. However, if the chains have as their lower energy shapes<sup>17</sup> that cannot pack on a lattice they simply get stuck. This is the basis of the glass transition. Because there is no energy (or entropy) change during the trapping process the glass transition is second-order. Because in liquid crystals there is an entropy change associated with the isotropic chains escaping

to the parallel alignment the isotropic liquid to nematic liquid crystal transition is first-order.

(3) The Ubiquitous Nature of the Transition Must Be Explained. Our explanation of glass formation is incomplete because it is applicable only to polymers (it is only for polymers that we can calculate the configurational entropy). A equilibrium theory is needed which treats low and high molecular weights on an equal footing. Configurational and communal entropy must somehow merge into the same concept; communal entropy being important at low molecular weights. Recent work suggests the possibility of a glassy phase even for spherical molecules<sup>17</sup>.

Another aspect of ubiquity is that some crystalline materials can show glassy behavior as metastable states. For polymers this is easily understood. There are so many ways to pack the molecules in the amorphous phase that the one (or several) crystalline configuration may never be sampled in the time scale of the experiments unless there is a strong energy preferring it. The question of sampling time is also an important question for low molecular weight (even for spherical molecules). Nucleation theory shows that there is an energetic barrier to crystal formation at low supercooling, while viscosity studies show there is a kinetic barrier to crystallization at high supercooling.

(4) The Kinetics of Glasses Must Be Qualitatively Explained. It is reasonable to suppose that the viscosity and the configurational entropy bear an inverse relationship to one another. As we observed in our resolution of Kauzmann's paradox flow consists in the ability of a system to move from one allowed configuration to another. It seems obvious that as the number of allowed configurations diminishes as we lower the temperature they become further separated in phase space and, consequently, it becomes more and more difficult to move from one to another. In the limit of  $S_c = 0$  flow becomes very difficult indeed. Speaking in the language of the microcanonical ensemble we would suppose that there were no flow. But because the system actually behaves in accordance with the canonical ensemble there are allowed configurations even below the glass temperature and flow, though highly restricted is still possible. These ideas need to be quantified and, in fact, a treatment by Adam and Gibbs<sup>18</sup> is an attempt along these lines.

(5) No Conceivable Alternative Exists. Granting that it is meaningful to discuss equilibrium properties of glasses the question of alternatives is the same as the question of whether we can evaluate the partition function more accurately. Obviously, improvements can always be made and any present theory will be replaced in time by more correct calculations.

In the next section we briefly indicate new directions.

### (IE) Improved Evaluation of the Partition Function Q

(1) Within the Context of the Mean Field Lattice Model. The theory which in Section (IC) gave such good results assumes a crude nearest neighbor model for the energy as a function of shape. The isomeric state model as developed by Volkenstein<sup>19</sup> and Flory<sup>20</sup> provides a more realistic description of chains and can be used to implement the more general version of the Gibbs-Di Marzio theory<sup>21</sup>. Also, the stiffness energy can be made a function of pressure<sup>22</sup>. Certain experiments seem to require this<sup>22</sup>.

(2) Within the Context of the Lattice Model. De Gennes<sup>23</sup> and des Cloiseaux<sup>24</sup> showed that the  $n=0$  vector model can be used to evaluate the statistics of polymer chains. One hopes that the method can be adapted to the case where the chain configurations are energy dependent. Nagle, Gujrati and Goldstein have argued, correctly I believe, that the time is ripe for better equilibrium theories of polymers, and have made some progress towards replacing the mean field version with more modern treatments<sup>25</sup>. Credit must be given to the enormous past successes of the mean field treatment, however.

(3) Within the Context of the Cell-Lattice Model. There are two points to be made. The first has to do with the usual assumption of separation of position and momentum variables in the classical phase integral. This is a bad assumption, especially when the quantity of interest is the entropy (SVT or EVT equations of state). It is known by everyone that the specific heat is given correctly only by a quantum treatment, even at moderately high temperatures. For polymers it is also a bad assumption because in polymers there is actually no separation of the phase integral into a product of a momentum part and a position part<sup>26</sup>. Now the lattice model does not require an assumption of separation even though most lattice treatments are concerned only with the configurational part of the phase integral and do in fact assume it. Our first point then is the applicability of the lattice model to the whole phase integral. It is therefore natural to add vibrational contributions to the lattice model in order to obtain as good an estimate of  $S_c$  as possible. As soon as this is done we are forced logically to go from a lattice model to a cell model because the vibrations of the segments can cause excursions beyond the boundaries of their original cells. We are thus faced early on with the problem of combining the lattice and cell models into a coherent overview. Our second point then is that the attempt to add vibrations forces us to consider the view that the cell and lattice models constitute an organic whole. As explained above in Sec. (ID 3) a proper cell-lattice model

would help us to quantify the ubiquity of glassification via the  $S_c = 0$  hypothesis.

(C) Computer Simulations. Computer simulations are an excellent way of mimicking the behavior of glasses. This is because there is little hope of solving the problems exactly. In the absence of energetics the combinatorial problem is equivalent to that of the  $n=0$  vector model, which is itself unsolved. When we add energetics the problem is even more intractable. Baumgardner has written a recent review which discusses modeling of amorphous phases<sup>27</sup>. An example of the utility of computer modeling is a recent paper by Yoon and Baumgardner which establishes that there is a first order transition from the amorphous liquid to crystalline phases even in the absence of volume changes<sup>28</sup>. It is required only that the trans configuration is the low energy configuration.

## (II) Nonequilibrium Considerations

Our aims in this section will be modest since the author feels that the problem of relaxation is not yet solved. We shall (1) show the underlying reason for the parallel behavior of thermodynamic and dissipative quantities; (2) clarify the meaning of order parameters, especially as they apply to glasses; (3) make some comments on the notion of collective variables and their use in linear response theory (generalized Langevin theory); and (4) discuss the William-Watts relation.

### IIA Parallel Behavior of Thermodynamic and Dissipative Variables

Because we are more familiar with first-order transitions rather than second-order transitions we shall consider them first. The (thermodynamic) volume and entropy change discontinuously when we go through the transition and so do dissipative quantities such as viscosity, diffusion coefficient and conductivity (mass, thermal, and electrical). Notice that for a first-order transition no one would say that the reason for the transition is the sudden increase in viscosity or in diffusion coefficient. Rather the sudden increase in viscosity is viewed as caused by the transition. Scientists were able to predict phase transition behavior without ever needing to think at all about dissipation. Yet even in this case there have been suggestions that the location of the transition can be defined in terms of dissipative quantities. For example, Sherwood has shown that a FCC crystal melts when the self diffusion coefficient reaches a critical value<sup>29</sup>.

Now consider the glass transition. The thermodynamic quantities  $V$  and  $S$  show an apparent second-order transition and concomitantly the dissipative quantities also show breaks in their slopes (as functions of  $T, P$ ). The viscosity in particular deserves discussion. It becomes so very large at the glass temperature

that it can be used to define  $T_g$ .  $T_g$  occurs at about  $10^{13}$  poise. At first it seems like a strange dichotomy. For first-order transitions we use a thermodynamic criteria even though a kinetic one exists, while for second-order transitions we use a kinetic criteria even though a thermodynamic one exists (the  $S_c = 0$  criterion).

The experimental viscosity of glasses at high viscosities has not been studied carefully because of the experimental difficulties associated with such measurements. Whether there is a break in the  $\eta$  vs.  $T$  curve and whether we can find materials for which the break occurs at different viscosities are important questions. A recent theoretical paper predicts a break<sup>30</sup>, and there is also experimental evidence. The important question is whether the break occurs always at the same value of viscosity. Were this to happen then there would be justification in using the  $\eta = 10^{13}$  poise criterion. If not then there is no more reason for using the criterion for glasses than for crystals.

One can see from the fluctuation dissipation theorem that there is indeed a reason for the parallel behavior in the breaks (as functions of  $T, P$ ) of the thermodynamic and the dissipative quantities. It is easy to prove that in general the dissipative quantities suffer the same kind of discontinuity as the thermodynamic quantities. The fluctuation dissipation theorem reads<sup>31</sup>

$$S_{i,j}(k, \omega) = 2kT\chi_{i,j}'(k, \omega) \quad (6)$$

where  $S_{i,j}(k, \omega)$  describes how fluctuations at  $r, t$  correlate with those at  $r', t'$ , and  $\chi_{i,j}(k, \omega)$  describes how a system responds at  $r', t'$  to a force or signal initiation at  $r, t$ .  $\chi$  can be viscosity, diffusion coefficient, dielectric response, etc., while  $S$  can be autocorrelations of velocity, force, polarization, etc. Thus, the dissipative quantities undergo the same kind of transition as the correlation functions. Now it is known that the correlation functions in the limit of  $k, \omega$  both equal to zero have the same discontinuities as the thermodynamic susceptibilities<sup>32</sup>. These latter quantities (i.e., specific heat, thermal expansion coefficient, etc.) have discontinuities of  $n$ th-order for  $n$ th-order transitions. Finally, we observe that correlation functions change smoothly as we vary  $r, t$  or  $k, \omega$ . This completes the proof. Previously we had used as a proof the observation that the Onsager kinetic coefficients are explicitly dependent on the thermodynamic susceptibilities<sup>33</sup> which display the proper transition behaviour.

This parallelism between the thermodynamic and dissipative quantities resolves the Kauzmann paradox in a profound way. Viscosity does not

intervene to save the thermodynamic day; rather viscosity and volume (as well as entropy) behave in a parallel fashion and, in fact, their behavior reflects the underlying second-order transition.

It also suggests that one might with profit follow the glass transition via dissipative quantities that are easier to measure than viscosity. Electrical conductivity has been used successfully<sup>34</sup> and shows a break at  $T_g$ .

### IIB Order Parameters

The concept of order parameters has been both used and misused in the study of polymer glasses, so it should be discussed. There is a difficulty in that different people mean different things by the term. There is nothing wrong with this, but it does mean that we must describe the various uses. Otherwise, our discussion would become confusing. In what follows we shall describe applications to glasses within an enumeration of various ways order parameters are defined.

#### Kinds of Order Parameters

(1) Equilibrium-Thermodynamic. Stanley<sup>35</sup> describes the use of density as an order parameter (OP). This is a useful concept in the neighborhood of a critical point since there is a critical exponent associated with density. De Gennes<sup>36</sup> shows that magnetization  $M$  or magnetic susceptibility  $\chi$  can be useful as OPs for liquid crystals. Any of the extensive variables from the conjugate pairs  $(V,P)$ ,  $(S,T)$ ,  $(N_i, \mu_i)$ ,  $(B,H)$ ,  $(E,D)$ ,  $(\tau_{ij}, \epsilon_{ij})$  can be used as an OP, as can also the derivatives of these extensive variables with respect to intensive variables. Since equations of state can always be expressed in terms of the fundamental susceptibilities (thermal expansion coefficient etc.) they have a special place as OPs. Apparently any extensive thermodynamic quantity or one trivially derived from it such as density, can be useful as an OP for describing behavior near a critical point.

This brings us to our first misuse of  $S$  as an order parameter for glasses. Simon apparently thought that the solid-liquid transition line terminated at a critical point just as the liquid-gas transition line does<sup>37</sup>. He attempted to use  $S$  as an order parameter to measure how deeply one is into the solid region just as one can use volume (or density) to measure how deeply one is into the liquid region when encircling the gas-liquid critical point. It was a brilliant idea that happens not to be true since there is no critical point along the solid-liquid line.

(2) Equilibrium But Not Strictly Thermodynamic Order Parameters. There are many equilibrium quantities which are not from the classic set of thermodynamic variables enumerated above. Yet, they are often used as OPs. One

example is the short range OP in a solid solution of A and B atoms which measures the number of A's surrounding B's and the number of B's surrounding A's compared to their random mixing values. Another example is the intensity of a density wave with given  $(k, \omega)$ . Such quantities are useful if there is a way to control or at least measure them experimentally, or if there is a way to calculate them from theory.

Phenomenological thermodynamic variables are connected to the underlying microscopic variables (if we restrict our considerations to the canonical ensemble) via the equation

$$F = -kT \ln Q, \quad Q = \sum_{\{i...j...\}} \exp(-E\{i...j...\}/kT) \quad (7)$$

where  $F$  is the Helmholtz potential,  $Q$  is the partition function and  $\{i...j...\}$  enumerates all microstates. Any summation variable in  $Q$  can be used as an OP. An example in polymers is the use of numbers of holes,  $n_0$ , (empty lattice sites in the lattice model) and the fraction of backbone bonds,  $f$ , flexed out of their lowest energy (usually trans) configurations<sup>34</sup>. One uses the maximum term method to evaluate  $Q$  and obtains a equation for  $F$  in terms of the thermodynamic variables as well as equations for the numbers of holes and flexes as functions of  $T, P$ . Because the maximum term method was used the equations determining  $n_0, f$  are equivalent to

$$\frac{\partial G(T, P, n_0, f)}{\partial n_0} = 0 \quad \frac{\partial G(T, P, n_0, f)}{\partial f} = 0 \quad (8)$$

These equations are obviously a special case of the Davies-Jones order parameters  $Z_i$ <sup>38</sup> which are determined at equilibrium by

$$\frac{\partial G(T, P, Z_i)}{\partial Z_i} = 0 \quad (9)$$

The Davies-Jones OPs are in turn a special case of the affinities of Prigogine and Defay<sup>39</sup>. In the Gibbs-Di Marzio theory of glasses  $n_0$  and  $f$  are continuous across the glass transition but their derivatives with respect to  $T, P$  are discontinuous. Even though there are two OPs the Ehrenfest relations hold. In the Davies Jones approach the OPs were determined by Eq. (9) above the  $T_g(P)$  but were constant below  $T_g(P)$ . This was shown to involve a contradiction<sup>40</sup> unless the OPs were not independent. The contradiction can be resolved only by replacing Eq. (9) by the time dependent set

$$\dot{Z}_i = L_{ij} \frac{\partial G(T,P,Z_j)}{\partial Z_j} \quad (10)$$

which describes just how the  $Z_i$  change with time. The  $\partial G/\partial Z_i$  are generalized forces. The assumptions involved in Eq. (10) are the same as those of the Onsager reciprocal relations. An important observation is that the dissipative coefficients  $L_{ij}(T,P)$ , which are given as expectation values of correlation functions of  $Z_i$  and  $Z_j$ , have the same behavior as functions of  $T,P$  as extensive variables<sup>40</sup>. Eq. (10) can be used to determine experimentally if the glass transition is only a kinetic phenomenon. One uses various  $T(t), P(t)$  histories and then measures  $Z_i, \dot{Z}_i$ . This enables one to determine if  $L_{ij}(T,P)$  show breaks at the glass transition.

Other OPs can be extracted from the partition function. The summation variable need not be one that is susceptible to the method of the maximum term. Allowed OPs include functions of OPs, integrals of summation variables, Fourier transforms, mean values and deviations about the mean of summation variables.

(3) Nonequilibrium Thermodynamic Order Parameters. The  $Z_i$  we defined above as well as time dependent experimental tags are examples. There seems to be little point in discussing these OPs unless we discuss the time dependent equations. We shall do some of this in the section on collective variables.

(4) Any Variable Which is a Measure of Symmetry Breaking. Haken<sup>41</sup> uses a more general concept of order parameter that is applicable to systems far from equilibrium. Any variable which is a measure of symmetry breaking can be an OP, but the variables need not be thermodynamic.

The general idea of an OP seems to be any variable that gives us a measure of how far we are from a unique place at which there is an onset of a qualitative difference in the symmetry of the system. Symmetry usually means spatial and/or temporal regularity, but its most general definition is through the symmetry operations of group theory.

### IIC Collective Variables<sup>2</sup>

We define a collective variable to be any function of the  $6N$  momentum and position variables of a system of  $N$  particles. The usefulness of collective variables is that many times the dynamics of a system can be adequately described at least in some of its aspects by a few equations with a few collective variables. The effective mass in solid state physics, the center of mass and the net force in planetary

orbit theory conservation laws on energy-momentum are all examples of the use of collective variables. Whenever one can justify the use of collective variables there is an enormous simplification. The collective variable concept has been used throughout history. Indeed, before the discovery of atoms all concepts were collective variables. Apple pie and motherhood, for example. Because of the hierarchical nature of the universe, concepts (and realities) at one level of the hierarchy are collective variables compounded from the concepts and realities of the lower levels of the hierarchy. The relevance of these remarks to glasses is simply that collective variables are used in their description. We wish to discuss the projection operator technique of Zwanzig and others<sup>42</sup> and offer a modest critique. Their technique provides the most direct method known to concentrate on the collective variables of interest by using projection operators to project out the slow variables (called gross variables by them and collective variables by us) and to place all other variables into the fluctuating force term. We feel a discussion of this method is best done in the context of a discussion of the concept of collective variables.

There is a fundamental theorem of collective variables<sup>43</sup>. If we have  $M$  functions  $Y_i(q_j, p_j)$  of  $6N$  variables  $q_j, p_j$  and the rank of their functional matrix is  $M-K$  then there are  $K$  relations among the  $Y_i$  that do not involve the  $q_j, p_j$ . The physical application of this theorem is simply that one can (and does) concern himself with the interrelationships among the  $Y_i$  without ever having to consider the  $q_j, p_j$ . In fact, until recently mankind hardly realized that his most primitive and primal concepts were collective variables. Yet, it is non-the-less true that the level of ideas on which our minds operate is the level of collective variables. An important fact about collective variables is that the connection among the collective variables and the original  $6N$  position-momentum variables cannot be reconstructed from a knowledge of the collective variables alone.

Now because the real world is described by differential equations we must discuss collective variables for differential equations. The simplest example is a linear matrix equation

$$\frac{d\vec{X}}{dt} = A \vec{X} \quad (11)$$

where  $\vec{X}$  is an  $N$  component vector and  $A$  and  $N \times N$  matrix. Now if the matrix is reducible then we can find a set of  $M$  new variables  $Y$ , which are linear functions of the  $N$  variables  $X$ , for which we have the relation

$$\frac{d\vec{Y}}{dt} = B\vec{Y} \quad (12)$$

where B is MxM. Notice that if we were to have started with Eq. (12) we would not have been able to recover Eq. (11). We are always in the position of knowing the  $Y_i$  and not the  $X_i$ , and of knowing Eq. (12) even though Eq. (11) is the more fundamental of the two. We cannot infer Eq. (11) from Eq. (12). This means that "collective variables" is not a reciprocal concept.

Now the variables of linear response theory are collective variables. This is seen most clearly in the projection operator technique of Zwanzig<sup>42</sup>. The generalized Langevin equation reads

$$\frac{d\vec{a}}{dt} = i\Omega \cdot \vec{a}(t) - \int_0^t \phi(\tau) \cdot \vec{a}(t-\tau) d\tau + \vec{f}(t) \quad (13)$$

where  $\vec{a}$  are m "slow" variables and the remaining 6N-m fast variables show up in the random force  $\vec{f}$ . If the random force were identically zero then the  $\vec{a}$  would correspond exactly to our collective variable concept. If, as is usually the case, the random force is not zero then the average values of the  $\vec{a}$  are collective variables. The projection operator method of linear response theory is most beautiful since it allows a method of generating collective variables. Its application to glasses, however, must wait on an answer to the following problems.

(1) The equations are not covariant. One does not in general recover a linear set of equations from a linear set. Consider for concreteness the two coupled linear equations

$$\frac{df}{dt} = L_{11} f + L_{12} N_0 \quad (14)$$

$$\frac{dN_0}{dt} = L_{21} f + L_{22} N_0$$

If we now make the substitution  $f = f, \dot{N}_0 = n_0$ , then the resulting equations are not linear! Maybe the variables of interest are not the linear set which would be obtained directly from linear response theory but rather the non linear set which would not be obtained directly from linear response theory. Obviously, it is important to know what the relevant variables are before we try to project them.

(2) Do we have a complete set of collective variables? Let us suppose that our complete set of slow collective variables is M, but that

we do not know this and project out a set of m variables ( $m < M$ ). This means that the random force is not a rapidly varying quantity compared to the m a's that we chose but that the force has variations of the same time scale as the a's. Obviously, the method does not work well unless we have identified a complete set of slow collective variables.

(3) Is the classification into fast and slow variables meaningful? For the classification to be meaningful the notion of slow variable must not be something that is a function of the time of observation. A meaningful measure of speed of decay is  $d \ln(a_i) / dt$ . If  $a_i$  is proportional to  $\exp(-\lambda t^\beta)$ , ( $\beta < 1$ ) i.e., a William-Watts distribution, then we can order the variables according to their slowness. However, if  $\beta$  is allowed to have values greater than 1 then the notion of slow or fast variables is time dependent and therefore invalid. In general, we would expect that there are times when the classification into slow and fast variables is meaningless and times when it is useful. The situation for glasses is not apparent.

(4) Is the fluctuating force Gaussian and are the random variables independent? For simplicity consider 2 random variables that are uncorrelated. An arbitrary transformation to 2 new random variables will generally result in a correlation between the new variables. This means that we cannot assume that the components of the generalized vector random force in the generalized Langevin equation are uncorrelated, unless we have reason to believe that our choice of variables is special. Once this is realized the simplicity of the Langevin approach is lost.

The above remarks show that an insight as to the nature of the relevant variables is required before we can profitably use linear response theory.

#### IID. The William-Watts Relation

The William-Watts distribution has been the subject of much recent discussion<sup>44</sup>. Valid insights into the causes of the nonexponential decay are being obtained. We wish only to suggest that the form of the WW distribution cannot be valid for all manners of susceptibilities. This can be seen clearly from a treatment of Di Marzio and Bishop which relates the mechanical and electrical susceptibilities<sup>45</sup>.

$$\frac{\epsilon(\omega) - \epsilon(\infty)}{\epsilon(0) - \epsilon(\infty)} = [1 - i\omega\eta(\omega)K] \quad (15)$$

where  $\epsilon(\omega)$  is the dielectric response,  $\eta(\omega)$  the complex shear viscosity and K a constant. This equation is a simple generalization of the Debye equation in which the zero frequency frictional coefficient for rotation of a sphere

is replaced by its frequency dependent value. It is valid as long as the concentration of dipoles is small. The point we wish to make is simply that if  $\epsilon(\omega)$  is a stable distribution then  $\eta(\omega)$  is not.

### References

1. E. A. Di Marzio, *Annals. N. Y. Acad. Sci.* 371, 1 (1981).
2. For example, see M. Gardner, "Extraordinary nonperiodic tiling that enriches the theory of tiles" *Sci. Amer.* January 1977, p. 10.
3. R. Penrose, *J. Inst. Math. and its application*, 7-8, 266 (1974).
4. R. Mosseri and J. F. Sadoc, *Proc. 2nd International Conf. on Struc. of Noncrys. Matls.*, P. H. Gaskell, J. M. Parker and E. A. Davis Eds. Taylor and Francis Inc., New York (1983) p. 137.
5. B. Mandelbrot, "The Fractal Geometry of Nature" (W. H. Freeman and Co., San Francisco 1982)
6. M. Hoare, *Ann. N. Y. Acad. Sci.* 271, 186 (1976).
7. L. W. Tilton, *J. Res. Nat. Bur., Stnds.*, 59, 139 (1957).
8. R. Zallen in "Fluctuation Phenomena," ed. E. W. Montroll and J. L. Lebowitz, (North-Holland, Amsterdam, 1979), p. 177.
9. K. Kubo, "Lectures in Theoretical Physics," Vol. 1, ed. by Brittin and Dunham (Interscience Pub., N.Y. 1959) pp. 120-203.
10. W. Kauzmann, *Chem. Revs.* 43, 219 (1948).
11. J. H. Gibbs and E. A. Di Marzio, *J. Chem. Phys.*, 28, 373 (1958).
12. A. R. Greenberg and R. P. Kusy, *Polymer*, 24, 513 (1983).
13. E. A. Di Marzio and J. H. Gibbs, *J. Poly. Sci.*, 1A, 1417 (1963).
14. E. A. Di Marzio, J. H. Gibbs, P. D. Fleming III and I. C. Sanchez, *Macromolecules*, 9, 763 (1976).
15. E. A. Di Marzio, *J. Res. Nat. Bur. Stnds.*, 68A, 611 (1964).
16. E. A. Di Marzio and F. Dowell, *J. Appl. Phys.*, 50, 6061 (1979).
17. B. Bagchi, C. Cerjan and S. A. Rice, *Theoretical Analysis of the Achievement of Random Close Packing of Hard Spheres*. Preprint.
18. G. Adam and J. H. Gibbs, *J. Chem. Phys.*, 43, 139 (1965).
19. M. V. Volkenstein, "Configurational Statistics of Polymeric Chains," (Interscience, N.Y. 1963).
20. P. J. Flory, "Statistical Mechanics of Chain Molecules," (Interscience, N.Y. 1969)
21. E. A. Di Marzio and J. H. Gibbs, *J. Chem. Phys.*, 28, 807 (1958).
22. K. D. Pae, C. L. Tang and E. S. Shin, *Bul. Amer. Phys. Soc.*, 29, 410 (1984).
23. P. G. de Gennes, *Phys. Lett.* A38, 339 (1972).
24. J. des Cloiseaux, *J. Phys. (Paris)* 36, 281 (1975).
25. P. D. Gujrati and M. Goldstein, *J. Chem. Phys.* 74, 2596 (1981).
26. M. L. Eidinoff and J. G. Aston, *J. Chem. Phys.* 3, 379 (1935); N. Go and H. A. Scheraga, *J. Chem. Phys.* 51 475 (1969); E. A. Di Marzio, 23rd IUPAC (Boston) 8 240 (1971).
27. A. Baumgardner, *Ann. Rev. Phys. Chem.* 35 000 (1984).
28. Do Y. Yoon and A. Baumgardner, *Phase Transition of Cubic Lattice Polymer Systems*, *Bul. Amer. Phys. Soc.*, 29 281 (1984); A. Baumgardner and Do Y. Yoon, *J. Chem. Phys.*, 79, 521 (1983).
29. J. Sherwood in *Specialist Periodical Report, Chem. Soc. London*, "Surface and Defect Properties" Vol. 2 1973.
30. V. G. Rostliashvili, A. R. Mekhoda, V. I. Irzhak, and B. A. Rosenberg, *J. Poly. Sci. Physics*, 22 000 (1984).
31. D. Forster "Hydrodynamic Fluctuations, Broken Symmetry, and Correlation Functions," (W. A. Benjamin, Inc. Reading, Ma. 1975).
32. H. B. Callen, "Thermodynamics," (John Wiley and Sons, Inc. 1960).
33. E. A. Di Marzio, *J. Appl. Phys.*, 45, 4143 (1974).
34. R. W. Warfield and B. Hartmann, *Polymer*, 21, 31 (1980).
35. H. E. Stanley, "Introduction to Phase Transitions and Critical Phenomena," (Oxford University Press, 1971).
36. P. G. de Gennes, "The Physics of Liquid Crystals," (Oxford University Press, 1974).
37. F. Simon, *Trans. Faraday Soc.*, 33 65 (1937).
38. R. O. Davies and G. O. Jones, *Adv. Phys.* 2, 370 (1953).
39. I. Prigogine and R. Defay, "Chemical Thermodynamics," (Longmans Green and Co., N. Y., 1954).
40. E. A. Di Marzio, *Macromolecules*, 10, 1407 (1977).
41. H. Haken, "Synergetics," (Springer-Verlag, N.Y., 1977).
42. See for example S. Nordholm and R. Zwanzig, *J. Stat. Phys.*, 13, 347, (1975).
43. Tullio Levi-Civita, "The Absolute Differential Calculus," (Blackie and Son, London 1926).
44. See for example M. F. Shlesinger and E. W. Montroll, *Proc. Nat. Acad. Sci.* 81 1280 (1984); A. K. Ragopal, K. L. Ngai, R. W. Rendell, and S. Teitler, *J. Stat. Phys.* 30 285 (1983); E. W. Montroll and J. T. Bendler, *J. Stat. Phys.*, 34, 129 (1984).
45. E. A. Di Marzio and M. Bishop, *J. Chem. Phys.*, 60, 3802 (1973).

MULTIPLE ORDERING PARAMETER MODELS OF THE GLASS TRANSITION  
AND APPROACHES TO EQUILIBRIUM

David Ng and J. J. Aklonis  
Loker Hydrocarbon Research Institute  
Department of Chemistry  
University of Southern California  
Los Angeles CA 90089-1661

Introduction

In modeling the viscoelastic behavior of high molecular weight polymers, distributions of relaxation or retardation times are always involved.<sup>1</sup> It is easy to understand the necessity for such distribution functions since, in these high molecular weight systems, various modes of motion of the molecules contribute to the measured response. Thus, short range motions which occur on a rapid scale as well as longer range motions which occur on a much longer time scale contribute significantly to the response of the system. The application of a distribution function formalism is a convenient way to treat such varied molecular time scales.

Although high molecular weight polymers usually form glasses, low molecular weight materials such as glycerol, ethanol and glucose, also exhibit vitreous states. In the last several years, there has been great interest in developing mathematical models to treat the varied and interesting kinetic aspects of glass transition behavior.<sup>2-10</sup> It has been found that multiple ordering parameter models which employ a distribution of recovery mechanisms have been quite successful in treating the behaviors of glasses. This is true for high molecular weight materials as well as for the lower molecular weight glass formers such as those mentioned above.

In this paper, we will present a brief exposition of a form of such multiple ordering parameter models which we feel is the easiest to understand<sup>3</sup> and will relate some of its successes as well as a few shortcomings. We will furthermore concentrate on one of these shortcomings, namely the difference between predicted and experimental behavior close to equilibrium and carefully investigate whether any set of parameters of the model can account for the approach toward equilibrium which is actually observed experimentally.

Multiple Ordering Parameter Models  
of the Glass Transition

In treating viscoelastic relaxation of polymers, a physical property such as the modulus, for example, is routinely partitioned as

$$E(0) = \sum_i E_i \quad (1)$$

$E(0)$  represents the short time limit of the tensile stress relaxation modulus. This value results from the contribution of many individual terms,  $E_i$ , each of which is associated with a specific molecular motion in the system.

In considering the kinetics of glass transition phenomena, it is convenient to define a variable which we have called  $\delta$

$$\delta = \frac{V(t) - V_\infty}{V_\infty} \quad (2)$$

where  $V(t)$  is the instantaneous value of the volume under any experimental conditions and  $V_\infty$  is the equilibrium volume under these conditions. When dealing with other extensive variables, similar definitions for  $\delta$  are possible. As was done for the stress relaxation modulus,  $\delta$  may also be partitioned as

$$\delta(0) = \sum_i \delta_{i,0} \quad (3)$$

where  $\delta(0)$  is the value of  $\delta$  immediately after the system has been perturbed from equilibrium by an "instantaneous" change in an intensive variable such as temperature or pressure, and  $\delta_{i,0}$  is the instantaneous contribution to the departure from equilibrium associated with the  $i$ th mode of molecular motion.

The time dependence of equation (1) is introduced by realizing that each mode of molecular motion takes place on its own effective time scale denoted by  $\tau_i$ . When treating the physics of the system properly, the time dependent stress relaxation modulus becomes



$$E(t) = \sum_i E_i e^{-t/\tau_i} \quad (4)$$

where each partial modulus value is weighted by a damped exponential involving the relaxation time of that particular mode of motion.

For volume relaxation of glasses, the situation is similar but not identical. For the simplest case involving system response after an instantaneous perturbation from equilibrium, the differential equation controlling the response of each molecular mechanism is

$$\frac{d\delta_i}{dt} = -\frac{\delta_i}{\tau_i} \quad (5)$$

Here,  $\delta_i$  is the contribution to the departure from equilibrium  $\delta$ , associated with the  $i$ th mode of molecular motion and  $\tau_i$  is the retardation time of that mode. The set of equations represented by equation (5) is very similar to the set of equations which were solved to yield equation (4). In equation (5), however, a very interesting and important coupling arises. Although not expressed explicitly in this equation, it is clear that each of the  $i$ th retardation times depend upon the overall temperature of the system. In a similar way, all of the multiple ordering parameter models employ a set of retardation times which depend on the overall departure of the system from equilibrium, i.e.  $\delta$ . Thus, the specific value of the  $\tau_i$ 's determine the time evolution of  $\delta$  and, at the same time, the value of  $\delta$  determines the magnitude of the retardation times. This circular coupling is the root of many of the interesting and important kinetic aspects of the glass transition.

To this point we have only considered the response of a system subject to an instantaneous perturbation from equilibrium. The model may be easily generalized to treat more complicated perturbations as

$$\frac{d\delta_i}{dt} = -\Delta\alpha_i q - \frac{\delta_i}{\tau_{i,r} a_T a_\delta} \quad (6)$$

where  $\Delta\alpha_i$  is given as  $\Delta\alpha_i = (\delta_{i,0}/\delta(0))(\alpha_l - \alpha_g)$

where  $\alpha_l$  is the coefficient of expansion of the liquid and  $\alpha_g$  is the coefficient of expansion of the glass. In equation (6)  $q$  is the heating or cooling rate and the retardation time is given a more general representation in which its structural and temperature dependencies are made clear as

$$\tau_i = \tau_{i,r} a_T a_\delta = \tau_{i,r} \exp[-\theta(T-T_r)] \exp[-(1-x) \frac{\theta\delta}{\Delta\alpha}] \quad (7)$$

where  $\tau_{i,r}$  is the value of the  $i$ th retardation time at the reference temperature  $T_r$  in equilibrium ( $\delta=0$ ).  $\theta$  is a material constant which characterizes a temperature dependence of each  $\tau_i$  under equilibrium conditions, and  $x$  is a

partition parameter ( $0 \leq x \leq 1$ ) which determines the relative contributions of temperature and structure to  $\tau_i$ .

### General Successes of Multi-Ordering Parameter Models

The kinetics of glass forming materials in the glass transition range are surprisingly varied. The general features of the kinetics have been presented several times recently<sup>3-10</sup> and will not be discussed at length again here. Nevertheless, it will be noted that these theories account for many aspects of the glass transition in a very satisfying way; these include the time dependence of glass transition phenomenon, the non-linearity of the kinetics, the asymmetry of behavior with respect to the sign of the perturbation evoking the response, and memory effects which are clearly evident. The existence of a distribution of retardation mechanisms whose time scales are coupled to the overall departure of the system from equilibrium is the crux of the underlying molecular mechanism responsible for these complicated aspects of the glass transition. It is very reassuring, in fact, that so many aspects of the complicated nature of the behavior of glasses can be so straightforwardly explained in terms of this simple model.

### Discrepancies Between Theory and Experiment

Models or theories are very important in science for many reasons. In part, their importance derives from their ability to explain or rationalize the apparently complicated results of many experiments in terms of but a few simple and plausible assumptions about the underlying fundamental processes. Perhaps even more importantly, however, models can be used to point out unexpected aspects of experimental results—results which signal that specific and maybe important modifications to the models must be made before the theory and experiment are in agreement.

As mentioned several times, the kinetic aspects of glasses in this interesting region are very complex. In this case, rather than being disappointed by the shortcomings of the model, one should be surprised at how much of the complicated behavior is actually explained by these simple multi-ordering parameter models. Nevertheless, it is still important to focus on the shortcomings of the models since here is where further success in our understanding of the glass transition can be won.

While we intend to concentrate on but one of the discrepancies in this paper, several groups<sup>3,8-10</sup> have noted apparent problems with the theory. In terms of a formulation of this multi-ordering parameter model involving a Williams-Watts distribution function, it seems clear that no single set of experimental parameters is totally successful in describing the behavior of any single glass forming system over a wide enough variety of conditions. In addition, while one might expect that the particular distribution function associated with

various extensive parameters such as volume or enthalpy might be different in any particular system, the formulation of these ordering parameter models suggests that the parameters controlling the specific values of each retardation time ( $\alpha$  and  $\theta$ ) should be the same for all extensive variables. This does not seem to be the case.<sup>8,10</sup>

In spite of shortcomings of this sort, there appears to us to be yet another major discrepancy between these theories and experiments which has the potential to force major modifications in the theories.

Many years ago, Kovacs<sup>11</sup> defined an effective retardation time, denoted as  $\tau_{\text{eff}}$

$$\tau_{\text{eff}}^{-1} = -\frac{1}{\delta} \frac{d\delta}{dt} \quad (8)$$

which could be easily measured from experimental data obtained by subjecting samples at equilibrium to "instantaneous" temperature jumps. These have been called simple approach experiments. Plotting this effective retardation time versus  $\delta$  for many simple approach experiments gives a very sensitive "fingerprint" of the kinetics of a particular glass former in its glass transition region. Kovacs<sup>11</sup> published accurate data on the behavior of polyvinylacetate and a portion of this data is reproduced in figure 1. On the figure long retardation times are low and short retardation times are high. The data represented here is all measured at 35°C. The data on the right hand side of the figure comes from contraction experiments involving subjecting the sample to rapid temperature decreases from higher temperatures (50, 40, and 37°C) to the experimental temperature of 35°C; the data on the left hand side of the figure is derived from expansion

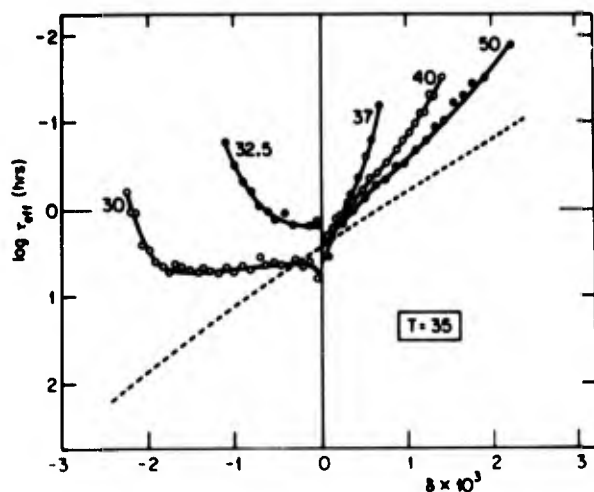


Figure 1:  $\log \tau_{\text{eff}}$  versus  $\delta$  for simple approach experiments on polyvinylacetate at 35°C (Reference 11). Dashed line shows typical single ordering parameter model behavior.

caused by subjecting the sample to a rapid temperature increase (from 30° and 32.5°C) to the experimental temperature, 35°C. Although, this is but a portion of Kovacs' data on polyvinylacetate, the richness of the response is obvious. In this figure, the dashed line denotes the dependence of a single relaxation time on  $\delta$  at constant temperature as given in equation (7) with reasonable parameters. It is abundantly clear that a single ordering parameter model does not have much success in rationalizing  $\tau_{\text{eff}}$  behavior for this typical glass forming system.

The feature of figure 1 upon which we wish to concentrate involves the behavior of this system as equilibrium is approached in expansion experiments, i.e., from  $\delta < 0$ . The results of two experiments are shown; it must be remembered that all experiments are carried out at 35°C and, although not shown in the figure, the time scales of the experiments are long involving the sample being subjected to the experimental temperature for periods of hours. The responses of the system to the temperature jumps from 30° and 32.5°C are markedly different. What is most interesting, however, is the enormous difference in behavior as equilibrium is approached. At values of  $\delta$  near  $10^{-4}$ , it is experimentally clear that the effective retardation time is dramatically different in each case—the effective retardation times differing by approximately a factor of 5 at a value of  $\delta = 10^{-4}$  in each experiment!

This behavior has certainly been noticed in the past. It is unexpected since, at such a small departure from equilibrium, the previous sample history would not be expected to exert such a strong influence on behavior. In fact, in their papers, Kovacs, et al.<sup>3</sup> commented on this point and indicated that, with the distribution function they have chosen to best fit the data for polyvinylacetate over a broad range of behavior, they had not chosen a set of parameters which will rationalize the strange behavior noticed in figure 1.

It seems to us, that others have disregarded this apparent discrepancy between theory and experiment. If the data are accurate (we are aware of no reason to assume they are not) any successful theory or model must show such markedly different behavior of  $\tau_{\text{eff}}$  as equilibrium is approached in expansion experiments starting from various temperatures.

We have, therefore, examined the intrinsic flexibility of multi-ordering parameter models as represented by equations (6) and (7) with respect to their abilities to generate  $\tau_{\text{eff}}$  behavior like that shown in figure 1 as equilibrium is approached in expansion experiments. We have tried to determine whether any set of experimental parameters involved in the model and any distribution function can give rise to such behavior.

### Distribution Functions of Varying Shapes

In order to investigate the influence of the shape of a distribution function on the approach toward equilibrium in expansion experiments, we have freely constructed functions which we feel represent all reasonable variations of shape which might give rise to the observed behavior. The actual shapes which must be considered are somewhat limited since, as equilibrium is approached, only the long term part of a distribution function is involved. Thus, more complicated distribution functions spanning longer time scales are of no interest.

The six distribution functions employed are denoted as A through F and are shown in the accompanying figures 2 through 7. Here the functions are presented as  $g(\tau)$  vs.  $\log \tau$ ; however, since the actual calculations were done using a discrete distribution, the normalization

$$1 = \sum_{i=1}^{100} g(\tau_i)$$

was applied to all distribution functions shown save function D which was represented by a thirteen point spectrum. The retardation times were chosen so as to be evenly spaced on a logarithm scale.

Distribution function A is a simple box extending over four decades of retardation time. The height of the box is determined by the normalization, and the retardation times are sufficiently closely spaced such that the behavior calculated is indistinguishable from that resulting from a continuous spectrum. Spectrum B is Gaussian and Spectrum C a two box function like that used previously by Kovacs et al.<sup>3</sup>

The Williams-Watts type distribution function has often been used because of its computational simplicity.<sup>4,8-10</sup> Here, rather than taking advantage of this feature, we have used the transform of the Williams-Watts function given by Lindsey and Patterson<sup>12</sup> which is shown in the figure and which is compatible with our particular calculational formulas. The essential shape similarity between distribution D and distribution C becomes clear when the functions are represented in this way.

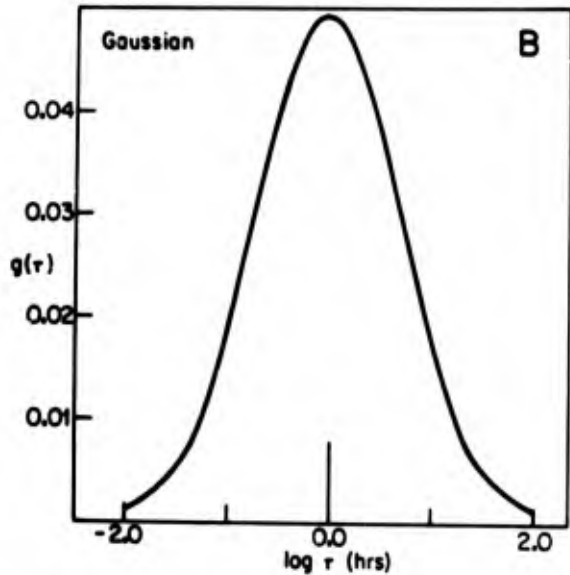


Figure 3: Gaussian distribution of retardation times with a full width at half peak maximum of two.

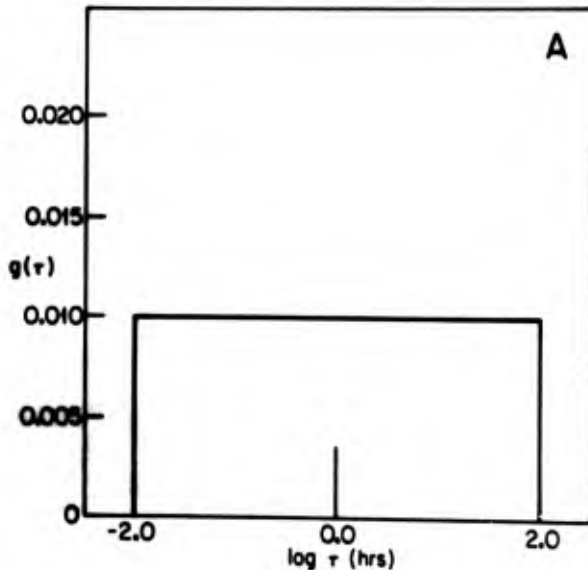


Figure 2: Single box distribution of retardation times.

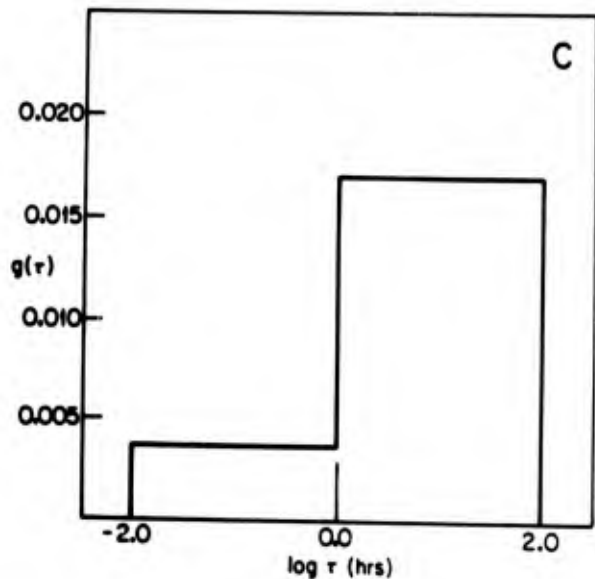


Figure 4: Two box distribution function used previously (Reference 3).

Finally two ramps were employed as distribution functions, one with positive slope and one with negative slope; both extended over four decades of relaxation time. Although behaviors associated with other distribution functions were in fact calculated, we feel that this selection of distribution functions is sufficient to make our point here.

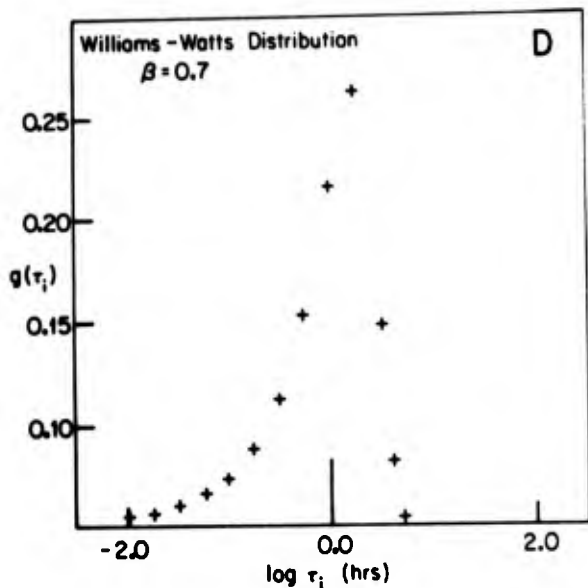


Figure 5: Williams-Watts distribution function  $\beta = 0.7$ .

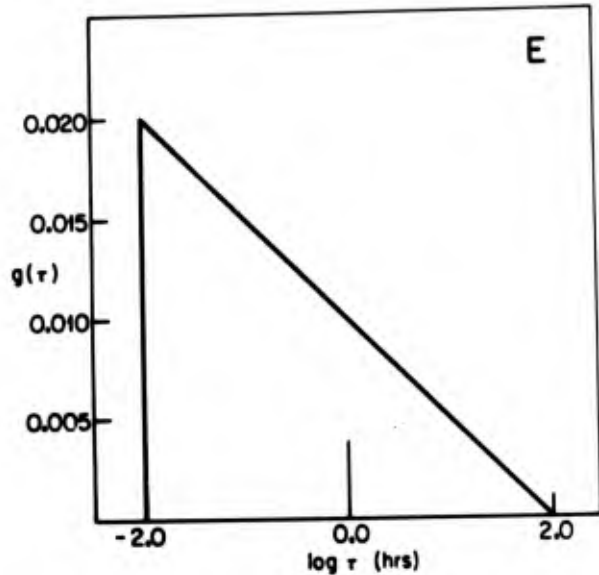


Figure 6: Ramp distribution function with a negative slope.

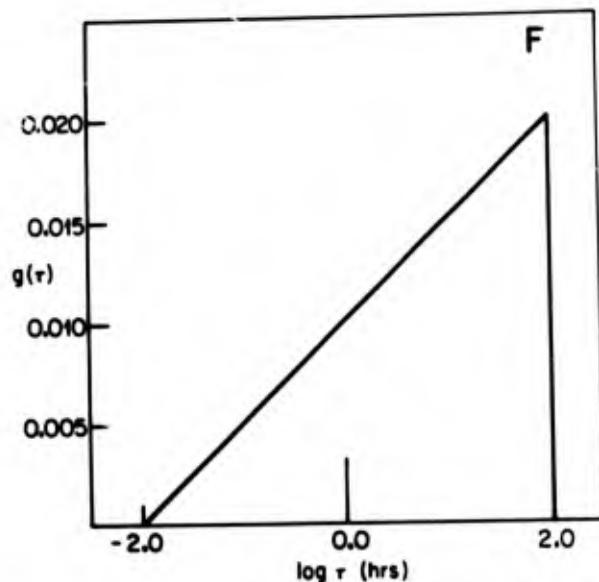


Figure 7: Ramp distribution with a positive slope.

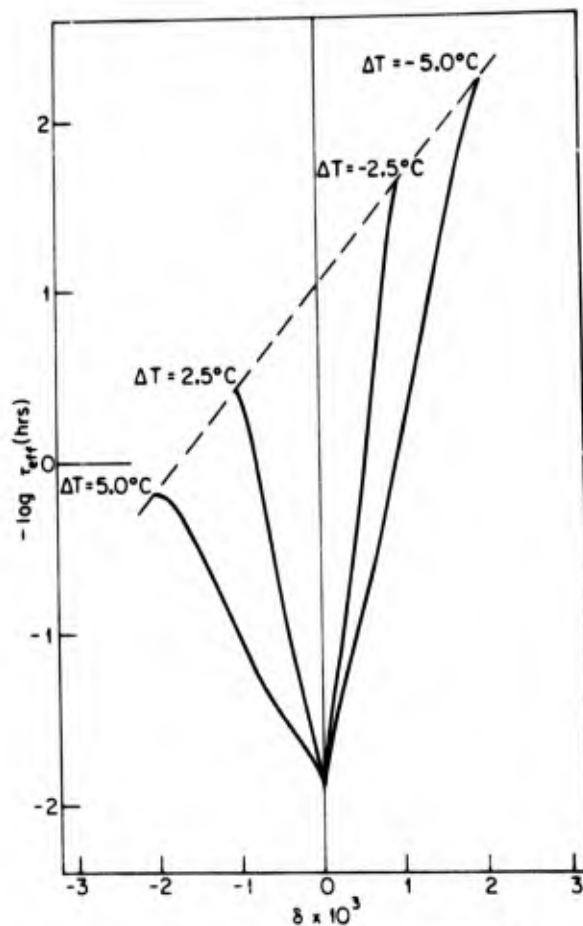


Figure 8: Typical  $\tau_{eff}$  behavior associated with the single box distribution (A).

Rather than varying both the distribution function shape and the parameters involved in equations (7) simultaneously, we will investigate the variations in behavior brought about by changes in distribution function shape and then consider changes in the other variables. At this point, reasonable values for the material parameters will be employed:

$$\theta = 1.0^{\circ}\text{K}^{-1}, \quad \Delta\alpha = 4 \times 10^{-4} \text{K}^{-1}, \quad \text{and } x = 0.4.$$

The simple approach behavior resulting from the six distribution functions identified in expansion and contraction from equilibrium at two or three temperatures above and below the experimental temperature is shown in figures 8 through 13. The influence of shape of the distribution is very clear. For example, the flat box distribution function A shown in figure 2 shows up as a rather featureless almost straight line  $\tau_{\text{eff}}$  plot in expansion (figure 8) whereas the Williams-Watts function (distribution D) has a much more complex  $\tau_{\text{eff}}$  structure (figure 11). Nevertheless, the feature of interest in this investigation is the variation in approach to equilibrium at small values of  $\delta$  in expansion experiments starting from different temperatures.

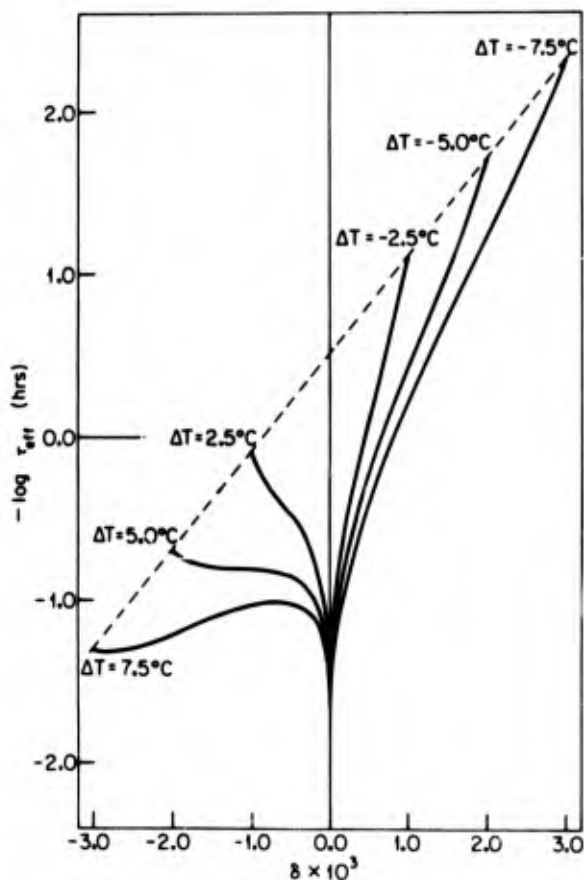


Figure 9: Typical  $\tau_{\text{eff}}$  behavior associated with the Gaussian distribution (B).

We suggest that quantitatively the differences between these curves at small values of  $\delta$  are essentially inconsequential as compared to the large variation seen in the experimental data. It is our contention that none of these distribution functions gives behavior which is of the type observed experimentally by Kovacs and depicted in figure 1. We were unable to generate a distribution function which gives behavior like that observed experimentally with the values of  $x$ ,  $\theta$  and  $\Delta\alpha$  stated above.

Since all of the simple approach behavior being considered takes place at a single temperature, the pure temperature dependence of the retardation times, as measured by the  $a_T$  term in equation (7), is of no interest. The structural dependent term, however, is important; it is a function of the time independent parameters  $x$ ,  $\theta$  and  $\Delta\alpha$ . For the sake of our further discussion in the next two sections of this paper, we will consider both  $\theta$  and  $\Delta\alpha$  to be fixed at  $1.0^{\circ}\text{K}^{-1}$  and  $4 \times 10^{-4} \text{K}^{-1}$  so that variations in the sensitivity of the retardation times to structure will result from changes in  $x$  alone. No loss of generality results from this simplification.

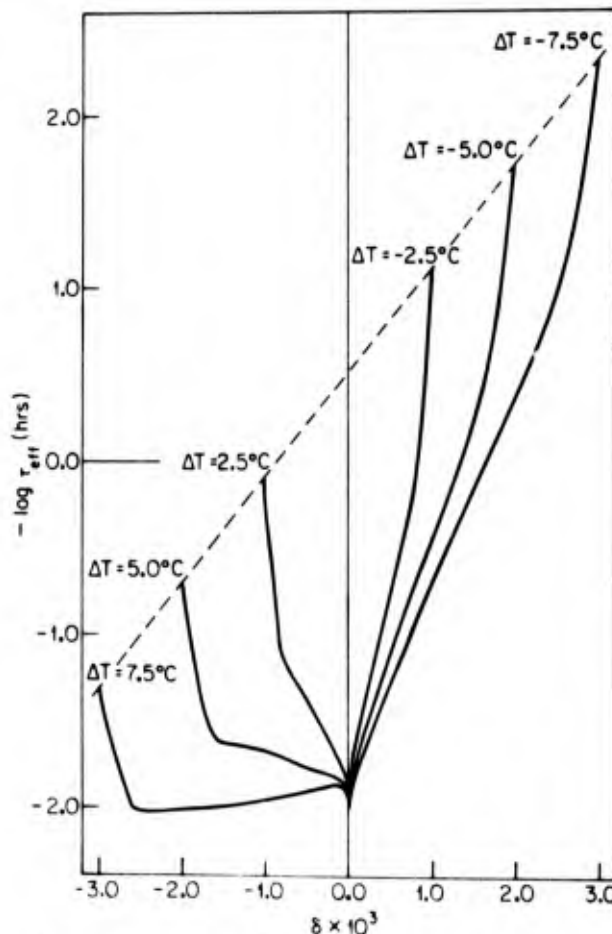


Figure 10: Typical  $\tau_{\text{eff}}$  behavior associated with the double box distribution function (C).

### Variation of Other Parameters

As mentioned above, there is but one other parameter which can be varied in the theory under these circumstances which will have an influence on the  $\tau_{eff}$  behavior, i.e., the value of  $x$  which gauges the structural dependence of each retardation time. In this section we will choose two other values of this parameter which represent near extremes of behavior. When  $x=0.95$ , a retardation time shifts very little with changes in  $\delta$ . On the other hand, when  $x=0.01$ , the sensitivity is quite extreme. Even though distribution functions B, C, D and F seemed to have the most interesting behavior in the previous section, here, for the sake of exposition, we will limit our consideration to the two box distribution function called C. The conclusions are identical for the other functions as well.

The  $\tau_{eff}$  behavior for this distribution function at these values of  $x$  is presented in figures 14 and 15. The values of  $x$  scan structural sensitivities which essentially cover the range of all possible variations. Comparison of figures 14 and 15 makes this clear. In figure 14, the initial  $\tau_{eff}$  value differs little whether the temperature jump evoking response is  $7.5^\circ$  or one third of this value. On the

other hand, in figure 15, a factor of two variation in the temperature jump results in the initial value of  $\tau_{eff}$  varying by almost a factor of 10.

Of all the  $\tau_{eff}$  plots shown, figure 15 would seem to have the most promise of duplicating experimentally observed behavior. Nevertheless, even with this extreme and perhaps unreasonable value of  $x$ , the variation in  $\tau_{eff}$  at very small departures from equilibrium is, once again, very much smaller than the factor of approximately 5 which was observed by Kovacs.<sup>11</sup>

Thus, we are forced to conclude that we have been unable to choose a distribution function and value of the partition parameter  $x$  which will generate behavior which is even remotely like that which has been reported experimentally. If the experimental data are accurate, we feel that this conclusion represents a major discrepancy between theory and experiment which deserves consideration. It is hard to imagine devising a reasonable mechanism within the framework of current multi-ordering parameter theories which will yield the experimentally observed behavior.

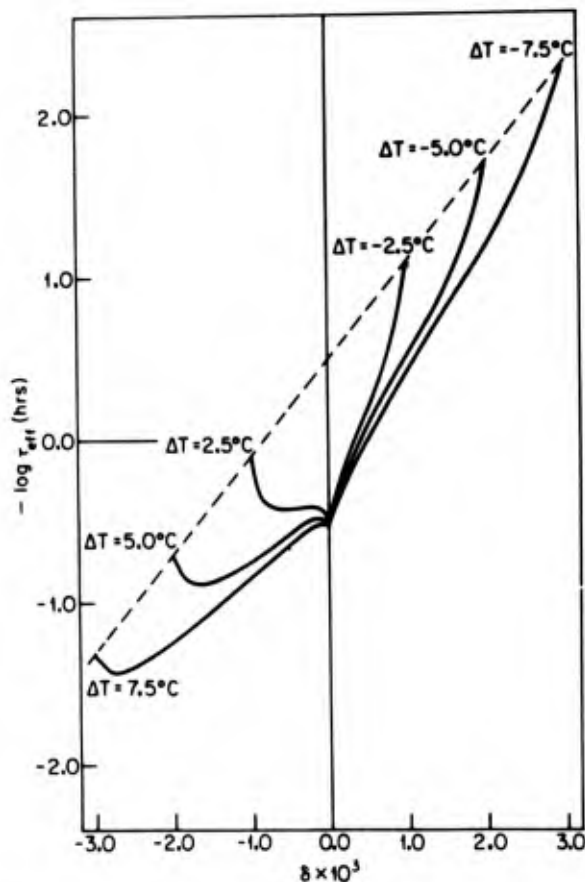


Figure 11: Typical  $\tau_{eff}$  behavior associated with the Williams-Watts distribution function (D).

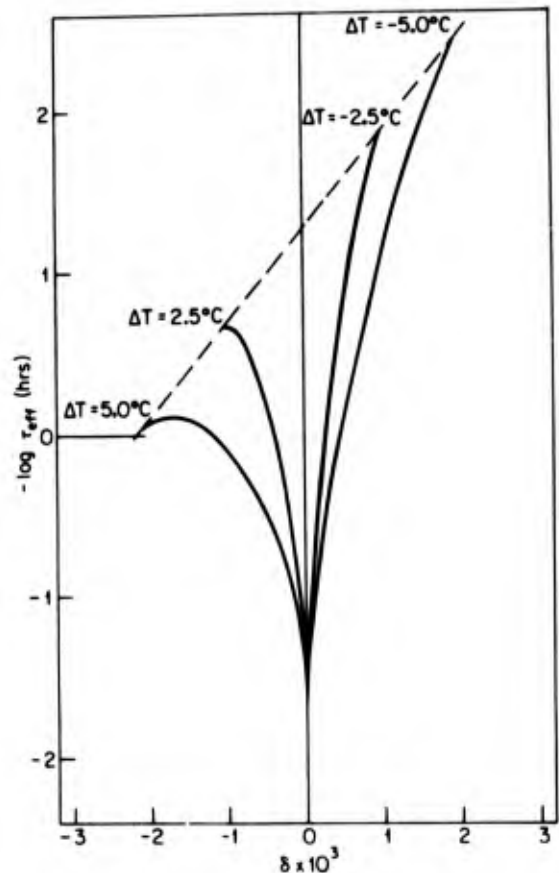


Figure 12: Typical  $\tau_{eff}$  behavior associated with a ramp with negative slope (E).

### A Possible Experimental Complication

In carrying out all simple approach experiments, it is presumed that the sample is in an equilibrium state before it is subjected to the "instantaneous" temperature jump. This condition is easily satisfied for contraction experiments where the equilibrium must be established at high temperatures and relaxation times are rapid. On the other hand, for expansion experiments where the equilibrium must be obtained at low temperatures, relaxation is very slow. It has been suggested that perhaps the large variation in relaxation times observed experimentally in expansion experiments by Kovacs actually resulted from inadequate annealing of the sample such that the samples aged at the lowest temperatures were actually not at equilibrium before the glass was subjected to a rapid temperature increase.

To explore the effect of such a possibility on experimentally observed  $\tau_{eff}$  behavior, we have simulated exactly this situation on the computer. Once again, the distribution function employed was the two box one shown in figure 4. The value of  $x$  was taken as 0.5 and  $\theta$  was increased to  $2.5^\circ \text{K}^{-1}$ . This larger than usual value for  $\theta$  was taken primarily for

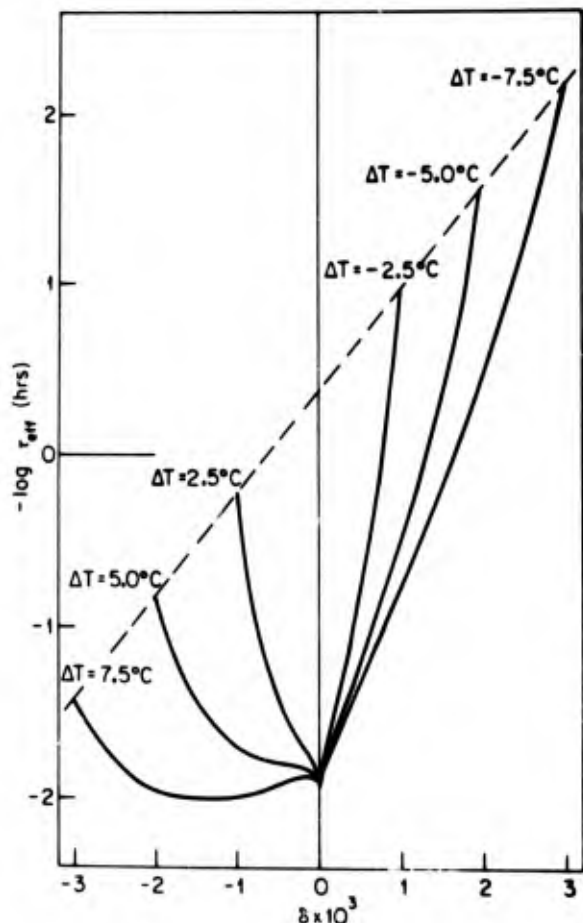


Figure 13: Typical  $\tau_{eff}$  behavior associated with a ramp with positive slope (F).

the sake of computational convenience since a large temperature dependence helped to emphasize the effect. The situation is somewhat similar to experiments which Kovacs has called memory experiments in the past. The procedure is depicted in figure 16. Initially the sample is at equilibrium at the reference temperature of  $300^\circ \text{K}$ . For simplicity we have assumed that the sample has a volume of exactly 1.0 cubic centimeters under these conditions. In the first experiment, the sample is quickly quenched to  $297.5^\circ \text{K}$ . It is annealed under these conditions for 10 hours which is a sufficiently long time to allow  $\delta$  to attain a value less than  $10^{-5}$  i.e., the sample is essentially at equilibrium. Next the sample is heated back to  $300^\circ \text{K}$  and  $\tau_{eff}$  is calculated as equilibrium is established. This behavior is shown as the  $\Delta T = 2.5^\circ \text{C}$  curve in figure 17. The  $\tau_{eff}$  behavior is as would be expected under these conditions, being similar to what was calculated earlier for this distribution function (figure 10). The reason that the behaviors depicted there and here are not identical is associated with the fact that  $\theta$  has been increased from 1.0 to 2.5 which makes the structural sensitivity, as well as the temperature sensitivity, more extreme.

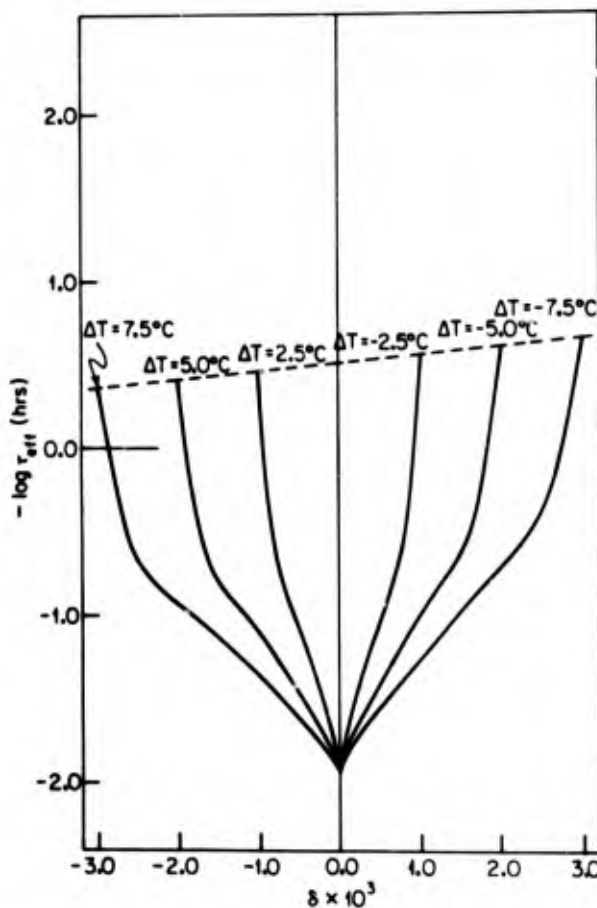


Figure 14:  $\tau_{eff}$  behavior with minimal structural sensitivity, i.e.,  $x=0.95$ ; double box distribution.

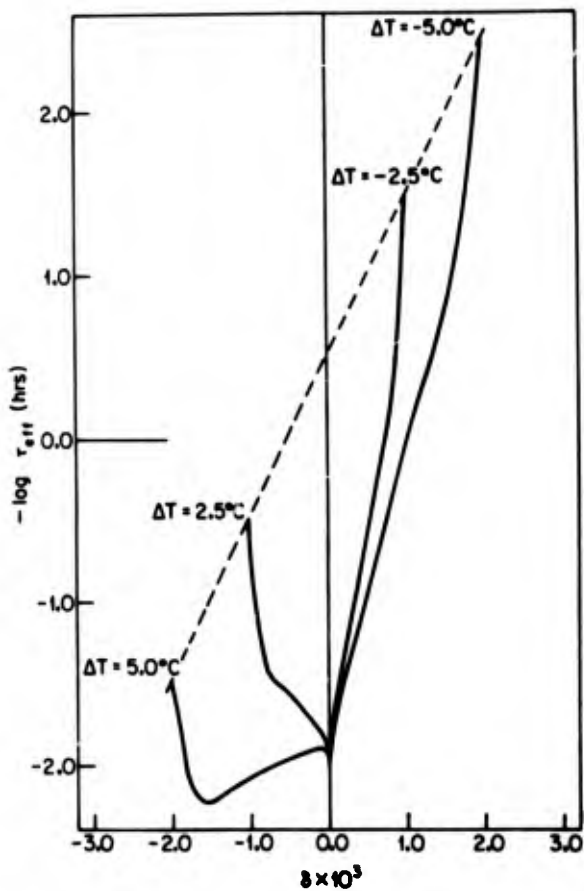


Figure 15:  $\tau_{\text{eff}}$  behavior with extreme structural sensitivity, i.e.,  $x=0.01$ ; double box distribution.

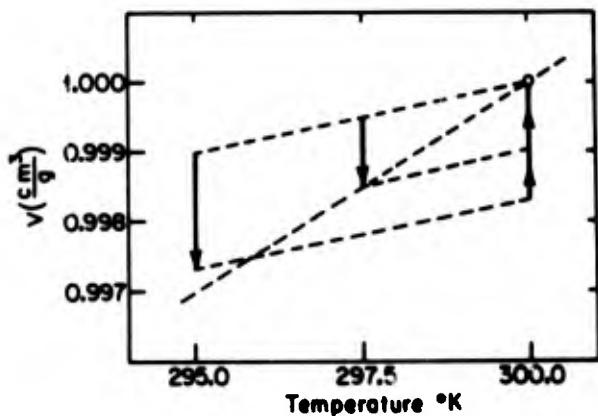


Figure 16: Volume versus temperature behavior for expansion experiments departing from various states. Solid lines represent time dependent volume adjustment. Equilibrium is virtually established during annealing at 297.5°K but not at 295.0°K.  $\alpha_l = 6.0 \times 10^{-4} \text{K}^{-1}$ ,  $\alpha_g = 2.0 \times 10^{-4} \text{K}^{-1}$ .

Referring back to figure 16, the lower temperature experiment takes place as follows: The sample, initially at equilibrium at 300°K is subjected to a rapid temperature quench to 295°K and is then allowed to anneal for  $10^3$  hours. This annealing time is much longer than that at 297.5°K. Nevertheless, because of the experimental parameters chosen, the system is still far from equilibrium. Thus, this is like the situation which has been suggested to be the case in Kovacs's expansion experiments. The  $\tau_{\text{eff}}$  behavior observed after the sample in this state is reheated rapidly to 300°K is also shown in figure 17. The behavior does not look at all like what is observed experimentally. Kovacs<sup>11</sup> found that the  $\tau_{\text{eff}}$  behaviors for expansion experiments starting from lower temperatures were much slower in approaching equilibrium than the  $\tau_{\text{eff}}$  behavior resulting from expansion experiments starting at higher temperatures. In this sample calculation, we see just the opposite situation. Here, the  $\tau_{\text{eff}}$  curves actually cross; the one associated with the

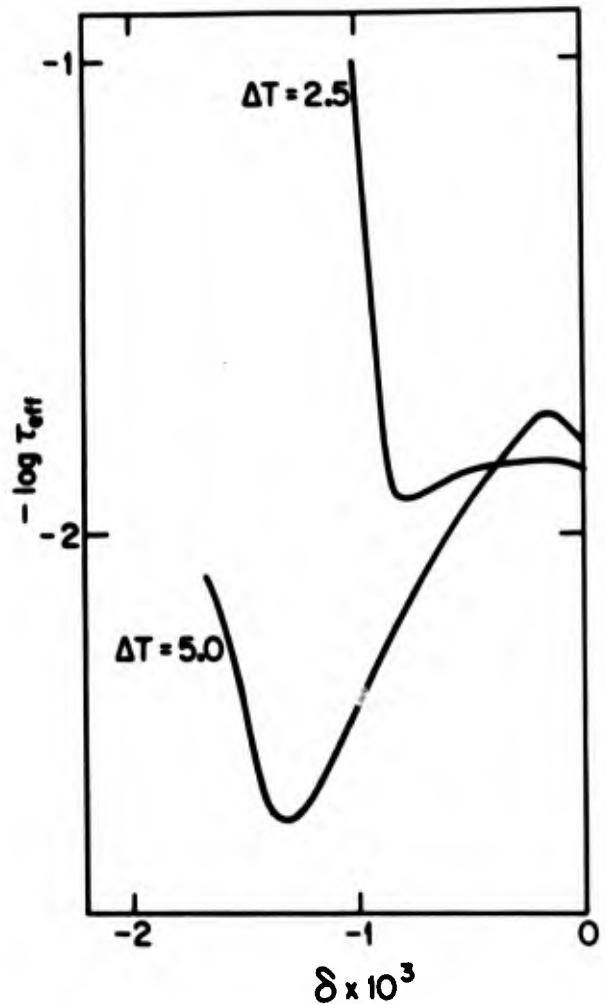


Figure 17:  $\tau_{\text{eff}}$  behavior for the two expansion experiments represented in Figure 16.



lower starting temperature actually approaching equilibrium with relaxation times shorter than those evidenced by the system subjected to the smaller temperature jump.

This behavior is contrary to what is observed experimentally; nevertheless, such behavior is consistent with this model and can be understood quite satisfyingly in terms of the data presented in figure 18. This is a representation of the state of the system in each expansion experiment depicted in figure 16 immediately after the temperature jump back to 300°K. If the system were close to equilibrium before the temperature jump, this representation looks like the distribution function. For the 2.5° temperature jump, one sees the two box distribution function shown as the dashed lined. On the other hand, if the system had not yet attained equilibrium before the application of the temperature increase, irrespective of the annealing time, then the situation changes somewhat. Because of the nature of this theory, the

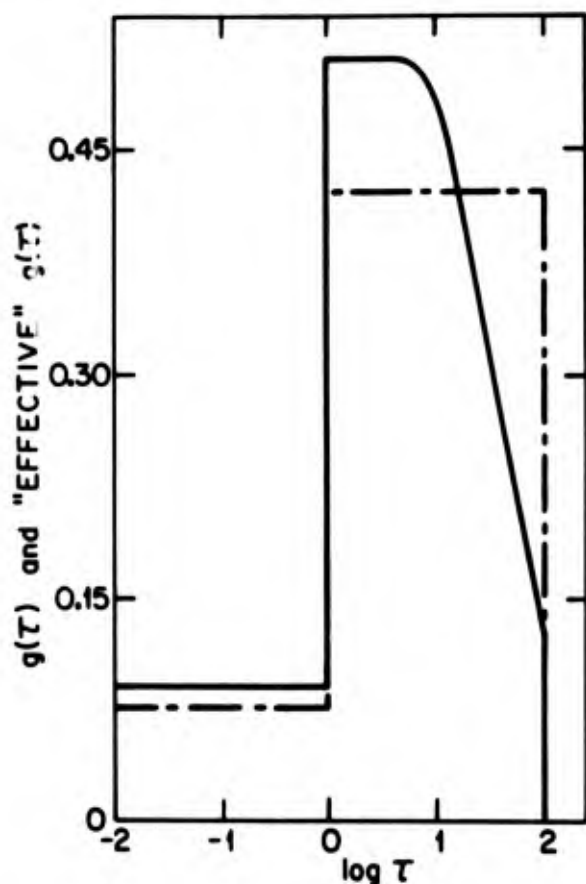


Figure 18: Normalized distribution of departures from equilibrium for the two expansion experiments represented in Figure 16 immediately after heating to 300°K. Solid line is for the experiment in which  $\Delta T = 5^\circ\text{C}$ .

non-attainment of equilibrium is associated primarily with the more slowly relaxing terms in the system. Since the two temperature jumps are of opposite sign in this particular experiment, the net departure from equilibrium at the beginning of the high temperature recovery is partitioned as shown by the solid line in figure 18. In this figure, it is clear that the slowest recovering processes are not strongly represented. In fact, an experiment starting from equilibrium with a distribution function which looked like that depicted by the solid line would give exactly the same  $\tau_{\text{eff}}$  behavior as that calculated for expansion with this more complicated set of experimental conditions. Since the long time portion of the distribution function is somewhat deleted, it makes sense that the effective retardation time behavior would show a more rapid approach to equilibrium.

These calculations show quite conclusively that any non-attainment of equilibrium of this sort will not give well separated  $\tau_{\text{eff}}$  approaches to equilibrium like those observed experimentally; rather, the behavior will be marked by  $\tau_{\text{eff}}$  curves which cross or come close to crossing, a situation markedly different from experimental behavior.

This exercise does suggest a manner in which the particular parameters of the multi-ordering parameter model may be chosen to mimic, at least roughly, Kovacs' result. If one could generate a situation like that depicted in figure 18 where the truncated "effective" distribution function were associated with the smaller temperature jump experiment while the non-truncated distribution function were associated with the larger temperature jump experiment, one would have a situation which would give rise to large discrepancies in approach toward equilibrium of the sort observed experimentally.

To make this point clear, we have carried out one additional calculation, the results of which are shown in figure 19. In order to devise a system which is further from equilibrium when annealed at a higher temperature than at a lower temperature (in spite of the fact that the annealing time is longer at the lower temperature) it is necessary to choose a rather unusual set of parameters. In our case  $\theta = 0.5^\circ\text{K}^{-1}$  and  $x=0.2$ . The small value of  $\theta$  is adopted since one needs a very small change in relaxation time resulting purely from temperature changes. As can be seen in figure 19, with these parameters the desired situation is attained. Since the maximum value of  $\delta$  for the large temperature jump experiment is close to  $-2 \times 10^{-3}$ , it is clear that the sample was about at equilibrium when annealed for  $10^3$  hours. On the other hand, if the smaller temperature jump experiment had reached equilibrium during its annealing time of 10 hours, the maximum value of  $\delta$  for this experiment would have been  $-1 \times 10^{-3}$ . The substantial difference here results from the

non-attainment of equilibrium during annealing for the small temperature jump experiment. It must be remembered virtually all of this non-attainment of equilibrium will manifest itself as a truncation the long retardation time portion of behavior. This fact is seen in the approach to equilibrium depicted in figure 19. Here a major discrepancy of the type observed by Kovacs experimentally is actually seen. Nevertheless, we do not feel that we have shown a situation in which multi-ordering parameter models of the type discussed herein can be used to explain Kovacs' data. It is quite clear from numerous experiments that  $\theta$  is not of the order of  $0.5^\circ\text{K}^{-1}$  but rather much closer to  $1.0^\circ\text{K}^{-1}$ . Without the small value of  $\theta$ , the kinds of  $\tau_{\text{eff}}$  plots shown in figure 19 would not arise using reasonable parameters. What is even more important, is the fact that the directly measured relaxational behavior associated with the annealing of a sample which would be described by these parameters would clearly shown an observant experimenter that the small temperature jump experiment needed more annealing time to reach equilibrium. Thus, it is not at all possible that the behavior we have calculated with this strange set of parameters explains or rationalizes the experimental results.

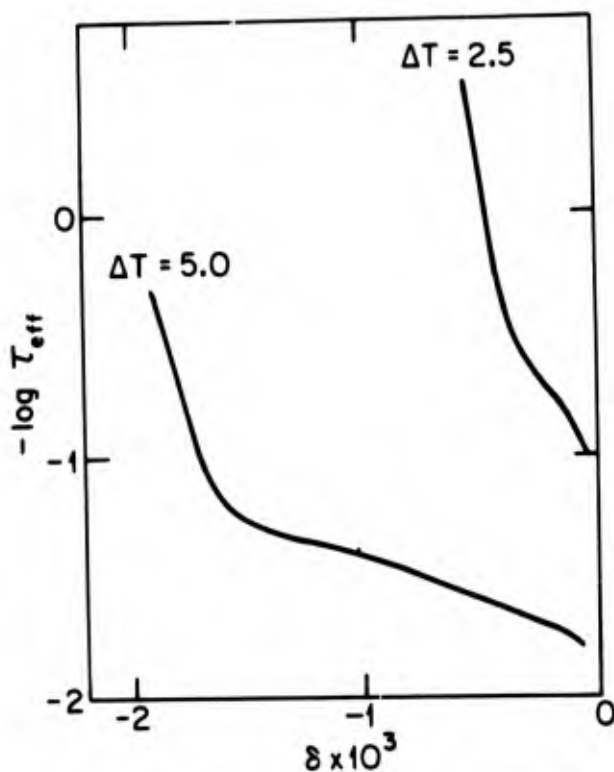


Figure 19:  $\tau_{\text{eff}}$  behavior for two expansion experiments. Conditions are the same as represented in Figure 16 except that  $\theta = 0.5^\circ\text{K}^{-1}$ ,  $x=0.2$  and annealing times were 10 hours at  $297.5^\circ\text{K}$  and  $10^3$  hours at  $295^\circ\text{K}$ .

## Conclusion

After much trial and error experimentation with parameters and distribution functions of current multi-ordering parameter models of glass, we have found a situation where we can mimic the type of unexpected  $\tau_{\text{eff}}$  behavior observed experimentally in simple approach expansion experiments as equilibrium is approached. However, this behavior could only be produced using parameters and assumptions which are not reasonable experimentally. Thus, we are forced to conclude that with any distribution function and with any set of experimental parameters which are reasonably consistent with experiment, multi-ordering parameter models do not give the type of  $\tau_{\text{eff}}$  behavior observed experimentally in simple approach expansion experiments and this is a major shortcoming of the model which has yet to be addressed.

## Acknowledgement

We would like to thank the U.S. Army Research Office for supporting this research on grant DAAG-29-82-K-0212.

## Bibliography

1. J.D. Ferry, *Viscoelastic Properties of Polymers*, 2nd ed., Wiley, New York, 1971.
2. O.S. Narayanaswamy, *J. Am. Ceram. Soc.*, **54**, 291 (1971).
3. (a) A.J. Kovacs, J.M. Hutchinson and J.J. Aklonis, *The Structure of Non-Crystalline Materials*, P.H. Gaskell, Ed., Taylor and Francis, 1977, p. 153.  
(b) A.J. Kovacs, J.J. Aklonis, J.M. Hutchinson and A.R. Ramos, *J. Polymer Sci.*, **17**, 1097 (1979).  
(c) J.J. Aklonis and A.J. Kovacs *Contemporary Topics in Polymer Physics*, Vol. 3, M.C. Shen, Ed., Plenum, 1979, P. 209.
4. C.T. Moynihan, A.J. Eastel and M.A. Debolt, *J. Am. Ceram. Soc.*, **59**, 12 (1976).
5. (a) K.L. Ngai, *Comments Solid State Physics*, **9**, 127 (1979).  
(b) K.L. Ngai, *Comments Solid State Physics*, **9**, 141 (1980).
6. (a) R.E. Robertson, *J. Polym. Sci., Part C*, **63**, 173 (1978).  
(b) R.E. Robertson, *J. Polym. Sci. Polym. Phys. Ed.* **17**, 597 (1979).
7. Ryong-Joon Roe, *J. Appl. Phys.* **48**, 4085 (1977).
8. T.S. Chow and W.M. Prest, *J. Appl. Phys.* **53**(10), 6568 (1982).
9. T.M. Hodge and A.R. Berens, *Macromolecules*, **15**, 762 (1982).
10. J.M. O'Reilly, *J. Appl. Phys.* **50**, 6083 (1979).
11. A.J. Kovacs, *Fortschr. Hochpolym. Forsch. (Adv. Polym. Sci.)*, **3**, 394 (1963).
12. G.P. Lindsey and G.D. Patterson, *J. Chem. Phys.* **73** (7), 3348 (1980).

# THE EFFECTS OF PHYSICAL AGING ON ENTHALPY RELAXATION IN POLYMERS.

## A PHENOMENOLOGICAL APPROACH

Ian M. Hodge  
BFGoodrich R&D Center  
Brecksville, Ohio 44141

### Abstract

Experimental and computer simulation enthalpy relaxation studies of physical aging in glassy polymers are described. The effects on aging of different thermal and nonthermal histories of the glass, such as cooling rate, hydrostatic pressure, vapor absorption and desorption, and tensile stress, are discussed. The effects of the same nonthermal perturbations applied during aging, and of aging time and temperature, are also presented. Information on aging is obtained from the amount of enthalpy lost during aging and how that enthalpy is recovered during heating to above the glass transition region. The rate of aging is increased by histories which raise the excess enthalpy of the glass, reflecting the nonlinearity of the aging kinetics. Hydrostatic pressure, absorbed vapor, and mechanical stress applied during aging slow down the rate of enthalpy loss. Depending on the chemical nature and history of the glass and the aging conditions, enthalpy recovery during heating occurs in temperature ranges centered from well below to just above the glass transition range. Recovery below  $T_g$  is shown to be a manifestation of the memory effects associated with nonexponential decay functions.

### Contents

1. Physical Aging
2. Phenomenology
3. Mathematical Modeling
4. Parameter Optimization and Fitting of Experimental Data
5. Comparison of Calculated and Experimental Results
  - 5.1 Thermal Histories
    - 5.1.1 Poly(vinyl chloride) PVC
    - 5.1.2 Polystyrene PS
    - 5.1.3 Poly(vinyl acetate) PVAc, poly(methyl methacrylate) PMMA, Bisphenol A polycarbonate PCarb
    - 5.1.4 Correlation of Parameters
  - 5.2 Preaging Nonthermal Histories
    - 5.2.1 Hydrostatic Pressure
    - 5.2.2 Mechanical Stress and Vapor Induced Dilatation
  - 5.3 Coaging Nonthermal Histories
6. Summary and Conclusions

## 1. Physical Aging

Glasses usually exist in a non-equilibrium state and relaxation towards equilibrium is commonly referred to as physical aging. Aging affects a large number of properties including but not restricted to density, enthalpy and entropy, creep compliance and modulus, dielectric permittivity and electrical conductivity. The term "physical" aging intimates that the changes in these and other properties occur in the absence of phase changes (e.g. crystallization) or chemical reactions (e.g. photochemical degradation).

Enthalpy is a convenient property to monitor physical aging with because of the availability of accurate and sensitive Differential Scanning Calorimetry (DSC) instruments. Enthalpy lost during aging is recovered during reheating to above  $T_g$ , and this recovery is usually manifested as a maximum in the heat capacity which occurs at temperatures ranging from well below to the upper edge of the glass transition region. An example of enthalpy recovery well below  $T_g$  is found in the pioneering study of PVC by Illiers (1), and recovery near  $T_g$  is exemplified by the early study of PS by Volkenstein and Sharonov (2). A large body of experimental data on the effects of physical aging on enthalpy relaxation in polymers has been published (1-23) and some generalizations can be made:

- (1) The effects of aging are removed on heating the glass above  $T_g$ .
- (2) The temperatures ( $T_e$ ) at which the heat capacity maxima ( $C_{p_{max}}$ ) appear increase approximately linearly with both annealing temperature ( $T_e$ ) and  $\log(\text{annealing time}, t_e)$ , when the aged glass is not too close to equilibrium. There are indications that  $T_{e_{max}}$  increases approximately with  $\log(\text{heating rate}, QH)$  (9), although this is not well established.
- (3) The magnitude of  $C_{p_{max}}$  increases approximately linearly with  $T_e$  and  $\log t_e$ , as does the enthalpy lost during aging,  $\Delta H_e$ , of which  $C_{p_{max}}$  is a crude measure.
- (4) As the aged glass approaches equilibrium deviations from these linear relations are observed until at equilibrium no changes with aging occur. At fixed  $t_e$ ,  $\Delta H_e$  and  $C_{p_{max}}$  pass through a maximum as a function of  $T_e$ , often when  $T_e$  is about 20K below  $T_g$ , and decrease to zero when  $T_e \gg T_g$ . At fixed  $T_e$ ,  $\Delta H_e$  and  $C_{p_{max}}$  become constant at long  $t_e$  as the aged glass approaches equilibrium.

For PVC, additional general features are found:

- (5)  $T_{e_{max}}$  is insensitive to the history of the glass before aging, such as cooling rate

(20), vapor induced swelling (20), hydrostatic pressure during cooling (4,16), and mechanical strain (16,20).

- (6)  $C_{p_{max}}$  and  $\Delta H_e$  are strong functions of history before aging. Histories which elevate the excess enthalpy before aging increase  $\Delta H_e$  and  $C_{p_{max}}$ .

The reproduction of these trends is an essential test of computer simulations of physical aging.

## 2. Phenomenology

The increased rate of aging as temperature approaches  $T_g$ , and the elimination of aging effects after heating to above  $T_g$ , suggest a close connection between aging and the glass transition phenomenon. This is confirmed by the successful application of glass transition phenomenology to physical aging by Kovacs and coworkers (24) and Hodge and Berens (25). In anticipation of this connection, we describe in this section the phenomenology of nonexponential, nonlinear relaxations in the glass transition region.

Glass transition kinetics are nonexponential in the sense that relaxation towards equilibrium is described by a nonexponential decay function  $\phi(t)$ . This is formally equivalent to a distribution of relaxation times  $g(\tau)$ , related to  $\phi(t)$  by

$$\phi(t) = \int_0^{\infty} g(\tau) e^{-t/\tau} d\tau \quad (1)$$

and normalized such that

$$\int_0^{\infty} g(\tau) d\tau = 1 \quad (2)$$

The moments of the distribution,  $\langle \tau^n \rangle$ , are given by

$$\langle \tau^n \rangle = \int_0^{\infty} \tau^n g(\tau) d\tau \quad (\text{for all } n) \quad (3a)$$

$$= \int_0^{\infty} t^{n-1} \phi(t) dt \quad n \geq 1 \quad (3b)$$

$$= (-1)^{|n|} \left. \frac{d^{|n|} \phi(t)}{dt^{|n|}} \right|_{t=0} \quad n \leq -1 \text{ (integer)} \quad (3c)$$

There is abundant experimental evidence for nonexponential relaxation in amorphous media. One consequence of nonexponentiality which has important consequences for physical aging is the memory effect. In essence, this effect describes the observation that relaxation from a particular state depends not only on what the state is, but also on how that state was reached. A classic example of this

in polymer glasses is the volume maximum with respect to time following two temperature steps of opposite sign observed by Kovacs (26). This effect is illustrated in Fig. 1, and it is instructive to analyze it. The thermal history consists of a downward temperature step of  $\Delta T_1$  to temperature  $T_1$  at time  $t_1$  from a starting temperature  $T$  at equilibrium, and an upward step of  $\Delta T_2$  to temperature  $T_2$  at time  $t_2$ .

The time dependence of volume for  $t > t_2$  is

$$V(t) = \Delta V_1 \phi(t-t_1) + \Delta V_2 [1 - \phi(t-t_2)] \quad (4a)$$

$$= \Delta V_1 \phi[(t_2-t_1) + (t-t_2)] + \Delta V_2 [1 - \phi(t-t_2)] \quad (4b)$$

where  $\Delta V_1$  and  $\Delta V_2$  are the changes in equilibrium volume corresponding to the temperature steps  $\Delta T_1$  and  $\Delta T_2$ . If  $\phi(t)$  is exponential and the relaxation times at  $T_1$  and  $T_2$  are  $\tau_1$  and  $\tau_2$ , then

$$V(t) = \Delta V_1 \exp\left[-\frac{(t_2-t_1)}{\tau_1} - \frac{(t-t_2)}{\tau_2}\right] + \Delta V_2 \left\{1 - \exp\left[-\frac{(t-t_2)}{\tau_2}\right]\right\} \quad (5a)$$

$$= \Delta V_2 + \exp\left[-\frac{(t-t_2)}{\tau_2}\right] \left\{\Delta V_1 \exp\left[-\frac{(t_2-t_1)}{\tau_1}\right] - \Delta V_2\right\} \quad (5b)$$

The expression in curly brackets in Eq. (5b) is independent of time so that  $V(t)$  decays exponentially and no maximum in  $V$  is observed. This is not necessarily the case if  $\phi(t)$  is nonexponential. To illustrate this we use a functional form for  $\phi(t)$  which has been found empirically to describe a large number of relaxation phenomena in a wide variety of amorphous material: the fractional exponential or Williams-Watts function (27)

$$\phi(t) = \exp[-(t/\tau_0)^\beta] \quad 1 \geq \beta > 0 \quad (6)$$

For this function the transformation from Eq. 5a to Eq. 5b cannot be made because

$$\left[\frac{t_2-t_1}{\tau_1} + \frac{t-t_2}{\tau_2}\right]^\beta \neq \left(\frac{t_2-t_1}{\tau_1}\right)^\beta + \left(\frac{t-t_2}{\tau_2}\right)^\beta \quad \beta \neq 1 \quad (7)$$

In these cases  $V(t)$  may pass through a maximum for  $t > t_2$ . This is illustrated in Fig. 1 where  $V(t)$  from Eqs. 4 and 6 is plotted for three values of  $\beta$ . The long time tails for smaller values of  $\beta$  seen in Fig. 1 result from longer average relaxation times: Eq. 3b gives for the first moment of the William-Watts function

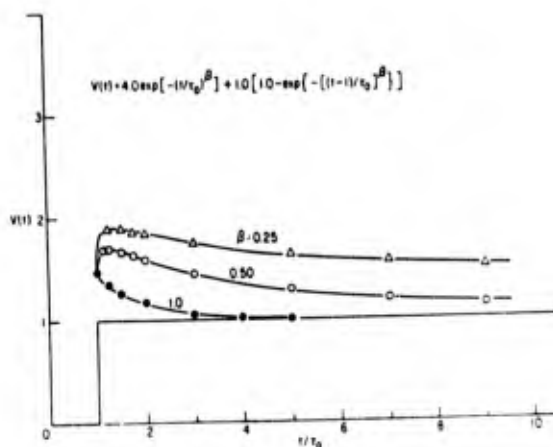


Figure One Calculated time dependences of volume following two temperature steps, for the indicated values of  $\beta$  (Eqs. 4,6).

$$\langle t \rangle = \frac{\tau_0}{\beta} \Gamma\left(\frac{1}{\beta}\right) = \tau_0 \Gamma(1 + 1/\beta) \quad (8)$$

where  $\Gamma$  is the gamma function. Thus  $\langle t \rangle / \tau_0 = 1, 2, 6$  for  $\beta = 1, 0.5, 0.25$  respectively.

In addition to being nonexponential the glass transition phenomenon is also nonlinear, in the sense that the functional form of  $\phi(t)$  changes with the degree of departure from equilibrium. Non-linearity can be conveniently treated by making the average relaxation time a function of "structure" as well as temperature. It is an additional convenience to treat the "structural state" of a system, as measured by a macroscopic property such as enthalpy, in terms of the fictive temperature,  $T_f$ , introduced by Toole (28). The fictive temperature of a system is the temperature at which the observed property would be the equilibrium value (usually obtained by extrapolation). Isothermal relaxation from a non-equilibrium state is then described by the decay of  $T_f$  toward  $T$ . It is worth noting that  $T_f$  measures only the relaxation component of a macroscopic property and that the fictive temperatures assessed from different properties of the same glass may differ. This is illustrated in Fig. 2 where two arbitrary properties are plotted schematically as a function of temperature. The fictive temperature of the glass immediately after cooling,  $T_f'$ , is the same for each property, but because of different relaxation behavior in the transition range  $T_f$  is different for each property at the same fictive temperature within the range. Thus glasses with the same fictive temperature arrived at by different paths may not have the same molecular configuration. The fictive temperature is a phenomenological convenience and is not an accurate measure of molecular structure.

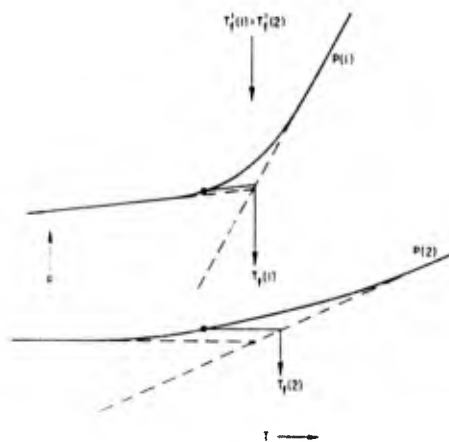


Figure Two Fictive temperature behavior for two arbitrary properties of the same material with the same thermal history.

A commonly used method for handling nonlinearity is that of Narayanaswamy and Gardon (29,30). The relaxation time (e.g.  $\tau_0$  in Eq. 6) is expressed as

$$\tau_0 = A \exp\left[\frac{x\Delta h^*}{RT} + \frac{(1-x)\Delta h^*}{RT_f}\right] \quad (9)$$

where A, x, and  $\Delta h^*$  are constants and R is the ideal gas constant. Note that for small departures from equilibrium,  $T_f \sim T$  and linear kinetics are recovered. The parameter x is a numerical measure of nonlinearity ( $1 \geq x > 0$ ;  $x=1$  for a linear relaxation). The parameter  $\Delta h^*$  determines the rate at which the frozen in fictive temperature,  $T_f'$ , changes with cooling rate QC (31-33):

$$\Delta h^*/R = -\partial \ln(QC) / \partial (1/T_f')_p \quad (10)$$

and is easily obtained from cooling rate data (see below). The preexponential parameter A is determined by  $T_g$  and  $\Delta h^*$ :

$$\ln A \sim -\Delta h^*/RT_g + \ln \tau_0|_{T_g} \quad (11)$$

The most important effect of nonlinearity on aging is that  $\tau_0$  in non-equilibrium glasses is shortened relative to that in the equilibrium state at the same temperature, because  $T_f' > T$ . Thus significant decreases in  $T_f'$  can occur over reasonably short times, i.e. physical aging occurs. Nonlinearity also results in self-retarding relaxation during cooling and isothermal aging, and a self-accelerating return to equilibrium during heating which may increase the heat capacity overshoot above  $T_g$ . Self retardation during aging has been shown by Struik (34) to give an

approximately linear relation between  $\log \tau$  and  $\log t_e$ , for an exponential relaxation.

### 3. Mathematical Modeling

Two basic approaches to modeling non-exponential and non-linear relaxation phenomena near and below the glass transition have been used, both of which rest on earlier work by Toole (28) and Narayanaswamy (29,30). The approach of Kovacs, Aklonis, Hutchinson, and Ramos (24) treats the non-exponential decay function as a sum of exponentials, with relaxation times and weighting factors given by summation versions of Eqs. (1) and (2). The departure from equilibrium is described by differential equations, one for each relaxation time. The resulting coupled, non-linear differential equations are solved for different thermal histories.

Another approach is due to Moynihan and coworkers (35,36). An extension of this approach to thermal histories which include aging has been described by Hodge and Berens (25), and is used here. The method treats cooling and heating as a series of temperature steps and isothermal hold times, and the response of  $T_f$  to each step is described by a decay function  $\phi(t)$ . As a matter of convenience and good accuracy,  $\phi(t)$  is assumed to be of the Williams-Watts form although any other functional form (including a sum of exponentials) could also be used. The Narayanaswamy expression for  $\tau_0$  in terms of T and  $T_f$  (Eq. 9) is used to define a reduced time  $t_r$  which is inserted into the argument of the decay function

$$t_r = \sum \Delta t_i / \tau_{0,i} \quad (12)$$

where i indexes the time intervals. For cooling and heating the time intervals are the isothermal hold times between temperature steps

$$\Delta t_i = \Delta T_i / Q_i \quad (13)$$

where  $\Delta T_i$  is the temperature step and  $Q_i$  is the cooling or heating rate. The total response to cooling and heating is obtained by Boltzman superposition of responses to each temperature step. This is valid when the reduced time is used and the nonlinearity is removed by continual updating of  $\tau_{0,i}$ . The expression for  $T_f$  is

$$T_{f,n} = T_0 + \sum_{j=1}^n \Delta T_j \left\{ 1 - \exp\left[-\left(\sum_{k=j}^n \frac{\Delta T_k}{Q_k \tau_{0,k}}\right)^\beta\right] \right\} \quad (14)$$

$$\tau_{0,k} = A \exp\left[\frac{x\Delta h^*}{RT_k} + \frac{(1-x)\Delta h^*}{RT_{f,k-1}}\right] \quad (15)$$

where  $T_{f,i}^n$  is the fictive temperature after  $n$  temperature steps and  $T_0$  is a starting temperature well above  $T_g$  at which equilibrium exists. For almost all of the calculations reported here constant temperature steps of 1K were used. The conditions under which this is inadequate are discussed later.

The normalized heat capacity  $C_p^N(T)$  is given by  $dT_{f,i}^n/dT$  and is calculated from the expression

$$C_p^N(T) = \frac{T_{f,i}^n - T_{f,i-1}^n}{T_i - T_{i-1}} \quad (16)$$

This is zero in the glassy state and unity in the rubber or liquid state.

Aging is inserted into the cooling cycle and the aging time  $t_e$  is divided into subintervals to allow for changes in  $T_f$  and  $T_0$  (25). For most of the calculations, 5 logarithmically even spaced subintervals per decade of aging time were used. During aging, Eq. (14) is modified by summing only the reduced time and truncating the Boltzman summation since no temperature steps occur during aging. The total thermal history consists of cooling at a constant rate from  $T_0$  to the aging temperature  $T_e$ , staying there for the aging time  $t_e$ , cooling again at the same rate to the minimum temperature (usually 300K) and heating at constant heating rate to well above  $T_g$ . This deviates somewhat from many experiments in which the sample is cooled to room temperature, placed in an annealing oven, cooled to room temperature again, transferred to a DSC instrument and heated. The differences appear to be negligible in most cases, however, since relaxation which occurs during transfer to and from the oven is generally small compared with that which occurs during aging. In any case for quantitative tests of the calculation procedure aging is performed in the DSC instrument, and the experimental thermal history exactly matches the history used in the calculations. The experimental variables which must be known are the cooling and heating rates and the aging time and temperature.

The use of 1K temperature steps for Boltzman integration is adequate when  $C_p^N$  does not exceed ca 2.0. For larger values of  $C_p^N$ , smaller temperature steps are required. In these cases the temperature step is varied according to  $C_p^N$  calculated for the previous step:

$$\Delta T_i = \frac{1}{C_p^N(T_{i-1})} \quad \text{if } C_p^N(T_{i-1}) > 1 \quad (17)$$

$$= 1 \quad \text{if } C_p^N(T_{i-1}) \leq 1$$

For very large values of  $C_p^N$  this procedure may

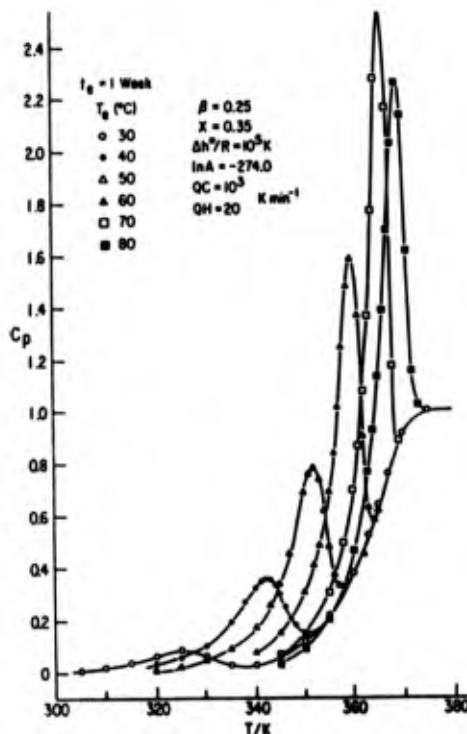


Figure Three Calculated temperature dependences of  $C_p^N$  as a function of aging temperature.

also be inadequate. However, thermal lag effects in DSC instruments would also affect these large heat capacities and quantitative comparison with experiment would therefore be difficult in any case.

It has been shown by Hodge and Berens (25) that the calculation procedure described above reproduces all of the experimental trends listed in Section 1. As an example, we show in Fig. 3 calculated curves of  $C_p^N$  for different values of  $T_e$  at constant  $t_e$ . The experimentally observed increase in peak height ( $C_p^N$ ) and shift to higher peak temperatures ( $T_{max}^N$ ) with  $T_e$  are reproduced. The peak height is calculated to pass through a maximum when  $T \sim T_g - 20$  and then decrease with  $T_e$  (observed experimentally). This maximum occurs because at low  $T_e$  the loss of enthalpy is restricted by long relaxation times, whereas at high  $T_e$  the relaxation time is sufficiently short that equilibrium can be reached ( $T_f = T$ ) and the loss of enthalpy is determined by how much  $T_f$  exceeds  $T$  at the start of aging. This excess decreases as  $T_e$  increases and eventually disappears when  $T_e$  is above  $T_g$ .

One of the more interesting effects of physical aging on enthalpy relaxation is the development of heat capacity peaks well below  $T_g$ , corresponding to enthalpy recovery in the glassy state. The earliest experimental observation of this phenomenon appears to be that of Illers (1) for PVC, and it has since

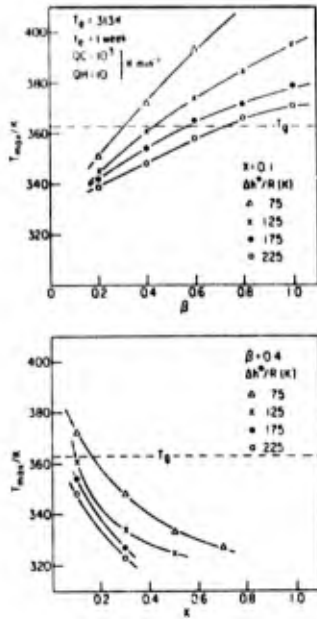


Figure Four Dependences of  $T_{max}^{max}$  on  $\beta$  and  $x$  for the indicated values of  $\Delta h^*$ . Parameter  $A$  varied with  $\Delta h^*$  to keep  $T_g$  fixed at 363K.

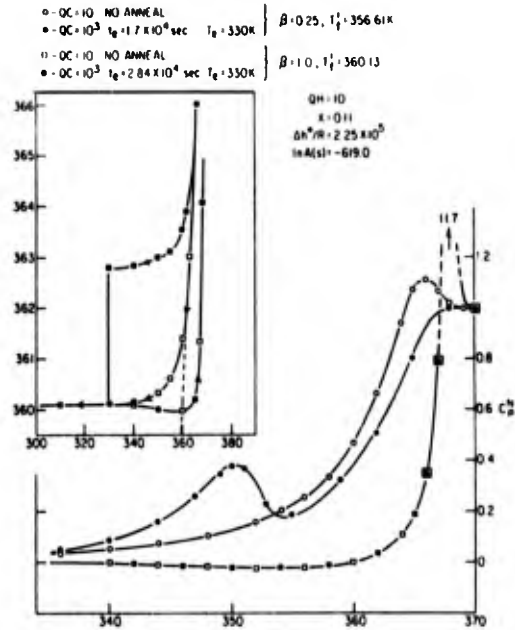


Figure Five Calculated temperature dependencies of  $C_p$  for a slow cooled and fast quenched plus aged glass for  $\beta = 0.25$  and  $1.0$ . Inset: Thermal histories expressed as  $T_f$  vs  $T$ .

been observed by others for PVC (3,5,15,20,37,39,41), PS (4,9,13,17,38,60,43,-44), and PMMA (22,41,42). The first theoretical explanation in terms of the glass transition kinetics was given by Kovacs et al. (24). Here we discuss the phenomenon in terms of the calculation procedure described above. First we establish the combinations of material parameters which produce sub- $T_g$  peaks by calculating the effects of the parameters  $x$  and  $\beta$  for different values of  $\Delta h^*$ . The pre-exponential factor  $A$  is varied with  $\Delta h^*$  to keep  $T_g$  constant. The results are shown in Fig. 4. Low values of  $\beta$  and high values of  $\Delta h^*$  and  $x$  favor peaks below  $T_g$ . For  $\beta=1$  no combination of parameters or thermal histories could be found which produced a sub- $T_g$  peak, suggesting that the memory effect associated with non-exponential decay functions is essential for sub- $T_g$  peak development. This is confirmed by calculated heat capacity scans of two glasses with the same  $T_f'$  arrived at by different paths: a slow cool, and a rapid quench followed by aging. These histories are displayed in Fig. 5 inset in the form of  $T_f$  vs.  $T$  plots. The corresponding heat capacity curves are shown in Fig. 5 for  $\beta = 0.25$  and  $1.0$ . For  $\beta=1$  the two histories produce identical curves, corresponding to the absence of any memory effect for an exponential decay function. For  $\beta=0.25$  the slowly cooled glass exhibits an overshoot above  $T_g$  and the aged glass a sub- $T_g$  peak. The sub- $T_g$  peak is analogous to the volume maximum following two temperature steps, observed by Kovacs (51) and discussed above, because cooling, aging, and

heating are qualitatively similar to two temperature steps separated by a waiting time (the times for cooling and heating are short compared with the aging time). In both cases the glass "remembers" the aging time or time between temperature steps when  $\beta \neq 1$ .

The lowering of  $T_{max}^{max}$  with increasing  $\Delta h^*$  and  $x$  also occurs for shorter aging times and lower aging temperatures. These variations in parameters and aging conditions correspond to the effective aging time,  $t_e/\tau$ , being shortened. This is demonstrated by combining Eq. (9) and (11) to give

$$\ln \tau_o = \frac{-\Delta h^*}{RT_g} + \frac{x\Delta h^*}{RT_e} + \frac{(1-x)\Delta h^*}{RT_f'} \quad (18)$$

where  $\tau_o$  ( $T_g$ ) has been put equal to 1 sec and the dependence of  $\tau$  on  $t$  has been neglected for simplicity. Since  $T_f' \approx T_g$ ,

$$\ln \tau_o \sim \frac{x\Delta h^*}{R} \left( \frac{1}{T_e} - \frac{1}{T_g} \right) \quad (19)$$

from which it is clear that increasing  $x$  and  $\Delta h^*$  and decreasing  $T_e$  all lengthen  $\tau$  and thus shorten the effective aging time  $t_e/\tau_o$ .

We conclude this section with a curious result associated with the effects of  $\Delta h^*$ . For linear relaxations in which the relaxation time is an Arrhenius function of temperature, and the functional form of the decay function is independent of temperature, the variable  $\ln \tau$  ( $\ln w$  in the frequency domain) is equivalent to  $\Delta h^*/RT$ . The temperature range of a



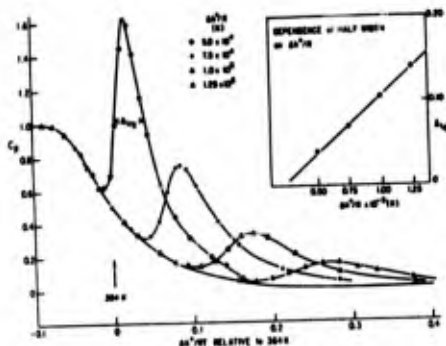


Figure Six Effect of  $\Delta h^*$  on aging peaks.  $QC = 10^3$ ,  $QH = 20$ ,  $t_e = 1$  week,  $T_e = 313K$ ,  $\beta = 0.25$ ,  $x = 0.35$ .

relaxation is therefore a function of  $\Delta h^*$  and it is of interest to see if such scaling occurs for nonlinear relaxations. Calculated  $C_p$  curves for different values of  $\Delta h^*$  (from ref. 25) are plotted as a function of  $\Delta h^*/RT$  in Fig. 6. The glass transition "background" is independent of  $\Delta h^*$  when plotted in this way but the aging peaks are not: their width at half height is a linear function of  $\Delta h^*$  (Fig. 6 inset). The linear relation is not understood, but the general phenomenon appears to be analogous to the superposition of volume maxima on a smoothly decaying background for different aging treatments [Kovacs (51)].

#### 4. Parameter Optimization and Fitting Experimental Data

Before comparing calculated and experimental results it is necessary to normalize the experimental data. The normalized heat capacity  $C_p^N(T)$  is given by

$$C_p^N(T) = \frac{C_p(T) - C_{pg}(T)}{C_{p1}(T) - C_{pg}(T)} \quad (20)$$

where  $C_p$ ,  $C_{p1}$ , and  $C_{pg}$  are the measured liquid and glassy heat capacities respectively. Linear extrapolations of  $C_{pg}$  and  $C_{p1}$  are made into the transition range, and it is important that the heat capacity be measured far outside the transition region to accurately assess the temperature dependences of  $C_{pg}$  and  $C_{p1}$ .

The fictive temperature immediately before heating,  $T_f'$ , is obtained by integrating  $C_p^N(T)$ , measured during heating, from well below to far above the transition range. The fictive temperature of the glass is obtained from the temperature axis intersection of the extrapolated high temperature integral (a straight line with unity slope). For this analysis it is desirable to keep the heating rate constant so that calibration of the DSC instrument is needed for only one heating rate. The experimental  $C_p^N(T)$  data are evalu-

ated every 1K and a computer file containing  $C_p^N$  over a 100K temperature range is created. For calculations using dynamically varying temperature steps (Eq. 17), which produce data at non-integer temperatures, values of  $C_p^N$  at integral temperatures are obtained by linear interpolation.

The Marquardt optimization procedure (45) was used by Hodge (22) and Hodge and Huvard (21) to obtain the best fit model parameters ( $A$ ,  $\Delta h^*$ ,  $x$ ,  $\beta$ ) from experimental data. The FORTRAN program for the Marquardt procedure was a modified version of that given by Kuester and Mize (46) and worked well in this application. The objective function  $\psi$  was

$$\psi = \sum_T [C_p^N(T) - \hat{C}_p^N(T)]^2$$

where  $C_p^N$  and  $\hat{C}_p^N$  are the experimental and calculated values of  $C_p^N(T)$ . This objective function has the advantage of placing the least weight on the smallest values of  $C_p^N$ , which have the greatest uncertainties because of uncertainties in  $C_{pg}$ . The initial trial values of  $x$  and  $\beta$  were 0.5 and the initial value of  $A$  was calculated from Eq. 11 with  $\ln \tau = 1.0$  at  $T_g$ . The best fit values of  $x$  and  $\beta$  were constrained to lie between 0.001 and 1.0 and  $\ln A$  was restricted to  $\pm 15$  of the initial estimate. The values of  $QC$ ,  $T_e$ ,  $t_e$ ,  $QH$ ,  $T_g$  (defined for convenience as the temperature at which  $C_p^N=0.5$ ), and  $\Delta h^*$  were input. The output consisted of best fit values for  $x$ ,  $\beta$ ,  $A$ , and  $\psi$ . The value of  $\Delta h^*$  was obtained either from the cooling rate dependence of  $T_f'$  (Eq. 10), or from the minimum in  $\psi$  as a function of input  $\Delta h^*$ . In all cases for which comparisons could be made, the two evaluations of  $\Delta h^*$  were in reasonable agreement ( $\pm 20\%$ ). In one case, discussed below, agreement was within 5%.

For PVC  $\psi$  is determined more by the glass transition data than the sub- $T_g$  peaks, and the optimization failed because the glass transition for PVC is broad and not easily reproduced. In this case,  $x$  and  $\beta$  were obtained by matching  $C_p^N$  and  $T_{max}$  of the sub- $T_g$  peaks for several aging times at a single aging temperature (see 5.1.1 for details).

#### 5. Comparison of Calculated and Experimental Results

##### 5.1 Thermal Histories

5.1.1 Poly(vinyl chloride) PVC. The value of  $\Delta h^*$  for PVC obtained from the cooling rate dependence of  $T_f'$  (Eq. 10) is 450 kcal mole<sup>-1</sup> (25). The  $T_g$  of ca 363K ( $C_p=0.5$ ,  $QC=40$ ,  $QH=10$ ) gives  $\ln A(\text{sec}) = -619.0$ . For the aging studies, very rapid quenching was needed to accelerate the development of sub- $T_g$

TABLE I

## Fit to Aging Data for PVC

( $\Delta h^* = 450 \text{ kcal mole}^{-1}$ ,  $\ln(A, \text{sec}) = -619.0$ ,  
 $x = 0.11$ ,  $\beta = 0.25$ ,  $QC = 2 \times 10^4 \text{ K min}^{-1}$ ,  
 $QH = 20 \text{ K min}^{-1}$ )

$T_e, ^\circ\text{C}$	$t_e, \text{hr}$	$C_p^N$		$T_{\text{max}}$	
		obsd	calcd	obsd	calcd
20	7	0.13	0.08	324	323
	27	0.14	0.12	328	327
	150	0.21	0.21	332	333
40	6	0.16	0.19	336	337
	24	0.33	0.31	341	341
	50	0.40	0.40	343	343
60	1	0.21	0.37	351	350
	7	0.66	0.76	357	355
	24	1.10	1.20	359	357
	50	1.60	1.60	360	359

peaks. This was achieved by pouring PVC powder (containing agglomerates of ca  $1 \mu\text{m}$  diameter particles) at ca  $120^\circ\text{C}$  into liquid nitrogen. Boiling of the nitrogen stopped after about 2 sec. Assuming Newtonian cooling (exponential decrease in temperature from ca  $400\text{K}$  to  $77\text{K}$  in 2 sec), a cooling rate through  $T_g$  of  $2 \times 10^4 \text{ K min}^{-1}$  was estimated. Aging at  $40^\circ\text{C}$  was analyzed to obtain values of  $x$  and  $\beta$  which gave the best overall fit to  $C_p^N$  and  $T_{\text{max}}$  for aging times of 6, 24, and 50 hours. The best fits were obtained with  $x=0.11$ ,  $\beta=0.25$ . Interestingly, the value of  $\beta$  is the same as that obtained from dielectric data (47). Although it is not expected that dielectric and enthalpy relaxation parameters would be exactly the same, the unusually small values of  $\beta$  for both properties lends credence to the enthalpy relaxation analysis. The best fit parameters and a comparison of experimental and calculated values of  $C_p^N$  and  $T_{\text{max}}$  for several aging times at three aging temperatures are summarized in Table I. The agreement is within experimental uncertainty, and it is shown below that the parameters in Table I also give a good account of the effects of non-thermal histories on aging at room temperature.

The value of  $\Delta h^*$  for PVC is very high, about four times larger than typical carbon-carbon bond energies. This suggests that at least five chain segments are involved in a relaxation event. The high value of  $\Delta h^*$  and small value of  $\beta$  contribute to the low  $T_{\text{max}}$  and well developed sub- $T_g$  peaks (Fig. 4). The small value of  $x$  would increase  $T_{\text{max}}$  but this is evidently outweighed by the opposite effects of  $\beta$  and  $\Delta h^*$ .

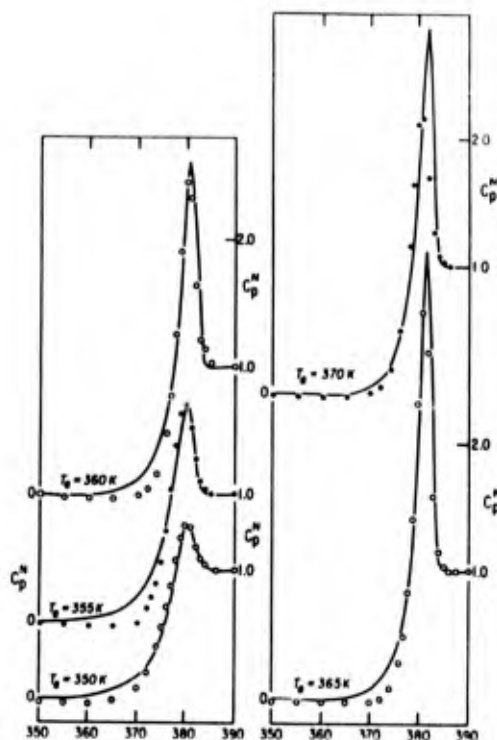


Figure Seven Comparison of experimental (points) and calculated (lines) data for a polydisperse polystyrene (ref 21), after aging for one hour at the indicated temperatures.

**5.1.2 Polystyrene (PS).** The value of  $\Delta h^*$  for a polydisperse polystyrene ( $M_w/M_n = 3.8$ ) obtained from the cooling rate dependence of  $T_g'$  is  $157 \text{ kcal mole}^{-1}$  (21). Analysis of a single thermal history with no aging gave a best fit value of  $165 \text{ kcal mole}^{-1}$  (21), in excellent agreement with the experimental value. Other parameters obtained from analysis of the same thermal history were  $\ln A(\text{sec}) = -216.6$ ,  $x=0.63$ ,  $\beta=0.68$ . These parameters accurately predict the response of  $C_p$  to other thermal histories, including those with aging, indicating that the glass transition kinetics determine the kinetics of physical aging down to about  $30\text{K}$  below  $T_g$  (the lowest aging temperature studied). A comparison of experimental and calculated  $C_p$  is given in Fig. 7. One hour anneals at temperatures down to ca  $30\text{K}$  below  $T_g$  did not produce sub- $T_g$  heat capacity maxima, in contrast to PVC which exhibited a well developed sub- $T_g$  peak when aged 1 hour about  $30\text{K}$  below  $T_g$  (see Table I).

Analysis of data obtained by Prest (48) for a monodisperse polystyrene, also for aging temperatures down to ca  $30\text{K}$  below  $T_g$ , produced a set of parameters similar to that obtained for the polydisperse material (50). However, analysis of data published by Chen and Wang (17) for another monodisperse polystyrene produced parameters which are more like those

TABLE II

## Enthalpy Relaxation Parameters

Material	lnA(sec) ±1	Δh*	x ±0.05	β	Reference
		(kcal mole <sup>-1</sup> ) ±10%		±0.05	
PVAc	-275.4	175	0.28	0.53	22
PVAc	-223.6	142.6	0.41	0.51	49
PVC	-619.0	450	0.11	0.25	25
PS	-216.4	165	0.43	0.68	21
PS	-457.0	350	0.12	0.39	21
PMMA	-355.7	275 (±20%)	0.22 (±0.1)	0.37 (±0.1)	22
PCarb	-353.6	300	0.22	0.54	22
As <sub>2</sub> Se <sub>3</sub>	-85.5	81.8	0.49	0.67	36
B <sub>2</sub> O <sub>3</sub>	-75.6	90	0.40	0.65	35
5P4E	-153.1	77	0.40	0.70	36

for PVC than for the two PS materials just discussed ( $\Delta h^*=350$  kcal mole<sup>-1</sup>,  $\ln A(\text{sec}) = -457.1$ ,  $x=0.12$ ,  $\beta=0.39$ ). Although this set of parameters is less reliable because data for only two thermal histories could be analyzed, no single set of parameters could be found which reproduced data for all materials. The parameters for the polydisperse material did not produce the sub-T<sub>g</sub> shoulder reported by Chen and Wang under any of several aging conditions which equaled or approximated the experimental conditions. Similarly, the parameters for the monodisperse material did not reproduce the annealing data for the polydisperse material.

The large difference in parameter values for the different polystyrenes is not well understood. However, the low aging temperature for the Chen and Wang experiments (about 60K below T<sub>g</sub>) compared with the other experiments (less than 30K below T<sub>g</sub>) suggests that the glass transition kinetics give a poor description of aging far below T<sub>g</sub>. This is confirmed by analysis of non-thermal histories for PS which involve perturbations at or near room temperature (see §5.2.2 below), which indicate that the Chen and Wang parameters are needed to give a satisfactory account of the data. This contrasts with PVC, for which a single set of parameters gives a good description of aging from T<sub>g</sub> down to room temperature. If this difference between PS and PVC with regard to their low temperature aging behavior is real, it is speculated that it reflects the difference in secondary relaxation temperatures (high for PS, low for PVC).

5.1.3 Poly(vinyl acetate) PVAc, Poly-(methylmethacrylate) PMMA, Bisphenol A polycarbonate PCarb. Poly(vinyl acetate) has been studied by Sasabe and Moynihan (49) for thermal histories with no aging, and by Hodge (22) for histories with and without aging. There is good agreement between the two sets of parameters (see Table II), and in both cases agreement between experimental and calculated results is comparable with that found for polystyrene (Fig. 7). Polycarbonate was studied by Hodge (22) who again obtained agreement between calculated and experimental data comparable with that found for PS. For PMMA Hodge (22) obtained significantly poorer agreement between observed and calculated data. The parameters for PCarb and PMMA are included in Table II. For all three materials aging temperatures lay between T<sub>g</sub> and ca T<sub>g</sub>-30K. Thus the possibility exists that, as for PS, different parameters would be obtained from analysis of low temperature aging data.

5.1.4 Correlation of Parameters. A summary of the best fit parameters for materials to which the Moynihan formalism has been applied is given in Table II. An inspection of this table reveals strong correlations between all four parameters, which are displayed in Fig. 8. These correlations are robust with respect to uncertainties in the parameters, as illustrated by the "best fit" parameters for PVAc obtained for values of  $\Delta h^*$  differing by ±15% from the experimental value (Fig. 8). These parameter values move along the correlation lines, so closely in fact that it raises the possibility that the correlations may be generated by the parameter uncertainties. However, the full range of parameters is far greater than the uncertainties and the correlations cannot be eliminated by forcing the parameters to their extreme values. Accordingly the correlations will be accepted as fact for the purpose of discussion.

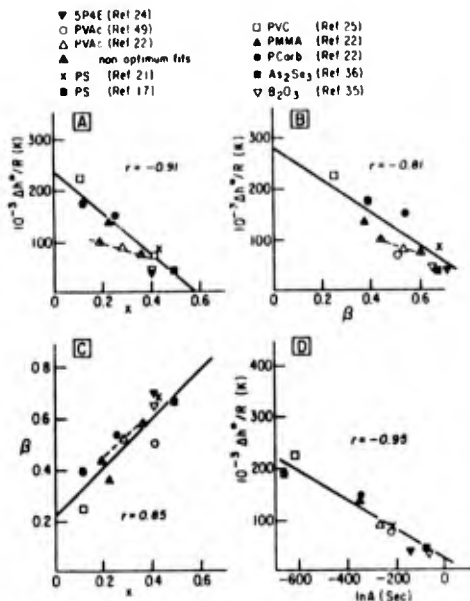


**Figure Eight** Correlations between best fit parameters for the indicated polymers and inorganic glasses. Nonoptimum parameters for PVAc indicate correlations between parameter uncertainties.

The correlation between  $A$  and  $\Delta h^*$  reflects the small range in  $T_g$  of the materials listed in Table II. We offer no molecular interpretation of this correlation since it is difficult to attach physical significance to values of  $A$  which can be as small as  $10^{-270}$  sec (!!!). The other correlations are consistent with commonly held views on the cooperative nature of the glass transition. To make the discussion concrete, we interpret  $\beta$  as a measure of the number of segments which can move statistically independent of adjacent segments (smaller values of  $\beta$  correspond to a larger number of segments). It is speculated that this number corresponds to a correlation length for some form of fluctuation. The involvement of many chain segments is expected to give a large activation energy, thus accounting for the inverse correlation between  $\beta$  and  $\Delta h^*$ . As noted above for PVC, the large activation energies for most polymers exceed C-C bond energies and therefore also demand the involvement of several chain segments. Relaxation events in which a larger number of chain segments participate might also be expected to be more affected by the molecular environment (i.e. "structure"). To the extent that the parameter  $x$  reflects the importance of molecular structure, relative to temperature, in determining the average relaxation time an inverse correlation between  $x$  and the number of chain segments per relaxation event might also be expected. This could account for the correlations between  $x$ ,  $\beta$  and  $\Delta h^*$ . These speculated relations between the number

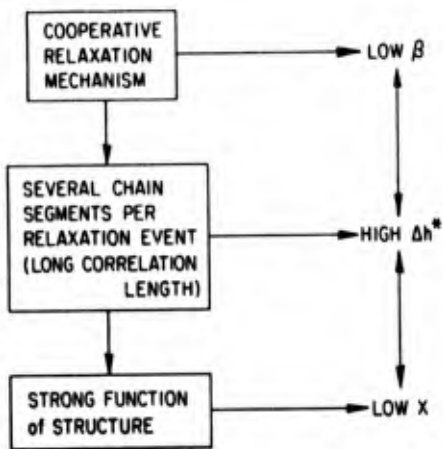


**Figure Nine** Schematic of speculated relations between model parameters and number of chain segments per relaxation event.

of chain segments per relaxation event and the parameters  $\beta$ ,  $\Delta h^*$ , and  $x$  are summarized in Fig. 9. Many more data on many more materials are needed to establish the generality of these correlations.

## 5.2 Preaging Non-Thermal Histories

Several studies of the effects of non-thermal perturbations on physical aging have been reported. We restrict ourselves here to the effects of hydrostatic pressure, mechanical stress, and vapor absorption. In this section we discuss the effects of perturbations which are removed before aging; studies in which the perturbations are maintained during aging are considered in section 5.3.

### 5.2.1 Hydrostatic Pressure.

We discuss two experimental investigations, of PVC (16,39) and PS (4). In both studies pressure was applied above  $T_g$ , maintained during cooling to the glassy state, and released before aging and reheating. The experimental heat capacity data of Prest and coworkers (16) for PVC, obtained after aging for 110 days at room temperature and atmospheric pressure, are shown in normalized form in Fig. 10a. The glass transition moves to slightly higher temperatures with pressure and the sub- $T_g$  peak becomes sharper and more asymmetric and moves to somewhat lower temperatures. Weitz and Wunderlich (4) studied the effects of hydrostatic pressure applied during cooling on enthalpy relaxation in PS, PMMA and the non-polymeric glasses phenolphthalein, sucrose, and  $KNO_3/Ca(NO_3)_2$ . Their normalized experimental data for PS are shown in Fig. 11a. Each sample was cooled at  $0.083K\ min^{-1}$  under various pressures, transferred to the DSC instrument, and heated at  $5K\ min^{-1}$  at atmospheric pressure. In some cases samples were

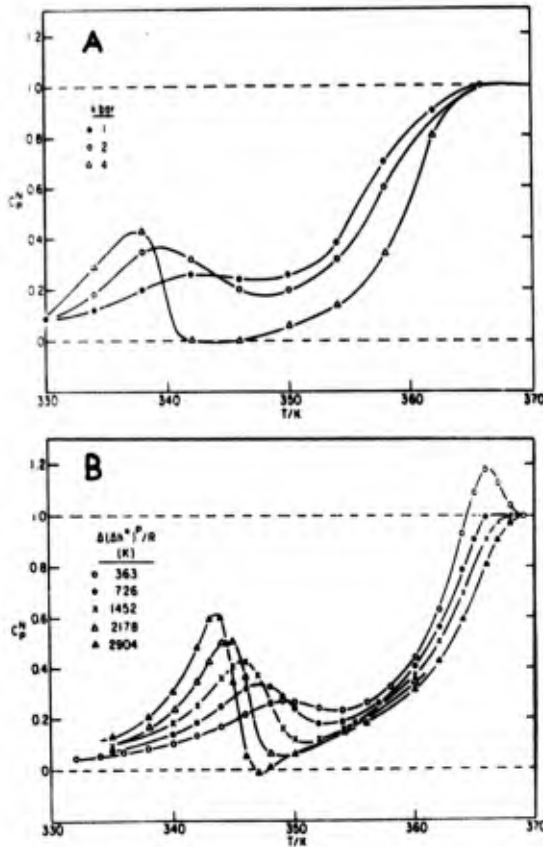


Figure Ten  $C_p^N$  data obtained at atmospheric pressure for PVC formed by cooling under the indicated hydrostatic pressures, and aged for 110 days at room temperature. (A) Experimental data after Prest and Roberts (16). (B) Calculated data using the calculation procedure  $\Delta P \sim \Delta(\Delta h^*)^P$  (see text).

stored at  $-10^\circ\text{C}$  for an unspecified time (presumably days or more) before scanning. Physical aging was not deliberately investigated in this study, but probably occurred during transfer of the sample to the DSC instrument and/or during storage at  $-10^\circ\text{C}$ . For calculation purposes these conditions were assumed to correspond to aging at 300K for 1 second.

Hydrostatic pressure  $P$  can be introduced into the calculation procedure in three equivalent ways. All start from the observation that  $P$  increases  $T_g$  by lengthening the average relaxation time, and all assume the parameters  $x$  and  $\beta$  to be independent of pressure. In the first method, the fictive temperature is decreased so that  $T_f < T$  at equilibrium when  $P > 0$ . In the second method the preexponential parameter  $A$  is increased with  $P$ . Equivalent changes ( $\Delta$ ) in  $T_f$  and  $\ln A$  are related by

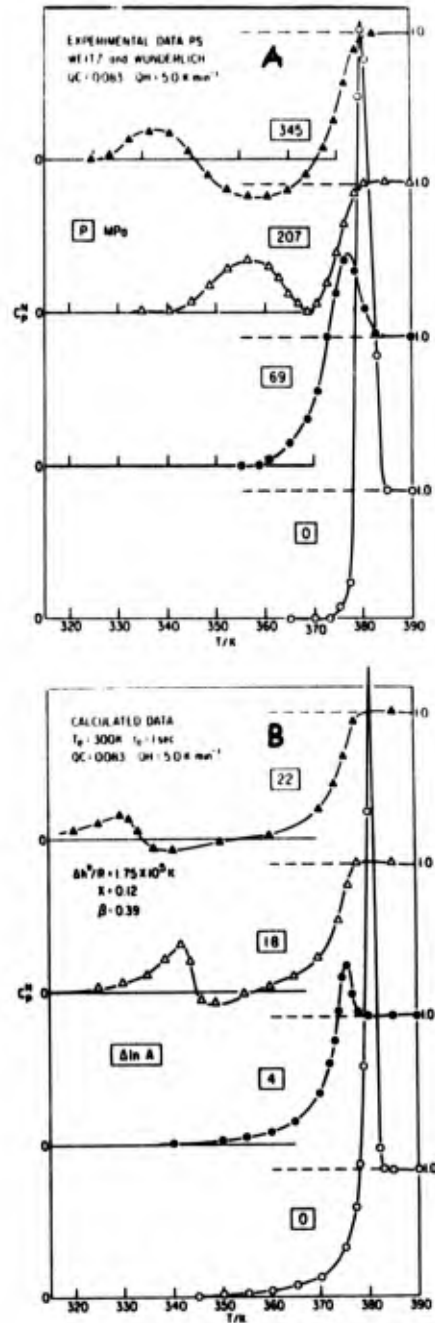


Figure Eleven  $C_p^N$  data obtained at atmospheric pressure for PS formed by cooling under hydrostatic pressure. (A) Experimental data after Weitz and Wunderlich (4). (B) Calculated data after aging 1 second at 300K, using calculation procedure  $\Delta P \sim \Delta \ln A^P$  (see text).

$$\Delta \ln A^P \sim \frac{(1-x)\Delta h^*}{RT_g^2} \Delta T_f^P \quad (21)$$

where the superscript  $P$  indicates changes due to pressure. Third, the activation energy is increased with pressure. Equivalent changes in  $\Delta \ln A^P$  and  $\Delta(\Delta h^*)^P$  are given by

$$\Delta \ln A^P \sim \frac{\Delta(\Delta h^*)^P}{RTg} \quad (22)$$

An approximate relation between  $\Delta T_f^P$  and  $\Delta P$  is readily derived. First,

$$\Delta \left( \frac{\partial H}{\partial P} \right)_T \sim -TV\Delta\alpha \quad (23)$$

where  $\alpha$  is the thermal expansion coefficient and  $\Delta$  now refers to changes at the glass transition. Inserting the relation  $\Delta(dH) = \Delta C_p dT$  into (22), and noting that

$$dT_f \sim \left( \frac{x}{1-x} \right) dT \quad (24)$$

gives

$$\frac{dT_f}{dP} \sim \frac{\Delta T_f^P}{\Delta P} \sim - \left( \frac{x}{1-x} \right) \frac{TV\Delta\alpha}{\Delta C_p} \quad (25)$$

In order to provide a reasonable test of the calculation procedure it is necessary to evaluate  $\Delta T_f^P/\Delta P$ . For PVC  $\Delta C_p \sim 0.07$  cal gm<sup>-1</sup>K<sup>-1</sup>,  $\Delta\alpha \sim 2 \times 10^{-4}$  K<sup>-1</sup>,  $V = 0.7$  gm cm<sup>-3</sup>,  $T_g = 363$ K,  $x = 0.11$ . Inserting these values into Eq. (25) gives

$$\Delta T_f^P/\Delta P \sim 2K \text{ kbar}^{-1} \quad (26)$$

The experimental pressure range (0-6 kbar) thus corresponds to  $\Delta T_f^P \sim 0-12$ K. Eq. (21) gives  $\Delta \ln A^P \sim 0-12$  for the same range, and  $\Delta(\Delta h^*) \sim 0-8.7$  kcal mole<sup>-1</sup>. Calculated normalized heat capacities are shown in Fig. 10b for  $\Delta(\Delta h^*)^P$ ; the parameters are those obtained from analysis of purely thermal histories for another PVC (Table II). The calculated curves using  $\Delta T_f^P$  and  $\Delta \ln A^P$  are very similar to those shown in Fig. 10b. Although only qualitative reproduction of experimental trends was aimed for in these calculations, the agreement is quantitatively very good.

To reproduce the PS data it was necessary to use the parameters obtained from the 320K annealing data of Chen and Wang (17) (see Table II). Insertion of the appropriate quantities onto Eq. (25) gave  $\Delta T_f^P/\Delta P \sim 2K \text{ kbar}^{-1} \sim 2 \times 10^{-2} K \text{ MPa}^{-1}$ . Eqs. (21)<sup>f</sup> and (22) give values of 1.1 kbar<sup>-1</sup> for  $\Delta \ln A^P$  and 0.82 kcal mole<sup>-1</sup> kbar<sup>-1</sup> for  $\Delta(\Delta h^*)^P$ . As for PVC, calculations using  $\Delta T_f^P$ ,  $\Delta \ln A^P$ , and  $\Delta(\Delta h^*)^P$  gave comparable results. Calculated results using  $\Delta \ln A^P$  are shown in Fig. 11b. The experimental trends are qualitatively reproduced, namely a decrease in overshoot at low pressures, the development of a sub-T<sub>g</sub> peak at intermediate pressures, and the development of an exothermic minimum between  $T_{max}^e$  and  $T_g$  at the highest pressures. Similar trends were observed experimentally by Yourtee and Cooper (40) and by Dale and Rogers (43). In view of uncertainties in the experimental aging

history and in the parameters for PS, the overall good agreement between calculated and experimental curves is regarded as indicating the essential correctness of the calculation procedure. The calculations indicate that significant room temperature/atmospheric pressure aging occurs in seconds for glasses prepared under high hydrostatic pressure, because of the small values of  $\tau_0$  following pressure release. The sub-T<sub>g</sub> peaks observed experimentally for PS are evidently physical aging peaks with the aging occurring during sample transfer from the pressure cell to the DSC instrument.

Data for nonpolymeric glasses exhibit a simple reduction in overshoot with pressure with no sub-T<sub>g</sub> peaks occurring, according to Weitz and Wunderlich (4). Insertion of parameters typical of nonpolymeric glasses (e.g. those for 5P4E listed in Table II) produced similar results - no sub-T<sub>g</sub> peaks were calculated to occur.

An interesting feature of the calculations for both PVC and PS is that shortened relaxation times in the glassy state are produced only after pressure release; the relaxation time before pressure release is longer than that for the atmospheric pressure vitrified glass. This implies that aging under pressure would be slow, which is observed experimentally (see 5.3).

**5.2.2 Mechanical Stress and Vapor Induced Dilation.** The effects of mechanical stress of various kinds (cold drawing, powder compaction) on physical aging and enthalpy relaxation in polymers have been observed by several investigators. The general effect is to accelerate aging. Several types of vapor and liquid adsorption and desorption treatments also hasten physical aging (14,20). The discussion here is restricted to data obtained by Berens and Hodge (20) for PVC, which are representative.

The influence of mechanical stress on aging is typified by data for PVC film which was slowly cooled (about 40K min<sup>-1</sup>) and then cold drawn beyond the yield point (to about 100% elongation). Samples were aged at 40°C for up to 140 hours. Sub-T<sub>g</sub> heat capacity peaks developed faster than in liquid nitrogen quenched PVC powder (estimated cooling rate 2x10<sup>4</sup>K min<sup>-1</sup>, see ref. 20 for details). These data are included in Fig. 12 as plots of  $C_p$  and  $T_{max}^e$  vs log t. The effects of swelling by absorbed penetrant are represented by aging data for PVC powder which was cooled at about 40K min<sup>-1</sup>, swollen by absorption of methyl chloride to a concentration sufficient to depress T<sub>g</sub> below room temperature, and vitrified by rapid desorption of the penetrant (in a few seconds, see ref. 20 for details). The rate of sub-T<sub>g</sub> peak development in this material, after aging at 40°C, was comparable with that observed for the liquid nitrogen

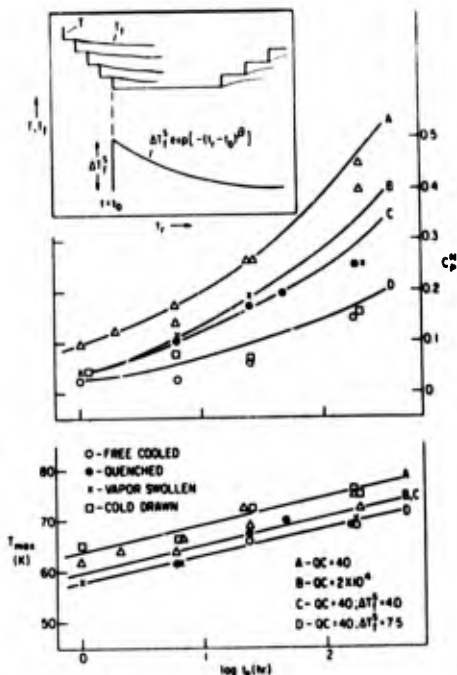


Figure Twelve Experimental  $N$  (points) and calculated (lines) values of  $C_p^{\max}$  and  $T^{\max}$  vs  $\log t_r$ , for PVC with the indicated preaging perturbations. Experimental data after Berens and Hodge (20). Inset: Schematic of calculation procedure.

quenched powder. These data are also displayed in Fig. 12.

Mechanical stress and vapor induced dilation are introduced into the calculation procedure in the same way. An instantaneous increase in  $T_f^S$ ,  $\Delta T_f^S$ , is assumed to occur as a result of the treatment, which decays with aging time and reheating according to

$$\Delta T_f^S(t_r) = \Delta T_f^S \exp[-t_r^\beta] \quad (27)$$

where  $t_r$  is the reduced time given by Eq. (12). This is superimposed on the response to the thermal history, Eqs. (14), (15). The two responses are coupled by their common dependence of  $\tau_0$  on  $T_f^S$ . It is assumed that the model parameters  $f$  are unaffected by cold drawing or swelling. The calculation procedure is displayed schematically in Fig. 12 inset.

A comparison of calculated and experimental data requires that  $\Delta T_f^S$  be evaluated. Its value was obtained by matching the calculated and smoothed experimental values of  $C_p^{\max}$  for an aging time of 24 hours at 40°C. The calculations are tested by comparing predictions of  $C_p^{\max}$  for other aging times, and  $T^{\max}$  for all times, with experiment. The calculated curves are shown as the solid lines in Fig. 12, and are in good overall agreement with experiment. In particular the experimen-

TABLE III

Effects of Hydrostatic Pressure Applied During Aging of PVC

Hydrostatic Pressure (MPa)	$\Delta T_f^S$	$C_p^{\max}$		$T^{\max}$	
		obsd	calcd	obsd	calcd
0	0	0.14	0.18	341	345
47	-2	0.07	0.11	333	332
94	-4	0.04	0.04	320	321

tal result that the vapor swollen and liquid nitrogen quenched powders age almost identically is reproduced. This is in apparent disagreement with the memory effects associated with a nonexponential decay function. However, the important concept in the memory effect is the reduced time taken to reach the starting value relative to the reduced evolution time. In both the liquid nitrogen quenched and vapor diluted glasses the elevated enthalpy at the start of aging is reached (from the equilibrium state above  $T_g$ ) essentially instantaneously compared with the aging time.

The good agreement of calculated and experimental results exhibited in Fig. 12 indicates that the calculation procedure is essentially correct. In particular, the agreement justifies the assumption that the model parameters are not affected by possible structural or conformational changes induced by cold drawing or methyl chloride plasticization.

5.3 Co-Aging Nonthermal Histories

The effects of hydrostatic pressure, tensile stress and vapor adsorption applied during aging, on enthalpy relaxation in PVC, have been investigated by Berens and Hodge (44). In all cases the development of sub- $T_g$  peaks is slowed down, corresponding to a lengthening of the average relation time. The peak temperature,  $T^{\max}$ , generally decreases although in some cases this is not evident until large perturbations are applied. The discussion here is restricted to the effects of approximately hydrostatic pressure, applied by a plunger to powdered PVC. The powder was cooled at about 40K min<sup>-1</sup> at atmospheric pressure before aging for 24 hours at 40°C under several pressures. A summary of  $C_p^{\max}$  and  $T^{\max}$  as a function of applied pressure is given in Table III.

The calculation procedure for coaging perturbations was to decrease  $T_f^S$  by an amount  $\Delta T_f^S$  during aging, or to increase  $A$  or  $\Delta h^*$  by a constant amount during aging. As before, the parameters  $x$  and  $\beta$  are assumed to be unaffected by pressure. This procedure guarantees

that  $\Delta H_e$  will diminish with pressure, so that barring an extreme narrowing of the sub-Tg peak  $C_p^{\text{max}}$  will also decrease. The accuracy of the calculation is assessed from the shift in  $T_{\text{max}}$ , and an assumed monotonic increase in the magnitude of  $\Delta T_f$  with pressure. Calculated values of  $C_p^{\text{max}}$  and  $T_{\text{max}}$  are compared with experimental values in Table III. The agreement in  $T_{\text{max}}$  is very good and there is an almost linear increase in  $\Delta T_f$ ,  $\Delta \ln A$ , and  $\Delta(\Delta h^*)^P$  with  $P$ . This agreement again indicates that the calculation procedure is essentially correct.

## 6. Summary and Conclusions

The effects of physical aging on enthalpy relaxation in polymers are generally well described by the phenomenology used to characterize the glass transition kinetics. The development of sub-Tg heat capacity maxima with aging in some materials, most notably PVC, has been shown to reflect the nonexponential decay function for enthalpy relaxation. The effects of nonthermal perturbations such as hydrostatic pressure, mechanical deformation, and vapor induced dilation can be calculated by simple extensions to the standard phenomenology. Perhaps surprising is the apparent invariance of the four parameters ( $A$ ,  $\Delta h^*$ ,  $x$ , and  $\beta$ ) with respect to temperature, pressure, deformation, and departure from equilibrium. It is known that these invariances are approximate but evidently any variations are incidental to, and not causative of, the enthalpic manifestations of physical aging. The correlations between the four parameters observed for several polymers need to be investigated in more detail. The success of the Marquardt optimization procedure for obtaining enthalpy relaxation parameters from experimental data should allow testing of correlations for a large number of materials, including but not restricted to other polymers. If the correlations successfully withstand further studies, a common physical origin for all the parameters would be indicated. A possible candidate is the number of chain segments per relaxation event, or perhaps a correlation length for fluctuations in conformation or similar measure of molecular structure.

## Acknowledgments

It is a pleasure to thank D. Puraty and F. Kunig for their experimental assistance, and G. Huvard for his contribution to the Marquardt optimization studies. I thank A. R. Berens, H. B. Hopfenberg, W. M. Prest, Jr. and J. M. O'Reilly for many helpful comments. Much of the work described here was supported by the National Science Foundation under the Industry-University Cooperative Research Program through Grant No. CPE-7920740. I thank The BFGoodrich Company for permission to publish.

## References and Notes

1. K. H. Illers, *Makromol. Chem.* **127** 1 (1969).
2. M. V. Volkenstein and Yu. A. Sharonov, *Vysokomol. Soed* **3** 1739 (1961).
3. C. R. Foltz and P. V. J. McKinney, *J. Appl. Sci.* **13** 2235 (1969).
4. A. Weitz and B. Wunderlich, *J. Polym. Sci. Polym. Phys. Ed.* **12** 2473 (1974).
5. A. Gray and M. Gilbert, *Polymer* **17** 44 (1976).
6. R. Straff and D. Uhlmann, *J. Polym. Sci., Polym. Phys. Ed.* **14** 1087 (1976).
7. T. E. Brady and S. A. Jabarin, *Polym. Eng. Sci.* **17** 686 (1977).
8. G. Ceccorolli, M. Pizzoli, and G. J. Pezzin, *Macromol. Sci. Phys.* **B14** 499 (1977).
9. I. G. Brown, R. E. Wetton, M. J. Richardson, and N. G. Savill, *Polymer* **19** 659 (1978).
10. Z. H. Ophir, J. A. Emerson, and G. L. Wilkes, *J. Appl. Phys.* **69** 5032 (1978).
11. M. J. Richardson and N. G. Savill, *Polym. J.* **11** 123 (1979).
12. J. M. O'Reilly, *J. Appl. Phys.* **50** 6083 (1979).
13. M. G. Wysgoski, *J. Appl. Polym. Sci.* **25** 1455 (1980).
14. A. R. Shultz and A. L. Young, *Macromolecules* **13** 633 (1980).
15. W. M. Prest, Jr., J. M. O'Reilly, F. J. Roberts, Jr., and R. A. Mesher, *Polym. Eng. Sci.* **21** 1181 (1981).
16. W. M. Prest, Jr. and F. J. Roberts, Jr., *Ann. N.Y. Acad. Sci.* **371** 67 (1981).
17. H. S. Chen and T. T. Wang, *J. Appl. Phys.* **52** 5898 (1981).
18. J. Menczel and B. Wunderlich, *J. Polym. Sci. Polym. Lett.* **19** 261 (1981).
19. C. Bauwers-Crowet and J.-C. Bauwens, *Polymer* **23** 1599 (1982).
20. A. R. Berens and I. M. Hodge, *Macromolecules* **15** 756 (1982).
21. I. M. Hodge and G. S. Huvard, *Macromolecules* **16** 371 (1983).



22. I. M. Hodge, *Macromolecules* 16 898 (1983).
23. U. Yilmazer and R. J. Farris, *J. Appl. Polym. Sci.* 28 3269 (1983).
24. A. J. Kovacs, J. J. Aklonis, J. M. Hutchinson, and A. R. Ramos, *J. Polym. Sci., Polym. Phys. Ed.* 17 1097 (1979).
25. I. M. Hodge and A. R. Berens, *Macromolecules* 15 762 (1982).
26. A. J. Kovacs, *Fortschr. Hochpolym. Forsch* 3 394 (1963).
27. This function can be traced back to Kohlrausch, but is often referred to as the Williams-Watts function following its application to dielectric relaxation by Williams and Watts [*Trans. Faraday Soc.* 66 80 (1970)]. It figures prominently in the mathematical modeling of physical aging described in section 3.
28. A. Q. Tool, *J. Am. Ceram. Soc.* 29 240 (1946).
29. R. Gardon and O. S. Narayanaswamy, *J. Am. Ceram. Soc.* 53 148 (1970).
30. O. S. Narayanaswamy, *J. Am. Ceram. Soc.* 51 621 (1971).
31. H. N. Ritland, *J. Amer. Ceram. Soc.* 37 370 (1954).
32. C. T. Moynihan, A. J. Easteal, and M. A. DeBolt, *J. Amer. Ceram. Soc.* 59 12 (1976).
33. C. T. Moynihan, A. J. Easteal, J. Wilder, and J. Tucker, *J. Phys. Chem.* 78 2673 (1974).
34. L. C. E. Struik, "Physical Aging in Amorphous Polymers and Other Materials", Elsevier, New York (1978).
35. M. A. DeBolt, A. J. Easteal, P. B. Macedo, and C. T. Moynihan, *J. Amer. Ceram. Soc.* 59 16 (1976).
36. C. T. Moynihan *et al.*, *Ann. N.Y. Acad. Sci.* 279 15 (1976).
37. H. P. Brown, G. M. Musindi, and Z. H. Stachurski, *Polymer* 23 1508 (1982).
38. R.-J. Roe and G. M. Millman, *Polym. Eng. Soc.* 23 318 (1983).
39. J. M. O'Reilly and R. A. Mosher, *J. Appl. Phys.* 51 5137 (1980).
40. J. B. Yourtee and S. L. Cooper, *J. Appl. Polym. Sci.* 18 897 (1974).
41. R. E. Wetton and H. G. Moneyppenny, *Br. Polym. J.* 7 51 (1975).
42. R. M. Kimmel and D. R. Uhlmann, *J. Appl. Phys.* 42 4917 (1971).
43. W. C. Dale and C. E. Rogers, *J. Appl. Polym. Sci.* 16 21 (1972).
44. A. R. Berens and I. M. Hodge, to be published.
45. D. M. Marquardt, *J. Soc. Indust. Appl. Math* 11 431 (1963).
46. J. L. Kuester and J. H. Mize, "Optimization Techniques with FORTRAN", McGraw-Hill: New York, 1973.
47. I. M. Hodge, unpublished analysis of literature data [Ishida, Y. *Kolloid Z.* 168 29 (1960)].
48. W. M. Prest, Jr., private communication.
49. H. Sasabe and C. T. Moynihan, *J. Polym. Sci.* 16 1447 (1978).
50. I. M. Hodge, unpublished results.
51. A. J. Kovacs, *J. Polym. Sci.* 30 131 (1958).

# **RELAXATIONS IN POLYMERS**

## THE CREEP BEHAVIOR OF AMORPHOUS POLYMERS

Dr. Donald J. Plazek  
Department of Metallurgical and Materials Engineering  
University of Pittsburgh  
Pittsburgh, Pennsylvania 15261

### INTRODUCTION

The mechanical response of most polymers is strongly dependent on the time or frequency of measurement. This time-dependence is beyond a change in the character of the material such as is caused, for example, by thermal-oxidative degradation. With the character of the material being constant its changing response with time is clearly due to the sluggish response of molecular mechanisms to applied tractions or strains. Two of the most common causes for the retardation of molecular responses are the extreme crowding experienced by supercooled liquids near their glass temperatures and the extremely complicated convolutions required of long threadlike molecules. Amorphous thermoplastic and elastomeric polymers display time-dependent mechanical responses for both reasons. Materials with a variable time dependent response in the present sense are said to be viscoelastic. The viscoelastic response is temperature dependent but this dependence is not involved in defining viscoelastic behavior. A dynamic modulus may change rapidly with temperature over several orders of magnitude as a result of the temperature dependence of its viscoelastic behavior. However, the temperature variation of the mechanical response does not constitute a viscoelastic behavior. All liquids that happen not to freeze upon being cooled are unavoidably destined to become glasses and hence are markedly viscoelastic at least in the neighborhood of their glass temperature,  $T_g$ . Although it is difficult to precisely characterize, it is clear that the structure of a liquid varies significantly with temperature. When the equilibrium form of the structure can no longer make a complete adjustment to a temperature change in the time allotted, the liquid is below its  $T_g$ . Thus the so-called "glass transition" is not a transition but is something not happening—the something being the maintenance of an equilibrium liquid structure with continual cooling. Glass temperatures are usually determined by establishing the temperature where the expansion coefficient, in a volume-temperature curve, or the heat capacity in a DTA or DSC\* curve show abrupt increases with temperature. Both curves should be determined at a constant rate of cool-

ing. The refractive index,  $n$ , of a liquid, which is proportional to the electron density and hence the mass density, can also be used as the experimental variable to determine  $T_g$ . Frequently the maximum found in the loss tangent as a function of temperature is identified as  $T_g$ . We cannot recommend this procedure since it is yet to be established which, viscoelastic mechanisms are intimately related to the molecular motions which are involved in a change in the structure of a liquid. The procedure has considerably less claim to validity when one is dealing with the non-crystalline portion of a crystalline polymer.

The role of the density in determining the rate at which irreversible processes (such as viscoelastic responses, changes in liquid structure, or crystallization above but near  $T_g$ ) occur in polymers or any other supercooled liquids can be appreciated by asking how such processes can take place over time scales which are literally dozens of orders of magnitude slower than the basic molecular step involved. Molecular vibrations occur at some  $10^{12}$  Hz and some of the rate processes referred to can persist for minutes, hours, months and far longer if the proper conditions are chosen. It seems clear that nearly all of the molecular vibrations are fruitless in responding to the pertinent forcing functions and that rare stochastic local density fluctuations are necessary for a combination of molecular motions to contribute a fruitful response. Thermal kinetic energy is usually involved in effecting the response but the amount must be considered sufficient to bring about the responding change in molecular positions when a local rarefaction of necessary magnitude occurs. Activation energy barriers to the motion are not involved since under conditions of great molecular crowding the geometrical barriers, when present, are too high to be overcome by the thermal kinetic energy present. Among the most convincing pieces of evidence against the direct influence of temperature in determining the magnitude of

\*DTA, differential thermal analysis, DSC, differential scanning calorimetry.

the rate processes to which we are alluding are the rate changes that occur during isothermal and isobaric volume contraction that can conveniently be observed some 10 to 20°C below the usual  $T_g$ . (1,2) The merit of the free volume rationale of rate processes in supercooled systems is testified to by the applicability and successes of the Doolittle equation which has its intrinsic volume dependence implicitly indicated by variations with temperature in the widely used Williams, Landel, and Ferry, WLF, equation. Discussion of the temperature dependences of the viscosity and viscoelastic responses will be given below.

The fundamental principal variable of viscoelasticity is time, and the material characterizing curves shift markedly on the time scale with temperature. The material variables and their effects on viscoelastic response that will be explored here are molecular weight and, to a lesser extent, its distribution; plasticizer concentration; and stereochemical structure. Most of the data that we personally have available is in the form of shear creep and creep recovery. With the aid of computer programs some of the data have been transformed into other viscoelastic functions and is available for contrasting comparisons. The discussion here will deal principally with the viscoelastic behavior in terms of creep compliance curves,  $J(t)$ , and the corresponding retardation spectra,  $L(\ln t)$

The creep experiment involves the sudden creation of a fixed level of stress in the previously relaxed material being studied. The ensuing monotonically increasing strain is measured as a function of the time following the "instantaneous" increase in stress level. At small strains and stresses the strain,  $\gamma(t)$ , at any time,  $t$ , sec., is proportional to the stress level,  $\sigma_0$ , dynes/cm<sup>2</sup> or N/m<sup>2</sup>. Then the strain per unit stress is a unique function of time and is called the creep compliance function,

$$J(t) = \gamma(t) / \sigma_0 = J_g + J_d \psi(t) + t/\eta \quad (1)$$

The creep compliance is usually decomposed into the three terms shown in Eq. (1).  $J_g$ , representing a recoverable deformation, is usually considered to be a constant, but in reality is the long time limiting value of preceding dispersions such as those attributed to the motion of side groups on the polymer chain. These are not normally seen at or above  $T_g$  because of their short response times. The second term,  $J_d \psi(t)$ , represents the principal time dependent recoverable deformation, where  $\psi(t)$  is the normalized retardation function which varies from 0 to 1 as the time,  $t$ , extends from 0 to  $\infty$  and  $J_d$ , the retarded compliance, is the normalization constant. All of the permanent deformation is represented by the  $t/\eta$  term, where  $\eta$  is the shear viscosity coefficient. This viscous deformation is the only deformation that we refer to as flow. Under constant stress conditions the permanent deformation accumulates linearly with the passage of time. It contributes additively not only to the creep compliance

function but also to the complex dynamic compliance. The viscoelastic functions that are rigidities are not so separable. The presence of permanent deformation in the creep response of a material distinguishes viscoelastic liquids from viscoelastic solids. That is, if  $\eta$  is infinite all of the creep response is ultimately recoverable and the material being measured is a viscoelastic solid. One can conclude that it contains an effective molecular network as is found in crosslinked elastomers.

The character of a creep response cannot be seen by looking at a linear plot of the results since qualitatively the response of all linear viscoelastic materials is the same in that the monotonically increasing deformation accumulated as a function of the time of creep has a monotonically decreasing velocity. The only qualitative difference between viscoelastic solids and liquids is that the long time limiting velocity is zero for solids and finite for liquids. The recoverable deformation of a viscoelastic liquid  $J_r = J_g + J_d \psi(t)$  can only be reliably determined by allowing the material to recover under zero stress conditions after creeping to steady state, where  $\psi(t) = 1$ . Zero stress is achieved by removing the traction that produced the state of stress. Mathematically, the recoverable compliance is also  $J(t) - t/\eta$ , but this difference all too quickly becomes less than the experimental uncertainty and therefore is valueless in the terminal region of response. Since there is no flow during recovery, the recoverable deformation has the same qualitative appearance as the creep deformation of a viscoelastic solid. The terminal velocity is zero. Our comments will be restricted to non-crosslinked amorphous polymers which are viscoelastic liquids.

When an experimentally determined creep compliance curve is plotted logarithmically, i.e.  $\log J(t)$  versus  $\log t$ , characteristic features immediately become apparent. These features can be seen in Figure 1 where plateaus in the response curve indicate the paucity of viscoelastic deformation mechanisms in the corresponding time scale regions. The regions of response in between plateau levels are called dispersions. A steep rise in  $J_r(t)$  indicates a high population of viscoelastic mechanisms. More often than not dispersions are referred to as transitions. The danger in this practice is the possibility of confusing transitions in a property with a supposed transition in the state of the material. In a linear viscoelastic response the state of the material is not changed; only the compliance or modulus of the material varies. If one is not simply studying the time dependent response, but is measuring, for example, a dynamic modulus and loss tangent while the temperature is varied, changes in the modulus level and peaks in the loss tangent can be encountered which may or may not reflect thermodynamic transitions in the material.

Most often a single type or group of molecular mechanisms contribute to a dispersion,

although overlap between groups of mechanisms is encountered. In Figure 1 the dotted lines indicate the three contributions to the creep compliance equation. The numbers indicate the various features that should be noted. The schematic curve shown semi-quantitatively represents the response of a linear amorphous polymer with a weight average molecular weight in the neighborhood of  $1.0$  to  $2.0 \times 10^5$ , and an ordinary spread in chain lengths, say, not far broader than the most random distribution. The primary softening transition or dispersion usually extends from a glassy level of  $1.0 \times 10^{-10}$   $\text{cm}^2/\text{dyne}$  ( $1.0 \times 10^{-9}$   $\text{m}^2/\text{N}$ ) to a rubbery level of  $3 \times 10^{-6}$   $\text{cm}^2/\text{dyne}$  ( $3 \times 10^{-5}$   $\text{m}^2/\text{N}$ ). This enormous rise is due to the retarded response of the threadlike polymer chain backbones. The response of the chain molecules has been described in terms of normal coordinate modes of motion; (3) now called Rouse modes. The extent of involvement of the polymer chain in this dispersion is limited to segments found between molecular entanglements. The presence of the rubbery plateau is the principal piece of evidence for the existence of a transient molecular network where the entanglements between molecules play the role of crosslinks. After delaying the response, the entanglements eventually slip and a subsequent dispersion follows. We will return to the nature of this terminal dispersion after the effect of chain length on  $J_r(t)$  is discussed. The final level of the recoverable deformation yields the steady state recoverable compliance,  $J_e^0$ , which next to the viscosity is the most common viscoelastic characterizing parameter referred to. The same symbol without the superscript is used to describe the terminal level of recoverable deformation of an elastomer which is a viscoelastic solid, only in this case it is called the equilibrium compliance. Numbers were intentionally left off the abscissa of Figure 1 since the values depend enormously on the temperature of measurement. If the measurement were carried out at the glass temperature,  $T_g$ , the first log time mark next to the left border would correspond to 0 or one second. Each subsequent mark would indicate the passing of an order of magnitude of time. Hence, the steady state response is attained some eleven decades of time later or after the passage of 30,000 years. (Note that if an estimate of the viscosity of the polymer is desired from Figure 1 the extrapolation of the  $t/\eta$  dotted line to  $\log t = 0$  yields  $-\log \eta$ :  $(\log J_r(t) = \log t - \log \eta)$ ).

Obviously a compliance curve as shown in Figure 1 is not measured directly. It is constructed by the temperature reduction procedure that was discovered by Leaderman (4) and further developed by Tobolsky and Andrews (5) and then by Ferry. (6) Figure 2 shows how this procedure works. Measurements are taken over the range of time or frequency that is possible and convenient with the instrument available; in this case creep runs extending from one second to slightly more than a day are indicated. Then, if the response curve does not change its shape with a change of temper-

ature, the curves obtained at different temperatures can be shifted horizontally to superimpose on a reference curve measured at a chosen reference temperature,  $T_0$ . Sometimes small vertical or magnitude shifts are also necessary. (7,8) The shape of the curve is maintained if all of the viscoelastic mechanisms involved have the same temperature dependence. Quite often the temperature dependence (really the volume dependence, see below) of all the mechanisms within a group contributing to a single dispersion is close to the same, but, in general, the temperature dependence of mechanisms from different groups is different. Generally, it is found that dispersions occurring at shorter times relative to any other dispersion will be less temperature sensitive; i.e. its apparent activation energy will be smaller. Figure 2 shows a secondary dispersion at times less than one second and indicates that the effect of the distribution of molecular weights is found in the terminal zone. A material with a broad distribution will show a far larger final dispersion in the recoverable compliance than that with a narrow distribution. The former will normally range from 20 to 50 times that of the rubbery plateau value while the latter will be as small as a factor of 2.5 to 3. The measure of the temperature dependence is the shift along the logarithmic time scale to accomplish the superposition of each temperature curve onto the reference temperature curve. The shift is identified as  $\log a_T$  where  $a_T^{-1}$  is the factor by which retardation times change when the temperature is changed from a general temperature,  $T$ , to the reference temperature,  $T_0$ . If the original temperature is higher than  $T_0$ , the creep rates are higher, so they must be slowed down to correspond to the response at the lower temperature,  $T_0$ . The reduced time is  $t/a_T$  and must be larger than  $t$ , which demands that  $a_T < 1$  and  $\log a_T < 0$ . For all  $T < T_0$ ,  $\log a_T > 0$ .

The time dependent recoverable component of the creep compliance has an alternate form which utilizes the concept of the distribution function of retardation times,  $L(\ln \tau)$ , which is often referred to as the retardation spectrum;  $\tau$ , the retardation time, is the material clock time. It is a measure of the population of viscoelastic mechanisms that are characteristic of the material. Using  $L(\ln \tau)$

$$J(t) = J_g + \int_{-\infty}^{\infty} L(\ln \tau) (1 - e^{-t/\tau}) d \ln \tau + t/\eta \quad (2)$$

Although it is not necessary, it can be helpful in appreciating the nature of  $L(\ln \tau)$  to know that this mathematical formulation was derived from the mechanical analogue called the Generalized Kelvin or Voigt Body; an infinite series of springs each in parallel with its own dashpot; included are two degenerate elements, a single series glassy spring to account for  $J_g$  and a single series dashpot to represent the permanent deformation,  $t/\eta$ , contribution. To find out the terminal value for the recoverable compliance,  $J_e^0$ , set  $t = \infty$  (any time greater than the time it takes  $\psi(t)$  to come close as one chooses to value of one). Then  $J_e^0 = J_r(\infty) = J_g + \int_{-\infty}^{\infty} L(\ln \tau) d \ln \tau \quad (3)$

The steady state recoverable compliance is simply the sum of the glassy compliance and the area under  $L(\ln\tau)$  when plotted linearly against  $\ln\tau$ . It is our opinion that the effects by variations of molecular and other material variables are best seen in the retardation spectrum,  $L(\ln\tau)$ . Since viscous flow does not contribute to  $L(\ln\tau)$  the long time effects of molecular orientation giving rise to recovery are not obscured as they are in most of the viscoelastic functions. The behavior of the viscosity can be analyzed separately.

#### MOLECULAR WEIGHT AND ITS DISTRIBUTION

##### A) Commercial Polymers

Many commercial polymers have molecular weight distribution which are slightly broader than a random distribution where the weight average molecular weight  $M_w$ , is twice as large as the number average,  $M_n$ . In Figure 3 we see the creep recovery behavior of such a polymer - a polystyrene produced by Arco/Polymers where  $M_n = 93,000$  and  $M_w = 220,000$ . The results from measurements at nine temperatures extending from slightly below  $T_g$ , where the glassy response is seen, up to  $87^\circ\text{C}$  above  $T_g$  where the attainment of steady state is seen. (9) The  $J(t)$  curves for the higher temperatures where viscous flow is appreciable are shown in Figure 4. The short dashed curves represent the corresponding recoverable contribution and the long-dashed lines the permanent viscous deformation. With  $100^\circ\text{C}$  chosen as the reference temperature the recoverable compliance curves are shifted horizontally to form the reduced curve shown in Figure 5. Little more can be said than that every feature of  $J_r(t)$  alluded to in Figure 1 is seen here including the substantial 30 fold increase of the deformation in the dispersion above the rubbery plateau level. Whereas a mechanical analogue model with a single retardation time would sweep through the largest part of a dispersion in little more than a decade of time, polymers as exemplified here require 6 decades of time.

In Figure 6 the reduced  $J_r(t)$  curve for the Dylene 8 sample is compared with two slightly higher molecular weight grades of polystyrene. For 8E,  $M_n = 104,000$ , and  $M_w = 260,000$ ; and for 8C,  $M_n = 122,000$  and  $M_w = 290,000$ . The small differences in molecular weight result in significant trends in the response. The primary dispersion is oblivious of the molecular weight differences of the samples. The other two features to be noticed is that that rubbery plateau is more strongly developed with increasing molecular weight and higher  $J_e$  is reached at a later time. The same results are compared on a linear basis in a semi-logarithmic plot in Figure 7 and it can be seen that the differences are substantial, especially in the terminal region.

In Figure 8 the retardation spectra derived from the recoverable compliance curves of Figure 6 are shown. For moderate to high molecular

weight polymers the common features of the distribution function,  $L$  are: 1) At short times near the glassy region of response  $L(\ln\tau) = 0.246 \delta \tau^{1/3}$ , which reflects the fact that the form of the creep in this region is Andrade Creep, (10,11a)  $J(t) = J_g + \delta t^{1/3}$ ; 2) In the following region a peak is found which, like the Andrade region, is independent of molecular weight at high molecular weights. This peak represents viscoelastic mechanisms which contribute to the primary softening dispersion. When the rubbery plateau is reached the preceding large concentration of deformation mechanisms is past and  $L(\ln\tau)$  diminishes. At sufficiently high molecular weights a well defined minimum is found; 3) a second peak, which is at least as big as and usually is much bigger than the first, is found beyond the minimum. This peak reflects the presence of mechanisms associated with the terminal dispersion approaching steady state. The position of the first peak on the time scale is largely determined by the  $T_g$  of the polymer and the position of the second peak moves out to longer times with increasing molecular weight and the breadth of the distribution. For polymers with narrow molecular weight distributions the second peak is only marginally greater than the first as will be seen below, but for high molecular weight polymers with broad distributions the terminal peak can be enormously higher and broader.

Near the maximum the first peak in  $L$  is usually symmetrical but the second peak is usually asymmetrical with the left or short side approach to the maximum often following the Andrade form, indicating that, the recoverable creep compliance has the form  $J_r(t) = J_N + \beta' t^{1/3}$ , where  $J_N$  is the rubbery plateau compliance and  $\beta'$  is a different characterizing constant than that found in the glassy region.

In Figure 8 most of the above features are seen except for the minimum between peaks. The Andrade region is found between  $\log t/a_T = 0$  and 3; the first softening dispersion peak between 3 and 8 and the terminal peak from 8 to 14. The molecular weights of these materials are not quite high enough for the two peaks to be completely resolved. The first peak appears to be a strong shoulder on the larger second peak.

A reduced curve for the creep compliance was not shown simply because the reduction procedure does not work well for  $J(t)$ , at least within  $20^\circ\text{C}$  of  $T_g$ . An example of this kind of reduction failure is present in Figure 9, with the creep compliance of a polystyrene with a narrow molecular weight distribution,  $M = 47,000$ . The time scale shift factors were calculated from viscosities, (7)  $\log a_T = \ln(T)/\ln(T_0)$

Further analysis revealed that the recovery curves reduced successfully with empirical shift factors and that  $J_r(t)$  had a different temperature dependence from that of the viscosity. This difference is the reason for the lack of reduction seen here. Note that if the

viscous deformation had not been analyzed separately and the results used in the reduction attempt the curves in Figure 9 could have been superimposed with a fair degree of success. Discrepancies might have been attributed to experimental uncertainties. Close examination reveals that the temperature dependence of the mechanisms contributing to the terminal dispersion of the recoverable compliance has the same temperature dependence as that of the viscosity. If stress relaxation measurements are made, where the decaying stress in a sample deformed to a fixed strain is monitored as a function of the time following the imposition of the strain, stress relaxation modulus curves are obtained. As mentioned above the contribution from viscous processes do not appear in an additive fashion and the inapplicability of the reduction process is not as readily discerned as it is from creep and recovery measurements.

### B. Polymers with Narrow Molecular Weight Distributions

The terminal region of response is far more dependent on the molecular weight distribution than it is on the molecular weight.<sup>(7)</sup> As a consequence of this fact the determination of the effect of the molecular weight on the viscoelastic response had to wait until the advent of anionic living polymers with their comparatively narrow molecular weight distributions. Even many of these research samples have proven not to be sufficiently narrow. Only the examining a series of samples of so-called "monodisperse" polystyrenes and examination of fractions of these has data been collected that appears to represent the unadulterated molecular weight dependence of  $J_r(t)$ .

In Figures 10, 11, 12, and 13 the reduced  $J_r(t)$  curves of part of a series of samples are shown. The recovery behavior of lowest molecular weight sample of the set, A-25,  $M_v = 47,000$  is shown in Figure 10. A single dispersion extending from the usual glassy level up to a steady state value of  $\log J_r(\infty) = 6.18$  is seen. The dispersion covers over 8 decades of time. The second dispersion you think you see is real for the sample, but sufficient evidence has been obtained to attribute it to a residual high molecular weight tail. In Figure 11 sample M102 with a molecular weight of 94,000 shows a  $\log J_e = -5.88$ . Only those readers with great perception and insight can clearly see the beginning of the development of a rubbery plateau at about  $10^6$  sec. In the response of polystyrene L-2,  $M_v = 189,000$ , the lack of complete superposition can be seen, but a rubbery plateau is clearly visible followed by a surprisingly small terminal dispersion. The steady state recoverable compliance has not increased with the increase in molecular weight;  $\log J_e = -5.90$ . This constancy of  $\log J_e$  persists in the behavior of polystyrene sample A-19,  $M_v = 600,000$ , as seen in Figure 13 where the rubbery plateau is well developed.

On the basis of predictions of the

dilute solution theory of Rouse<sup>(3)</sup>  $J_e^0$  was expected to be proportional to the first power of the molecular weight and the surprising molecular weight independence of  $J_e^0$  at high molecular weights was discovered by Tobolsky, Aklonis and Akovali in 1965.<sup>(12)</sup> A number of investigators has followed up and individually confirmed this observation. However as seen together in Figure 14 the functionality of the dependence of  $J_e^0$  on  $M$  is not altogether clear. If we single out our own results which cover the entire measured range of molecular weights we see in Figure 15 that at low molecular weights, below  $10^5$ , the Rouse theory prediction adapted to bulk polymers<sup>(13)</sup> is followed except for a possible deviation at very low molecular weights. Since the Rouse theory does not apply to very short chains the deviation is not surprising. In fact we are surprised by the excellent agreement with a theory originally intended for isolated molecules. Above a molecular weight of about 100,000, the  $J_e^0$  values become completely independent of chain length. To explain this we have coupled the questions: why is  $J_e^0$  independent of molecular weight and why is the ratio  $J_e^0/J_N$  so small? The best samples indicate that the steady state recoverable compliance,  $J_e^0$ , which reflects the maximum degree of molecular orientation per unit stress is between 2.5 to 3 times larger than the rubbery plateau compliance,  $J_N$ . The latter is determined by the molecular weight per entangled unit,  $M_e$ , which is inversely proportional to the number of chains in the transient network,  $\nu$ . Using the kinetic theory expression for the rubberlike response of the transient entanglement network we have

$$J_N = M_e / \rho RT (1 - 2M_e/M) \quad (3)$$

where  $M_e = N_A \rho V / \nu$ ;  $N_A$  is Avogadro's number;  $\rho$  is the density;  $V$ , the volume;  $R$ , the gas constant; and  $T$ , the absolute temperature in Kelvins. The parenthetical expression is the usual correction for loose ends<sup>(14)</sup> where  $M$  is the number average molecular weight. This expression, derived for crosslinked systems is more accurate for the entanglement network than for a crosslinked network because the unavoidable presence of trapped entanglements in a crosslinked material is not accounted for by the theoretical expression. For the entanglement network itself is no such interference.

Returning to our double question, it must be kept in mind that since we are restricting ourselves to linear behavior, the total number and distribution of entanglements in the material remains constant during the measurement. The entanglement level is determined dynamically; entanglements cease to exist when polymeric chains diffuse apart and new ones are created when two molecules diffuse into the same domain. Thus, we are dealing with a dynamic equilibrium (between the rate of disentangling and the rate of entangling) which is unaffected by our measurement, but when an entanglement comes apart it affects our measurement. Statistically it is replaced by a newly formed entanglement arising from the free diffusion process. The network chains associated with the new-born

entanglement have not had the opportunity to come to their new "equilibrium" states of orientation and therefore they must go through the motions associated with the first peak of the retardation spectrum. In the mean time they do not support their share of the load and when distributed among the older network chains an additional increment to the deformation is made resulting in an increase in  $J_r(t)$ . The time for the diffusion of the entanglement to the center of the molecule must be involved in establishing its full network status or  $J_e^0$  would necessarily decrease with increasing molecular weight if the time for re-establishment to full status would be fixed by the position of the first peak in  $L$  since the rate of disentanglement is diminished with the increasing viscosity as the chain length is increased. The  $J_e^0$  level then also represents an entanglement network response which is determined by the concentration of effective network chains (or entangled units). For the present then we have to accept that polymers are telling us that between 1/3 to 1/2 of the entanglements are effective at steady state.

For polystyrene with a molecular weight of 600,000 (i.e. A-19)  $J_N$  was found to be  $4.9 \times 10^{-7}$  cm<sup>2</sup>/dyne by integrating under the first peak of  $L$  ( $\ln \tau$ ), see Figure 16. With Equation (3) one finds that this corresponds to  $M_e = 14,000$ . From  $J_e = 1.59 \times 10^{-6}$  an effective molecular weight per entangled unit  $M_e^0 \approx 41,000$  is obtained. The entanglement network is well developed when the molecular weight of a polymer is over  $5 \times 10^5$ . The two peaks in  $L$  ( $\ln \tau$ ) are well separated for A-19 as shown in Figure 16. The development of the second peak in  $L$  ( $\ln \tau$ ) as the molecular weight increases can be seen in Figure 17 where the samples have the following viscosity molecular weight averages A-25, 47,000; M102, 94,000; L-2, 190,000; A-19, 600,000; A-16, 600,000. Slight time scale adjustments, labeled  $a_M$  were made to bring about the best superposition of the short time end of the spectrum. The shape of the spectrum below  $\log \tau/a_{T,M} = 6$  is independent of molecular weight for all samples greater than 30,000. The position on the time scale is a function of the  $T_g$  of the polymer and hence the number average molecular weight and any plasticizing impurities present. The second peak appears to grow out of the first and move rapidly toward longer times until a fairly deep minimum separates them. We can see in Figure 18 by examining the  $J_r(t)$  and  $L_A$  curves with the filled points how the maxima in  $L$  ( $\ln \tau$ ) are in an approximate line with the half point levels (on a linear scale - 0.3 log units below the plateaus) of the  $J_r(t)$  curves and how the minimum reflects the flattest portion of the rubbery plateau. The sample represented here is the narrow distribution polystyrene PC-6A with  $M_v = 840,000$ .

We will not go into detail concerning the lower molecular weight samples that show no entanglement effect because the details are in the literature.(15) One reduced curve of a

lower molecular weight sample A61,  $M_v = 16,000$ , is shown in Figure 19 to illustrate the features that are characteristic of the low end of the molecular weight scale. A single dispersion is seen extending from the glassy level out to the steady state level. The  $J_e$ 's surprisingly are temperature dependent. Reduction obtains a short times and small compliances but the curves from different temperatures separate as steady state is approached. It is seen that  $J_e$  decreases with decreasing temperature, which is unexpected and unexplained except that we suspect the difference in the temperature dependences between the  $J_r(t)$  and  $\eta$  is involved in changing the position of the steady state balance between orientation and diffusion processes.  $J_e$  does approach a high temperature asymptote as the temperature sensitivities approach one another. The level of the high temperature asymptote does not rise above the predicted Rouse level; see Figure 15. Also note that the  $T_g$  for this sample is 92°C and at the same reduction temperature of 100°C which was used for the higher molecular samples the response is shifted more than two orders of magnitude toward shorter times. Glass temperatures for the very high molecular weight samples are close to 98°C. The retardation spectrum, not shown here, has only one maximum between the glassy region and steady state.

#### PLASTICIZER CONCENTRATION

It has been known for a long time that plasticizers and other diluents depress the  $T_g$  severely. Most plasticizers are supercooled liquids themselves and are therefore glass-formers. In many instances their  $T_g$  is in the neighborhood of -60°C. When added to a glassy polymer at any higher temperature the plasticizer is bringing with it, so to speak, a great deal of free volume which is responsible for the solution having a much lower  $T_g$  than the bulk polymer.

It has also been known that the effective molecular weight of a polymer appears lower in solution by virtue of the separation of molecules; i.e. one must go to a higher molecular weight to see entanglement effects.(16) The system Polystyrene-Tricresyl Phosphate (or equivalently Tritolyl Phosphate) has been studied over the entire composition range (17) The polystyrene was the PC-6A whose bulk (pure) response is shown in Figure 18. The depression of  $T_g$  is illustrated in Figure 20 where the value decreases from 98°C to -70°C. In the mid concentration range two  $T_g$ 's were observed, which suggests the presence of two phases but no other evidence of phase separation was noted and a similar effect in the system polystyrene-toluene has been reported (18). Since toluene is an extremely good solvent for polystyrene, phase separation does not appear to be likely there. The drop in  $T_g$  with increasing diluent is accompanied by comparable shifts in the viscosity response as is shown in Figure 21. The concentration of polymer is indicated as weight



per cent.

The viscoelastic behavior of polymer solutions has been studied extensively by Ferry, and his co-workers in both the dilute and concentrated ranges. (7) Elsewhere little attention has been given to the study of the viscoelastic response (as defined above) of polymer solutions over wide ranges of concentration. A number of studies of temperature variation have been made that did not include the measurement of the time dependence and as a result yielded little information. The study being referred to here shows with some clarity the metamorphosis of the retardation spectrum with large scale changes in the concentration of diluent. It has become clear that the following concentration variable linearly obscures the pattern of change in somewhat the same manner as does an examination of a viscoelastic response as a function of linear time or frequency. The information content is precisely the same but is considerably more apparent with logarithmic variations of the independent variable.

Since the time scale of response varies enormously with dilution because of the  $T_g$  depression, a corresponding state comparison of the response curves is desirable. Normally this would be the behavior at the glass temperature. In this case, because of the  $T_g$  ambiguity, we have chosen to match the position of the principal or first peaks of  $L(\ln\tau)$  of the various solutions on the time scale. The comparison is shown in Figure 22 where the time scale is that of the pure PC-6A at a reference temperature of 100°C. It is immediately clear that the change in  $L$  with the addition of the first fifty per cent of plasticizer is trivial insofar as its shape is concerned. The rubbery plateau is shortened as diluent is added. This is reflected by the decrease in the separation of the maxima in proportion to the 3.4 power of the volume fraction of solvent. Hence a decrease of about one logarithmic unit on the time scale in the peak separation from 100% to 55% polymer is barely noticeable. The vertical shift or increase in magnitude is approximately a square dependence on the concentration. By the time three fourths of the polymer is replaced by solvent the shape of the curve is considerably altered as the peaks merge. At 10% polymer the merger is complete and the individual peaks have lost their identity as they would have with a reduction of the molecular weight by a factor of 10. There are no entanglement effects on the one per cent level and there is one narrow peak in  $L$  that reflects viscoelastic mechanisms involving the polymer. The 1.25% solution does have two peaks in its spectrum but the low one at short reduced retardation times is that of the solvent alone. The plasticizer behavior is completely Andrade creep up to the maximum in  $L$  at  $\log \tau/a_T$  at  $-1.5$ .

The corresponding  $J_r(t)$  curves are seen in Figure 23 in slightly shifted positions (because of a different attempt for a cor-

responding state). The dashed line through the 1.25% recovery curve has a slope of one. Where the  $J_r(t)$  curve matches this slope there is no information concerning the retardation spectrum, i.e.  $L$  is immeasurably small. No detectable viscoelastic mechanisms are present in that region of the time scale. Notice the gap in  $L$  in Figure 22. A slope of one in a log-log plot of  $J(t)$  or  $J_r(t)$  versus  $t$  is the highest possible observable slope in the response of a linear viscoelastic material. The slope of one means the velocity is constant. Constant velocity in creep is often taken as evidence of the achievement of steady state. This is a misguided conclusion. If a creep curve has a constant velocity within experimental limits the correct conclusion is that no information about  $L$  is available from that creep curve. Information concerning  $L$  may very well be present in the recovery curve in the same region of time scale. When  $\psi(t) = 1$  or when  $L$  has gone to zero for the last time steady state has been reached. Experimentally it can be difficult to be sure steady state is achieved. Creep curves can be encountered that have log-log slopes greater than one--reflecting the presence of acceleration. This behavior puts it outside the boundaries of linear viscoelasticity and indicates a structural collapse of some sort within the material.

The recovery curves in Figure 23 contain the same information indicated by the spectra in the preceding figure but we don't believe it is as apparent. Four of the corresponding creep curves are presented in Figure 24 with the recoverable components indicated by dashed lines. For samples with entanglements, the pure polystyrene and the 55% solution, the onset of measurable viscous flow coincides with the beginning of the terminal dispersion. This coincidence is in accord with the contention that the terminal dispersion is tied in with the rate of disentanglement. The  $J(t)$  curve for the 10% solution serves as a warning pointing to a possible misinterpretation of creep compliance curves as well as some of the other viscoelastic functions. The slight plateau in  $J(t)$  could be mistaken for a rubberlike plateau from which one might attempt to estimate the molecular weight per entangled unit. From the fact that  $J_r(t)$  shows but one dispersion, and therefore  $L$  but one peak, it is clear that knowledge concerning the entanglement network cannot be extracted. For those familiar with dynamic moduli Figure 25 is presented where the real  $G'$ , and imaginary  $G''$ , components of the complex dynamic shear modulus,  $G^* = G' + iG''$ , shown along with the loss tangent,  $\tan \delta = G''/G'$ , of the 10% solution as a function of the reduced radian frequency,  $\omega a_T = 2\pi\nu a_T$ ;  $\nu$  is the ordinary frequency in Herz. Seeing the  $\log G'$  curve, one certainly would be tempted to claim the presence of an entanglement plateau at the level of  $10^4$  dynes/cm<sup>2</sup>. The above discussion shows this to be ridiculous. The retardation spectrum or  $J^*$  must be examined before such conclusions can be drawn. The final comment we wish to make concerning Figure 24 is that the

viscous component of the creep of the 1.25% solution does not become negligible with decreasing time until the glassy level is reached.

The concentration dependence of  $J_e$  of polystyrene PC-6A is shown in Figure 26. The sources of the data are indicated in its legend. At concentrations of polymer greater than  $\text{Log } C$  ( $\text{g}/\text{cm}^3$ ) = -0.6 the slope is in the neighborhood of -2 indicating a  $C^{-2}$  dependence and at the lower concentrations indicated it shifts to an inverse first power. At still lower concentrations a maximum is expected and to its left a direct first power dependence is theoretically predicted. (3,19,20)

#### MOLECULAR WEIGHT REVISITED

Since the form of the viscoelastic response of a polymer is little affected by an appreciable addition of plasticizer while  $T_g$  is severely depressed, it is possible to extend the investigation of the effect of molecular weight to higher values while diminishing the threat of thermal degradation. Such an extension was attempted as depicted in the diagram in Figure 27. A series of 55% solutions of high molecular weight polystyrenes in TCP was studied to determine if the molecular weight independence of  $J_e$  persisted. (21) The spectra obtained are presented in Figure 28. Here again the general features listed above are seen; the glassy Andrade region; the softening dispersion peak; the deepening minimum; and the retreating terminal peak with increasing molecular weight preceded by a second Andrade region in the rubbery plateau. Even with the substantially lowered  $T_g$  steady state was not achieved with the two highest molecular weight samples (7.0 and 43 million). An extrapolation technique was required to estimate  $J_e$  and the terminal region of  $L(\ln\tau)$ . Reduced steady state recoverable compliances,  $J_e^0$ , from three different studies are presented in Figure 29 as a function of  $M\phi$ , where  $\phi$  is the volume fraction of polymer. The conclusion reached was that the drawn line represents the true behavior of monodisperse samples and that  $J_e^0$  continues to be independent of molecular weight to indefinitely high values of  $M$ . Any residual molecular weight dispersion increases the recoverable compliance above the monodisperse level. This fact coupled with knowledge that samples with molecular weights above a million tend to be somewhat broader alloys one to suspect that the points above the line are somewhat in error.

One of the most familiar of the polymer property laws is the Fox and Flory equation (22)

$$\eta = KM^{3.4} \quad (4)$$

for samples with molecular weights above a critical value,  $M_c$ , where the effect of entanglements makes its appearance. The value of  $M_c$ , the break-point in a log-log plot of viscosity versus molecular weight, for polystyrene is 33,000. Since the length of the rubbery plateau as well as its height is a function of the entanglement network, attempts

have been made to connect it to the viscosity-molecular weight relationship. (13,12,7) For broad distribution polymers there has been no successful proposition. In Figure 30 the results from the same three studies indicated in the diagram of Figure 27 (15,17,21) yield an expression for the recoverable deformation of narrow distribution polymers which is completely parallel to the viscosity law. The length of the rubbery plateau is best measured by the separation of the maxima in  $L(\ln\tau)$ . Thereby we are considering the ratio of the two most dominant retardation times,

$$\tau_{m,2}/\tau_{m,1} = (M/M_c)^{3.4} \quad (5)$$

or  $\Delta \log \tau_m = -3.4 \log M_c + 3.4 \log M$

Therefore for narrow distribution polymers one can write

$$\eta = KM^{3.4} \quad M > M_c \quad (4)$$

$$\tau_{m,2} = K'M^{3.4} \quad M > M_c, \text{ where } K' = \tau_{m,1}/M_c \quad (7)$$

Earlier attempts at characterizing the molecular weight dependence of the length of the rubbery plateau were carried out in terms of monomeric friction coefficients and terminal relaxation times. (13,12,7) It is not clear how they correspond to the above expression. The corresponding expression for  $\tau_{m,2}$  for a broad distribution polymer will depend on the form and breadth of the distribution, but will be a much stronger function of the molecular weight. Perhaps a high moment of the molecular weight, such as  $M_z$  or higher, will be appropriate if the position of the softening dispersion peak is kept as the reference. Note that the  $M_c$  in Equations (4) and (7) are the same. The second peak in  $L(\ln\tau)$  appears at the molecular weight where entanglements start influencing the viscosity; see the intercept in Figure 30.

#### STEREOCHEMICAL VARIATION

It has been observed by Karasz, Bair and O'Reilly (23) that asymmetrical vinylidene polymers like polymethylmethacrylate, PMMA, and poly  $\alpha$  methyl styrene, PaMS exhibit large variations in their  $T_g$ 's with changes in their stereo-regularity or tacticity. Their corresponding vinyl counterparts, polymethylacrylate, PMA, and polystyrene, PS, do not. Extreme steric hindrance and a resulting tendency toward helical conformations even in the melt apparently are behind the variations observed. It has been demonstrated that the viscoelastic response of PMMA is profoundly affected by the stereochemical form. (24-28) The lack of an effect in the vinyl polymers is yet to be demonstrated. Figure 31 shows the abrupt manner in which  $T_g$  rises with increasing syndiotactic pair content. (29) Commercial PMMA has a syndiotactic pair content of about 75%. From 50% to 100% syndiotacticity the  $T_g$  increase is slightly more than 10°C. The curve is drawn through points determined on samples that have no measurable tendency toward

block formation.

The  $J_r(t)$  behavior of a commercial PMMA (27) sample with a viscosity average molecular weight of  $7.6 \times 10^5$  is presented in Figure 32. Reduction worked well over the entire range of response. Three items should be noted. The glassy compliance indicated is exceptionally high; the material has a soft glass. The rubbery plateau is rather low, corresponding to an  $M_e$  of 4700, and the rubbery plateau is extremely broad. It is as broad and as flat as any in the literature.  $T_g$  for this material is about 117°C. The retardation spectrum obtained from this recovery curve is shown in Figure 33. Well developed Andrade regions are seen above and below a symmetrical central peak. The sample is a whole polymer (as opposed to a fraction) with a broad molecular weight distribution. Steady state was not achieved even at 189°C so the peak associated with the second or terminal dispersion was not reached. Previously we conjectured that the two Andrade regions derived from a common group of viscoelastic mechanisms, but having seen how the Andrade region in the rubbery plateau moves out continually toward longer times with increasing molecular weight (see Figure 28) no connection is seen at present.

Methacrylates with intermediate variations of tacticity have been studied but the principal dramatic differences can be seen if the behavior of the virtually 100% isotactic form is examined in Figure 34. The molecular weight of the polymer ( $M_w = 6.1 \times 10^5$ ) is nearly as high as that of the above commercial PMMA, yet, instead of a well developed rubberlike plateau, there is none. Such a response has not previously been seen and has not been explained even in the most qualitative sense. We can only imagine that the molecules are in a helical conformation which imparts such rigidity to the molecule that normal entangling is precluded. Another apparent difference is the glassy compliance which is clearly about three times smaller than that of the commercial material. This harder glass is a reflection of the fact that the side groups along the polymer chain backbone are not free to move independently. The mechanical  $\beta$  mechanism is virtually absent from highly isotactic PMMA. (24) Dielectric measurements (30) support this contention. A feature that is not obvious in Figure 34 is that this material did not flow; i.e. the  $t/\eta$  contribution is missing from  $J(t)$  and therefore  $J(t)$  is indistinguishable from  $J_r(t)$ . Non-crosslinked, amorphous polymers have on rare occasion been observed not to flow at temperatures far above their  $T_g$ . (31) This phenomenon has been linked to the presence of long chain branches.

The retardation spectra of the two PMMA samples discussed above along with that of an ideally atactic PMMA polymer are shown in Figure 35. The ideally atactic polymer has 25% isotactic triads, 25% syndiotactic triads and 50% heterotactic triads and no tendency

for block formation. The behavior of the spectra for the commercial and atactic samples appears to be similar in the molecular weight independence region. The faster response of the commercial polymer might be an intrinsic property of the higher  $T_g$ , since as will be shown below the form of the volume dependence, i.e. the apparent temperature dependence, suggests that the curves are at their true corresponding state volumes. A corresponding first peak in  $L(\ln\tau)$  is compatible with the slight shoulder seen on the huge concentration of viscoelastic mechanisms which is responsible for the absence of the rubberlike plateau.

#### TEMPERATURE DEPENDENCES

The shift factors for all of the  $J_r(t)$  curves of the narrow distribution polystyrene samples of differing molecular weight fall on one typical looking curve when the reference temperature is  $T_g$  and the values for  $\log a_T$  are plotted as a function of  $T - T_g$  as seen in Figure 36. The sensitivity to temperature always becomes dramatically greater as the  $T_g$  is approached from above. The same kind of curve is observed if we examine the variation of the viscosity of the polystyrenes with temperature, Figure 37. Though qualitatively the same as the  $a_T$  curve from the  $J_r(t)$  response, they represent different temperature dependences. These kinds of temperature dependence curves for glass-forming systems were first noted by M.L. Williams (32) to have the same functionality when plotted in the manner of Figure 36. Shortly after the "universal" Williams, Landel and Ferry, WLF, equation was proposed (33) and rationalized in terms of the fractional free volume concept of A. Doolittle. The WLF equation is

$$\log a_T = \frac{-C_1 (T - T_0)}{C_2 + T - T_0} \quad (8)$$

where  $T_0$  is any chosen reference temperature which can be  $T_g$ , and  $C_1$  and  $C_2$  are characterizing constants which can be related to free volume parameters. Williams, Landel and Ferry showed how, assuming volume temperature linearity, Equation (8) can be derived from the Doolittle equation

$$\eta = A e^{b/\phi_f} \quad (9)$$

where the relative free volume,  $\phi_f = v_f/v_0 = (v - v_0)/v_0$ . The volume is  $v$ , the occupied volume is  $v_0$  and the free volume,  $v_f$ , is their difference,  $v - v_0$ .  $A$  and  $b$  are characterizing constants. In addition they showed that an alternate form is, the Vogel (34) Tamman and Hess (36) Fulcher, (35) VFTH, equation

$$\eta = A \exp c/(T - T_\infty) \quad (10)$$

where  $A$ ,  $c$  and  $T_\infty$  are characterizing constants. Extrapolation of the metastable equilibrium volume-temperature line to  $T_\infty$  yields the operational occupied volume,  $v_0$  since this represents the hypothetical state of the supercooled liquid where the viscosity is infinite. In log form

$\log \eta = \log A + c/2.303 (T - T_{\infty})$   
 so that a plot of  $\log \eta$  versus  $1/(T - T_{\infty})$  should yield a straight line. Repeated guesses for  $T_{\infty}$  have to be made until all the data points lie on a straight line. If positive curvature results the guess for  $T_{\infty}$  was too low and negative curvature indicates that it was too high. A resulting sigmoidal shaped curve indicates that no fit is possible. Most all of the polymer rate data in the literature can be fitted to these expressions. The  $J_r(t)$  shift factor data from Figure 36 are replotted in Figure 38 according to the VFTH equation. The quality of fit to the form of the equation is easy to judge in this straight line representation. Within experimental uncertainty it can be seen that the recoverable compliances of polystyrenes with molecular weights from  $10^3$  to  $10^6$  have the same free volume dependence. A comparable plot for the viscosities of these same samples showed puzzling variations in form. However when the product  $\eta J_e$  was plotted accordingly the results seen in Figure 39 are obtained. Details are given in the legend. This product represents a characteristic time of the material and appears to be a more fundamental irreversible or rate process variable than the viscosity. The parallel lines shown in Figure 39 makes the same statement as the single line of Figure 38. The free volume parameters describing the temperature dependence of the two kinds of deformation, recoverable and non-recoverable, however, are different. (15)

If we finally examined the temperature of dependence of the recoverable compliance of the PMMA samples with differing tacticity we note that in spite of some of the striking differences in the form of their viscoelastic responses their dependence on temperature relative to corresponding state temperatures,  $T_0 \approx T_g$ , is identical; see Figure 40. The surprising fact is that their common form of temperature dependence is unique in the realm of high molecular weight polymers. It does not fit the free volume form over the entire temperature range of measurement. The dotted line in Figure 40 represents the best fit of the low temperature data to a WLF curve. Up to the present all of the other high polymer temperature dependence data can be fitted to the free volume expressions. The difference of the PMMA behavior at this time is not understood.

Nearly all of our data, comments and conclusions concerned polystyrene and polymethylmethacrylate, but there is ample reason to expect most of the conclusions to be applicable to a great many linear amorphous polymers.

#### References

- 1) A.J. Kovacs, R.A. Stratton and J.D. Ferry, *J. Phys. Chem.*, 67, 152 (1963).
- 2) D.J. Plazek and J.H. Magill, *J. Chem. Phys.* 45, 3038 (1966).
- 3) P.E. Rouse, Jr., *J. Chem. Phys.* 21, 1272 (1953).
- 4) H. Leaderman, *Textile Res. J.*, 11, 171 (1941).
- 5) A.V. Tobolsky and R.D. Andrews, *J. Chem. Phys.*, 13, 3 (1945).
- 6) J.D. Ferry, *J. Am. Chem. Soc.*, 72, 3746 (1950).
- 7) J.D. Ferry, *Viscoelastic Properties of Polymers*, 2nd ed., Wiley, New York, 1970.
- 8) D.J. Plazek and A.J. Chelko, Jr., *Polymer*, 18, 15 (1977).
- 9) D.J. Plazek and P.K. Agarwal, *Proc. VII Internat. Cong. on Rheology, Gothenburg, Sweden*, p. 488, 1976.
- 10) E.N. da C. Andrade, *Proc. Roy. Soc. (London)* A84, 1 (1910).
- 11a) D.J. Plazek, *J. Colloid Sci.*, 15, 50 (1960).
- 11b) D.J. Plazek, *Polymer J.* 12, 43 (1980).
- 12) A.V. Tobolsky, J.J. Aklonis, and G. Akovali, *J. Chem. Phys.*, 42, 723 (1965).
- 13) J.D. Ferry, R.F. Landel, M.L. Williams, *J. Appl. Phys.*, 26, 359 (1955).
- 14) P.J. Flory, *Principles of Polymer Chemistry*, Cornell University Press, Ithaca, N.Y., 1953.
- 15) D.J. Plazek and V.M. O'Rourke, *J. Polymer Sci.*, A-2, 9, 209 (1971).
- 16) G.C. Berry and T.C. Fox, *Adv. Polymer Sci.* 5, 261 (1968).
- 17) E. Riande, H. Markovitz, D.J. Plazek, and N. Raghupathi, *J. Polymer Sci. Symp.* 50, 405 (1975).
- 18) G. Braun and A.J. Kovacs, *Proc Conf. on Physics of Non-Crystalline Solids*, J.A. Prins, Ed. North Holland, Amsterdam, 1965, p. 303.
- 19) S. Kusamizu, L.A. Holmes, A.A. Moore, and J.D. Ferry, *Trans. Soc. Rheol.* 12:4, 559 (1968).
- 20) L.A. Holmes and J.D. Ferry, *J. Polymer Sci. Part C*, 23, 291 (1968).
- 21) N. Raghupathi, Ph.D thesis, University of Pittsburgh, 1975.
- 22) T.G. Fox and P.J. Flory, *J. Am. Chem. Soc.* 55, 221 (1951).

- 23) F.E. Karasz, H.E. Bair and J.M. O'Reilly, *J. Phys. Chem.*, 69, 2657 (1965).
- 24) J.K. Gillham and S.J. Stadnicki, *Polymer Preprints*, 15, 562 (1974).
- 25) W.G. Gall and N.G. McCrum, *J. Polymer Sci.*, 50, 489 (1961).
- 26) J. Heijboer, In Physics of Non-Crystalline Solids, North Holland, Amsterdam, p. 231 (1965).
- 27) D.J. Plazek, V. Tan and V.M. O'Rourke, *Rheol. Acta.*, 13, 367 (1974).
- 28) D.J. Plazek and N. Raghupathi, *Polymer Preprints*, 15, 53 (1974).
- 29) T.G. Fox, T. Altares, Jr., K.G. Mayhan, and S.P.S. Yen, Technical Documentary Report No. ML-TDR-64-286, Part III (1966), From Mellon Institute, Pittsburgh, PA. 15213, to Air Force Materials Lab., Wright Patterson Air Force Base, OH 45433.
- 30) G.P. Mikhailov and T.I. Borisova, *Polymer Sci. USSR*, 2 387 (1961).
- 31) D.J. Plazek, W. Dannhauser, and J.D. Ferry, *J. Colloid Sci.*, 16, 101 (1961).
- 32) M.L. Williams, *J. Phys. Chem.*, 59, 95 (1955).
- 33) M.L. Williams, R.F. Landel, and J.D. Ferry, *J. Am. Chem. Soc.*, 77, 3701 (1955).
- 34) H. Vogel, *Physik, Z.*, 22, 645 (1921).
- 35) G.S. Fulcher, *J. Amer. Chem. Soc.*, 8, 339 (1925).
- 36) G. Tamman and G. Hesse, *Z. anorg. allg. Chem.*, 156, 245 (1926).
- 37) H. Odani, N. Nemoto, and M. Kurata, *Bull. Inst. Chem. Res., Kyoto University*, 50, 117 (1972).
- 38) Y. Einaga, K. Osaki, M. Kurata, and M. Tamura, *Macromolecules*, 4, 87 (1971).

#### ACKNOWLEDGEMENT

The financial support of the National Science Foundation under the Polymer Program Grant DMR76-09804 and the Chemical Process Program CPE80-24713 is appreciated and acknowledged.

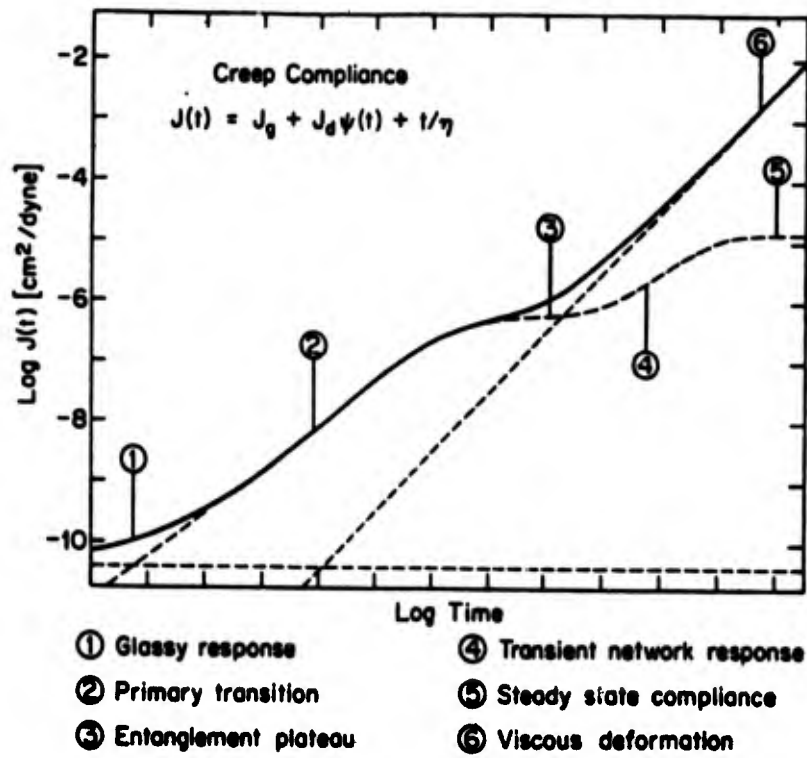


Figure 1. Schematic creep compliance curve,  $J(t)$ ,  $\text{cm}^2/\text{dyne}$  or  $\text{m}^2/\text{N}$ , as described in text.

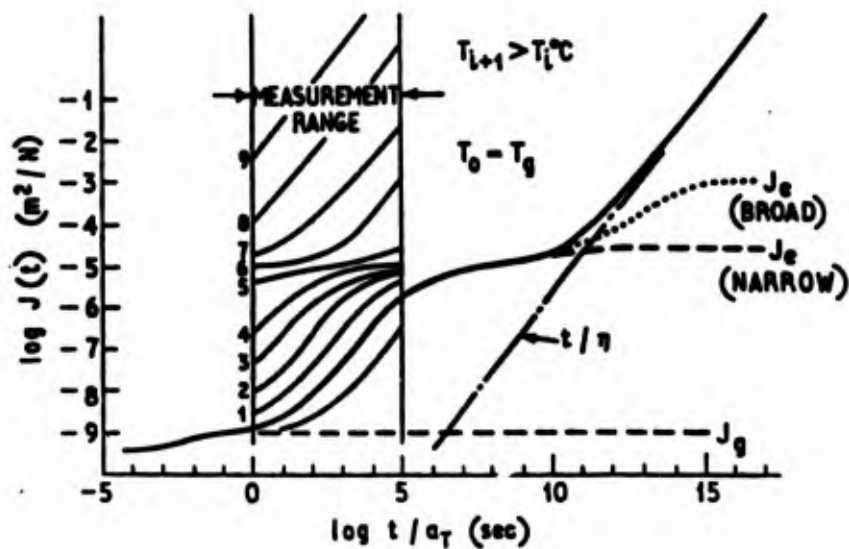


Figure 2. Schematic creep and recovery curve illustrating the temperature reduction process and the extent of recovery found for polymers with narrow and approximately random molecular weight distributions.

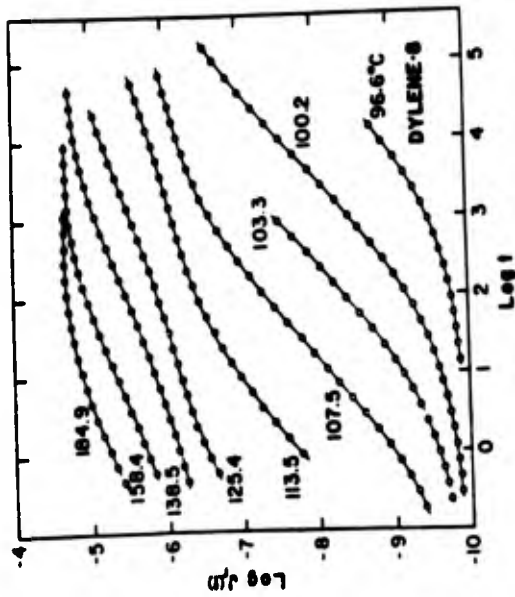


Figure 3. Logarithmic plots of the measured recoverable compliance,  $J_r(t)$ ,  $\text{cm}^2/\text{dyne}$  versus time,  $t$ , second, for a commercial polystyrene with  $M_n = 93,000$  and  $M_w = 220,000$  at the indicated temperatures.

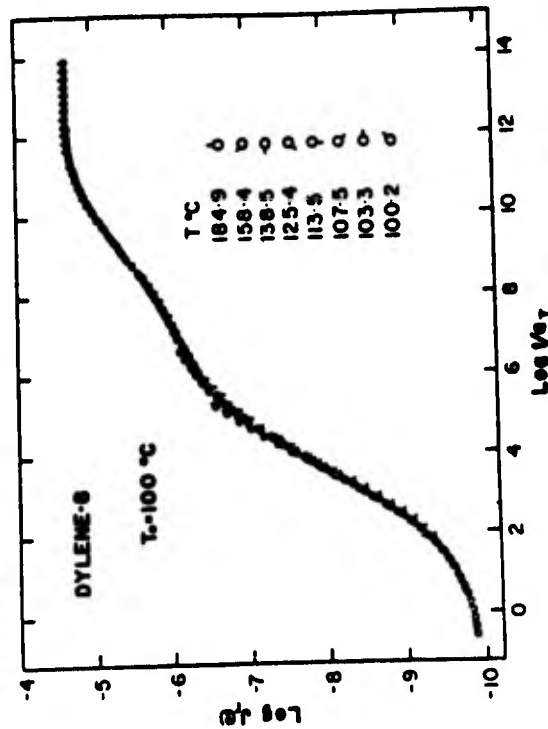


Figure 5. Logarithmic reduced recoverable compliance curve for the Dylene-8 sample;  $a_T$  is the shift factor for the recoverable compliance. Reference temperature  $T_0 = 100^\circ\text{C}$ .

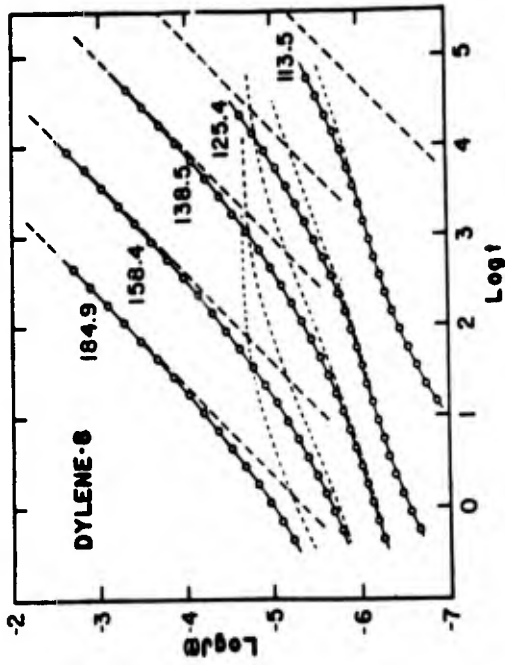


Figure 4.

Logarithmic plot of creep compliance,  $\text{cm}^2/\text{dyne}$ , versus time, second for Dylene-8 at the indicated temperatures in degree centigrade. Short dash lines are recovery curves, long dash lines represent the viscous contribution to the creep compliance.

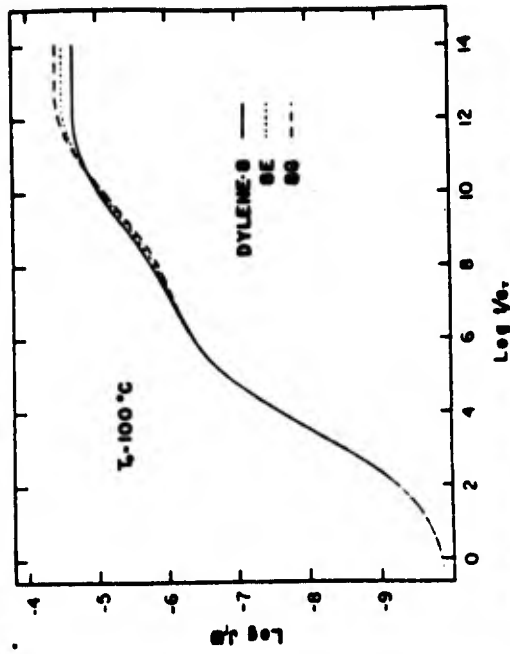


Figure 6.

Comparison of the reduced recovery curves of Dylene samples at the reference temperature,  $100^\circ\text{C}$ .  $J_r(t)$  -  $\text{cm}^2/\text{dyne}$ ,  $t/a_T$  in seconds. Molecular weights of 8, 8E and 8G are given in the text. Dylene 8 is normally used for injection molding, 8E, for extrusion and 8G for biaxially oriented film.

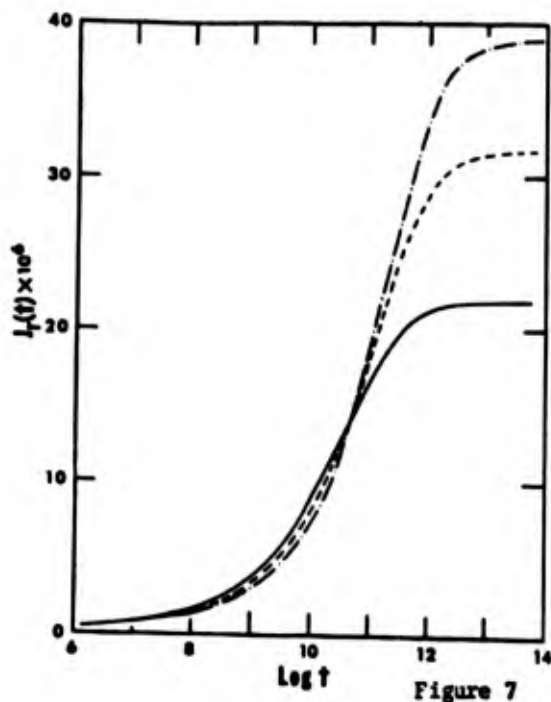


Figure 7

Plots of reduced recoverable compliance versus reduced log time of Dylene samples. Reference temperature  $T_0 = 100^\circ\text{C}$ . The curves are identified by the key in Figure 6; 8G has the highest molecular weight and the highest steady state compliance.

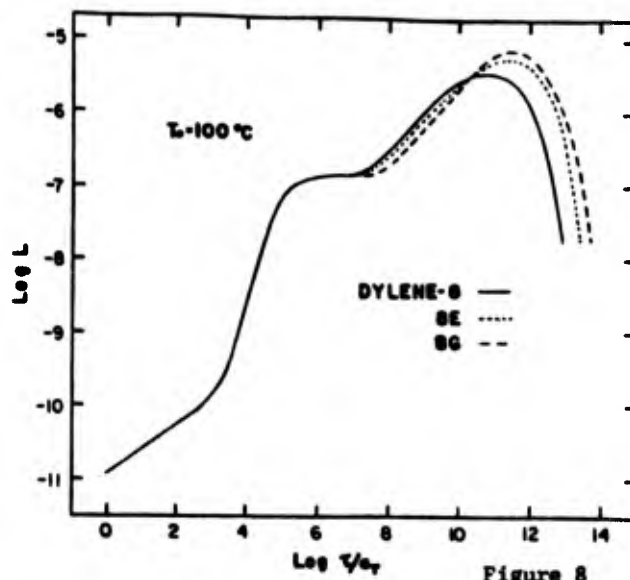


Figure 8

Comparison of the retardation spectra (logarithmic plot,  $L$  in  $\text{cm}^2/\text{dyne}$ ,  $\tau/a_T$  in sec.) of Dylene samples at the reference temperature of  $100^\circ\text{C}$ .

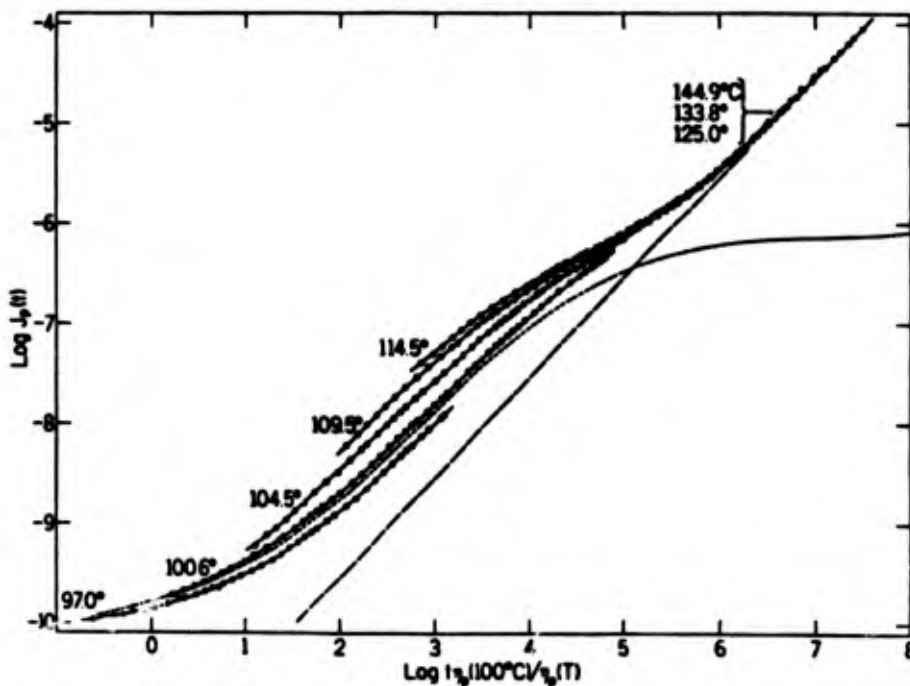


Figure 9.

Logarithmic plot of creep compliance,  $J_p(t)$  against reduced time scale  $t/a_T$ ,  $a_T = \eta_p(T)/\eta_p(T_0)$ ,  $T_0 = 100^\circ\text{C}$ . Failure of temperature reduction is indicated. Long-dashed line is the  $100^\circ$   $t/\eta$  contribution. Short-dashed line is the reduced recoverable compliance curve.



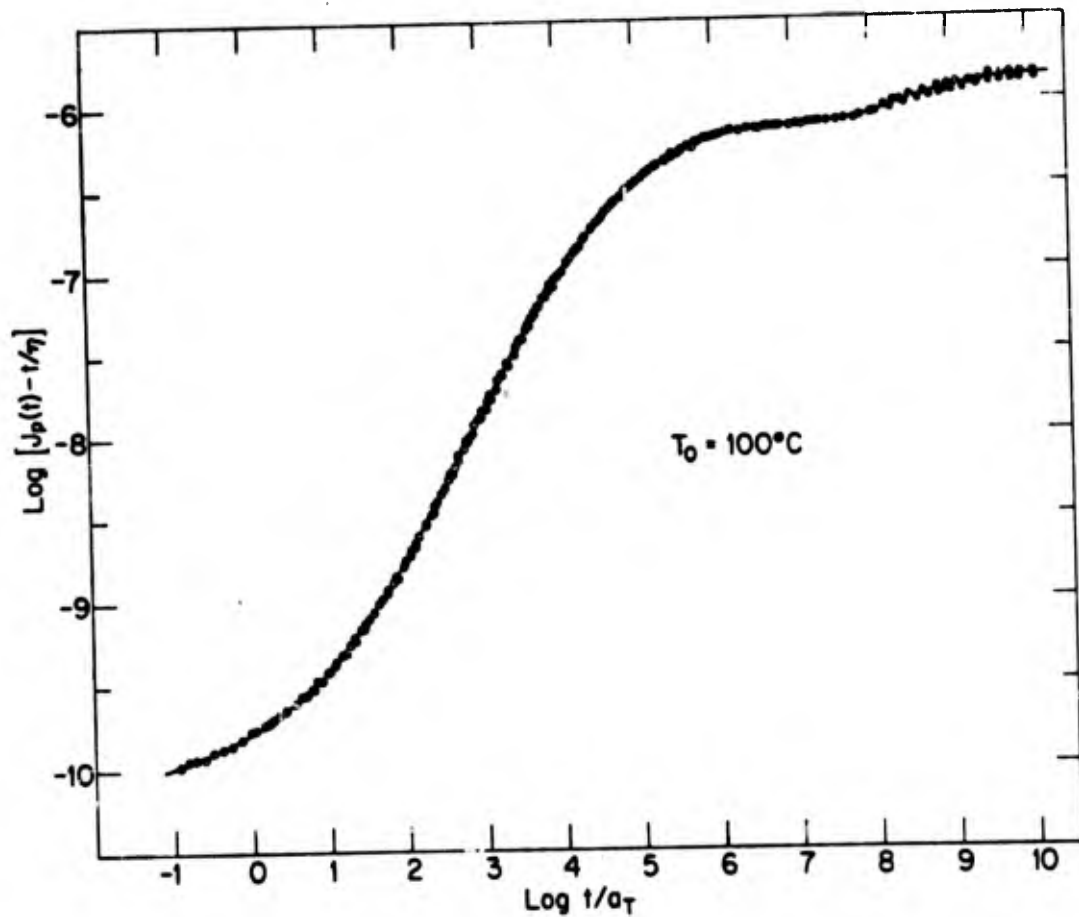


Figure 10

Logarithmic plot of recoverable compliance,  $J_r(t) = J_p(t) - t/\eta$ , against reduced time,  $t/a_T$ , reduced to  $100^\circ$ . The dispersion observed at reduced times greater than  $10^8$  sec is believed to be due to the presence of a high molecular weight tail in the sample and does not represent the behavior of the

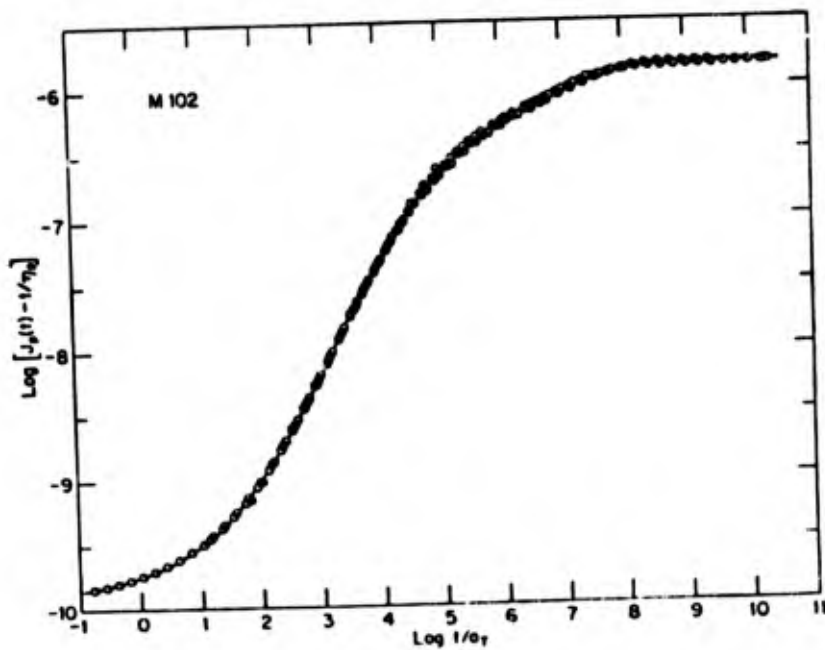


Figure 11.

Logarithm of reduced recoverable compliance of M-102 (mol wt. = 94,000) presented as a function of reduced time.  $T_0 = 100^\circ\text{C}$ . Temperatures of measurement are:  $97.9^\circ$ ,  $\odot$ ;  $102.9^\circ$ ,  $\ominus$ ;  $105.7^\circ$ ,  $\odot$ ;  $109.4^\circ$ ,  $\odot$ ;  $113.4^\circ$ ,  $\odot$ ;  $119.4^\circ$ ,  $\ominus$ ; and  $134.1^\circ\text{C}$ ,  $\odot$ .

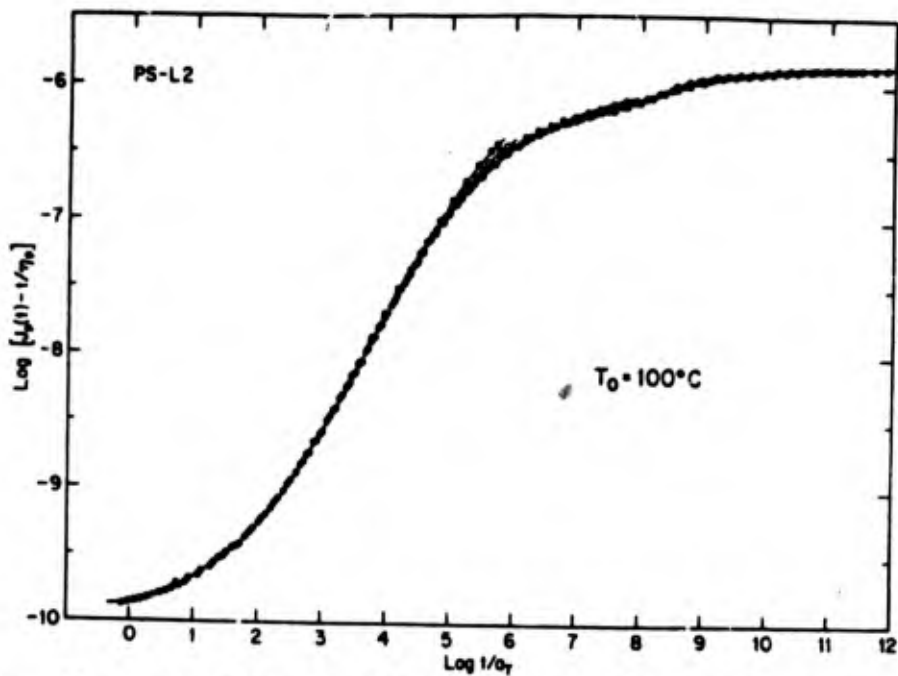


Figure 12. Logarithmic plot of  $J_p(t) - t/\eta_0$  of L-2 versus reduced time,  $t/a_T$ . Temperature of reduction  $T_0 = 100^\circ\text{C}$ . Temperatures of measurement are:  $100.7^\circ, \odot$ ;  $102.9^\circ, \ominus$ ;  $105.1^\circ, \odot$ ;  $109.4^\circ, \odot$ ;  $113.7^\circ, \odot$ ;  $116.0^\circ, \odot$ ;  $119.7^\circ, \odot$ ;  $144.9^\circ, \odot$ ;  $160.3^\circ, \otimes$ .

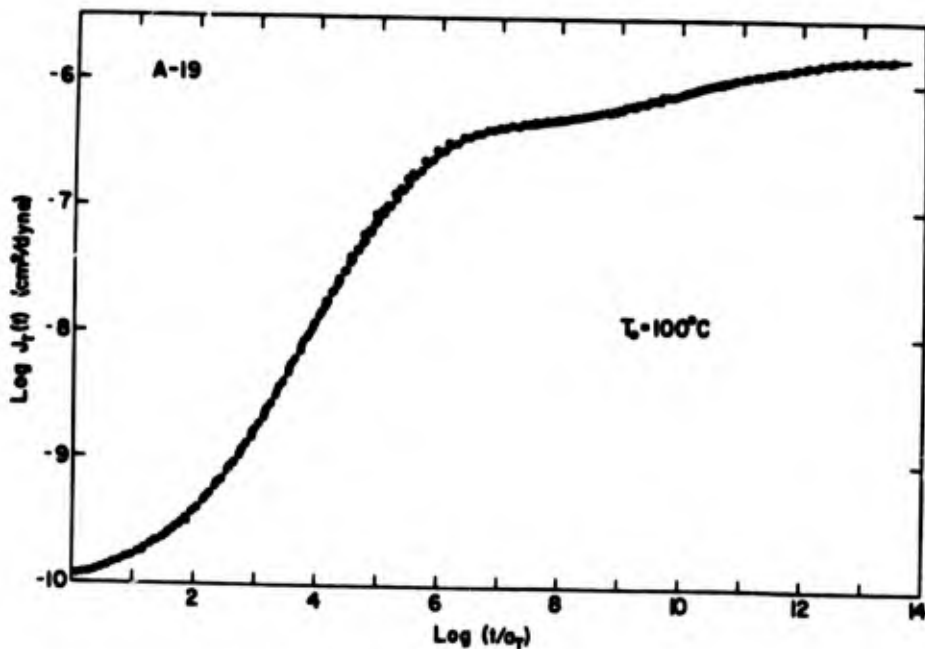
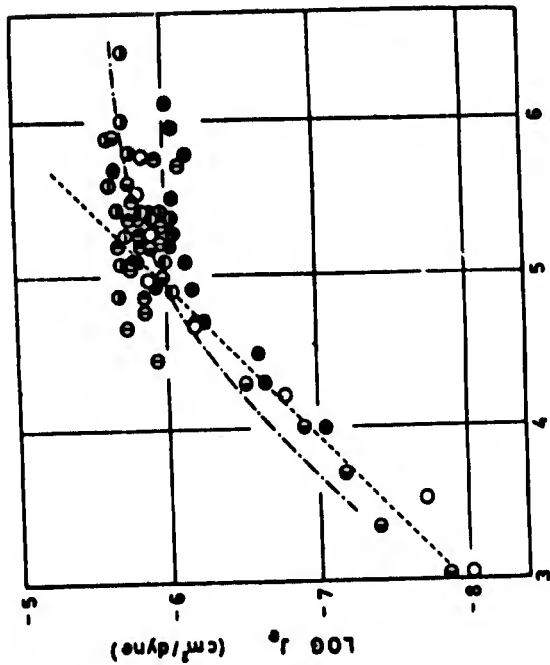


Figure 13.  $\text{Log } J_r(t)$  versus  $\text{Log } t/a_T$  for A-19 ( $M_v = 600,000$ ). Reduction reference temperature  $T_T = 100^\circ\text{C}$ . Temperatures of measurement are:  $100.6^\circ, \odot$ ;  $103.0^\circ, \ominus$ ;  $105.0^\circ, \ominus$ ;  $109.4^\circ, \odot$ ;  $112.4^\circ, \odot$ ;  $119.4^\circ, \odot$ ;  $144.6^\circ, \ominus$ ;  $160.0^\circ, \odot$ ;  $180.0^\circ, \odot$ .



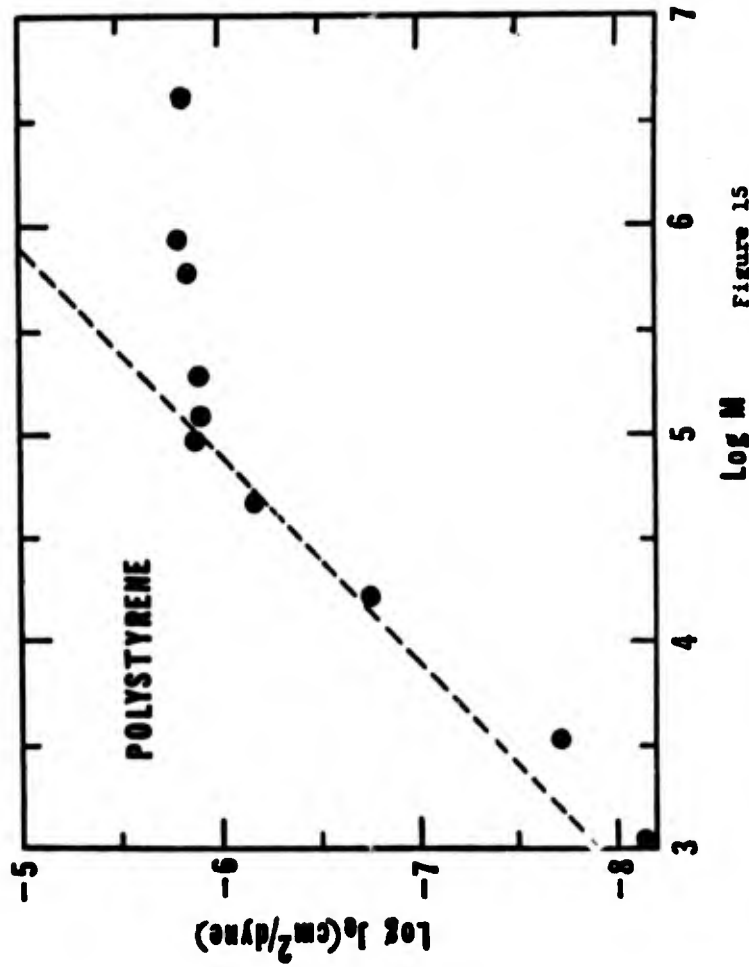
LOG  $M_w$

The logarithmic plot of  $J_e$  at 160°C against  $M_w$  for polystyrene.

- Plazek-O'Rourke;
- O'Reilly-Prest;
- ⊖ Tobolsky et al;
- ⊕ Akovali;
- ⊙ Mieras-Rijn. The dotted and the chain lines represents the Rouse prediction and the Graessley-Segal equation, respectively.
- Mills-Nevin
- ⊙ Murakami et al.
- ⊖ Nemoto;
- ⊙ Onogi et al.

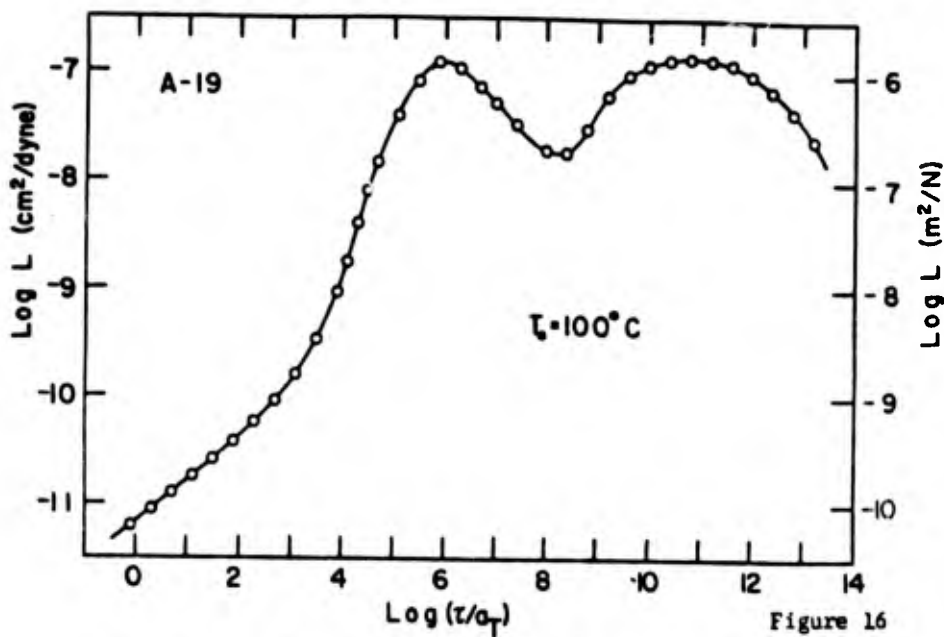
FIGURE 14

Literature values for the steady state recoverable compliance of narrow molecular weight distribution polystyrenes of differing molecular weights; taken from reference 37.



Log M Figure 15

Polystyrene steady state recoverable compliance,  $J_e$ , values presented as a logarithmic function of molecular weight; values from references 15 and 17.



The retardation spectrum for polystyrene A-19 ( $M_v = 600,000$ ) plotted as a function of the reduced retardation time. The reference temperature,  $T_0 = 100^\circ\text{C}$ .

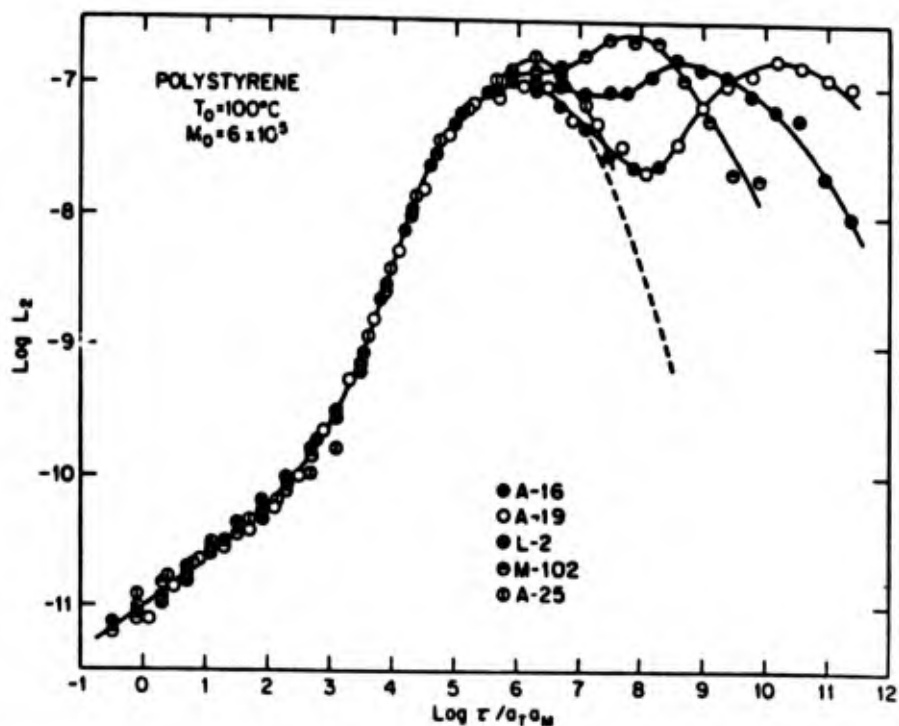


Figure 17. Second approximation values of the retardation spectra for polystyrene samples A-25,  $M_v = 47,000$ ; M102,  $M_v = 94,000$ ; L-2,  $M_v = 189,000$ ; A-19,  $M_v = 600,000$ ; and A-16,  $M_v = 800,000$  plotted logarithmically against the reduced time scale where  $a_T$  is the temperature reduction factor and  $a_M$  is the effective number average molecular weight factor which reflects differences in  $T_g$ . The reference temperature,  $T_0 = 100^\circ\text{C}$  and the reference molecular weight is  $6.0 \times 10^5$ .

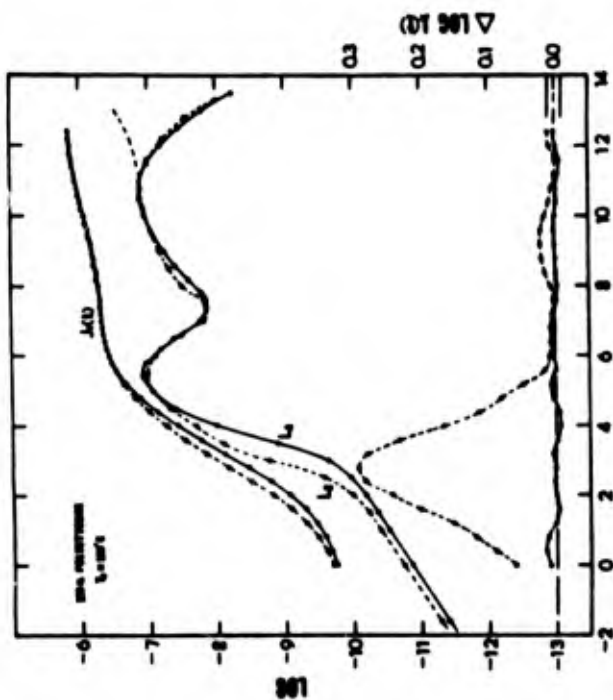


Figure 18

Composite logarithmic plot of recoverable compliance and spectrum of undiluted polystyrene, PC-6a. Points read from reduced experimental curve. Dashed and solid lines calculated from  $L_2$  and  $L_A$ , respectively. Logarithm of second approximation to retardation spectrum,  $L_2$ , open circles, and accepted spectrum,  $L_A$ , solid circles, plotted against the logarithm of reduced retardation time,  $\tau/a_T$ . At bottom, difference curves of the logarithms of the measured and calculated compliances which are shown above. Open circles calculated with  $L_2$  and solid circles with  $L_A$ . The dashed line segment at long times for  $L_2$  reflects the weak polydispersity dispersion which has been eliminated in most of the analysis.  $T_0=100^\circ\text{C}$ .

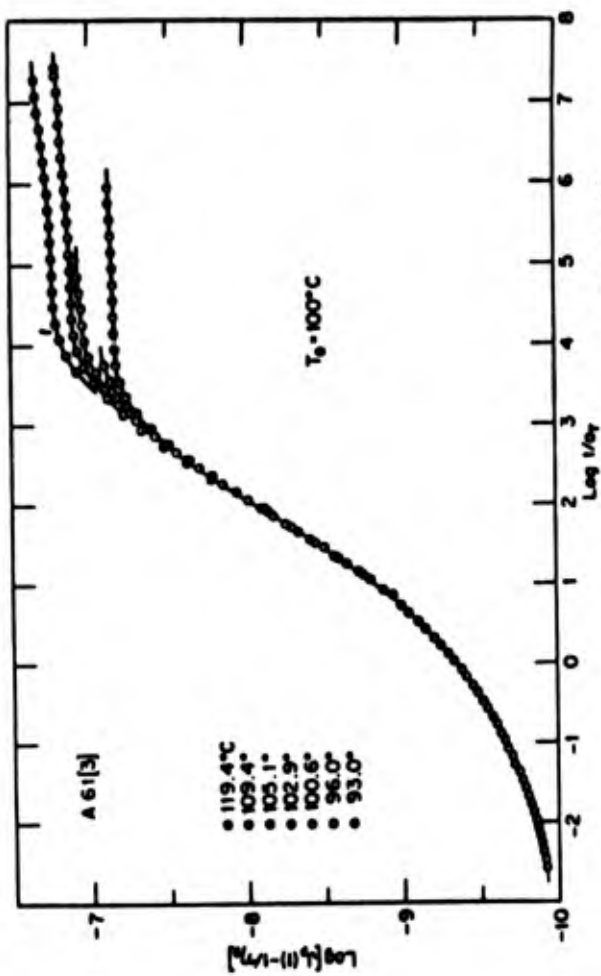


Figure 19

Plots of the recoverable compliance curves against the logarithm of the reduced time,  $t/a_T$  (sec). Temperature-dependent horizontal shift factors,  $a_T$ , relative to  $100^\circ\text{C}$ , have been empirically determined to give best superposition below knees of curves.

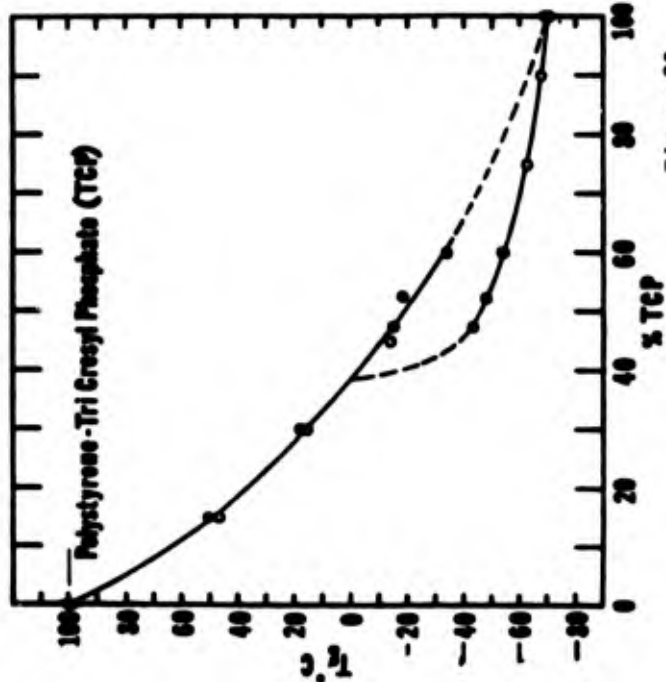


Figure 20

Concentration dependence of glass temperature of solutions of polystyrene, PC-6a, in m-tricresyl phosphate. Solid circles are DTA results. Other points by DSC and dilatometry. Plotted temperatures are corrected to be equivalent to dilatometric determination.

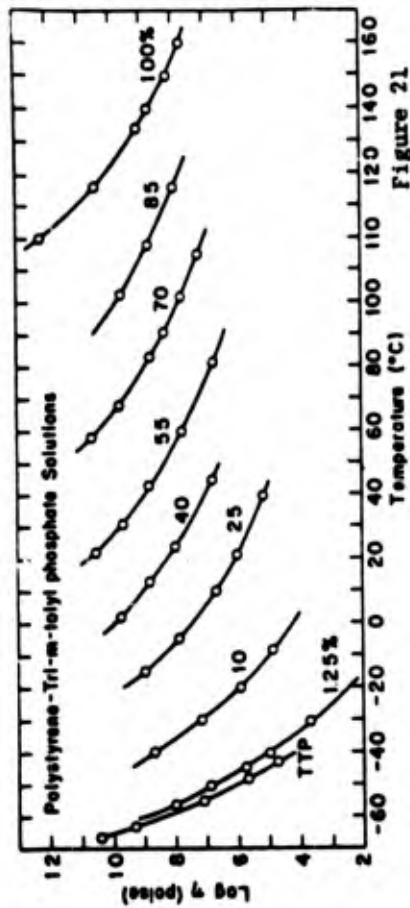


Figure 21

Logarithm of the viscosity plotted against temperature for polystyrene, PC-6a, TCP, and seven solutions. Concentrations are indicated in weight %.

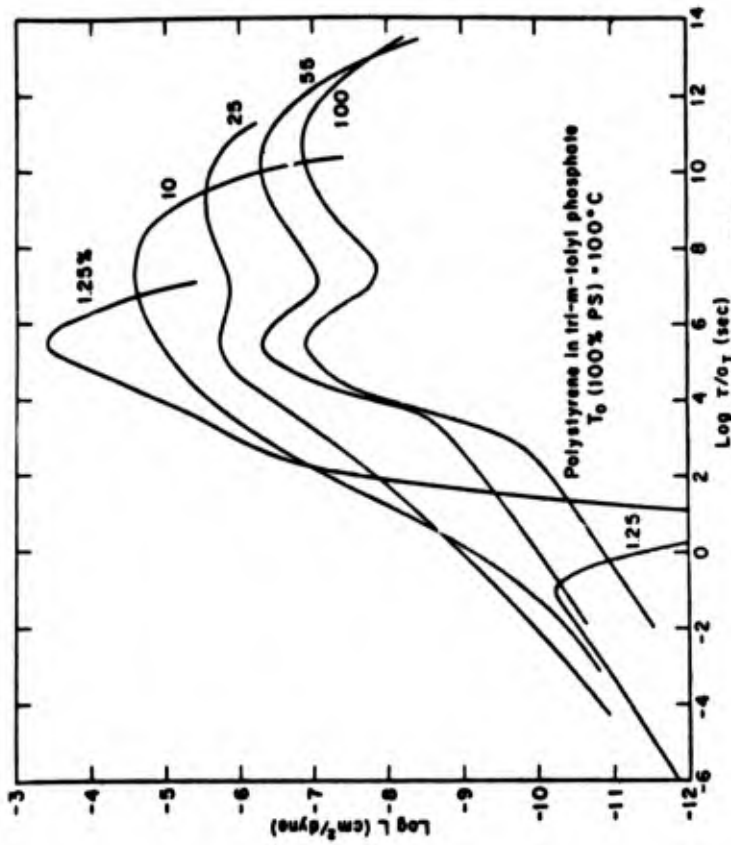


Figure 22

Comparison plot of retardation spectra with all solutions having a common time at the peak of primary dispersion as a corresponding state criterion. The pure polymer at 100°C is used as standard state and reference temperatures  $T_0$  for the solutions are chosen accordingly.

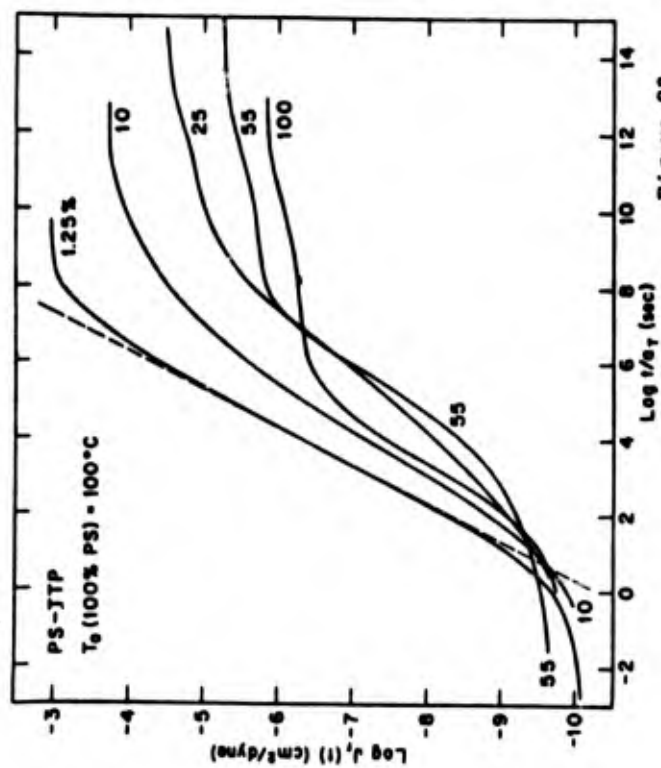


Figure 23

Corresponding state plot of reduced recoverable compliance curves for undiluted polymer and 4 solutions (according to the Andrade creep criterion, i.e. matching the glassy level Andrade creep regions). Dashed line is drawn with a slope of one.

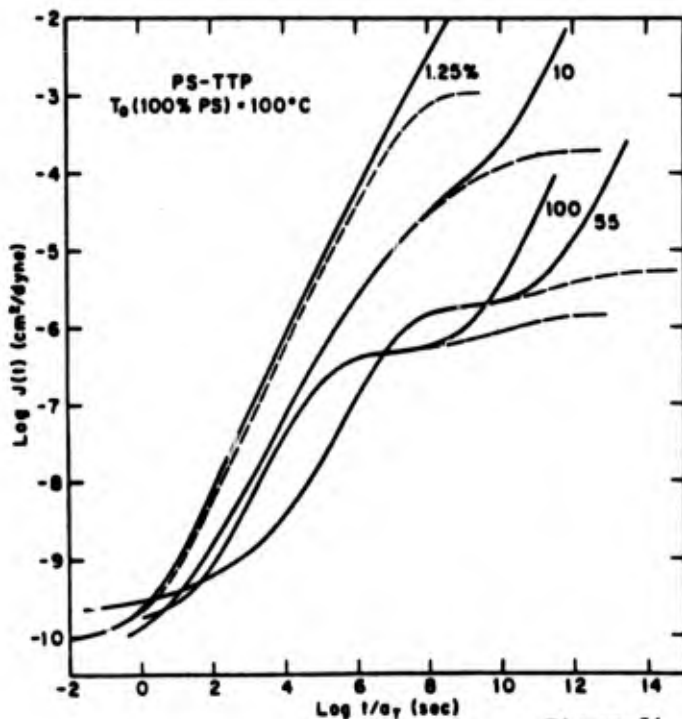


Figure 24

Corresponding state plot of reduced creep compliance,  $J(t)$ , of polystyrene, PC-6a, and 3 solutions (according to the Andrade creep criterion). Dashed lines are recoverable compliance curves.

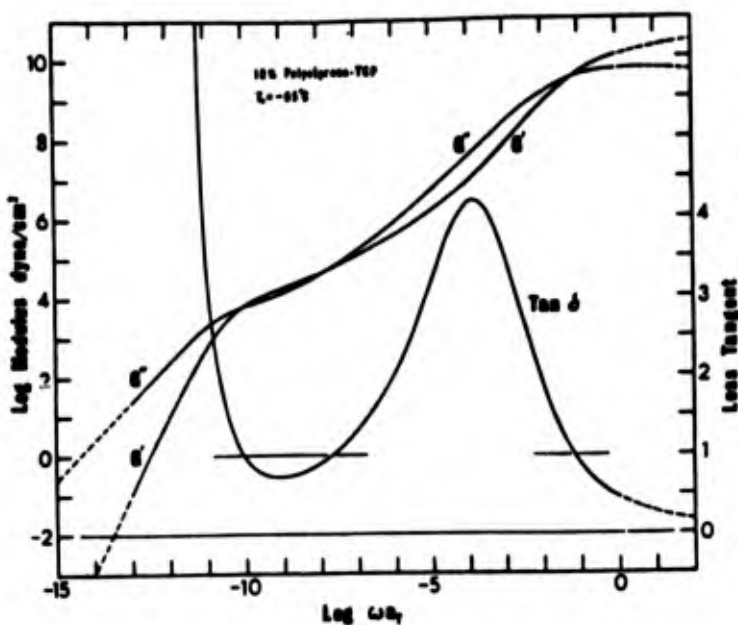


Figure 25. Logarithmic plots of the real,  $G'$ , and the imaginary,  $G''$  components of the complex dynamic shear modulus,  $G^*$ , for a 10% solution of polystyrene, PC-6a ( $M_v = 860,000$ ) against the reduced frequency scale, Reference temperature,  $T_0 = -65^\circ\text{C}$ . The corresponding loss tangent curve is presented linearly as a function of  $\log \omega a_T$ .

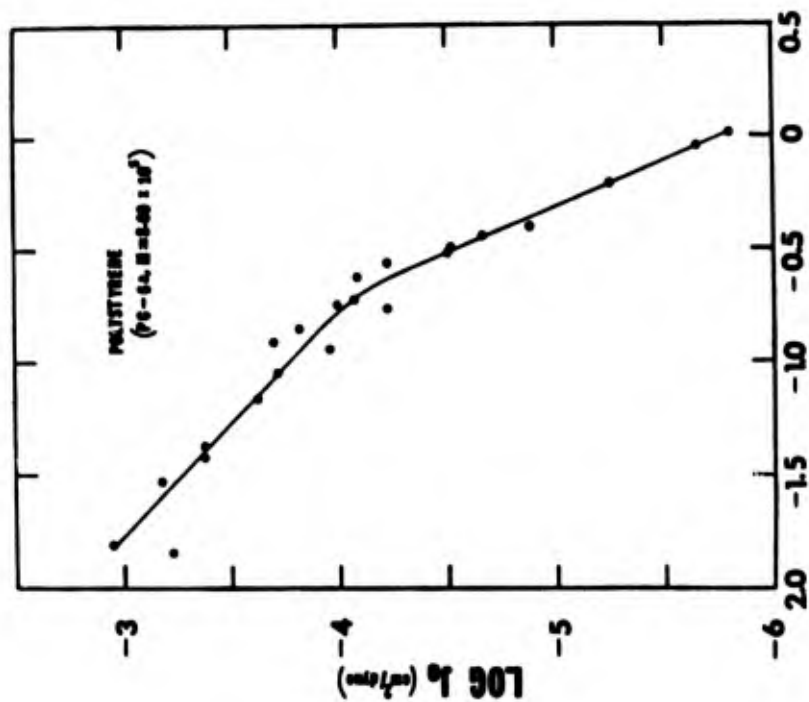


Figure 26

Logarithmic plot of steady-state recoverable compliance,  $J_e$ , as a function of concentration, g/cm<sup>3</sup>. ●, reference 17; ○, reference 20; ○, reference 19; ○, reference 38.

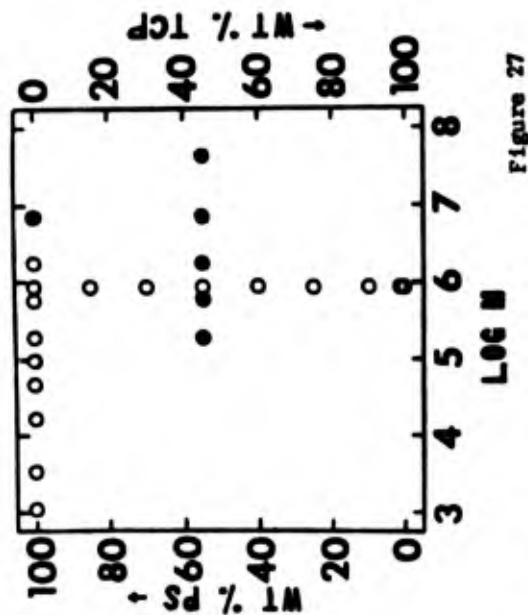


Figure 27

Diagram indicating the extent to which the system polystyrene-TCP has been studied in references 15, 17, and 21.

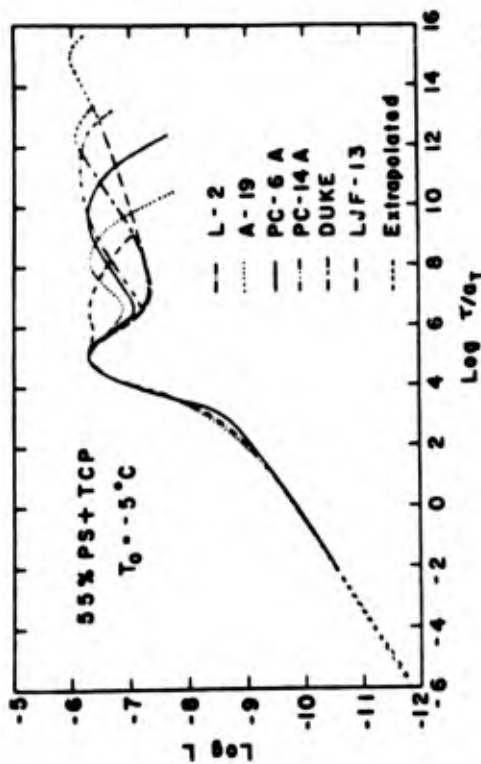


Figure 28

Comparison of retardation spectra (logarithmic plot,  $L$  in cm<sup>2</sup>/dyne,  $\tau/a^2$  in sec), of solutions of polystyrene. Molecular weights of samples are as follows: L-2,  $1.89 \times 10^5$ ; A-19,  $6.0 \times 10^5$ ; PC-6a,  $8.60 \times 10^5$ ; PC-14a,  $1.80 \times 10^6$ ; DUKE,  $7.1 \times 10^6$ ; LJF-13,  $43.7 \times 10^6$ . Reference solution is PC-6a.



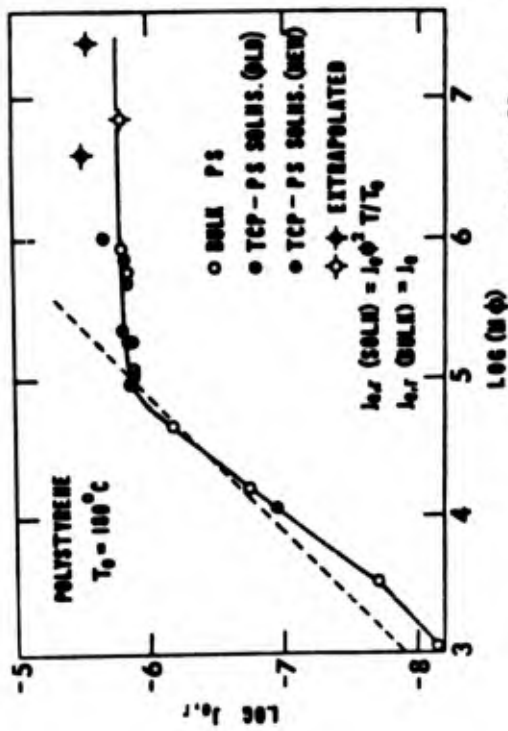


Figure 29

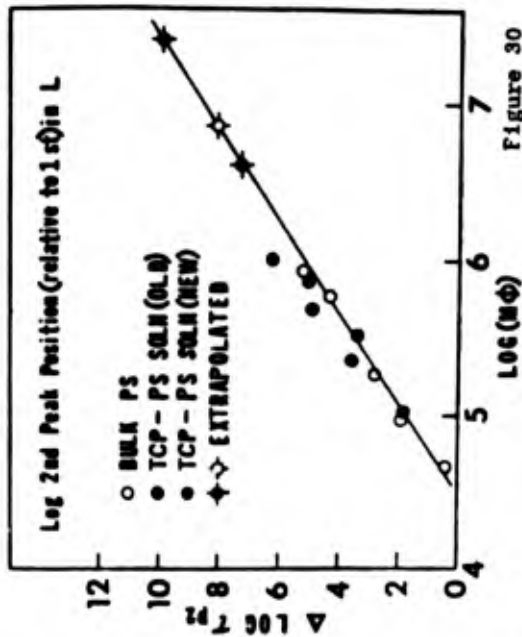


Figure 30

Logarithmic plot of the reduced recoverable compliance,  $J_e'$  ( $\text{cm}^2/\text{dy}$ ) vs. the product  $\phi'$  ( $M\phi$ ).  $\phi$  is the volume fraction of the polymer.  $\circ$  reference (15),  $\bullet$  Reference (21),  $\diamond$  Reference (17). The dotted line indicates the Rouse prediction.

Logarithmic plot of the second peak position relative to 1st on time scale in L vs. ( $M\phi$ ) product ( $\phi$  is volume fraction) for polystyrene system.

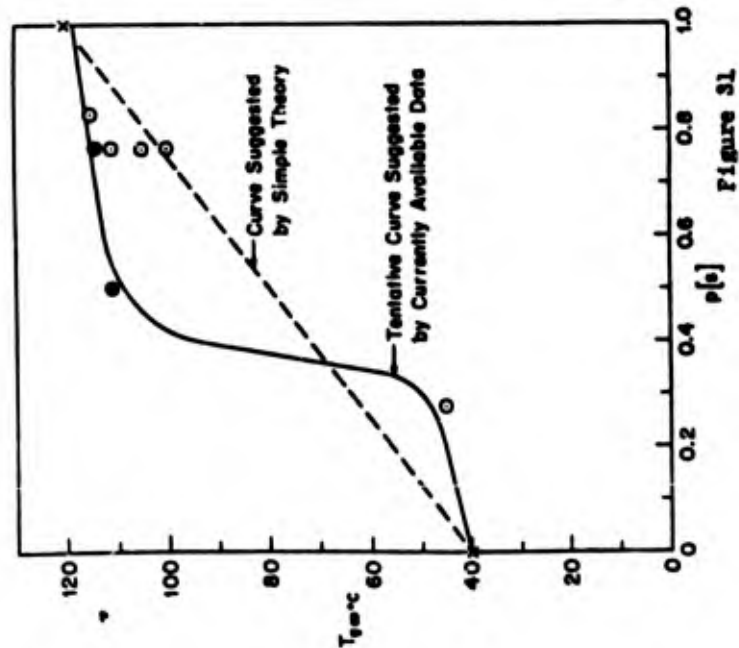


Figure 31

The glass temperature,  $T_g$ , of polymethylmethacrylate, PMMA, shown as a function of the fraction of syndiotactic pair placements. From reference (29). The  $\infty$  subscript indicates the high molecular weight asymptote value.

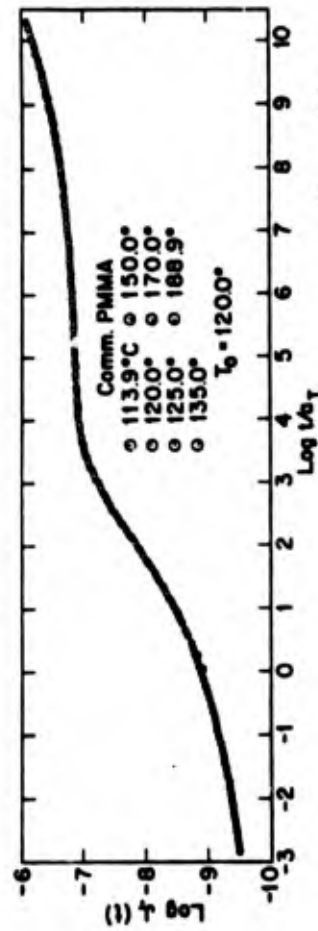
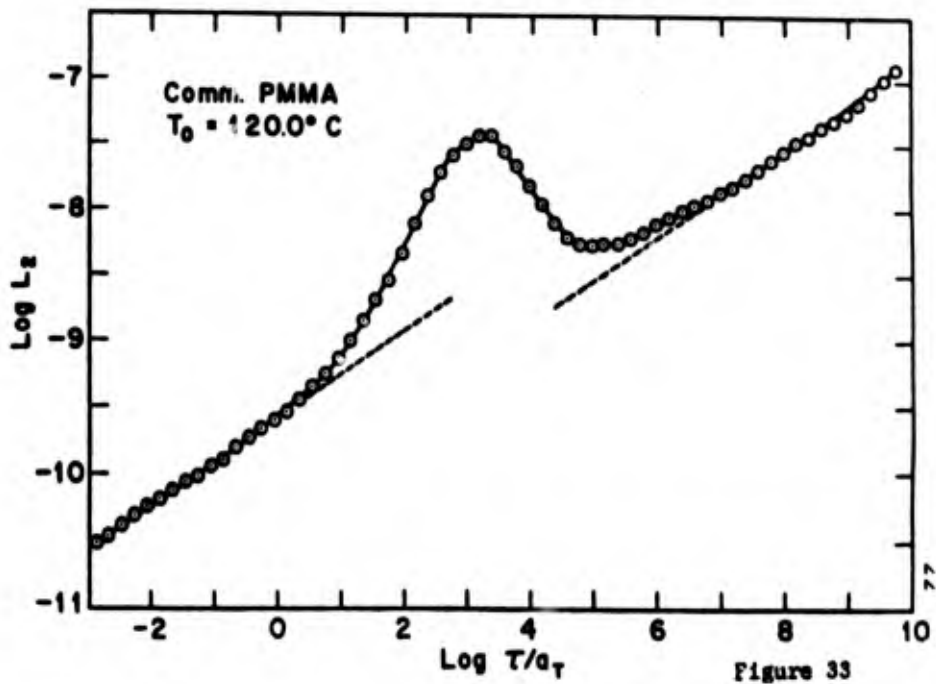
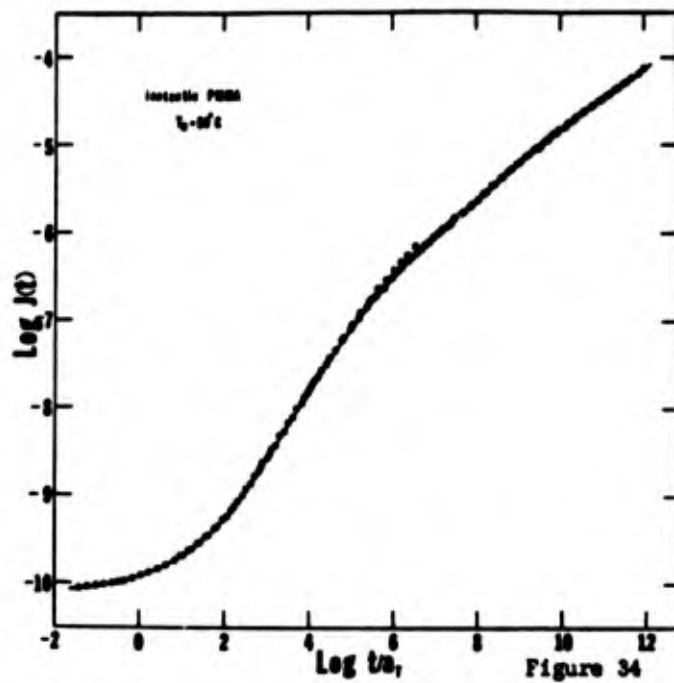


Figure 32

The logarithm of the reduced recoverable creep compliance  $J_r(t)$  of commercial PMMA plotted as a function of the logarithmic reduced time scale. Reference reduction temperature,  $T_0 = 120^\circ\text{C}$ .



Second approximation to the retardation spectrum (distribution function of retardation times) of a commercial sample of polymethylmethacrylate, ( $M_v = 760,000$ ) shown versus the reduced retardation time. The reference temperature,  $T_0 = 120^\circ\text{C}$ .



The shear creep compliance of isotactic polymethylmethacrylate ( $M_v = 610,000$ ) presented as a function of reduced time. The reference temperature,  $T_0 = 50^\circ\text{C}$

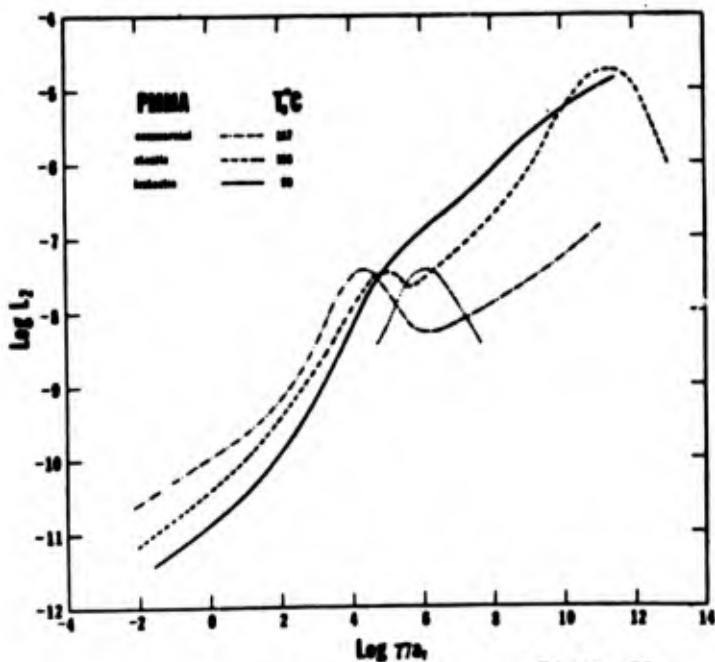


Figure 35

Second approximation to the retardation spectra of three PMMA samples of differing stereoregularity plotted as a function of reduced retardation time at their respective corresponding state temperatures. Corresponding states determined with their temperature dependence curves.

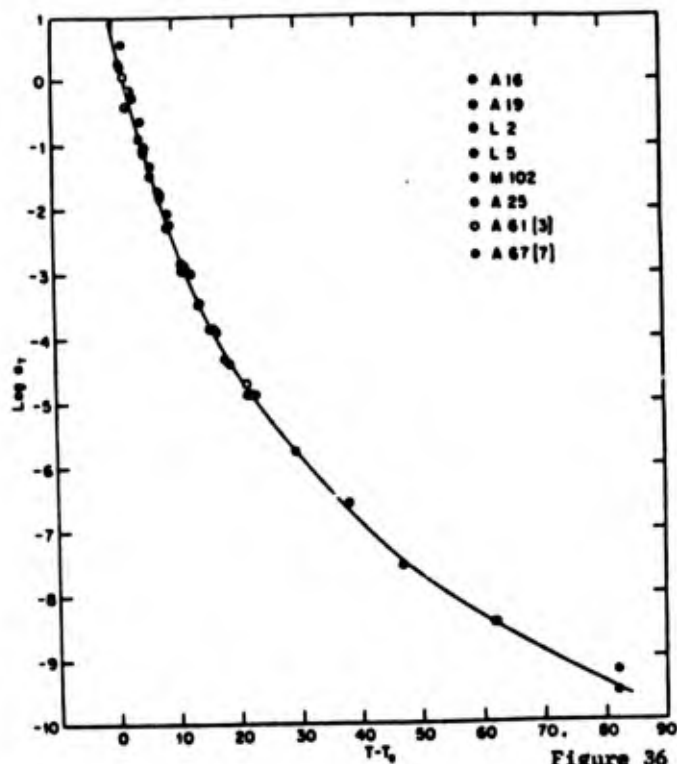


Figure 36

Temperature dependence shift factors obtained from  $J_r(t)$  curves of the polystyrene samples A67,  $M_v = 1100$ ; A61,  $M_v = 16,000$ ; A25,  $M_v = 47,000$ ; M102,  $M_v = 94,000$ ; L5, 122,000; L-2, 190,000; A19, 6000,000; A16, 800,000 presented as a function of the temperature difference  $T - T_g$ . The reference temperature  $T_0$  in each case is  $T_g$ .

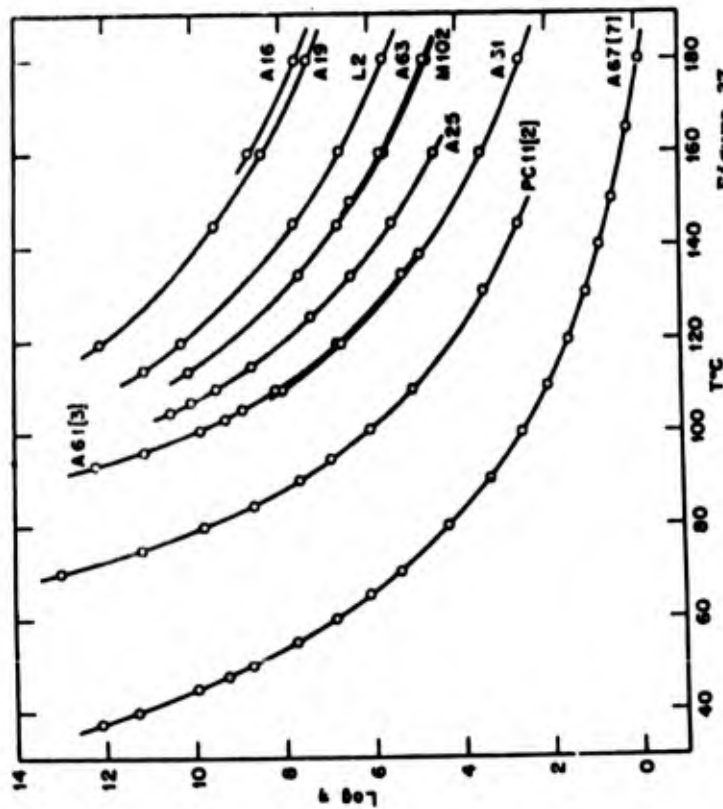


Figure 37

Plots of the logarithm of the viscosity  $\eta$  (poise) vs. temperature  $T$ . Molecular weights of indicated samples are as follows: A-67 [7] -- 1100; PC-11[2] -- 3300; A-61 -- 15,700; A-61[3] -- 16,400; A-58 -- 20000; A-25[4-6] -- 47000; M-102 -- 94000; A-63 -- 104000; L-5[5,8] -- 122000; L-2 -- 190000; A-19[7-12] -- 600,000; A-16[5] -- 800000.

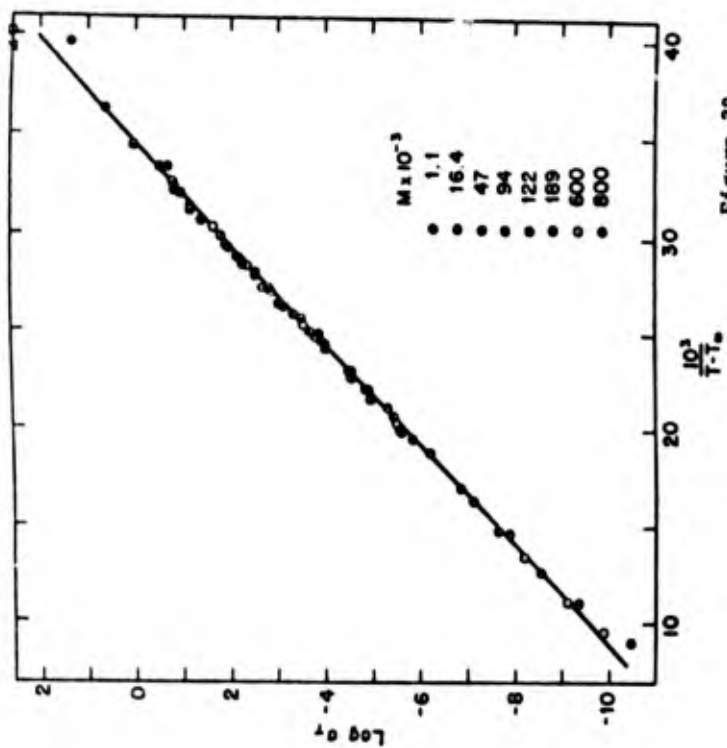


Figure 38

Recoverable compliance shift factors  $a_T$  plotted semilogarithmically against  $10^3/(T-T_g)$  for samples of indicated molecular weight. For each sample the reference temperature for reduction is  $T_g$  so that  $a_T = 0$  at  $T = T_g$ . Equation of line is:  $\log a_T = -13.46 + 389/(T-T_g)$ .

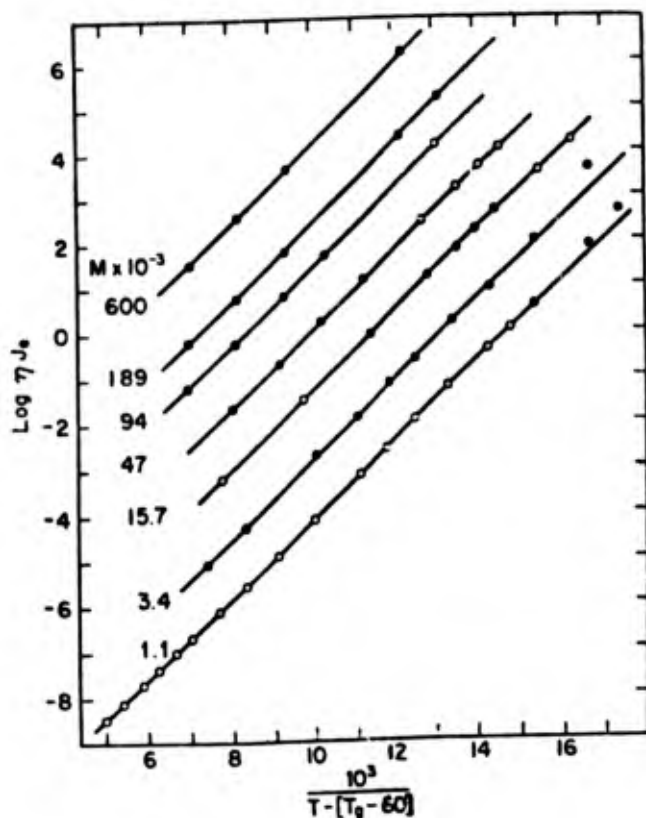


Figure 39. Semilogarithmic plots of the product of the viscosity of  $\eta$  (poise) and the equilibrium recoverable compliance  $J_e$  ( $\text{cm}^2/\text{dyne}$ ) against the reciprocal of the temperature,  $T - [T_g - 60^\circ\text{C}]$ . Viscosities for all plotted points were measured. (●)  $J_e$  measured, (⊗)  $J_e$  extrapolated or interpolated from creep data; (○) extrapolations to permit calculations of  $J_e$ . Molecular weights of samples are shown. The line for  $M = 1100$  has been drawn parallel to that for  $M = 3400$ .

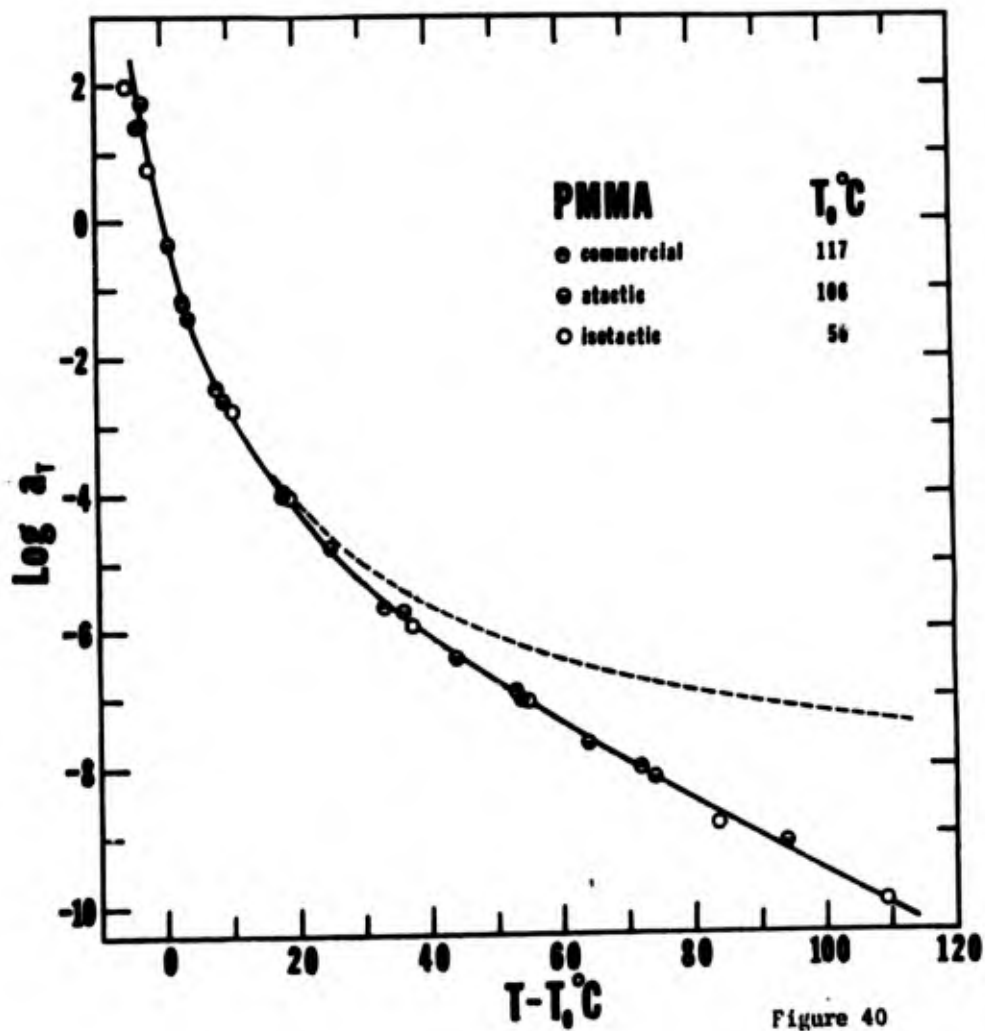


Figure 40

Temperature shift factors,  $a_T$ , for three stereochemical isomers shown logarithmically as a function of temperature,  $T$ , relative to a reference temperature  $T_0$ , where  $T_0 \cong T_g$ . The dashed line is the best fit WLF equation at the lower temperatures.

# LIGHT SCATTERING SPECTROSCOPY OF PURE FLUIDS NEAR THE GLASS TRANSITION

G. D. Patterson  
AT&T Bell Laboratories  
Murray Hill, New Jersey 07974

## Abstract

Light scattering is due to spatial fluctuations of the dielectric tensor  $\epsilon$  of the fluid. In liquids these fluctuations are dynamic. As the liquid approaches the glass transition some of these fluctuations become very slow. Dynamic light scattering is one of the most powerful tools in the study of the distribution of relaxation times associated with molecular motion in liquids near the glass transition. In the present paper I will summarize the experimental results obtained by light scattering spectroscopy of pure fluids near the glass transition.

## Introduction

The incident light in a light scattering experiment is characterized by a well defined frequency  $\omega_0$  and wavevector  $\vec{q}_i$ . Light which is scattered through an angle  $\theta$  in the scattering plane is characterized by a wavevector  $\vec{q}_s$  and a frequency spectrum  $S(\vec{q}, \omega)$  where  $\vec{q} = \vec{q}_s - \vec{q}_i$  is called the scattering vector with magnitude

$$q = \frac{4\pi n}{\lambda} \sin \frac{\theta}{2}$$

where  $n$  is the refractive index of the fluid and  $\lambda$  is the wavelength of the incident light in a vacuum. The dielectric fluctuations can be represented as  $\vec{q}$  dependent amplitudes according to

$$\Delta\epsilon(\vec{q}) = \int_V \Delta\epsilon(\vec{r}) \exp(i\vec{q}\cdot\vec{r}) d\vec{r} \quad (1)$$

where the integral is over the scattering volume. Light is scattered through an angle  $\theta$  only by fluctuations characterized by  $\vec{q}$  for that scattering angle.

The fluctuation amplitudes are a function of time in liquids and can be described by a relaxation function

$$\phi(\vec{q}, t) = \frac{\langle \Delta\epsilon(\vec{q}, 0) \Delta\epsilon(\vec{q}, t) \rangle}{\langle \Delta\epsilon^2(\vec{q}) \rangle} \quad (2)$$

The spectral density  $S(\vec{q}, \omega)$  of the scattered light is related to the relaxation function for the fluctuations by

$$S(\vec{q}, \omega) = \frac{1}{2\pi} \int_{-\infty}^{+\infty} e^{-i\omega t} \phi(\vec{q}, t) dt \quad (3)$$

When the time scale for the fluctuations is faster than  $10^{-6}$ s it is customary to measure the frequency spectrum of the scattered light directly. When the fluctuations are slower than that, the relaxation function is obtained by measuring the intensity autocorrelation function

$$C(\vec{q}, t) = \frac{\langle I(\vec{q}, t) I(\vec{q}, 0) \rangle}{\langle I \rangle^2} = 1 + A \phi(\vec{q}, t) \quad (4)$$

where  $A$  depends only on experimental parameters such as the coherence area of the scattered light and the discrete sample time used to measure the digital autocorrelation function. The experimental measurement of the frequency spectrum<sup>1</sup> or the relaxation function<sup>2</sup> has been described extensively elsewhere. In this article we will focus on the results of light scattering studies and their importance for the understanding of the glass transition.

The incident light can also be polarized and the scattered light analyzed. If the incident light is polarized vertically (V) with respect to the scattering plane and the scattered light is observed with vertical polarization (VV), the symmetry of the fluctuations that lead to light scattering is longitudinal. In the HV (VH) configuration the symmetry is transverse.

The dielectric tensor fluctuations can be expressed as

$$\Delta\epsilon = \sum_i \left( \frac{\partial\epsilon}{\partial A_i} \right) \Delta A_i \quad (5)$$

where the  $A_i$  are scalar or tensor variables which couple to the dielectric tensor. The equilibrium dielectric tensor is a scalar and depends primarily on the density  $\rho$  of the liquid. The other major source of light scattering in pure fluids is the inherent optical anisotropy of the molecules. Fluctuations in the orientation of the molecules leads to local birefringence in the liquid and hence to light scattering. In this paper we will consider only these two sources of light scattering.

The complete phenomenological theory of light scattering by a liquid has been presented by Rytov<sup>3</sup>. In this paper we will consider the spectrum due to longitudinal density fluctuations and the spectrum due to pure orientation fluctuations. For a more complete discussion of light scattering from liquids see Ref. 4.

### Theory

The phenomenological theory of light scattering by longitudinal density fluctuations is expressed in terms of the mechanical and thermal moduli of the liquid. These are the modulus of compression  $K$ , the shear modulus  $G$ , the thermal modulus  $\frac{\rho C_V}{T}$  where  $C_V$  is the specific heat at constant volume and  $T$  is the temperature, and the quantity  $\kappa\alpha_T$  where  $\alpha_T$  is the thermal expansion coefficient. The mechanical moduli occur in the combination known as the longitudinal modulus  $M = K + \frac{4}{3}G$ . The spectrum also depends on the thermal conductivity  $\kappa$ . The exact expression for the spectrum is given by

$$S_r(q, \omega) = \frac{-k_B T}{2\pi i \omega} \left[ \frac{\gamma^2 C q^2}{\Delta} - c.c. \right] \quad (6)$$

where  $k_B$  is Boltzmann's constant,

$$\gamma = \frac{\partial\epsilon}{\partial\rho}, C = \frac{\rho C_V}{T} + \frac{\kappa q^2}{i\omega T}, \Delta = (Mq^2 - \rho\omega^2)C + K^2\alpha_T^2 q^2,$$

and c.c. denotes the complex conjugate. The spectral features depend on the roots of the dispersion equation  $\Delta=0$ .

The simplest model for a liquid is a compressible, viscous fluid. The longitudinal modulus can be expressed as

$$M = K_0 + i\omega(\gamma_V + \frac{4}{3}\gamma_S),$$

where  $K_0 = 1/\beta_T$  is the static modulus of compression and  $\beta_T$  is the isothermal compressibility,  $\eta_V$  is the volume viscosity and  $\eta_S$  is the shear viscosity. There are then three roots of the dispersion equation. There will be a central line called the Rayleigh peak with linewidth  $\Gamma_r = \frac{\eta_V^2}{\rho C_r}$

where  $C_p$  is the specific heat at constant pressure. There will also be two shifted features called the Brillouin peaks with splitting  $\pm\Delta\omega_1 = qV_1$  and linewidth  $\Gamma_1$  where  $V_1$  is the longitudinal sound velocity. Brillouin scattering is due to scattering by sound waves of wavevector  $\vec{q}$ . The linewidth is determined by the lifetime of the sound waves. The sound velocity is given by

$$V_1 = \left[ \frac{K_0\gamma}{\rho} - \frac{\Gamma_r^2}{q^2} \right]^{1/2}$$

and the linewidth by

$$\Gamma_1 = \frac{q^2}{2\rho}(\gamma_V + \frac{4}{3}\gamma_S) + \frac{\eta_V^2}{2\rho C_r}(\gamma-1)$$

where  $\gamma = C_p/C_V$  is the ratio of specific heats which expresses the ratio of adiabatic to isothermal moduli. Sound waves are adiabatic in organic liquids. The contribution to the Brillouin linewidth due to direct conduction of heat is very small and will be ignored in the further discussion. This three peak structure was first predicted by Landau and Plazcek<sup>5</sup>. The predictions of the theory are quite good for atomic fluids like argon, but they break down completely for fluids near the glass transition.

As the liquid approaches the glass transition the viscosities become very large. This would mean that the Brillouin peaks would be too wide to observe. In fact they are quite sharp near  $T_g$ . The simple theory also predicts that the sound velocity decreases as the Brillouin linewidth increases which is the reverse of the actual experimental observations. The prediction for the Rayleigh peak remains good over the entire liquid range, but it is very difficult to measure the linewidth. In the further discussion we will ignore the Rayleigh peak, except to note that the adiabatic modulus must be used for the Brillouin peaks.

Real liquids are viscoelastic. After a step change in the volume the pressure takes time to approach its equilibrium value. The apparent longitudinal modulus then becomes a



function of time and changes from its initial value  $M_\infty$  to its final value  $\gamma K_0$ . The difference  $M_R$  is called the relaxation modulus. In the simplest case the relaxation can be characterized by a single relaxation time  $\tau$ . The simplest form for the modulus which yields the correct qualitative behavior for the longitudinal sound velocity and Brillouin linewidth is  $M = \gamma K_0 + \frac{M_R i \omega \tau}{1 + i \omega \tau}$ .

The Brillouin linewidth is then predicted to go through a maximum and the sound velocity increases as  $\tau$  increases. In addition a new central feature is predicted. This dynamic central peak was first described theoretically by Mountain<sup>6</sup> and is picturesquely called the Mountain peak. The linewidth of the new central peak depends on  $1/\tau$ . The intensity of the Mountain peak depends on the dispersion in the sound velocity due to the finite relaxation time. While the correct qualitative behavior of  $\Gamma_1$  is predicted, the quantitative predictions near the glass transition are very bad. Near  $T_g$  the relaxation time must be very long and the simple theory predicts that the Brillouin linewidth would be unobservably small. In fact the value of  $\Gamma_1$  near the glass transition is a substantial fraction of its value at its maximum. The Mountain peak is also predicted to be a single Lorentzian peak since there is only a single relaxation time. The observed Mountain peak is highly non-Lorentzian (or highly non-exponential in the time domain). This means that a distribution of relaxation times must be invoked to explain the results.

The adiabatic longitudinal modulus can in general be represented as

$$M^*(\omega) = \gamma K_0 + M_R \int_0^\infty \frac{\rho(\tau) i \omega \tau}{1 + i \omega \tau} d\tau \quad (7)$$

where  $\rho(\tau)$  is the distribution of relaxation strengths for all the processes which relax longitudinal stress. The \* denotes that  $M$  is complex and can be decomposed into a real part  $M'$  and an imaginary part  $M''$ . The sound velocity is then given by

$$V_l = \left( \frac{M'(\Delta\omega_1)}{\rho} \right)^{1/2} \text{ and the linewidth by}$$

$\Gamma_1 = \frac{q^2 M''(\Delta\omega_1)}{2\rho \Delta\omega_1}$ . The explicit expression for the linewidth is then

$$\Gamma_1 = \frac{q^2 M_R}{2\rho} \int_0^\infty \frac{\rho(\tau) \tau}{1 + \Delta\omega_1^2 \tau^2} d\tau \quad (8)$$

As long as  $\Delta\omega_1 \tau \ll 1$  for all  $\tau$  the Brillouin linewidth is determined by

the average relaxation time

$$\Gamma_1(0) = \frac{q^2}{2\rho} M_R \langle \tau \rangle \quad (9)$$

Near the glass transition many of the processes which relax the longitudinal stress have relaxation times that are too long to contribute to  $\Gamma_1$  but enough fast processes persist to keep the linewidth measureable. The Mountain spectrum is now predicted to be of the form

$$S_M \approx \int_0^\infty \frac{\rho(\tau) \tau}{1 + \omega^2 \tau^2} \frac{\Delta\omega_1^2 \tau^2}{1 + \Delta\omega_1^2 \tau^2} d\tau \quad (10)$$

Only those processes with sufficiently long relaxation times contribute fully to the Mountain spectrum since only those processes lead to dispersion in  $M'$ . All these features will be illustrated with actual data below.

Molecular orientation is a microscopic quantity so that a purely phenomenological theory would have no macroscopic variable which leads to light scattering. In the limit of rotational diffusion molecular orientation fluctuations give rise to a depolarized (HV) central Lorentzian spectrum whose width is determined by the orientational relaxation time. Such times have been observed to follow the empirical relation

$$\tau_{or} = \frac{C \eta}{T} + \tau_0 \quad (11)$$

where  $C'$  depends only on the size and shape of the molecule and  $\tau_0$  accounts for the observed finite intercept in a plot of  $\tau_{or}$  against  $\frac{\eta}{T}$ . As the glass transition is approached the viscosity becomes very large and the orientation relaxation time must become very large if rotational diffusion is the only mechanism. In fact the observed relaxation functions for orientational motion near the glass transition are highly non-exponential. Further discussion on this topic will be deferred until the results have been presented.

### Experimental Results

The Rayleigh-Brillouin spectrum has now been studied as a function of temperature and pressure in many liquids from high temperatures down to the glassy region. A thorough review of Brillouin linewidth studies is available<sup>7</sup>. The Rayleigh-Brillouin spectrum of a typical<sup>8</sup> viscoelastic liquid over its entire liquid range is shown in Figure 1. As the liquid is cooled the Brillouin splitting and linewidth increase. The Brillouin linewidth goes through a maximum while the splitting

# 2,4,6-TMH

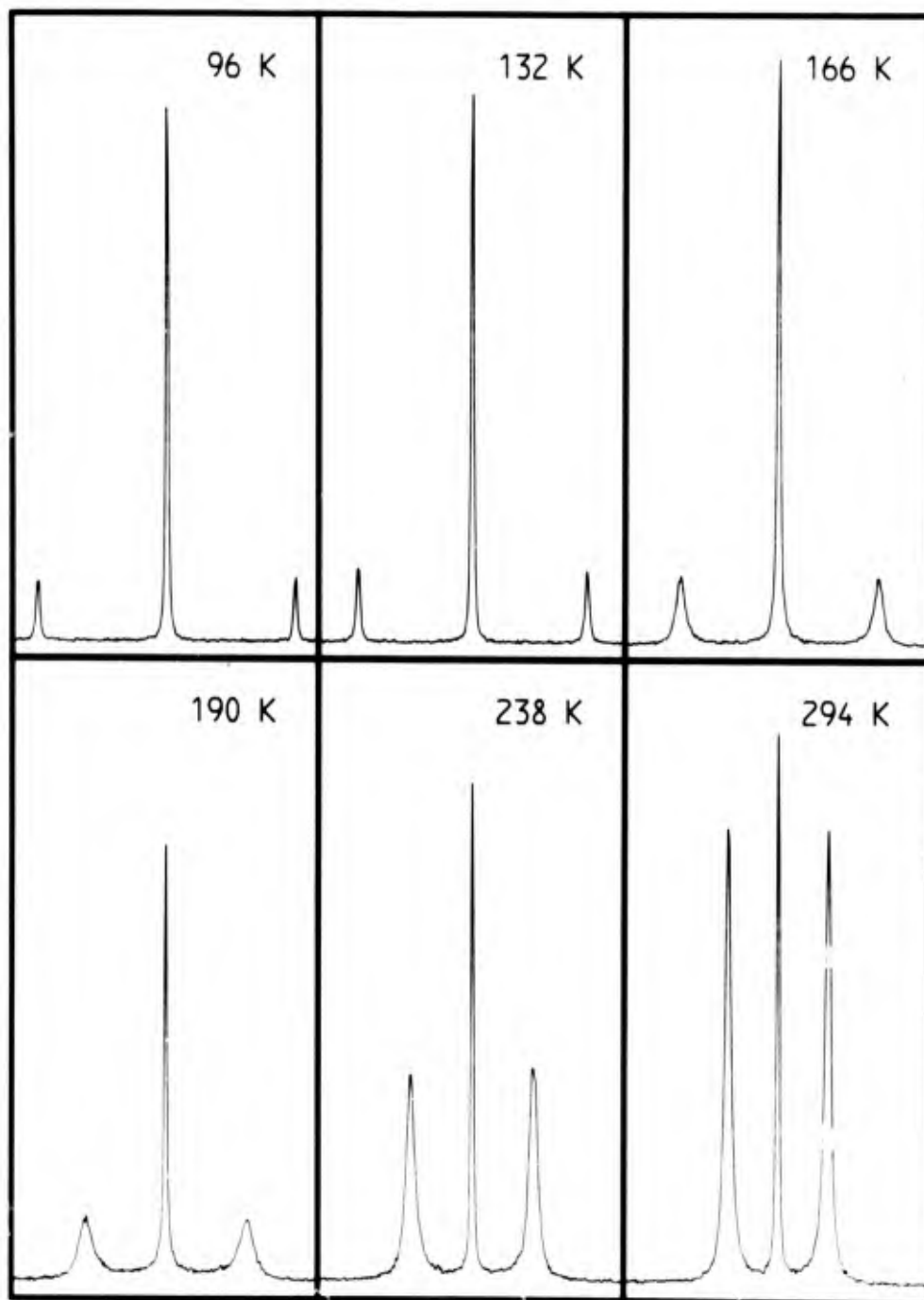


Figure 1. Rayleigh-Brillouin spectra of 2,4,6-trimethylheptane at six different temperatures that span the full range of viscoelastic behavior. This liquid was chosen because almost all the intensity is due to longitudinal density fluctuations. At the highest temperature (294 K) the spectrum is typical of a low viscosity liquid. The sample is in the glassy state at 96 K. The frequency scale is the same for each frame and is equal to 27.1 GHz.

increases monotonically. One spectrum in the glassy state is also shown, but it does not look qualitatively different than the spectrum for an equilibrium fluid near  $T_g$ . In the region of the Brillouin linewidth maximum the Mountain peak is evident in the spectrum. At lower temperatures it becomes the major component of the Rayleigh-Brillouin spectrum. The contributions from the Rayleigh and Brillouin peaks can be subtracted from the spectrum and the Mountain peak obtained by itself. The results are shown in Figure 2. The spectrum is highly non-Lorentzian at all temperatures. At the lowest temperatures the half-width of the spectrum is too narrow to be resolved directly in the frequency domain. However, significant intensity persists in the wings of the spectrum all the way out to the frequency of the Brillouin splitting. It is these high frequency processes which keep the Brillouin linewidth measurable near  $T_g$ .

The low frequency part of the Mountain spectrum near the glass transition can be studied by photon correlation spectroscopy. A typical relaxation function is shown in Figure 3. The relaxation function  $\phi^2(t)$  is plotted against  $\log t$ . The function is highly non-exponential but can be well described by the empirical function<sup>9</sup>

$$\phi(t) = \exp\left(-\frac{t}{\tau}^\beta\right) \quad (12)$$

where  $0 < \beta \leq 1$  is a measure of the width of the distribution of relaxation times implied by the non-exponential decay. The relaxation function can be characterized by the average relaxation time  $\langle \tau \rangle$  which for the empirical function is given by  $\langle \tau \rangle = \frac{\tau}{\beta} \Gamma(1/\beta)$  where

$\Gamma(x)$  is the gamma function. The average relaxation time is observed to follow the empirical relation

$$\langle \tau \rangle = \exp\left(\frac{A + BP}{T - T_0}\right)$$

where  $T_0$  is an empirical temperature well below  $T_g$ . A typical result for  $\langle \tau \rangle$  is plotted logarithmically against  $1/T$  in Figure 4.

The distribution of relaxation times necessary to describe the observed relaxation function is at least several decades in width. However, for many materials the shape of the relaxation function (as characterized by the empirical parameter  $\beta$ ) is invariant to changes in temperature, pressure or dilution with a small molecule<sup>2</sup>. Although the value of  $\beta$  changes from one material to another the insensitivity to the thermodynamic state suggests a type of universality for the glass

transition phenomenon.

Dynamic mechanical studies of polymers near the glass transition usually consist of measuring  $G'$  and  $G''$  as a function of temperature and frequency over a wide range. Corresponding measurements of the frequency dependent dielectric constant yield values of  $\epsilon'$  and  $\epsilon''$ . Just as the Brillouin linewidth is observed to go through a maximum, the imaginary part of  $G$  and  $\epsilon$  goes through a maximum as a function of frequency or temperature. For some materials more than one maximum is observed. The lower frequency (higher temperature) maximum is called the primary glass relaxation (or  $\alpha$  process), while the higher frequency (lower temperature) maximum is called the secondary glass relaxation (or  $\beta$  process). If the frequencies of maximum dielectric or mechanical loss (where  $\epsilon''$  or  $G''$  is a maximum) are plotted against  $1/T$  the primary glass relaxation data follow the same sort of empirical law as the average relaxation time determined by light scattering<sup>10</sup>. The secondary relaxation data follow an Arrhenius temperature dependence. However, this apparently simple behavior masks the fact that the shape of the relaxation function associated with the secondary relaxation is changing with temperature and is very much broader than the primary relaxation. The two relaxation processes do appear to merge at high temperatures or frequencies.

The light scattering relaxation functions observed for the alkyl methacrylates change shape dramatically as the glass transition is approached<sup>2,11,12</sup>. The relaxation function observed for poly(ethyl methacrylate) (PEMA) near  $T_g$  is shown in Figure 5. It is over 7 decades wide. The apparent value of  $\beta$  changes from 0.4 at high temperatures to 0.16 at 70 °C. This behavior is also observed for poly(methyl methacrylate) (PMMA). The average relaxation times observed for PEMA and PMMA are consistent with the mechanical relaxation data and have the same temperature dependence as that found for the primary glass relaxation. This is because the average relaxation time  $\langle \tau \rangle$  is dominated by the longest relaxation times associated with the primary process. Because the relaxation function is monotonically decreasing and very broad it is not obvious how to separate the decay into more than one component. Until recently the data was not of high enough quality to attempt to calculate the distribution of relaxation times directly from the

# 2,4,6-TMH

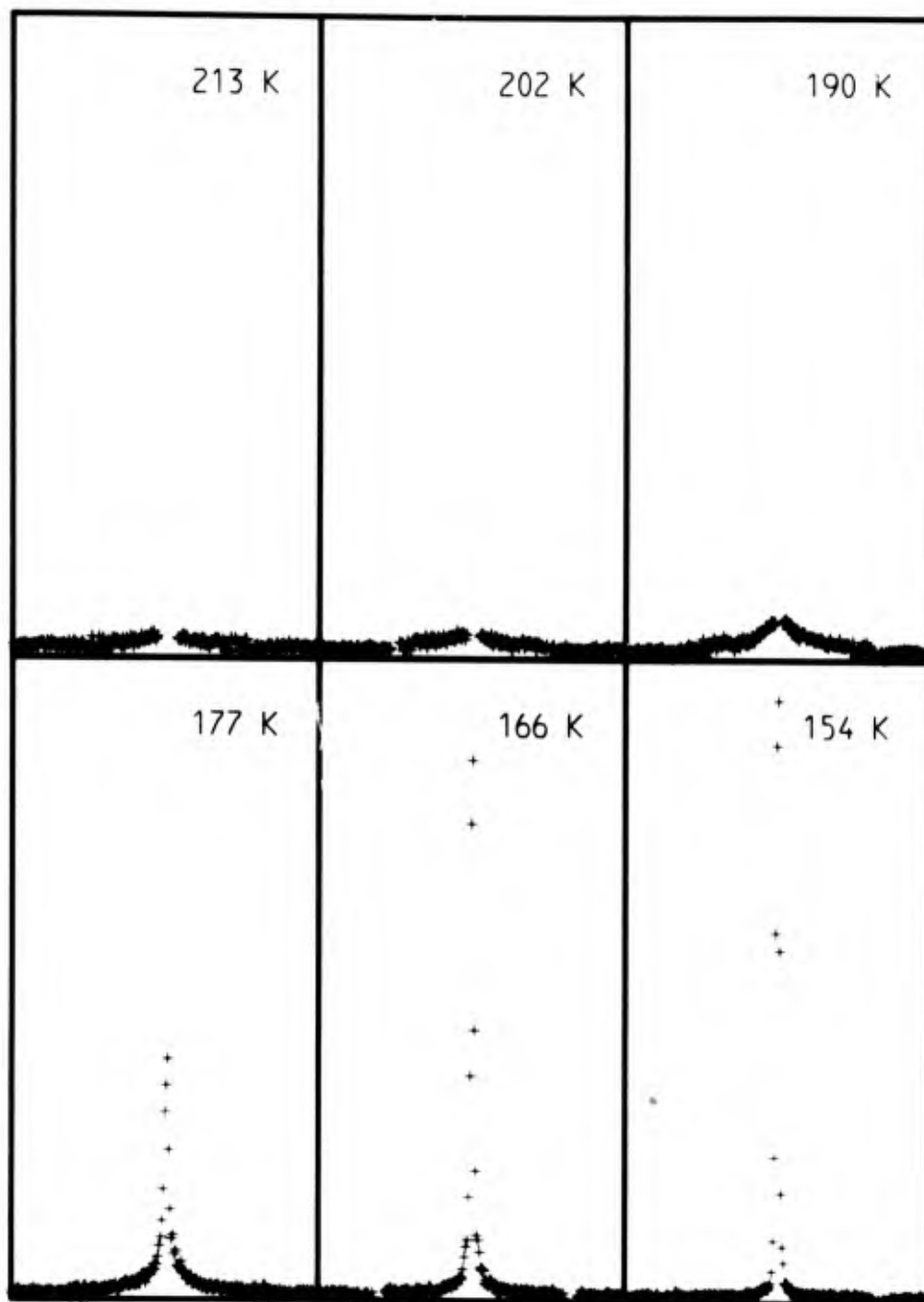


Figure 2. Mountain spectra for 2,4,6-TMH at six temperatures spanning the Brillouin linewidth maximum. The spectra are highly non-Lorentzian at all temperatures. At the lowest temperatures the half width of the peak is too narrow to be resolved in the frequency domain, but significant intensity persists in the wings of the spectrum.

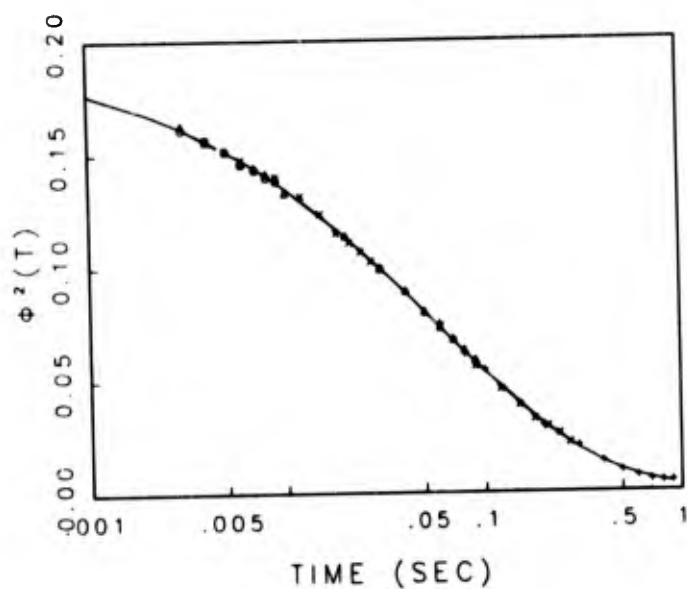


Figure 3. A typical relaxation function  $\phi^2(t)$  plotted versus  $\log t$  for longitudinal density fluctuations observed near the glass transition. The line is the best calculated empirical function  $\phi(t) = \exp(-t/\tau)^\beta$ .

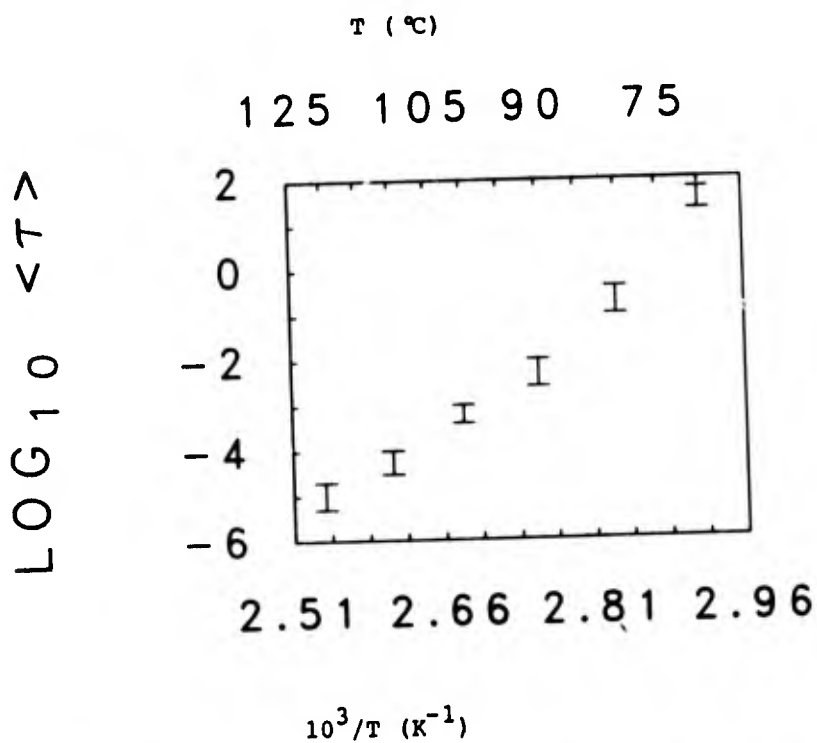


Figure 4. Average relaxation time  $\langle \tau \rangle$  plotted against  $1/T$  for poly(ethyl methacrylate) (PEMA). The data follows the empirical law  $\langle \tau \rangle = \langle \tau \rangle_0 \exp(A/T - T_0)$ .

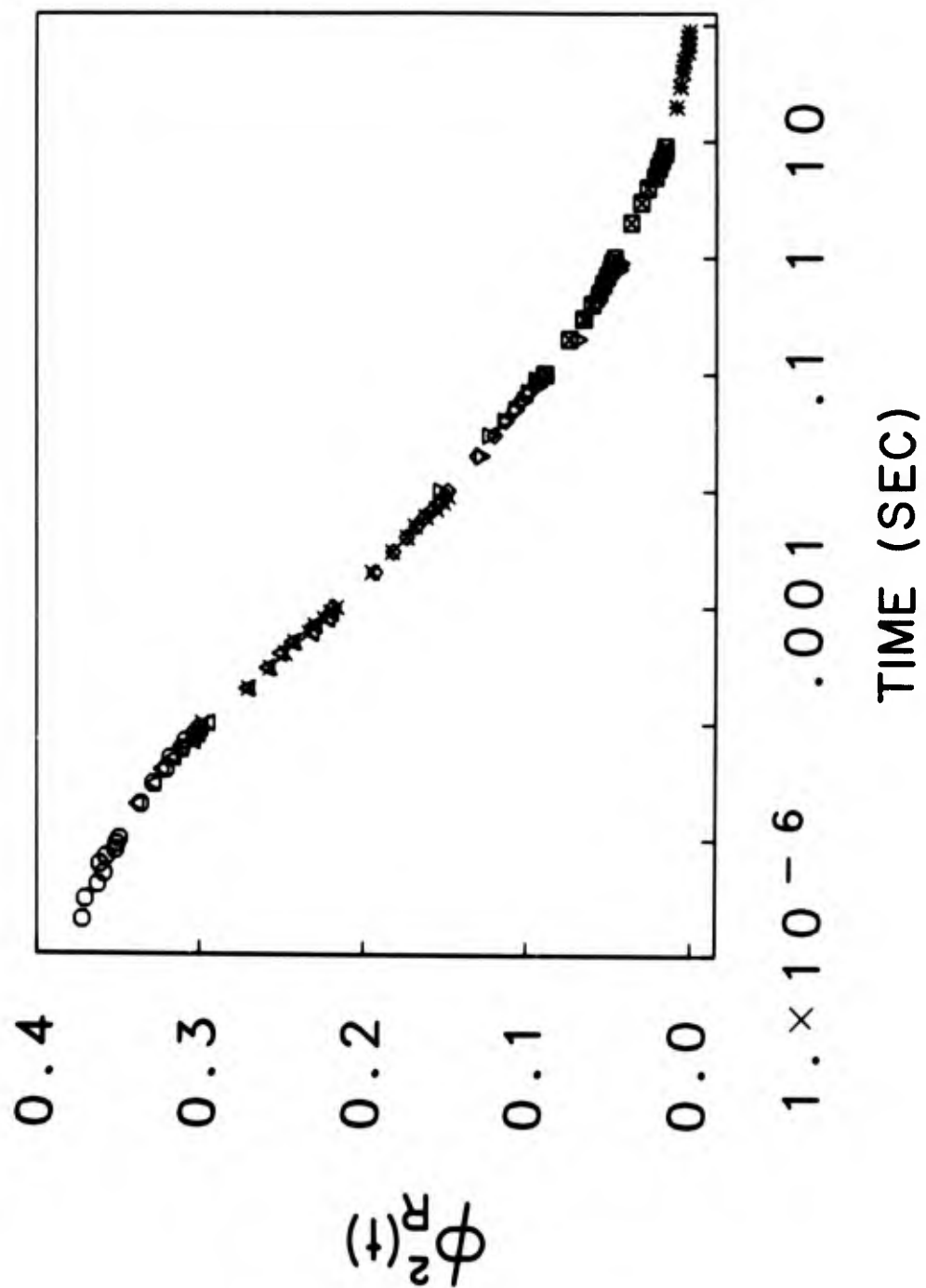


Figure 5. Relaxation function  $\phi^2(t)$  plotted versus  $\log t$  for PEMA at 70°C. The value of  $\beta$  is very low (0.16) and indicates that both the primary and secondary glass relaxation are contributing to the observed relaxation function.

data. However, this has now been accomplished<sup>13</sup>.

Extensive studies of the depolarized Rayleigh scattering of polystyrene near the glass transition have also been carried out<sup>14-17</sup>. The same empirical function used to describe the shape of the Mountain peak works well for the orientational fluctuations observed by depolarized Rayleigh scattering. The average relaxation time also obeys the same empirical law as that observed for the Mountain peak or normal mechanical or dielectric relaxation studies. However, the average relaxation time is approximately two decades longer than that determined directly from mechanical measurements. The longitudinal modulus depends on both the modulus of compression and the shear modulus. Part of the shear modulus is due to the coupling between orientation and shear<sup>18</sup>. Thus, the depolarized Rayleigh scattering is sensitive to only part of the full distribution of relaxation times that determine the longitudinal modulus. For chain molecules the overall reorientation of the chain or of some shorter segment is much slower than the local chain rearrangements that dominate the relaxation modulus near the glass transition. But the rate of orientational relaxation is determined by the rate at which the local rearrangements take place so that the same non-exponential relaxation function with the same temperature dependence is observed.

Although the observed relaxation function in polystyrene does not change shape as a function of temperature, pressure or dilution, there is at least 20% of the initial decay that is too fast to observe with a correlator. Attempts to observe this component directly in the frequency domain were unsuccessful because it is expected to be very broad. The strong sharp peak due to the slow processes makes it very difficult to separate the small potential differences between the wings of the central peak and any other real small contribution. However, the value of the relaxation function  $\phi(t)$  observed at  $10^{-6}$  s requires that there be faster processes present. The best evidence for their existence is the finite value of the Brillouin linewidth observed in polystyrene near the glass transition<sup>19</sup>.

Another way to observe the presence of processes with relaxation times substantially faster than those associated with the primary process is to use pressure to increase  $\langle \tau \rangle$  to  $10^6$

s. The sample is allowed to equilibrate for a week and is then measured. Some of the fluctuations are too slow to relax during the  $10^4$  s necessary to obtain the data and contribute as if they were elastic sources of light scattering. This complicates the analysis, but there is a very broad decay evident in the results<sup>20</sup>.

Part of the observed relaxation function near the glass transition seems to behave in a universal manner with temperature and pressure. This part is well described by the empirical relaxation function with values of  $\beta$  in the range 0.3-0.7. The shorter time (higher frequency) part changes shape with temperature and may be well separated from the longer time primary glass relaxation. Only by considering the full relaxation function will a consistent picture of the dynamics of liquids near the glass transition emerge. Light scattering is helping to provide the experimental basis for a deeper understanding of the glass transition.

#### References

- (1) G. D. Patterson, in *Methods of Experimental Physics*, ed. R. A. Fava, **16A**, 170 (1980).
- (2) G. D. Patterson, *Adv. Polymer Sci.*, **48**, 125 (1983).
- (3) S. M. Rytov, *Sov. Phys. JETP*, **31**, 1163 (1970).
- (4) G. D. Patterson, *J. Phys. Chem.*, to be published.
- (5) L. Landau and G. Placzek, *Phys. Z. Sowjetunion*, **5**, 172 (1934).
- (6) R. D. Mountain, *J. Res. Nat. Bur. Stds.* **70A**, 207 (1966).
- (7) G. D. Patterson, *CRC Crit. Rev. of Solid State and Mat. Sci.*, **9**, 373 (1980).
- (8) P. J. Carroll and G. D. Patterson, *J. Chem. Phys.*, to be published.
- (9) G. Williams and D. C. Watts, *Trans. Faraday Soc.*, **66**, 80 (1970).
- (10) N. G. McCrum, B. E. Read and G. Williams, *Anelastic and Dielectric Effects in Polymeric Solids*, London, Wiley, 1967.
- (11) G. D. Patterson, J. R. Stevens and C. P. Lindsey, *J. Macromol. Sci.*-

Phys., B18, 641 (1980).

- (12) G. D. Patterson, P. J. Carroll and J. R. Stevens, J. Poly. Sci. Polym. Phys. Ed., 21, 613 (1983).
- (13) P. J. Carroll and G. D. Patterson, J. Chem. Phys., to be published.
- (14) G. D. Patterson, C. P. Lindsey and J. R. Stevens, J. Chem. Phys., 70, 643 (1979).
- (15) C. P. Lindsey, G. D. Patterson and J. R. Stevens, J. Polym. Sci. Polym. Phys. Ed., 17, 1547 (1979).
- (16) G. D. Patterson, J. R. Stevens and P. J. Carroll, J. Chem. Phys., 77, 622 (1982).
- (17) G. D. Patterson, P. J. Carroll and J. R. Stevens, J. Polym. Sci. Polym. Phys. Ed., 21, 605 (1983).
- (18) G. D. Patterson and C. P. Lindsey, J. Appl. Phys., 49, 5039 (1978).
- (19) G. D. Patterson, J. Polym. Sci. Polym. Phys. Ed., 15, 579 (1977).
- (20) G. D. Patterson and P. J. Carroll, J. Polym. Sci. Polym. Phys. Ed., 21, 1897 (1983).



## RELAXATION IN CRYSTALLINE POLYMERS

Philip L. Taylor

Department of Physics  
Case Western Reserve University  
Cleveland, Ohio 44106

### Abstract

A discussion is given of the problems involved in developing a theoretical understanding of the dynamics of phase transformations in crystalline polymers. These ideas are illustrated by a description of approaches taken in studying three simple materials -- polyvinylidene fluoride, polytetrafluoroethylene, and polybutylene terephthalate. In the first case one is studying the rotation of a planar molecule, in the second the unwinding of a helix, and in the third the longitudinal motion involved in the stretching of a coiled chain.

### Introduction

Although we seldom give the question much thought, our lives are in fact surrounded by changes of state of polymeric systems. Every time we smile or frown, our skin, which is itself a biopolymer, relaxes and restores to our face the form it had before the smile lit it up or the frown disfigured it. The mythical East Wind that is said sometimes to blow and freeze on the faces of unlucky individuals the scowl or frown that was to be found there would be a representation of the effects to be felt if the relaxation phenomenon were to cease. In the realm of synthetic polymers, the act of sitting down while wearing a pair of stretch jeans induces a change of phase from one crystalline form of a polymer known as PBT to another form which has a longer crystal axis dimension; the act of standing up while wearing the same pair of stretch jeans then, through the same happy piece of technology, allows one to display no wrinkled knees or other unesthetic bagginess, but to show the world a smooth face. When we throw an egg into the frying pan to cook breakfast, few of us are aware that if the pan is lined with PTFE, then a couple of crystal-crystal phase transitions will occur in this Teflon lining as the pan is heated above room temperature.

In the scientific study of phase transitions and of their time dependence in polymers we will be concerned with two kinds of motion. Because a polymeric molecule exists in the form of a long chain, it is useful to divide the types of motion that the molecule may undergo into motions parallel to the chain direction and motions that do not involve translation of the chain in its own direction. These other motions can be lateral translations or, more commonly, rotations about the chain axis. A third category, in which one discusses the time dependence of the polymerization process itself, will not be discussed at length here. In relation to this type of phenomenon we could, for instance, investigate the process of solid state polymerization. Here a single crystal formed from a monomer can be induced to polymerize by the action of ultraviolet or gamma radiation. Then new chemical bonds are formed, and what had been a lattice of small chemical units becomes an ordered array of long chains over a time and with a time dependence that will vary with temperature, pressure, and the chemical environment.

Polymers, being as ubiquitous and complex as they are, provide a rich source of study for relaxation processes. This very richness, however, forces us to restrict our attention in a paper such as this to a few illustrative examples. Here we will look at two simple polymers in which chain rotation is important, and one in which longitudinal motion of the polymer chain is of great interest.

### Polyvinylidene Fluoride

Polyvinylidene fluoride, also known as PVF<sub>2</sub>, is a remarkable material in that it can be produced in a form in which it has a spontaneous electric dipole moment. Unlike ceramic ferroelectrics, in which the moment arises from an instability in the phonon spectrum of a non-polar material, PVF<sub>2</sub> consists of a flexible chain composed of units of fixed dipole moment of about  $7 \times 10^{-30}$  coulomb-meters. The particular phase in which PVF<sub>2</sub> shows these effects is known as the  $\beta$  phase, and is shown schematically in Fig. 1.

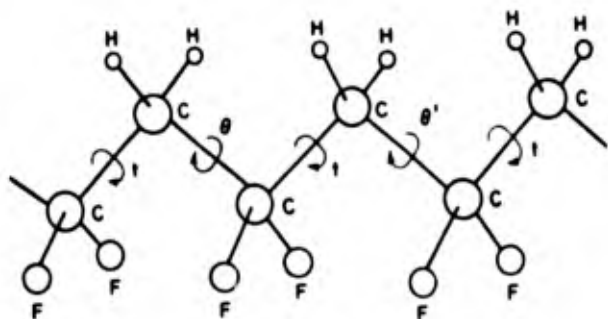


FIG. 1. Molecular structure of poly(vinylidene fluoride).

The great technological interest in  $\beta$ -PVF<sub>2</sub> arises from the fact that one may make transducers and other devices of large area from it. It may be produced in complex shapes, is easily cut without damage, and is light and flexible. It requires no complex mounting process, is chemically stable and mechanically strong, and can handle large electrical power. Its density is sufficiently low that it has a better acoustical match to water than most other ferroelectrics. Its piezoelectric properties make it useful in hydrophones, loudspeakers and optical modulators, while its pyroelectricity lends itself to use in infrared detectors, radiometers, and intrusion detectors.

As produced by drawing from the more stable  $\alpha$  phase, a film of  $\beta$ -phase material will consist of randomly oriented domains. In order to obtain useful aligned material, this sample is exposed to large electric fields at modestly high temperatures, a process known as poling. To understand the process by which the chains rotate about their axes to align themselves with the applied field has been a challenging task in theoretical polymer physics.

The first model to be studied was one introduced by Aslaksen (1), in which the polymer chain rotates by 180° about its axis. The second model followed a more recent suggestion by Kepler and Anderson (2), who noticed that a rotation by 60° might also occur. Both these models led to results that were at great variance with the experimental results as known at the time. Fortunately, this uncomfortable situation was relieved by some more careful experimentation, which showed that a theory based on one of these models had in fact predicted the observed relaxation time for the poling process.

The first model considered the situation shown in Fig. 2, in which a domain wall separates oppositely polarized regions of a crystallite. A phenomenological Hamiltonian may then be proposed of the form

$$H = T + U,$$

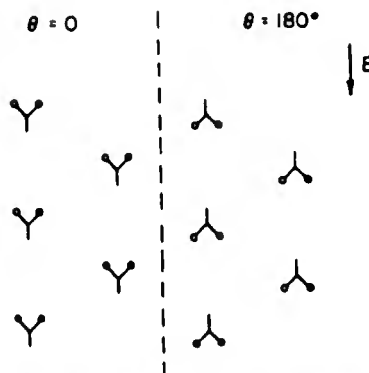


FIG. 2. At the boundary between oppositely polarized regions some chains are in a neutral environment for which the energies of either of two opposite orientations are approximately equal.

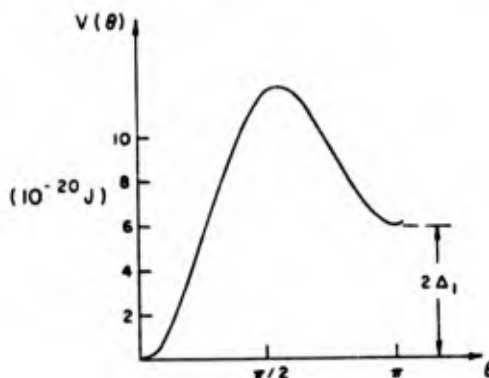


FIG. 3. Interchain contribution to the potential energy of a monomer unit of PVF<sub>2</sub> as a function of angle of rotation about its chain axis. The unit is located at the center of the orthorhombic unit cell of the  $\beta$  phase. All neighboring chains are aligned at  $\theta = 0$ .

where

$$T = \frac{1}{2} I \sum_i \dot{\theta}_i^2 \quad (1)$$

and

$$U = \sum_i [A_1(1 - \cos\theta_i) + A_2(1 - \cos 2\theta_i) + \frac{1}{2} k(\theta_i - \theta_{i+1})^2] \quad (2)$$

where  $I$  is the moment of inertia of a monomer unit about the center-of-mass axis of the chain and the dot signifies differentiation with respect to time. The first two terms in  $U$  represent the combined influence of the local crystalline order (that is, the interchain potential) and an applied electric field. They constitute a potential having minima at  $\theta = 0$  and  $\pi$ , providing  $4A_2 > |A_1|$ . In practice, even with large applied electric fields, this condition is satisfied. The last term in  $U$  represents the torsional rigidity of the chain. The interchain potential for a monomer unit of a chain at the center of the  $\beta$ -phase unit cell is shown as a function of the rotational angle  $\theta$  about its axis in Fig. 3.

The time variation of  $J_i$ , the angular momentum of the  $i^{\text{th}}$  unit, defined as

$$J_i = I\dot{\theta}_i \quad (3)$$

obeys a Langevin equation of the form

$$\dot{J}_i = -\partial U/\partial \theta_i - \lambda J_i + F_i(t). \quad (4)$$

This equation is the dynamical equation of the system supplemented by a damping term  $-\lambda J_i$  and a Brownian-motion term  $F_i(t)$ .

Aslaksen (1) had pointed out that any polymer chain in the crystal field of its neighbors has two locally stable orientations, in one of which, the stable orientation, the polarization of the chain was parallel to that of its neighbors, and in the other of which it was antiparallel to the neighbors' orientation. For this reason he suggested that poling involved a possible reversal of orientation of the polarization of a crystallite, rather than wholesale rotations of crystallites. The poling field would then lower the energy of the metastable antiparallel orientation of the chain polarizations in such a way as eventually to reverse the orientations of all polymer chains within a crystallite. The advantage of this picture is that the topological structure of a polymer sample is preserved, and large-scale motions of polymer chains, corresponding to changes of orientation of the local crystal axes, are avoided.

When the potential defined in Eq. (2) is inserted in Eq. (4) one obtains a set of coupled nonlinear differential equations of motion which have not been solved analytically, even in the absence of the thermal-fluctuation term. There are, however, some known special solutions to the equation that is obtained by taking the continuum limit of Eq. (2) at zero temperature. That is, one replaces the difference

$$\theta_{i+1} - 2\theta_i + \theta_{i-1} \quad \text{by the differential}$$

$a^2 \partial^2 \theta / \partial x^2$  with  $a$  the repeat distance along the chain direction  $x$ , and ignores the thermal term  $F(t)$ . The equation that results,

$$I\ddot{\theta} = -A_1 \sin \theta - 2A_2 \sin 2\theta + ka^2 (\partial^2 \theta / \partial x^2) - \lambda I \dot{\theta}, \quad (5)$$

is known as the double sine-Gordon equation. (3)

To this equation there are the "kink" solutions, which describe the motion of the boundary between two regions of the chain, in one of which  $\theta \approx 0$  and in the other of which  $\theta \approx \pi$ . In the present case the potential energy is lower for  $\theta \approx \pi$  and so this region advances at the expense of the region in which  $\theta \approx 0$ . This is illustrated in Fig. 4.

The approximation that yields the double sine-Gordon equation has a number of obvious weaknesses. One knows, for example, that the

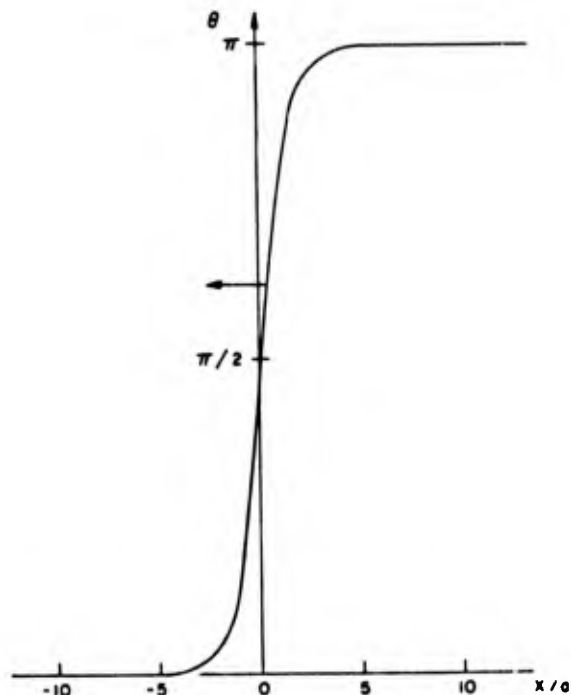


FIG. 4. Solution of the double sine-Gordon equation represents a kink traveling to the left.

poling process is temperature dependent, and so the exclusion of the Brownian-motion term  $F(t)$  from Eq. (4) allows only a zero-temperature result to be predicted. One must also expect the discrete nature of the polymer chain to play a significant role in the motion of a kink of polarization.

In view of these inadequacies of the analytical approach, a series of computer experiments were performed in which the discrete nature of the chain and the thermal fluctuations were taken into account. A chain of 40 monomer units was chosen for study, in accord with experimental observations of lamellar thickness (2). The equations of motion, Eqs. (4), were solved by linearization and direct integration over a small time increment  $\Delta t$ . The thermal forces were included by adding an impulse of fixed magnitude  $(2\lambda I k_B T / \Delta t)^{1/2}$  but of random sign during each time increment. Because of the random nature of the force, all the finite-temperature experiments were performed repeatedly and average values taken.

A computer experiment was then performed to determine the waiting time  $t_w$  that on average elapses between application of the field  $E$  and passage of a kink into the crystallite along a given chain. The results of this study are shown in Fig. 5, in which  $t_w$  is plotted as a function of inverse temperature for various fields. The approximately linear behavior suggests that a picture of thermally activated kink creation is valid, with

$$t_w = \Lambda e^{B/T}.$$

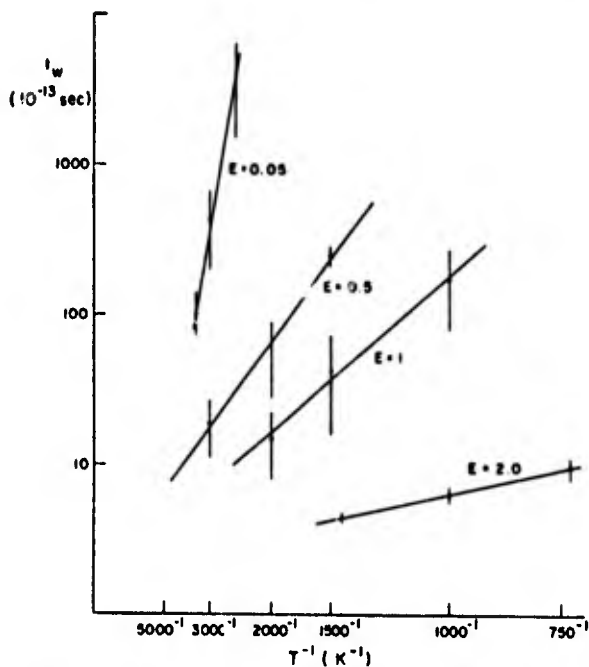


FIG. 5. Logarithm of the average waiting time  $t_w$  for creation of a  $180^\circ$  kink is shown as a function of  $T^{-1}$  for various fields  $E$  in units of  $10 \text{ GV m}^{-1}$ .

The "attempt frequency"  $\Lambda^{-1}$ , found from the common extrapolations of the lines to infinite temperature, yields a value of about 7 THz, which is to be compared with the figure of 8.4 THz obtained by multiplying twice the librational frequency at zero wave number of 2.1 THz by a further factor of 2 to allow for the two ends of the chain. The activation energy  $h\kappa_p$ , found from the slope of these lines, can be interpreted satisfactorily in terms of the contributions of the various terms in the Hamiltonian given in Eqs. (1) and (2).

The average waiting time for a chain to reverse its electric polarization under typical poling conditions ( $T=373 \text{ K}$ ,  $500 \text{ MV m}^{-1}$ ) and in a neutral crystal environment is predicted by this model to be of the order of  $7 \times 10^4 \text{ sec}$ . The theoretical poling time for the entire sample will clearly be much larger than this, and of the order of days or weeks. Because poling had been observed to occur in periods of a few minutes, there was clearly some inadequacy in the model.

The clue to the alternative mechanism for poling came from the orthorhombic nature of  $\text{PVF}_2$ . The closeness of the structure to a hexagonal form led Kepler and Anderson (2) to make an ingenious suggestion of an alternative mechanism of poling, namely that a rotation of the chains through  $60^\circ$  rather than  $180^\circ$  plus a small distortion of the lattice might be the correct model. This possibility is illustrated in Fig. 6, in which the boundary between such

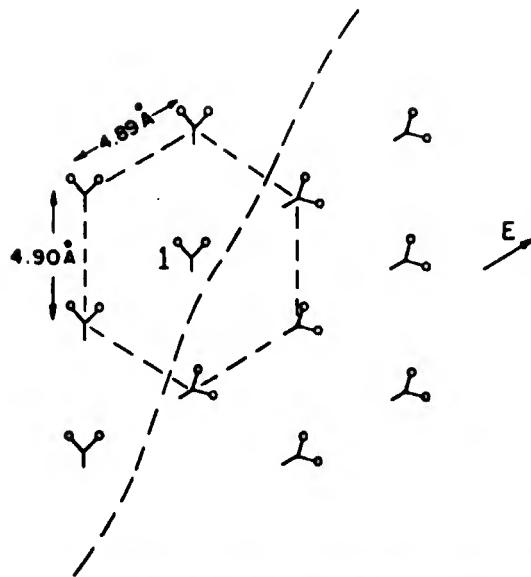


FIG. 6. Boundary between regions of  $\beta$ -phase  $\text{PVF}_2$  differing in direction of polarization by  $60^\circ$ .

twinned regions is shown. Some support for such a mechanism has recently been given in the form of infrared studies in which the optical properties of a  $\text{PVF}_2$  surface were shown to be modified by poling (5). A simple reversal of chain orientation through  $180^\circ$  would presumably have left these unchanged.

In this model the potential barrier to rotation was greatly reduced, and poling proceeded much more rapidly than in the previous case. In fact, the predicted poling time was now reduced to be of the order of microseconds to milliseconds (6). We had escaped from the frying pan of having predicted a poling time too long by three orders of magnitude only to land in the fire of a prediction apparently too short by six orders of magnitude. It was thus a welcome resolution when Furukawa and Johnson (7), in a careful set of measurements of the poling process, concluded that relaxation to the poled state occurs in times of the order of microseconds. Subsequent analysis (8) showed that the detailed form of the growth of the polarization with time was matched quite closely by this model of propagating kinks. Thus were we rescued from the ribald comments of our critics.

#### Polytetrafluoroethylene

Teflon, or PTFE, is well known for its "non-stick" properties. Eggs, in principle, can be fried in a pan lined with PTFE and then removed with no adhering traces left behind. This same slipperiness that makes Teflon unwilling to bind to other substances shows up also in the ease with which the polymer chain can rotate about its crystalline axis. Early

experiments (9) established that under atmospheric pressure PTFE exists in the form of helical chain molecules. At least three solid phases have been identified at atmospheric pressure (9,10), with two structural phase transitions occurring at 19°C and 30°C. While early x-ray studies found a commensurate  $13_6$  helix as the conformation of the low-temperature phase (phase II), recently Clark et al. (11) have concluded from careful examination of electron diffraction data that this helix is, in fact, incommensurate.

A number of theoretical studies (12-16) have been conducted on the conformation and phase transitions of PTFE. However, no comprehensive theory exists of the conformations in the different phases or of the phase transitions of PTFE. It has been speculated that the phase transitions may be modeled as incommensurate-commensurate (IC) transitions.

One route to a Hamiltonian for the PTFE system that might yield insight into the phase diagram of this polymer is through molecular mechanics. The basic problem in this approach is the determination of universally applicable parameters characterizing the nonbonded interactions. Such parameters are never really universal and do not produce very accurate results, energy differences of  $1 \text{ kcal mol}^{-1}$  being barely significant in calculations using this method. (The barrier between the right- and left-handed helices in PTFE is estimated to be about  $2 \text{ kcal mol}^{-1}$ .)

This being the case, Banerjee (17) has formulated a model in which the most basic elements of the Teflon chain are present, but in which the mathematics is sufficiently tractable to permit solution of the relevant equations.

While Teflon has a molecular structure similar to the  $\text{PVF}_2$  shown in Fig. 1, but with all the hydrogen atoms replaced by fluorines, a simple model of this system may be visualized as a linear array of canted "arrows" or "spins" of equal size, each free to rotate in a plane perpendicular to the line joining the arrows, as shown in Fig. 7. The angle that the  $j^{\text{th}}$  arrow makes with a certain fixed direction, defined as the z-direction, is  $\phi_j$ . Each arrow interacts with its nearest neighbors with a potential energy of the form:

$$W(\phi_{n+1}, \phi_n) = -\cos(\phi_{n+1} - \phi_n - \alpha) \quad (6)$$

Here  $\alpha$  is a measure of the degree of natural cantedness of the system. In other words, to minimize this energy in the absence of other forces the arrows form a helix, and  $\alpha$  is a measure of the pitch of that helix. These arrows, or  $\text{CF}_2$  units, are also subject to an external symmetry-breaking field which represents the effect of interchain interactions. The potential energy of the  $j^{\text{th}}$  arrow in the presence of the external field is given by:

$$V(\phi_j) = -\gamma \cos(2\phi_j) \quad (7)$$

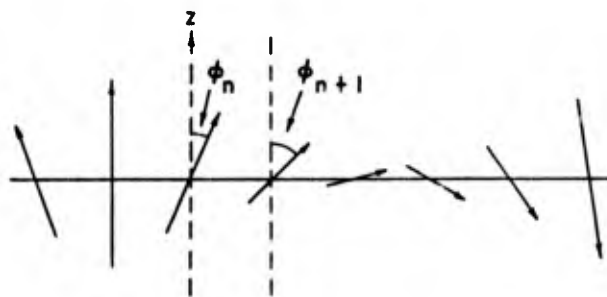


FIG. 7. In the helical molecule of PTFE successive  $\text{CF}_2$  units are oriented at angles  $\phi$  to the crystal z axis.

The constant  $\gamma$  characterizes the strength of the interchain forces, and hence the pressure. Under the influence of this pressure term alone, i.e. with no nearest-neighbor interaction, the ground state configuration would have all the arrows aligned parallel or anti-parallel to the z-direction.

The total Hamiltonian for the array of arrows is then

$$H = -\sum_n \{ \cos(\phi_{n+1} - \phi_n - \alpha) + \gamma \cos(2\phi_n) \} \quad (8)$$

The conditions for a ground state configuration may be found simply by minimizing the total energy with respect to the set of variables  $\{\phi_n\}$ . Differentiating the total Hamiltonian with respect to  $\phi_n$  and setting the derivative equal to zero gives an infinite set of equations:

$$\begin{aligned} \sin(\phi_{n+1} - \phi_n - \alpha) - \sin(\phi_n - \phi_{n-1} - \alpha) \\ = 2\gamma \sin(2\phi_n) \end{aligned} \quad (9)$$

Solutions to Eq. (9) yield configurations for which the energy is a local extremum. Of these, a subset are minimum energy configuration and a further subset of these are the ground state configurations.

The equations determining the condition for a ground state, Eq. (9), transform, in the continuum limit, to a non-linear second-order differential equation. It is quite common in dealing with second-order differential equations to reduce each to two coupled first-order differential equations. A similar operation can be carried out with the difference equations. In fact, such a procedure applied to the discrete sine-Gordon equation gives rise to the well-known and much-studied standard map, also referred to as the Taylor-Chirikov (18) map or the Frenkel-Kontorova map. In the case of Eq. (9) this reduction can be effected as follows.

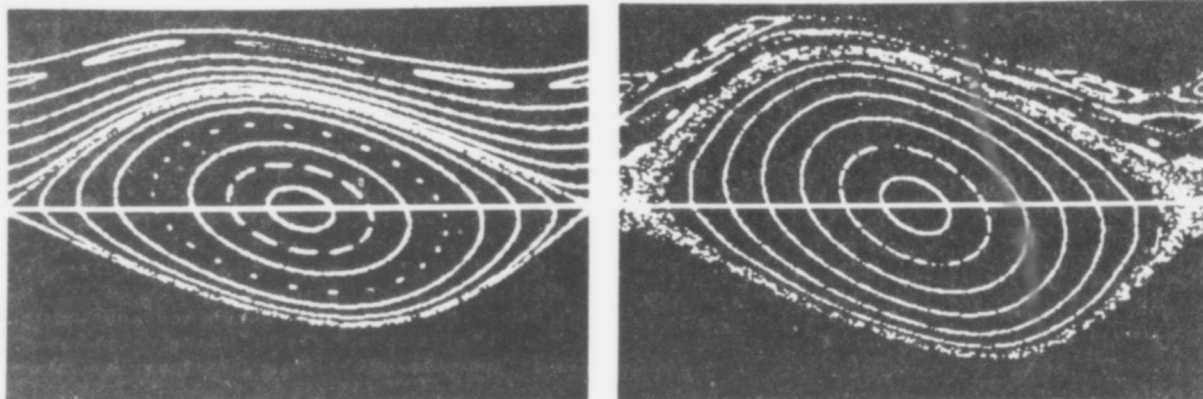


FIG. 8. A plot of  $s(\phi)$  shows how the angle between successive  $\text{CF}_2$  units varies with the angle between a  $\text{CF}_2$  unit and the crystal axis. The left-hand figure shows commensurate states as isolated rings or dots; the right-hand figure shows that at higher pressure chaotic states exist for which  $s$  is not a simple function of  $\phi$ .

A new variable  $s_n$  is defined through the equation

$$s_n = \sin(\phi_{n+1} - \phi_n - \alpha) \quad (10)$$

Then Eq. (9) can be rewritten in terms of  $\phi_n$  and  $s_n$  as

$$s_n - s_{n-1} = 2\gamma \sin 2\phi_n \quad (11)$$

Together, Eqs. (10) and (11) form a pair of equations analogous to a pair of coupled first-order differential equations.

The variable  $\phi$  is defined as modulo  $\pi$  and lies in the range  $[0, \pi]$  while the variable  $s$  is restricted to lie in the range  $[-1, +1]$  in order that the inverse sine be well defined. With these restrictions, Eqs. (10) and (11), which we rewrite here for convenience in the form

$$\phi_{n+1} = \phi_n + \alpha + \sin^{-1} s_n \quad (12)$$

$$s_{n+1} = s_n + 2\gamma \sin 2\phi_{n+1} \quad (13)$$

define a mapping of a part of the surface of a cylinder onto itself. This mapping, which can be expressed as

$$G(\phi_n, s_n) \rightarrow (\phi_{n+1}, s_{n+1}) \quad (14)$$

can be trivially shown to be area-preserving.

While no complete solution is possible, Banerjee was able to make a number of conjectures within the context of this simple model of PTFE. One of the most interesting ideas results from the observation that increasing pressure induces a commensurate phase to form at certain energies, but that there is an accompanying region of chaotic states of higher energy.

This is shown in Fig. 8, which is a map of  $s_n$  as a function of  $\phi_n$ . In (a) the pressure is low, and the continuous lines are indicative of an incommensurate system, with all possible values of  $\phi$  occurring, although for some energies these lines have broken up into rings, which are characteristic of commensurate states. At higher pressures, as shown in (b) the commensurate states are surrounded by a chaotic region in which  $s_n$  is not restricted to be a finitely valued function of  $\phi$ . One may speculate that these disordered states may play a crucial role in permitting rapid relaxation of one phase of PTFE to another as the temperature or pressure is varied.

#### Polybutylene Terephthalate

This almost-unpronounceable polymer is usually known as PBT, although some workers refer to it as PTMT, which is an abbreviation for the totally unpronounceable alternative name of polytetramethylene terephthalate. The repeat unit of the polymer chain consists of the terephthalate part, which is a benzene ring with a couple of carbon dioxides attached on opposite sides, and a linking butylene piece of connected  $\text{CH}_2$  units, as shown in Fig. 9.

The interesting properties of PBT reside in the fact that the butylene part has two possible conformations that are very close in energy. One of these is an extended conformation, in which the carbon atoms form a planar zig-zag, while the other has the butylene segment slightly coiled up. Luckily (for the wearers of stretch jeans) the coiled conformation has the lower energy, and is thus the stable form. It takes only a modest stress, however (and modesty is not an unimportant concept in this area) to produce a transition to the extended form.

The crucial aspect of this transition from the coiled conformation, which is known as

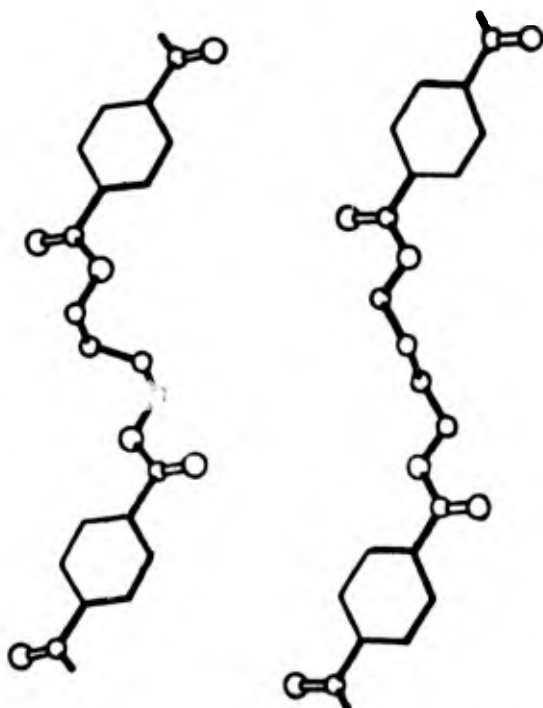


FIG. 9. Chain conformation in the  $\alpha$  (left) and  $\beta$  (right) forms of PBT.

$\alpha$ -PBT, to the extended  $\beta$ -PBT is that it appears to be totally reversible. On removal of the stress from the  $\beta$  chain, the  $\alpha$  chain is recovered. This property makes PBT almost unique among the simple polymers, and poses a challenge to theoretical analysis.

The fact that this stretchable property of PBT does represent a true crystal-crystal phase transition has now been demonstrated by a number of experimental techniques. Perhaps the most convincing of these is the type of dynamical x-ray measurement now possible using synchrotron radiation. There one can see the disappearance of some diffraction spots and the appearance of others as the crystal is strained over periods of a few milliseconds, the transition being apparently complete at strains of about ten per cent.

Very little is yet known about the detailed mechanism by which this polymer expands and contracts, although some competing models are starting to be suggested. Vandana Datye (19) has studied the question of whether neighboring benzene rings in adjacent chains remain linked to each other, or whether one chain can translate along its axis like a worm in a tunnel. Preliminary results seem to indicate that a model of linked chains yields better predictions for the stress at the critical point than does the alternative; these calculations, however, were only performed within a mean-field model, and so too great a reliance should not be placed on them.

## Conclusions

While crystalline polymers are an increasingly important object of scientific study, a large number of unanswered questions remain. In particular, the dynamical processes that come into play when crystal-crystal phase transitions take place represent an area immersed in, at best, controversy and, at worst, ignorance. The experimental information now being provided by more powerful and sophisticated instruments and techniques present us with an as yet uncompleted patchwork of clues as to the microscopic processes occurring. The development of a true theoretical understanding of the nature of relaxation in crystalline polymers will remain a challenge for some years to come.

## Acknowledgements

This work was supported by the Materials Research Laboratory program of the N.S.F. under grant DMR81-19425 and by the Army Research Office under grant DAAG29-83K-0168.

## References

- (1) E. W. Aslaksen, *J. Chem. Phys.* **57**, 2358 (1972).
- (2) R. G. Kepler and R. A. Anderson, *J. Appl. Phys.* **49**, 4490 (1978).
- (3) S. Duckworth, R. K. Bullough, P. J. Caudrey, and J. D. Gibbon, *Phys. Lett.* **57A**, 19 (1976).
- (4) J. E. McKinney, G. T. Davis, and M. G. Broadhurst, *J. Appl. Phys.* **51**, 1676 (1980).
- (5) D. Naegle and D. Y. Yoon, *Appl. Phys. Lett.* **33**, 132 (1978).
- (6) H. Dvey-Aharon, T. J. Sluckin and P. L. Taylor, *Phys. Rev.* **B21**, 3700 (1980).
- (7) T. Furukawa and G. E. Johnson, *Appl. Phys. Lett.* **38**, 1027 (1981).
- (8) J. D. Clark and P. L. Taylor, *Phys. Rev. Lett.* **49**, 1532 (1982).
- (9) C. W. Bunn and E. R. Howells, *Nature* **174**, 549 (1954).
- (10) C. A. Sperati and H. W. Starkweather, Jr., *Fortschr. Hochpolym.-Forsch* **2**, 465 (1961).
- (11) Edward S. Clark, J. J. Weeks, and R. K. Eby, *ACS Symposium Series* **141**, 183 (1980).
- (12) J. J. Weeks, I. C. Sanchez, R. K. Eby, and C. I. Poser, *Polymer* **21**, 325 (1980).
- (13) T. W. Bates and W. H. Stockmayer, *J. Chem. Phys.* **45**, 2321 (1966).
- (14) T. W. Bates, *Trans. Faraday Soc.* **63**, 1825 (1967).
- (15) T. W. Bates and W. H. Stockmayer, *Macromolecules* **1**, 12 (1968).
- (16) T. W. Bates and W. H. Stockmayer, *Macromolecules* **1**, 17 (1968).
- (17) A. Banerjee, Ph.D. thesis, Case Western Reserve University, 1983.
- (18) B. Chirikov, *Phys. Rep.* **52**, 265 (1979).
- (19) V. K. Datye and P. L. Taylor, *Bull. Am. Phys. Soc.* **29**, 408 (1984).

# MEASUREMENT OF THE TORQUE AND NORMAL FORCE IN TORSION IN THE STUDY OF THE THERMOVISCOELASTIC PROPERTIES OF POLYMER GLASSES

Gregory B. McKenna

Polymers Division  
National Bureau of Standards  
Washington, D. C. 20234

## Abstract

The simultaneous measurement of the torque and normal force responses in torsion experiments on viscoelastic materials provides multidimensional (multiaxial) data from a single simple test geometry. Two sorts of experimental programs are chosen as examples of the utility of these measurements in materials characterization. In the first, results from the literature are used to show how the torque and normal force data can be used to test constitutive relations in an efficient way. Data are presented which support the important theoretical prediction that in two step torsional deformations where the magnitude of the second step is one-half the magnitude of the first step, the normal stress response is predicted to be independent of the duration of the first step and equal to the single step response to a deformation of the same magnitude as the second step.

The second program involves a study of physical ageing in a freshly quenched polymer glass. The simultaneous measurement of the normal force and the torque provides an additional probe of the effects of the changes in volume accompanying ageing on the viscoelastic response of the glass. Results are presented which show, not only that the torque and normal force "age" differently, but also that the ageing behavior of the derivatives of the strain potential function is such that the classical picture of ageing needs to be reevaluated.

## Introduction

Early in this century, Poynting (1) carried out some elegant experiments in which he twisted steel wires and simultaneously measured length and volume changes. The length change effect has become widely known as the Poynting effect while the measurement of volume changes has been largely ignored\*. The Poynting effect has an analogue if one performs torsion experiments and holds the sample length constant: a normal force is measured on the ends of the sample. The implications of the Poynting effect and its

\*In recent work, Matsuoka, et al. (2) have measured length and diameter changes of solid polymers subjected to torsional deformations.

analogue normal force are well understood in terms of finite or second order elasticity theories (3,4) and have been extensively studied in the physics and rheology of polymer solutions, melts (5,6) and elastomers (4,7,8). It is only recently that work has been carried out to measure simultaneously the torque and normal force (or length change) of materials which are considered to be rigid solids such as glassy polymers (2,9,10) and highly deformable (plastic) metals (11,12,13).

In this paper we discuss the usefulness of normal force measurements which are made simultaneous with torque measurements when viscoelastic solids are subjected to stress relaxation histories. First we will show how the normal force data can be used as a consistency check in studying proposed constitutive relations which describe the torsional data. Second the use of normal force measurements will be shown to add an extra dimension to conventional physical ageing experiments (e.g., measurement of the evolution of the viscoelastic properties of a glass after a quench from above  $T_g$ ).

## Experimental Tests of Constitutive Relations

### The BKZ Constitutive Relation

In 1963 a single integral constitutive relation for non-linear viscoelastic materials was proposed by Bernstein, Kearsley and Zapas (14). This BKZ relation was formulated based upon the idea of an "ideal elastic fluid" and has proven an excellent model in the study of the viscoelastic behavior of polymeric melts and solutions.

In general, for an incompressible material, the stress,  $\sigma_{ij}(t)$  for any deformation history is described by the following constitutive relation (14,15):

$$\sigma_{ij}(t) = -p\delta_{ij} + \int_{-\infty}^t \{U_1(I_1, I_2, t-\tau) B_{ij}(t, \tau) - U_2(I_1, I_2, t-\tau) B_{ij}^{-1}(t, \tau)\} d\tau \quad (1)$$

where  $p$  is the hydrostatic pressure,  $\sigma_{ij}$  is the Kronecker delta,  $B(t, \tau)$  is the relative left Cauchy-Green deformation tensor,  $I_1$  and  $I_2$  are the invariants of  $B$ ,  $U$  is the strain potential function,  $U_1 = \partial U / \partial I_1$ , and  $U_2 = \partial U / \partial I_2$ .



The important feature of the BKZ theory was that from the determination of the material functions ( $U_1$  and  $U_2$ ) in single step stress relaxation histories; the behavior in more complicated deformation histories could, in principle, be described. For example Zapas and Craft (16) successfully used the single step stress relaxation behavior in simple extension and the BKZ theory to describe the behavior in multiple step, constant rate of stretch (load & unload) and creep and recovery experiments. (See Figures 1-3). Zapas and Phillips (17) successfully correlated the single step relaxation responses in shear of a polymer solution to the observed non-linear response for relaxation after cessation of steady shearing flows (Fig. 4). Thus, the BKZ theory has proven to be an excellent model of the non-linear viscoelastic behavior of polymeric materials. Its failings will be discussed subsequently, but first we show some results for the theory which are necessary in understanding the importance of simultaneous measurements of torque and normal force responses to study constitutive models.

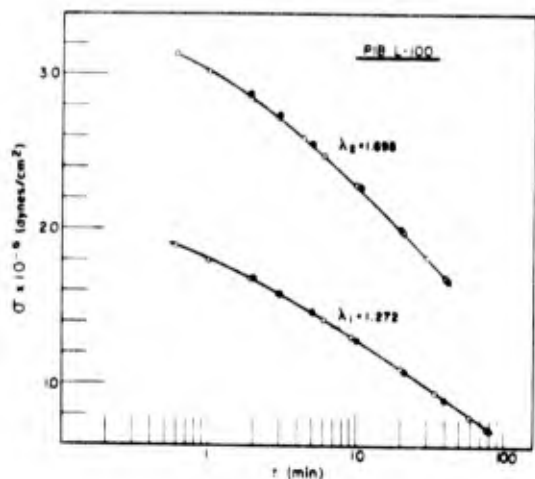


Figure 1. Comparison of BKZ prediction (black circles) with experimental results (open circles) in two step stress relaxation experiment on polyisobutylene in which the second step is greater than the first (16).

Although the BKZ theory postulates the existence of a strain potential function,  $U$  (which is similar to the strain energy function common to finite elasticity theories), Bernstein (15) has shown that for specific geometries of deformation one need only obtain the single step stress relaxation response of the system in that geometry and over the relevant range of time and magnitude of deformation in order to be able to describe arbitrary deformation histories in the same geometry. This obviates the necessity of actually determining  $U_1$  and  $U_2$  in many practical situations.

Thus, for example, in simple shear experiments:

$$\sigma_{12}(t) = \int_{-\infty}^t [\dot{\gamma}(t) - \dot{\gamma}(\tau)] G_*(\dot{\gamma}(t) - \dot{\gamma}(\tau), t - \tau) d\tau \quad (2)$$

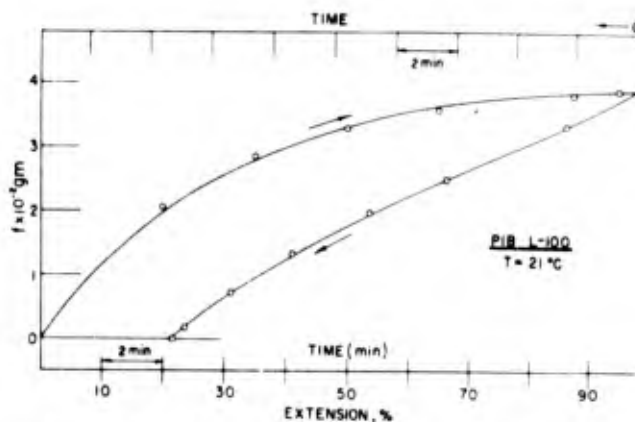


Figure 2. Comparison of BKZ prediction (open circles) with experimental results (solid line) for constant rate of strain in polyisobutylene (16).

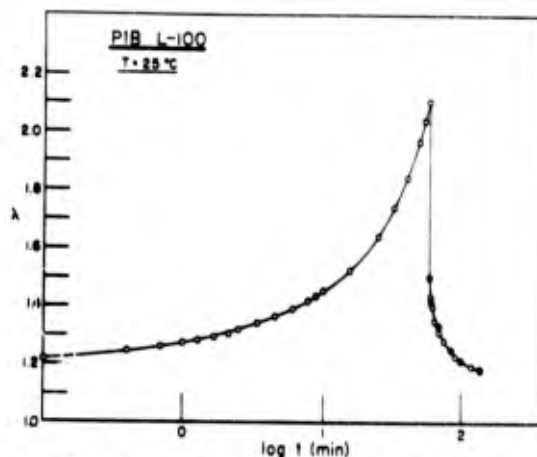


Figure 3. Comparison of BKZ prediction (black circles) with experimental results (open circles) for creep and recovery of polyisobutylene (16).

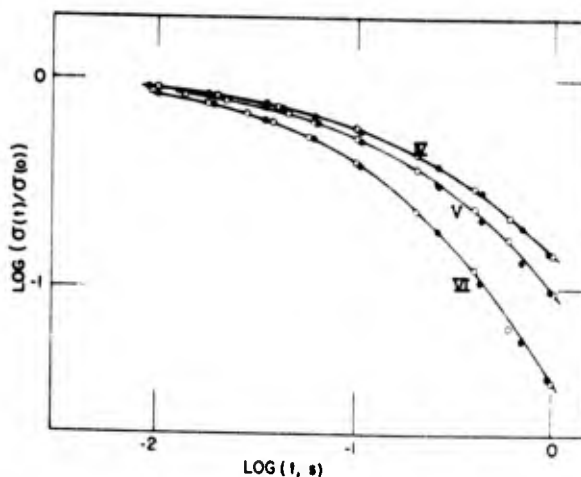


Figure 4. Comparison of BKZ prediction (black circles) for stress relaxation after steady shear with experimental results (open circles) for polyisobutylene. (IV)  $\dot{\gamma} = 0.177 \text{ s}^{-1}$ ; (V)  $\dot{\gamma} = 1.11 \text{ s}^{-1}$ ; (VI)  $\dot{\gamma} = 5.56 \text{ s}^{-1}$

where  $\sigma_{12}(t)$  is the shear stress response at time  $t$ ,  $\gamma(t)$  and  $\gamma(\tau)$  are the shear strains at times  $t$  and  $\tau$  respectively,  $G(\gamma, t)$  is the single step stress relaxation response at strain  $\gamma$  and time  $t$ , and  $G_* = \partial G / \partial t$ .

In torsional experiments (see Figure 5), the shear strain,  $\gamma$ , is a function of radial position,  $r$ , in the cylinder. In this case we must integrate over the cylinder cross section and find that the torque response  $T(t)$  is [9]:

$$T(t) = \int_{-\infty}^t K_*(\psi(t) - \psi(\tau), t - \tau) d\tau \quad (3)$$

where  $\psi$  is the angle of twist per unit length and  $K_*$  is analogous to  $G_*$  in eq. 2 only it includes the integration over the geometry, i.e.,

$$K_*(\psi, t) = -2\pi\psi \int_0^R G_*(\psi r, t) r^3 dr \quad (4)$$

and we note here that  $G_* = 2(U_1 + U_2)$  (5)

where the  $U_i$ 's are the derivatives of the BKZ strain potential function described previously (Eq. 1).

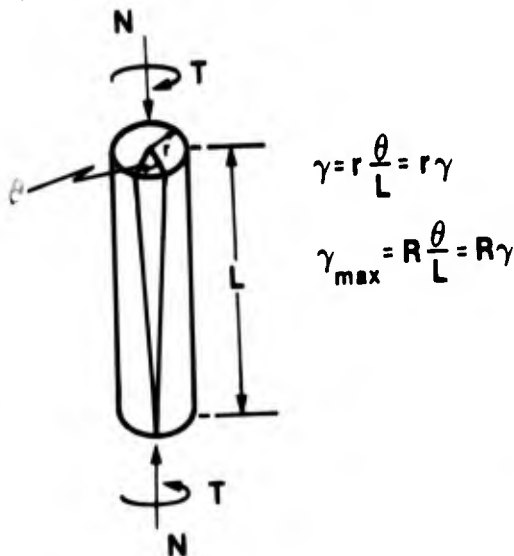


Figure 5. Torsion of a cylinder.

Similarly, one can find the normal force response in torsion:

$$N(t) = \int_{-\infty}^t H_*(\psi(t) - \psi(\tau), t - \tau) d\tau \quad (6)$$

where now  $H$  is the single step normal force relaxation function and is written as

$$H_*(\psi, t) = 2\pi\psi^2 \int_0^R L_*(\psi r, t) r^3 dr \quad (7)$$

where  $L_*$  in terms of the BKZ strain potential function is:

$$L_* = U_1 + 2U_2 \quad (8)$$

For single step stress relaxation histories described by

$$\psi(\tau) = 0 \quad \text{for } -\infty < \tau < 0$$

$$\psi(\tau) = \psi \quad \text{for } \tau \geq 0$$

the torque response is:

$$T(t) = \int_{-\infty}^0 K_*(\psi, t - \tau) d\tau = K(\psi, t) \quad (9)$$

thus, it is shown that  $K(\psi, t)$  represents the single-step torque response at a constant angle of twist (strain) and time,  $t$  where  $K(\psi, \infty) = 0$ . We note that  $K$  is an odd function in  $\psi$ , i.e.,  $K(\psi, t) = -K(-\psi, t)$ . Similarly, it can be shown that the normal force response to a single step history is

$$N(t) = H(\psi, t) \quad (10)$$

where we note that  $H$  is an even function in  $\psi$ , i.e.,  $H(\psi, t) = H(-\psi, t)$ .

For a two step strain history given by (see Figure 6)

$$\psi(\tau) = 0 \quad \text{for } -\infty < \tau < -t_1$$

$$\psi(\tau) = \psi_1 \quad \text{for } -t_1 \leq \tau < 0$$

$$\psi(\tau) = \psi_2 \quad \text{for } 0 \leq \tau$$
(A)

we obtain the torque response as

$$T(t) = K(\psi_2, t + t_1) + K(\psi_2 - \psi_1, t) - K(\psi_2 - \psi_1, t + t_1) \quad (11)$$

and the normal force response as

$$N(t) = H(\psi_2, t + t_1) + H(\psi_2 - \psi_1, t) - H(\psi_2 - \psi_1, t + t_1) \quad (12)$$

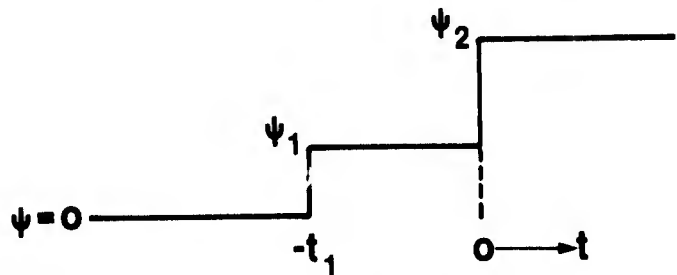


Figure 6. Two step deformation history.

Now as it turns out, it is in two step strain histories where the second step in strain is less than the first step in strain that the BKZ theory fails. Some of the first data showing this was obtained in the laboratories of the National Bureau of Standards by R. W. Penn (18). In his experiments, Penn twisted high purity aluminum wires and applied the BKZ theory to describe complicated strain histories from the single step stress relaxation response (Fig. 7). As can be seen in Figure 8, when the loading increases, the theory and experimental results agree reasonably well. On the other hand, if the sample is unloaded half way (i.e.,  $\gamma_2 = 1/2 \gamma_1$ ) the BKZ theory, while correctly predicting a maximum in the shear stress response, is unable to quantitatively describe the behavior (Fig. 9). Subsequently, Zapas (17)

carried out similar experiments on a solution of polyisobutylene and found that the BKZ theory was unable to predict the second step response (see Fig. 10).

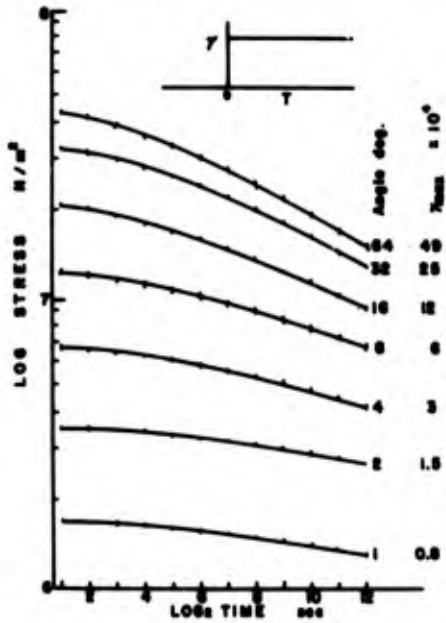


Figure 7. Single step stress relaxation of aluminum wire subjected to different angles of twist (18).

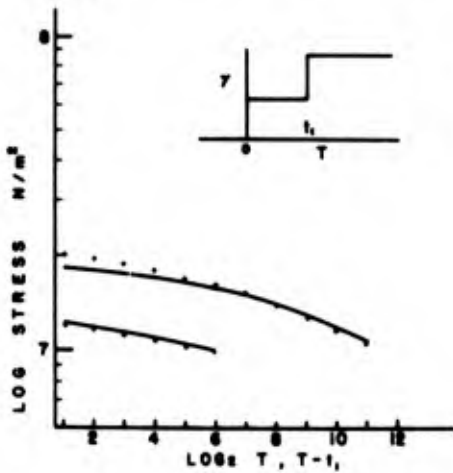


Figure 8. Comparison of BKZ prediction (solid line) with experimental results (black circles) for two step stress relaxation experiment in torsion of aluminum (18).

Though the BKZ theory does not correctly describe all deformation histories, its inherent simplicity and the power of the model have led to many efforts to modify the BKZ theory, without changing its fundamental structure (19,20, 21). In the following we will look at one such model and show how simultaneous measurement of torque and normal force responses proved an efficient method of testing a modified form of the theory.

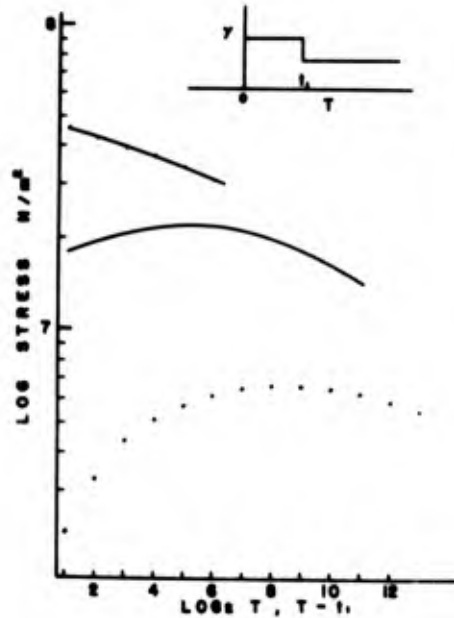


Figure 9. Comparison of BKZ prediction (solid line) with experimental results (black circles) for "half-step" torsional stress relaxation of aluminum (18).

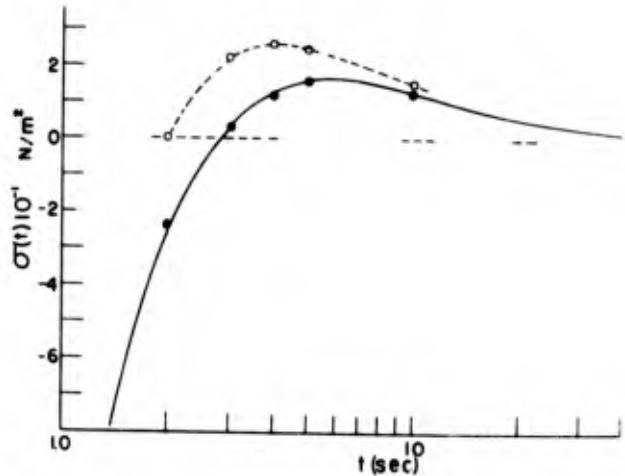


Figure 10. Comparison of BKZ prediction (open circles) with experimental results (black circles) for "half-step" shear stress relaxation of a polyisobutylene solution. The solid line represents the modified BKZ prediction (21).

#### A Modified Form of the BKZ Constitutive Equation

One attempt to correct the "faults" of the BKZ theory was proposed by Zapas (21) in 1974. He introduced a "material clock" function into the memory term of the kernel in the BKZ constitutive equation. This function "shifted" the material memory in a fashion which depended on the previous strain history. In what follows we will follow the development used in (9) for the torque and normal force responses in the modified BKZ theory.

In the original BKZ theory, the effect of the material configuration at all previous time,  $\tau < t$ , was taken to work in the same fashion as an elastic potential with the configuration at time,  $\tau$ , being the preferred configuration. Furthermore, the effect was one of a fading memory which depends upon the time elapsed between time,  $\tau$ , and the present time,  $t$ , i.e.,  $t-\tau$ . In the modified theory the memory depends on the previous strain history. For torsional histories the memory for the modified BKZ is given by:

$$\int_{\tau}^t \dot{\phi}(\psi(t), \psi(\tau), \psi(\xi), t-\xi) d\xi \quad (13)$$

where  $\dot{\phi}$  is the derivative of  $\phi$  with respect to the argument  $t-\xi$ . In the present work we take  $\phi(\psi(t), \psi(\tau), \psi(\xi), t-\xi)$  to be independent of  $\psi(\tau)$ . Then the torque response to a general history can be written as:

$$T(t) = -4\pi \int_{-\infty}^t \int_0^R \{ \psi(t) - \psi(\tau) \} \{ G_* [ (\psi(t) - \psi(\tau)) r, \int_{\tau}^t \dot{\phi}(\psi(t), \psi(\xi), t-\xi) d\xi ] \} \dot{\phi}(\psi(t), \psi(\tau), t-\tau) r^3 dr d\tau \quad (14)$$

and similarly for the normal force:

$$N(t) = 2\pi \int_{-\infty}^t \int_0^R \{ \psi(t) - \psi(\tau) \}^2 \{ L_* [ (\psi(t) - \psi(\tau)) r, \int_{\tau}^t \dot{\phi}(\psi(t), \psi(\xi), t-\xi) d\xi ] \} \dot{\phi}(\psi(t), \psi(\tau), t-\tau) r^3 dr d\tau \quad (15)$$

where the function  $\phi$  has the following properties:

$$\begin{aligned} \phi(\psi(t), \psi(\xi), \infty) &= 0 \\ \phi(\psi(t), \psi(\xi), 0) &= 0 \\ \text{and } \phi(\psi(t), \psi(\xi), t) &= t \text{ when } \psi(t) = \psi(\xi) \end{aligned}$$

and the functions  $G_*$  and  $L_*$  are defined as:

$$G_* = 2(U_1 + U_2); \quad L_* = U_1 + 2U_2 \quad (16)$$

where the  $U_1$  and  $U_2$  are as in the BKZ theory but now with the memory terms corresponding to the modified form, i.e.,

$$U_1(\gamma, t) = U_1(\gamma, \int_{\tau}^t \dot{\phi}(\gamma(t), \gamma(\xi), t-\xi) d\xi) \quad (17)$$

With the given definitions of  $\phi$  we can obtain the dependence of  $G_*$  and  $L_*$  (or  $U_1$  and  $U_2$ ) on strain as in the unmodified BKZ theory. Then from two-step histories the function  $\phi$  can be evaluated.

Following the procedure used in the above discussion of the unmodified BKZ theory for the single step stress relaxation torque and normal force responses we get  $T(t) = K(\psi, t)$  and  $N(t) = H(\psi, t)$ , respectively. For the two-step history (A) the results are:

$$T(t) = K(\psi_2, t+\zeta) + K(\psi_2 - \psi_1, t) - K(\psi_2 - \psi_1, t+\zeta) \quad (18)$$

$$N(t) = H(\psi_2, t+\zeta) + H(\psi_2 - \psi_1, t) - H(\psi_2 - \psi_1, t+\zeta) \quad (19)$$

where, again,  $K$  and  $H$  are the single step stress relaxation responses at the appropriate arguments and  $\zeta$  is given by

$$\zeta = \int_t^{t+t_1} \dot{\phi}(\psi_2, \psi_1, \theta) d\theta \quad (20)$$

There are two interesting points to be made here. First, note that the function  $\zeta$  is the same for the torque and normal force responses. This means that the same function required to fit the two step torsional data must fit the normal force data. This is a strong reason for simultaneous measurement of torque and normal force in the two step experiment because a function  $\zeta$  can always be found to fit the torque (or shear) data. Now, the same function must also fit the normal force data for the theory to be valid for these histories. In the subsequent section we will present the experimental results showing how this works.

Second, if we carry out a two step experiment in which  $\psi_2 = 1/2 \psi_1$  (what we call a half step strain history), due to the fact that  $H$  is an even function in  $\psi$  the normal force response is given as:

$$N(t) = H(\psi_2, t) \quad (21)$$

thus, we find that in this history  $N(t)$  is independent of the duration of the first step and equal to the single step response at a deformation amplitude,  $\psi_2$ , of the second step. This result is also given by the unmodified BKZ theory. The torque response does, however, depend upon the first step duration (through  $\phi$ ) and is given by:

$$T(t) = 2K(\psi_2, t+\zeta) - K(\psi_2, t) \quad (22)$$

Using the modified theory, Zapas (21) was able to describe experiments which the BKZ theory did not successfully describe. In figure 10 are compared the BKZ, modified BKZ and experimental data for a 19.3% polyisobutylene solution in cetane. As can be seen, the modified theory successfully describes the behavior. However, because of experimental limitations, Zapas was unable to carry out normal stress measurements in stress relaxation experiments and, therefore the theory could not be further tested without going to more complicated strain histories. As a result, the description of two step shear stress data with the modified BKZ theory could be criticized as "curve fitting". In order to test the modified theory, we carried out experiments on PMMA tubes as described in the following section (9,10).

#### Simultaneous Measurement of the Torque and Normal Force in Torsion

Experimental. We conducted our experiments (9) on cast cylindrical tubes of poly(methylmetha-

crylate) (PMMA), which were obtained from a commercial supplier\*.

The nominal tube inner diameter was 2.54 cm and the nominal outer diameter was 3.81 cm. The tubes were cut to 15.2-cm length and machined to an outer diameter of 3.33 cm on a lathe so that the outer and inner surfaces were coaxial. Tube diameters varied somewhat from specimen to specimen, but each cylinder was measured individually to the nearest 0.0025 cm and these values used for all subsequent calculations.

Gel permeation chromatography of c.e tube indicated that this manufacturer's cast acrylic has a number average molecular weight of approximately 546,000 and a narrow molecular weight distribution as indicated by an  $M_w/M_n$  of 1.17. It is expected that these values could vary from sample to sample, but no effort was made to examine such variations.

All tests were conducted at room temperature ( $24 \pm 1$  °C) using an Instron\*\* tension-torsion test machine. This machine is a servohydraulic system interfaced with a Hewlett-Packard\*\* 2100 minicomputer for control and data acquisition.

Single-step and multiple-step stress relaxation tests were conducted at various angular displacements. During the test normal force, torque, linear displacement, and angular displacement voltages were acquired as a function of time. Data were obtained at times from 0.05 to 10,000 seconds.

Two sets of experiments were performed. In one, tests were conducted on samples which had undergone no previous known strain history. Tests were conducted on PMMA which had been mechanically conditioned by cycling through a prescribed strain history. Single-step and two-step strain histories were applied to the samples. The time to reach the desired strain varied with the strain amplitude. The time to obtain a strain of 0.03 was less than 0.05 sec while the time to reach a strain of 0.06 was approximately 0.10 sec. For this reason the short time data at high strains may be somewhat unreliable.

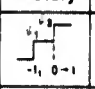
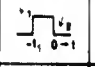
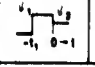
\*The equations for a tube are similar to those for a solid cylinder, however, the geometry is integrated from  $R_1$  to  $R_2$  rather than from 0 to  $R$ . The problem is briefly discussed in (10) and the results of Eqs. 11,12, and 18-23 are unchanged.

\*\*Certain commercial materials and equipment are identified in this paper in order to specify adequately the experimental procedure. In no case does such identification imply recommendation or endorsement by the National Bureau of Standards, nor does it imply necessarily the best available for the purpose.

In several cases the diameter was monitored for possible changes on samples tested at high strain amplitudes. No changes were observed within the measurement capability of the calipers used (0.0025 cm). No attempt was made to internally pressurize the tubes.

We also carried out experiments on a polyisobutylene solution (19.3% in cetane) using a parallel-plate arrangement (diameter = 7.0 cm, gap = 3.0 mm) in a Rheometrics Mechanical Spectrometer\*\*. The steps were introduced with the aid of dc voltage supply which could be varied to obtain the desired machine response (10). The two step strain histories studied are shown in Table 1 along with the equations which describe the torque and normal force responses.

Table 1. Two Step Strain Histories

Type	History	1	2	N(t)	T(t)
I.		$\psi$	2	$H(2\psi, t+\zeta) + H(\psi, t) - H(\psi, t+\zeta)$	$K(2\psi, t+\zeta) + K(\psi, t) - K(\psi, t+\zeta)$
II.		$\psi$	0	$H(\psi, t) - H(\psi, t+\zeta)$	$-K(\psi, t) + K(\psi, t+\zeta)$
III.		$\psi$	2	$H(\psi_2, t)$	$2K(\psi_2, t+\zeta) - K(\psi_2, t)$

Results and Discussions. In the following discussion it is important to keep in mind that, for all of the strain histories described, the shear stress (torque) response can be fitted using the modified form of the BKZ theory. From the values for  $\zeta$  (or  $\phi$ ) determined from this fitting procedure it is then possible to predict the normal stress response in the same strain history. If the normal stress response is successfully predicted it shows that the theory works for the strain histories involved and the theory has a predictive rather than merely a descriptive capability (if only the shear response is considered).

Figure 11 shows the normal stress response to a Type I history in which  $\psi_2 = 2\psi_1$  ( $\gamma_2 = 2\gamma_1$ ). Also shown are the BKZ and modified BKZ predictions. As can be seen the experimental results agree with the modified theory. Figure 12 shows the measured normal stress response along with the BKZ and modified BKZ predictions for a Type II history in which  $\psi_2 = 0$ . Again the modified theory quite successfully predicts the measured normal stress response. (We note here that for PMMA the regular BKZ theory, obviously, does not describe the torque response in two step histories).

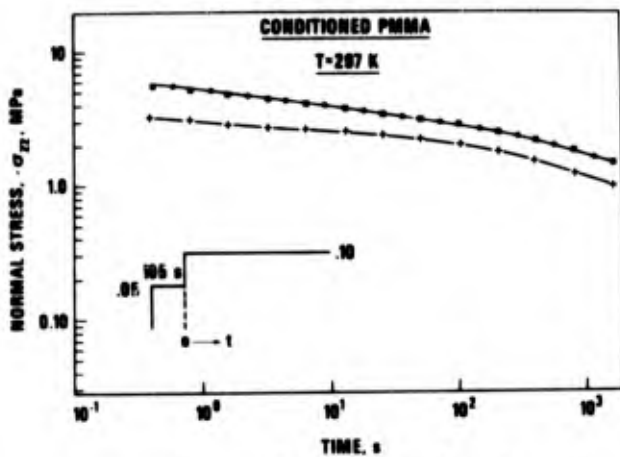


Figure 11. Second step normal stress response for a two step torsional history for PMMA in which  $2\gamma_1 = \gamma_2$ . BKZ theory (+); modified BKZ theory (●); experimental data (■) (9).

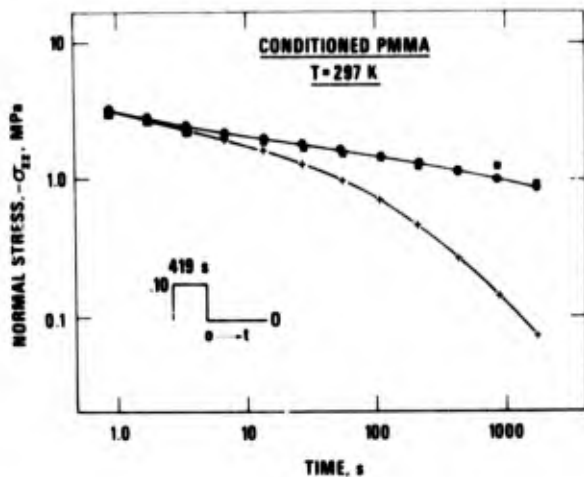


Figure 12. Second step normal stress response for a two-step history for PMMA in which  $\gamma_2=0$ . BKZ theory (+); modified BKZ theory (●); experimental data (■) (9).

The success of the modified BKZ theory in describing the Type I and Type II strain histories on the conditioned PMMA is very encouraging. However, the usefulness of measuring normal forces simultaneous with the torque can be seen to be important from the following, unique results, which we reported several years ago (9,10) and which are predicted both by the modified BKZ and the regular BKZ theories. In the half-step, Type III strain history, we recall that the BKZ theory could not describe the shear stress response (Figs. 9,10,11) but that the modified theory corrects this deficiency (Figs. 10,13). However, both theories predict that the normal stress response in this history is the same as in a single step experiment at a deformation amplitude equal to that of the second step (see eq. 21 and Table 1). Until 1979 (9,10) no one had noticed this interesting prediction. In Figure 14 we show a comparison between the second step response at  $\gamma_2=0.03$  ( $\gamma_1=0.06$ ) compared with the single step

response for  $\gamma=0.03$ . As can be seen there is no difference between the data points within experimental error. In Figure 15 we show a similar result for the PIB solution. Another check on this prediction is to test whether or not the response is independent of the first step duration,  $t_1$ . As can be seen in Fig. 16, this is indeed the case over a range of  $t_1$  from 3.28 to 1678 seconds. It is interesting that the BKZ type theories correctly predict that the normal stress behavior in the half-step (Type III) history is independent of the duration of the first step. This suggests that the structure of the BKZ-type theories is quite a good one. We note here that this response constrains the multiple integral expansion form of constitutive relation in such a fashion (by suppressing odd terms) that Coleman (22) felt that it would be useful to expand about the BKZ model instead.

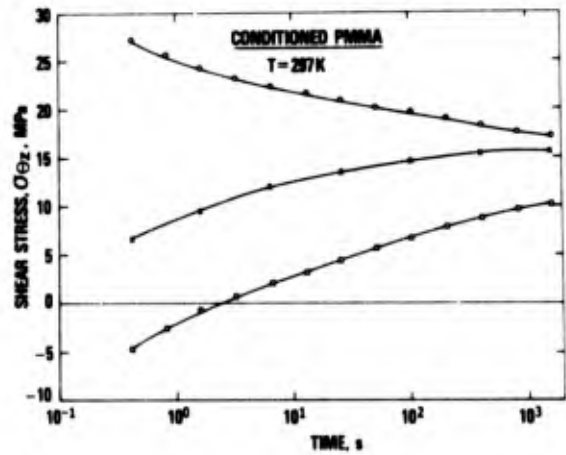


Figure 13. PMMA torque response in single-step stress relaxation history with  $\psi=1.81$  rad/m (o) compared with the second step response in a "half-step" history with  $\psi_1=3.62$  rad/m,  $\psi_2=1.81$  rad/m,  $t_1=419$  s (□). Also shown is the BKZ prediction (x) (10).

One other point about measuring the torque and normal force responses simultaneously is demonstrated in the following negative result. The "as received" PMMA which we tested could not be successfully described using the modified BKZ theory (9). In spite of the ability to describe the shear data in a Type II ( $\gamma_2=0$ ) strain history, the normal stress data could not be described. This is shown in Fig. 17. Without normal force data we would not have been able to state emphatically that as received PMMA cannot be described by this constitutive relation.

In summary, then, the simultaneous measurement of torque and normal force during stress relaxation experiments in constant length torsion is an efficient means for evaluating constitutive

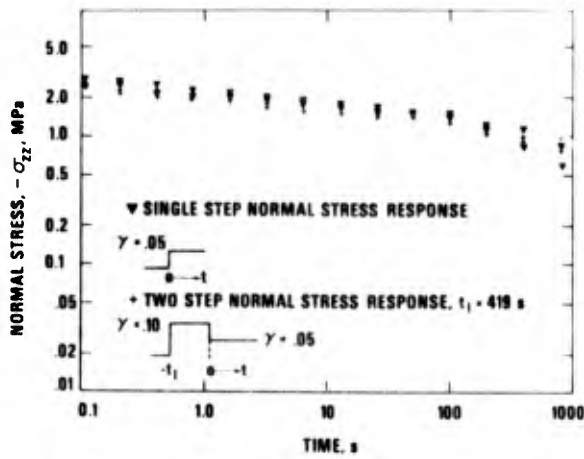


Figure 14. Second step normal stress response for a "half-step" stress relaxation history in which  $\gamma_1=2\gamma_2$  compared with the single step stress relaxation response at strain,  $\gamma_2$ . The triangles represent the single step response at  $\gamma=0.05$ ; the crosses represent the second step response at  $\gamma_2=0.05$  (9).

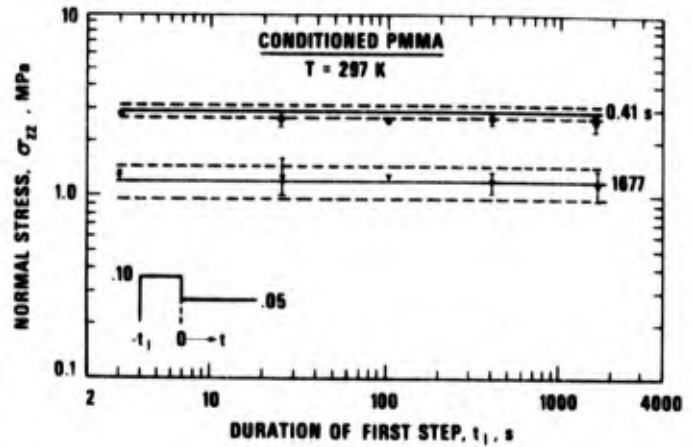


Figure 16. PMMA normal stress response in "half-step" torsional stress relaxation history vs. duration of first step  $t_1$ .  $\gamma_1=0.10$ ;  $\gamma_2=0.05$ . Solid lines show mean values for single step responses with  $\gamma=0.05$ . Dotted lines represent single standard deviation for single step response based on five replicate tests (10).

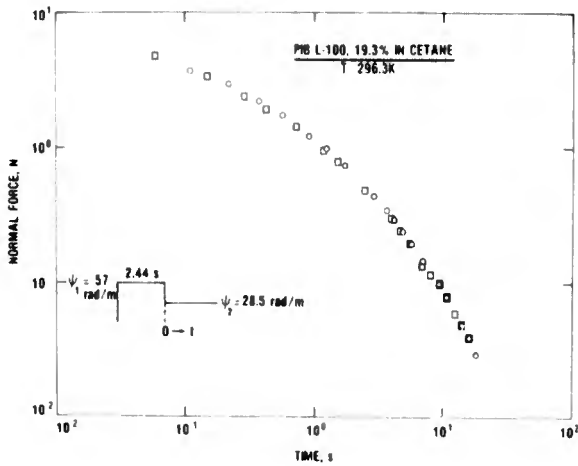


Figure 15. Polyisobutylene (19.3% in cetane) normal force response in a single step torsional stress relaxation history with  $\psi=28.5$  rad/m ( $\square$ ) compared with the second step response when  $\psi_2=1/2\psi_1=28.5$  rad/m ( $\circ$ ) (10).

relations, as shown by the contrasting results for the "as received" and the "mechanically conditioned" PMMA. In addition the simultaneous measurement of torque and normal force responses led to the interesting discovery that if the second step torsional deformation is half that of the first step ( $\psi_2=1/2\psi_1$ ) then the normal stress response on the second step is the same as the single step normal stress response at this deformation, i.e.,  $\psi=\psi_2$  and independent of the duration of the first step.

In the next section we show how simultaneous measurement of torque and normal force responses can serve as a useful probe of the viscoelastic response of glassy polymers as a func-

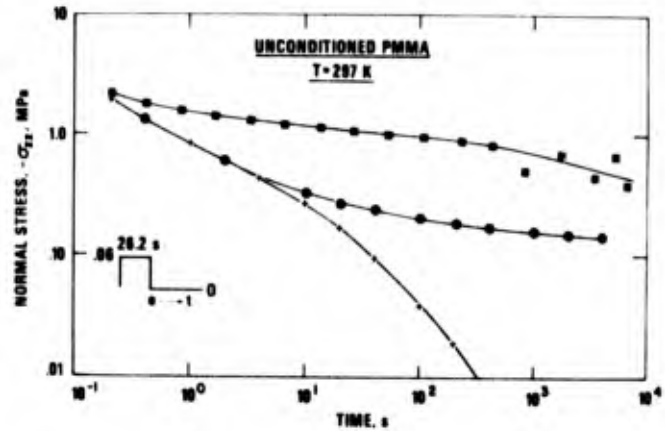


Figure 17. Second step normal stress response for unconditioned PMMA in a two step history in which  $\gamma_2=0$ . BKZ theory (+); modified BKZ theory ( $\bullet$ ); experimental data ( $\blacksquare$ ) (9).

tion of their physical state or structure after a quench from above  $T_g$  to below,  $T_g$ .

#### Torque and Normal Force Responses as Probes of Physical Ageing in Glassy Polymers

##### The Classical Picture of Ageing

Upon isobaric cooling through their glass transition range, undercooled liquids are known to depart from their thermodynamic equilibrium (23). This is illustrated schematically in Fig. 18. Non-equilibrium glassy structures are inherently unstable since they evolve spontaneously towards their equilibrium structure which depends only upon  $T$  (and  $P$ ) (23). This approach towards structural equilibrium is clearly reflected in the time dependence of the

volume and enthalpy of the glass as well as by its mechanical (viscoelastic) properties. Fig. 19 shows typical volume recovery curves for a polymer glass and Figure 20 shows how the relaxation modulus changes with increasing ageing time. This behavior was first evidenced by Kovacs, et al. (24) and subsequently named "physical ageing" by Struik (25) in his extensive work on a large number of glass forming materials.

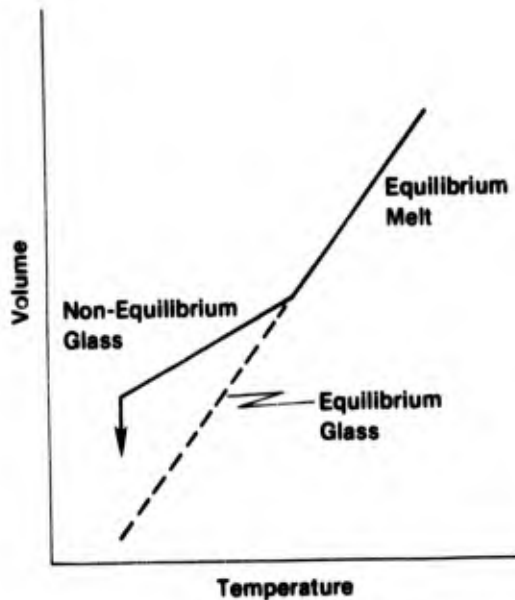


Figure 18. Schematic of volume temperature behavior of a glass.

Although Kovacs, et al. (24) could not account for the changes observed in the dynamic viscoelastic properties of a poly(vinyl acetate) glass with the time,  $t_e$ , elapsed after quenching, by a simple shift of the relaxation spectrum along the time (frequency) axis, Struik's (25) data, taken in creep, strongly suggest that ageing can be described quite accurately by merely shifting the retardation spectrum of the glass towards longer times. We refer to Struik's widely read treatise (25) for our "Classical Picture of Physical Ageing".

The classical picture of ageing, as formulated by Struik, is based on the postulate that as the volume of the glass decreases with increasing ageing time (c.f. Fig. 19) after a quench, the change in the glassy structure (free volume) changes the relaxation (or retardation) spectrum only by shifting it along the time axis by an amount  $t_e$ . The amount of the shift per decade of time,  $\mu$ , is found [from considerations of the autoretarding nature of the approach curves (of Figure 19) and free volume-molecular mobility arguments] to be less than or equal to unity, i.e.,

$$\mu = d \log a / d \log t_e \leq 1 \quad (23)$$

where  $\log a$  denotes the shifts along the logarithmic time axis required to superpose the

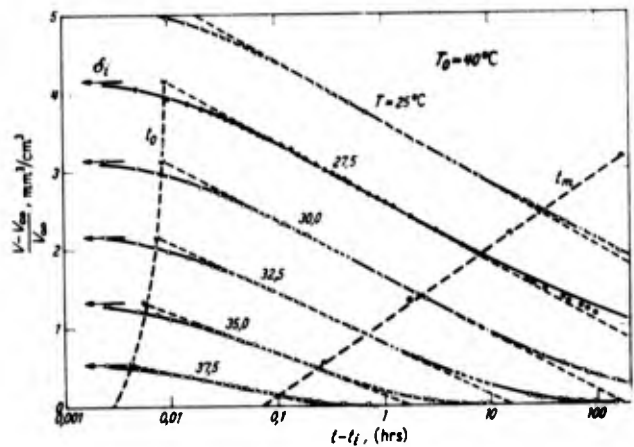


Figure 19. Isothermal volume recovery of polyvinyl acetate quenched from above  $T_g$  to temperature indicated. Note that over a large range in time, the slope,  $\beta = -d(v - v_e) / v_e / d \log t$  is constant and nearly independent of temperature. (After Kovacs (23) with permission).

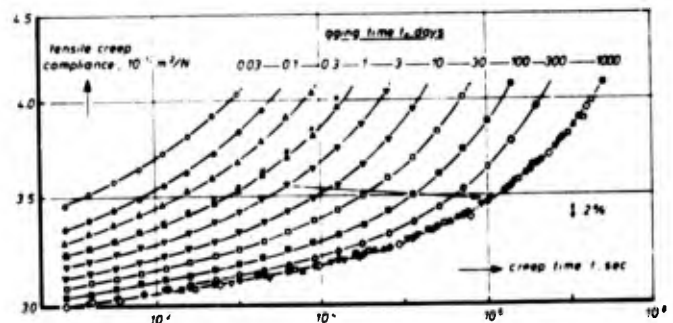


Figure 20. Small strain tensile creep of a PVC glass quenched from 90 °C ( $T_g + 10$  °C) to 20 °C at various ageing times,  $t_e$ , after the quench. (After Struik (25), with permission).

creep compliance,  $J(t, t_e)$  or relaxation modulus,  $G(t, t_e)$  curves measured at increasing values of  $t_e$  to that obtained at a reference ageing time  $t_e^0$ . Struik further notes that, in the so-called ageing range,  $\mu=1$ . His arguments are detailed in Appendix D of Reference (25).

In the classical picture of ageing, the above arguments are valid in the small deformation, linear viscoelastic range when the duration,  $t_1$ , of the relaxation or creep test is small relative to the ageing time, i.e.,  $t_1 / t_e \leq 0.10$ .

Struik has also investigated the change with ageing of the large stress (or deformation) properties of polymer glasses. He reports two additional phenomena: (i) Creep at large stresses "erases" (partially or completely) the effect of previous ageing (thus "rejuvenates" the glass by shifting its retardation spectrum towards shorter times) (see Figure 21) and, (ii) The rate of ageing,  $\mu$ , decreases dramatically as the stress increases (see Fig. 22).



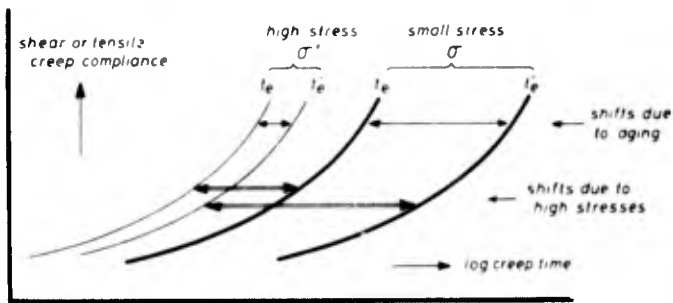


Figure 21. Schematic of the relative effects of ageing on the small stress and large stress creep behavior of a glass (after Struik (25), with permission).

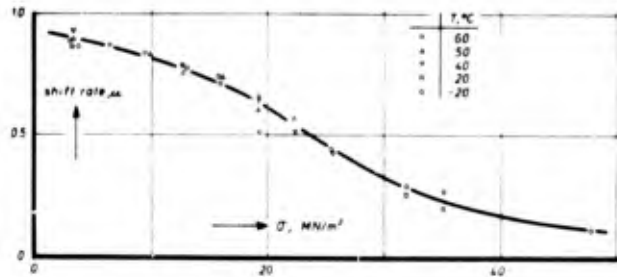


Figure 22. Variation of the "double logarithmic" shift rate with maximum shear stress for PVC quenched from 90 °C to various temperatures (after Struik (25), with permission).

Within a fair approximation, both of these effects are claimed to be virtually independent of temperature and the geometry of the deformation (tensile or shear) regardless of the chemical nature of the polymer. Struik (25) tentatively attributed these results to an increase of the free volume of the sample created by the deformation, i.e., by the mechanical energy dissipated by the system.

Although the Struik picture of ageing is still contested (26,27,28), it does serve as a useful reference to understand at least qualitatively, the model. In what follows, we will show what happens when the ageing phenomenon is studied in torsion and both the torque and normal force responses are measured simultaneously (29,30). As will be shown, the measurement of the normal force response provides an additional piece of information, which makes simple interpretation of ageing data along the lines of Struik's arguments quite difficult.

#### Comparison of the Effect of Ageing on Torque and Normal Force Responses

**Analysis.** From Section II we know that single step stress relaxation experiments carried out in torsion at constant length results in torque and normal force responses. In order to analyze the effects of ageing on the single step data in the non-linear viscoelastic range, we chose to use a reduced torque,  $T_R(t)$ , and a

reduced normal force,  $N_R(t)$ , defined as follows:

$$T_R(t) = T(t)/\pi R^3 \gamma \bar{G}/2 \quad (24)$$

where  $T(t)$  is the measured torque at time,  $t$ ,  $R$  is the radius of the cylinder,  $\gamma = \psi/R$  where  $\psi$  is the angle of twist per unit length and  $\bar{G}$  is the secant modulus in torsional stress relaxation.

$$N_R(t) = 2N(t)/\pi R^2 \gamma^2 \quad (25)$$

where  $N(t)$  is the measured normal force.  $N_R(t)$  is analogous to a second order relaxation modulus. Variation of  $T_R$  with  $\gamma$  implies non-linear behavior while that of  $N_R$  implies that higher than 2nd order terms are also operative (7,9,31).

In studying the effects of physical ageing on the  $T_R(t)$  and  $N_R(t)$  responses, we will make use of the Struik "double logarithmic shift rate",  $\mu$  defined in eq. 23 but now there will be a  $\mu$  which corresponds to the torque response and one which corresponds to the normal force response.

As discussed subsequently, our results showed unexpectedly that the torque and normal force responses "age" differently. We therefore found it useful to take advantage of a "scaling law" derived by Penn and Kearsley (7) to decompose our torque and normal force responses into more "fundamental" quantities which are, for viscoelastic materials, analogous to the derivatives of the strain energy function in rubber elasticity. The development follows reference 32: a. The Strain Potential Function Derivatives. For simple viscoelastic materials, Rivlin (33) has shown that for certain deformation histories, such as those obtained in single step stress relaxation experiments, isochronal data can be treated in the same manner as equilibrium data for elastic materials. For incompressible materials he showed that the stress in any deformation can be described using two material functions which are functions of time,  $t$ , and the invariants in the principal stretches,  $I_1$  and  $I_2$ . Though one need not assume the existence of a strain energy (or potential) function to describe single step stress relaxation histories, we shall use the BKZ-type notation presented in Section II.

In the BKZ theory of an elastic fluid (14) the existence of a time dependent strain potential function is postulated. If we consider single step stress relaxation deformations, then we can define isochronal values for the derivatives of the strain potential function as follows:

$$W_i(t) = \partial W / \partial I_i(I_1, I_2, t) = \int_{-\infty}^t \partial U / \partial I_i(I_1, I_2, t-\tau) d\tau \quad (26)$$

where  $U$  is the potential function of the BKZ theory and the  $I_i$ 's are the  $i^{\text{th}}$  invariants of the left relative Cauchy deformation tensor,  $t$  is present time and  $\tau$  is past time.

For torsion of an elastic rod with fixed ends, Penn and Kearsley (7) showed that the derivatives of the strain energy function can be determined from torque and normal force measurements. By a similar analysis for a viscoelastic (BKZ) rod we can find values for the  $W_1(t)$  defined above:

$$W_1(t) + W_2(t) = 1/4\pi\psi R^4(3T + T_\psi) \quad (27)$$

$$W_1(t) + 2W_2(t) = -1/\pi\psi^2 R^4(N + \psi N_{\psi,2}) \quad (28)$$

where  $R$  is the radius of the rod,  $\psi$  is the angle of twist per unit length, and  $N$  is the total normal force required to keep the length constant.  $T_\psi = \partial T / \partial \psi$  and  $N_{\psi,2} = \partial N / \partial (\psi^2)$ .

Equations 27 and 28 can be solved simultaneously for  $W_1(t)$  and  $W_2(t)$  as functions of both twist and time.

McKenna and Zapas (32) have determined  $W_1(t)$  and  $W_2(t)$  from the torque and normal force data obtained in single step stress relaxation experiments for the unconditioned PMMA described in Section II. Their results showed that  $W_1(t)$  is negative and increases towards zero (or even becomes positive) as either strain or time increase (Fig. 23).  $W_2(t)$  on the other hand is positive, much greater in magnitude than  $W_1(t)$ , and decreases towards zero as time or deformation increase (Fig. 24). The differences in the time and deformation behavior of  $W_1(t)$  and  $W_2(t)$  will be seen to be important in understanding the results of the ageing experiments described subsequently.

In studying the behavior of a polymer glass which is ageing, it is now necessary to do the scaling law analysis for  $W_1(t, t_e)$  and  $W_2(t, t_e)$  where  $t_e$  is the ageing time. It is then possible to determine how  $W_1$  and  $W_2$  shift with ageing time.

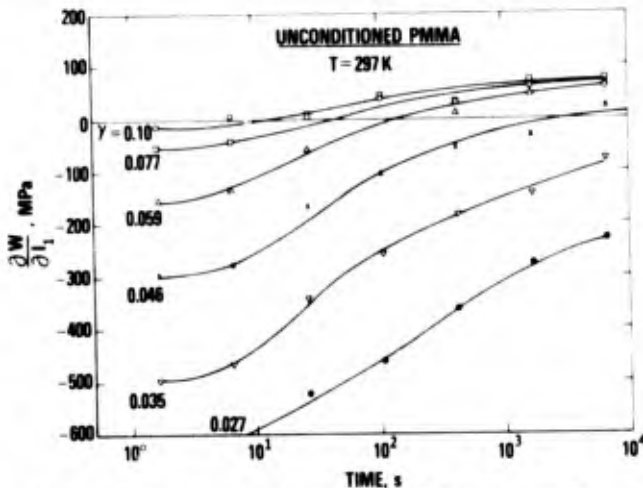


Figure 23.  $W_1$  as a function of time at various strain levels (as indicated) for PMMA.

Experimental. Specimens of an industrial grade PMMA ( $M_w = 1.3 \times 10^6$ ) were machined into 50 mm long cylinders with a 4.5 mm diameter along the 30 mm long gauge section. Both ends of the 10 mm

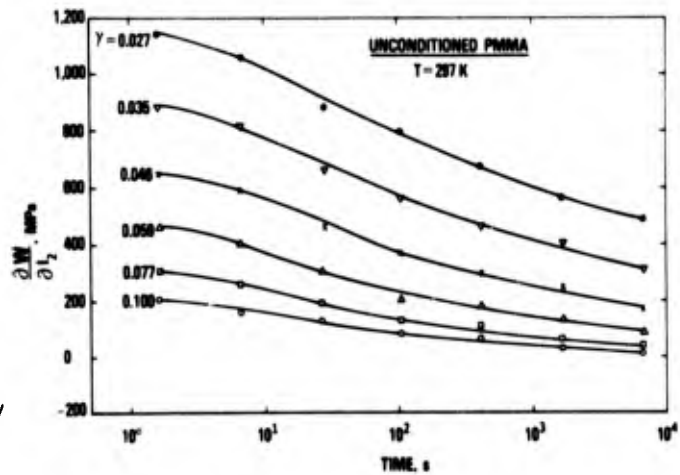


Figure 24.  $W_2$  as a function of time at various strain levels (as indicated) for PMMA.

diameter cylinder were pierced by concentric holes (5 mm in diameter 7.5 mm in depth) for accurate centering of the specimen into the Rheometrics Dynamic Mechanical Spectrometer (RDMS). The samples were heated to  $T_0 = 120^\circ\text{C}$  for 30 minutes, prior to each mechanical testing, and quenched to different  $T_1$  values (40, 60 and  $80^\circ\text{C}$ ) in the RDMS oven. The moment of the quench defines the origin of the ageing time,  $t_e$ , of the specimens.

Stress relaxation was measured with such samples submitted to the same deformation,  $\gamma = \psi R$ , at increasing ageing times. The relaxation tests, during which torque,  $T$ , and normal force,  $N$ , were recorded continuously, lasted only approximately  $0.1 \times t_e$  to reduce errors due to simultaneous structural recovery (see Struik (25)).

Results. Figure 25 depicts two families of stress relaxation "isotherms" for  $T_R$  at  $T_1 = 40^\circ$  and  $60^\circ\text{C}$ , both obtained in the linear range ( $\gamma = 0.0027$ ) at various ageing times, as indicated. Clearly, these relaxation curves cannot be superposed by simple horizontal shifts, even within each family of isotherms, nor can the isotherms be superposed with an additional vertical shift. In fact, at both temperatures the  $T_R(t)$  isotherms appear to rotate counterclockwise with increasing  $t_e$ , and the negative slope:  $s = -dT_R/d \log t$ , at comparable  $t_e$ , is always slightly larger at  $40^\circ$  than at  $60^\circ\text{C}$ . These features are in contradiction with the classical picture of ageing of Struik (25), but they are consistent with the results recently obtained by Guerdoux and Marchal (34) in dielectric, and by Guerdoux et al. (35) in dynamic mechanical investigations with a similar PMMA. Figure 26 represents three families of  $T_R(t)$  isotherms obtained at  $T_1 = 80^\circ\text{C}$ , at three different deformation levels, as indicated. This figure reveals a more classical behavior than Figure 25, since for any fixed value of  $\gamma$  the  $T_R(t)$  curves are superposable within a good approximation by simple horizontal shifts. Moreover, the  $T_R(t)$



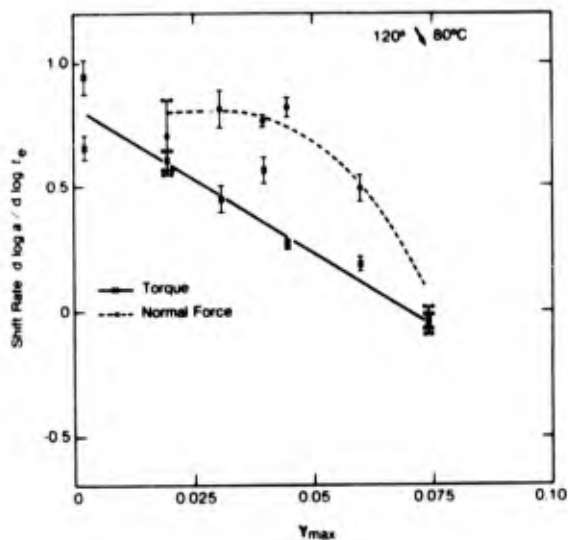


Figure 28. D formation dependence of the shift rates for  $T_R$  and  $N_R$  at 80 °C (29,30).

Table 2. Mechanical and Volumetric Ageing Parameters for PMMA (29,30)

$T_1$ (°C)	$10^4 \times B$ ( $\text{cm}^3 \text{g}^{-1}$ )	$\gamma_{\text{max}}$	$\mu(T_R)$	$\mu(N_R)$
40	3.6	0.0027	0.17-0.44 <sup>a</sup>	b
		0.039	0.17	0.51
60	3.7	0.0027	0.40-0.80 <sup>a</sup>	b
		0.039	0.25	0.66
80	3.5	0.0027	0.94	b
		0.0027	0.66	b
		0.020	0.61	0.71
		0.031	0.45	0.82
		0.040	0.56	0.77
		0.045	0.27	0.82
	0.060	0.19	0.49	
	0.074	-0.06 <sup>c</sup>	-0.03 <sup>c</sup>	

<sup>a</sup>The relevant  $T_R$  isotherms were not superposable. The figures indicate the approximate range of shift rates at the shortest and largest  $t$  values investigated (see Fig. 2).

<sup>b</sup>Normal force could not be measured at these small deformations.

<sup>c</sup>Negative  $\mu$  values at high values of  $\gamma$  suggest some strain softening is occurring.

An analysis of the torque and normal force response to determine  $W_1(t, t_e)$  and  $W_2(t, t_e)$  as described in the previous section was undertaken to examine the effects of ageing on  $W_1$  and  $W_2$ . As can be seen from Figure 29, not only are the shift rates for  $W_1$  and  $W_2$  different, but that for  $W_1$  is greater than unity at strains less than  $\gamma = 0.05$ , and the variation of  $\mu$  with deformation is greater for  $W_1$  than for  $W_2$ . These results do not fit in with the classical picture of ageing as discussed below.

**Discussion.** The results reported by McKenna and Kovacs (29,30) on the ageing behavior of PMMA reveal a few, though significant, discrep-

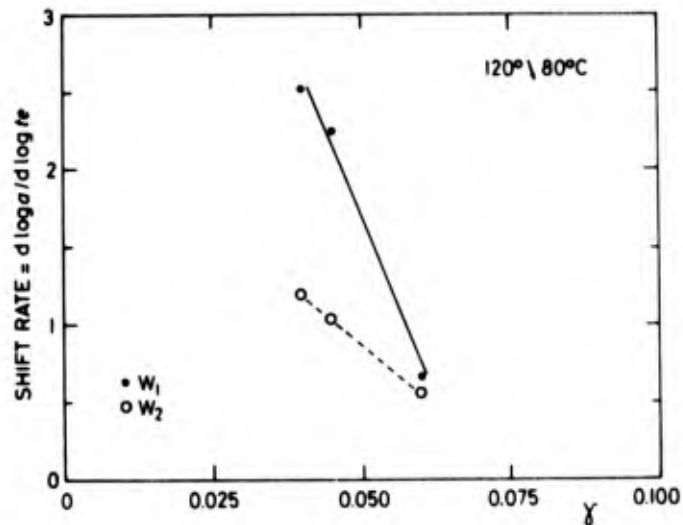


Figure 29. Deformation dependence of the shift rates for  $W_1$  and  $W_2$  at 80 °C.

ancies as compared to the general picture emerging from Struik's investigations (25). In the linear viscoelastic range, the  $T_R(t)$  relaxation isotherms, measured at increasing ageing times, cannot be superposed by mere shifting along the time axis below some critical temperature range ( $60^\circ < T_C < 80^\circ \text{C}$ ). This critical temperature range decreases, however, as the deformation increases. Such effects may be accounted for by a change with increasing ageing time in the shape of the relaxation spectrum at short times (24). This change in shape may arise from the fact that the contribution of the secondary relaxation processes varies with  $T_1$  (36). These processes are in fact known to display a much smaller temperature sensitivity than do the main retardation processes controlling the glass transition (25), and presumably similar differences exist for the structure dependence of these relaxations. Furthermore, the shift rate for the torque relaxation function,  $T_R(t)$ , decreases much more rapidly with increasing deformation than does that of the normal force relaxation function  $N_R(t)$ . This difference in shift rates for the torque and normal force responses increases with decreasing temperature (cf. Figs. 26-28 and Table 2), and implies that the molecular processes controlling the torque (shear) response are less sensitive to changes in structure (free volume) during ageing than are those determining the normal force response.

Decomposition of the torque and normal force into  $W_1(t)$  and  $W_2(t)$  gives an interesting result which requires further study for definite interpretation. However, the following can be said: (a) the finding that  $W_1(t)$  and  $W_2(t)$  show different shift rates implies that the molecular processes which are responsible for  $W_1(t)$  are affected differently by changes in glassy structure (free volume) than are the processes responsible for  $W_2(t)$ , (b) the result is consistent with the finding of McKenna and Zapas (32,37) discussed previously

in which the time dependence of  $W_1(t)$  and  $W_2(t)$  are different. Since the torque response is a function of  $W_1(t)$  and  $W_2(t)$  [c.f. eqs. 3-8] and the normal force response is a function of  $W_1(t)$  and  $2W_2(t)$ , the shift rates for  $W_1$ ,  $W_2$ ,  $T_R$  and  $N_R$  can all be different. This accounts for the observation that at  $\gamma < 0.05$   $\mu_T \leq 1$  and  $\mu_{N_R} \leq 1$  while  $\mu_{W_1} > 1$  and  $\mu_{W_2} \approx 1$ , and (c), the observation that the shift rate  $\mu$  for  $W_1(t)$  can be  $> 1$

implies that the Struik (25) arguments that  $\mu \leq 1$  need to be reevaluated because they apply to the kinetics of the volume relaxation and should, therefore, be independent of the viscoelastic property for which  $\mu$  is measured.

### Summary

Simultaneous measurement of the torque and normal force in solid materials gives additional information concerning their behavior which can only be obtained, otherwise, by carrying out a large number of experiments in various testing geometries. This procedure, then, has been shown to be useful in testing constitutive laws which have been used to "fit" torsional data. Thus, in Section II (9) we showed how a modified BKZ theory could be used to describe two step torsional (shear stress) stress relaxation data simply from the existence of an extra term (material clock) in the equation. By adding the measure of normal force it was shown that the behavior of "mechanically conditioned" PMMA could be well described by the modified theory while the same measurements on "as received" PMMA showed that this material did not follow the modified BKZ equations.

In addition, the normal force measurements were important in discovering (9,10) a fundamental material behavior which is also predicted by the BKZ and modified BKZ theories. That is, the normal stress (force) response to a two step strain history in which the second step strain is half the first step is predicted to be independent of the duration of the first step and identical to the responses to a single step history at the strain level of the second step.

It was also shown in Section III (28) that the torque and normal force responses can be used as probes of the physical ageing process in glassy polymers. The results show that the structure (free volume) of the glass affects the torque and normal forces differently since the rate of change (shift rate) of the torque with time after quench (ageing time) paralleling known changes in the volume of the specimen is different than that of the normal force. Decomposition of the torque and normal force data into the strain energy (potential) function derivatives,  $W_1(t)$  and  $W_2(t)$  using a scaling law approach (7) results in the interesting finding that the shift rate,  $\mu$ , for  $W_1(t)$

is different from that of  $W_2(t)$ , which implies that the effects of glassy structure (free volume) on  $W_1(t)$  and  $W_2(t)$  are different. Furthermore, it was found that  $\mu > 1$  for  $W_1(t)$ , implying that Struik's (25) argument that  $\mu \leq 1$  is incorrect.

The findings summarized in this article were made because of the ability to measure simultaneously the torque and normal force responses in torsional stress relaxation experiments. They show that it is important to carry out experiments in a multi-dimensional geometry. Such experiments can be used for testing constitutive laws in a relatively efficient manner. They can also serve as probes of other phenomena, such as physical ageing, by allowing one to observe two material responses simultaneously. Further work is continuing in this laboratory with the goal of resolving the questions raised by the experiments and analyses presented here.

### References

- (1) J. H. Poynting, Proc. Roy. Soc. (London), A86, 534 (1912).
- (2) T. T. Wang, H. M. Zupko, L. A. Wyndon and S. Matsuoka, Polymer 23, 1407 (1982).
- (3) F. D. Murnaghan, Finite Deformation of an Elastic Solid, J. Wiley & Sons, NY. (1951).
- (4) R. S. Rivlin and D. W. Saunders, Phil. Trans. Roy. Soc. (London) A243, 251 (1951).
- (5) R. B. Bird, R. C. Armstrong and O. Hassager, Dynamics of Polymeric Liquids: Vol. I Fluid Mechanics, J. Wiley & Sons, NY (1977).
- (6) W. R. Schowalter, Mechanics of Non-Newtonian Fluids. Pergamon Press, NY (1978).
- (7) W. Penn and E. A. Kearsley, Trans. Soc. Rheology, 20, 227 (1976).
- (8) G. B. McKenna and L. J. Zapas, Polymer 24, 1495 (1983).
- (9) G. B. McKenna and L. J. Zapas, J. Rheology 23, 151 (1979).
- (10) G. B. McKenna and L. J. Zapas, J. Rheol. 24, 367 (1980).
- (11) B. Wack, J. Mecanique 20, 737 (1981).
- (12) A. M. Freudenthal and M. Ronay, Proc. Roy. Soc. (London), A292, 14 (1966).
- (13) C. G'Sell, S. Boni and S. Shrivastava, J. Mater. Sci. 18, 903 (1983).
- (14) B. Bernstein, E. A. Kearsley and L. J. Zapas, Trans. Soc. Rheology, VII, 391 (1963).

- (15) B. Bernstein, *Acta Mechanica* II, 329 (1966).
- (16) L. J. Zapas and T. Craft, *J. Res. NBS*, 69A, 541 (1965).
- (17) L. J. Zapas and J. C. Phillips, *J. Res. NBS*, 75A, 33 (1971).
- (18) R. W. Penn, National Bureau of Standards, Unpublished Data.
- (19) B. Bernstein and A. Shokooh, *J. Rheol.* 24, 189 (1980).
- (20) M. H. Wagner and H. M. Laun, *Rheol. Acta*, 17, 138 (1978).
- (21) L. J. Zapas, "Nonlinear Behavior of Polyisobutylene Solutions", in *Deformation and Fracture of High Polymers*, ed. by H. H. Kausch, J. A. Hassell and R. I. Jaffee, Plenum Press, 381 (1974).
- (22) B. D. Coleman and L. J. Zapas, 53rd Annual Meeting of the Society of Rheology, Louisville, KY, 1981.
- (23) A. J. Kovacs, *Fortschr. Hochpolym.-Forsch.*, Bd. 3, 394 (1963).
- (24) A. J. Kovacs, R. A. Stratton, and J. D. Ferry, *J. Chem. Phys.* 67, 152 (1963).
- (25) L. C. E. Struik, *Physical Ageing in Amorphous Polymers and Other Materials*, Elsevier, Amsterdam (1978).
- (26) F. A. Myers, F. C. Cama and S. S. Sternstein, *Ann. N. Y. Acad. Sci.* 249, 94 (1972).
- (27) W. M. Prest, F. J. Roberts, Jr., and I. Hodge, Proc. 12th North American Thermal Analysis Society Conf. Williamsburg, VA, 1983, pp. 119.
- (28) C. K. Chai and N. G. McCrum, *Polymer* 21, 706 (1980).
- (29) G. B. McKenna and A. J. Kovacs, *Polymer Preprints* 24, 100 (1983).
- (30) G. B. McKenna and A. J. Kovacs, *Polymer Eng. Sci.* (to be published).
- (31) G. B. McKenna and L. J. Zapas, *Polymer* 24, 1495 (1983).
- (32) G. B. McKenna and L. J. Zapas, "Viscoelastic Behavior of Poly(methyl methacrylate) Prediction of Extensional Response from Torsional Data", in *Rheology, Vol. 3: Applications*, ed. by G. Astarita, G. Marrucci and L. Nicolais, Plenum Press, New York, 299 (1980).
- (33) R. S. Rivlin, *Quart. Appl. Math.*, 14, 83 (1956).
- (34) L. Guerdoux and E. Marchal, *Polymer* 22, 1199 (1981).
- (35) L. Guerdoux, R. A. Duckett and D. Froelich, *Polymer* (in press).
- (36) J. C. Wittmann and A. J. Kovacs, *J. Polym. Sci. C*, 15, 4443 (1969).
- (37) G. B. McKenna and L. J. Zapas, 49th Annual Meeting of the Society of Rheology, Houston, TX (1978).

## Nonlinear Viscoelastic Behavior of Glassy Polymers

K. L. Ngai  
Naval Research Laboratory  
Washington, D.C. 20375

and

A. F. Yee  
General Electric Corporate Research and Development  
Schenectady, NY 12345

We have extended a linear viscoelastic model to the nonlinear viscoelastic regimes of amorphous polymers. This is done by introduction of the structural state of relaxation and its dependence on strain. For any strain or stress history, the structural state of relaxation is evolving as a function of time, we are led to a constitutive equation for stress and strain. A new set of experiments has been designed and implemented for polycarbonate to verify the ideas and predictions of the model. The experimental data supports the basic premise of the model and brings out several of its predicted features. Some measurements in nonlinear viscoelasticity by other workers are reviewed and are shown to be consistent with the model. Comparisons are made between our model of nonlinear viscoelasticity with several established models. There are some common features as well as differences. Our model, based on fundamental mechanism of relaxation, provides a more microscopic foundation of the features of nonlinear viscoelasticity of amorphous polymers.

### INTRODUCTION

The mechanical properties of materials under finite or large deformations are of interest both from a fundamental and from a practical point of view. Materials of interest include metals, ceramics, plastics, textile fibers, inorganic glasses, elastomers, etc. In this work we limit our discussions to glassy polymers below their glass transition temperatures. Linear viscoelasticity based on the Boltzmann superposition principle, which describes well the behavior of glassy polymers at small strains, is no longer adequate at large strains. Therefore, a nonlinear viscoelasticity description needs to be constructed. Several nonlinear viscoelastic theories proposed in the past years have been reviewed by various workers.<sup>1,2</sup> These theories,<sup>3-16</sup> if used properly, can be useful in making predictions. However, it seems more advances have to be made before we have a satisfactory description that provides physical insight into the problems. There apparently is still plenty of room for contributions to be made in this area. This view is shared by Ward in his recent review<sup>17</sup> where he stated "There is not at present a representation of nonlinear viscoelasticity which gives an adequate description of the behavior and provides some physical insight into the origins of this behavior."

A new approach to nonlinear viscoelasticity of amorphous polymers is proposed here which first puts its emphasis on the fundamental origin, that is, a mechanism of nonlinear viscoelastic relaxation on the "molecular" level. This enables us to construct a nonlinear viscoelastic model in which the stress-strain response functional is proposed to have a specific form derivable from the molecular mechanism. In contrast, in most existing nonlinear viscoelastic theories the response functionals or functions are not derived from a physical basis and are left as empirical, to be determined by experiments. After the new approach has been presented, we shall discuss experimental data that give support to the model. Then, we shall review the various theories and models of nonlinear viscoelasticity proposed by others in the past. For the purpose of comparing our model with others, we consider only theories that are either specifically designed for or claimed to be applicable to amorphous polymers below the glass transition temperature. This restriction is necessary because the mechanism, and hence the model to be described here, is appropriate for amorphous polymers and may not be applicable to elastomers, polymer melts, etc. Although the approach with some modifications should be useful there also. In the future, we shall

return to the nonlinear viscoelasticity of these other systems.

## MODEL FOR RELAXATION

In glassy polymers, relaxation of a primitive species such as the primary ( $\alpha$ ) or the secondary ( $\beta$ ,  $\gamma$ , etc.) relaxations are responsible for many of the mechanical and dielectric properties. The traditional treatment of the relaxation<sup>17,18</sup> of any of these primitive species follows the conventional picture of transition in the presence of a heat bath. The transition rate is a constant  $W \equiv 1/\tau_0$ , independent of time. The constant,  $\tau_0$ , is often called the relaxation time. In glassy polymers the mechanical relaxation properties cannot be explained by a single relaxation time. Almost without exception, theoretical models<sup>19</sup> have invoked a distribution of relaxation times ascribed to one cause or another. We may add that what is proposed is an "inhomogeneous" distribution of relaxation times. In other words, for various reasons that invariably can be traced to randomness, one primitive species is said to relax with a relaxation time different from that of another.

In an approach<sup>21-24</sup> that departs at the outset from the traditional one, it was recognized that, in general, a primitive species does not relax with a constant relaxation rate  $W_0$ . Instead, the relaxation rate is time-dependent. Let us examine where the time-dependence of the relaxation rate comes from. Consider a primitive relaxation species in a glassy polymer. We can think of the primitive species as one or a few repeat units of a polymer chain, or a molecular moiety, or a side group, etc. As usual, the primitive species couples to the heat bath, through which relaxation of the primitive species with a constant relaxation rate  $W_0$  is now possible. In any of the above-cited examples of primitive species in a glassy polymer, in addition to the heat bath, these species couple also to many nearly degenerate (energy-wise) configurations of the polymer solid. After an initial period of time in which the primitive species has proceeded to relax, this coupling will cause concomitant adjustments of the configurations. Put another way, the initial relaxation of the primitive species will switch on a new coupling with the rest of the polymer, causing transitions between the near degenerate configurations to entail. These transitions which necessarily accompany the relaxation of the primitive species due to the coupling of the latter to its environs will slow down the relaxation process. The way that these accompanying transitions slow down the relaxation is by making the initial constant relaxation rate a function of time, in particular, a decreasing function of time,  $W(t)$ , at long times. The decrease in relaxation rate at long times (i.e.  $W(t) < W_0$ ) slows down the relaxation process by modification of the simple exponential decay to slower decreasing functions of time. There is

an alternative but equivalent description in terms of entropy evolution of the near degenerate configuration levels. Before relaxation of the primitive species takes place, these configurations are at thermodynamic equilibrium and hence attained the maximum value of the entropy. After relaxation of the primitive species has been initiated, its coupling with the configurations will drive them away from thermodynamic equilibrium by causing transitions among them. The entropy of the configurations which has the maximum value initially can only decrease. From theory,<sup>25</sup> the relaxation rate of the primitive species is  $\infty \exp(-F/RT) = \infty \exp(-\Delta H/RT) \exp(\Delta S/R)$ . Since entropy will decrease,  $\Delta S$  is negative. The relaxation rate is reduced from the primary rate of  $W \equiv \infty \exp(-\Delta H/RT)$  by the factor  $\exp(\Delta S/R)$ . In general,  $\Delta S$  is a function of time. Hence we can see from the entropy evolution following relaxation of the primitive species that its relaxation rate in glassy polymers will be reduced from its primary value. The reduction is a function of time and the exponential relaxation,  $\exp(-t/\tau_0)$ , will be modified and slowed down. Thus it is inappropriate to start with exponential relaxation with a time-independent relaxation time,  $\tau_0$ , to describe relaxation of a primitive species in glassy polymers. Each primitive species has a fundamental reason to relax nonexponentially with a time-dependent relaxation rate. Hence the traditional approach to describe relaxation of macroscopic quantities in glassy polymers by invoking an inhomogeneous distribution of time-independent relaxation times cannot be justified even though it is widely used.

After pointing out that relaxation rate is fundamentally time-dependent, one may ask how the time-dependence can be calculated. A full review of the calculations is outside the scope of this work. Only a skeletal description of the essential steps and results will be given here. For details, the reader is referred to References 20 and 24. The results to be described follow from a model of near degenerate configuration levels we have constructed. Although we know very little about the rather complicated configuration levels, there is a fundamental physical principle related to energy level repulsion that gives us information on the distribution of energy level spacings. For practically most condensed matter, including glassy polymers, the spacing distribution is always linear in energy at small energies. The interactions between the levels switched on by the primitive species after it starts to relax is a random variable. The distribution of this random interaction should be the same for all levels provided all level spacings involved are small. Knowledge of this distribution is difficult to obtain, and this is typical in amorphous and/or disordered materials where quantification of randomness is always difficult. We are not doing any better in ascertaining the distribution of the random interaction. Fortunately, even without any information of the actual distribution, we can



still proceed to obtain useful results and predictions of how the relaxation of the primitive species is modified. One has to pay a price, although not a dear one, of introducing parameters into the theory. The key parameter needed is  $n$ , which is the product of the average of the square of the random interaction variable and the proportionality constant of the linear (in energy) level spacing distribution. The quantity  $n$  is a combined measure of the strength of coupling of the primitive species to the configuration levels and the density of these levels. The linear spacing distributions which start at an energy  $E_c = h\nu_c$  ( $h$  is the Planck's constant) and extends down to zero energy decrease in entropy with time according to  $-n \ln(\omega t)$ . This reduces the relaxation rate to  $\omega_c^n (\omega t)^{-n}$ . At energies exceeding  $E_c$ , the level spacing distribution no longer increases linearly with energy. It levels off and then cuts off exponentially. The entropy decrease of these levels with spacings larger than  $E_c$  has no characteristic time dependence. We incorporate their contribution and call it  $-\Delta S_c$ . The reduced relaxation rate has the form of:

$$W(t) = W_0 e^{-\Delta S_c/R} (\omega_c t)^{-n}, \quad 0 \leq n < 1 \quad (1)$$

Substitution of the time-dependent relaxation rate given by Eq. (1) into the relaxation equation for primitive species,  $P$ , gives

$$dP/dt = -W(t)P \quad (2)$$

and on integration of Eq. (2), the primitive species relaxes according to

$$P = P_0 \exp(-t^{1-n}/(1-n)\exp(-\Delta S_c/R)\omega_c^n \tau_0) \quad (3)$$

This can be written as a pair of equations:

$$P = P_0 \exp[-(t/\tau_p)^{1-n}] \quad (4a)$$

and

$$\tau_p = [(1-n)\exp(-\Delta S_c/R)\omega_c^n \tau_0]^{1/1-n} \quad 0 \leq n < 1 \quad (4b)$$

Equation (4a) has the form of a fractional exponential function which has been repeatedly suggested<sup>26-31</sup> in the past as empirical relaxation functions. The compliance functions corresponding to the relaxation functions in the form of Eq. (4a) can be traced to Kohlrausch who in 1866 suggested a fractional exponential creep compliance function. Apparently Pierce in 1923 was the first to suggest directly the fractional exponential relaxation function which we rewrite in the familiar form of

$$P = P_0 \exp[-(t/\tau)^\beta], \quad 0 < \beta \leq 1 \quad (5)$$

In the field of dielectric relaxation, Williams and Watts<sup>31</sup> were the first to suggest Eq. (5) as a useful empirical function. In the field of amorphous polymers, Eq. (5) is often referred to as the Williams and Watts function even though mechanical relaxations are considered. We shall follow this custom.

Our model has led us to derive the Williams and Watts function from a microscopic and mechanistic approach, i.e., Eq. (4a). There is, in addition, another prediction given by Eq. (4b) that is entirely new. It gives a physical meaning to the measured effective relaxation time,  $\tau_p$ , by relating it to the microscopic primary<sup>P</sup> relaxation time,  $\tau_0$ , in a well-defined and quantitative manner. Equation (4a) and Eq. (4b) are coupled predictions. By coupled we mean that if the fractional exponential time dependence of Eq. (4a) gives a good fit to the time or frequency dependence of the experimental data for a choice of  $n$  and  $\tau_p$ , then these same  $n$  and  $\tau_p$  appear in Eq. (4b). Even with these same sets of  $n$  and  $\tau_p$  already determined via Eq. (4a), the abundance<sup>P</sup> of extra parameters,  $\Delta S_c$ ,  $\omega_c$  and  $\tau_0$  makes Eq. (4b) not difficult to be satisfied. In other words the extra prediction given by Eq. (4b) does not appear to lend extra validity to the model. However, this weakness is only apparent. To see this, let us stress the meaning of Eq. (4b) which is a restatement of the basic physics of the model. The primary microscopic relaxation time,  $\tau_0$ , of the primitive species is modified by the mechanism to  $\tau_p$ . The latter can be deduced readily from experimental data. Along with this modification, the dependences of  $\tau_0$  on thermodynamical variables such as temperature  $T$ , on molecular variables such as molecular weight, etc., will also be modified for  $\tau_p$ . For example, if  $\tau_0$  is thermally activated with activation enthalpy  $E_A$  so that

$$\tau_0 = \tau_\infty \exp(E_A/RT) \quad , \quad (6)$$

then

$$\tau_p = \tau_\infty^* \exp(E_A^*/RT) \quad (7)$$

where  $E_A^*$ , the activation enthalpy of  $\tau_p$  is related to  $E_A$  by

$$E_A^* = E_A/(1-n) \quad (8)$$

in which only  $n$  appears. This provides a stringent test since  $n$  can be obtained from experimental data. Such a prediction between the apparent activation enthalpy,  $E_A^*$ , and the microscopic activation enthalpy has been verified in many instances. For amorphous polymers below  $\tau_0$ , the most detailed study<sup>32</sup> was on the  $\gamma$ -relaxation of chloral-polycarbonate, a derivative of bisphenol-A-polycarbonate. In glassy chloral-polycarbonate measurements of NMR and dynamic mechanical relaxations have been made. Both sets of data are well fitted by Eq. (4a) with  $n=0.8$ . The primitive relaxation species involved has been identified by NMR techniques to involve phenylene ring rotation about the chain axis. Yet, the dynamic mechanical results suggest that the primitive species is at least one repeat unit. Thus an apparent contradiction existed. Both of these molecular motions have been studied by Hartree-Fock calculations and the activation enthalpy is found to be about 10 kJ/mol. in both cases. Earlier the same relaxation has been studied by

NMR in dilute solutions<sup>33</sup> of chloral-polycarbonate. In the most dilute solutions, it was found that the activation energy measured is close to about 10 kJ/mol. In this case, we have a rather clear situation. The activation energy based on theoretical molecular calculations is known. Further, in dilute solutions, the chain-chain interactions in the bulk are absent. One may then expect the measured activation energy of about 10 kJ/mol. can be taken as approximately that of the primitive species. Now with  $E_A \cong 10$  kJ/mol. known and  $n=0.8$  for the same relaxation in the glass, we can make an additional prediction based on Eq. (8) that the activation energy observed in bulk chloral should be about 50 kJ/mol. This is indeed the case. The apparent contradiction was resolved by considering a type of motion that was consistent with all the experimental observations and theoretical calculations.

We shall give a few more examples that lend strong support to Eq. (4b). These examples are restricted to the domain of polymeric systems, although some nonpolymeric glasses will also be included in the discussion. We shall illustrate that predictions of Eq. (4a) and (4b) are able to explain widely different features of polymer systems in the glassy, transition, rubbery plateau and terminal relaxation regions. Discussions will be brief because we do not intend to write a review here but rather cite them to bring out the universal nature of the mechanism. Consider monodisperse, linear, flexible polymers in the melt region. At sufficiently high molecular weights,  $M_c$  the chains entangle with each other. Through the entanglements, each polymer chain couples to the rest, i.e. configurations of other chains. The bare Rouse modes of relaxation of each polymer chain are given by the familiar expression

$$\tau_{oi} = \frac{M^2}{i^2} \left[ \frac{a^2 \zeta_0}{6\pi^2 M^2 kT} \right], \quad i=1, 2 \dots \quad (9a)$$

Note that

$$\tau_{oi} \propto M^2 \quad (9b)$$

The fundamental mechanism now works through the entanglement coupling, shifting each of the bare Rouse relaxation modes,  $\tau_{oi}$ , to the apparent  $\tau_{pi}$ . The degree of cooperativity of the Rouse mode decreases rapidly with the index  $i$ . Since the degree of cooperativity gives a measure of the coupling strength of the bare Rouse mode to the configurations, we expect that the fractional exponent,  $n_i$ , for mode  $i$  will be largest for  $i=1$  and decreases rapidly to zero as  $i$  increases. From the prediction of Eq. (4b), rewritten now in the form

$$\tau_{pi} = [(1-n_i) \exp(-\Delta S_i/R) \omega_c^{n_i} \tau_{oi}]^{1/(1-n_i)} \quad (10a)$$

$$\tau_{pi} \propto M \quad (10b)$$

it follows that the shift of  $\tau_{oi}$  to  $\tau_{pi}$  to longer times is the most significant. It is well known from Rouse's work that the bare  $i=1$  mode makes a major contribution to the flow viscosity. The nonlinearity of the magnitude of the shift obtained through exponentiation in Eq. (10) will enhance further the dominance of the shifted  $i=1$  Rouse mode. Thus the terminal relaxation region can be considered to be almost entirely due to one mode with relaxation time,  $\tau_p$ , and exponent,  $n_1$ . Its contribution to stress relaxation is

$$G(t) = G_N^0 \exp(-(t/\tau_{p1})^{1-n_1}) \quad (11)$$

which implies a steady-state viscosity

$$\eta = G_N^0 \tau_{p1} \Gamma[1/(1-n_1)] / (1-n_1) \quad (12a)$$

with

$$\eta \propto \tau_{p1} \propto M^{2/(1-n_1)} \quad (12b)$$

where  $\Gamma$  denotes the gamma function. The product of the plateau modulus and the recoverable compliance can be calculated directly. The expression is

$$J_e G_N^0 = (1-n_1) \Gamma[2/(1-n_1)] / \Gamma^2(1/(1-n_1)) \quad (13)$$

So far we have outlined the predictions on various measurable quantities of melt rheology. The tests come from analyses of experimental data. The test of Eq. (4b), now in the form of Eq. (11), comprises making comparisons of terminal relaxation frequency or dependence with the family of fractional exponential relaxation functions to see if there is an  $n$  value that gives a good fit to the data; and, if so, determine it. We have examined<sup>34</sup> monodisperse linear, flexible entangled polymer melts and concentrated solutions, using stress relaxation data  $G(t)$ , dynamic data  $G'(\omega)$ ,  $G''(\omega)$ , and creep compliance data  $J(t)$ . We found that without exception, each set of data is well fitted by the appropriate viscoelastic functions derivable from Eq. (11) for some  $n$  value. It is remarkable that good fits are obtained for most of the data for values of  $n$  lying between 0.4 and 0.47. Now with  $n_1$  fixed, at least inside an interval, we can test critically Eq. (4b) via Eqs. (12b) and (10b). That is, with the  $n_1$  values determined, do they predict a viscosity which has the molecular weight dependence of the form  $M^{3.4}$  found for most polymers? This is indeed a discriminating test because, with the allowable values of  $n_1$  already decided, there are no other adjustable parameters. It is easy to verify that for  $n_1=0.4$ , Eq. (12b) predicts that

$$\eta \propto M^{3.3}, \quad J_e G_N^0 = 2.05 \quad (14)$$

and for  $n = 0.47$ ,

$$\eta \propto M^{3.8}, \quad J_e G_N^0 = 2.63 \quad (15)$$

These predictions are in very good agreement with data. By going through this example, we hope the reader has acquired a better understanding of the general applicability of the coupling mechanism in relaxation, and how the relaxations of the bare microscopic primitive species (which in here is the terminal Rouse mode) are slowed down, resulting in a shift of the effective relaxation time  $\tau_p$  that appears in the fractional exponential relaxation function to a much longer time than the original  $\tau_{oi}$ .

Brief mention will be made on conductivity relaxation of  $Li^+$  ion in lithium-borate glasses.<sup>36,37</sup> A nonexact version of the work will be given for the sake of simplicity. The conductivity relaxation is described by the electric modulus function  $M^*(\omega) = M'(\omega) - iM''(\omega)$  which can be deduced from dielectric relaxation measurements. The primitive species is the  $Li^+$  ion. The relaxation process is the hopping motion of the  $Li^+$  ion from site to site. The coupling of the  $Li^+$  ion to the configuration levels causes the hopping relaxation rate to be time-dependent and has the generic form of Eq. (1). Indeed the measurements<sup>38</sup> show again that  $M^*(\omega)$  is well fitted by Eq. (4a) with  $n \approx 0.48$ . In this system, we can design a very stringent test of the second relation of Eq. (4b) by studying the isotope mass dependence.

One has a choice of  $^6Li$  or  $^7Li$  isotope in sample preparation. The temperature dependence of the hopping relaxation has the Arrhenius form. The activation energy as well as the value of  $n$  is independent of the isotope, as expected. The isotope mass dependence of  $\tau_o$  is

known. The simplest relation of  $\tau_o^{(7)}/\tau_o^{(6)} = \sqrt{7/6} \approx 1.08$  is expected. Then Eq. (4b) predicts that the observed  $\tau_p$  as well as the resistivity  $\rho$  (the electric analogue of flow viscosity) will have an enhanced isotope mass dependence of

$$\rho^{(7)}/\rho^{(6)} = \tau_p^{(7)}/\tau_p^{(6)} = (\tau_o^{(7)}/\tau_o^{(6)})^{1/(1-n)} \quad (16)$$

This is another unambiguous test of Eq. (4b), since in Eq. (16) only  $n$ , predetermined by fitting to  $M^*(\omega)$ , appears. The experimental data are in quantitative support of Eq. (16), thus verifying once more that the time dependent transition rate mechanism is appropriate.

Before we enter into the discussion of nonlinear viscoelasticity, it would be helpful to bring out clearly the concept of "structural state" implied by the present model of relaxation. The configuration levels that play a central role in modifying primitive species relaxation in a manner according to Eqs. (4a) and (4b) depend on the "structure" of the condensed matter in which the primitive species are immersed. This leads to another idea of checking Eqs. (4a) and (4b). Suppose we modify the "structure" of the condensed matter in one way or another, while the primitive species is kept the same. Then the configuration levels

as well as their strength of coupling to the same primitive species will be changed for the modified structure. We use the term "structural state" to describe the set of parameters  $\{n, \omega_c, \Delta S_c\}$  which essentially characterizes the configuration levels and their coupling to the primitive species. Structures modified differently will have different structural states. Their effective  $\tau_p$ 's will be related

differently to the same  $\tau_o$  because the sets  $\{n, \omega_c, \Delta S_c\}$  are different. Consider the example that  $\tau_o$  is thermally activated with  $\tau_o = \tau_{\infty} \exp(E_o^o/RT)$ . Let  $j=1,2, \dots$  index the different structures that are obtained by modifications of the original which we label by  $j=0$ . Then,  $n_j$  of the structural states  $\{n_j, \omega_{cj}, \Delta S_{cj}\}$  being all different, Eq. (4b) implies that

$$\tau_{pj} = \tau_{oj}^* \exp(E_{Aj}^*/RT) \quad (17)$$

where

$$E_{Aj}^* = E_A / (1-n_j) \quad (18)$$

Equation (18) can be restated as follows: The product  $E_{Aj}^*(1-n_j)$  is invariant and is the actual microscopic activation energy of the primitive species. An example of structural modification is the absorption of different amounts of water in polymers. In several studies,<sup>38,39</sup> Eq. (18) has been verified. Another example is dilution. Solutions of polycarbonates studied by Jones and coworkers<sup>33</sup> on the  $\gamma$ -relaxation are in accord with Eq. (18) as mentioned earlier already. Variation of temperature and pressure, or physical aging for a long enough time period will also modify the structure and the structural state. These modifications often take place most importantly when the temperature is near  $T_g$ . When near  $T_g$ , structural changes in most polymers and many, though not all, glasses are accompanied by volume changes or configurational entropy changes. A free volume<sup>40,41</sup> or configurational entropy<sup>42</sup> rationalization of the relaxation rate of the primitive species,  $\tau_o$ , suggest that  $\tau_o$  will also change with structural changes. In these circumstances, in addition to the structural state specification, we should add the information about  $\tau_o$ . We write it as  $\{n_j, \omega_{cj}, \Delta S_{cj}; \tau_{oj}\}$ . The relaxation rate is given by Eq. (1) and the effective  $\tau_p$  is still obtained from  $\tau_{pj}$  by Eq. (4b)--since the mechanism is universal, it is always operative. Other treatments of relaxation have usually neglected this;  $\tau_p$  is mistaken to be just  $\tau_{oj}$ . The nonexponential nature of the relaxation is accounted for, as an afterthought, to be due to a distribution of  $\tau_{oj}$ 's. To justify Eq. (4a), one needs to find an additional reason why the assumed distribution of  $\tau_{oj}$ 's is always such that they lead to Eq. (4a).

Most workers in relaxation of amorphous polymers and glasses have recognized the structure dependence of relaxation, especially near

T. The structure has been described by a fictive temperature,  $T_f$ , introduced by Toole,<sup>43</sup> or by deviation of volume,  $\delta$ , from equilibrium, considered by Kovacs.<sup>44</sup> We shall use  $\Sigma$  to label the structure with the understanding that  $\Sigma$  can be identified with  $T_f$  or with  $\delta$  wherever it is appropriate. Replacing the index j by a functional dependence on  $\Sigma$ , the structural state dependence on structure is specified in general by the set:

$$\{n(\Sigma), w_c(\Sigma), \Delta S_\gamma(\Sigma); \tau_o(\Sigma)\} \quad (19)$$

in the context of the present model. In the literature, for example, the dependence of  $\tau_o$  on structure has been proposed by Narayana-<sup>45</sup> to have the form of

$$\tau_o = A \exp\left(\frac{x\Delta h^*}{R} + \frac{(1-x)\Delta h^*}{RT_f}\right) \quad (20)$$

where x, lying between zero and one, is a parameter. Kovacs et al.<sup>46</sup> have proposed the form

$$\tau_o = \tau_r \exp[\theta(T_r - T)] \exp[-\theta(1-x)(T_f - T)] \quad (21)$$

which takes into account the dependence of  $\tau_o$  on the structure. The nonexponential nature of the relaxation process is then attributed to the existence of a distribution of relaxation times. Moynihan, et al.<sup>47</sup> have empirically used the fractional exponential functions with a temperature or structure independent  $\beta \equiv 1-n$  to model the distribution. Kovacs et al. have used a two-box distribution which gives approximately the same results as that of a fractional exponential for some value of  $\beta$ . It is important to emphasize that much of the important aspects of relaxation have been recognized by these workers and others. We come into this area by making a contribution to the understanding of the origin of the nonexponential nature of the relaxation, tracing it to a fundamental mechanism, and pointing out that structure dependence comes not only through  $\tau_o$  but also through  $n$ ,  $w_c$  and  $\Delta S_\gamma$ . That  $n$  is structure dependent is easy to check with experimental data. Torsional creep data of polystyrene<sup>35</sup> undergoing physical aging shows that  $n$  increases significantly as aging time increases, and indicates that  $n$  is structure dependent. Similar observations have been made on creep data of polyvinylchloride<sup>48</sup> and polypropylene.<sup>48,49</sup> Stress relaxation data of polystyrene<sup>48</sup> and silicate glasses<sup>48</sup> also exhibit the same behavior. Dielectric relaxation data on a number of glasses and polymers near  $T_g$  show that  $n$  for the primary relaxation is a function of  $T$ . In all these instances it is remarkable that not only  $n$  changes with  $T$ , but the relaxation proceeds according to Eq. (4a) at all temperatures. This is suggestive of the existence of a physical mechanism like the one discussed here.

## MODEL FOR NONLINEAR VISCOELASTICITY

The purpose of a lengthy discussion of the model for relaxation in the previous section is dual. First, we have given several examples to support the general applicability of the fundamental mechanism of relaxation described by Eqs. (1) or (4a) and (4b). These will facilitate the reader's understanding, especially in the construction here of an approach to nonlinear viscoelasticity. Second, some rudimentary concepts associated with the model for relaxation have been brought out and discussed. The most important concept is the structural state of relaxation specified by  $\{n(\Sigma), w_c(\Sigma), \Delta S_\gamma(\Sigma); \tau_o(\Sigma)\}$  where  $\Sigma$  denotes the structure. The variables that specify the structural state are a function of the structure itself. At time  $t'$  if the material is subjected to a step change of temperature or strain, etc., and if the structure is held constant thereafter to be  $\Sigma(t') \equiv \Sigma'$ , then the structural state of relaxation will modify the relaxation of a primitive species from the rate of  $\tau_o^{-1}(\Sigma)$  to

$$W(\Sigma', (t-t')) = \tau_o^{-1}(\Sigma') \exp(-\Delta S_\gamma(\Sigma')/R) (w_c(\Sigma')(t-t'))^{-n(\Sigma')} \quad (22)$$

for  $t > t'$ . If the structure  $\Sigma$  is also changing with time, then the structural state of relaxation is an implicit function of time. The momentarily relaxation rate will acquire an additional dependence on time through  $\Sigma(t)$ , i.e.

$$W(\Sigma(t), (t-t')) = \tau_o^{-1}(\Sigma(t)) \exp(-\Delta S_\gamma(\Sigma(t))/R) (w_c(\Sigma(t))(t-t'))^{-n(\Sigma(t))} \quad (23)$$

Although we have not explicitly written down for  $t > t'$  the dependence of  $\tau_o$  on the thermodynamic variables such as pressure or temperature, yet such dependences must be included in cases where pressure or temperature variations are involved. This is important for enthalpy recovery in step changes of temperature<sup>44,50</sup> and for continuous cooling and heating as in a D.S.C. experiment.<sup>47,51</sup>

As an example let us consider the classical volume recovery experiment of Kovacs.<sup>44,46</sup> A finite temperature jump near  $T_g$  from  $T$  to  $T'$  at  $t=0$  is entailed by structural relaxation which can be monitored by the volume recovery to its equilibrium value of  $V_\infty$  for temperature  $T$ . It simplifies matters if the instantaneous structure  $\Sigma(t)$  can be specified by the volume  $V(t)$  or by the volume deviation  $\delta(t) \equiv (V(t) - V_\infty)/V_\infty$  from equilibrium. The primitive species is now the relaxation responsible for structure or volume change near  $T_g$ . The time development of  $\delta(t)$  with the relaxation rate of Eq. (23) is governed by the differential equation

$$d\delta(t)/dt = -W(\delta(t), t) \delta(t) \quad (24)$$

which has the self-consistent solution of

$$\delta(t)/\delta(t=0) = \exp\left\{-\int_0^t dt' W(\delta(t'), t')\right\} \quad (25)$$

where

$$\delta(t=0) = (V(t=0) - V_\infty)/V_\infty \quad (26)$$

and

$$W(\delta(t), t) = \tau_0^{-1}(\delta(t), T) \exp(-\Delta S_\gamma(\delta(t))/R) [\omega_c(\delta(t))t]^{-n(\delta(t))} \quad (27)$$

Equation (25) can be solved numerically. The solutions have the features of asymmetry, nonlinearity and memory effects as pointed out by Aklonis and Kovacs.<sup>3,2</sup> Application has been made to polyvinylacetate.<sup>50</sup>

We shall be using a generalization of the expression on the right hand side of Eq. (25) repeatedly in this work. The generalized form takes into account that the step change occurs at  $t'$ . It has the form of

$$\exp\left\{-\int_{t'}^t dt'' W(\Sigma(t''), t''-t')\right\} \equiv \phi(t, t'; \Sigma(t'')) \quad (28)$$

From now on we need not indicate the temperature explicitly. This is because in considering nonlinear viscoelasticity the temperature is often kept constant throughout a stress-strain history.

With most of the tools at hand, we are ready to build a model for nonlinear viscoelasticity. To make things simpler, we consider an amorphous polymer in some state which does not change with time or changes with time so slowly that within any of the time periods of interest, the state remains in effect the same. An example of this is a well annealed sample with the structure approaching near that of equilibrium such that structure relaxation would be negligible in the time period of interest. This initial state can be considered free of stress or strain. If at some time,  $t_0$ , a step increase of strain is imposed on the sample. For  $t > t_0$ , the sample is then under a constant strain  $\epsilon_0$ . Since the material is viscoelastic, the resultant stress will relax from an instantaneous value according to

$$\sigma(t) = \epsilon_0 M(t-t_0) \quad t > t_0 \quad (29)$$

where  $M(t)$  is the stress relaxation modulus. The single step increment in strain corresponds to a strain history of

$$\epsilon(t) = \epsilon_0 \theta(t-t_0) \quad (30)$$

where  $\theta(t)$  is the unit step function,  $\theta(t)=0$  for  $t < 0$  and  $\theta(t)=1$  for  $t > 0$ . We can consider a more general strain history. The immediate generalization is the imposition of an arbitrary number of increments  $\epsilon_i$  in strain at times  $t_i$ ,  $i=0, 1, 2, \dots, N$ .<sup>1</sup> If the stress

relaxation can be accurately described by the linear superposition of responses

$$\sigma(t) = \sum_i \epsilon_i \theta(t-t_i) M(t-t_i) \quad (31)$$

for the same  $M(t)$ , and if  $M(t)$  is a function of time only and is independent of the strain magnitude  $\epsilon$  in Eq. (29), then the relaxation is linear viscoelastic. The modulus  $M(t)$  is related to relaxation processes in the molecular level of description. That  $M(t)$  is independent of strain magnitude and strain history is equivalent to the same independences of the molecular relaxation processes. The latter proceeds in general according to the relaxation function given by Eq. (28). Therefore, in the regime of linear viscoelasticity, the structure  $\Sigma$  is not modified by any of the strain magnitudes considered, and it remains unchanged throughout any strain history.

Large strain magnitudes that invalidate linear viscoelasticity in causing both the dependence of  $M(t)$  on  $\epsilon_0$  and breakdown of linear superposition in the form of Eq. (31) may be attributed partly to changes in structure. A change of structure will lead to a dependence of  $M(t)$  on  $\epsilon_0$  caused by the implicit dependence of the primitive species relaxation rate on  $\Sigma$ , as can be seen in Eq. (23). This, together with the change of  $\Sigma$  with time, make linear superposition with the same relaxation modulus function impossible. To construct a model of nonlinear viscoelasticity, we consider the dependence  $\Sigma_\infty(\epsilon)$  of the equilibrium structure on strain  $\epsilon$ . The initial state has been assumed to be at equilibrium with structure  $\Sigma_\infty(\epsilon=0)$ . If at time  $t=0$ , the sample is subjected to a large strain increment  $\epsilon_0$ . The strain history is given by  $\epsilon(t) = \epsilon_0 \theta(t)$ . For  $t < 0$ ,  $\Sigma(t) = \Sigma_\infty(\epsilon=0)$  and for  $t > 0$ ,  $\Sigma(t)$  relaxes from the initial structure  $\Sigma_\infty(\epsilon=0)$  toward the final equilibrium structure  $\Sigma_\infty(\epsilon_0)$ . The primitive molecular process that is responsible for the structural relaxation relaxes with the rate of Eq. (23) that is dependent on the instantaneous structure  $\Sigma(t)$  through the parameters of the structural state,  $\tau_0$ ,  $\omega$ ,  $\Delta S_\gamma$  and  $n$ . If  $\Sigma$  can be represented by a scalar such as the fictive temperature,  $T_f$ , of Toole,<sup>4,3</sup> or the equilibrium volume,  $V_\infty$ , of Kovacs,<sup>4,1</sup> then the relaxation of  $\Sigma$  for the strain history of  $\epsilon = \epsilon_0 \theta(t)$  follows the differential equation

$$d\Sigma(t)/dt = -W(\Sigma(t), t)\Sigma(t) \quad (32)$$

The solution of which, consistent with the boundary conditions,

$$\Sigma(t) = \Sigma_\infty(\epsilon_0) + (\Sigma_\infty(\epsilon=0) - \Sigma_\infty(\epsilon_0)) \exp\left\{-\int_0^t dt' W(\Sigma(t'), t')\right\} \quad (33)$$

With a fictive temperature representation of structure, the solution can be written as

$$T_f(t) = T_{f\infty}(\epsilon_0) + (T_{f\infty}(\epsilon=0) - T_{f\infty}(\epsilon_0)) \exp\left\{-\int_0^t dt' W(T_f(t'), t')\right\} \quad (34)$$

We shall use  $\Sigma$  as well as  $T_f$  for the designation of structure from this point on.

The stress relaxation modulus  $M(t)$  associated with the same primitive molecular relaxation process is given by

$$M(t) = M_R + (M_U - M_R) \exp\left\{-\int_0^t dt' W(T_f(t'), t')\right\} \quad (35)$$

where  $M_U$  and  $M_R$  are the unrelaxed and relaxed stress moduli respectively. If more than one primitive relaxation process is involved in the time period of interest, then we have to sum over their contributions in Eq. (35). If there is absence of variation of  $T_f$  with time so that all the relaxation parameters of the structural state are constant, moreover, if  $M_R$  and  $M_U$  are independent of the stress magnitude, then  $M(t)$  is a function of time only. The linear superposition of responses can hold and we have linear viscoelasticity. In general  $T_f$  evolves with time, and both  $M_R$  and  $M_U$  can depend on strain magnitude when the latter is large. Consideration of the dependences of  $M_R(\epsilon)$  and  $\Delta M(\epsilon) \equiv (M_U - M_R)$  on  $\epsilon$  from a fundamental point of view is beyond the scope of this work. The stress relaxes as

$$\sigma(t) = M(t)\epsilon_0 = M_R(\epsilon_0)\epsilon_0 + \Delta M(\epsilon_0)\epsilon_0 \exp\left\{-\int_0^t dt' W(T_f(t'), t')\right\} \quad (36)$$

If we define the fractional departure of the fictive temperature from equilibrium as

$$\Delta T_f(t, \epsilon_0) = [T_f(t) - T_{f\infty}(\epsilon_0)] / [T_{f\infty}(\epsilon_0) - T_{f\infty}(\epsilon_0)] \quad (37a)$$

According to Eqs. (34) and (28)

$$\Delta T_f(t, \epsilon_0) = \exp\left\{-\int_0^t dt' W(T_f(t'), t')\right\} \equiv \phi(t, 0; T_f(t')) \quad (37b)$$

Then on comparing Eq. (34) with Eq. (36), we obtain

$$\sigma(t) = M_R(\epsilon_0) + \Delta M(\epsilon_0) \cdot \Delta T_f(t, \epsilon_0) \quad (38)$$

relating the stress relaxation to the structural relaxation.

### Multiple Steps

An  $N$  step strain history described by

$$\epsilon(t) = \sum_{i=1}^N \epsilon_i \theta(t-t_i) \quad (39)$$

and  $t_i < t_{i+1}$  for  $i=1 \dots N-1$  will be considered by generalizing the one step result. Here  $\epsilon_i$  can be positive or negative, so long as  $\epsilon(t) \geq 0$  for all  $t \geq 0$ .

Let  $\epsilon_F = \sum_{i=1}^N \epsilon_i$ , which is the final strain at  $t > \max\{t_i\}$ . Then by superposition of the  $1 \leq i \leq N$  relaxation of the structure to each of

the  $N$  steps, it can be verified that the fictive temperature will relax according to:

$$T_f(t) = T_{f\infty}(\epsilon_F) + \sum_{j=1}^{N^*} (\Delta T_{f\infty})_j \exp\left\{-\int_{t_j}^t dt' W(t'-t_j; T_f(t'))\right\} \quad (40)$$

where

$$(\Delta T_{f\infty})_1 = T_{f\infty}(\epsilon=0) - T_{f\infty}(\epsilon_1) \quad (41)$$

and

$$(\Delta T_{f\infty})_j = T_{f\infty}(\epsilon_{j-1}) - T_{f\infty}(\epsilon_j) \quad (42)$$

for  $2 \leq j \leq N$ . The star superscript for the summation reminds us that if  $t_k < t < t_{k+1}$ , then the sum over  $j$  goes from 1 to  $k$  only.

The development of stress with time can be obtained by superposition of expressions given in Eq. (36) with the result

$$\sigma(t) = \sum_{j=1}^{N^*} M_R(\epsilon_j) \epsilon_j + \sum_{j=1}^{N^*} \Delta M_j \epsilon_j \exp\left\{-\int_{t_j}^t dt' W(t'-t_j; T_f(t'))\right\} \quad (43)$$

where

$$\Delta M_j = \Delta M\left(\sum_{i=1}^j \epsilon_i\right) \quad (44)$$

### Continuous Strain History

Having the result for a number of finite steps, we are ready to generalize it to infinitesimal steps and continuous strain history. The generalizations of Eq. (40) and Eq. (43) can be written down immediately for a strain history of  $\epsilon(t)$ ,  $t \geq 0$  and  $\epsilon=0$  for  $t < 0$ . The structural relaxation proceeds as

$$T_f(t) = T_{f\infty}(\epsilon(t)) - \int_0^t dt' \frac{dT_{f\infty}}{d\epsilon} \frac{d\epsilon}{dt'} \exp\left\{-\int_{t'}^t dt'' W(t''-t'; T_f(t''))\right\} \quad (45)$$

while the stress relaxation goes as

$$\sigma(t) = \int_0^t dt' M_R(\epsilon) \frac{d\epsilon}{dt'} + \int_0^t dt' \Delta M(\epsilon) \frac{d\epsilon}{dt'} \exp\left\{-\int_{t'}^t dt'' W(t''-t'; T_f(t''))\right\} \quad (46)$$

For the particular case of increase in strain starting from  $t=0$  at a constant strain rate  $\dot{\epsilon}$ , as encountered in yield studies,  $d\epsilon/dt$  in Eqs. (45) and (46) is a constant.

Equation 46 can be used to obtain creep in the nonlinear regime. For example, for a single step increase  $\sigma_0$  in load from zero load at  $t'=0$  we can regard the strain on the right hand side of the equation to increase exactly as that corresponding to the creep experiment. Then the stress on the left hand side must remain constant at  $\sigma_0$ . The creep strain  $\epsilon(t)$  can be obtained by solving the two simultaneous

integral-differential equations (45) and (46) with  $\sigma(t)$  set identically equal to  $\sigma_0$ . This consideration can be generalized to multiple steps or continuous loading history. The simultaneous equations can be solved numerically by a high speed computer. Results of such computations will be obtained in the future. In lieu of the numerical results, we give a physical description of nonlinear creep here. After the application of a large load  $\sigma_0$ , the strain initially increases exactly as the compliance function  $J_{\Sigma_0}$  for the structure

$\Sigma_0$ . Creep compliance is related to the relaxation modulus  $M_{\Sigma_0}$  by the relation

$$\int_0^t J_{\Sigma_0}(\tau) M_{\Sigma_0}(t-\tau) d\tau = t \quad (47a)$$

which can be derived from Eq. (47) if  $T_f$  or  $\Sigma$  remains unchanged and neglecting the first term on the right hand side. After an increment in time  $\delta t$ , the strain has increased by  $\delta \epsilon_1$ . If  $\delta \epsilon_1$  is large enough such that  $\Sigma_0(\delta \epsilon_1)$  is different from  $\Sigma_0$ , and if  $\delta t_1$  is long enough so that the structure  $\Sigma(\delta t_1) \equiv \Sigma_1$  at  $\delta t_1$  has departed from  $\Sigma_0$ , then the structural state of relaxation is modified and as a consequence the relaxation modulus is changed to  $M_{\Sigma_1}$ . For a

next increment in time  $\delta t_2$ , the creep compliance will follow  $J_{\Sigma_1}(t)$ , obtainable by inverting

$$\int_0^t J_{\Sigma_1}(\tau) M_{\Sigma_1}(t-\tau) d\tau = t \quad (47b)$$

After  $\delta t_2$  the strain will be incremented by  $\delta \epsilon_2$  and the structure changed to  $\Sigma(\delta t_2) \equiv \Sigma_2$ .

Then, for another increment in time  $\delta t_3$ , the creep will have compliance function  $J_{\Sigma_2}(t)$

that can be obtained by inversion of the formal relation with  $M_{\Sigma_2}$  and so on. In other words,

the creep compliance is composed of "pieces" from the family of curves  $J_{\Sigma_i}(t)$ . For  $\sum_{j=1}^i \delta t_j < t$

$< \sum_{j=1}^{i+1} \delta t_j$ , we take the piece from  $J_{\Sigma_i}(t)$ . This

is illustrated by Fig. 1. If  $\delta t_i$  is taken as infinitesimals, the vertical jumps between pieces is also infinitesimal. Passing to the limit of a large number of infinitesimal pieces, the  $J(t)$  for nonlinear creep can be constructed as the curve defined by the squares in the figure. Note that  $n(\Sigma_{i+1}) < n(\Sigma_i)$ . When we return to nonlinear creep in the next section, these discussions will be useful for understanding the experimental data. It is also worth noting that if dependence of  $T_{f\infty}$  or  $\Sigma_{\infty}$  on  $\epsilon$  is known, and if the structural state dependences  $n(T_f)$  etc. on  $T_f$  or  $\Sigma$  is known by stress relaxation measurements, then we can predict creep behavior at long times.

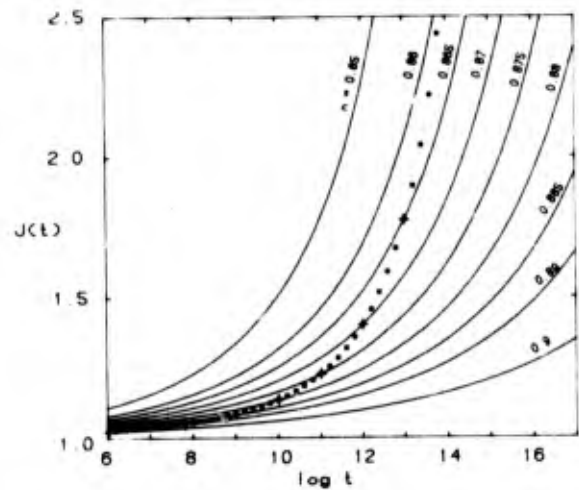


Fig. 1. A family of creep curves  $J_{\Sigma_i}(t)$  generated from an equation like Eq. (47a) with  $M_{\Sigma_i}(t)$

taken to have the form of Eq. (3) with  $n$  a function of  $\Sigma_i$ . At time  $t_i$ , if the structure is  $\Sigma_i$ , the creep compliance is taken from the  $J_{\Sigma_i}$  curve at  $t_i$  as illustrated by the crossed squares.

#### FEATURES OF THE MODEL

We shall bring out the salient features of the model through discussions of its predictions and the comparisons of these predictions with experimental data. New experimental evidence to support the basic premise of the model will be presented first. This is followed by a selected review of relevant experimental data available in the open literature and the interpretation of these in the context of the model.

The physical picture behind the model is the strain induced structural change with time, resulting in the structure moving towards a new equilibrium structure  $\Sigma_{\infty}(\epsilon)$ , where  $\epsilon$  is the step increase in strain at  $t=t'$ . Associated with each of the transient structure  $\Sigma(t)$  is the structural state of relaxation specified by the set  $\{n(\Sigma), w(\Sigma), \Delta S_{\Sigma}(\Sigma); \tau_0(\Sigma)\}$ ; and the relaxation proceeds with the rate of Eq. (23). If sufficiently long time has elapsed such that  $\Sigma$  has settled into  $\Sigma_{\infty}$ , then the structural state will assume the final constant values of  $\{n(\Sigma_{\infty}), w(\Sigma_{\infty}), \Delta S_{\Sigma}(\Sigma_{\infty}); \tau_0(\Sigma_{\infty})\}$ . If we probe the relaxation state of the equilibrium structure at  $t=t'$  without modifying it any further, then the relaxation with the time dependence of

$$\exp\left[-\frac{1-n(\Sigma_{\infty})}{1-n(\Sigma)}(t-\hat{t})\right] \exp(-\Delta S_{\Sigma}(\Sigma_{\infty})/R)(w_c(\Sigma_{\infty}))^{n(\Sigma_{\infty})} \tau_0(\Sigma_{\infty}) \quad (48)$$

should be observed for  $t > \hat{t}$ . Let us clarify this statement further because it is rather important. Probing the relaxation state of the equilibrium structure without modifying the

structure means the measurements of the viscoelastic relaxations made have not induced any structural change throughout the duration of the measurements. We can envisage using measurements like conventional nuclear magnetic resonance (NMR) of the spin lattice relaxation times  $T_1$  or  $T_{1\rho}$  in the rotating frame, dielectric relaxation, photon correlation spectroscopy, thermal stimulated current spectroscopy, creep and stress relaxation etc. as probes. It is immediately obvious that all these measurements, except the mechanical relaxations will not induce any change of structure. Even the mechanical relaxation measurements will not modify the structure further provided the additional strain or stress imposed is sufficiently small. That is, although we are dealing with the subject of nonlinear viscoelasticity, linear viscoelastic measurements with small strain or stress can be made and used to characterize the structural state of relaxation at the equilibrium structure. The idea of characterization of the structural state of nonlinear viscoelastic amorphous polymers by a technique of another kind, such as light scattering, is attractive though not pragmatic at this time. It is far more convenient to use small strain induced stress relaxation since essentially the same experimental set-up can be used. Characterization of relaxation state can be generalized to a transient structure  $\Sigma(t)$  at any  $t$  provided the change in  $\Sigma(t)$  during the period of time necessary for making the measurements is negligible. If this condition is satisfied, the measurements for characterization can be thought of as a snapshot taken of the transient structure  $\Sigma(t)$ . To make easy reference to the small strain stress-relaxation measurements, and to avoid confusion with the large strain stress response, we shall call the former "tickle" measurements or runs.

#### EXPERIMENTAL EVIDENCE

The experiments are designed to verify the predictions of the model in the case of large strains. Uniaxial tensile experiments are used for convenience, even though shear experiments are somewhat easier to interpret. In the experiment, an initial strain is applied in the form of a ramp. After some time  $t_s$  has elapsed, the structure has approached essentially a constant state, and it is probed with an additional small strain step, i.e., a "tickle." It is this tickle step that is analyzed in terms of Eq. (48). This experimental procedure is schematically illustrated in Figs. 2 and 3. The time necessary for the structure to reach a constant state  $t_s$  is simply determined by the application of a series of small tickles, each of which is analyzed in terms of Eq. (48). When the coupling parameter  $n$  becomes constant to within the experimental error, then  $t_s$  is considered to have been reached. The experimental details are given in the following sections.

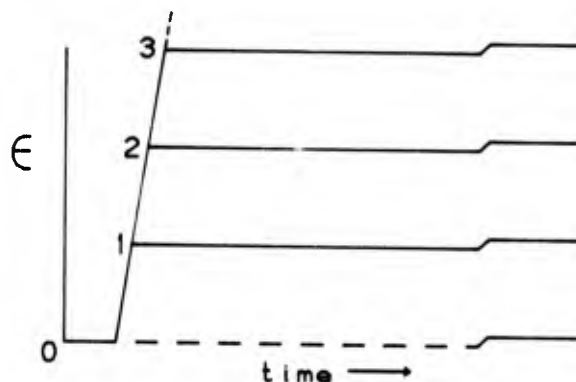


Fig. 2. An initial large strain is first applied and followed by an additional small strain step ("tickle") after an elapsed time,  $t_s$ .

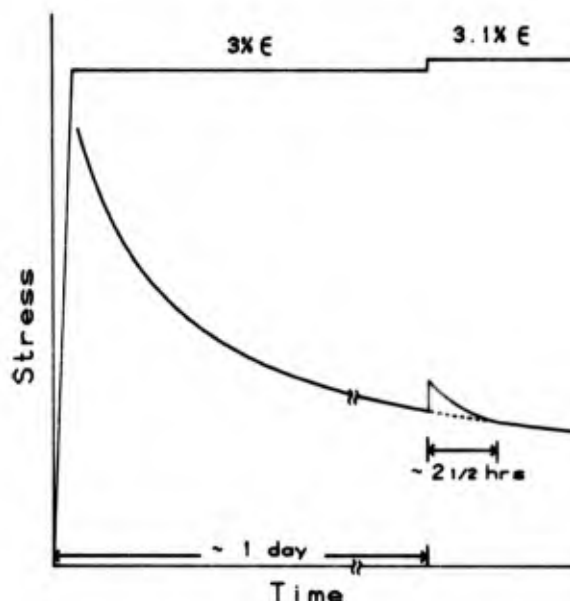


Fig. 3. Stress relaxation as a function of time (thick curve) that corresponds to the strain history of Fig. 2 and redrawn for 3% initial strain and 0.1% tickle. The elapsed time is approximately 1 day.

#### Specimen Preparation

The polymer selected for these studies was BPA-polycarbonate in the form of 2.5mm-thick extruded sheets made from Texan thermoplastic resin produced by the General Electric Co. The molecular weight of this material has been determined by GPC using methylene chloride as the solvent and polystyrene as standard.  $M_n$  was found to be about 30,000 and  $M_w$  about 10,000. A small amount of orientation existed in the as-received sheets as judged by the amount of birefringence, which was quite uniform. Most of the experiments were performed on the as-received material without further treatment. Both the tensile modulus and the tensile yield strength were found to be inde-



pendent of the extrusion direction. In DSC measurements, the as-received material exhibited enthalpy overshoot indistinguishable from quenched materials. The  $T_g$  of these materials was found by DSC at  $20^\circ \text{min}^{-1}$  to be  $147^\circ \text{C}$ . ASTM D638 Type I tensile specimens were prepared from the sheets with a template and a high-speed router. The specimen edges were carefully polished. A thin coating of liquid rubber was applied to the entire specimen to prevent crazing.

#### Testing Equipment and Procedure

The specimens were tested in a special high response servo-hydraulic testing machine manufactured by Instron Corp. This machine and the associated data acquisition equipment have been described elsewhere. Special high frequency response high sensitivity extensometers were attached to the specimen in both the longitudinal and the transverse directions. Uniaxial strain was applied to the specimens in either stroke or strain control at the rate of  $2 \text{ sec}^{-1}$ . Thus a 5% strain was applied in about 25 msec. The load, longitudinal and transverse strains, and the stroke (displacement) signals were simultaneously recorded onto a Norland Model 3001 digital oscilloscope. The data acquisition intervals were controlled by a logarithmic timer. During this first strain step data were recorded from 0.1 sec to  $10^5$  sec. To determine  $t_s$  the relaxation behavior was probed by the application of a small 0.1% strain step (tickle) after some time had elapsed from the initial application of the first strain step. This procedure was carried out as follows: the testing machine was set to stroke control (if it was not already in that mode); then the load and strain amplifiers were reset to zero and the sensitivities were increased by a factor of ten. The machine was then reverted to strain control, and a 0.1% strain step was applied in 2 msec. Data acquisition, again at logarithmic time intervals, was resumed from 0.1 to  $10^4$  sec. After some experimentation it was found that  $t_s \approx 10^3$  sec. The results reported here, unless otherwise noted, were obtained after  $10^3$  sec. The tests were conducted in an environmental chamber providing temperature stability of  $\pm 0.5^\circ$  in the  $10^3$  sec. interval. The load cell was thermally isolated from the test chamber and kept at  $31 \pm 1^\circ \text{C}$ .

#### Results

The first step stress relaxation at various strain levels at  $35^\circ \text{C}$  are shown in Fig. 4. The true stress values are shown as the changes in cross-sectional area have been taken into account. Each of the curves was obtained from fresh specimens with nominally identical thermal history. These curves demonstrate clearly that the material is in the nonlinear regime. Figure 5 is a plot of the isochronous modulus at various strain levels. These data are consistent with the observations of Yannas and co-workers,<sup>53</sup> that the linearity limit in poly-

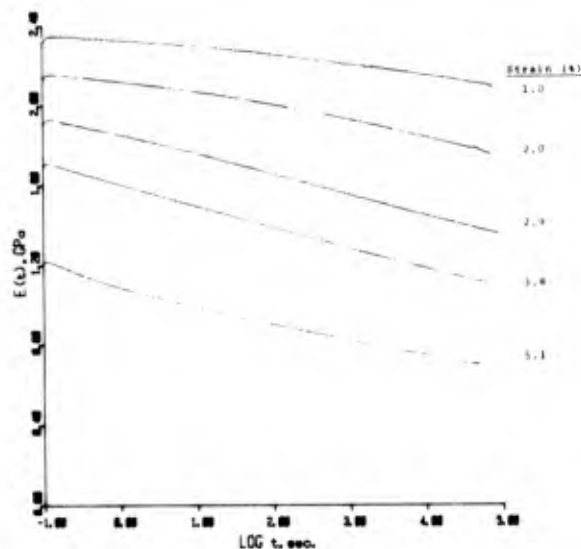


Fig. 4. First step true stress relaxation at various strain levels at  $35^\circ \text{C}$ .

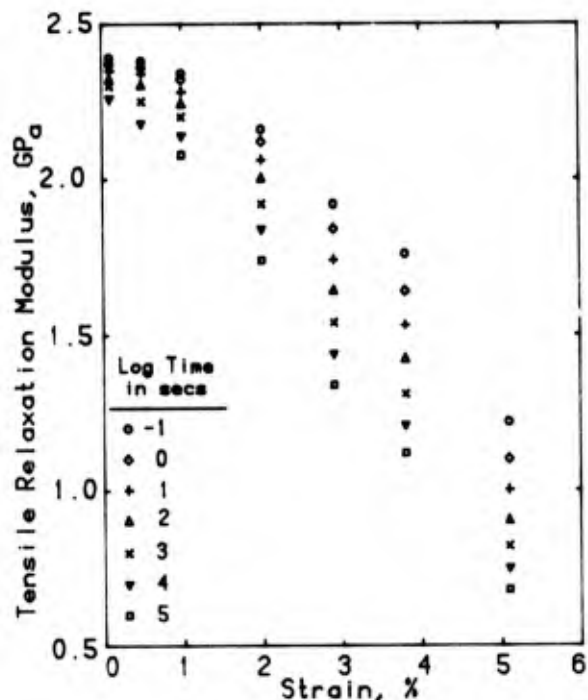


Fig. 5. Plot of the isochronous modulus at various strain levels.

carbonate is about 1% strain (see Figs. 6a-c). Note also that except at the lowest strain levels, the curves cannot be fitted to a fractional exponential function. The failure of the fractional exponential function to describe the nonlinear stress relaxations is consistent with the notion, advanced in earlier sections of this paper, that the structure in the glass is continuously relaxing (Eq. 36).

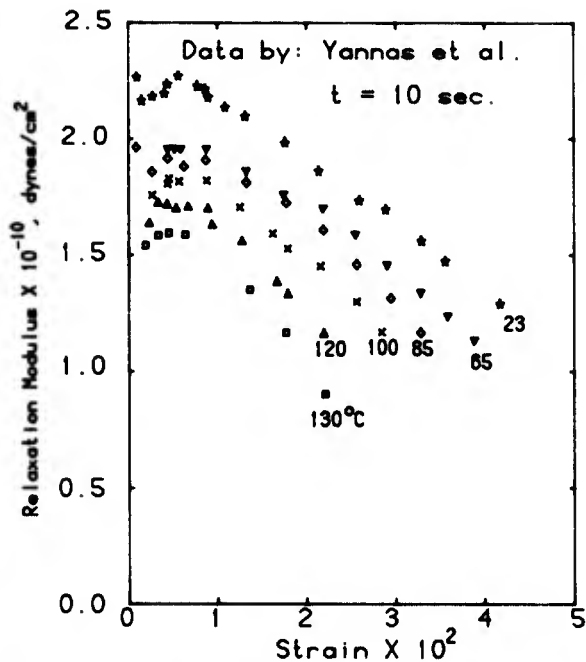


Fig. 6a. Isochronous relaxation modulus data of polycarbonate by Yannas, Sung and Lunn (Ref. 53) replotted against strain at different temperatures ( $t=10$  sec.).

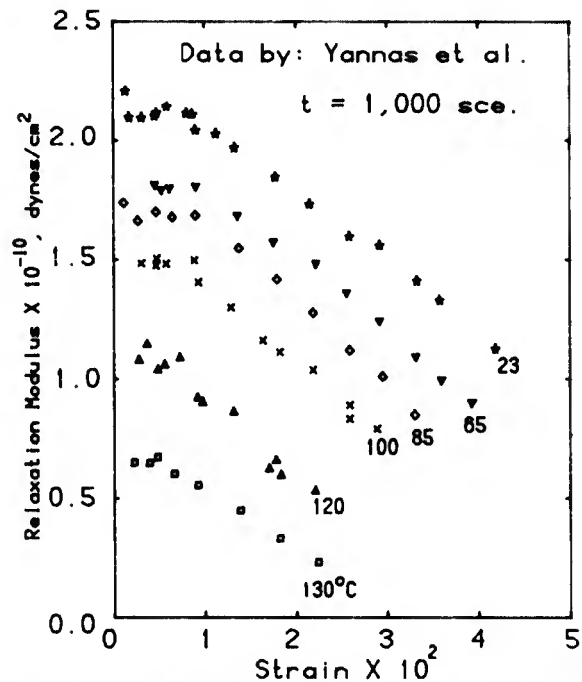


Fig. 6c. Isochronous relaxation modulus data of polycarbonate by Yannas et al. replotted against strain at different temperatures ( $t = 1000$  sec.).

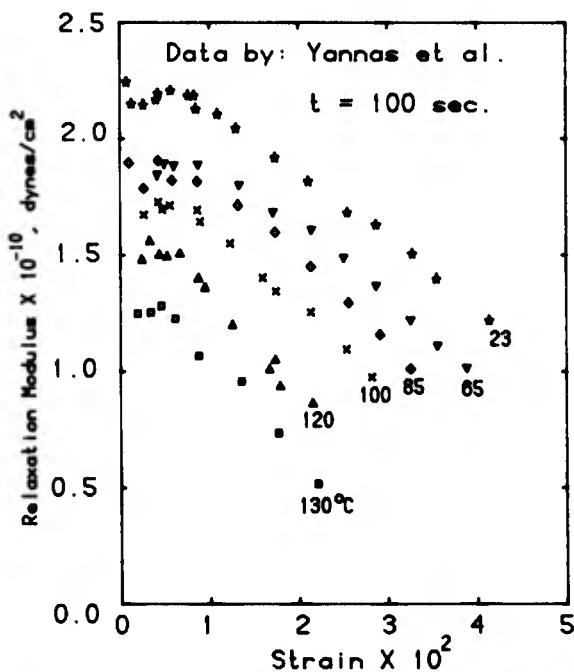


Fig. 6b. Isochronous relaxation modulus data of polycarbonate by Yannas et al. replotted against strain at different temperatures ( $t = 100$  sec.).

To determine the time required for the structure to stabilize,  $t_s$ , small, 0.1% tickle strains were applied at various times  $t_I$  from

the application of the first strain step. Figure 7 is a collection of these results at  $t_I = 3.3, 8, 27,$  and  $45.5$  hrs. for a first step strain of 4%. Although the coupling parameter  $n$  for the best fit is shown for each of the curves, deviations from fractional exponential behavior are significant for  $t_I = 3.25$  and 8 hrs. These results simply indicate that within the second step time scale of  $10^4$  sec, the structure is still changing rapidly at these values of  $t_I$ . These results also demonstrate that after approximately  $10^5$  sec, the structure has stabilized to the point where  $n$  becomes constant to within experimental error. This series of experiments has shown that a choice of  $t_s = 10^5$  sec is appropriate.

The stress relaxation results from the tickle runs are shown in Fig. 8. Since the second step is superimposed on the first step, the results shown are for the combined stresses. Since the stress due to the first step is changing very slowly on this time scale, the effect is rather insignificant. Figure 9 compares the net second step relaxation, obtained by subtracting off the first step stress extrapolated from  $t_I = 1 \times 10^5$  to  $t_I = 1.1 \times 10^5$  sec, against the gross stress relaxation. It is clear that the difference between the two curves is small, and essentially the same parameter  $n$  is obtained in both cases. The data in Fig. 8 indicate that the effect of increasing strain is to systematically change the shape of the relaxation curves, as well as to shift the effective

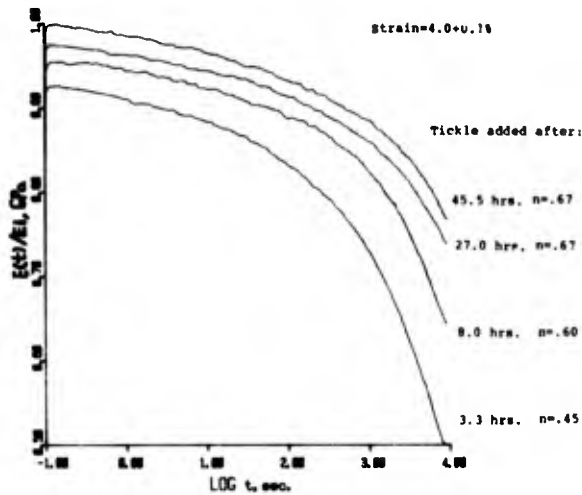


Fig. 7. Stress relaxation data for a total strain of 4.0±0.1% for determination of the time required for the structure to stabilize after a first step strain of 4%.

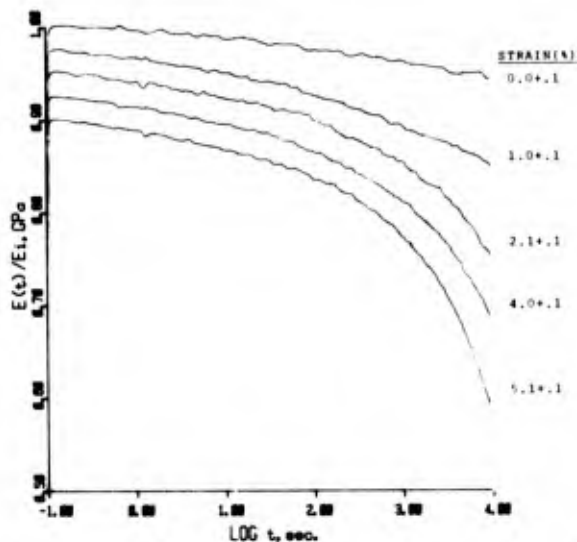


Fig. 8. Stress relaxation data from the tickle runs.

relaxation times to much shorter times. The fact that these curves cannot be shifted onto a master curve by any combination of vertical and horizontal shifts is obvious from the gross difference in the shapes of the curves. These curves, however, can be fit very well to Eq. (48) with little systematic deviation. Figure 10 plots the coupling parameter  $n$  against strain. The approximately linear dependence is remarkable. Even more striking is that when extrapolated to  $\epsilon=6\%$ , which is roughly the yield strain of polycarbonate at 35°C and moderate strain rates, a value of  $n \approx 0.6$  is obtained. From dielectric measurements it is known that  $n \approx 0.6$  for the  $\alpha$  relaxation ( $T_g$ ) of polycarbonate. This implies that the elevated strain at incipient yield induces

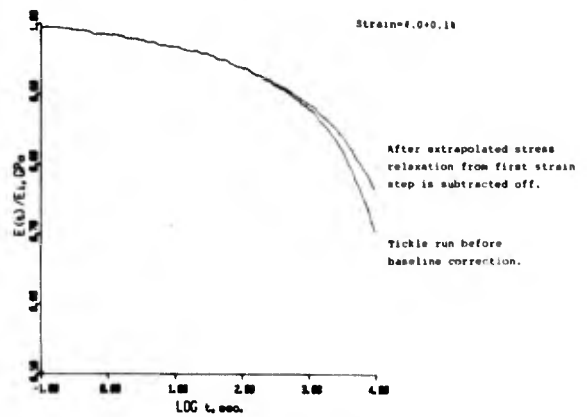


Fig. 9. Net second step relaxation obtained by subtracting off the first step stress.

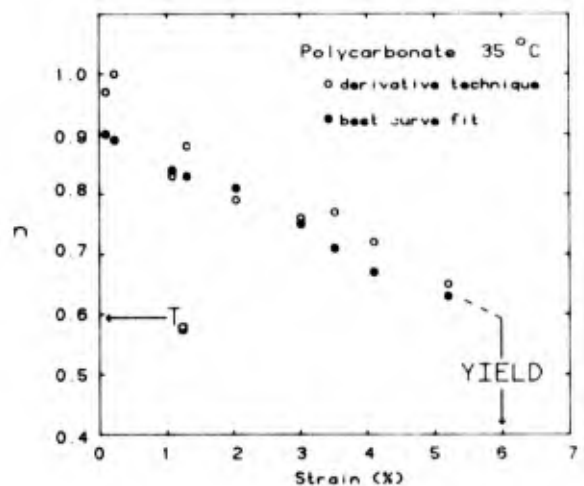


Fig. 10. The coupling parameter  $n$  plotted against strain.

a structure that relaxes in the same manner as the polymer at its  $T_g$ . This result is consistent with the concepts advanced in section III, and with the model proposed by Robertson for yielding in glassy polymers. The effective relaxation times  $\tau_p$ , which can be obtained from both the curve fitting and Eq. (46), are shown in Fig. 11. Remarkably,  $\tau_p$  has been shifted by almost twelve decades of  $P$  time. This is, of course, the reason why polycarbonate, at temperatures well below  $T_g$ , behaves almost like an elastic material at small strains, but is capable of undergoing large shear flow at yield.

#### Discussion of Experimental Data

The purpose of this work is to establish the basis of the nonlinear viscoelasticity model, discuss the concepts and making overall comparisons with experimental data. In contrast to the tickle runs, during which an

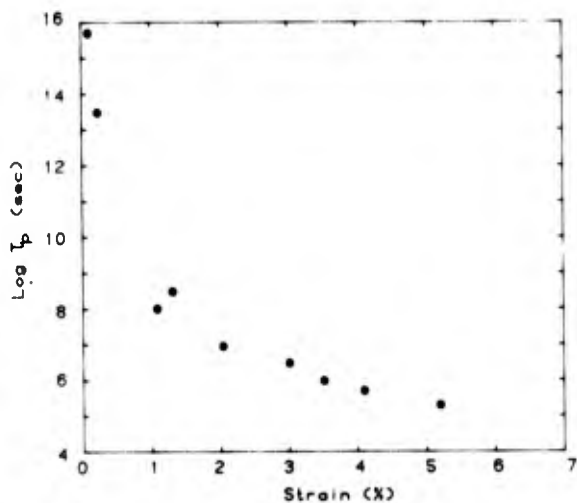


Fig. 11. The effective relaxation time  $\tau_p$  plotted against strain.

approximately constant structure  $\Sigma_\omega(\epsilon)$  is maintained throughout, the nonlinear stress relaxation in the period of  $10^{-1}$  to  $10^5$  sec witnesses the evolution of the structure from  $\Sigma_\omega(\epsilon=0)$  to  $\Sigma(\epsilon)$ . From Eqs. (38), (37b), (35), (28) and (27), it follows that the logarithmic derivative

$$\frac{d}{d(\log t)} \{ \log d\sigma/dt \} \quad (49)$$

may not have a constant value because the structural state of relaxation changes with time. If the variation of  $n(\Sigma(\epsilon, t))$  dominates, then the time dependence of the logarithmic derivative reflects that of  $n(\Sigma(\epsilon, t))$ . The data for  $\epsilon$  ranging from 1.1 to 5.1% when analyzed this way are indeed consistent with a continuous decrease of  $n(\Sigma(\epsilon, t))$  as  $t$  increases. This provides evidence for the evolution of the structural state of relaxation. We observe also that if  $\epsilon_1 < \epsilon_2$  then

$$n(\Sigma_\omega(\epsilon_1)) > n(\Sigma_\omega(\epsilon_2)) \quad (50)$$

and

$$n(\Sigma(\epsilon_1, t_1)) > n(\Sigma(\epsilon_1, t_2)) \quad (51)$$

if  $t_2 > t_1$ . These properties require that, for stress relaxation, the strain and time dependences of the response are not separable. They suggest also that at low strains and/or at short times, the response is linear viscoelastic. This is so because under one or both of these conditions, the structure has hardly been modified. However, at higher strains and at long times, the behavior is nonlinear. The stress relaxation data at various strain levels are in accord with this picture of viscoelastic behaviors. We shall discuss other nonlinear viscoelastic measurements of amorphous polymers with these properties in mind. Note that these properties germane to amorphous polymers and glasses below  $T_g$  may be irrelevant for elastomers, crystalline polymers, metals, etc. At this time, it cannot be ruled out that some but not all of the properties established here for amorphous polymers may be applicable to other

materials. Nonetheless, we shall exercise caution in limiting our considerations to amorphous polymers and glasses.

The tensile creep data of unplasticized polyvinylchloride at 20°C by Turner<sup>16</sup> offers another set of evidence for the time development of structural state of relaxation. However, before we discuss Turner's nonlinear creep data, it would be worthwhile to examine the linear viscoelastic properties of glassy PVC. In particular we choose to present the data of Cama and Sternstein,<sup>2,54</sup> who conducted linear stress relaxation experiments in pure torsion at shear strains between the values of 0.6% and 1.5%. In Cama's thesis,<sup>54</sup> the quantity (see Eq. (49) for comparison)

$$-d \log G(t)/d \log t$$

measured at 30, 100, 500 and 1000 minutes is tabulated. The isochronal values of  $-d \log G(t)/d \log t$  are nearly the same for shear strains between the values of 0.6% and 1.5%. If  $G(t)$  is a fractional exponential,  $\exp[-(t/\tau_p)^{1-n}]$ , then

$$-d \log G(t)/d \log t = (1-n)(t/\tau_p)^{1-n}$$

and a plot of the logarithm of  $-d \log G(t)/d \log t$  versus  $\log t$  will be a straight line with slope  $1-n$ . In Fig. 12, we have plotted in this manner several sets of the data by Cama and Sternstein. It can be seen that good linear relations are obtained. In Fig. 13, the  $G(t)$  data for different samples are plotted together with fits by the fractional exponentials. In any case the data support the fractional exponential time dependence of linear stress relaxation in glassy unplasticized and plasticized PVC. This information will be useful for the discussion of nonlinear creep data of PVC to follow.

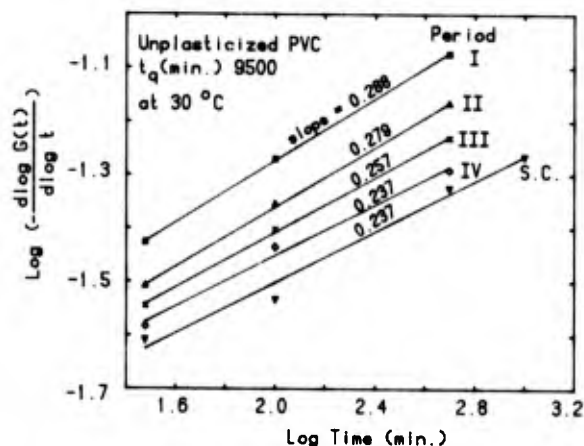


Fig. 12. A  $-d \log G(t)/d \log t$  vs  $\log t$  plot of unplasticized PVC data of Cama and Sternstein.

We have presented the formulation for nonlinear creep in the previous section III. During creep, the structure and hence the structural state of relaxation will evolve with time after a step increase  $\sigma_0$  in load. Turner's

data are replotted as creep compliance  $\epsilon(t)/\sigma_0$  as a function of time for various  $\sigma_0$  in Fig. 14, and as a function of applied load  $\sigma_0$  at various times in Fig. 15. Similar data on polycarbonate reported by Yannas et al.<sup>53</sup> is shown in Figs. 16a and 16b. By inspection of Figs. 15 and 16, it is clear that the time dependence of the creep compliance changes with the load level. The stress and time dependences of creep are therefore not separable, as noted by Turner. The cause for the nonseparability of stress and time dependences of creep is the same as that for stress relaxation. It is the evolution of structure and the dependence of the rate of evolution on stress level. The nonseparability in the main is the consequence of the inequalities:

$$n(\Sigma(\sigma_1, t)) > n(\Sigma(\sigma_2, t)), \text{ if } \sigma_2 > \sigma_1 \quad (51)$$

and

$$n(\Sigma(\sigma_1, t_1)) > n(\Sigma(\sigma_1, t_2)), \text{ if } t_1 < t_2 \quad (52)$$

Here  $\Sigma(\sigma_1, t)$  stands for the structure at time  $t$  after a step increase in stress of magnitude  $\sigma_1$  has been applied at  $t=0$ . Equation (51) essentially says that the time dependence of the creep compliance at one stress level cannot be obtained from the other at a different stress level by an appropriate shift in time scale. The structure evolution is different in the two cases and as a result the creep curves bear no simple relationship to each other.

The plots of Figs. 15 and 16 illustrate the existence of a linear region at short times and low stresses. In the linear region, the creep compliance is approximately independent of stress at sufficiently low stresses. This follows as a consequence of the model. At short times and low stress levels, the structure has not undergone any change that is significant enough to alter the structural state of relaxation.

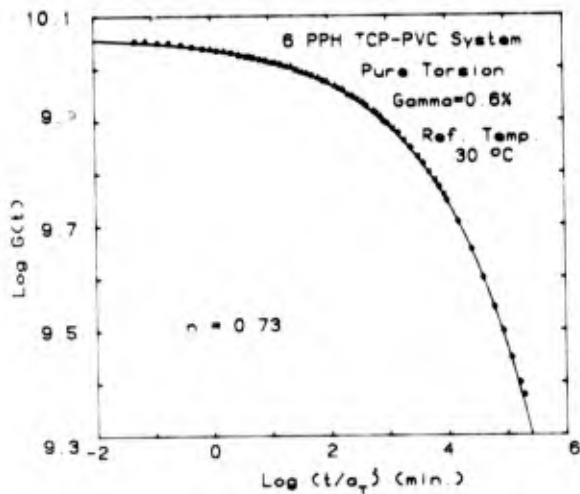


Fig. 13a. Stress relaxation data of plasticized 6PPH TCP-PVC by Cama and Sternstein, and fit to a fractional exponential with  $n=0.73$ .

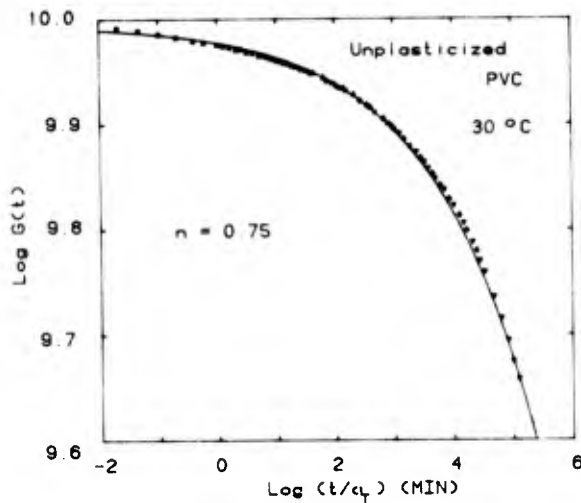


Fig. 13b. Stress relaxation data of unplasticized PVC by Cama and Sternstein and fit to a fractional exponential with coupling constant  $n=0.75$ .

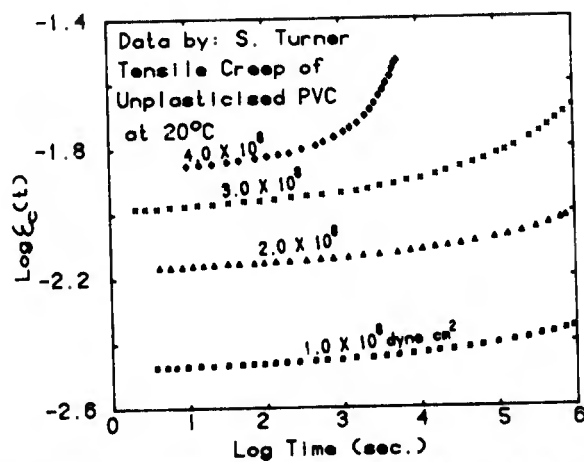


Fig. 14. Turner's tensile creep data of unplasticized PVC replotted as creep compliance versus  $\log t$  for various step increase in load.

On the other hand, for the same stress levels and time scales, the recovery compliance  $J_r(t-t_1)$  may now be dependent on stress and hence is nonlinear. Recovery involves the application of a stress  $\sigma_0$  at zero time followed by its removal at time  $t_1$ . The recovery compliance at time  $t$ ,  $J_r(t-t_1)$ , is defined as the difference between the compliance  $J_1(t)$ , at time  $t$  if the initial stress is applied continuously and the compliance,  $J_2(t)$ , at time  $t$  if the same initial stress applied at zero time is removed at time  $t_1$ . For a linear viscoelastic material, if the former is  $J(t)$ , then the latter is  $J(t)-J(t-t_1)$  and

$$J_r(t-t_1) = J(t) - [J(t) - J(t-t_1)] = J(t-t_1) \quad (53)$$

Returning to nonlinear viscoelasticity and the case that at some low stress  $\sigma_0$  for times shorter than  $t_{max}$ , the creep compliance is approximately independent of stress. If the stress  $\sigma_0$  is removed at  $t_1$  and  $t_1 \gg t_{max}$ , then

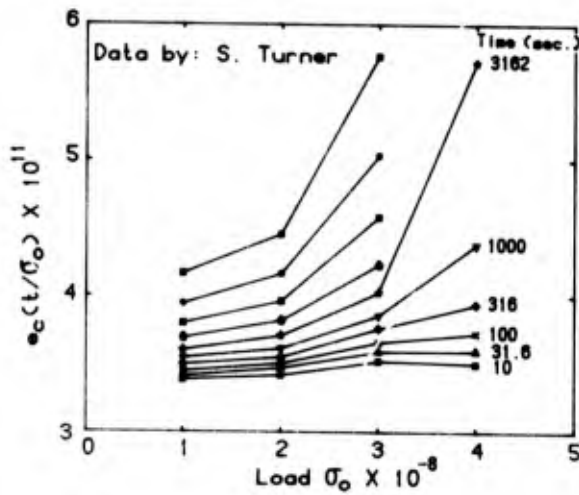


Fig. 15. Turner's tensile creep data of unplasticized PVC replotted as creep compliance versus applied load at various times.

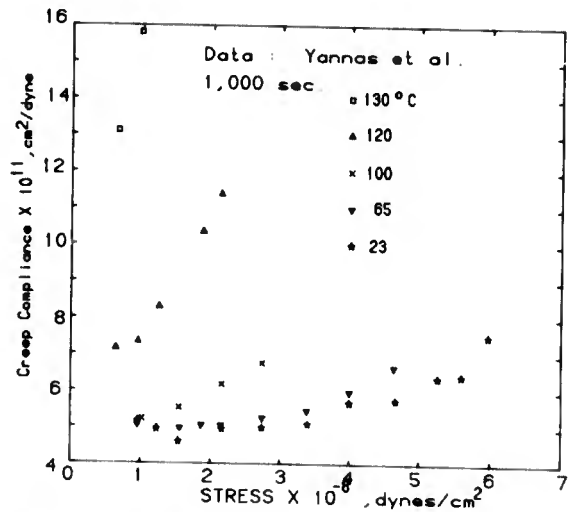


Fig. 16b. A replot of isochronous creep compliance data of polycarbonate by Yannas and Lunn versus stress at various temperatures at  $t=1000$  sec.

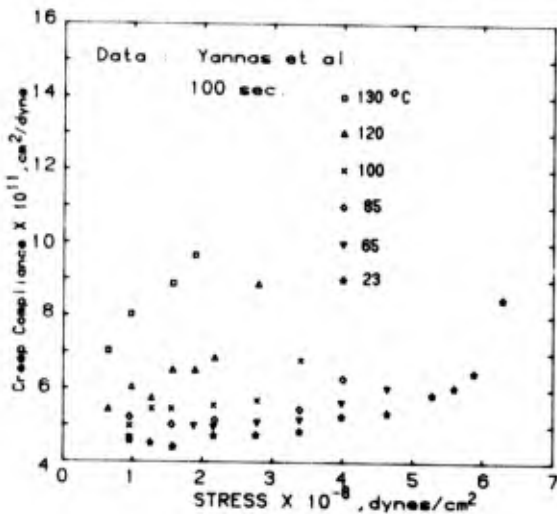


Fig. 16a. A replot of isochronous creep compliance data of polycarbonate by Yannas and Lunn versus stress at various temperatures at  $t=100$  sec.

during the period of time,  $t_1 - t_{\max}$ , the structure could have had enough time to change significantly and furthermore continues to change after  $t_1$ . Let us examine the effect of this structural change on the recovery compliance. If the structure changes from  $\Sigma(\sigma=0, t=0)$  to  $\Sigma_1 \equiv \Sigma(\sigma_0, t_1)$ , then the structural state of relaxation at  $t_1$  will satisfy

$$n(\Sigma(\sigma_0, t_1)) < n(\Sigma(\sigma_0, t)) \quad (54)$$

At short times after  $t_1$  such that for all  $t > t_1$  that further structural change can be ignored, we have  $J_2 = J_1(t) - J_{\Sigma_1}(t - t_1)$  and

$$\begin{aligned} J_r(t - t_1) &= J_1(t) - [J_1(t) - J_{\Sigma_1}(t - t_1)] \\ &= J_{\Sigma_1}(t - t_1) \end{aligned} \quad (55)$$

where  $J_{\Sigma_1}(t - t_1)$  is the creep compliance function at  $t > t_1$  for the structure  $\Sigma_1$ . Equation (54) together with similar inequalities for the other structural state parameters leads to the inequality

$$J_{\Sigma_1}(t - t_1) > J_1(\Delta t) \quad (56)$$

where, to avoid confusion, we have used  $\Delta t$  to represent the increment of time starting from zero time and has the same magnitude as the difference  $t - t_1$ . Combining Eq. (55) with Eq. (56), we obtain

$$J_r(t - t_1) > J_1(\Delta t) \quad (57)$$

which is a restatement of the phenomenon that (1) creep and recovery curves are not identical, the recovery compliance is larger than the creep compliance at short times, and (2) the recovery compliance is not independent of stress at stress levels that the creep compliance is independent of stress. The latter follows directly from Eq. (55) and the dependence of  $\Sigma_1$  on stress.

In a two-step loading program with a stress  $\sigma_0$  at  $t=0$  followed by an additional stress  $\sigma_0$  at time  $t=t_1$ , the additional creep is defined by the difference of the observed creep and the creep for a one-step loading only at  $t > t_1$ . For  $t > t_1$ , the second step in loading will cause the structure to change further, resulting in

$$n(t, 2\text{-steps}) < n(t, 1\text{-step}) \quad (58)$$

and this will cause the additional creep curves to be in excess of the initial creep, as is often observed in experiments.

It is important to reemphasize that a key prediction of the model given by Eqs. (51) and

(52) is consistent with commonly observed nonlinear viscoelastic behavior of amorphous polymers.

#### COMPARISONS WITH OTHER MODELS

In this work we seek a model of nonlinear viscoelasticity that is based on the complex time dependences of relaxations of molecules and chains in glassy polymers. The latter are traceable to a very fundamental mechanism of relaxation of any primitive species in a complicated structure or environment such as glasses. The rate of relaxation depends on the structure. Large strain deformation modifies the structure. There are well-defined predictions of the fundamental mechanism that have been proven repeatedly in several areas of polymer physics and glass sciences. On application of the fundamental mechanism, these predictions lead to the construction of a model for nonlinear viscoelasticity. The structure evolution with time is self-consistently related to the time dependences of stress or creep strain, and both can be calculated for any strain or stress program. Thus the nature of this model is different from all other models reviewed in several recent articles. It is also a unified model, relating some basic physics of nonlinear viscoelasticity to those in apparently unrelated physical phenomena in polymeric or nonpolymeric systems. Equations (43), (27) and (28) in conjunction with Eq. (40) provide an explicit expression, derivable from first principles, for the general constitutive equation often written as

$$\sigma(t) = \int_{-\infty}^t F[\epsilon(\tau)] \quad (59)$$

which states that the stress at time  $t$  is a function  $F$  of the strain at all previous times  $\tau$ . This should be contrasted with most other approaches where kernel functions, which are used to approximate the functional, are left to be determined by a basic experiment such as one-step strain increase, or are postulated as an empirical function. The remarks made here and throughout this section about other models and approaches should not be viewed as promotions of the present model as being superior. These other models have their own advantages and serve different useful purposes. Rather, we would like to think of our physical and mechanistic approach to play the role of complementing and/or supplementing some of these engineering, rheological and other microscopic approaches. That is, our emphasis is on basic physical mechanism and on constructing a nonlinear model from this basis up. This is the angle that none of engineering and rheological approaches has taken. There is no doubt in our minds that proven successful rheological approaches such as the modified Bernstein, Kearsley and Zapas (BKZ) theory<sup>13</sup> for an incompressible elastic fluid probably will be able to correlate the data from the type of step plus tickle experiments presented in this work for glassy polymers. After all, McKenna and

Zapas<sup>14,15</sup> have demonstrated the applicability of a modified BKZ theory to PMMA below  $T_g$ . It is worthwhile to discover the reason why an incompressible elastic fluid theory should work for compressible glassy polymers (and to metals such as aluminum). Our work may provide some clue to this query. When formulated specifically to apply to amorphous polymers, the constitutive equation (46) obtained bears some similarity to the BKZ<sup>13</sup> and the Schapery<sup>11</sup> equations, although there are also some differences. The similarity may account for the success of BKZ in describing stress relaxation in amorphous polymers. The differences, such as the kernel  $\exp\{-\int_t^t dt'' W(t''-t'; T_f(t''))\}$  in Eq. (46) which has an inseparable dependence on strain and time, help to remove difficulties that the original BKZ and the Schapery theories may encounter. The emergence of our way of description of nonlinear viscoelasticity does not take away any of the merits of these and other theories. On the contrary, it lends them some support by providing them with a fundamental basis. This is the theme we shall adhere to throughout this section.

As a first example, we cite that power laws for creep strain as a function of time are often found to be appropriate for nonlinear viscoelasticity. Turner,<sup>16</sup> Van Holde<sup>35</sup> and Findley<sup>56</sup> and co-workers have all proposed the empirical expression

$$e(t) = e_0(\sigma) + A(\sigma)t^m \quad (60)$$

for the creep strain under a constant stress  $\sigma$ . Here  $e_0$  and  $A$  are functions of  $\sigma$  and  $m$  and are considered to be material constants. Our approach provides a justification for Eq. (60). This follows from Eq. (47a) and the fractional exponential  $\exp(-t/\tau_p)^{1-n}$  time dependence for  $M(t)$ . The creep compliance can be well approximated by Eq. (60) at short times, where  $m=1-n$ .

Schapery's model<sup>11</sup> introduced nonlinearity by modifying the Boltzmann's single integral stress relaxation or creep compliance functions by an appropriate shift in time scale. For stress relaxation, he proposed that

$$\sigma(t) = h_e G_r e(t) + h_1 \int_{-\infty}^t \Delta G(\rho-\rho') \frac{d}{d\tau} h_2 [e(\tau)] d\tau \quad (61)$$

where  $\Delta G(t) = G(t) - G_r$ ,  $G_r$  is the relaxed modulus and the reduced time  $\rho$  is the so-called reduced time defined by

$$\rho = \rho(t) = \int_0^t dt' / a_e [e(t')] \quad , \quad a_e > 0 \quad (62)$$

and

$$\rho' = \rho(t) = \int_0^t dt' / a_e [e(t')] \quad (63)$$

$h_e$ ,  $h_1$ ,  $h_2$  and  $a_e$  are material properties which are functions of strain. By inspection of Eq. (61), one can see that the strain and time dependence of the stress relaxation response of Schapery are separable. This is inadequate for description of nonlinear viscoelastic response of glassy polymers as mentioned in the previous section and by Turner.<sup>16</sup>

The stress relaxation given by Eqs. (45) and (46) according to our model cannot be written in Schapery's representation. The product

$$\Delta M(\varepsilon) \exp\left\{-\int_{t'}^t dt'' W(t''-t'; T_f(t''))\right\} \quad (64)$$

of the kernel in Eq. (46) cannot be cast into Schapery's form of

$$h_1 \frac{dh_2}{de} \Delta G \left[ \int_{t'}^t dt'' / a_e [e(t'')] \right] \quad (65)$$

There are at least two reasons for this. First is the dependence of  $W$  on the difference  $(t''-t')$  and the second is the variation in the form of the function  $W$  with  $t''$  according to

$$\begin{aligned} W(t''-t'; T_f(t'')) &= \tau_0^{-1} (T_f(t''), T) \\ \exp(-\Delta S_c(T_f(t''))/R) &[\omega_c(T_f(t'')) \\ (t''-t')]^{-n} & (T_f(t'')) \end{aligned} \quad (66)$$

Moreover  $T_f(t'')$ , obtainable by solution of Eq. (45), depends on the strain history of previous times. It is a functional of  $\varepsilon(t)$ . All these cause the inseparability of strain and time. These make it impossible to cast expression (64) as the time scale transformation of a function which is Schapery's representation.

The larger the strain at  $t''$  is, the more the structural state of relaxation parameters  $\tau_0$ ,  $\Delta S_c$ ,  $\omega_c$  and  $n$  at  $t''$  will accelerate the relaxation rate  $W$  in Eq. (66). This effect is taken into account by an appropriate shift in time scale by Schapery. Under certain conditions and for some strain programs this representation may be adequate for stress relaxation. However it is important to bear in mind that Eq. (61) has neglected some other aspects that may become important at large strains and at long times.

The original BKZ theory<sup>4</sup> has a similar problem as the Schapery representation. The kernels  $m(t-\tau)$ ,  $a(t-\tau)$  and  $b(t-\tau)$  that enter into the original fluid theory are fixed. Zapas<sup>13</sup> has modified the original BKZ theory by including dependence on previous strain history. An elegant treatment of this has been given by McKenna and Zapas.<sup>14,15</sup> The stress response of the modified BKZ theory is no longer separable in strain and time. This is achieved by replacing the fading memory which depends upon the time difference  $t-\tau$  by

$$\int_{\tau}^t \dot{\phi}(\Psi(t), \Psi(\tau), \Psi(\xi), t-\xi) d\xi \quad (67)$$

where  $\dot{\phi}$  is the derivative of the function  $\phi$  with respect to the time argument,  $t-\xi$ . Although the modified BKZ is still an incompressible fluid theory, it is so sophisticated that no doubt much of the physics of nonlinear viscoelasticity of glassy polymers has been incorporated. McKenna and Zapas<sup>14,15</sup> have demonstrated its utility in normal and shear stress responses of PMMA. Direct comparison between our approach with the modified BKZ

theory cannot be made because the latter is based on an incompressible fluid. Nevertheless, interpreting our results of Eqs. (45) and (46) as much as possible in terms of a memory, it is not difficult to see that there are some similarities with the modified BKZ representation. The modified BKZ, like the original BKZ theory, does not give explicitly the response function but leaves it to be determined by a single-step stress relaxation experiment. The memory dependence on the previous history is also evaluated by two-step strain experiments. Our model, in which an attempt has been made to give the form of the response function explicitly, may be viewed as complementary to the modified BKZ theory.

The most general representation of nonlinear viscoelasticity is given by Green and Rivlin in their multiple integral theory. The constitutive equation in its one-dimensional form is written as

$$\begin{aligned} \sigma(t) &= \int_{-\infty}^t G_1(t-\tau) \dot{\varepsilon}(\tau) d\tau + \int_{-\infty}^t \int_{-\infty}^t G_2(t-\tau_1, \\ & t-\tau_2) \dot{\varepsilon}(\tau_1) \dot{\varepsilon}(\tau_2) d\tau_1 d\tau_2 + \int_{-\infty}^t \int_{-\infty}^t \int_{-\infty}^t \\ & G_3(t-\tau_1, t-\tau_2, t-\tau_3) \dot{\varepsilon}(\tau_1) \dot{\varepsilon}(\tau_2) \dot{\varepsilon}(\tau_3) \\ & d\tau_1 d\tau_2 d\tau_3 + \text{higher order terms} . \end{aligned} \quad (68)$$

The  $G$  functions are not given a priori and are to be taken as empirical functions of time. The first term is the Boltzmann's superposition linear term. The second and the higher order terms take into account nonlinear behavior. This representation is complicated, and, often for practical applications, only the lowest order terms are retained. A three-term approximation has been adopted by Onaran and Findley.<sup>56</sup> Kinder and Sternstein<sup>12</sup> pointed out that published creep data require terms of higher order. In Eq. (68) all the  $G$  functions depend on the time differences  $t-\tau_i$  only. Pipkin and Rogers<sup>8</sup> proposed a reformulation of Eq. (68) by generalizing the  $G$  functions to be a function of both elapsed time  $t-\tau_i$  and strain  $\varepsilon(\tau_i)$ . They wrote the constitutive equation as

$$\begin{aligned} \sigma(t) &= \int_{-\infty}^t G_1[t-\tau, \varepsilon(\tau)] \dot{\varepsilon}(\tau) d\tau \\ &+ \int_{-\infty}^t \int_{-\infty}^t G_2[t-\tau_1, \varepsilon(\tau_1), t-\tau_2, \varepsilon(\tau_2)] \\ & \dot{\varepsilon}(\tau_1) \dot{\varepsilon}(\tau_2) d\tau_1 d\tau_2 \\ &+ \text{higher order terms} . \end{aligned} \quad (69)$$

The hope is that in this manner fewer lower order terms need to be retained than in the original Green-Rivlin representation for an adequate description. In particular, if only the first term need be retained such that

$$\sigma(t) = \int_{-\infty}^t G[t-\tau, \varepsilon(\tau)] \dot{\varepsilon}(\tau) d\tau \quad (70)$$

the model becomes simple and attractive. It is a single integral constitutive equation that preserves the additivity of incremental strain effects in the Boltzmann superposition sense but allows for nonlinear effects. Equation



(70) is termed the nonlinear superposition theory by Sternstein.<sup>2</sup> It is instructive to discuss our constitutive equation (46) as a nonlinear superposition theory. Equation (46) cannot be written exactly in the form of Eq. (70) because the kernel in Eq. (46) is not a function of  $\varepsilon(\tau)$  but a functional of  $T_f(\tau')$  of the entire strain history  $0 \leq \tau' < t$ . Nonetheless, with this difference explicitly written out as

$$\sigma(t) = \int_{-\infty}^t G[t-\tau, \int_{t=0}^t [T_f(\tau')] ] \dot{\varepsilon}(\tau) d\tau \quad (71)$$

where

$$G[t-\tau, \int_{t=0}^t [T_f(\tau')] ] \equiv M_R(\varepsilon(\tau)) + \Delta M(\varepsilon(\tau)) \exp\left[-\int_{t=0}^t d\tau' W(t'-\tau; T_f(t'))\right] \quad (72)$$

we obtain an analogous nonlinear superposition theory.  $G$  in Eq. (71) is now a functional of the structure  $T_f(\tau')$ , which, according to our model, can change with time in the nonlinear region.

## CONCLUSIONS

We have offered an alternative way of looking at the phenomena of nonlinear viscoelasticity in glassy polymers. Starting out from a microscopic, physical and mechanistic approach to relaxation time dependences, nonlinear creep and stress relaxation are predicted and a constitutive equation is constructed. The possibility of structural change with time for a glassy polymer under nonlinear stress or strain is pointed out. The instantaneous creep/relaxation rates are structure dependent. The structure evolution with time, when solved self-consistently, then leads to the prediction of nonlinear creep and stress relaxation. The approach proposed here is justified by experimental data which support the idea of a time dependent structural state to relaxation and its dependence on strain. Some published data of nonlinear creep and stress relaxation are analyzed and used to give additional evidence for the present point of view. The approach and its results are consistent with some of the most sophisticated representations of nonlinear viscoelasticity, though there are differences. It provides some physical insight into several rheological approaches.

## References

1. I.M. Ward, Mechanical Properties of Solid Polymers, 2nd ed., John Wiley & Sons, New York (1983).
2. S.S. Sternstein, "Mechanical Properties of Glassy Polymers," Treatise on Materials Science and Technology, Vol. 10B, ed. J.M. Schultz (Academic Press, New York, 1977).
3. A.E. Green and K.S. Rivlin, Arch. Rat. Mech. Anal. 1, 1 (1957).
4. B. Bernstein, E.A. Kearsley and L.P. Zapas, Trans. Soc. Rheol. 7, 391 (1963).
5. K.F. Nolte and W.N. Findley, Trans. Soc. Rheol. 15, 111 (1971).
6. I.M. Ward and E.T. Onat, J. Mech. Phys. Solids 11, 217 (1963).
7. K. Onaran and W.N. Findley, Trans. Soc. Rheol. 9, 299 (1965).
8. A.C. Pipkin and T.G. Rogers, J. Mech. Phys. Solids 16, 59 (1968).
9. F.J. Lockett and S. Turner, J. Mech. Phys. Solids 19, 201 (1971).
10. M.G. Brereton, S.G. Croll, R.A. Duckett, and I.M. Ward, J. Mech. Phys. Solids 22, 97 (1974).
11. R.A. Schapery, Polym. Eng. Sci. 9, 295 (1969).
12. D.F. Kinder and S.S. Sternstein, Trans. Soc. Rheol. 20, 119 (1976).
13. L.J. Zapas, in Deformation and Fracture of High Polymers, ed. H.H. Kausch, J.H. Hassell, and R.I. Jaffee (Plenum, New York, 1974).
14. G.B. McKenna and L.J. Zapas, J. Rheol. 23, 151 (1979).
15. G.B. McKenna and L.J. Zapas, J. Rheol. 24, 367 (1980).
16. S. Turner, Ch. 4 in The Physics of Glassy Polymers, ed. R.N. Haward, ed. Wiley, 1973; Polymer Eng. Sci. 6, 306 (1966).
17. K. Blum, Density Matrix Theory and Applications (Plenum Press, New York, 1981).
18. B. Fain, Theory of Rate Processes, 20, Lecture Notes in Chemistry (Springer-Verlag, Berlin, 1980).
19. N.G. McCrum, B.E. Read and G. Williams, An Elastic and Dielectric Effect in Polymeric Solids (John Wiley & Sons, London, 1967).
20. K.L. Ngai, Comments Solid State Phys. 9, 127 (1979); 9, 141 (1980).
21. A.K. Rajagopal, K.L. Ngai, R.W. Rendell and S. Teitler, J. Stat. Phys. 30, 285 (1983).
22. K.L. Ngai and A.K. Rajagopal, Non-Debye Relaxations in Condensed Matter, ed. T.V. Ramakrishnan (World Scientific, Singapore, 1984).
23. S. Teitler, A.K. Rajagopal and K.L. Ngai, Phys. Rev. A26, 2906 (1982).

24. A.K. Rajagopal, S. Teitler and K.L. Ngai, *J. Phys. C* (in press).
25. S. Glasstone, K.J. Laidler and H. Eyring, *The Theory of Rate Processes* (McGraw Hill, New York, 1942).
26. R. Kohlrausch, *Pogg. Ann.* (3) 12, 292 (1847).
27. F.T. Pierce, *J. Textile Inst.* 14, T390 (1923).
28. J. DeBast and P. Gilard, *Phys. & Chem. of Glasses* 4, 117 (1963).
29. C.R. Kurkjian, *Phys. & Chem. of Glasses* 4, 128 (1963).
30. I.L. Hopkins, *Phys. Chem. of Glasses* 4, 117 (1963).
31. G. William and D.C. Watts, *Trans. Faraday Soc.* 66, 80 (1970).
32. A.A. Jones, J.F. O'Gara, P.T. Ingelfield, J.T. Bendler, A.F. Yee and K.L. Ngai, *Macromolecules* 16, 658 (1983).
33. J.F. O'Gara, S.G. Desjardins and A.A. Jones, *Macromolecules* 14, 63 (1981); 12, 1136 (1979).
34. K.L. Ngai and R.W. Rendell, *Polymer Preprints*.
35. D.J. Plazek, K.L. Ngai and R.W. Rendell, *Polymer Eng. Science* (in press).
36. H.L. Downing, H. Jain and N. Peterson
37. K.L. Ngai, R.W. Rendell and H. Jain, submitted to *Phys. Rev. B*.
38. H.W. Starkweather, *Macromolecules* 15, 320 (1982).
39. H.W. Starkweather and J.J. Chang, *Macromolecules* 15, 752 (1982).
40. A.K. Doolittle, *J. Appl. Phys.* 22, 1471 (1951); *ibid.* 23, 236 (1951).
41. M.L. Williams, R.F. Landel and J.D. Ferry, *J. Am. Chem. Soc.* 77, 3701 (1955).
42. J.H. Gibbs and E.A. DiMarzio, *J. Chem. Phys.* 28i, 373 (1958).
43. A.Q. Toole, *J. Res. Nat. Bureau Standards* 37, 73 (1946).
44. A.J. Kovacs, *Fortschr. Hochpolym. Forsch.* 3, 394 (1964).
45. O.S. Narayanaswamy, *J. Amer. Ceram. Soc.* 54, 491 (1971).
46. A.J. Kovacs, J.J. Aklonis, J.M. Hutchinson and A.R. Ramos, *J. Polym. Sci., Phys. Edition* 17i, 1097 (1979).
47. C.T. Moynihan, P.B. Macedo, C.J. Montrose, P.K. Gupta, M.A. Debolt, J.F. Dill, B.E. Dom, P.W. Drake, A.J. Esteal, P.B. Elterman, R.P. Moeller, H. Sasabe and J.A. Wilder, *Ann. New York Acad. Sci.* 279 (1976).
48. K.L. Ngai, in *Non-Debye Relaxations in Condensed Matter* (World Scientific, Singapore (1984)).
49. C.K. Chai and N.G. McCrum, *Polymer* 21, 706 (1980).
50. J. Bendler and K.L. Ngai, *Macromolecules* (in press).
51. R.W. Rendell, T.K. Lee and K.L. Ngai, *Polym. Eng. Sci.* (in press).
52. J. Aklonis and A. Kovacs,
53. I. V. Yannas and A. C. Lunn, *Macromol. Sci.-Phys.* B4, 603 (1970); I.V. Yannas, N-H Sung and A.C. Lunn, *ibid.*, B5, 487 (1971).
54. F.J. Cama, Ph.D. Thesis, Rensselaer Polytechnic Institute, 1974.
55. K. Van Holde, *J. Polymer Sci.* 24, 417 (1957).
56. W.N. Findley, J.S. Lai, and K. Onaren, *Creep and Relaxation of Nonlinear Viscoelastic Materials* (North-Holland Publishing Co., Amsterdam, 1976).

# **METALLIC GLASSES**

COMPARISON OF FLOW AND STRUCTURAL RELAXATION IN AMORPHOUS ALLOYS WITH  
PHYSICAL AGING IN AMORPHOUS POLYMERS

A. I. Taub

General Electric Corporate Research and Development  
Schenectady, NY 12301

Abstract

Structural relaxation has a strong effect on the flow behavior of amorphous alloys. Increases in viscosity of more than 7 orders of magnitude are commonly observed during isothermal annealing of these materials. This increase in the flow resistance has been attributed to the equilibration of the atomic structure and is therefore similar in nature to the physical aging process exhibited by amorphous polymers. In this paper, data on the effect of preannealing on the subsequent stress relaxation behavior of amorphous alloys is reanalyzed by the technique used for amorphous polymers as summarized by Struik. While some discrepancies are found, it appears that a general characteristic of amorphous materials is a linear time dependence for the flow resistance. The shift rate for polymers is about unity below  $T_g$  and the viscosity of amorphous alloys and inorganic glasses increases linearly with time. This linear relation is characteristic of a self-retarding process and is therefore consistent with the general model that explains the increase in the flow resistance in terms of the equilibration of the atomic structure.

Introduction

There have been numerous investigations of the kinetics of flow and structural relaxation in melt-quenched amorphous alloys since their discovery some 25 years ago (1) and our understanding of the behavior of these materials has increased tremendously. These research efforts have been conducted primarily by metallurgists rather than by the more traditional investigators of amorphous materials and this has resulted in a method of presenting experimental data that differs significantly from that used in polymer and inorganic glass science. This has made interdisciplinary communication difficult even though the basic phenomenon reported for the metallic glasses are strikingly similar to those found in other amorphous systems. In this paper, an attempt will be made to reformulate the flow data of amorphous alloys into a format that is consistent with that used for amorphous polymers.

First, since this paper will emphasize those aspects of the flow behavior that deal with structural relaxation, a brief overview of the model that has been developed to explain the effects of structural change on flow will be presented. Then a summary will be made of the existing data on the flow of amorphous alloys using the terminology that has been developed by the metallurgists. The data on structurally stabilized specimens will be reviewed to lay the groundwork for the more complex data on the effects of structural relaxation. Finally, the latter will be reformulated for comparison with the physical aging data for amorphous polymers.

The Metallurgists Viewpoint

Structural State Definitions.

Almost every intrinsic property of amorphous alloys has been shown to vary as the structure changes (2,3), with perhaps the most dramatic effect being the change in the flow resistance. The origin of the effect of structural change on the viscosity can be explained with the aid of Figure 1 which illustrates the variation of the viscosity of a glass forming alloy with temperature. Consider the alloy at a temperature above the melting temperature  $T_m$ . The atomic structure and physical properties of the alloy in this regime are determined by the equilibrium state. If the alloy is cooled below  $T_m$ , its atomic structure continuously adopts configurations dictated by equilibrium, until the region of the glass transition temperature  $T_g$  is reached. At some temperature near  $T_g$ , the atomic configuration begins to "freeze." That is, the resistance to atomic motion becomes large enough to restrict structural rearrangement, resulting in the time required for the atoms to adopt their equilibrium configurations becoming greater than the time allowed by the cooling process. The atomic structure then begins to deviate from the configuration required by equilibrium. As the temperature continues to decrease, the resistance to atomic motion increases even more and the time required for structural rearrangements becomes larger. Eventually, significant structural change on the time scale of the cooling process ceases and the

atomic configuration is "frozen in." Curve a in Figure 1 represents the isoconfigurational (i.e. - constant structure) viscosity of the alloy in the as-quenched condition.

Subsequent heat treatment of the alloy at temperatures below  $T_g$  allows the atomic structure to approach its equilibrium configuration before crystallization commences. This results in a shift of the isoconfigurational curves towards the equilibrium curve, as shown schematically in Figure 1. This shift is manifested as an increase in the viscosity of the alloy.

The viscosity of a glass forming alloy is therefore not a unique function of temperature in the range  $T < T_g$ . One must distinguish between the viscosities of the metastable equilibrium liquid, the isoconfigurational glass and the crystallized alloy. In this paper we will concentrate on the glassy state. Within this regime, distinction must still be made between those tests that involve a preanneal of the glass to stabilize its structure during subsequent flow testing and those tests in which the structure of the glass is continuously changing. We examine first flow in a structurally stabilized glassy alloy.

**Flow in Structurally Stabilized Specimens.**

Figure 2a shows a typical strain vs time plot obtained from a creep test of an amorphous alloy following a long term preanneal at the testing temperature (5). The anneal is required to stabilize the structure of the alloy and will be described in more detail later. Following the definitions of Nowick and Berry (6), the strain response of the material is divided into three components as shown in Table I.

TABLE I

Component	Recoverable	Time-Dependent
Ideal Elasticity	Yes	No
Anelasticity	Yes	Yes
Viscoelasticity	No	Yes

The instantaneous elongation  $\gamma_0$  is characterized by ideal elasticity. The steady state strain  $\gamma_p$ , established in this case after about 50 hours, is viscoelastic. The anelastic contribution  $\gamma_a$  is responsible for the transient flow that occurs before the steady state condition is established. Separate discussions of each of these flow components, including reference to the effects of structural relaxation, follow.

**Ideal Elasticity.** The instantaneous elongation measured on loading specimens has been shown to be completely reversible on unloading ( $\gamma_0 = -\gamma_0'$ ) and to vary linearly with the applied load. Structural changes in the amorphous state have been shown to affect the elastic stiffness

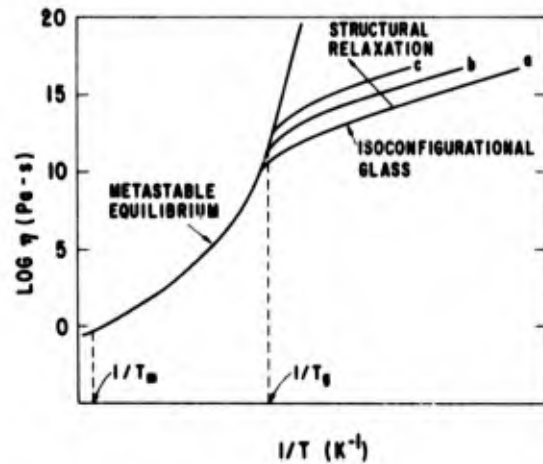


Figure 1. Schematic plot of the temperature dependence of the viscosity in a glass forming alloy during quenching and reheating. Curve a represents the deviation of the viscosity from the equilibrium curve during the quench. Curves b and c illustrate the shift in the isoconfigurational viscosity towards the equilibrium curve during annealing. (from ref. 4)

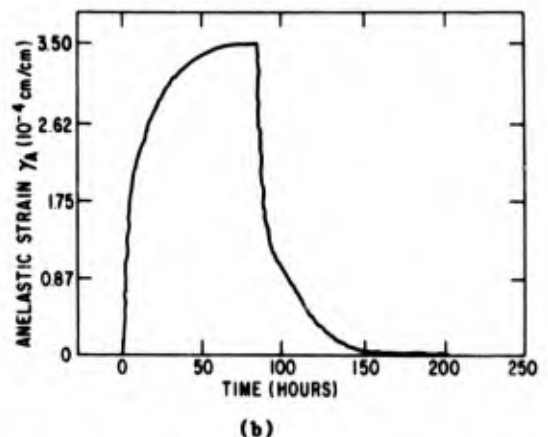
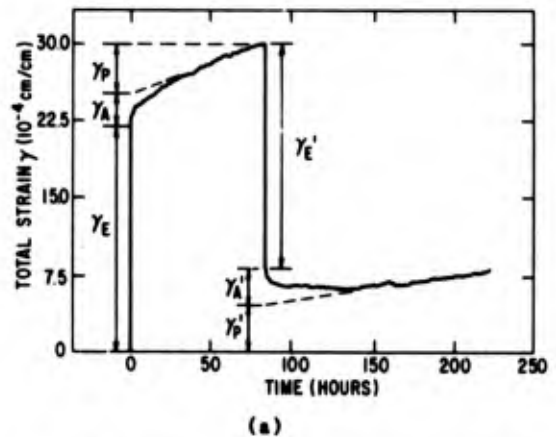


Figure 2. Strain response to stress cycle from 35 to 71 to 35 MPa. Sample preannealed at testing temperature of 500 K for 575 hours. (a) Total strain. (b) Anelastic strain obtained by subtracting the ideal elastic and viscoelastic strains. (from ref. 5)

of metallic glasses (7). Increases in modulus approaching 10% relative to the as-quenched condition, have been reported for many systems annealed near the glass transition temperature (8).

**Anelasticity.** Figure 2b shows the anelastic component of the total strain of Figure 2a obtained by subtracting the ideal elastic and viscoelastic contributions. The time-dependent, transient nature of the flow is evident. In this case, additional anelastic flow is not resolvable after approximately two days. The figure also illustrates the recoverability of the anelastic flow. In the test, the stress was cycled from 35 to 71 to 35 MPa and complete recoverability of the anelastic strain is verified ( $\gamma_a = -\gamma_a'$ ). The linearity of the anelastic strain with stress and the superposition of the anelastic strains has also been verified (5).

It has been shown that the anelastic strain cannot be described as a simple exponential decay but that successful fits to the data can be obtained with a spectrum of relaxation times. Argon and Kuo (9) have measured this spectrum for several alloys by performing recovery creep experiments on structurally stabilized specimens. The specimens were first mechanically polarized by creep over a long period of time at  $T = 150K$ , followed by cooling under stress to 200K and removal of the stress. The temperature was then increased incrementally and the degree of creep recovery measured. The data was analyzed to obtain activation energy spectra. The spectra are continuous functions rising sharply from very low values ( $\sim 20$  kcal/mole) to peak cut-off values at about 45-55 kcal/mole.

More extensive studies of the anelastic behavior of amorphous alloys using dynamic testing methods such as the vibrating reed technique have been performed to study the anelastic energy spectra in more detail (10). These studies have shown that the anelastic energy spectrum is very sensitive to the degree of structural relaxation in the alloys (11). However, the anelastic flow component measured in creep and stress relaxation tests appears to be only weakly affected by structural relaxation (12).

**Viscoelasticity.** The viscoelastic flow exhibited by structurally stabilized specimens is characterized by a constant strain rate. Referring to Figure 2a, the viscoelastic component is shown to contribute throughout the test, although constant strain rate, steady state flow is not fully established until after the decay of the anelastic transient.

The viscoelastic flow has been found to vary linearly with stress at low stresses while exhibiting power law dependence at higher values of stress (13). This behavior has been shown to be consistent with Eyring's (14) transition state model which predicts a stress ( $\tau$ )-strain rate ( $\dot{\gamma}$ ) relation of the form (15-17):

$$\dot{\gamma} = \dot{\gamma}_0 \text{SINH} \left[ \frac{\tau \gamma_0 \Omega_f}{2kT} \right] \quad (1)$$

$\gamma_0 \Omega_f$  is the volume strain element where  $\gamma_0$  is the measure of the local shear strain that an atomic scale volume  $\Omega_f$  undergoes when contributing to flow. The experimental determinations of this parameter show a strong temperature and composition dependence (13,18-20).

Viscoelastic flow is strongly affected by structural change in the alloy. Changes in the viscoelastic strain rate due to structural change of more than 7 orders of magnitude are commonly observed (21-23). The origin of the effect of structural change on the viscosity was explained qualitatively in the previous section. In the following section this aspect will be reviewed in greater detail.

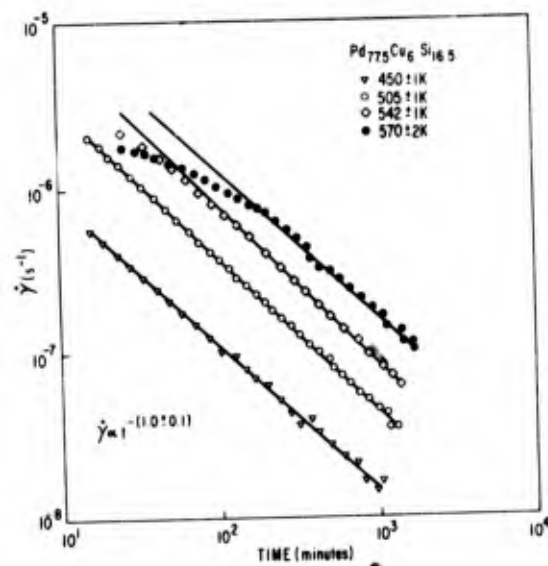


Figure 3. Equivalent strain rate as a function of test time for a sample creep tested from the as-cast condition at the indicated temperatures. (from ref. 22)

**Flow With Accompanying Structural Relaxation.**

In contrast to the flow behavior of structurally stabilized amorphous alloys discussed above, the flow of unannealed specimens does not attain a steady state condition. Rather, the strain rate  $\dot{\gamma}$  continues to decrease throughout the test as shown in Figure 3 for a sample of  $\text{Pd}_{77.5}\text{Cu}_6\text{Si}_{16.5}$  creep tested in the as-quenched condition. At the lower temperatures, the strain rate varies inversely with time from the start of the tests:  $\dot{\gamma} \sim t^{-1}$ . At the higher temperatures a similar decrease is observed, but only after an initial transient period of approximately thirty minutes.

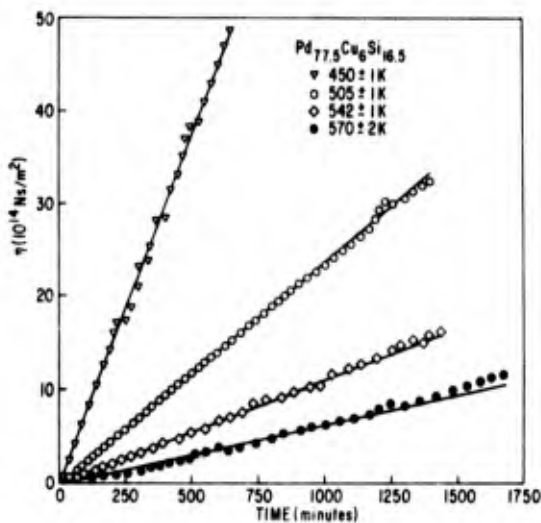


Figure 4. Viscosity as a function of test time at the indicated temperatures. (from ref. 22)

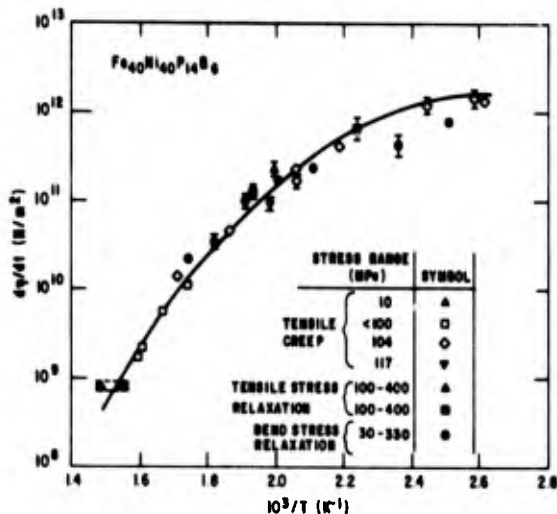


Figure 5. Rate of change of viscosity with time as a function of temperature, as measured in tensile creep, tensile stress relaxation and bend stress relaxation tests. The testing stress ranges are indicated. (from ref. 30)

Since the flow of these alloys has been shown to be Newtonian at low stresses, it has been more convenient to examine the viscosity  $\eta = \tau/\dot{\gamma}$ , rather than the strain rate. It should be pointed out that this viscosity is only the "apparent" viscosity and not the true viscoelastic viscosity since the testing procedure precludes subtraction of the anelastic contribution from the total strain rate. Figure 4 shows that the viscosity increases linearly with time at all the temperatures tested. In fact, the viscosity relaxation exponent  $n = d(\ln \eta)/d(\ln t)$  for a wide range of alloy compositions has been found to be nearly unity ( $0.9 < n < 1.0$ ) in the temperature range  $T < T_g - 20$  (22-28).

The viscosity increase observed in creep experiments is also manifested in stress relaxation

tests (23). As the preannealing time is increased, the viscosity of the sample increases and correspondingly, the stress relief kinetics slow down. This leads to a shifting of the stress relaxation curves to longer times. When the magnitude of this shift is related to the changes in the viscosity due to the preannealing treatment, the viscosity is found to increase linearly at a rate that is consistent with that measured during creep testing.

In Figure 5, the rate of viscosity change with time  $\dot{\eta}$  for amorphous  $\text{Fe}_{40}\text{Ni}_{40}\text{P}_{14}\text{B}_6$ , is plotted against inverse temperature. The data indicate that the measured values of  $\dot{\eta}$  are independent of the testing method (tensile creep and tensile and bend stress relaxation) and the investigator (22,24,25,29,30), prior thermal treatment of the alloy (5,22,26,31), and the magnitude of the testing stress (5,22,32). The non-Arrhenius form of the data is consistent with that observed on a wide range of amorphous alloys (27-28).

We now address an apparent paradox in the data. The viscosity relaxation has been shown to proceed continuously during testing of unannealed specimens. It has also been shown that even if a specimen has been given a preanneal, the viscosity continues to increase during subsequent flow testing at a rate that is the same as that measured on unannealed specimens. Yet, in the previous section, data on structurally stabilized specimens was presented in which a steady state strain rate (i.e. - constant viscosity) was attained. It is important therefore to define what is meant by a "stabilized" structure. It has been established that the structure relaxes and that the viscosity changes continuously during isothermal annealing. However, since the rate of viscosity increase  $\dot{\eta}$  is a constant, the fractional rate of viscosity increase  $d(\ln \eta)/dt$  decreases as the test proceeds. If a specimen is annealed until the fractional rate of viscosity change becomes less than about 5% per day, then short time testing (<1 hour) at the annealing temperature can be performed under "pseudo" steady-state conditions. Further, if the testing temperature is below the preanneal temperature, then testing over longer periods is allowed since the relaxation rate is lower at the lower temperature.

This technique of establishing "pseudo" constant structure conditions has proved very useful in determining the temperature dependence of the constant structure (isoconfigurational) viscosity. It has been demonstrated that if a specimen is annealed until the fractional rate of viscosity change becomes less than 10% per day, then one can lower the temperature, measure the viscosity and then raise the temperature back to the anneal temperature and find that the viscosity has not changed from its original value. The viscosity can also be reproduced after higher temperature cycling if the measurements are made in a short time. The return to the original viscosity value at the end of the test

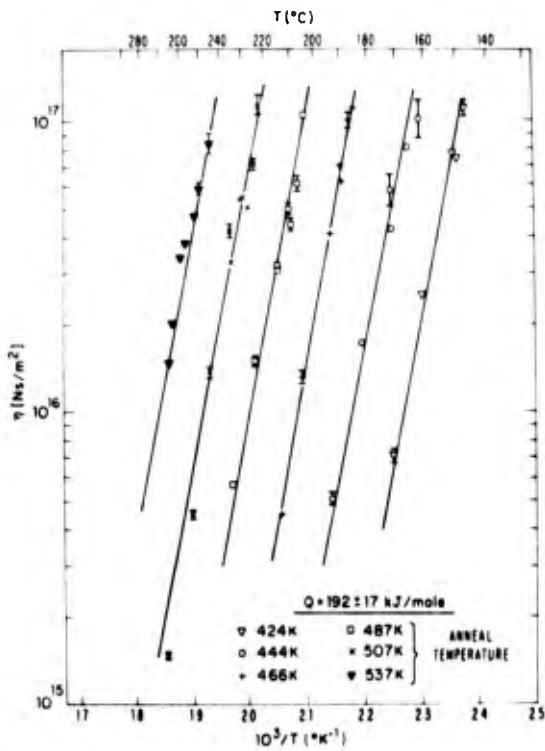


Figure 6. Isoconfigurational viscosities of glassy Pd<sub>82</sub>Si<sub>18</sub> obtained after stabilizing anneals at the indicated temperatures. (from ref. 26)

implies that negligible structural change occurred during the temperature cycle. This ability to reproduce viscosity measurements during temperature cycling is the operational definition of isoconfigurational measurements. The tests are not truly at constant structure, rather the irreversible structural change during the test is negligible.

Figure 6 shows the isoconfigurational viscosity data for a Pd<sub>82</sub>Si<sub>18</sub> specimen that was structurally stabilized in the manner described above, at successively higher temperatures. As expected, the isoconfigurational curves are seen to shift in the direction of the equilibrium curve with increasing annealing temperature. A constant activation energy was obtained  $Q=192 \pm 17$  kJ/mole. Further studies have shown that this activation energy is unaffected by the magnitude of the applied stress during both the stabilizing preanneal and the isoconfigurational testing (4,31).

All of the available isoconfigurational data are shown in Figure 7. The existing equilibrium data is included for completeness. Temperature normalization has been applied to facilitate comparison between alloys. The agreement of the experimental data with the schematic illustration of Figure 1 is readily apparent. It has recently been shown that the activation energy for isoconfigurational flow does not remain constant over the entire temperature range but that

it increases with temperature (curve g). The change in activation energy is small at low temperatures, but it increases rapidly as the glass transition temperature is approached. This trend is similar to that found for  $Q_{\eta}$ .

#### Reformulation of the Data.

In the previous section, the basic phenomenon associated with the flow behavior of amorphous alloys have been presented with distinction made between those experiments done under conditions of "pseudo" steady-state and those performed under conditions where the structure of the alloy changed continuously during the tests. The structural changes and their effect on the flow behavior are described generally as an equilibration of the atomic configuration. In that sense, the observations made are analogous to the physical aging that occurs in amorphous polymers. Accordingly, in this section the structural relaxation data will be reformulated

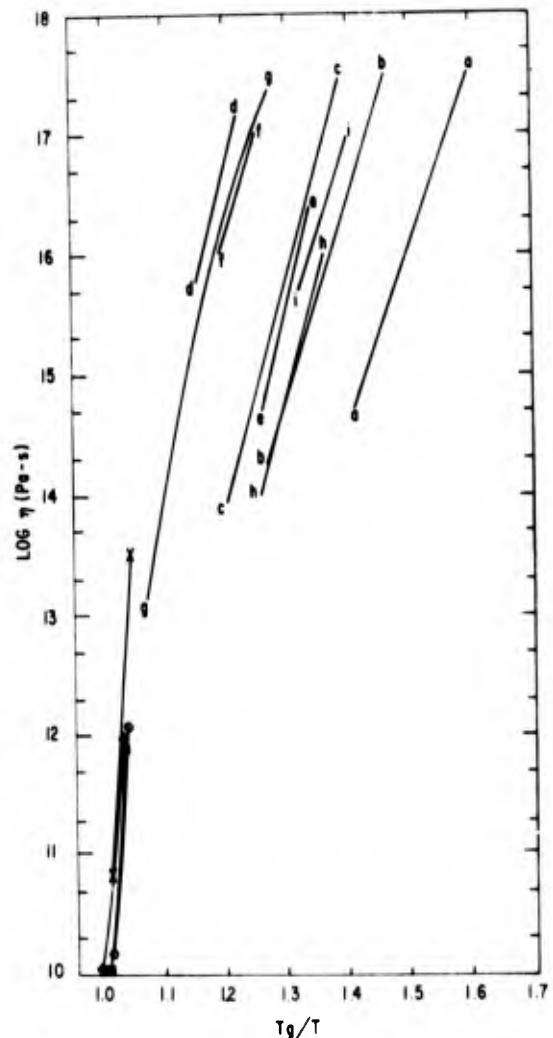


Figure 7. The available isoconfigurational and equilibrium viscosity data as measured in creep tests. Reduced-temperature scaling is used. For those alloys which do not exhibit a glass transition, the temperature at the onset of crystallization is used. (from ref. 28)



into a format that is consistent with that used in the polymer literature so that direct comparison can be made with that data. In particular, comparison will be made between the amorphous alloy data summarized above and the corresponding small-strain properties of amorphous polymers summarized in the recent monograph by Struik (33).

Figure 8 shows the relaxation modulus  $G(t) = \sigma(t)/\gamma$  (34) for several as-quenched samples of amorphous  $Pd_{77.5}Cu_{6.5}Si_{16}$  tested in bending at 498K after the indicated preanneals at the testing temperature for the indicated times  $t_e$  (23). The middle curve gives the result of a superposition of the data by a horizontal shift in the direction indicated by the arrow. In agreement with the results of Struik on many amorphous polymers, the data can be reduced to a master curve by a horizontal shift. Continuing with Struik's analysis, the horizontal shifts between successive stress relaxation curves are noted by an acceleration factor  $a$ , which is taken as positive for a shift to the left. In Figure 9, the acceleration factor relative to the 420 second preanneal is plotted against the aging time. The acceleration factors for tests performed at 523K are also shown in the figure. The aging can be characterized by the shift rate  $\mu = d(\ln a)/d(\ln t)$ . In this case,  $\mu$  is found to be reasonably close to unity,  $\mu = 0.80$ .

Similar analyses were done for amorphous  $Fe_{40}Ni_{40}P_{14}B_6$  (see Figure 9) and  $Pt_{40}Ni_{40}P_{20}$ . These alloys exhibited shift factors considerably less than unity. For the FeNiPB alloy, both tensile and bend stress relaxation test data were analyzed and found to be in good agreement. The shift factors are plotted in Figure 10 as a function of temperature. The data for several amorphous polymers as reported by Struik are also included in the figure.

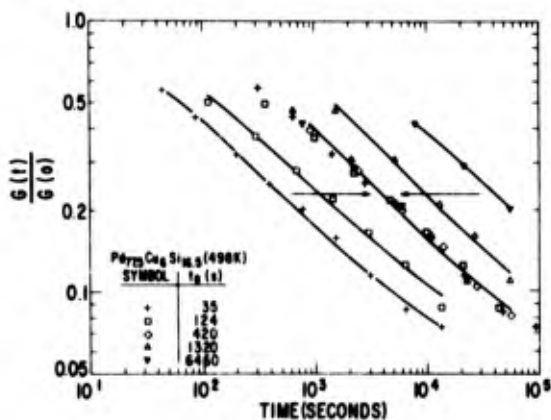


Figure 8. Bend stress relaxation data for PdCuSi. The specimens were preannealed at the test temperature for the indicated times. The data is shifted horizontally in the directions indicated to superimpose on the curve for  $t_e = 420$  seconds. (after ref. 23)

As Figure 10 illustrates, the aging behavior of all polymers is very similar. The shift rate  $\mu$  is zero above  $T_g$  where the material is equilibrated. Just below  $T_g$ , it rapidly increases to about unity, remaining unity over a wide temperature range below  $T_g$ . At low temperatures, the aging begins to cease and  $\mu$  decreases. This lower temperature decrease in  $\mu$  is associated with secondary relaxation in the materials (motion of side groups or parts of chain segments compared to motion of the segments as a whole) and may not have an analog in amorphous metallic alloys. The data for the latter is too limited to draw any significant conclusions on the temperature dependence of the shift factor. However, the reason for the differences in  $\mu$  between the alloys cannot be merely a function

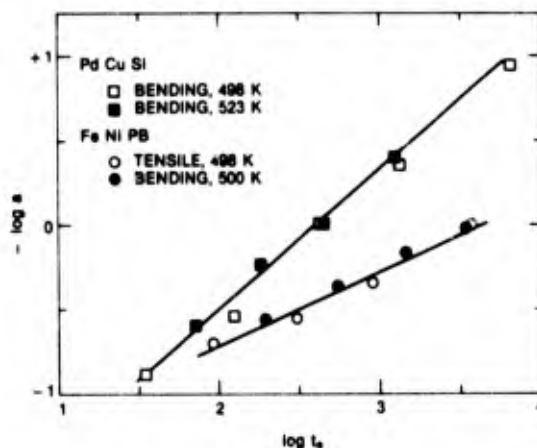


Figure 9. Acceleration factor as a function of annealing time  $t$  for the data of Figure 8. Additional data for PdCuSi at 523 K and FeNiPB is included.

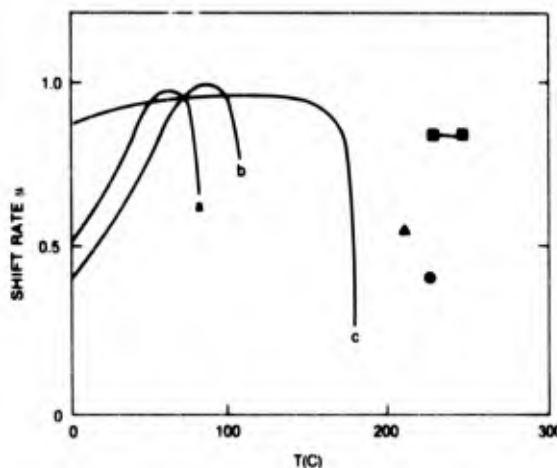


Figure 10. Shift rate  $\mu$  as a function of temperature for amorphous polystyrene (a), PMMA (b), polysulphone (c), FeNiPB ( $\bullet$ ), PdCuSi ( $\blacksquare$ ), and PtNiP ( $\blacktriangle$ ). (after ref. 33)

of the testing temperature, since the glass transitions for FeNiPB and PdCuSi are close, making the difference  $T - T_g$  for the two alloys small.

### Discussion

The structural relaxation process described above is by nature a self-retarding mechanism. That is, as the atomic structure equilibrates, the viscosity of the material increases. This viscosity increase is a reflection of the decreasing mobility of the atoms ( $M \sim 1/\eta$ ). As the atomic mobility decreases, the ability of the structure to continue relaxing decreases, and therefore the structural relaxation rate decreases. The large viscosity changes that are observed (>7 orders of magnitude) are associated with relatively small changes in the density and radial distribution functions, indicating that the process is in fact strongly self-retarding.

Struik shows that for systems with strong self-delaying effects, when the system is far from equilibrium as is the case for the amorphous alloy data presented in this paper, the mobility is expected to decrease linearly with the reciprocal of time ( $\mu \sim 1$ ). Then, since the acceleration factor is proportional to the mobility of the material which is in turn inversely proportional to the viscosity, one obtains:

$$\mu = -d(\log a)/d(\log t_e) = -d(\log \eta)/d(\log t_e) \sim 1$$

One then expects the shift rate  $\mu$  determined from the acceleration factors to be the same as the slope of the  $\log \eta - \log t_e$  curves. For the PdCuSi alloy, the shift in the relaxation curves has previously been explained quantitatively by a linear increase in the viscosity during the preanneal (23) in agreement with a shift rate  $\mu$  of nearly unity as determined in the previous section. For the PtNiP and FeNiPB, as well as for every other amorphous alloy investigated, linear viscosity-time kinetics have also been observed. Yet for these alloys  $\mu$  is considerably less than unity. The reason for this discrepancy is not clear at this time.

A linear viscosity-time dependence is not unique to amorphous alloys. Several investigators have reported linear time kinetics for several inorganic glasses (35-37). In fact, for the inorganic glasses, the true viscosity (35) was measured as compared to the "apparent" viscosity reported for the amorphous alloys. This was accomplished by subtracting out the contributions to the elongation due to the contraction associated with the free volume decrease as the atomic configurations adopt their equilibrium states and the elongation due to anelasticity. Unfortunately, we are not aware of corresponding preannealing studies on inorganic glasses to check for agreement in the value of  $\mu$  calculated from viscosities and by the shift technique.

### Conclusions

Structural relaxation has been shown to have a very strong effect on the flow behavior of amorphous alloys. Increases in the viscosity of more than 7 orders of magnitude are commonly observed during isothermal annealing of these materials. The kinetics of this process are well established and characterized by a linear increase in the viscosity with annealing time.

This increase in the flow resistance has been attributed to the equilibration of the atomic structure and is therefore similar in nature to the physical aging process exhibited by amorphous polymers. That process has been studied quite extensively, but the method of analyzing the data differs significantly from that used in the amorphous alloy literature so that comparison between the two systems has been difficult.

In this paper, the existing data on the effect of preannealing on the subsequent stress relaxation behavior of amorphous alloys was reanalyzed by the technique used for amorphous polymers as summarized by Struik. The data on PdCuSi was found to exhibit a shift rate  $\mu$  of approximately unity, in agreement with the data for many amorphous polymers. This value of  $\mu$  is consistent with the linear viscosity-time kinetics found previously for this alloy. However, two other amorphous alloys were analyzed in a similar manner, and although they also exhibit linear viscosity-time kinetics, the calculated values of the shift rate  $\mu$  were significantly less than one. The reason for this discrepancy is unclear.

In general, it appears that the evolution of the flow resistance of amorphous materials is characterized by a linear time relation. The shift rate for polymers is about unity below  $T_g$  and the viscosity of amorphous alloys and inorganic glasses increases linearly with time. This linear relation is characteristic of a self-retarding process and is therefore consistent with the general model that explains the increase in the flow resistance in terms of the equilibration of the atomic structure.

### References

- (1) W. Klement, Jr., R.H. Willens, and P. Duwez, *Nature* 187 (1960) 809.
- (2) T. Egami, V. Vitek, and D. Srolovitz, *Proc. 4th Int. Conf. on Rapidly Quenched Metals*, T. Matsumoto, and K. Suzuki, ed., Japan Institute of Metals, Sendai, Japan, (1982) 517.
- (3) A.L. Greer, *J. Non Cryst. Solids* 61-62 (1984) 737.
- (4) F. Spaepen and A.I. Taub in "Amorphous Alloys," ed. F.E. Luborsky, Butterworths, Boston (1983) 231.
- (5) A.I. Taub and F. Spaepen, *J. Mat. Sci.* 16 (1981) 3087.

- (6) A.S. Nowick and B.S. Berry, "Anelastic Relaxation in Crystalline Solids", Academic Press, New York, 1972.
- (7) H.S. Chen, Rep. Prog. Phys. 43 (1980) 353.
- (8) H.S. Chen, J. Appl. Phys. 49 (1978) 3289.
- (9) A.S. Argon and H.Y. Kuo, J. Non Cryst. Solids 37 (1980) 241.
- (10) B.S. Berry in "Metallic Glasses," Am. Soc. Metals, Metals Park, OH (1978) 161.
- (11) N. Morito and T. Egami, J. Non Cryst. Solids, 61-62 (1984) 973.
- (12) J. Haimovich and T. Egami, Mat. Sci. Engng. 61 (1983) 89.
- (13) A.I. Taub, Acta Met. 28 (1980) 633.
- (14) H. Eyring, J. Chem. Phys. 4 (1936) 283.
- (15) F. Spaepen, Acta Met. 25 (1977) 407.
- (16) F. Spaepen, in "Physics of Defects," R. Balian, M. Klemen and J.-P. Poirier, ed., Les Houches Lectures XXXV, 133, North Holland, Amsterdam (1981).
- (17) A.S. Argon, Acta Met. 27, (1979) 47.
- (18) A.I. Taub, Scripta Met. 17 (1983) 873.
- (19) A.I. Taub, Acta Met 30 (1982) 2117.
- (20) J.C.M. Li, ref. 2, 1335.
- (21) A.I. Taub and F. Spaepen, Scripta Met 13 (1979) 185.
- (22) A.I. Taub and F.E. Luborsky, Acta Met 29 (1981) 1939.
- (23) A.I. Taub and F.E. Luborsky, Mat. Sci. Engng. 56 (1983) 157.
- (24) J.P. Patterson and D.R.H. Jones, Acta Met 28 (1980) 675.
- (25) P.M. Anderson, III and A.E. Lord, Mater. Sci. Engng. 44 (1980) 279.
- (26) A.I. Taub and F. Spaepen, Acta Met 28 (1980) 1781.
- (27) A.I. Taub and J.L. Walter, J. Non Cryst. Solids 61-62 (1984) 811.
- (28) A.I. Taub and J.L. Walter, Mat. Sci. Engng. 62 (1984) 249.
- (29) T. Takemori, T. Mizoguchi and T.R. McGuire, Mat. Res. Bull. 15 (1980) 81.
- (30) A.I. Taub, Acta Met 30 (1982) 2129.
- (31) S. Tsao and F. Spaepen, ref. 2, 463.
- (32) A.I. Taub and F. Spaepen, Scripta Met 13 (1979) 883.
- (33) L.C.E. Struik, "Physical Aging in Amorphous Polymers and Other Materials," Elsevier Scientific Publishing, New York (1978).
- (34) J.D. Ferry, "Viscoelastic Properties of Polymers," John Wiley and Sons, New York (1970).
- (35) A.L. Zijlstra, Phys. Chem. of Glasses 4 (1963) 143.
- (36) H.R. Lillie, J. Am. Ceram. Soc. 16 (1933) 619.
- (37) P.M. Prod'homme, Rheol Acta 12 (1973) 337.

# **SPIN GLASSES**

## RECENT EXPERIMENTAL ADVANCES IN SPIN GLASSES

C. Y. Huang  
Los Alamos National Laboratory  
Los Alamos, NM 87545

We present a working definition and a general description of a spin glass. A number of different systems, including metals, semiconductors, and insulators, are discussed. This review presents the current status of experimental spin-glass research with special emphasis on the extent to which the results of this research yield information on spin dynamics. We review the salient features of a series of recent experimental results, published in the past five years, on the susceptibility, magnetization, heat capacity, high-pressure effects, phonon-thermal conductivity, neutron scattering, nuclear, electron, and muon spin resonance. The successful applications of the fractional exponential relaxation function to the frequency dependence of the susceptibility and the time dependence of the thermoremanent magnetization are demonstrated. Concerning the possible existence of the phase transition at the susceptibility cusp temperature, we summarize the experimental evidences.

### I. INTRODUCTION

Studies of the magnetic properties of dilute transition metal alloys have been a subject of interest for half a century. As early as 1931, Shih (1) investigated the magnetic susceptibility  $\chi$  of dilute alloys of iron in gold (AuFe). With the advent of the Kondo effect, this one-impurity problem prompted intensive studies in the 1960's of those alloys with "non-interacting" or very dilute 3d-magnetic impurities dissolved in non-magnetic metallic hosts. In 1971, Cannella, Mydosh, and Budnick (2) observed rather sharp cusp-like peaks in the low-field ac magnetic susceptibility  $\chi(T)$  for a series of low-concentration (~1 at %) AuFe alloys. This observation has stimulated many experimentalists as well as theoreticians. Later, this peaking in  $\chi(T)$  was used as one of the signatures marking an alloy as being a spin glass.

Conventional spin glasses are dilute magnetic alloys such as CuMn, or AgMn or AuFe, in which the 3d-magnetic moments interact via the long-range RKKY interactions. Because the magnetic impurities are distributed randomly, the sign and size of the interaction is very sensitive to the inter-impurities distance. As a result, contradictory ordering between two magnetic moments depending on two different paths, called "frustration," (3) takes place. This encounter of competing positive and negative alignments is essential to the formation of the spin glass state. Spin glasses exhibit rather unusual properties (4-17). As pointed out previously, one observes a sharp cusp in  $\chi(T)$  at the "freezing temperature" (conventionally

denoted as  $T_f$ ,  $T_g$ ,  $T_0$ , or  $T_{sg}$ ). Mössbauer measurements on Fe in AuFe showed a hyperfine splitting roughly at  $T_f$ , thereby suggesting the formation of static or quasi-static internal fields below  $T_f$  owing to frozen-in spins (18). Even though neutron scattering studies (19) have shown the absence of long-range magnetic order, many authors have attempted to interpret these anomalies as evidence of a phase transition. The suggestion of a possible phase transition at  $T_f$  has challenged an entire generation of theorists in understanding this new but different kind of "transition." In the absence of an external magnetic field, the magnetic contribution to the specific heat  $C$  has been observed only as a broad maximum (20) well above  $T_f$  and there is no anomaly in  $C$  around  $T_f$  as one would normally expect for a phase transition. However, very recently anomalies near  $T_f$  have been observed (21) in  $\partial(C/T)/\partial T$  and  $\partial^2(C/T)/\partial T^2$ . Nevertheless, some authors have recognized that spin glasses are very complex systems, and they treat the problem from a dynamic, metastable point of view, assuming a "progressive freezing" of spins throughout the sample upon lowering the temperature below  $T_f$ .

In this review, only experiments pertinent to dynamics published in the last five years will be discussed in detail, and the choice of the experiments to be reviewed simply results from the prejudice of the author. Readers who wish to obtain more detailed and complete information on the subject are referred to some earlier review papers [Refs. 3-17, 22-27]. Also, an expanded version of the present paper is in preparation for publication in the

II. LOW-FIELD AND LOW-FREQUENCY SUSCEPTIBILITY

1. Metallic Spin Glasses

A metallic spin glass is commonly a dilute metallic magnetic alloy in which the dominant interactions are the long-range RKKY interactions. The first measurements of low-field (~5 G) and low-frequency (155 Hz) susceptibility,  $\chi(T)$ , were carried out on metallic AuFe by Cannella et al. (2) Figure 1 shows their results of four AuFe alloys. The remarkable feature of this low-field measurement is the occurrence of a sharp, cusp-like peak in each  $\chi(T)$ . This cusp-like peak has been observed in many dilute alloys (28). Cannella and Mydosh (29) also investigated the effect of applied magnetic fields on the susceptibility. Fields of only ~100 G destroy the sharp susceptibility peaks and produce broader maxima similar to those observed by Tholence and Tournier (30). The occurrence of the sharp peak has prompted many theorists (31,32) to believe that there exists a new kind of phase transition at  $T_f$ , below which magnetic moments are frozen into thermal equilibrium orientations but with no average long-range order, and thus the system is in the so-called spin-glass phase.

2. Insulating Spin Glasses

EuS is an insulator and is well known as an ideal Heisenberg ferromagnet, whose crystallographic symmetry is cubic. The localized, spin-only moments ( $7\mu_B$ ) of the  $\text{Eu}^{2+}$  ions ( $8S_{7/2}$ ) are coupled to their neighbors via isotropic exchange interactions. The first-neighbor ferromagnetic interaction ( $J_1$ ) dominates the indirect (via the S ions) antiferromagnetic second-neighbor exchange interaction ( $J_2$ ), and their ratio is  $J_2/J_1 = -1/2$ . When EuS is diluted with non-magnetic, isostructural SrS, magnetic moments grouped into finite clusters are effectively decoupled from the ferromagnetic alignment within the long-range ferromagnetic order. As the dilution proceeds, eventually ferromagnetism breaks down and the spin glass "order" sets in, as a result of the "frustration" effect.

Maletta and his co-workers (33-37) have investigated the magnetic properties of insulating  $\text{Eu}_x\text{Sr}_{1-x}\text{S}$  alloys. Figure 2 displays the ac susceptibility at 117 Hz for four spin glass samples of  $\text{Eu}_x\text{Sr}_{1-x}\text{S}$ . All these curves exhibit strong maxima, defining  $T_f$ .

III. SCALING

Recently, Barbara et al. (38-40) studied two spin glasses: polycrystalline 4.6 at % Mn in Cu and amorphous 37% Gd in Al. They have used a SQUID magnetometer to measure the dc susceptibility,  $\chi(H)$ , up to 50 kG. They argued that the nonlinear susceptibility  $\chi_5$  behaves like  $H^{2/3}$  at  $T_f$ . Accordingly, they used the following scaling relation for the non-

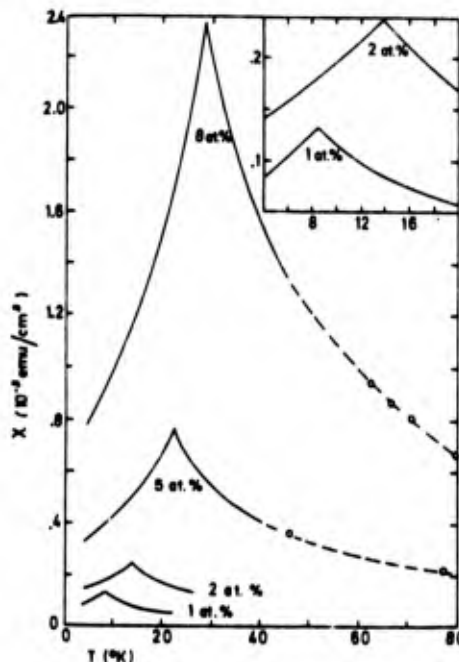


Figure 1. Low field susceptibility  $\chi(T)$  for alloys of AuFe with Fe concentration = 1, 2, 5, and 8 at %. (Ref. 2).

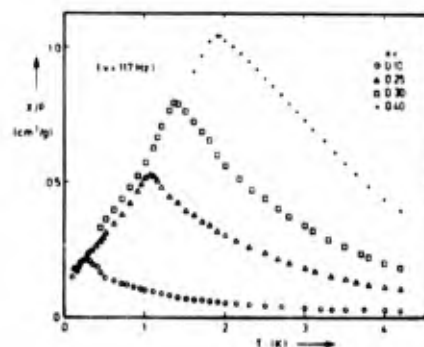


Figure 2. Temperature dependence of the ac susceptibility in  $\text{Eu}_x\text{Sr}_{1-x}\text{S}$  with different Eu concentration x (Ref. 33).

linear susceptibility:

$$\chi_5(H, \underline{t}) = \chi_0(\underline{t}) - M/H = H^2/\delta' f(\underline{t}/H^2/\phi') \quad (1)$$

where  $\underline{t} = (T - T_f)/T_f$ ,  $\chi_0 = \chi(H \rightarrow 0)$ , and  $f(y)$  is a scaling function, in which

$$f(y) \rightarrow \text{const.}, y \rightarrow 0,$$

$$f(y) = y^{-\gamma'}, y \rightarrow \infty,$$

$$\phi' = \gamma' \delta' / (\delta' - 1) \equiv \beta' \delta' \quad (2)$$

As shown in Fig. 3, their data for the case  $T > T_f$  converge toward a single curve for the two samples. They find

$$\begin{aligned} \gamma' &= 3.8 \pm 0.5, & \delta' &= 6.1 \pm 0.2 \\ \psi' &= 4.0 \pm 0.5 & & (37\% \text{ GdAl}); \\ \gamma' &= 3.4 \pm 0.4, & \delta' &= 4.1 \pm 0.2, \\ \psi' &= 5.0 \pm 0.5, \\ \beta' &= 1.1 \pm 0.2 & (4.6\% \text{ MnCu}) \end{aligned}$$

For the sake of self-consistency, they also employed another parametric form for  $\chi$  in the critical region (39):

$$\chi(H, \underline{t}) = \chi_p - A \underline{t}^{\beta'} - [B(\underline{t}^{\gamma'}/H^2) + CH^{-2/\delta'}]^{-1}, \quad \text{for } \underline{t} > 0, \quad (3)$$

where  $\chi_p$  is the peak value of  $\chi$  at  $T_f$ . By fitting about 500 data points for  $0 < H < 2000$  G, they got  $\beta' = 93 \pm 0.04$ ,  $\gamma' = 2.7 \pm 0.1$ ,  $\delta' = 5.7 \pm 0.2$ . These scaling results support the possibility of a second-order phase transition at  $T_f$ .

#### IV. HEAT CAPACITY

##### 1. Metallic Spin Glasses

In the last section, we have assumed that there is a phase transition between spin-glass and paramagnetic behavior. The question is whether a phase transition is observed in the thermodynamic sense or just a rapid change in the dynamics of the spin system. One of the

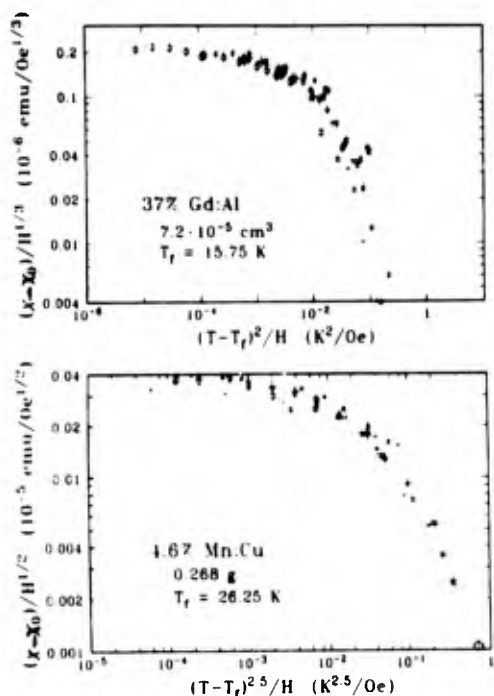


Figure 3. Scaling fits according to Eq. (1) for the non-linear susceptibility as a function of field and temperature above  $T_f$ . For GdAl and MnCu samples, respectively, large circles represent data at 16 and 26.5 K; small x's, 16.4 and 27; large x's, 17 and 27.5; crosses, 18 and 28; small circles, 20 and 29; equals signs, 30 and 30; U's, 40 and 40; and O's, 50 and 50 (Ref. 38).

earliest experimental investigations was by Wenger and Keesom (20,41) who measured the magnetic heat capacity of AuFe and CuMn metallic spin glasses. At  $T_f$ , there is no cusp-like peak. In order to investigate the low-temperature behavior, Fogle et al. (21,42) have measured the heat capacity down to  $\sim 50$  mK. They subtracted off the lattice and hyperfine contributions to obtain the magnetic heat capacity. The low-temperature data conform to  $\Delta C = \gamma T + \Delta T^2$ . Fogle et al. (21) concluded that, to within experimental error, the leading term in the low temperature heat capacity is a concentration independent linear term  $\gamma T$ , with  $\gamma = 1.8$  mJ/mole-K $^2$ . They (42) suggested that the  $T^2$  term might be due to the presence of a finite density of magnon-like collective excitations (43-45). Numerical calculations (43) on metallic spin glasses have confirmed the linear dependence of  $C(T)$  on  $T$ .

##### 2. Insulating Spin Glasses

Meschede et al. (37) have measured the heat capacity of insulating  $\text{Eu}_x\text{Sr}_{1-x}\text{S}$  with  $x = 0.40$  and 0.54 from 0.3 to 10 K with fields up to 1.00 T (10 kG). The  $x = 0.40$  sample is a spin glass with  $T_f = 1.7$  K. Similar to a metallic spin glass, the specific heat curve displays a broad maximum well above  $T_f$ , no singularity at  $T_f$ , and a linear temperature dependence at low temperature. Below 0.45 K, the specific heat per Eu ion at zero field can be fitted with the relation

$$C^*(T) = \gamma T + \Delta T^{-2}, \quad (4)$$

where  $\gamma/\text{kg} = 0.49 \pm 0.01 \text{ K}^{-1}$  and  $\Delta^2/\text{kg} = (2.6 \pm 0.4) \times 10^{-3} \text{ K}^2$ .  $\text{Eu}_{0.54}\text{Sr}_{0.46}\text{S}$  becomes ferromagnetic at  $T_c' = 5.0$  K and "re-enters" from a ferromagnetic state into a spin-glass state at  $T_f' = 2.0$  K. At  $T_c'$ , there is a broad maximum. Again there is no anomaly at  $T_f'$ .

Because the specific heat of both metallic and insulating spin glasses has a linear term in  $C^*(T)$  at low temperature, Meschede et al. (37) conjectured that this linear term exists independent of the type of magnetic coupling and of the concentration of magnetic ions. Furthermore, in view of the fact that both dielectric and metallic glasses have linear dependencies of  $C(T)$ , these authors surmised that the  $\gamma T$  law of  $C(T)$  might be a universal property of "disordered" solids at low temperature.

For the reentrant  $\text{Eu}_{0.54}\text{Sr}_{0.46}\text{S}$  sample, at  $B = 1.00$  T and below 0.65 K,  $C^*$  fits well with the relation

$$C^* = A T^{3/2} + \Delta T^{-2}, \quad (5)$$

which is a common relation for a ferromagnet in a small field at low temperature. Here  $A/\text{kg} = 0.25 \pm 0.01 \text{ K}^{-3/2}$ , which is much larger than the value,  $A/\text{kg} = 0.03 \text{ K}^{-3/2}$ , for ferromagnetic EuS. One can conclude that a high field ( $B > 1.00$  T) suppresses the low-temperature spin-glass phase in  $\text{Eu}_{0.54}\text{Sr}_{0.46}\text{S}$

and induces ferromagnetic ordering.

### 3. Phase Boundary

Recently, de Almeida and Thouless (46) showed that the Sherrington-Kirkpatrick (SK) model for classical Ising spins exhibits an instability for purely random interactions in the presence of a magnetic field. This instability has been interpreted as a phase transition line, called an AT line, marking the onset of freezing of the spin component longitudinal to the field (47). Gabay and Toulouse (48) have extended this calculation to obtain the phase boundary for classical  $m$ -component spins. This instability line is called the GT line and is given by

$$\tau \equiv 1 - T_f(H)/T_f(0) = 0.23(g\mu_B H/J)^2 \quad (6)$$

for  $\tau \ll 1$ , where  $g$  is the  $g$ -factor,  $\mu_B$  the Bohr magneton,  $T_f(H)$  the critical temperature in a field  $H$ , and  $J \equiv k_B T_f(0)$ . The transverse spin ordering considered in the GT line is not detectable in susceptibility measurements but it is accompanied by a specific-heat anomaly of "third-order character."

Fogle et al. (21) have measured the specific heat of 2790-at-ppm CuMn sample from 0.3 to 30 K at various fields up to 75 kG. Their results are displayed in Fig. 4. As shown, there is no obvious anomaly in the  $C/T$  vs  $T$  curves at  $T_f$  as indicated by the arrow. However, there is structure in  $d(C/T)/dT$  and  $d^2(C/T)/dT^2$  as exhibited in Figs. 4(b) and (c), respectively. The anomaly is shifted to a lower temperature in an applied field. Accordingly, it is reasonable to assume that the  $H$ - $T$  dependence of the anomaly is related to that of the phase boundary. The dotted curves in Fig. 4 represent the background heat capacity obtained by fitting the data to a six-term polynomial. The resulting anomaly in  $\Delta C/T$ , which is the difference between the experimental points and the background, is shown in Fig. 4(d). The anomaly does not show the sharp cusp required for a transition third-order character predicted by the theory. This "broadening" might be caused by an inhomogeneous distribution or clustering of the Mn atoms. As exhibited, the amplitude of the anomaly decreases with increasing field. This is in agreement with the theory because the order of the longitudinal components increases with decreasing temperature and increasing field, thus reducing the entropy change associated with the appearance of transverse order. The temperature at which this anomaly takes place,  $T_M$ , is found to be proportional to  $H^2$ , as shown in the inset of Fig. 4. However, the proportionality constant is smaller by a factor of 2.5 than the theoretical value given in Eq. (6). In conclusion, in spite of some quantitative discrepancies, the qualitative agreement between mean-field theory and experiment is striking and seems to constitute persuasive evidence of reality for the transverse ordering and the relevance of the mean-field theory to

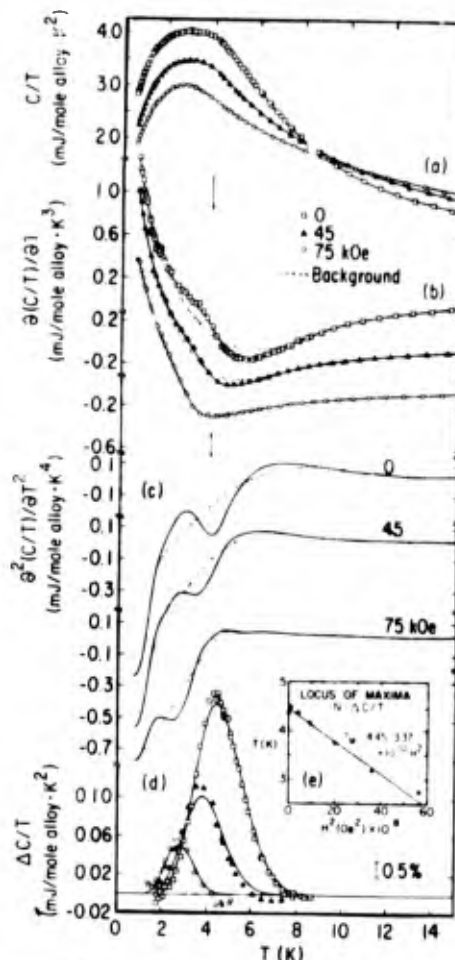


Figure 4. Spin-glass heat capacity,  $C$ , and derived quantities for 2790-at-ppm CuMn. The solid curves represent spline fits. The dotted curves in (a) - (c) represent the background heat capacity. The anomaly  $\Delta C$ , is shown in (d), and the locus of its maxima in (e). The arrows represent the freezing temperature at  $H = 0$  (Ref. 21).

real spin glasses.

### V. HIGH PRESSURE EFFECTS

The magnetic properties in a "disordered" system are in general very insensitive to pressure. As a result, the high pressure effects on a spin glass are expected to be weak. The first attempt was made on the effect of pressure on the electrical resistivity,  $\rho(T)$  (49-51). In spite of the strong dependence of  $\rho$  on pressure, the absence of the anomaly in  $\rho(T)$  at  $T_f$  made the results less tangible.

In order to augment the pressure effect, it is helpful to use an exchange-enhanced host. Pd is such a host. In particular, its conduction electron density of states at the Fermi energy varies very strongly with pressure (52). For  $Pd_{1-c}Mn_c$  with  $c < 3$  at %, giant moment ( $\sim 7.5 \mu_B$ ) ferromagnetism prevails. However,



Mn nearest neighbors are coupled, producing Mn-Mn antiferromagnetic exchange. When  $c > 4$  at %, the probability of having two Mn atoms at first, second, and third nearest-neighbor sites increases. Verbeek et al. (53) investigated the alloys,  $(\text{Pd}_{0.9965}\text{Fe}_{0.0035})_{1-x}\text{Mn}_x$ , in which the master alloy,  $\text{Pd}_{0.9965}\text{Fe}_{0.0035}$ , is a strong giant-moment ferromagnet with an effective moment as high as  $\approx 10 \mu_B$ . At a very low Mn concentration, the system is a ferromagnet, as demonstrated by the solid curve for  $x = 0.01$  in Fig. 5. At a high Mn concentration, short-range Mn-Mn antiferromagnetic exchange competes with the long-range ferromagnetic interaction, supplying the "frustration" with the appearance of the spin-glass phase at  $T_f$ , as exhibited in Fig. 5.  $\chi(T)$  for  $x = 0.065$  shows a typical cusp. However, for  $0.03 < x < 0.06$ , an alloy is a reentrant spin glass, which becomes a ferromagnet at  $T_c'$ , followed by a transition to a spin-glass state at  $T_f'$ . As an example,  $\chi(T)$  for  $x = 0.05$  is shown in Fig. 5. Figure 6 shows the magnetic phase diagram for the three distinct systems with  $x = 0.01, 0.05,$  and  $0.065$ , have been studied (54) under high pressure  $P$  up to 20 kbar. The pressure effects on  $\chi(T)$  are as displayed in Fig. 5. The pressure dependencies of  $T_c$  for the  $x = 0.01$  ferromagnet,  $T_f$  for the  $x = 0.065$  spin glass, and  $T_f'$  and  $T_c'$  for the  $x = 0.05$  reentrant spin glass are given in Fig. 7. To the accuracy of the experiment, all of them are linear in  $P$ . This linear relationship is understandable, because 20 kbar is only a small pressure in comparison with the internal atomic forces.

The results presented above can be understood as follows: the increase in the Mn concentration breaks the infinite ferromagnetic cluster at its weakest links, giving rise to an increase of the "frustration" in magnetic interactions. Therefore,  $dT_c/dx < 0$ ,  $dT_c'/dx < 0$ ,  $d\chi(T_f)/dx < 0$ ,  $dT_f'/dx > 0$ ,

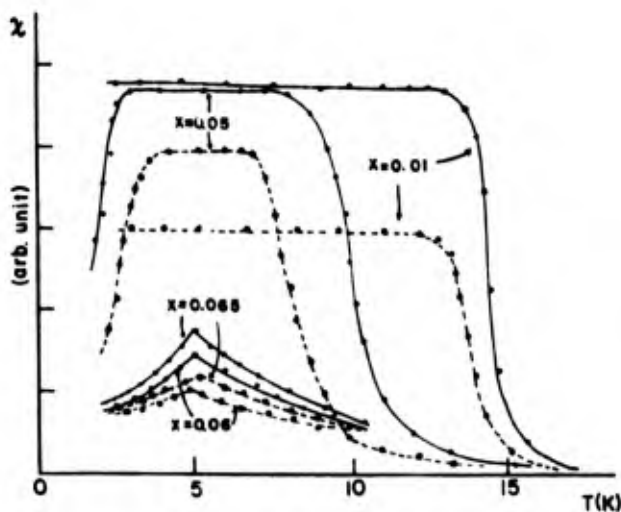


Figure 5. Temperature dependence of  $\chi$  of  $(\text{Pd}_{0.9965}\text{Fe}_{0.0035})_{1-x}\text{Mn}_x$ . The solid curves for samples at 1 bar and dashed curves are at 20 kbar (Ref. 55).

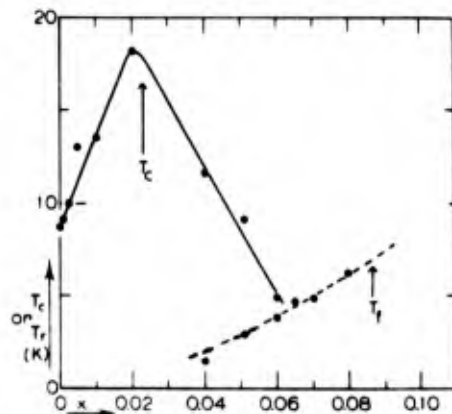


Figure 6. Collection of experimental data for the magnetic phase diagrams of  $(\text{Pd}_{0.9965}\text{Fe}_{0.0035})_{1-x}\text{Mn}_x$  (Ref. 54).

$dT_f/dx > 0$ . The application of high pressure in effect increases Mn - Mn short-range interactions. In consequence, one expects  $d\chi(T_f)/dP < 0$ ,  $dT_c/dP < 0$ ,  $dT_c'/dP < 0$ ,  $dT_f'/dP > 0$ , and  $dT_f/dP > 0$ . The pressure effect is small, as expected:  $dT_c/dP = -31 \pm 1 \text{ mK/kbar}$  for  $x = 0.01$  and  $dT_f/dP = +27 \pm 2 \text{ mK/kbar}$  for  $x = 0.065$ . Hardebusch et al. (56) have measured the dc magnetic susceptibility of a 3 at % AgMn spin glass under hydrostatic pressure up to 15 kbar. They have found  $dT_f/dP = +42 \pm 4 \text{ mK/kbar}$ , which is comparable with the values obtained in PdFeMn discussed above. Similar pressure effect in amorphous  $(\text{Fe}_{1-x}\text{Mn}_x)_{75}\text{P}_{16}\text{B}_6\text{Al}_3$  has been obtained by Chu et al. (57).

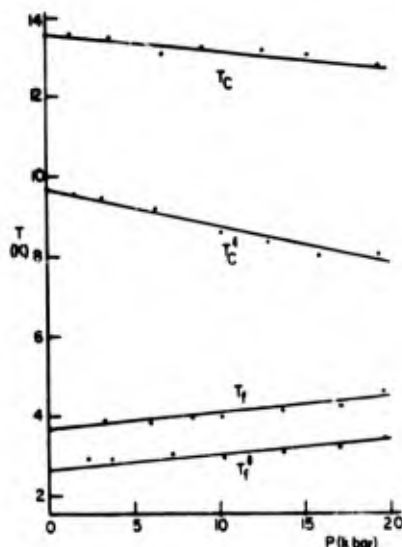


Figure 7. The pressure dependence of  $T_c$ ,  $T_c'$ ,  $T_f$ , and  $T_f'$  (Ref. 55).

## VI. PHONON-THERMAL CONDUCTIVITY

As pointed out in Secs. IV. 1 and 2, a linear temperature dependence of the magnetic heat capacity similar to the heat capacity in disordered solids has been found at low temperature. In analogy to the structural two-level systems (TLS) introduced by Anderson et al. (58) and Phillips (59) for understanding the properties of disordered, non-magnetic materials, a theory of magnetic two-level systems (MTLS) was proposed to describe the low temperature behavior of a spin glass. An MTLS is associated with a cluster of spins having two equilibrium positions, with the moments pointing parallel or antiparallel to an easy axis of magnetization. Free rotations of the clusters are blocked by anisotropy barriers, as shown in Fig. 8, and the dynamics of a spin glass is then expected to be dominated by thermal activation processes. A phenomenological description of the non-ergodic properties of a spin glass below  $T_f$  utilizing MTLS has been presented by Souletie and his co-workers (10,60).

In order to give direct evidence that the MTLS does exist, Wassermann and his collaborators (61,62) measured the phonon-thermal conductivity,  $\kappa(T)$ , of amorphous  $(\text{Pd}_{77.5-x}\text{Cu}_6\text{Si}_{16.5})\text{M}_x$  (with  $M = \text{Mn, Fe, and Co}$ ) down to  $\sim 0.3$  K at  $B = 0$  and 5 T. In an amorphous metal, the residual electrical resistance is very high, and hence, the electronic contribution to  $\kappa(T)$  is negligible. Consequently, the phonon thermal conduction  $\kappa^{\text{ph}}(T)$  arises from three scattering processes: (a) phonon-electron, (b) phonon-structural TLS, and (c) phonon-MTLS scatterings.  $\kappa^{\text{ph}}(T,B)$  is enhanced by  $\sim 8\%$  for the  $x = 10$  sample below 4 K and  $\sim 30\%$  for the  $x = 15$  sample at  $\sim 0.4$  K, when  $B$  increases from 0 to 5 T. For the Fe samples,  $\kappa^{\text{ph}}(T,B)$  at 1 K is enhanced by about 5% and about 10% for  $x = 10$  and 15, respectively. However, for the Mn samples, no enhancement has been observed. The orbital contribution to the magnetic moment is zero for Mn (S-State), and increases from Fe to Co. Hence, based on the increasing enhancement of  $\kappa^{\text{ph}}(T,B)$  from Mn to

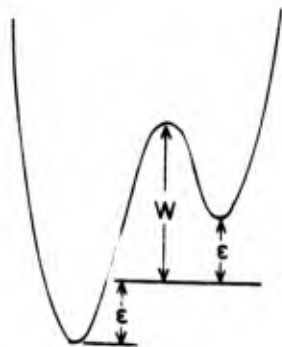


Figure 8. An asymmetrical double well potential.  $W$  is the height of the barrier and  $c$  represents the splitting (Ref. 60).

Fe and then to Co, it is concluded that the spin-orbit interaction is responsible for the coupling of the phonons to the MTLS. The enhancement of  $\kappa^{\text{ph}}$  in a high field is not limited only to these metallic amorphous spin glasses. A similar enhancement has been observed in insulating single crystalline  $\text{Eu}_x\text{Sr}_{1-x}\text{S}$  spin glasses (63).

## VII. FREQUENCY DEPENDENCE OF $\chi(\nu)$

### 1. Frequency Dependence of $T_f$

One of the first indications of the unusual properties of spin glasses was the unexpected observation of the frequency dependence of  $T_f$  (64-83,14,33,36) in almost all the spin glasses studied to date, including such diverse systems as  $\text{AgMn}$  (80),  $\text{Al}_2\text{Mn}_3\text{Si}_3\text{O}_{12}$  (83), small iron particles in an amorphous alumina matrix (82), granular Fe- $\text{Al}_2\text{O}_3$  films (77), and others. Figure 9 shows the temperature dependence of the real part of  $\chi$ ,  $\chi'$ , for  $\text{Eu}_{0.44}\text{Sr}_{0.56}\text{S}$  measured at 17, 198, and 2103 Hz (78). It is clear that  $T_f$  increases with increasing frequency  $\nu$ .  $T_f$  in these insulating spin glasses can be measured at microwave frequencies. In Fig. 10 data are shown for  $\text{Eu}_{0.43}\text{Sr}_{0.57}\text{S}$  taken at 840 MHz. The 9-GHz data (78) are displayed in Fig. 11. Because the Arrhenius law gives unphysical results, Tholence instead employed the empirical Vogel-Fulcher law (68):

$$\nu = \nu_0 \exp[-E_a/k_B(T_f - T_0)] \quad (7)$$

where  $\nu$  is the measured frequency. For  $\text{Eu}_x\text{Sr}_{1-x}\text{S}$ ,  $\nu_0$  is  $10^{13} \text{ s}^{-1}$ , and other parameters,  $T_0$ ,  $E_a$ , and  $T_f$ , are presented as a function of  $x$  in Fig. 12. Strickman and Wolfarth (84) proposed that  $T_0$  arises from inter-cluster coupling. In some cases,  $\nu$  can be extended up to  $\sim 10^{11} \text{ s}^{-1}$  using neutron scattering (85,86).  $\text{CuMn}$  is such an example. Figure 13 gives the frequency dependence (68) of  $T_f$  in  $\text{CuMn}$ . However, recent experiments

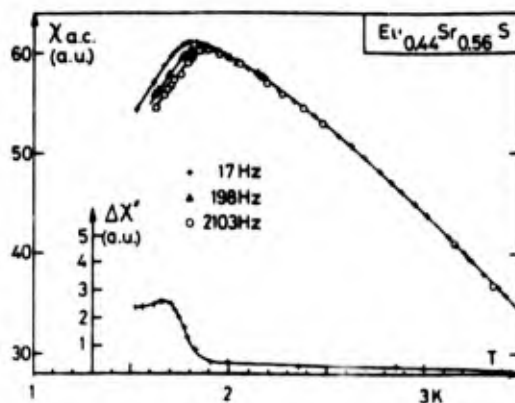


Figure 9. AC susceptibility of  $\text{Eu}_x\text{Sr}_{1-x}\text{S}$  for  $x = 0.44$  and  $\nu = 17, 198, 2103$  Hz. The thermal variation  $\Delta\chi''$  of the imaginary part is shown for  $\nu = 17$  Hz (Ref. 78).

on Au-B at % Fe (74) and on PrPo.85 (69) show that at very low frequency  $T_f$  reaches a minimum and becomes independent of  $\nu$ . This discrepancy is understandable because the free volume concept used in obtaining the Vogel-Fulcher law for an ordinary glass is not readily applicable to a spin glass and because the energy involved in a spin glass (i.e., the exchange energy) is of the order of  $k_B T$ , while that in an ordinary glass is much larger than  $k_B T$ .

In a recent paper, Singh et al. (36) reported their  $\chi'$  measurements of  $\text{Eu}_x\text{Sr}_{1-x}\text{S}$  spin glasses from 0.1 to 12 GHz. They found that  $T_f$ , the peak of  $\chi'(T)$ , increases with  $\nu$  up to 0.5 GHz but then decreases with increasing  $\nu$  for  $\nu > 0.5$  GHz. However, the maximum in  $\chi'(T)$  is observed only up to  $\sim 1$  GHz. Moreover, they observed a pronounced dip in the  $\chi'$  vs  $T$  curve instead of a maximum for their  $x = 0.43$  sample at  $\nu = 8.3$  and 12.2 GHz. They interpreted this anomalous frequency dependence in terms of the coexistence of both fast and slow spin relaxation times in the freezing processes associated with small-size ferromagnetic clusters and spin-glass type of order, respective-

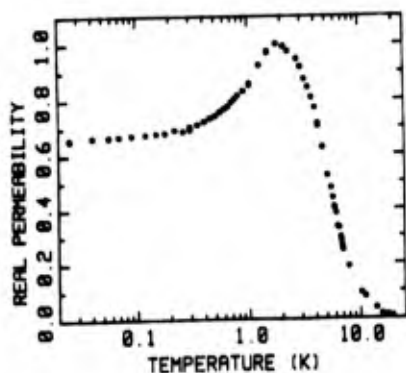


Figure 10. Normalized real part of permeability for  $\text{Eu}_{0.43}\text{Sr}_{0.57}\text{S}$  at 840 MHz as a function of temperature at  $B = 0$  G (Ref. 79).

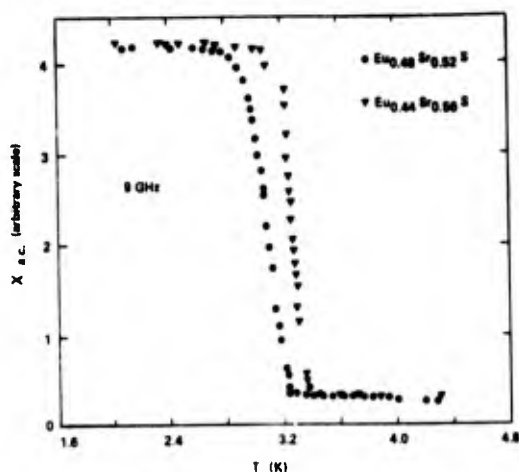


Figure 11. Thermal variation of the ac susceptibility of  $\text{Eu}_x\text{Sr}_{1-x}\text{S}$  for  $x = 0.44$  and  $0.48$ , measured at 9 GHz (Ref. 78).

ly. They concluded that, in order to understand the phenomenon of spin-glass freezing, one should also consider the change of size and relaxation time of ferromagnetically correlated regions with temperature.

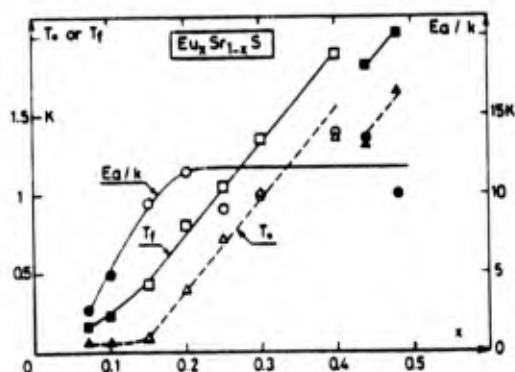


Figure 12.  $T_f(\nu = 10 \text{ Hz})$  and the parameters  $T_0$ ,  $E_a/k_B$  deduced from the fit of  $T_f(\nu)$ , by a Vogel-Fulcher law:  $\nu = \nu_0 \exp E_a/k_B(T_f - T_0)$  are shown (Ref. 78).

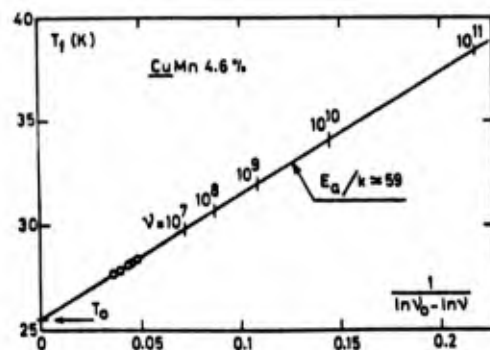


Figure 13. Plot of  $T_f$  vs  $1/(\ln \nu_0 - \ln \nu)$  for  $\text{Cu} - 4.6 \text{ at } \% \text{ Mn}$  with  $\nu_0 = 10^{13} \text{ s}^{-1}$  (Ref. 68).

## 2. Spectral Distribution of Relaxation Times

In order to explain his neutron scattering data, Murani (87) was the first to propose that there is a wide distribution of relaxation times,  $\tau$ . At high (room) temperature, for a very dilute alloy, the density of relaxation times,  $N(\tau)$ , is represented by a delta-function peak, whereas  $N(\tau)$  for a sample with a moderate concentration (a few %) of Mn atoms is broadened. With decreasing temperature, the spectrum evolves continuously towards longer relaxation times, and the peak in  $N(\tau)$  also moves towards longer times.

Recently, Wenger and his collaborators (14,81) measured both  $\chi'$  and  $\chi''$  in a number of spin glasses at various frequencies. According to Casimir and du Pré (88,89),

$$\chi' = \chi_S + (\chi_T - \chi_S)/(1 + \omega^2\tau^2) \quad (8a)$$

$$\chi'' = \omega\tau(\chi_T - \chi_S)/(1 + \omega^2\tau^2) \quad (8b)$$

where  $\chi_T$  is the isothermal susceptibility in

the limit  $\omega \rightarrow 0$  and  $\chi_C$  the adiabatic one in the limit  $\omega \rightarrow \infty$ . At  $\omega = 1/\tau$ ,  $\chi'$  will have an inflection point, whereas  $\chi''$  will show a maximum. This maximum thus provides a method for determining the average relaxation time constant  $\tau_{AV}$  for each temperature. According to Eq. (8),  $\chi''$  should follow a  $\text{sech}(2\ln\omega\tau)$  dependence for a single relaxation time and will be considerably broadened if a distribution of  $\tau$ ,  $g(\tau)$ , is present. Therefore  $\chi''$  could provide the dynamics of the spin freezing near  $T_f$  more than  $\chi'$ . Wenger also found the Argand diagrams,  $\chi''$  vs  $\chi'$ , for  $(\text{Ho}_2\text{O}_3)_{0.08}(\text{B}_2\text{O}_3)_{0.92}$  at several temperatures around  $T_f$ . The curves cannot be described as semicircles (indicative of a single relaxation time) but as arcs of semicircles. He followed the analysis of Cole's plots for the dielectric susceptibility, and found, for all temperatures,  $g(\tau) = (b/\sqrt{\pi})\exp(-(b\ln\tau/\tau_{AV})^2)$ , with  $b = 0.23$  and  $\tau_{AV} = 1.5 \times 10^{-8} \exp(4.4/T)$  s. It is essentially a single Gaussian distribution. As a result, the spin freezing in this Ho glass can be interpreted within the Néel picture of superparamagnetic relaxation (90). Furthermore, he pointed out that  $T_f$  in this spin glass follows an Arrhenius-like  $k_B T_f = -E/2\ln\pi\tau_0$ , with  $E/k_B = 6.6$  K and  $\tau_0 = 4.5 \times 10^{-9}$  s. Figure 14 exhibits (81) the absorption  $\chi''$  of a  $(\text{Eu}_0.2\text{Sr}_0.8\text{S})$  spin glass with  $T_f(10 \text{ Hz}) = 640$  mK. There is no clearly observable maximum in  $\chi''$  over the frequency range investigated, thus implying a broad distribution of relaxation times. The Argand diagram displayed in Fig. 15 supports this conclusion, because none of these three figures can be described as semicircles. From these curves, one can conclude that a broad distribution of  $\tau$  is present even for  $T > T_f$ .  $g(\tau)$  becomes even broader as  $T$  approaches  $T_f$  and it remains very broad for  $T < T_f$ . Wenger (14) found a distribution function for  $(\text{CoO})_{0.4}(\text{Al}_2\text{O}_3)_{0.1}(\text{SiO}_2)_{0.5}$ . As shown in Fig. 16, a dramatic increase of long relaxation times for  $T < 6$  K is visible.  $g(\tau, T)$  is essentially constant over  $2\ln\tau$  at  $T < 4.2$  K so that logarithmic time dependencies can

be expected for long-time relaxation measurements.

### 3. Fractional Exponential Relaxation Function

In a dielectric crystalline system, a relaxation species (an electric dipole) in contact with a heat bath relaxes exponentially as  $\phi(t) = \exp(-t/\tau_0)$  after a disturbance. In an ordinary glass or a polymer, the Hamiltonian of the system is very complex, leading to a distribution of energy level spacings, which is linear in energy from a zero energy difference up to an upper cut-off energy,  $\hbar\omega_c$ , followed by a plateau at intermediate energies but an exponential decrease at high energies. In Ngai's model(91), relaxation of a relaxation species to the heat bath is accomplished via the level spacing excitations. Thus, the relaxation function is modified (91):

$$\phi(t) = \exp(-t/\tau_D)^{1-n}, \quad (9)$$

$$\tau_D = (\omega_c^2 \tau_0)^{1/(1-n)}, (\omega_c t \gg 1), \quad (10)$$

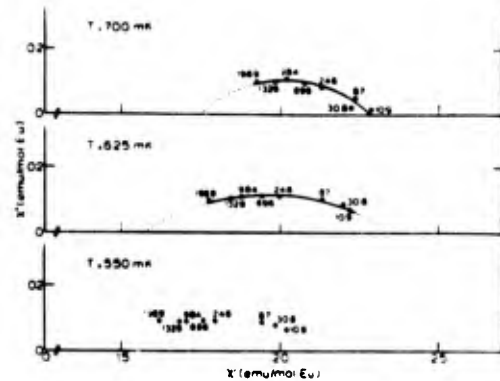


Figure 15. Argand diagram for  $\text{Eu}_0.2\text{Sr}_0.8\text{S}$  at three different temperatures. The lines are computer fit to the data points assuming a symmetric diagram (Ref. 81).

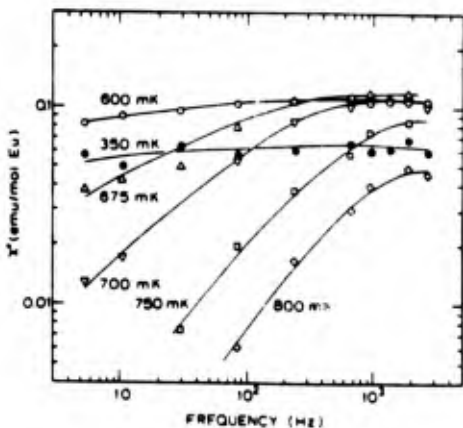


Figure 14.  $\chi''$  as a function of frequency for different temperatures. The solid lines are a visual guide (Ref. 81).

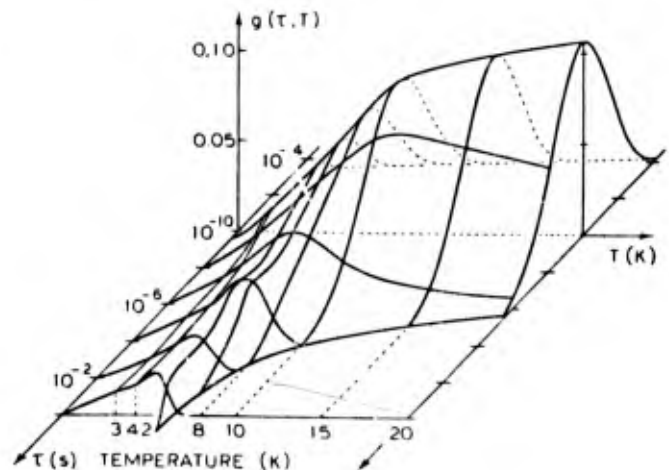


Figure 16.  $g(\tau, T)$  of a cobalt spin glass (Ref. 14).

where  $0 < n < 1$ , with  $n \equiv \underline{a}|V|^2$  in which  $V$  is the coupling between a relaxation species and the level spacing excitations, and  $\underline{a}$  is a constant. Equations (9) and (10) have been successfully applied to dielectric, optical, recombination, mechanical, volume, enthalpy, conductivity relaxation, and other measurements, independent of the relaxation species, such as an electron, ion, dipole, molecular moiety, polymer segment or polymer chain (92). In this case, the distribution function of relaxation times can be obtained through the identity  $\int g(\tau) \exp(-t/\tau) d\ln\tau = \exp(-t/\tau_p)^{1-n}$ . Accordingly, a larger  $n$  corresponds to a broader spectrum.

Very recently, Ngai et al. (93) applied Eqs. (9) and (10) to spin glasses. In this case, the level spacing excitations arise from the spin-glass Hamiltonian of the form  $H = -\sum_{ij} J_{ij} S_i S_j - \sum_i H S_i$ . The relaxation scheme is displayed in Fig. 17.  $n$  is a function of  $T$ ,  $H$ , thermal and magnetic history, etc. Far above  $T_f$ ,  $n$  is zero or nearly zero, and the effective relaxation time,  $\tau_p$ , shifts with  $T$  in an Arrhenius way:  $\tau_\infty \exp E_A/k_B T$ , where  $\tau_\infty$  and  $E_A$  are, respectively, the inverse of the attempt frequency and the activation energy. As  $T$  approaches  $T_f$ ,  $n$  increases,  $g(\tau)$  broadens, and  $\tau_p$ , as well as the mean relaxation time  $\langle \tau \rangle = \int \tau g(\tau) d\ln\tau = [\tau_p/(1-n)] \Gamma[1/(1-n)]$ , departs from the Arrhenius law. Here  $\Gamma(x)$  is the gamma function. For a crystalline magnet, Eq. (8) can be rewritten as

$$\chi^*(\omega, T) = \chi_S + (\chi_T - \chi_S) FT(d/dt) \exp(-t/\tau) \equiv \chi' - i\chi'' \quad (11)$$

where  $FT$  stands for Fourier transform. In analogy, Ngai et al. (93) used for spin glasses

$$\chi^*(\omega, T) = \chi_S + (\chi_T - \chi_S) \times FT [d/dt] \exp[-(t/\tau_p)^{1-n}] \quad (12)$$

Figure 18 shows the real and imaginary parts of Eq. (12) with  $n = 0.7$  for all  $T$ ,  $\tau_\infty = 10^{-10}$  s,

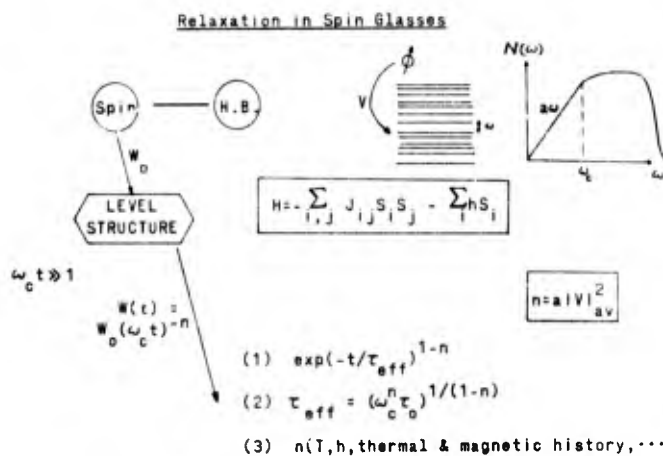


Figure 17. Relaxation in a spin glass (Ref. 93).

$\omega_c = 10^{10}$  rad/s,  $E_A/k_B = 2.1$  K. Here  $(\chi_T - \chi_S)$  is taken to be  $C/T$  and is the equilibrium Curie law of a paramagnet. These simulated results resemble those for  $(\text{Ho}_2\text{O}_3)_{0.08}(\text{B}_2\text{O}_3)_{0.92}$  measured by Wenger (14). In addition to the similarity of the shapes to the measured  $\chi'(T, \omega)$  and  $\chi''(T, \omega)$ , Eq. (12) also predicts correctly the relative sizes of  $\chi'$  and  $\chi''$ , the Arrhenius relation between  $T_f$  and  $\nu$ , and the sizable shift of the  $\chi''$  maximum to lower temperature than  $T_f(\nu)$  for each of the  $\nu$ 's considered. In analogy to its counterpart in ordinary glasses, this Ho glass is classified as a type B spin glass because  $n$  is independent of  $T$  and  $T_f$  varies with  $\nu$  according to the Arrhenius law.

In a type A glass,  $n$  varies with  $T$ . Figure 19 displays a typical variation of  $n$  with  $T$ .  $\chi'$  and  $\chi''$  have been acquired (93) with  $\omega_c = 10^{10}$  rad/s,  $\tau_\infty = 10^{-10}$  s,  $E_A = 2T_f$ , and  $T_f = 800$  mK at 16 kHz. The  $\chi'(T)/\chi''(T)$  ratio is smaller than that for the Ho glass, and the relation between  $T_f$  and  $\nu$  is not Arrhenius but resembles the Fulcher-Vogel behavior. These results are therefore applicable to  $\text{CuMn}$  and  $\text{Eu}_x\text{Sr}_{1-x}\text{S}$  spin glasses as discussed in Ref. 93. Because  $n$  depends on  $H$  and thermal history, Eq. (12) can explain the field dependence to be discussed in the next chapter. Furthermore, because  $n$  is much less temperature dependent at lower temperature, it is understandable that  $T_f$  does not obey the Fulcher-Vogel law but reaches a minimum at very low frequency (69,74). In consequence, Eq. (12) is capable of interpreting the frequency, field, and temperature dependencies of  $\chi'$  and  $\chi''$ .

## VIII. MAGNETIZATION

### 1. Remanance and Irreversibilities

In 1974, Tholence and Tournier (94) discussed the occurrence of a remanent magnetization and an irreversible susceptibility in a spin glass below  $T_f$ : They measured the

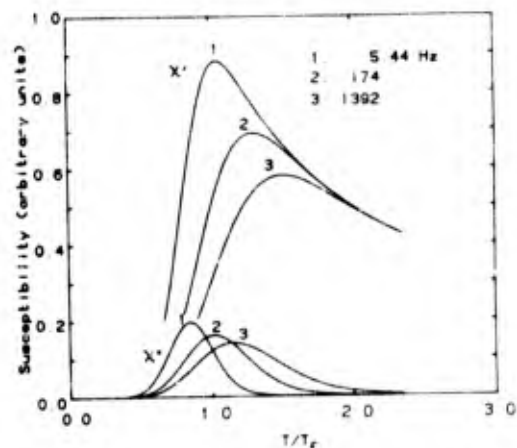


Figure 18.  $\chi'$  and  $\chi''$  obtained by calculation (see text for parameters) for the purpose of simulation of a type B spin glass (Ref. 93).

isothermal remanent magnetization (IRM) by cycling an external field  $0 \rightarrow H \rightarrow 0$ , and then measuring the magnetization. The thermoremanent magnetization (TRM) was also measured by cooling a spin glass from  $T > T_f$  to  $T < T_f$  in a field  $H$  followed by setting  $H = 0$ . These TRM and IRM have been interpreted in terms of the magnetic two-level systems (10,60). It is easy to see that these IRM and TRM are responsible for the presence of the displaced M-H hysteresis loop (4) below  $T_f$ .

Nagata et al. (95) have acquired the susceptibilities of two CuMn spin glasses deduced from the magnetization measured at a low static field. After cooling the samples in zero field (less than 0.05 G), cusp-like peaks were observed at  $T_f$ .

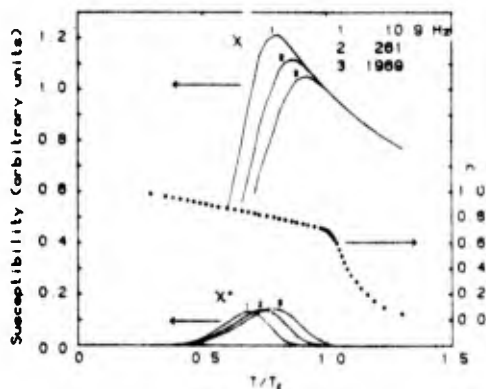


Figure 19.  $\chi'$  and  $\chi''$  obtained by calculation (see text for parameters) for the purpose of simulation of a type A spin glass (Ref. 93).

## 2. Time Dependence of TRM

Guy investigated the time dependence of TRM (96). He found that the magnetization changes with  $t$  according to

$$M(t) = M_0 - S \ln t \quad (13)$$

where  $S$  is a constant. He interpreted this time dependence in terms of Néel's superparamagnetic relaxation. However, Ferré et al. (97) found for other spin glasses that their data fit better with the power law,  $TRM(t) \propto t^{-n}$ , initially proposed by Binder (98), than Eq. (13). This slow response to a change in magnetic field is known as magnetic viscosity.

In place of the  $\ln t$  and power laws, one can use a fractional exponential relaxation function. In this case

$$TRM(t) = \sigma_{TRM}(T) = \sigma_0 \exp[-(t/\tau_D)^{1-n}] \quad (14)$$

Chamberlin et al. (99) very recently tried to fit the TRM data of their Ag-2.6 at % Mn + 0.46 at % Sb spin glass sample to Eq. (14). In order to improve the fitting accuracy, as shown in Fig. 20(a), they plotted  $\log[-d(\sigma_{TRM})/dt]$  vs  $\log(t)$  at  $T/T_f = 0.771, 0.856, 0.897,$  and

0.966. These authors obtained  $n = 0.694, 0.740, 0.766,$  and  $0.831$  for these four temperatures, respectively. To see the accuracy of the fitting, in Fig. 20(b) is plotted  $\log(\sigma_{TRM})$  against  $t^{1-n}$ . As demonstrated, the fractional exponential relaxation function can properly describe the time dependence of  $TRM(t)$ . The values of  $n$  and  $\sigma_0$  thus obtained are displayed against  $T/T_f$  in Fig. 21(a) and (b). The beautiful fit of the fractional exponential relaxation function to the data as presented in Fig. 20 calls for the need of more experiments near  $T_f$ , above and below, in order to acquire  $\tau_D$  and thus to understand the freezing process near  $T_f$ .

Chamberlin et al. (99) assumed that  $\tau_D$  can be written in terms of two temperature-independent parameters  $\underline{C}$  and  $\omega$  as  $\underline{C}\omega^{1-n} = (1-n)/\tau_D^{-n}$ . Based on their data, they found that  $\log(\underline{C}\omega^{1-n})$  is linear in  $(1-n)$  with  $\underline{C} = 0.59 \pm 0.05$  and  $\omega = (3 \pm 1) \times 10^{-6} \text{ s}^{-1}$ . This value of  $\underline{C}$  is close to  $e^{-\gamma}$  ( $\gamma =$  Euler's constant) based on the Ngai theory (91). However, Ngai and Rajagopal (100) pointed out that Chamberlin et al. in obtaining  $\underline{C}$  had made an additional assumption, namely,  $\omega_c \propto 1/\tau_0 \propto \omega$ , which is not compatible with the Ngai theory.

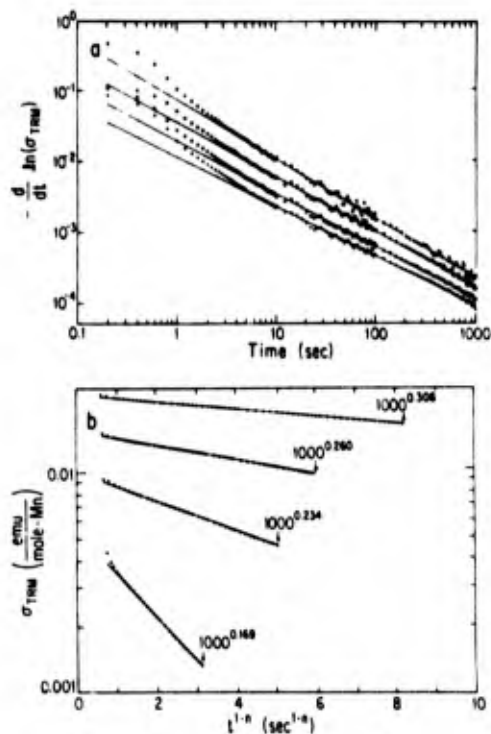


Figure 20. Determination of the time fractional exponent  $n$ . (a) Log-log plot of the derivative of the logarithm of  $\sigma_{TRM}$  as a function of time at four temperatures:  $T/T_f = 0.771, 0.856, 0.897,$  and  $0.966$ . The slopes greater than 5 seconds given  $n$ . (b) Semi-log plot of  $\sigma_{TRM}$  as a function of time raised to the  $(1-n)$  power. The solid lines are the best fits to Eq. (14) to the data (Ref. 99).

### 3. The de Almeida-Thouless (AT) Transition Line

In Sec. IV-3, the GT line obtained from the heat capacity data (21) was presented. In addition, many papers based on magnetic measurements have appeared (101-113). One of the characteristic magnetic properties of spin-glass systems is the magnetic viscosity. Because most of the experimental findings related to this viscosity have been reproduced by Monte Carlo calculations (114-116), Yeshurun et al. (102) have utilized this property for identification and characterization of the AT line. They investigated the time dependence of the magnetization in an amorphous  $(\text{Fe}_{0.64}\text{Mn}_{0.36})_{75}\text{P}_{16}\text{B}_6\text{Al}_3$  spin glass ( $T_f = 41$  K) at various values of  $H$ . From 1 minute to 12 minutes after a step increase of the field to some value  $H$ , their data can be fitted to an expression

$$M(t) = M_0 + S \ln t \quad (13)$$

The relaxation rate,  $S(H)$ , increases with  $H$ , peaks at  $H_m(T)$ , then decreases and vanishes at  $H_c(T)$ . As a fixed value of  $H$ ,  $S$  increases with  $T$ , peaks at  $T_m(H)$ , and then decreases and vanishes at  $T_c(H)$ . The magnitude of the peak of  $S$ ,  $S_m$ , increases and its temperature  $T_m$  decreases with increasing field. The lines described by  $T_m(H)$  and  $T_c(H)$  coincide with the  $H_m(T)$  and  $H_c(T)$  lines within experimental error. Figure 22 is the summary of their results. The dashed curve (p) is found via parabolic extrapolation to a zero value of  $S(H)$ .

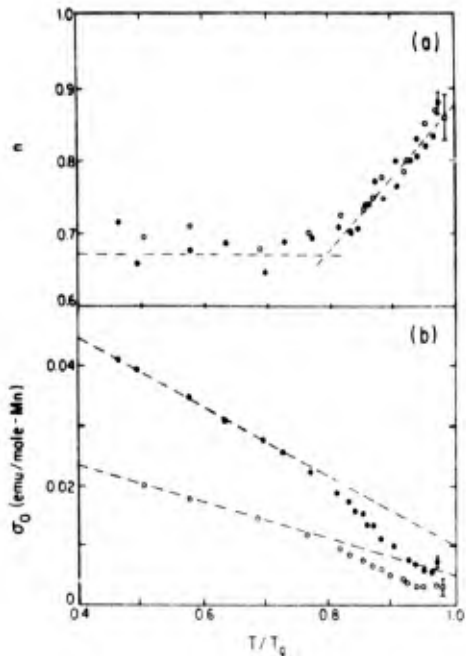


Figure 21. (a) The temperature dependence of  $n$ . The dashed lines are guides for the eye. (b) The temperature dependence of  $\sigma_0$  (Ref. 99).

Yeshurun et al. (102) found that the parabolic dependence of  $S$  on  $H$  fails at high fields above  $H = H_t$ , where  $S$  levels off and then decreases slowly to zero. This "tail" is then extrapolated to  $S = 0$  by fitting the high field data to a power law,  $S \propto (1 - H/H_c)^{\nu'}$ , where  $1 < \nu' < 1.5$ . The solid curve (t) in Fig. 22 describes the  $H$ - $T$  relation obtained by this vanishing of the tail ( $S = 0$ ). Thus, line (p) is the border line between two viscous regimes in the  $H$ - $T$  diagram, whereas line (t) separates viscous and nonviscous regimes. Because there are no theoretical reasons for a change in viscous characteristics between two viscous regimes, these authors identify line (t) as the AT line.

They also measured  $H_m$ , the field at which  $S$  is maximum at a given temperature. In terms of the freezing temperature  $T_g$ , they obtained that  $H_m$  varies as

$$H_m = 1360 (1 - T/T_g)^{1.5 \pm 0.1} \text{ Oe} \quad (15a)$$

for  $\text{CuMn}$ , and

$$H_m = 250 (1 - T/T_g)^{1.8 \pm 0.2} \text{ Oe} \quad (15b)$$

for  $\text{Fe}_{10}\text{Mn}_{170}\text{P}_{20}$ . The theoretical AT line<sup>46</sup> is given by

$$H_{AT}(T) = (2kT_g/\sqrt{5} \mu)(1 - T/T_g)^{3/2} \\ = (10120 \text{ Oe})(1 - T/T_g)^{3/2} \quad (15c)$$

where  $\mu = (2S)\mu_B = 5 \mu_B$  and  $T_g = 3.455$  K have been used for their  $\text{CuMn}$  sample. Aside from a factor of 7 in the prefactor, the experimental result for  $\text{CuMn}$ , Eq. (15a), agrees reasonably with the theoretical equation, Eq. (15c).

In addition to metallic spin glasses, insulating systems have also been investigated. Paulsen et al. (109) measured  $\chi'$  and  $\chi''$  of a spherical  $\text{Eu}_{0.4}\text{Sr}_{0.6}\text{S}$  sample from 7 to 5000 Hz with a SQUID magnetometer. The midpoint of the transition in  $\chi''$  is chosen as the definition for the AT transition because it closely corresponds to the peak of  $\chi'$  at  $T_f$  in the absence of an external field. The transition field at low temperature has been found to vary approximately as  $(1 - T/T_g^0)^\alpha$ , with  $\alpha \approx 3/2$ , where  $T_g^0$  is the zero-field transition temperature. This temperature dependence has the same form for  $\text{CuMn}$  given by Eq. (15a). Again the observed prefactor was 5-9 times smaller than the theoretical prediction given by Eq. (15c).

Nevertheless, very recently Wenger and Mydosh (111) pointed out that the GT line given by Eq. (6) and the AT line by Eq. (15c) can be obtained from the superparamagnetic model (117).

### IX. NEUTRON SCATTERING

Many review papers on the use of neutron scattering to study spin glasses have appeared (9,10,45,85-87,118-121). In this chapter, only some papers with salient features will be discussed.

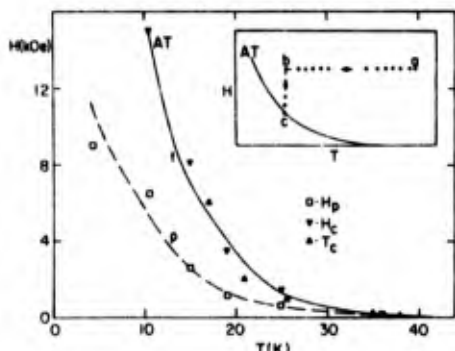


Figure 22. T-H phase diagram for  $(\text{Fe}_{0.64}\text{Mn}_{0.36})_{75}\text{P}_{16}\text{B}_6\text{Al}_3$ . Line (p) is the loci of  $S = 0$  found via parabolic extrapolation of  $S(H)$ . The solid line (t) is the AT line. Inset describes schematically a field-cooled process. At a point b, above the AT line, the field is turned off. A rapid relaxation to c is followed by a logarithmic decay in the spin-glass phase (Ref. 102).

### 1. Small Angle Neutron Scattering and Other Techniques

Murani and Heidemann (122) measured the elastic cross-sections of  $\text{Cu} - 8$  at % Mn at  $q = 0.17, 0.29$  and  $0.56 \text{ \AA}^{-1}$  at various values of the elastic energy resolution  $\Delta E$ . For a given  $q$ , the cross-section for  $\Delta E \sim 1.5 \text{ \mu eV}$  is nearly temperature independent at high temperatures but begins to increase markedly below about  $47 \pm 2 \text{ K}$ . For  $\Delta E \sim 25 \text{ \mu eV}$ , the marked increase of the cross-section begins at  $55 \pm 3 \text{ K}$ , and when  $\Delta E \sim 250 \text{ \mu eV}$ , this temperature increases to  $75 \pm 5 \text{ K}$ . Because the elastic scattering cross-section is proportional to the Edward-Anderson (EA) order parameter (122), the temperature around which the marked increase in the elastic scattering cross-sections occurs may be regarded as the freezing temperature corresponding to the time constant (i.e.,  $\Delta E$ ) of the measuring probe. Thus, the freezing temperature decreases with the decrease of  $\Delta E$  or the increase of the measurement time constant. Murani (123) also measured the spin-spin correlation function as a function of energy for  $q = 0.08 \text{ \AA}^{-1}$  at 300 K for several  $\text{CuMn}$  spin glasses. He showed that the Lorentzian spectral function fits well with the data for the 1.1 and 3.0 % samples, but it does not do as well at higher concentrations, in particular at the high-energy wings. He (87) interpreted this discrepancy in terms of a wide spectral distribution of relaxation times evolving continuously with decreasing temperature, devoid of any critical behavior, either speeding up or slowing down, at any finite temperature including  $T_f$ .

### 2. Neutron Spin Echo (NSE)

In addition to the ac susceptibility, which probes the  $10^{-5} - 10^2 \text{ s}$  time scale at zero wave number  $q = 0$ , neutron scattering is another

technique which can provide fully model-independent information, because neutrons probe directly the Fourier transform  $S(q, \omega)$  of the spin-spin correlation function  $\langle S(r, t) S(0, 0) \rangle$ . In particular, NSE spectroscopy allows one to observe directly the evolution of correlations in the time domain of  $10^{-12}$  to  $10^{-8} \text{ s}$  at wave number ranging from  $0.04$  to  $0.4 \text{ \AA}^{-1}$ , thus providing both the space (momentum) and time variations at the same time.

The neutron scattering cross-section is directly proportional to the spin-spin correlation function  $S(q, \omega)$ , where  $q$  and  $\omega$  are the neutron momentum change and energy change, respectively. In NSE,  $S(q, t)$  is directly measured, and it is related to  $S(q, \omega)$  by the cosine Fourier transform

$$S(q, t) = \int S(q, \omega) \cos \omega t \, d\omega. \quad (16)$$

It can be rewritten as

$$S(q, t) = S(q) s(q, t), \quad (17)$$

where  $S(q) = S(q, t=0)$  is the static correlation function or structure factor related to the short-range order (SRO), and  $s(q, t)$  contains the dynamic information, with  $s(q, t=0) = 1$ . The ac susceptibility is related to these quantities by

$$\chi(\nu) \propto \lim_{q \rightarrow 0} S(q) [1 - s(q, t)] / k_B T, \quad (18)$$

with  $t = 0.7/2\nu$ . Here  $[1 - s(q, t)]$  is the fraction of spins, which can respond to an external field within  $t$  and thus contributes to  $\chi$ . NSE is capable of measuring both  $S(q)$  and  $s(q, t)$  directly. Hence it allows the identification of both the static and dynamic contributions to  $\chi$ , if the  $q \rightarrow 0$  limit can be evaluated. In this section we present a summary of Mezei's NSE results (85,86).

For  $\text{CuMn}$ , the  $s(q, t)$  spectra are independent of  $q$  at small  $q$  ( $< 0.4 \text{ \AA}^{-1}$ ) and they show no singularity. In Fig. 23 are shown the results for  $\text{Cu} - 5$  at % Mn. The thick line represents the simple exponential decay,  $\exp - \gamma t$

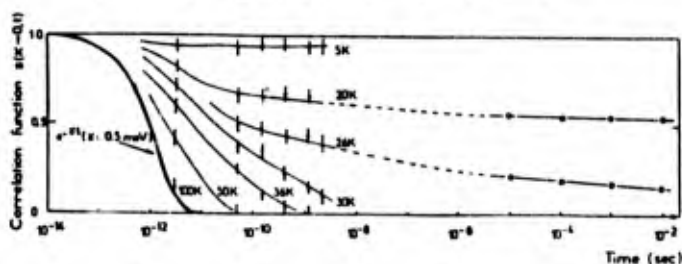


Figure 23. Spin relaxation,  $s(q, t)$ , in  $\text{Cu} - 5$  at % Mn at various temperatures. Data points for  $t < 10^{-8} \text{ s}$  were measured by NSE at  $q = 0.093 \text{ \AA}^{-1}$  [Ref. 124], those for  $t > 10^{-6} \text{ s}$  were calculated from ac susceptibility data [Ref. 68]. Except for the line for 100 K which is exponential, all other lines are just guides to the eye.



with  $\gamma = 0.5$  meV. Thus, all the  $s(q,t)$  curves demonstrate much slower decays than the exponential one, and they are compatible with the Monte Carlo result (114),  $s(q,t) \approx \text{const} - \ln t$ . These slow decays suggest that  $s(q,t)$  arises from a broad distribution of relaxation times. Similar results have been found for Cu - 1 and 10 at % Mn (125) and  $\text{La}_{0.7}\text{Er}_{0.3}\text{Al}_2$  (126).

Mezei et al. (126) have found that the spin relaxation time for  $T > T_f$  could be described by the Arrhenius relation,  $\tau = \tau_0 \exp E/k_B T$ , by assuming that the broad distribution of  $\tau$  results from a broad distribution of activation energies  $E$  via a relation (125)

$$s(q,t) = E_m \int_0^{E_m} \exp[-t/\tau_0 \exp(E/k_B T)] dE, \quad (19)$$

where a constant distribution of  $E$ 's in the interval  $(0, E_m)$  has been assumed. However, at  $T < T_f$  for CuMn and  $T < 10$  K for  $\text{La}_{0.7}\text{Er}_{0.3}\text{Al}_2$ , the data deviates severely from the Arrhenius relation, Eq. (19). Mezei, et al. (126) suggested that this failure of Eq. (19) to fit the data might be a consequence of the onset of the strong ferromagnetic short-range order,  $S(q)$ , at low temperature.

As pointed out previously,  $s(q,t)$  is independent of  $q$  below the moderate  $q$  value of about  $0.4 \text{ \AA}^{-1}$ , i.e., the spin relaxation does not exhibit a "kinematical slowing-down" (127). This is possible only when the relaxation is due to spin-nonconserving forces (usually spin-orbit or dipole interaction), and the spin dynamics in this range of  $q$  is not determined by the Heisenberg exchange interaction, which is a spin-conserving exchange interaction, as one would normally expect. Therefore, the relaxation process includes the Korringa relaxation mechanism (128) serving as an intermediate step in the  $q \rightarrow 0$  limit, followed by a spin non-conserving conduction electron-lattice relaxation.

The open circles illustrated in Fig. 23 were obtained from the ac susceptibility data (68) for Cu - 5 at % Mn by means of Eq. (18). These calculated points for  $t > 10^{-5}$  s join very nicely the NSE results obtained for  $t < 10^{-8}$  s. Conversely, ac susceptibilities can be calculated from Eq. (18) using the NSE results. Figure 24 shows the calculated susceptibilities at 0.1, 2.5 and 40 GHz (85,86), along with the measured 10 Hz ac susceptibility.  $T_f$  at 0.1 GHz is about 15% higher than that measured at 10 Hz, in agreement with the frequency dependence of the Fulcher-Vogel law (68). Based on the above discussion, it is clear that the appearance of the susceptibility cusp is a dynamic phenomenon resulting from the slowing-down of the spin relaxation with decreasing temperature. Above  $T_f$ , this slowing-down can be described as a thermally activated process following the Arrhenius law with a broad distribution of activation energies, without showing the singular character of critical fluctuations. The slowing-down continues through and below  $T_f$  with a faster-than-Arrhenius-type temperature

dependence.

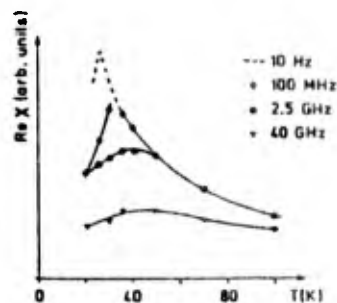


Figure 24. High frequency ac susceptibility of Cu - 5 at % Mn spin glass calculated from the NSE results in Fig. 23. The continuous lines are guides to eye, and the dashed line shows the directly measured 10 Hz ac susceptibility (Ref. 85, 86).

In view of the success of the application of the fractional exponential relaxation function in the susceptibility (Sec. VII-3) and TRM (Sec. VIII-2), one is tempted to fit  $s(q,t)$  to this function in order to obtain the temperature- and  $q$ -dependence of the fractional exponent,  $n(q,T)$ . However, the data, as presented in these figures, are not precise enough to make this fitting procedure meaningful.

## X. NUCLEAR MAGNETIC RESONANCE (NMR)

### 1. In an Applied Field

Host NMR in spin glasses has been investigated by several authors. The first of these investigations was by MacLaughlin and Allou (MA) (129) who studied  $^{63}\text{Cu}$  NMR in dilute CuMn (0.1 - 0.4 at %) alloys at temperatures near the freezing temperature  $T_g$ . They have shown that through  $T_g$  there are gradual decreases in the longitudinal and transverse NMR relaxation times,  $T_1$  and  $T_2$ , respectively, accompanied by a progressive diminution in the resonance intensity. They also found that the relaxation signal varies non-exponentially, but rather like  $\exp(-t/T_1)^{1/2}$ . Levitt and Walsted (LW) (130) measured the linewidth  $\Delta H$  for  $^{63}\text{Cu}$  in 0.96 at % Mn at 25.5 MHz. They found that  $\Delta H(T)$  follows the Brillouin function  $B_{5/2}(T)$ , for  $T \gg T_g$  (10 K), and falls below it at low temperature. They interpreted this decrease for  $T < T_g$  as arising from short-range order effects. Similar broadening of  $\Delta H$  below  $T_g$  has been observed by MA (131).

From spin-echo decays, LW acquired  $T_2$ . Their data showed that  $T_2$  decreases sharply just above  $T_g$  followed by a gradual increase as  $T$  is lowered from 4.2 to 1.6 K. For  $T > T_g$ ,  $T_2$  is believed to arise from the rapidly modulated hyperfine-field fluctuations, which contribute to the spin-echo decay rate,  $T_2 \approx \gamma^2 H_{hf} \tau_c$ , where  $\gamma$  is the gyromagnetic ratio,  $H_{hf}$  the hyperfine field, and  $\tau_c$  the Mn spin-correlation time.  $\tau_c$  becomes longer near  $T_g$ , resulting in shorter  $T_2$ . Both LW and MA

concluded that the lost intensity near  $T_g$  results from an experimental difficulty that the unobserved nuclei possess very short spin-echo decay times  $T_2$  so that the echo from those nuclei decays before the spectrometer has recovered from rf pulse overload.

$T_1$  can yield information on the transverse fluctuating fields experienced by the nuclear spins at the Larmor frequency  $\omega_n$ . Bloyet et al. (132) measured down to 2 mK the shape of the copper nuclear magnetization recovery  $M(t)$  on Cu - 12, 20 and 43 ppm with  $T_g = 29, 44, \text{ and } 87$  mK, respectively. They found that the magnetization recovery shape varies from an exponential decay for  $T \gg T_g$  to  $\exp [a - (a^2 + t/\tau_n)^{1/2}]$  for  $T < T_g$ .

## 2. In Zero Applied Field

For  $T \ll T_g$ , the spin system is "frozen", and the RKKY fields on a given shell of near-neighbor (nn) nuclei from a Mn impurity are well defined, although randomly distributed in direction. Accordingly, Alloul (133,134) was able to detect the spin echo signals of the first (A) and fourth (B) nn shells in zero applied field  $H_0$  on a Cu-1 at % Mn spin glass at  $T = 1.25$  K  $\ll T_g$  (10 K) after field-cooling the sample in a field  $H_{cool} = 10$  kG, which established the saturated remanent magnetization. Here, the local hyperfine fields (134) seen by the nuclei on the first and fourth shells are  $H_L = 50 \pm 5$  kG and  $10 \pm 0.2$  kG, respectively, based on the measurements in the paramagnetic regime of dilute CuMn. For a given resonance with an applied rf field  $H_1$ , the effective rf field  $H_1^{eff} = \eta \cdot H_1$  seen by the nuclei is enhanced in zero dc field. He found the enhancement factors to be  $\eta = 38 \pm 6$  and  $8 \pm 1$  for resonances A and B, respectively. His data exhibit that the enhancement of rf field and signal intensity depend strongly on the magnetic history of the sample; they increase with the remanent magnetization and vanishes if the sample is zero-field cooled.

This enhancement factor is believed to be related to the transverse electronic rf magnetization  $\sigma_t = \chi_t H_1$  induced by the rf field  $H_1$ , where  $\chi_t$  is the transverse susceptibility.  $\sigma_t$  in turn induces an rf local field  $H_1' = \eta_t H_1$  on the nuclei, and hence,  $\eta = |\eta_t \pm 1|$ . Alloul (133,134) assumed that, like a single domain ferro- or ferri-magnet, Mn spins are rigidly bound together and an applied magnetic field induces a collective rotation of the electronic magnetization, which is limited by the anisotropy field,  $H_A$ . Furthermore, Alloul and Hippert (135) interpreted the displaced M-H hysteresis loop (4) in terms of a mixture of the unidirectional and uniaxial anisotropies.

Alloul and his co-workers (136) also measured zero field transverse nuclear spin relaxation time,  $T_2$ , for near-neighbor  $^{63}\text{Cu}$  shells of Mn in  $\text{Cu}_{1-x}\text{Mn}$  alloys with  $x = 0.1, 0.2, 0.4, 1.35$  and  $4.7$  at % for  $T \ll T_g$  in a temperature range from 25 mK to 1.3 K. Even at high temperature, they observed that the decays

for a given sample were slightly nonexponential with a shape independent of nuclear site and temperature.

## XI. ELECTRON SPIN RESONANCE (ESR)

In order to explain the "spin glass transition," in analogy to the theory of superparamagnetic relaxation (137), Tholence and Tounier (94) proposed the superparamagnetic (SPM) model, in which a spin glass consists of an assembly of ferro- or antiferro-magnetic grains coupled by anisotropy forces arising from the dipolar and exchange interactions between spins. In this model, the "transition" is not a phase transition but rather a nonequilibrium freezing phenomenon in which the grains become blocked when their relaxation times are longer than the measurement time  $\tau_m$ , which is, like superparamagnetism, governed by the Arrhenius law (94):  $\tau_m = \tau_0 \exp E_A/k_B T$ , where  $\tau_0^{-1}$  is the attempt frequency, and  $E_A$  the activation energy. Here the freezing temperature  $T_f$  is frequency-dependent. On the contrary, in the phase transition picture of the EA model, the time correlation function  $q(t) = \langle S_a(t) \cdot S_a(0) \rangle$ , where  $\langle \dots \rangle$  denotes the thermal average and the bar signifies the average over the spins, behaves like (138,139)  $q(t) \sim \exp -a't$ , with  $a' \sim (T - T_f)$ , for  $T > T_f$ . In addition, Kinzel and Fischer (140), based on their calculations of the dynamical susceptibility, were the first to notice that a large number of different relaxation times results near  $T_f$ . They also obtained that long relaxation times become more important as  $T \rightarrow T_f$ , and  $q(t) \sim t^{-1/2}$ . Ma and Rudnick (141) employed the time-dependent Ginzburg-Landau model, instead of the replica method, to investigate the spin-glass phase. These authors found that  $q(t)$  has a  $t^{-1/2}$  long-time tail not only at  $T_f$  but also in the spin-glass phase, in agreement with the results obtained from Monte Carlo simulations by Binder and Stauffer (142). By means of Huber's result (143) that the correlation function can be expressed as  $q(t) = \langle S \cdot S \rangle \exp -Lt$ , with the Onsager kinetic coefficient

$$L = (1/NS^2) \int_0^\infty \langle \dot{S}_a(t) \cdot \dot{S}_a(0) \rangle dt,$$

when the decay rate of  $\langle \dot{S}(t) \cdot \dot{S}(0) \rangle$  is much faster than that of  $q(t)$ , Salamon and Herman (144) showed that the relaxation rate  $1/T_2 \propto L/T_x$  diverges as  $(T - T_f)^{-1}$  near  $T_f$ . Recently, in terms of the mean-field theory, Sompolinsky (145) assumed that the time-persistent spin-spin correlation function does not decay exponentially with a single relaxation time but rather with a distribution of many relaxation times, and pointed out that the order parameters are sums of a large number of contributions from a broad continuum of time scales ranging from the extreme static to the finite limits. Sompolinsky and Zippelius (146) concluded from their calculations that, approach-

ing  $T_f$  from above, spin fluctuations slow down with a relaxation time varying as  $(T - T_f)^{-1}$ , and that the time correlation function below  $T_f$  decays like  $t^{-\nu}$ , with  $\nu(T) = 1/2$  at  $T_f$  but decreasing with decreasing  $T$ .

Among many techniques, ESR has been utilized intensively to investigate the spin dynamics of spin glasses. The first ESR study was made by Owen et al. (147) on  $\text{CuMn}$  in 1957. Their work already comprised many indications of spin glass behavior, even though the broadening and the shift of the resonance line to lower fields along with hysteresis and field cooling effects below the "ordering" temperature were attributed to antiferromagnetism.

The first ESR experiment investigated from the view point of a spin glass was made by Salamon and Herman (144,148). They obtained the relaxation rate  $T_2^{-1}$  for a sphere of  $\text{Cu}_7\text{Mn}_{25}$  ( $T_f = 115$  K) by measuring the ESR spectra at 9.4 GHz. To analyze the data, they assumed the exchange-narrowing model that yields the Lorentzian lineshape. As shown in Fig. 25,  $T_2^{-1}$  increases drastically as  $T$  is lowered. They have shown that the Onsager kinetic coefficient  $L$  diverges as  $(T - T_f)^{-1}$  as  $T$  approaches  $T_f$  from above, as expected from the theory of Ma and Rudnick (141). The same temperature dependence has also been observed for some  $\text{AgMn}$  spin glasses by Dahlberg et al. (149). Very recently, Levy et al. (150) employed the Mori-Kawasaki formalism to calculate the linewidth from the Dzyaloshinsky-Moriya anisotropy interaction (151), and their results for the linewidth and the g-shift show the correct trend in comparison with the experimental curves for  $\Delta g = 2.6$  at % Mn. On the contrary, Jamet and Malozemoff (152) interpreted the g-shift and the broadening on their amorphous  $\text{GdAl}$  spin glasses in terms of the inhomogeneity arising either from a locally increased Gd concentration or from a configurational order. They attributed the drastic increase of the linewidth at low temperature to the partial blocking of the local field. Bhagat et al. (153), in place of the exchange-narrowing model, proposed an empirical formula for the linewidth.

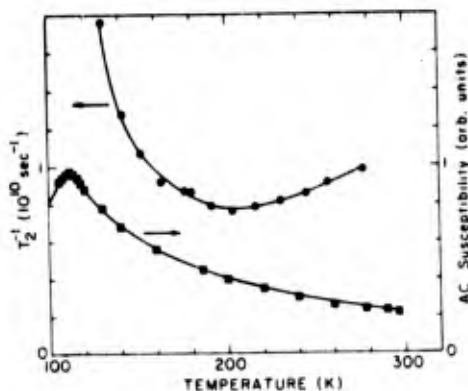


Figure 25. ESR relaxation rate  $T_2^{-1}$  and ac susceptibility of quenched  $\text{Cu}_7\text{Mn}_{25}$  (Ref. 144).

Usually, the exchange-narrowed Lorentzian lineshape develops into a Gaussian one when the spin fluctuations slow down. Several authors (154-158) have noted that the lineshape is strongly distorted even well above  $T_f$  and it is neither Lorentzian nor Gaussian, although many workers have fitted their observed resonant line to the Lorentzian lineshape in order to extract the linewidth  $\Delta H$  and g-shift  $\Delta g$ .

When the applied field is weak compared with the local field, or equivalently when  $\Delta H$  is comparable with the resonant field, the Zeeman energy can no longer be used as the unperturbed energy and the perturbation method conventionally employed in analyzing ESR data is no longer appropriate. This problem was investigated by Kubo and Toyabe (159) using a stochastic model for the local field. Hou and his coworkers (155-157) were the first to use the Kubo-Toyabe results to account for their distorted spectra. These authors (159) made use of the Gaussian-Markoffian model in which the correlation function of the internal fields,  $H_i(t = x, y, z)$ , takes the form  $\langle H_i(t)H_i(0) \rangle = (\Delta/\gamma)^2 \exp(-t/\tau)$ , where  $\Delta/\gamma$  is the width of the Gaussian distribution whose mean is zero,  $\gamma$  the gyromagnetic ratio, and  $\tau$  the correlation time. (This exponential time dependence may not be applicable to spin glasses, because the decay either follows a power law (160) or a fractional exponential function as discussed in Sec. VII-3 and  $\tau$  is broadly distributed.)

Following the method of Hayano et al. (161), Hou et al. (156,157) made use of the strong collision model in which the system evolves in time in a random but static field, jumping after a mean time  $\tau$  in a configuration into a new one, and calculated the resonance shape function in terms of the resonant field  $H_0$ ,  $\Delta$ , and  $\tau$ . Note that the width and the position of this new resonance function are in agreement with those obtained in the extreme narrowing limit when  $\Delta_1 \ll 1$ , a condition violated near  $T_f$ .

In an ordinary magnetic resonance experiment, the rf field is linearly polarized - i.e., it can be decomposed into both positively and negatively circularly polarized waves, thus giving rise to both resonance and antiresonance. When the resonant field and linewidth are comparable, both the resonance and antiresonance spectra contribute to the lineshape. For this purpose, Sugawara et al. (162) used the sum of the Bloch equations with the positive and the negative frequency contributions. However, this method is not correct near the slowing-down region, because the Bloch equations are correct only for the exchange-narrowed region.

Very recently, Hou et al. (155-157) made their ESR measurements on amorphous metallic ribbon samples of  $\text{Fe}_x\text{Ni}_{80-x}\text{P}_{20}$  ( $x = 8, 10$ , and 16) at 1.1 and 9.3 GHz. In order to minimize the skin effect giving rise to the mixing of the real part of the magnetic susceptibility,  $\chi'(\omega)$ , into the absorption spectrum, they thinned their samples down to  $\sim 10$   $\mu\text{m}$ , which is

about one skin depth. Owing to broad linewidths and distorted lineshapes, Hou et al. (155-157) measured the absorption spectra directly, in order to avoid spurious peaks originating from the usual derivative method with low frequency field modulation (157). Figures 26(a) and (b) illustrate the ESR absorption spectra for Fe<sub>8</sub>Ni<sub>72</sub>P<sub>20</sub> at 9.3 GHz and 1.1 GHz plotted against the internal frequency  $\omega_{in} = \gamma H_{in}$ , where  $H_{in}$  is the internal field, which is the external field minus the demagnetization field. As displayed, as temperature is lowered, the exchange-narrowed line at  $T = 2T_f$  broadens, shifts to the lower field, becomes asymmetric, and develops an absorption below  $T_f$  even at zero field. Thus, it is incorrect to take the field at which the maximum of an absorption spectrum takes place as the resonant field. In particular, at 1.1 GHz, as demonstrated in Fig. 26(b), the lineshape distorts progressively as  $T$  is lowered, and the linewidth becomes greater than the resonance field. It is clear that the negative frequency contribution is substantial. If one takes the derivative of the 1.1 GHz absorption data at  $T = 0.44 T_f$  with respect to the field, one could obtain a shape which looks like a distorted absorption lineshape normally expected in the derivative method. Hence the "resonant" field and linewidth thus acquired would be erroneous. This fact points to the need of measuring the ESR absorption directly, instead of the derivative method conventionally employed, in particular when the line is broad and distorted.

By fitting the absorption spectra to the Kubo-Toyabe theory, Hou et al. (156,157) acquired the relaxation rate  $\nu = 1/\tau$  and the rms amplitude of the random local fields  $\Delta$ . As shown by the straight lines in Fig. 27, for  $T > 1.15T_f$  the relaxation rates for both  $x = 8$  and 10 can be expressed by  $\nu = b(T - T_f)$  with  $b = 9.1 \times 10^9 \text{ s}^{-1}\text{K}^{-1}$  at 9.3 GHz. Similarly, at 1.1 GHz,  $b = 2.95 \times 10^{10} \text{ s}^{-1}\text{K}^{-1}$ . However, it is interesting to note that the relaxation rate does not diverge as  $T \rightarrow T_f$ , contradicting the theoretical predictions discussed above. Instead, for  $T < 1.15 T_f$ , the variation of  $\nu$  vs temperature is very moderate.

In the spin-glass regime, the resonant field is shifted from  $\omega/\gamma$ , and the new resonant frequency is given by (163)

$$\omega = [\omega_r + (\omega_r^2 + 4\omega_f^2)^{1/2}]/2,$$

where  $\omega_r/\gamma$  is the resonant field in the absence of the anisotropy,  $\omega_f/\gamma = \sqrt{K/x}$  is the anisotropy field. Hou et al. (156) analyzed their data and obtained the temperature dependence of the anisotropy energy,  $K(T) = K(0)(1 - T/T_f)$  with  $K(0) = 8.8 \times 10^3$  and  $9.5 \times 10^3 \text{ erg/cm}^3$  at 9.3 GHz for  $x = 8$  and 10, respectively, and  $K(0) = 3.9 \times 10^3$  and  $4.0 \times 10^3 \text{ erg/cm}^3$  at 1.1 GHz for these two samples.

Monod and Berthier (164) measured the ESR signals in the derivative mode on Cu - 1.35 and 4.7 % Mn samples at low and zero field in the frequency range from  $\sim 1$  GHz to  $\sim 2$  GHz after the samples were field-cooled down to 1.25 K at

$H_{cool} = 13 \text{ kG}$ . They found that the resonance frequency is linear in the applied field,  $H_0$ , i.e.,  $\omega = \gamma H_0 + \omega_a$ , where  $\omega_a$  is 1250 MHz (or equivalently 445 G) for the 1.35 % sample and is 1440 MHz (515 G) for the 4.7 % sample.  $\omega_a$  was attributed to the macroscopic anisotropy field.

Schultz et al. (165), on the other hand, investigated ESR on Cu - 10 at % Mn cooled to 1.8 K in the absence of an applied field ( $H_{cool} = 0$ ). In the field range from  $H_0 = 300$  to 800 G, they also found that the resonance frequency from 8.8 to 9.6 GHz is linear in  $H_0$ , but the slope,  $d\omega/dH_0$ , is only a half of that observed by Monod and Berthier (164) discussed above. Schultz et al. (165) further considered a simple hydrodynamic free energy including uniaxial anisotropy  $-K(\hat{N} \cdot \hat{n})^2/2$ , where  $\hat{N}$  and  $\hat{n}$  are, respectively, the directions of the cooling field  $H_{cool}$  and the remanent magnetization,  $M_r$ . This free energy takes the

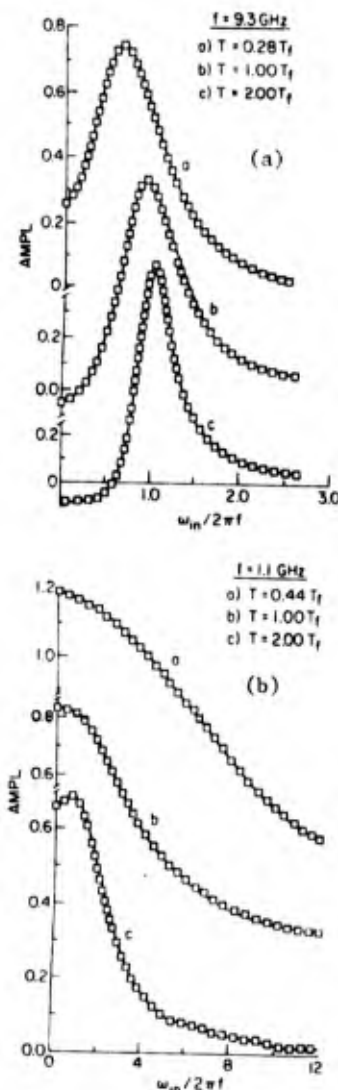


Figure 26. (a) Absorption spectra for Fe<sub>8</sub>Ni<sub>72</sub>P<sub>20</sub> at 9.3 GHz and (b) at 1.1 GHz plotted against the internal frequency  $\omega_{in} = \gamma H_{in}$  (Ref. 156.)

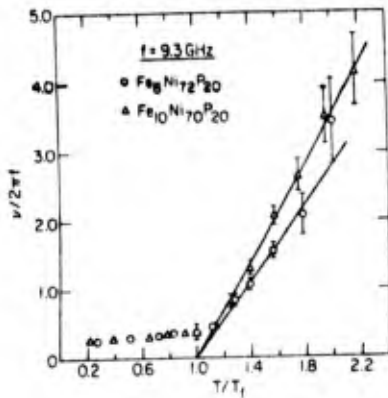


Figure 27. Relaxation rates  $\nu$  at 9.3 GHz for  $\text{Fe}_8\text{Ni}_{12}\text{P}_{20}$  ( $T_f = 18$  K) and  $\text{Fe}_{10}\text{Ni}_{10}\text{P}_{20}$  ( $T_f = 23$  K) vs  $T$  (Ref. 156).

following simple form:

$$F = (\hat{M} - M_r \hat{n})^2 / (2x_\perp) + (x_\parallel^{-1} - x_\perp^{-1}) \cdot (\hat{M} \cdot \hat{n} - M_r) / 2 - K (\hat{M} \cdot \hat{n}) / 2 - \hat{M} \cdot \hat{H} \quad (20)$$

By linearizing the equations of motion, this vector model yields the following two resonant frequencies  $\omega^\pm$ :

$$\omega^\pm / \gamma = \pm \left[ (1 + \xi) H / 2 - M_r / (2x_\perp) \right] + \left\{ \left[ (1 - \xi) H / 2 + M_r / (2x_\perp) \right]^2 + K / x_\perp \right\}^{1/2} \quad (21)$$

where  $\xi \equiv | -x_\parallel / x_\perp |$ . Figure 28(a) illustrates the ESR derivative signals observed by Schultz et al. (165) on a  $\text{Cu} - 8$  at % Mn, 0.3 at % Ni sample at 9.37 GHz at 20 K when they increased (solid curve) and decreased (dashed) the external field. The structure at  $\sim 3.3$  kG is due to the DPPH markers. By lowering the temperature to 1.4 K, they observed the ESR signal at 9.126 GHz as shown in Fig. 28(b), thus identifying the new  $\omega^-$  mode. According to their model, this second resonance mode is present when the anisotropy frequency  $\gamma \sqrt{K(T)} / x$  exceeds the spectrometer frequency. For the  $\omega^+$  mode, Eq. (21) can be solved for  $K$ . They obtained  $K(T) = K(0)(1 - \beta T / T_g')$ , where  $\beta = 0.67 \pm 0.07$ ,  $T_g'$  is the temperature at which the peak of the magnetization measured at  $\sim 3$  kG takes place, and  $K(0) = \tilde{a} C_{\text{Mn}}^2 + b_1 C_{\text{Mn}} C_1$ , in which  $C_{\text{Mn}}$  and  $C_1$  are concentrations of Mn and another impurities, respectively,  $\tilde{a} = 115 \pm 5$  and  $b_1 = 3050 \pm 300$  for nickel. However, these authors were not able to explain the angular dependence of their new  $\omega^-$  resonance spectrum. Later, the phenomenological vector model of Schultz et al. (165) was placed on more solid theoretical foundations by Henley et al. (163) and Saslow (166) making use of the triad model of Halperin and Saslow (167). In this model, the anisotropy energy is determined by the orientation of a spin triad relative to a reference triad, and the macroscopic internal degrees of freedom associated with the anisotropy are assumed to be represented by an orthonormal triad

instead of a unit vector. In addition to  $\text{CuMn}$ , ESR measurements on  $\text{AgMn}$  spin glasses have been made by Machado da Silva et al. (168). They have analyzed their results following the method used by Schultz et al. (165), and have obtained  $K(T)/K(0) = 1 - \beta T / T_g$ , with  $\beta = 0.78 \pm 0.08$ .

Hoekstra et al. (158) also made the ESR measurements employing the derivative method at 1 and 3 GHz for  $\text{Cu} - 2$  and 5 at % Mn samples. They were not able to observe any signal for the zero field-cooled samples. They pointed out that the absence of Ni in their samples is not crucial, and that a fixed field and variable frequency experiment is more appropriate to search for the  $\omega^-$  mode than the conventional operation in which the spectrometer frequency is kept fixed with a varying external field. Very recently, Hoekstra et al. (169) observed the ESR derivative signals on  $\text{CuMn}$  with Mn concentrations at 2, 3.5 and 5 at % at 1.1, 3.4, 4.0 and 9.5 GHz. They found that the anisotropy constants  $K$  obtained from ESR results when the applied field is parallel to the cooling field are in agreement with those determined by the transverse susceptibility and the torque measurements, but the  $K$  values determined from the remanence reversal of dc magnetization are smaller by a factor of  $\sim 2$ . They interpreted this discrepancy in terms of the breakdown of the rigid-body spin rotations assumed by many authors. Furthermore, they have not been able to observe the  $\omega^-$  mode even though their spectrometers were sensitive enough to observe it.

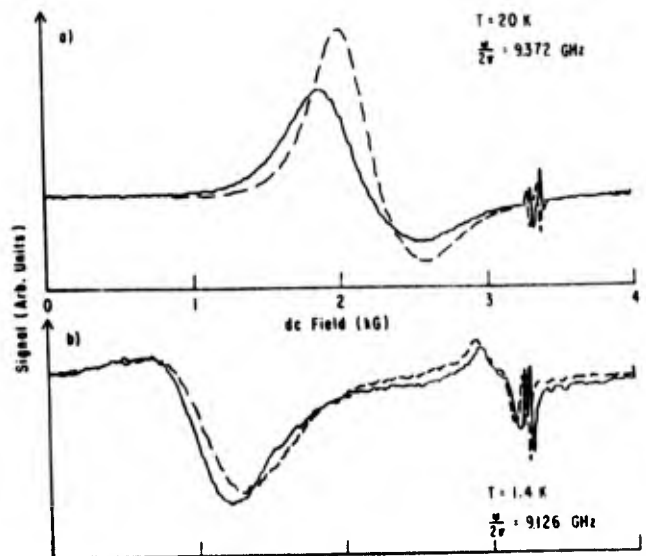


Figure 28. Traces of the ESR derivative signals vs the dc field for  $\text{Cu} - 8$  at % Mn and 0.3 at % Ni. The solid curves are for increasing field, and the dashed curves for subsequent decreasing. The structures at 3.3 kG is due to the DPPH markers. (a) The usual  $\omega^+$  mode is observed at  $T = 20$  K. (b) The new  $\omega^-$  mode is observed at 1.4 K (Ref. 165).

## XII. MUON SPIN ROTATION AND RELAXATION ( $\mu$ SR)

Several meson factories, such as TRIUMF (Vancouver), SIN (Zurich), CERN (Geneva), and LAMPF (Los Alamos), produce high intensity polarized positive muon beams. A positive muon has a mass of about 200 times that of an electron. When it is stopped in an interstitial site in a solid, its spin ( $1/2$ ) precesses within its lifetime ( $2.2 \mu\text{s}$ ) about the resultant of the external field and internal fields. When the external field is perpendicular to the beam direction, and hence, the spin direction, one can observe a coherence precession of muon spins. In the presence of random local fields, the depolarization of the muon polarization takes place, resulting in a damped precession. This method is analogous to conventional magnetic resonance. The depolarization rate is related to  $1/T_2$  in magnetic resonance, giving rise to a width,  $\underline{W} = (\gamma_\mu T_2)^{-1}$ , where  $\gamma_\mu$  is the muon gyromagnetic ratio,  $2\pi \times 1.35 \times 10^4$  s/G. This method was first applied to CuMn and AuFe spin glasses by Fiory and his coworkers (170). The Larmor precession frequency of the  $\mu^+$  spin owing to the external transverse field is disturbed by the direct magnetic dipolar fields from the magnetic impurities as well as the contact field from conduction electrons polarized by the RKKY interactions by means of the s-d exchange interaction  $J_{sd}$ . However, the dipolar field is stronger than the RKKY field by a factor of  $2E_F/J_{sd}$ , which is about 10 for CuMn (170). In Fig. 29,  $\mu^+$  depolarization width  $\underline{W}$  for Cu - 0.7 at % Mn is shown as a function of temperature for various values of the transverse applied magnetic field. Note the abrupt rise in  $\underline{W}$  near  $T_g$  determined from the low field susceptibility. For conventional magnetic resonance, any inhomogeneity in fields causes a broadening in the resonance linewidth, and hence the abrupt increase of  $\underline{W}$  in  $\mu$ SR near  $T_g$  was explained in terms of the freezing of Mn moments in random directions (170).

Positive muons are produced nearly 100% polarized, and hence an experiment can be carried out even in the absence of any external magnetic field. This property is important because an external field disturbs a spin glass. For this reason, a zero-field  $\mu$ SR technique should be appropriate for the study of the spin dynamics in a spin glass. Those readers interested in the details of this technique are referred to the original papers on this subject (161,171-173). This technique is capable of measuring the spin correlation time in a range from  $\sim 10^{-11}$  to  $\sim 10^{-5}$  s, in contrast to the ranges from  $\sim 10^{-13}$  to  $\sim 10^{-10}$  s for neutron scattering,  $\sim 10^{-10}$  to  $\sim 10^{-8}$  s for the Mössbauer effect, and  $\sim 10^{-5}$  to  $\sim 10^2$  s for the ac susceptibility measurement. This time range is essential in studying the critical slowing-down in a spin glass near  $T_g$ .

The first application of this new zero-field  $\mu$ SR technique to spin glasses was the measurements of the correlation times in AuFe and CuMn spin glasses (171). In these experi-

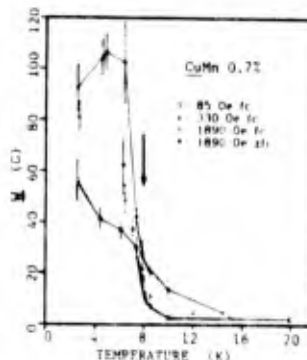


Figure 29.  $\mu^+$  depolarization rate, expressed as a linewidth, plotted against temperature for Cu - 0.7 at % Mn for several values of applied transverse magnetic fields. The arrow indicates the position of  $T_f$  (Ref. 170).

ments the muon spin relaxation functions were measured as a function of temperature. Figure 30 illustrates the time dependence of the muon spin relaxation functions,  $G_z(t)$ , for Au - 1 at % Fe at various temperatures above and below the freezing temperature ( $T_g = 9.1$  K). Owing to the absence of an external field, the Kubo-Toyabe theory (159) described in Chap. XI was employed. In a dilute alloy, magnetic impurities are randomly distributed. As a result, the random fields acting on  $\mu^+$  were assumed to be distributed according to the Lorentzian distribution previously obtained by Walstedt and Walker (174). The solid lines in Fig. 30 represent the fits of this model relaxation function to the data. This fitting procedure yields the correlation time  $\tau$  of Fe (or Mn) in AuFe (or CuMn). The results are plotted in Fig. 31; clearly  $\tau$  exhibits an abrupt variation around the freezing temperature  $T_g$ , increasing from  $\sim 10^{-10}$  s at  $1.2T_g$  to  $\sim 10^{-6}$  s at  $0.8T_g$ . As shown by the dashed curve, the data near  $T_g$  do not agree with the theoretical prediction,  $\tau = T/(T - T_g)$ , discussed in the last chapter. However, they fit well with the temperature dependence,  $\tau = [T/(T - T_g)]^2$ , as illustrated by the solid curve. A similar temperature dependency has also been observed for AgMn (175). In addition to these crystalline alloys, recently an amorphous metallic spin glass Pd<sub>75</sub>Fe<sub>5</sub>Si<sub>20</sub> has been studied (176). Interestingly, the correlation time above  $T_g = 15.5 \pm 0.3$  K, follows the same temperature dependence as that for CuMn:  $\tau = 1.8 \times 10^{-10} \times [T/(T - T_g)]^2$  s. To date, there is no theory to account for this unusual temperature dependence. The data for AuFe and CuMn can alternatively be fitted to the following Arrhenius form:

$$\tau = \tau_0 \exp(E_a/k_B T), \quad (22)$$

with  $E_a = 20k_B T_g$  and  $\tau_0 \sim 10^{-15}$  s. In addition, this Arrhenius law can also reasonably describe the temperature-data for  $\tau$  of insulating (CoO)<sub>40</sub>(Al<sub>2</sub>O<sub>3</sub>)<sub>10</sub>(SiO<sub>2</sub>)<sub>50</sub> (177). This ambiguity in the temperature dependence points to the need

of higher quality data in order to have any meaningful comparison with theory.

Below  $T_g$ , Uemura (173) followed the EA model and introduced an order parameter  $Q$  in the following way including both static and dynamic local fields:

$$\langle S(t)S(0) \rangle / \langle S(0)^2 \rangle = Q + (1 - Q) \exp(-t/\tau) \quad (23)$$

This is certainly a better approximation than the one using only a single exponential function.

In regard to the successful application of the fractional exponential relaxation function to account for the frequency dependence of  $\chi(T)$  described in Sec. VII-3 and the time dependence of TRM demonstrated in Sec. VIII-2, the zero-field  $\mu$ SR relaxation function,  $G_z(t)$ , has been calculated (178) employing the Kubo-Toyabe theory with the correlation function varying with time as  $\exp-(t/\tau)^{1-\alpha(T)}$ . In terms of the random local field width  $\Delta$ ,  $G_z(t)$  can be expressed as the form of the Fourier transform as follows:

$$G_z(t) = FT f(s), \quad (24)$$

where

$$f(s) = \sum_{l=0}^{\infty} [(-1)^l / s] (1/l!) (\underline{v}/s)^{l(1-\alpha)}$$

$$\times \left\{ \Gamma[1 + l(1-\alpha)]/3 + (2/3) \sum_{m=0}^{\infty} [(-1)^m / 2^m m!] \right.$$

$$\times (\Delta/s)^{2m} \Gamma[2m + l(1-\alpha)]$$

$$\left. \times [1 - (\Delta/s)^2 (1 - l + l\alpha + 2m)(2 + l - 2\alpha + 2m)] \right\}, \quad (25)$$

where  $\underline{v}(=1/\tau)$  is the relaxation rate. The fitting of the data to this form is currently in progress.

In conclusion,  $\mu$ SR, like NMR and ESR, is model-dependent. Furthermore, it is well known that the electronic properties near the site of the muon stopped inside the sample are greatly disturbed, accompanied by a lattice distortion around the site. In addition, it has been shown that (179)  $\mu^+$  in Cu is not at rest but hops around below  $\sim 7$  K. This hopping makes any  $\mu$ SR data analysis impossible, because the analysis normally assumes that  $\mu^+$  is at rest at a site within its lifetime. It is likely that  $\mu^+$  hops in Ag and Au as well. This suggests that amorphous systems are more suitable for the study of the spin dynamics in spin glasses. Notwithstanding, in order to have any meaningful comparison of  $\mu$ SR data with any model, it is essential to accumulate data of high quality as well as high statistics.

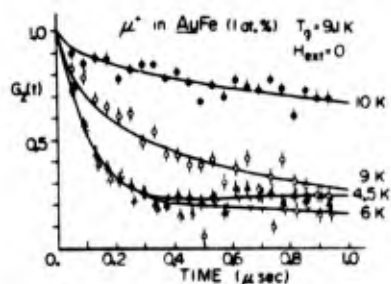


Figure 30. Zero-field muon spin relaxation functions  $G_z(t)$  for Au - 1 at % Fe. Solid curves are the theoretical curves (Ref. 171).

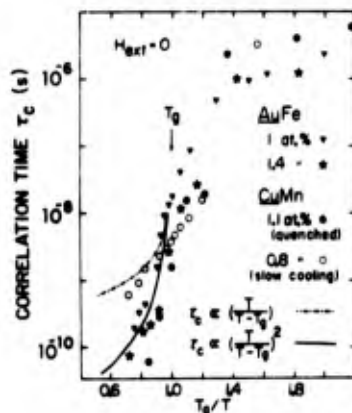


Figure 31. Correlation times  $\tau_c$  for AuFe, AgMn, and CuMn spin glasses (Ref. 171).

### XIII. CONCLUSIONS

In this paper, we have presented some experimental results for and some against the existence of the phase transition at  $T_f$ , and the new  $\omega^-$  ESR mode below  $T_f$  in a spin glass. The situation is very well described by a paragraph from a twenty-six-hundred-year-old Chinese classic, called the Tao-te ching (Classic of the Way and Virtue) translated as follows:

Is there a difference between yes and no?  
Is there a difference between good and evil?  
Must I fear what others fear? What nonsense!  
Other people are contented, enjoying the feast,  
But I alone am drifting, not knowing where I am.  
Like a new-born babe before it learns to smile,  
I am alone, without a place to go.  
Oh, I drift like the waves of the sea,  
Without direction, like the restless wind.

However, the Tao-te ching also says:

Knowing ignorance is strength.  
Ignoring knowledge is sickness.  
If one is sick of sickness, he is not sick.

The experimental work on spin glasses in the past five years has demonstrated to us that we are sick of sickness. Therefore, we are confident that a more effective understanding of the spin glass will soon appear.

#### ACKNOWLEDGEMENTS

I thank A. Arrott, R. J. Borg, J. D. Boyer, J. H. Brewer, H. S. Chen, M. K. Hou, D. L. Huber, R. A. Klemm, F. Mezei, A. P. Murani, J. A. Mydosh, K. L. Ngai, N. E. Phillips, A. K. Rajagopal, J. J. Rhyne, N. Rivier, J. Rudnick, M. B. Salamon, J. L. Tholence, Y. Uemura, C. E. Violet, E. F. Wassermann, and L. E. Wenger for many useful discussions. In particular, I would like to thank the late Prof. J. H. Van Vleck for stimulating discussions when I started to investigate the relaxation problem in the spin glass. I am also grateful to W. E. Keller, J. H. Huang, and E. H. Huang for their critical reading of the manuscript. This work was supported by the U. S. Department of Energy.

#### REFERENCES

1. J. W. Shih, Phys. Rev. **38**, 2051 (1931).
2. V. Cannella, J. A. Mydosh, and J. I. Budnick, J. Appl. Phys. **42**, 1689 (1971).
3. G. Toulouse, Comm. on Phys. **2**, 115 (1977).
4. J. A. Mydosh, A.I.P. Conf. Proc. **24**, 131 (1977); in Amorphous Magnetism II, ed. by R. A. Levy and R. Hasegawa (Plenum Press, New York, 1977) page 73; J. Magn. Mater. **7**, 237(1978); in Ferromagnetic Materials, ed. by E.P. Wohlforth (North-Holland, Amsterdam, 1980) Vol. I, page 1.
5. G. Heber, Appl. Phys. **10**, 101 (1976).
6. J. Souletie, J. Phys. (Paris) **39**, C2-3 (1978).
7. P.A. Beck, Progr. Mat. Sci. **23**, 1 (1978).
8. A. Blandin, J. Phys. (Paris) **39**, C6-1499 (1978).
9. A. P. Murani, J. Phys. (Paris) **39**, C6-1517 (1978).
10. R. Rammal and J. Souletie, in Magnetism of Metals and Alloys, ed. by M. Cyrot (North-Holland, Amsterdam, 1982) page 379; J. Souletie, J. Phys. (Paris) **44**, 1095 (1983).
11. K. H. Fischer, Phys. Stat. Sol. (b) **116**, 357 (1983).
12. H. Alloul, in Heidelberg Colloquium on Spin Glasses (Springer-Verlag, Berlin, 1983) page 18.
13. J. A. Mydosh, *ibid.* page 38.
14. L. E. Wenger, *ibid.*, page 60.
15. R. Omari, J. J. Prejean, and J. Souletie, *ibid.*, page 70.
16. R. A. Brand, V. Manns, and W. Keune, *ibid.*, page 79.
17. H. Maletta, *ibid.*, page 90.
18. C. E. Violet and R. J. Borg, Phys. Rev. **149**, 541 (1966).
19. A. Arrott, J. Appl. Phys. **36**, 1093 (1965); H. Malletta and W. Felsch, Phys. Rev. B **20**, 1245 (1979).
20. L. E. Wenger and P. H. Keesom, Phys. Rev. B **11**, 3497 (1975).
21. W. E. Fogle, J.D Boyer, R. A. Fischer, and N. E. Phillips, Phys. Rev. Lett. **50**, 1815 (1983); W. E. Fogle, J. D. Boyer, N.E. Phillips, and John Van Curen, *ibid.*, **49**, 1653 (1982).
22. K. Binder, J. Phys. (Paris) **39**, C6-1527 (1978); Festkörperprobleme (Advances in Solid State Physics) ed. by J. Treusch (Vieweg, Braunschweig, 1977) Vol. XVII, page 55; in Fundamental Problems in Statistical Mechanics, ed. by E. G. D. Cohen (North-Holland, 1980) Vol. V., page 21.
23. J. Joffrin, in La Matière Mal Condensée, ed. by R. Balian, R. Maynard, and G. Toulouse (North-Holland, 1979).
24. P. W. Anderson, *ibid.*
25. S. Kirkpatrick, *ibid.*
26. Heidelberg Colloquium on Spin Glasses, ed. by J. L. van Hemmen and I. Morgenstern (Springer-Verlag, Berlin, 1983).
27. G. S. Grest, C. M. Soukoulis, and K. Levin, in Magnetic Phase Transitions, ed. by M. Ausloos and R. J. Elliott (Springer, Berlin, 1983) page 183; J. Appl. Phys. **55**, 1634 (1984).
28. V. Cannella and J. A. Mydosh, Proc. Int. Conf. Magnetism, Vol. 2, Moscow, Nauka, page 74 (1974).
29. V. Cannella and J. A. Mydosh, Phys. Rev. B **6**, 4220 (1972).
30. J. L. Tholence and R. Tournier, J. Phys. (Paris) **32**, C1-211 (1971).
31. S. F. Edward and P. W. Anderson, J. Phys. F **5**, 965 (1975).
32. D. Sherrington and S. Kirkpatrick, Phys. Rev. Lett. **35**, 1792 (1975); S. Kirkpatrick and D. Sherrington, Phys. Rev. B **17**, 4384 (1978).
33. H. Maletta and W. Felsh, Phys. Rev. B **20**, 1245 (1979).
34. H. Malletta and W. Felsch, Z. Physik B **37**, 55 (1980).
35. H. Malletta, J. Appl. Phys. **53**, 2185 (1982).
36. G. P. Singh, M. von Schickfus, and H. Malletta, Phys. Rev. Lett. **51**, 1791 (1983).
37. M. Meschede, F. Steglich, W. Felsch, H. Malletta, and W. Zinn, Phys. Rev. Lett. **44**, 102 (1980).
38. B. Barbara, A. P. Malozemoff, and Y. Imry, Phys. Rev. Lett. **47**, 1852 (1981).
39. A. P. Malozemoff, Y. Imry and B. Barbara, J. Appl. Phys. **53**, 7672 (1982).
40. A. P. Malozemoff, S. E. Barnes, and B. Barbara, Phys. Rev. Lett. **51**, 1704 (1983); B. Barbara, A. P. Malozemoff, and S. E. Barnes, J. Appl. Phys. **55**, 1655 (1984).
41. L. E. Wenger and P. H. Keesom, Phys. Rev.



- B 13, 4053 (1976), AIP Conf. Proc. 29, 233 (1975).
42. W. E. Fogle, J. C. Ho, and M. E. Phillips, J. Phys. (Paris) 39, C6-901 (1978).
  43. L. R. Walker and R. E. Walstedt, Phys. Rev. Lett. 38, 514 (1977).
  44. D. L. Huber, in Excitations in Disordered Systems, NATO Advanced Study Series, ed. by M. F. Thorpe (Plenum Press, 1982) page 463.
  45. T. Giebultowicz, B. Lebech, B. Buras, W. Minor, H. Kepa, and R. R. Galazka, J. Appl. Phys. 55, 2305 (1984).
  46. J. R. L. de Almeida and D. .. Thouless, J. Phys. A 11, 983 (1978).
  47. M. Gabay and G. Toulouse, Phys. Rev. Lett. 47, 201 (1981).
  48. G. Toulouse and M. Gabay, J. Phys. (Paris), Lett. 42, L103 (1981); G. Toulouse, M. Gabay, T. C. Lubensky, and J. Vannimenus, *ibid.* 42, L109 (1982); D. M. Cragg, D. Sherrington, and M. Gabay, Phys. Rev. Lett. 49, 158 (1982); M. Gabay, T. Garel, and C. De Dominicis, J. Phys. C 15, 7165 (1982).
  49. J. S. Schilling, J. Crone, P. J. Ford, S. Methfessel, and J. A. Mydosh, J. Phys. F 4, L116 (1974); Phys. Rev. B 14, 4368 (1976); Europhysics Conf. Abstracts, Vol. I, 23 (1975).
  50. W. M. Star, Phys. Lett. 26A, 502 (1968); J. Ray, G. Chandra, and A. W. Shaikh, Proc. LT 15, Vol. II, 912 (1972).
  51. M. P. Yunus and D. Lazarus, Phys. Rev. B 19, 1039 (1979).
  52. E. Fawcett, D. B. McWhan, and R. C. Sherwood, Sol. Stat. Commun. 6, 509 (1969).
  53. B. H. Verbeek, G. J. Gieuwenbuys, H. Stocker, and J. A. Mydosh, Phys. Rev. Lett. 40, 586 (1978).
  54. J. A. Mydosh, G. J. Nieuwenhuys, and B. H. Verbeek, Phys. Rev. B 20, 1282 (1979).
  55. M. K. Wu, R. G. Aitken, C. W. Chu, C. Y. Huang, and C. E. Olsen, J. Appl. Phys. 50, 7356 (1979).
  56. U. Hardebusch, W. Gerhardt, and J. S. Schilling, Phys. Rev. Lett. 44, 352 (1980).
  57. C. W. Chu, M. K. Wu, B. J. Jin, W. Y. Lai, and H. S. Chen, Phys. Rev. Lett. 46, 1643 (1981).
  58. P. W. Anderson, B. I. Halperin, and C. M. Varma, Philos. Mag. 25, 1 (1972).
  59. W. A. Phillips, J. Low Temp. Phys. 7, 351 (1972).
  60. J. J. Prejean and J. Souletie, J. Phys. (Paris) 41, 1335 (1980).
  61. D. M. Herlach, E. F. Wasserman, and R. Willnecker, Phys. Rev. Lett. 50, 529 (1983); Magn. Magn. Mater. 31-34, 1404 (1983).
  62. E. F. Wassermann and D. M. Herlach, J. Appl. Phys. 55, 1709 (1984).
  63. C. Arzoumanian, P. A. de Goer, B. Salce, and F. Holtzberg, J. Phys. (Paris), Lett. 44, L39 (1983).
  64. H. V. Löhneysen, J. L. Tholence, and R. Tournier, J. Phys. (Paris) 39, C6-922 (1978).
  65. J. L. Tholence, F. Holtzberg, H. Godfrin, H. V. Löhneysen, and R. Tournier, *ibid.* 928.
  66. H. Maletta, W. Felsch, and J. L. Tholence, J. Magn. Magn. Mater. 9, 41 (1978).
  67. J. L. Tholence, in Trends in Physics, ed. by I. A. Dorobantu, page 747 (1981).
  68. J. L. Tholence, Sol. Stat. Commun. 35, 113 (1980), and references therein.
  69. M. Guyot, S. Foner, S. K. Hasanain, R. P. Guertin, and K. Westerholt, Phys. Lett. 79A, 339 (1980).
  70. C. A. M. Mulder, A. J. van Duyneveldt, and J. A. Mydosh, Phys. Rev. B 23, 1384 (1981).
  71. A. P. Malozemoff and Y. Imry, Phys. Rev. B 24, 489 (1981).
  72. L. Lundgren, P. Svedlindh, and O. Beckman, J. Magn. Magn. Mater. 25, 33 (1981).
  73. L. Lundgren, P. Svedlindh, and O. Beckman, J. Phys. F 12, 2663 (1982).
  74. L. Lundgren, P. Svedlindh, and O. Beckman, Phys. Rev. B 26, 3990 (1982).
  75. L. Lundgren, P. Svedlindh, P. Nordblad, and O. Beckman, Phys. Rev. Lett. 51, 911 (1983).
  76. L. Lundgren, P. Svedlindh, and O. Beckman, 31-34, 1349 (1983).
  77. D. Fiorani, J. L. Tholence, and J. L. Dormann, *physica* 107B, 643 (1981).
  78. F. Holtzberg, T. L. Francavilla, C. Y. Huang, and J. L. Tholence, J. Appl. Phys. 53, 2229 (1982).
  79. H. F. Hess and K. DeConde, *Physica* 108B, 1285 (1981).
  80. J. L. Tholence, *ibid.* 1287.
  81. D. Hüser, L. E. Wenger, A. J. van Duyneveldt, and J. A. Mydosh, Phys. Rev. B 27, 3100 (1983).
  82. J. L. Dormann, D. Fiorani, J. L. Tholence, and C. Sella, J. Magn. Magn. Mater. 35, 117 (1983).
  83. P. Beauvillain, C. Dupas, J. P. Renard, and P. Veillet, J. Magn. Magn. Mater. 31-34, 1377 (1983).
  84. S. Strickman and E. P. Wohlfarth, Phys. Lett. 85A, 467 (1981).
  85. F. Mezei, J. Appl. Phys. 53, 7654 (1982).
  86. F. Mezei, J. Magn. Magn. Mater. 31-34, 1327 (1983).
  87. A. P. Murani, J. Magn. Magn. Mater. 22, 271 (1981).
  88. H. B. G. Casimir and F. K. du Pré, *Physica* 5, 507 (1938).
  89. P. Debye, Polar Molecules (Dover, New York, 1945).
  90. L. Néel, Adv. Phys. 4, 191, (1955).
  91. K. L. Ngai, Comments Solid State Phys. 9, 127, 141 (1979).
  92. K. L. Ngai, in Non-Debye Relaxations in Condensed Matter, ed. by T. V. Ramakrishnan (World Scientific, Singapore, 1984).
  93. K. L. Ngai, A. K. Rajgopal and C. Y.

- Huang, 29th Conf. Magn. Magn. Mater., Nov. 8-11, 1983, Pittsburgh, PA, USA; J. Appl. Phys. 55, 1714 (1984).
94. J. L. Tholence and R. Tournier, J. Phys. (Paris) 35, C4-229(1974).
  95. S. Nagata, P. H. Keesom, and H. R. Harrison, Phys. Rev. B 19, 1633 (1979).
  96. C. N. Guy, J. Phys. F 8, 1306 (1978); F 7, 1505 (1977); F 5, L242 (1975).
  97. J. Ferré, J. Rajchenbach, and H. Maletta, J. Appl. Phys. 52, 1697 (1981).
  98. K. Binder, J. Phys. (Paris) 39, C6-1527 (1978).
  99. R. V. Chamberlin, G. Mozurkewich, R. Orbach, Phys. Rev. Lett. 52, 867 (1984).
  100. N. L. Ngai and A. K. Rajagopal, Phys. Rev. Lett. 53, 1024 (1984); R. V. Chamberlin, G. Mazurkewich, and R. Orbach, *ibid.* 1025.
  101. R. V. Chamberlin, M. Hardiman, L. A. Turkevich, and R. Orbach, Phys. Rev. B 25, 6720 (1982).
  102. Y. Yeshurun, L. J. P. Ketelsen, and M. B. Salamon, Phys. Rev. B 26, 1491 (1982).
  103. M. B. Salamon and J. L. Tholence, J. Appl. Phys. 53, 7684 (1982).
  104. J. L. Tholence, and M. B. Salamon, J. Magn. Magn. Mater. 31-34, 1340 (1983).
  105. M. B. Salamon and J. L. Tholence, *ibid.* 1375.
  106. I. A. Campbell, D. Arvantis, and A. Fert, Phys. Rev. Lett. 51, 57 (1983).
  107. N. Bontemps, J. Rajchenbach, and R. Orbach, J. Phys. (Paris), Lett. 44, L47 (1983).
  108. J. Rajchenbach and N. Bontemps, *ibid.* L799.
  109. C. Paulsen, J. A. Hamida, S. J. Williamson, and H. Maletta, J. Appl. Phys. 55, 1652 (1984).
  110. J. Rajchenbach, and N. Bontemps, *ibid.* 1649.
  111. L. E. Wenger and J. A. Mydosh, Phys. Rev. B 29, 4156 (1984).
  112. P. Monod and H. Bouchiat, J. Phys. (Paris), Lett. 43, L45 (1982).
  113. A. Berton, J. Chaussy, J. Odin, R. Rammal, and R. Tournier, *ibid.* L153.
  114. K. Binder and K. Schröder, Phys. Rev. B 14, 2142 (1976).
  115. W. Kinzel and K. Binder, Phys. Rev. B 19, 4595 (1979).
  116. C. Dasgupta, S. K. Ma, and C. K. Hu, Phys. Rev. B 20, 3837 (1979).
  117. W. F. Brown, Phys. Rev. 130, 1677 (1963).
  118. A. P. Murani, J. Appl. Phys. 49, 1604 (1978).
  119. G. Aeppli, S. M. Shapiro, H. Maletta, R. J. Birgeneau, and H. S. Chen, J. Appl. Phys. 55, 1628 (1984).
  120. J. J. Rhyne, in Magnetic Phase Transitions, ed. by M. Ausloos and R. J. Elliott (Springer, Berlin, 1983), page 241.
  121. H. Maletta, G. Aeppli, and S. M. Shapiro, Phys. Rev. Lett. 48, 1490 (1982); J. Magn. Magn. Mater. 31-24, 1367 (1983).
  122. A. P. Murani and A. Heidemann, Phys. Rev. Lett. 41, 1402 (1978).
  123. A. P. Murani, *ibid.* 1406.
  124. F. Mezei and A. P. Murani, J. Magn. Magn. Mater. 14, 211 (1979).
  125. A. P. Murani, F. Mezei, and J. L. Tholence, Physica 108B, 1283 (1981).
  126. F. Mezei, A. P. Murani, and J. L. Tholence, Sol. Stat. Commun. 45, 411 (1983).
  127. P.G. de Gennes and J. Villain, J. Phys. Chem. Solids 13, 10 (1960).
  128. A. P. Murani, J. Magn. Magn. Mater. 25, 68 (1981).
  129. D. E. MacLaughlin and H. Alloul, Phys. Rev. Lett. 36, 1158 (1976).
  130. D. A. Levitt and R. E. Walstedt, Phys. Rev. Lett. 38, 178 (1977).
  131. D. E. MacLaughlin and H. Alloul, Phys. Rev. Lett. 38, 181 (1977).
  132. D. Bloyet, E. Varoquax, C. Vibet, O. Avenel, and M. P. Berglund, Phys. Rev. Lett., 40, 250 (1978).
  133. H. Alloul, Phys. Rev. Lett. 42, 603 (1979).
  134. H. Alloul, J. Appl. Phys. 50, 7330 (1979).
  135. H. Alloul and F. Hippert, J. Magn. Magn. Mater. 31-34, 1321 (1983).
  136. H. Alloul, S. Murayama, and M. Chapellier, *ibid.* 1353.
  137. C. P. Bean, J. Appl. Phys. 26, 1381 (1955).
  138. S. F. Edwards and P. W. Anderson, J. Phys. F 6, 1927 (1976).
  139. K. H. Fischer, Sol. Stat. Commun. 18, 1515 (1976).
  140. W. Kinzel and K. H. Fischer, Sol. Stat. Commun. 23, 687 (1977).
  141. S. K. Ma and J. Rudnick, Phys. Rev. Lett. 40, 589 (1978).
  142. K. Binder and D. Stauffer, Phys. Lett. 57A, 177 (1976).
  143. D. L. Huber, J. Phys. Chem. Solids 32, 2145 (1971).
  144. M. B. Salamon and R. M. Herman, Phys. Rev. Lett. 41, 1506 (1978).
  145. H. Sompolinsky, Phys. Rev. Lett. 47, 935 (1981).
  146. H. Sompolinsky and A. Zippelius, Phys. Rev. B 25, 6860 (1982).
  147. J. Owen, M. E. Browne, V. Arp, and A. F. Kip, J. Phys. Chem. Solids 2, 85 (1957).
  148. M. B. Salamon and R. M. Herman, Sol. Stat. Commun. 31, 781 (1979).
  149. E. D. Dahlberg, M. Hardiman, R. Orbach, and J. Souletie, Phys. Rev. Lett. 42, 401 (1979).
  150. P. M. Levy and C. Morgan-Pond and R. Raghavan, Phys. Rev. Lett. 50, 1160 (1983).
  151. P. M. Levy and A. Fert, Phys. Rev. B 23, 4667 (1981); P. M. Levy, C. Morgan-Pond, and A. Fert, J. Appl. Phys. 53, 2168 (1982).
  152. J. P. Jamet and A. P. Malozemoff, Phys. Rev. B 18, 75 (1978); A. P. Malozemoff and J. P. Jamet, Phys. Rev. Lett. 39,

- 1293 (1977).
153. S. M. Bhagat, M. L. Sparo, and J. N. Lloyd, Sol. Stat. Commun. 38, 261 (1981).
154. D. Fiorani, N. Nogues, and S. Viticoli, Sol. Stat. Commun. 41, 537 (1982).
155. M. K. Hou, M. B. Salamon, and T. A. L. Ziman, J. Appl. Phys. 55, 1723 (1984).
156. M. K. Hou, M. B. Salamon, and T. A. L. Ziman, to be published in Phys. Rev. B.
157. M. K. Hou, Ph. D. Thesis, University of Illinois at Urbana-Champaign, 1984 (unpublished).
158. F. R. Hoestra, K. Barbeschke, M. Zomack and J. Mydosh, Sol. Stat. Commun. 43, 109 (1982).
159. R. Kubo and T. Toyabe, in Magnetic Resonance and Relaxation, ed. by R. Blinc (North-Holland, Amsterdam, 1967) page 810.
160. K. Binder, Z. Phys. B 26, 339 (1977).
161. R. S. Hayano, Y. J. Uemura, J. Imazato, N. Nishida, T. Yamazaki, and R. Kubo, Phys. Rev. B 20, 850 (1979).
162. K. Sugawara, C. Y. Huang, and B. R. Cooper, Phys. Rev. B 28, 4955 (1983).
163. C. L. Henley, H. Sompolinsky, and B. I. Halperin, Phys. Rev. B 25, 5849 (1982).
164. P. Monod and Y. Berthier, J. Magn. Magn. Mater. 15-18, 149 (1980).
165. S. Schultz, E. M. Gullikson, D. R. Fredkin, and M. Tovar, Phys. Rev. Lett. 45, 1508 (1980); J. Appl. Phys. 52, 1776 (1981).
166. W. Saslow, Phys. Rev. Lett. 48, 505 (1982).
167. B. I. Halperin and W. M. Saslow, Phys. Rev. B 12, 2154 (1977).
168. J. M. Machado da Silva and H. Abe, J. Magn. Mang. Mater. 31-34, 1351 (1983).
169. F. R. Hoekstra, G. J. Gieuwenhuys, K. Barbeschke, and S. E. Barnes, Phys. Rev. B 29, 1292 (1984).
170. A. T. Fiory, AIP Conf. Proc. 29, 229 (1976); D. E. Murnick, A. T. Fiory, and W. J. Kossler, Phys. Rev. Lett. 36, 100 (1976).
171. Y. J. Uemura, T. Yamazaki, R. S. Hayano, R. Nakai, and C. Y. Huang, Phys. Rev. Lett. 45, 583 (1980).
172. Y. J. Uemura, Hyp. Int. 8, 739 (1981).
173. Y. J. Uemura, Ph.D. thesis, University of Tokyo, 1981 (unpublished); Y. J. Uemura and T. Yamazaki, Physica 109 & 110B, 1915 (1982).
174. R. E. Walstedt and L. R. Walker, Phys. Rev. B 9, 4857 (1974).
175. J. A. Brown, S. A. Dodds, T. L. Estle, R. H. Heffner, M. Leon, D. E. MacLaughlin, C. E. Olsen, and M. E. Schillaci, Hyp. Int. 8, 763 (1981).
176. J. H. Brewer, D. P. Spencer, C. Y. Huang, Y. J. Uemura, and H. S. Chen, Bull. Am. Phys. Soc. 29, 338 (1984).
177. Y. J. Uemura, C. Y. Huang, C. W. Clawson, J. H. Brewer, R. F. Kiefl, D. P. Spencer, and A. M. de Graff, Hyp. Int. 8, 757 (1981).
178. M. K. Hou and C. Y. Huang, to be published.
179. C. Clawson, K. M. Crowe, S. E. Kohn, S. S. Rosenblum, C. Y. Huang, J. L. Smith, and J. H. Brewer, Phys. Rev. Lett. 51, 114 (1983).

# **ELECTRICAL RELAXATIONS IN IONIC CONDUCTORS**

# RELAXATION BY "FAST" IONS IN VISCOUS LIQUIDS AND GLASSES

C. A. Angell  
Department of Chemistry  
Purdue University  
West Lafayette, Indiana 47907

## Abstract

The phenomenology of relaxation of electrical and mechanical stress in inorganic amorphous phases by a subset of the system's particles, the "fast" monovalent cations, is examined. The decoupling of monovalent cation motions from those of the host quasi-lattice is defined by a relaxation time ratio, and the factors determining its value are examined. The relaxation functions for total structure and fast ion relaxations are both non-exponential,  $\phi(t) = \exp - ([t/\tau]^\beta)$ , and the departures from exponentiality are dependent on temperature above  $T_g$ . Interestingly enough, temperature effects the fractional exponents  $\beta$  in opposite ways. Finally, the component of the total mechanical relaxation spectrum due to fast ion motion is compared with the electrical relaxation and the origin of its much greater width is discussed.

## Introduction

Among certain of the glass-forming ionic liquids described in the previous set of "comments" by the author, are those cases in which a subset of the ions have a much higher intrinsic mobility than the remainder. The distinction between subset mobilities becomes greatly exaggerated as these liquids approach the glassy state and the relative mobilities may differ by as many as 12 orders of magnitude at the  $10^\circ \text{ min}^{-1}$  glass transition temperature. Such materials are of technological interest as solid electrolytes, and are currently being intensively investigated. In this account we discuss some of the intrinsic features of interest in these materials, and the chemical factors which permit their existence. We will also discuss short and long time aspects of the fast ion motion and mechanical manifestations of their existence. It will be seen that the mechanical relaxations have characteristics much in common with those which determine the electrical conductance.

It is a matter of academic interest that the Stokes-Einstein equation

$$D_i = kT/6\pi\eta r_i \quad (1)$$

in which  $\eta$  is the diffusion coefficient of species  $i$ , and  $r_i$  is its ionic radius, predicts that the electrical conductivity due to the ionic motion manifested by  $D_i$  should become very small as a glassy state is approached because the glassy state is defined by the arrival of the viscosity at values of the order  $10^{12}$ - $10^{13}$  poise. The fact that fast ion conductors exist implies that the coupling between species in liquids which is at the root of the Stokes-Einstein equation has ceased to be important in some cases. It is the job of the materials scientists to understand and quantify this decoupling process.

## The Decoupling Index $R_\tau$ and Its Origin

In a recent article (1) the author showed how the decoupling phenomenon could be quantified in simple terms using a decoupling index defined by the ratio of the structural relaxation time to the electrical relaxation time. Each relaxation time is defined as a Maxwell relaxation time through the ratio of the ordinary linear response coefficient, viscosity, or specific resistivity respectively, to the appropriate modulus:

$$\tau_s = \eta_s/G_\infty, \quad \tau_\sigma = \rho/M_\infty \quad (2)$$

where  $G_\infty$  is the (infinite frequency) shear modulus, and  $M_\infty$  the (infinite frequency) electrical modulus,  $M_\infty = (\epsilon_\infty \epsilon_0)^{-1}$ . In a few cases the data necessary to define both relaxation times over a considerable range of temperature are available, hence the behavior of their ratio can be depicted. An example is given in Figure 1. Note how the decoupling process develops rapidly with decreasing temperature.

In the general case the decoupling index can at least be determined at the glass transition temperature since the structural relaxation time is known to be of the order  $10^2$  seconds at this point and the conductivity relaxation time can be determined at the same temperature using an extrapolation of conductivity data which have normally been measured as a function of temperature over a range of temperatures below  $T_g$ . The electrical modulus is usually within

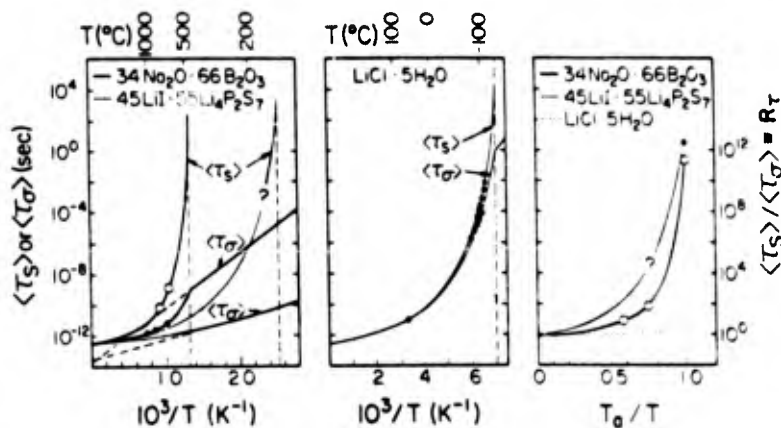


Figure 1. Relaxation times for shear and electrical stresses and for selected glass-forming liquids. Glass transition temperatures, where the conductivity relaxation time changes its temperature dependence are indicated by vertical dashed lines. The ratio of structural to conductivity relaxation times,  $R_T$ , shown in the third part of the figure, defines the decoupling index, see ref. 1.

a factor of 2 of the value  $1 \times 10^{12}$  volt<sup>-1</sup> coulomb<sup>-1</sup>.

The data shown in Figure 1 reveal, see Fig. 1(c), that the decoupling index  $R_T$  can differ by some 11 orders of magnitude from one glass to another, even when the mobile species is the same ( $\text{Li}^+$ ).

To understand the chemical differences which lead to these enormous changes in decoupling of ionic motions we survey the electrical conductivities of a variety of glasses of different compositions. For a decoupling index of unity, the data used to construct Figure 1 indicate that the conductivity at the glass transition temperature should be of the order of  $10^{-14} \text{ohm}^{-1} \text{cm}^{-1}$  at the glass transition temperature. The value at some convenient temperature, for example room temperature, will depend not only on the decoupling index but on the position of the comparison temperature, ambient in this case, to the glass transition temperature. For most of the glasses of interest, the latter is above room temperature and may vary widely from system to system. Thus, the conductivity at room temperature is not a reliable index of the decoupling appropriate to the system in question. However, it is the commonly available quantity, and also the quantity of practical interest as far as electrochemical applications of fast ion conductors are concerned; thus we will examine it in Figures 2 and 3 for any trends which may be evident. Figure 2 which is taken from J. L. Souquet's review paper (2) from the 1981 (Gatlinburg) Fast Ion Conductor Conference shows that for a variety of systems consisting of a compound containing a monovalent cation and a Lewis acid, the conductivity at fixed temperature rises exponentially with the concentration of the monovalent cation containing compound mole fraction. Clearly the conductivity depends on the presence of the low charge density cation, but the origin of the observed slope remains a matter of some controversy. A number of workers (3-5) interpret the

observation initially made by Ravaine and Souquet (3) that  $\log \sigma / \log a_{M_2O} = 1/2$

( $a_{M_2O}$  = activity of  $M_2O$ ) in terms of a precondition for mobility based on the dissociation of the alkali metal from some trap state on the surrounding ligands. The implication is that the conductivity is determined primarily by a thermodynamic equilibrium effect, the mobility of the cations in the "free" or dissociated state being approximately the same for all compositions. Figure 2 shows that the conductivity is greater, the less highly charged and the more polarizable the surrounding anions

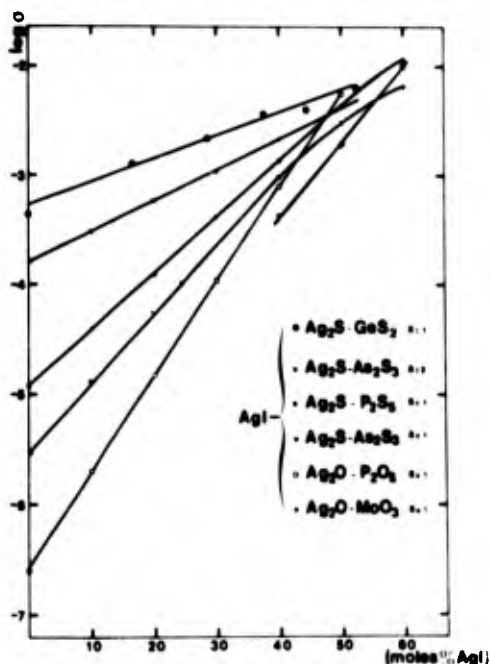


Figure 2. Silver cationic conductivity as a function of AgI content for several glassy systems, from ref. 2, reprinted by permission.

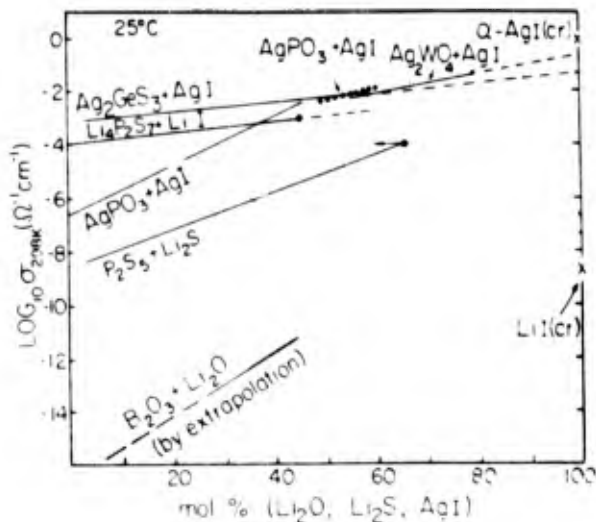


Figure 3. Room temperature conductivity and its composition dependence for various  $\text{Li}^+$  and  $\text{Ag}^+$  conductors, showing highest  $\sigma_0$  cases of each class. (Adapted from ref. 1.)

are. Thus the highest conductivities amongst the alkali metal-containing glasses are found in systems containing large mole fractions of the appropriate iodide. In the absence of iodide ions, it seems clear that sulfide ions lead to higher conductivities than do the corresponding oxide ions. Hunter and Ingram argue, however, that the conductivity of glass derived from different base glasses by addition of halides, sulfates, etc. depend more on the final monovalent cation fraction than on the anion present (6).

Figure 4, which compares the temperature dependence of conductivities of  $\text{Na}_2\text{O} \cdot 3\text{SiO}_2$  with that of the best alkali metal conducting glass  $57\text{Li}_4\text{P}_2\text{S}_7 \cdot 43\text{LiI}$  (7), shows that the higher conductivities of the glasses containing the more polarizable anions are only partly due to a greater decoupling of cation motions in such systems: the conductivities at  $T_g$  ( $\tau_s = 10^2$  sec) in the two cases illustrated, differ by only ~1 order of magnitude. The other important effect is the temperature at which the glass transition (which arrests the liquid structure and causes the conductivity activation energy to adopt a temperature-independent value) occurs.

Comparing the different monovalent cations, it appears that both size and polarizability effects play a role.  $\text{Li}^+$  and  $\text{Na}^+$  are both mobile compared with the larger alkali metal ions, while  $\text{Ag}^+$  which is of similar size to sodium but considerably higher polarizability, conducts about an order of magnitude better at room temperature. However, since the glass transition temperatures are different and higher for the alkali metal than for the  $\text{Ag}^+$  glasses, the differences in decoupling indexes are not as great as might be judged from Figures 2 and 3. The same comment may be made for comparisons

of the two group 1(b) cations  $\text{Ag}^+$  and  $\text{Cu}^+$ . Although  $\text{Ag}^+$ -containing glasses are the better conductors at room temperature, this situation reverses at higher temperatures at least for some compositions (8).

It is easier, in some ways, to determine what factors increase the coupling, hence decrease the performance of fast ion conductors, since the effects can be dramatic. Some interesting recent results in this respect are those of E. I. Cooper and the author on high LiI content salt mixtures (9). Compositions were devised in which all the anions were iodide (hence were expected to be favorable to high degrees of decoupling according to Figures 2 and 3) while 70% of the cations were  $\text{Li}^+$ . Contrary to initial expectations, this mixture, which had a glass transition below room temperature, proved to be a very highly coupled system. The reason is, evidently, that in this type of system where the second cation is a large organic cation rather than a small Lewis acid cation, the lithium cations are the most competitive in the system hence themselves establish the "matrix" which determines the fluidity. In other words it is the counter polarization of the anion matrix by the strong Lewis acid cations,  $\text{P}^{5+}$ ,  $\text{B}^{3+}$ , etc. which is primarily responsible for the decoupling of monovalent cations in the systems depicted in Figures 2 and 3. How this effect is to be quantified must remain for future work to determine.

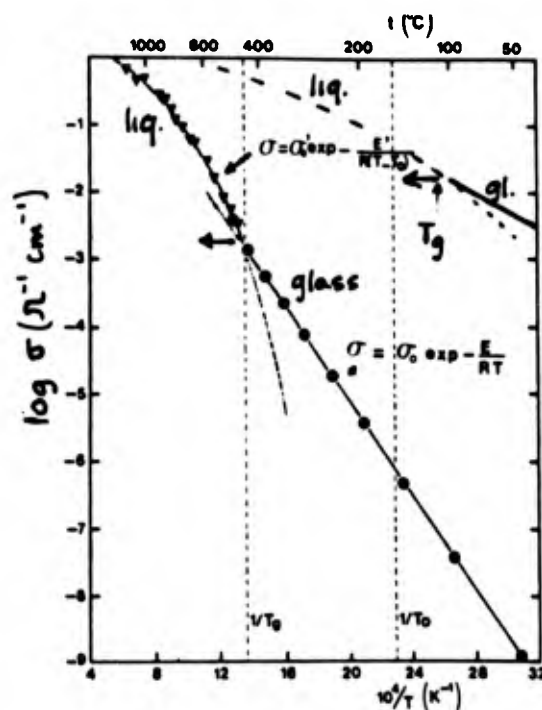


Figure 4. Variation of specific conductivity with temperature in liquid and glassy states for  $\text{Na}_2\text{O} \cdot 2\text{SiO}_2$  and  $57\text{Li}_4\text{P}_2\text{S}_7 \cdot 43\text{LiI}$  showing how, for equal decoupling at  $T_g$ , conductivity at ambient temperature depends on  $T_g$ .

Within a single system, the decoupling index can evidently pass through a maximum value if the concentration of monovalent cations is increased sufficiently. This is implied in several cases and has been observed clearly and quantified, in the case of the  $\text{Na}_2\text{O} + \text{B}_2\text{O}_3$  glasses (10) where a maximum decoupling is found at ~45%  $\text{Na}_2\text{O}$  (maximum room temperature conductivity is found at ~55%  $\text{Na}_2\text{O}$ ).

#### Short and Long Time Cation Motions in Fast Ion Conductors

Computer simulation studies of fast ion conducting glasses show that, as in the case of the crystalline materials, ions spend the majority of their time oscillating anharmonically about fixed quasi-lattice positions. The less frequent hopping or, rather, drifting motions which carry them from one site to an adjacent one, occur in a relatively short period, usually in cooperation with the concerted movement of another cation into the vacated site.

The oscillatory motions give rise to an absorption in the far infrared which has been observed and discussed by a number of workers including the author and colleagues (11-15), see Figure 5. The far infrared absorption can be related to the longer time diffusive motions through an absorption vs. frequency log-log plot (13), as depicted in Figure 6. The relation between the measurements obtained in different frequency regimes by different methods is obtained by converting the optical absorption coefficient, which is related to the energy loss per unit length measure, into an energy loss per cycle. The loss per cycle  $\epsilon''$ , is related to the conductivity by

$$\epsilon''(f) = \sigma(f)/e_0\omega \quad (3)$$

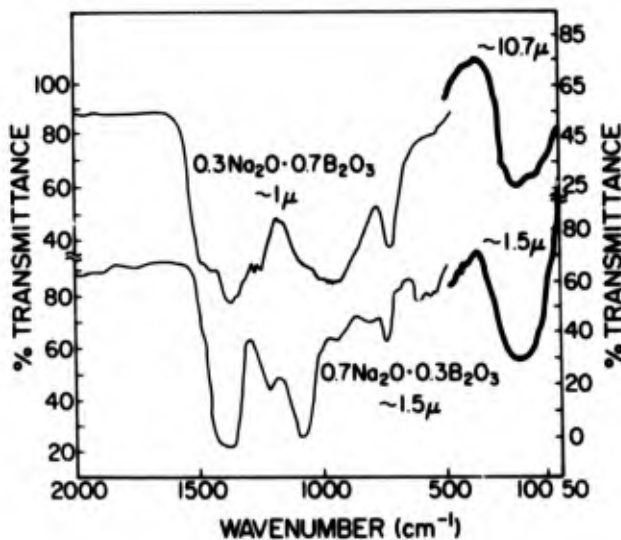


Figure 5. Mid and far infrared spectra of  $\text{Na}_2\text{O} + \text{B}_2\text{O}_3$  glasses from thin film studies - see ref. 15.

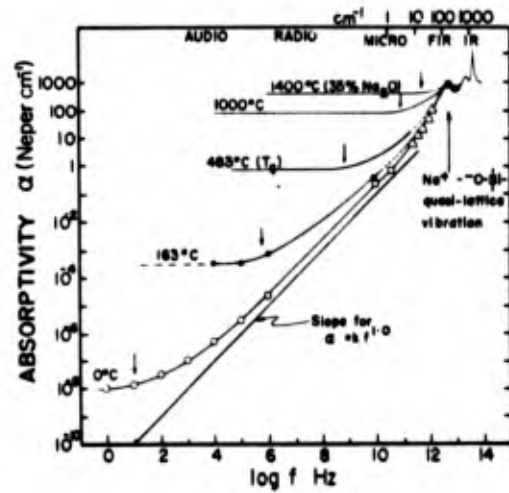


Figure 6. Experimental frequency spectrum for  $\text{Na}^+$  ion motions in  $\text{Na}_2\text{O} \cdot 3\text{SiO}_2$  glass and liquid state at different temperatures. For alkali silicate glasses,  $\sigma(f) \approx 1.01 \times 10^{-2}\alpha(f)$  (adapted from ref. 13).

and the final relation is (16)

$$\alpha(f) = \sigma(f)/cn(f)e_0 \quad (4)$$

The plot in Figure 6 shows that the two regimes, far infrared absorption and 0-10 MHz conductivity, are connected by a regime passing the microwave region with approximately unit slope. If the glassy structure contains microphase regions of high conductivity, these will be revealed as inflections or even plateau regions in this latter regime. However, these have not been reported except in deliberately formed biphasic materials (17).

Figure 4 may be regarded as a sort of density of states diagram for fast ion motions in the vitreous materials. As the temperature increases, the d.c. conductivity plateau mounts higher and higher on the diagram and tends (usually only in the mobile liquid state) to cover the region up to the far IR peak. The latter thus essentially determines the limiting high value for ionic conductivity in vitreous media.

#### Frequency Spectra for Conductivity and Longitudinal Relaxations

The a.c. characteristics of fast ion motion in vitreous materials are best displayed using a complex electrical modulus  $M^*$  representation of the results of a.c. bridge, or equivalent network analyzer, results. A recent data set on the imaginary part  $M''$  of a fast silver ion conducting glass (18,19) at various temperatures, superimposed to give a master plot, is compared with similar but unsuperimposed data (real and imaginary parts) for a classical sodium silicate glass (20) in Figure 7. If the conductivity relaxation process could be described by a



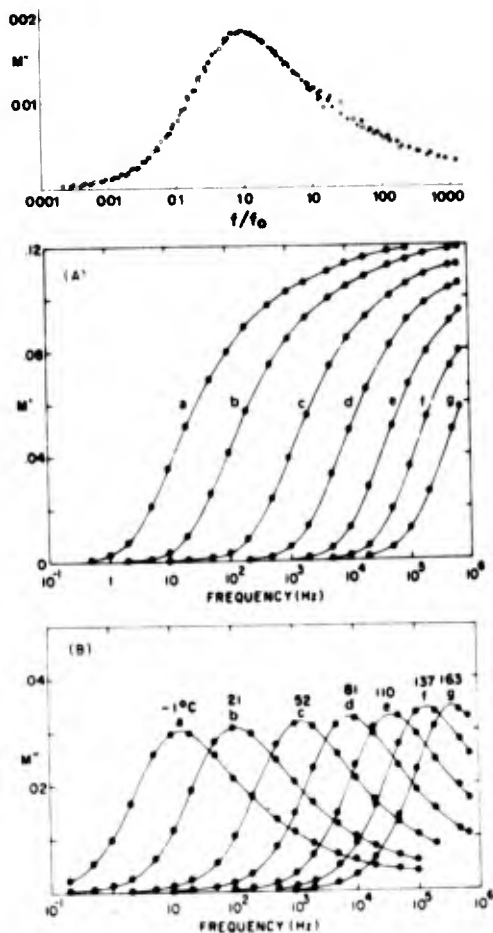


Figure 7. Comparison of electrical modulus loss spectra for a fast ion conducting glass, silver  $4\text{AgI}\cdot\text{Ag}_3\text{AsO}_4$  (a master plot for data (18) covering the  $-104$  to  $-157^\circ\text{C}$  range) with individual isothermal spectra for a classic alkali ion conducting glass  $\text{Na}_2\text{O}\cdot 3\text{SiO}_2$  (20). For the latter case the real part  $M'$  of the modulus is also shown. Note that in Eq. (1)  $\epsilon_\infty = 1/M'_\infty$ .

single relaxation time, the loss spectra  $M''$  vs.  $f$  would have full width at half height of 1.12 decades. It is clear that the spectral response function is not so described. In fact, rather than an exponential decay function, the fractional exponential form

$$\Theta(t) = \exp - ([t/\tau]^\beta) \quad (6)$$

is required. The value of the coefficient  $\beta$  is typically in the vicinity of 0.5 though considerable variations are possible. Interestingly enough, despite the great difference in composition, the modulus spectra for classical alkali silicate and AgI-based fast conducting glasses are almost identical.

Attempts have been made in the recent literature to interpret the width of the observed modulus spectra in terms of distributions of molecular environments (21), though this issue is far from clear in view of the latter observation.

In the extreme dilution limit for alkali cations in Lewis acids such as  $\text{SiO}_2$  and  $\text{GeO}_2$ , (which are extremely poor conductors) the modulus spectra narrow up, and the process can be correctly described by a single relaxation time (22,23).

An interesting situation arises when the temperature is raised above  $T_g$ . In the supercooled liquid range, the relaxation spectra tend to broaden (i.e.  $\beta$  decreases) with increasing temperature (24), just the opposite effect from that observed for the shear relaxation process. The two variations are contrasted in Figure 8 for the case of  $6\text{KNO}_3\cdot 4\text{Ca}(\text{NO}_3)_2$  (which is not a fast ion conductor but is the only case for which both relaxation processes have been fully characterized in the liquid and glassy states). The temperature dependence for each process is Arrhenius in character for some  $40^\circ\text{C}$  above  $T_g$  where the conductivity relaxation spectrum is broadening. The structural relaxation spectrum seems to be "frozen" in this region though the data are not of great precision.

#### Mechanical Relaxation due to Fast Ion Motion

Mechanical stresses imposed on a vitreous material can be relaxed by the localized displacement of ions, and since in a fast ion conducting glass there are many such ions, a substantial mechanical response may be expected in the frequency regime characteristic of the fast ion motion. Representing the electrical conductivity of a fast ion conducting glass, for example,  $0.6\text{AgPO}_3\cdot 0.4\text{AgI}$ , by its conductivity relaxation time defined by Eq. (2), we find that a mechanical relaxation observed using the commonly available frequencies of mechanical spectrometers (5-100 Hz) would only be expected at

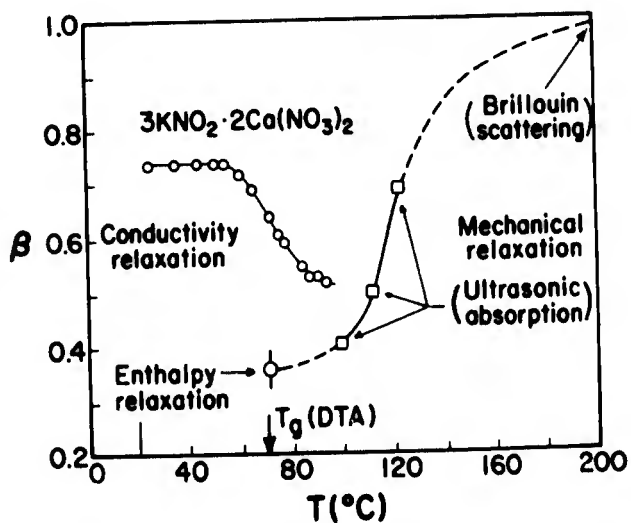


Figure 8. Comparison of the Eq. (6) exponent for relaxation of electrical stresses by mobile ions (conductivity relaxation) and mechanical stress by bulk viscosity (bulk or structural relaxation) for the case of  $2\text{Ca}(\text{NO}_3)_2\cdot 3\text{KNO}_3$  liquid and glass. [Data from refs. 24 and 25.]

temperatures of about  $-150^{\circ}\text{C}$  (1). Such relaxations have recently been observed in this laboratory and a representative example of the temperature scan for the glass  $0.6\text{ AgPO}_3\text{-}0.4\text{ AgI}$  is shown in Figure 9. Compared with the mechanical relaxation is the corresponding electrical modulus relaxation obtained by taking constant frequency cuts from a figure of the type of Figure 7 (19).

One observes that the most probable relaxation time for electrical stresses is almost identical with that of the mechanical relaxation, though the curve in temperature is much narrower in the latter case. The origin of the increased width at low temperatures, which implies an increasing spectral width at high frequencies for a constant temperature spectrum, is not clear. Since the mechanical loss approaches zero at the high temperature end, the increased width at high temperatures in the mechanical relaxation case is not obviously due to residual relaxation motions from the principal viscous process which is arrested at the (higher) glass transition temperature. It is worth noting, however, that sub- $T_g$  relaxations observed for molecular liquids by dielectric methods are characteristically much broader than the primary relaxation process (26). These broad relaxations also have an Arrhenius temperature dependence hence may be, in some sense, related phenomena.

It should be obvious that systems in which the ionic motions are fully coupled to the viscous motions, low temperature mechanical relaxations due to alkali motion will not be observed. Cases of practical importance to which this observation will apply are the polymer solvent + salt "solid electrolytes" now much in focus as separators for ambient temperature electrochemical cells. In these "solid electrolytes" the conductivity occurs within a locally liquid electrolyte which obtains its mechanical stability from the entanglement of the polymer chains. The glass transition temperatures for these materials are in fact far below room temperature and the decoupling index determined at the glass transition temperature is of the order of 100. It is only by having service temperature far above  $T_g$  that such materials are of any practical utility.

#### Summary

These comments have indicated something of the range of behavior available for study in solid amorphous materials with mobile ion species. Much information on systems containing mixed cations and mixed anions, either of which may affect the characteristic relaxation spectra and decoupling characteristics, remains to be obtained. Interest in these systems continues to grow and many new insights into their behavior may be expected in the future.

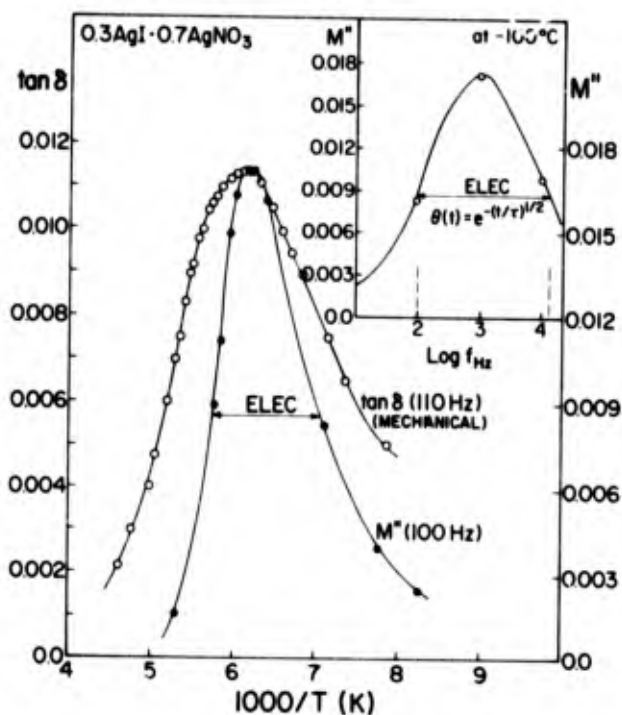


Figure 9. Comparison of 110 Hz mechanical and 100 Hz electrical loss vs. temperature curves ( $\tan \delta = E''/E'$ , and  $M''$  respectively) for  $0.3\text{ AgI}\cdot 0.7\text{ AgPO}_3$  glass, showing broader mechanical response, implying the existence of both fast and slow dynamic mechanical processes which do not transport charge. The normal character of the electrical relaxation is shown in the insert (c.f. Fig. 7). [Data taken from ref. 19.]

#### Acknowledgment

The author is indebted to his co-workers E. I. Cooper, C. Liu, S. W. Martin and S. Tamaddon for many discussions and to C. Liu for permission to show key results from his detailed mechanical-electrical relaxation studies on AgI-AgPO<sub>3</sub> and AgI-AgBO<sub>2</sub> glasses, and infrared studies on which Na<sub>2</sub>O + B<sub>2</sub>O<sub>3</sub> glasses, which are currently being published elsewhere. Our overall program has been supported in different aspects by NSF-MRL Grant No. DMR 7302643A01, DOE EPRIP Grant No. DE 100448 and ONR Agreement No. N0014-76-C-0035.

#### References

- (1) C. A. Angell, *Solid State Ionics* **9**610, 3 (1983).
- (2) J. L. Souquet, *Solid State Ionics* **5**, 77 (1983); *Ann. Rev. Mat. Sci.* **11**, 211 (1981).
- (3) D. Ravaine and J. L. Souquet, *Phys. Chem. Glasses* **18**, 27 (1977).
- (4) C. T. Moynihan and A. V. Lesikar, *J. Non-Cryst. Solids* **38**39, 371 (1980).
- (5) M. Tomazawa in *Treatise on Materials Science and Technology*, vol. 12, eds. M. Tomazawa and R. H. Doremus, Academic Press, New York, 1977, pp. 335-342.

- (6) C. C. Hunter and M. D. Ingram, *Solid State Ionics* (in press '84).
- (7) R. Mercier, J.-P. Malugani, B. Fays and G. Robert, *Solid State Ionics* 5, 663 (1981).
- (8) C. L. Liu and C. A. Angell, *Solid State Ionics* 11, 0000 (1984) (in press).
- (9) E. I. Cooper and C. A. Angell, *Solid State Ionics* 9610, 617 (1983).
- (10) S. W. Martin and C. A. Angell, *Commun. Am. Ceram. Soc.* 1984 (in press).
- (11) G. J. Exarhos, P. J. Miller and W. M. Risen, *J. Chem. Phys.* 60, 4145 (1974).
- (12) P. C. Taylor, S. G. Bishop, D. L. Mitchell, *Phys. Rev. Lett.* 27, 414 (1971).
- (13) J. Wong and C. A. Angell, *Glass: Structure by Spectroscopy*, Marcel Dekker, New York, 1976, Chapter 11.
- (14) C. A. Angell, L. Boehm, P. A. Cheeseman and S. Tamaddon, *Solid State Ionics* 5, 659 (1981).
- (15) C. Liu and C. A. Angell, *Mat. Res. Bull.* (to be published).
- (16) T. S. Moss, *Optical Properties of Semiconductors*, Butterworths, London, 1961, p. 2.
- (17) L. Boehm and C. A. Angell, unpublished work.
- (18) (a) R. J. Grant, M. D. Ingram, L. D. S. Turner and C. A. Vincent, *J. Phys. Chem.* 82, 2838 (1978).  
 (b) M. Lazzari, C. A. Vincent and E. Scrosati in *Fast Ion Transport in Solids*, North Holland, Amsterdam, 1979, p. 713.
- (19) C. Liu and C. A. Angell, *Solid State Ionics* (submitted for publication).
- (20) V. Provenzano, L. P. Boesch, V. Volterra, C. T. Moynihan and P. B. Macedo, *J. Am. Ceram. Soc.* 55, 492 (1972).
- (21) D. Ravaine and A. F. Wright, *Phys. Chem. Glasses* 24, 31 (1983).
- (22) M. Tomazawa, J. F. Cordaro and M. Singh, *J. Mater. Sci.* 14, 1945 (1979).
- (23) K. Simmons and J. Simmons, *J. Am. Ceram. Soc.* 62, 479 (1979).
- (24) F. S. Howell, R. Bose, C. T. Moynihan and P. B. Macedo, *J. Phys. Chem.* 78, 639 (1974).
- (25) C. A. Angell and L. M. Torell, *J. Chem. Phys.* 78, 937 (1983).

# NMR, ELECTRICAL RELAXATION, AND HIGH PRESSURE ELECTRICAL CONDUCTIVITY IN ION CONDUCTING POLYMERS

Steven G. Greenbaum  
Hunter College of CUNY, New York, New York 10021

John J. Fontanella  
U. S. Naval Academy, Annapolis, Maryland 21402

Recent nuclear magnetic resonance (NMR), electrical relaxation, and high pressure electrical conductivity studies of ion conducting polymers are reviewed. Most of the work discussed is that concerned with poly(ethylene oxide) (PEO) though some recent results concerning poly(vinyl acetate) are also described. A survey of experimental  $^1\text{H}$ ,  $^7\text{Li}$ ,  $^{19}\text{F}$ , and  $^{23}\text{Na}$  NMR data for ion conducting polymers based on PEO reveals some features that are commonly observed in superionic solids, such as motional narrowing in the temperature region of enhanced conductivity. The NMR activation energies are generally lower than those for conductivity, indicating the presence of localized motional processes. Previous electrical relaxation data along with new results for  $\text{PEO}_{4.5}:\text{NaI}$  and  $\text{PEO}_{4.5}:\text{LiCF}_3\text{SO}_3$  make it clear that PEO complexed with different salts exhibits different electrical relaxation spectra. Changes in chain structure are detected along with multiphase behavior. Also, new results are presented for the effect of high pressure on the electrical conductivity of poly(propylene oxide) complexed with alkali metal salts. Those results eliminate some ambiguities associated with previous high pressure electrical conductivity studies of PEO.

## Introduction

Ion conducting polymers represent a class of materials of intense current interest. These materials are being considered for use as the electrolyte in solid state batteries. Battery development is, in fact, progressing rapidly.(1) Most of the work to date has centered on poly(ethylene oxide) (PEO). The first reports of fast ion conduction in PEO were due to Wright and co-workers.(2-4) Extensive work, however, began after the paper by Armand and co-workers.(5) Since then, there have been many studies of this polymeric solid electrolyte(6-39) along with reports of others such as poly(propylene oxide)(5), polyacrylonitrile,(40) poly(vinylidene fluoride),(40) poly(tetra-methylene oxide),(41) poly(ethylene succinate),(42) and poly(vinyl acetate) (PVAc).(43)

Dielectric relaxation (DR) and nuclear magnetic resonance (NMR) techniques have been productively employed in studying fast ion processes in "traditional" solid electrolytes such as silicates, titanates, or aluminas which provide a framework for mobile monocations (e.g.  $\text{Li}^+$ ,  $\text{Na}^+$ ,  $\text{K}^+$ , or  $\text{Ag}^+$ ), or those of the heavy metal halide type (e.g.  $\text{PbF}_2$ ,  $\text{ZrF}_4$ ) whose ionic conductivity is attributable to a partially disordered sublattice above some critical temperature. The primary reason is that both techniques are powerful tools for probing the local environment of ions. Another compelling reason for focussing on DR and NMR effects can be found in current theories concerning the apparent universality of low-frequency

fluctuations, dissipation, and relaxation properties of condensed matter.(44) For example, fundamentally different measurements such as spin-lattice relaxation times and dielectric loss have shown remarkable similarity with respect to both temperature and frequency dependence for a wide variety of materials.(45) Consequently, both techniques have begun to be applied to ion-conducting polymers.

The study of DR in polymers has been going on for many years and there are several books on the topic.(46-48) Consequently, there already exists a considerable body of information on DR in "pure" PEO.(49-55) In fact, indications of fast ion conduction in PEO can be found in many of the early papers on "pure" PEO. For example, Ishida et al. attribute some of their observations to ionic conduction.(51) However, as is often the case, many questions about the origin of the relaxation phenomena remain. For example, it is easy to find at least four different interpretations of the  $\gamma$  relaxation (47,55-60) not to mention three different nomenclatures ( $\beta$ (56),  $\beta_a$ (51), and  $\gamma$ (46,47)).

In the DR section of the present paper, recent results by one of the authors concerning DR in ion conducting PEO(37-39) will be reviewed and new results will be presented. Further, recent high pressure electrical conductivity studies in PEO(36) will be discussed along with some recent new results for poly(propylene oxide). There is not a great deal of published NMR work on ion conducting polymers at the present time. Some recent results will be discussed along with material drawn from earlier studies.

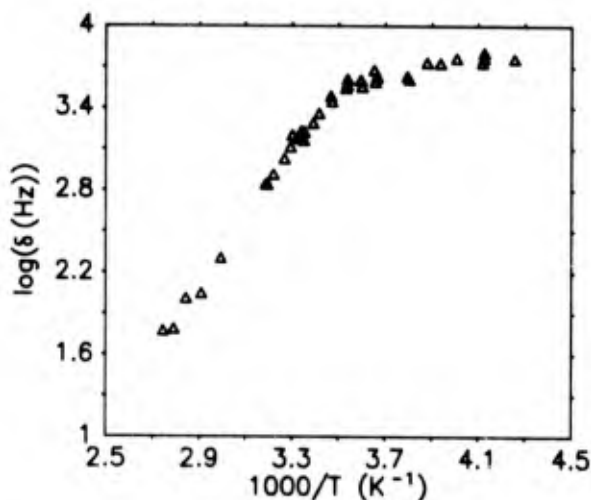


Fig. 1. Arrhenius plot of  ${}^7\text{Li}$  linewidth (in Hz) in PEO-polyurethane- $\text{LiClO}_4$  network (from ref. 32).

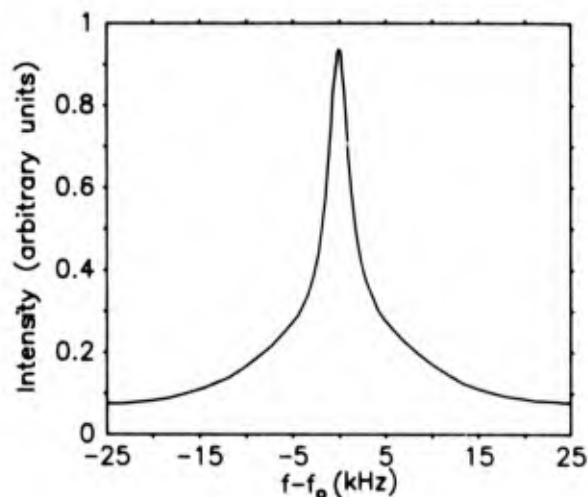


Fig. 2. Proton NMR lineshape of uncomplexed PEO ( $\text{MW } 5 \times 10^6$ ) at  $35^\circ\text{C}$ ,  $f_0=400$  MHz.

## Discussion

### Nuclear Magnetic Resonance

NMR studies of solid electrolytes have yielded important insights into both structural and dynamic properties, and several reviews of this rapidly growing field are in existence. (61-64) The power and versatility of the technique derive from the short-range nature of the nuclear quadrupole and dipole-dipole interactions. The quadrupole interaction occurs for nuclei with nuclear spin  $I > 1$  (e.g.  ${}^7\text{Li}$ ,  ${}^{23}\text{Na}$ ) subject to an electric field gradient (efg) generated by a surrounding charge distribution of lower than tetrahedral symmetry. Quadrupole effects thus constitute a sensitive probe of local bonding arrangements. For nuclei with spin  $I=1/2$  (e.g.  ${}^1\text{H}$ ,  ${}^{13}\text{C}$ ,  ${}^{19}\text{F}$ ) the nuclear dipole-dipole interaction is the predominant line-broadening mechanism since chemical shift effects usually provide a negligible contribution to broadening in the materials under consideration. The same argument applies to nuclei with  $I > 1/2$  situated in a highly symmetric charge distribution which yields a zero efg.

If atoms or ions can execute thermally activated motion, the dipolar fields experienced by their nuclei will be modulated with some characteristic "jump" frequency,  $\omega_j$ . When  $\omega_j$  exceeds the rigid dipolar linewidth  $\omega_D$ , the nuclei sense a partially averaged dipolar field which gives rise to a phenomenon known as motional narrowing. Thus linewidth versus temperature measurements can yield important qualitative information about ionic or atomic motion. The nuclear spin-lattice relaxation time  $T_1$  characterizes the nucleus' return to thermal equilibrium following a radio-frequency induced NMR transition, and as such, is also an effective probe of motional processes. The Bloembergen, Purcell, and Pound (BPP) treatment of nuclear relaxation (65) predicts a  $T_1$  minimum in the  $T_1$  vs. temperature curve, corresponding

to  $\omega\tau=1$  where  $\omega$  is the NMR frequency and  $\omega\tau=1$ . Another useful feature of  $T_1$  measurements is that activation energies for ionic (or atomic) motion can be readily extracted from the data for simple Arrhenius behavior:

$$\omega_j = \omega_0 \exp(-EA/kT).$$

An important consideration in the context of solid electrolyte studies concerns the fact that  $T_1$  is sensitive to local motion as well as long range transport processes and therefore does not always yield activation energies consistent with those determined by other techniques such as electrical conductivity.

High cationic mobilities in PEO-lithium salt complexes have been inferred from the observation of motional narrowing in  ${}^7\text{Li}$  NMR spectra. (5,26) In  $\text{PEO}_4:\text{LiCF}_3\text{COO}$  a single absorption line with no apparent quadrupole broadening is observed. The line begins to narrow at about  $15^\circ\text{C}$  and gradually decreases in width, becoming liquid-like at about  $100^\circ\text{C}$ . (26) Similar behavior has been noted in  $\text{LiClO}_4$ -containing complexes. (32) An Arrhenius plot of the  ${}^7\text{Li}$  linewidth temperature dependence is shown in Fig. 1 (data taken from ref. 32). The high temperature region of the curve yields an activation energy of about 11 kcal/mol which is somewhat lower than the conductivity activation energy of about 21 kcal/mol in the same temperature region. This discrepancy may be partly attributable to NMR's sensitivity to localized motion.

Proton NMR can shed light on the dynamics of the polyether chains just as  ${}^7\text{Li}$  NMR can for  $\text{Li}^+$  motion. The  ${}^1\text{H}$  absorption spectrum of uncomplexed PEO at  $35^\circ\text{C}$  is shown in Fig. 2 ( $f_0=400$  MHz). The most striking feature of the lineshape is its two-component nature, a narrow Lorentzian superimposed on a broad gaussian. The broad component is identified with the relatively rigid  $\text{CH}_2$  segments in the crystalline phase while the narrow line arises from flexible

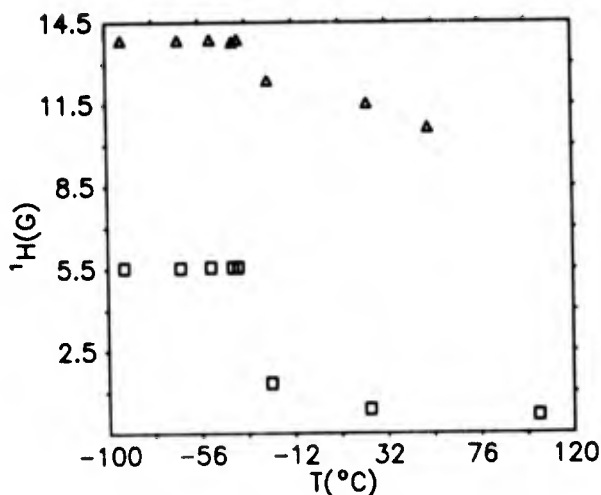


Fig. 3. Proton NMR linewidth (in gauss) vs. temperature in  $\text{PEO}_4:\text{LiCF}_3\text{COO}$ . Both components are shown (from ref. 26).

$\text{CH}_2$  segments in the elastomeric phase.  $^1\text{H}$  spectra of complexed PEO also exhibit two-phase behavior, with a somewhat broader crystalline component linewidth than that observed in pure PEO (approximately  $35^\circ\text{C}$ ). Fig. 3 demonstrates that motional narrowing also occurs for protons in  $\text{PEO}_4:\text{LiCF}_3\text{COO}$  (data taken from ref. 24). The temperature of the onset of the narrowing appears to be the same for both phases (approximately  $30^\circ\text{C}$ ), with the elastomeric phase exhibiting a greater motional effect.

A plot of  $^1\text{H}$   $T_1$  vs.  $1000/T$  for  $\text{PEO}_{4.5}:\text{NaClO}_4$  is shown in Fig. 4. From the local minimum occurring at about  $65^\circ\text{C}$ , a motional correlation time of about 400 ps can be inferred. It should be noted that both the broad and narrow  $^1\text{H}$  components of  $\text{PEO}_{4.5}:\text{NaClO}_4$  have approximately the same  $T_1$  value, indicating the presence of an efficient spin-diffusion mechanism.(66)

Berthier et al.(27) have found that  $^{19}\text{F}$  in  $\text{PEO}_8:\text{LiCF}_3\text{SO}_3$  also exhibits an NMR spectrum consistent with the presence of both a crystalline and an elastomeric phase. The linewidths associated with each phase differ sufficiently to allow computation of their relative concentrations as a function of temperature. The temperature dependences of the fractions of protons and fluorines in the crystalline phase of  $\text{PEO}_8:\text{LiCF}_3\text{SO}_3$  are shown in Fig. 5 (data taken from ref. 27). The discontinuity in the proton curve at 328 K is attributed to the melting of uncomplexed crystalline PEO. The absence of a similar feature in the fluorine curve indicates that the fraction of crystalline complex remaining above 328 K is salt-rich. It is of interest to note that certain PEO complexes such as  $\text{PEO}_8:\text{LiClO}_4$  exhibit no crystallinity above the melting point of pure PEO.(27)

$^{23}\text{Na}$  in  $\text{PEO}_{4.5}:\text{NaClO}_4$  produces a single-component lineshape with no detectable quadrupole broadening, even at temperatures as low as  $-100^\circ\text{C}$ . This finding is consistent with fourfold coordination of the  $\text{Na}^+$  ion which has

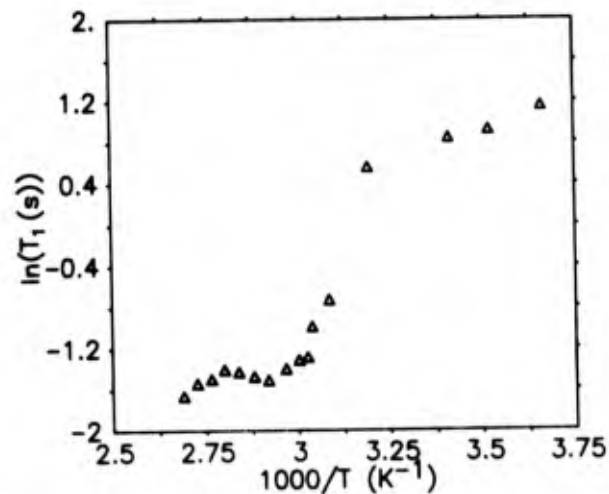


Fig. 4.  $^1\text{H}$   $T_1$  vs.  $1000/T$  in  $\text{PEO}_{4.5}:\text{NaClO}_4$ .

also been suggested by other investigations.(17) However,  $\text{PEO}_{10}:\text{NaI}$  does yield a quadrupole broadened  $^{23}\text{Na}$  spectrum (only the central  $1/2, -1/2$  transition is observed at low temperature(27)) which suggests that variations in stoichiometry (and/or anion) will affect the average coordination of the cation.

Finally, poly(vinyl acetate) complexed with  $\text{LiClO}_4$  also shows motionally narrowed  $^7\text{Li}$  NMR spectra.(43) Fig. 6 displays the temperature dependences of the full-width-at-half-maximum (FWHM)  $^7\text{Li}$  linewidth and  $^7\text{Li}$   $T_1$ . The similarity between PVAc- and PEO-based complexes (with respect to  $^7\text{Li}$  linewidths) suggests corresponding qualitative similarities of ion mobilities and perhaps transport mechanisms in the two different materials. The  $T_1$  data points yield an activation energy of  $0.11 \pm 0.03$  eV, about an order of magnitude less than the conductivity value which, again, is indicative of local motional processes sufficient for nuclear relaxation.

#### Electrical Relaxation

DR studies provide an alternative, often complementary method of probing the motion of ions and their local environments, and has been applied to the study of polymers by many workers. In the experiments performed by the author, values of the conductance,  $G$ , and capacitance,  $C$ , were determined using a fully automated micro-processor controlled bridge constructed by CGA Associates, Cleveland, Ohio. The bridge operates at five audio frequencies over the range 100-10,000 Hz in equal logarithmic intervals and is interfaced with an Apple IIe computer. Some of the measurements are two terminal while others are three terminal using the parallel plate guard ring configuration.(67) Aluminum electrodes are evaporated onto the faces of the samples. The bridge is usually operated in the "conductance" mode where  $G/\omega$  and  $C$  are read directly representing the equivalent parallel conductance and capacitance of the material. In general,

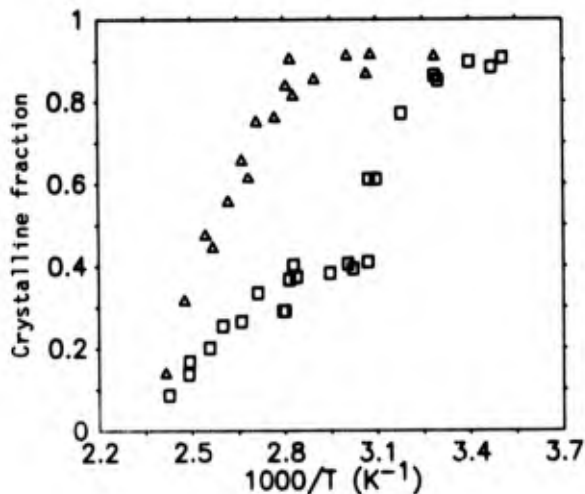


Fig. 5. Fractions of protons (squares) and fluorines (triangles) in the crystalline phase of  $\text{PEO}_8:\text{LiCF}_3\text{SO}_3$  (from ref. 27).

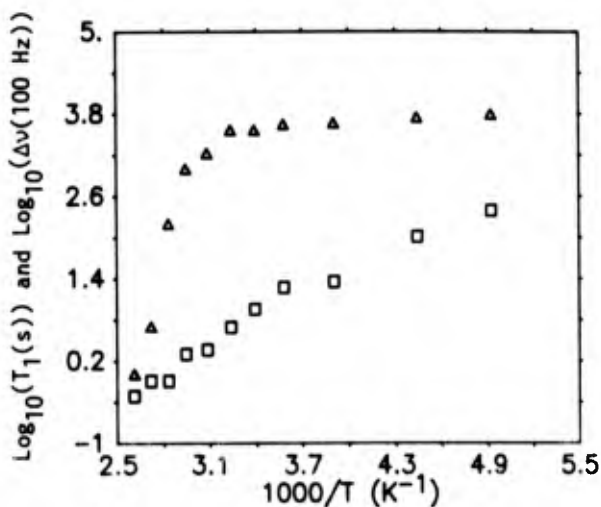


Fig. 6. Temperature dependences of  $^7\text{Li}$  linewidth (triangles) and  $T_1$  (squares) in  $\text{PVAcg}:\text{LiClO}_4$  (from ref. 43).

the value of the real part of the dielectric constant,  $\epsilon'$ , is determined at 300K and 1000 Hz using:

$$C = \epsilon_0 \epsilon' A/d \quad (1)$$

where  $A$  is the area of the plates and  $d$  is their separation.  $\epsilon_0$  is the permittivity of free space. In the absence of an experimental value for the linear thermal expansion coefficient, values of  $\epsilon'$  at all other temperatures and frequencies are determined from:

$$\epsilon'_T = \epsilon'_{300} C_T/C_{300} \quad (2)$$

Values of  $\epsilon''$  are then calculated from:

$$\epsilon'' = \epsilon' G/C\omega \quad (3)$$

and in some cases this is transformed to a conductivity via:

$$\sigma = \epsilon'' \epsilon_0 \omega \quad (4)$$

One important feature of the measurement system is that eight samples can be placed in the same sample holder which allows careful inter-comparison of samples.

Typical results for  $\epsilon''$  vs.  $T(\text{K})$  at low temperatures for "pure" PEO are shown in Fig. 7. (37) Two relaxations are observed in agreement with the literature. The first relaxation,  $\alpha_a$ , has been unambiguously associated with the glass transition.(46,47) The identification of the second relaxation,  $\gamma$ , is not so clear from the literature. It has been variously attributed to a "crankshaft mechanism,"(57,58) "3-bond" or "4-bond" motions,(59,60) "chain end hydroxyl groups"(47) or the " $\text{tg}+\text{t} \rightleftharpoons \text{tg}-\text{t}$ " transition.(55) In previous papers on dielectric relaxation in ion containing PEO(37-39) the data were interpreted in terms of the " $\text{tg}+\text{t} \rightleftharpoons \text{tg}-\text{t}$ " transition. However, by preparing deuterated samples of PEO, the authors have recently

obtained evidence that the  $\gamma$  relaxation in PEO is more likely to be due to hydroxyl groups at least some of which are probably at chain ends as suggested by Hedvig.(47) That data will be presented elsewhere. There is, however, one feature of the  $\gamma$  relaxation which is well documented. That is that the  $\gamma$  relaxation is essentially independent of the degree of crystallinity.(51) Consequently, in the discussion below concerning the  $\gamma$  relaxation, it is assumed that no distinction can be made between crystalline and amorphous phases of a given composition.

Figs. 8 and 9 show the relaxation spectrum for  $\text{PEO}_{4.5}:\text{NaSCN}$  and  $\text{PEO}_{4.5}:\text{KSCN}$ . The results for  $\text{PEO}_{4.5}:\text{LiSCN}$  are similar to those for  $\text{PEO}_{4.5}:\text{NaSCN}$ . There are no traces of  $\alpha_a$  in any of the complexed materials. This shows that no amorphous pure PEO exists in any of the complexed materials. This is confirmed by differential scanning calorimetry studies.(68) In most cases, however, a thermal event is observed at about  $60^\circ\text{C}$  which is usually attributed to pure crystalline PEO. These materials, of course, are not fully complexed.

Next, as seen in Fig. 8, the  $\gamma$  relaxation for  $\text{PEO}_{4.5}:\text{NaSCN}$  is very similar to that for "pure" PEO. At first sight this would appear to be due to pure PEO. However, the materials are not very conductive(37) in agreement with the literature for highly complexed material. Further, the intensity of the peak is not diminished over that for "pure" PEO. Consequently, it was concluded(37) that the structure of the complexed polymer is not significantly different from that of "pure" PEO. The current interpretation of these results is that the sodium ions are smaller than the helical tunnel radius,(22) and this, combined with the linear configuration of the anion do not produce severe distortions in the polymer chains. More recent work by the authors show that there are, indeed, small differences between the DR spectrum for  $\text{PEO}_{4.5}:\text{NaSCN}$  and

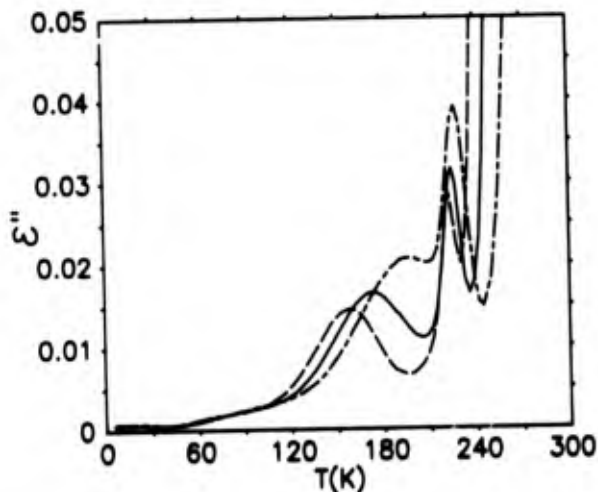


Fig. 7.  $\epsilon''$  vs.  $T(K)$  for "pure" PEO (from ref. 37). The frequencies are: dash, 100 Hz; solid, 1,000 Hz; chain link, 10,000 Hz.

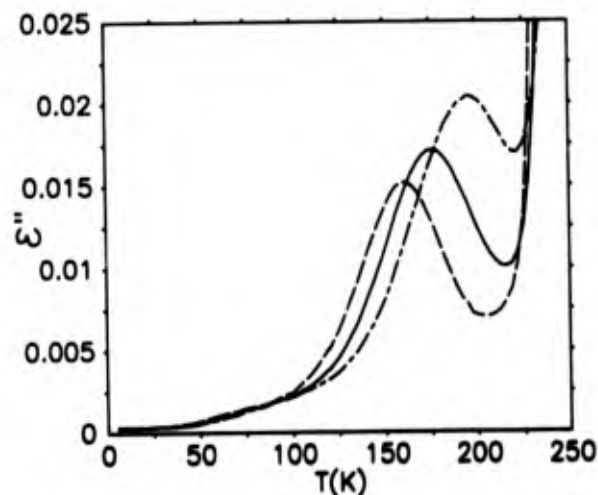


Fig. 8.  $\epsilon''$  vs.  $T(K)$  for  $PEO_{4.5}:NaSCN$  (from ref. 37). The frequencies are: dash, 100 Hz; solid, 1,000 Hz; chain link, 10,000 Hz.

that for "pure" PEO confirming that the peak is indeed attributable to complexed material and thus supporting the conclusions of the earlier report.(37) The new work will be presented in detail elsewhere.

However, as can be seen in Fig. 9, for  $PEO_{4.5}:KSCN$ , there is a drastic change in the  $\gamma$  relaxation region with at least three peaks being observed. Consequently, it was concluded(37) that the chains contain severe local distortions. This trend has recently been confirmed by the x-ray work of Hibma.(28)

A second example of large changes in the  $\gamma$  relaxation region is shown in Fig. 10 where some results for  $PEO_{4.5}:LiCF_3SO_3$  are plotted. At least three relaxations are seen, none of which corresponds to the  $\gamma$  relaxation in "pure" PEO or to those observed in  $PEO_{4.5}:KSCN$ , for example. These results are interesting because there has been a great deal of work on this material. Careful studies of the variation of these relaxations with salt concentration are presently being carried out in an attempt to better understand the structure of these materials and hence gain insight into the origin of the various relaxations.

A final example of the type of relaxation phenomena observed in these materials is shown in Fig. 11 where  $\epsilon''$  vs.  $T(K)$  is plotted for  $PEO_{4.5}:NaI$ . The results are interesting as the temperature variation of the two relaxations is very similar to that observed for those in  $PEO_{4.5}:LiCF_3SO_3$ . Further work is necessary concerning this result.

As is apparent from the discussion thus far, the main thrust of the work to date has been to use DR to learn about materials. However, work has also begun toward using the materials to learn about DR. In particular, efforts are being made to evaluate the data in the light of various recent theories of DR.(44,45,69,70) An example of some preliminary results in this area are given in Fig. 12 via a "universal" plot of DR for the  $\gamma$  relaxation in "pure" PEO. That

plot is constructed by best-fitting only five frequencies at a variety of temperatures. The best-fit curve is the theoretical form usually employed by Jonscher.(69,70) A new, fully-automated complex impedance measuring assembly operating at seventeen approximately equal logarithmic frequency intervals over the frequency range 10-100,000 Hz is currently operational and will make it easier to obtain plots such as Fig. 12.

#### High Pressure Electrical Conductivity

Of primary importance for these materials is the electrical conductivity. Typical high temperature conductivities are shown in Fig. 13. In order to gain information concerning electrical transport in these materials, the effect of high pressure on the electrical conductivity has been studied. The results for  $PEO(36)$  can be summarized as follows.

The magnitude of the variation of the electrical conductivity with pressure, and hence activation volume given by:

$$v = -kT(\partial \ln G / \partial P) \quad (5)$$

scale with the size of both the anion and cation. The simplest interpretation of this is that both the anions and cations are mobile. This agrees with several recent works concerning this material.(9,10,12,13,23) One of the ambiguities associated with these results, however, is that PEO is a multiphase system. For example, "pure" crystalline PEO forms easily and thus one must be concerned with the effects of pressure on the phase equilibrium. In order to eliminate this ambiguity, studies have recently been carried out on the effects of pressure on sodium salts in Parel (Hercules, Inc.), a highly elastomeric material consisting mostly of poly(propylene oxide) (PPO). The effects of pressures up to 0.3 GPa on the conductivity in this material are shown in Fig.



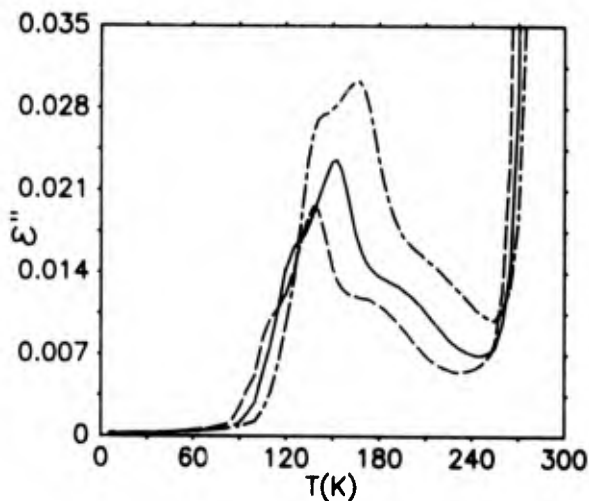


Fig. 9.  $\epsilon''$  vs.  $T(K)$  for  $PEO_{4.5}:KSCN$  (from ref. 37). The frequencies are: dash, 100 Hz; solid, 1,000 Hz; chain link, 10,000 Hz.

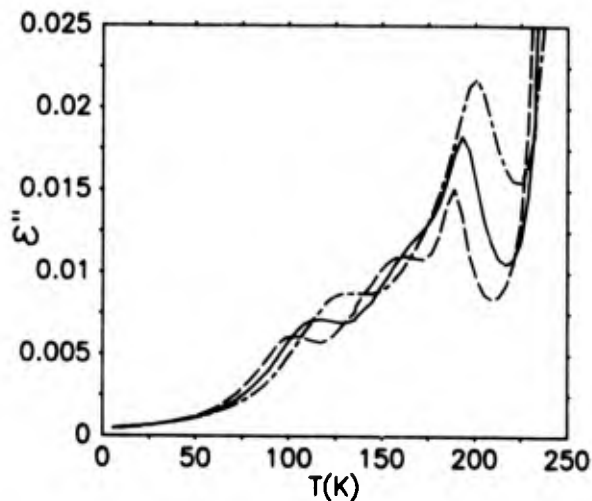


Fig. 10.  $\epsilon''$  vs.  $T(K)$  for  $PEO_{4.5}:LiCF_3SO_3$ . The frequencies are: dash, 100 Hz; solid, 1,000 Hz; chain link, 10,000 Hz.

14. It is clear that the activation volume is much larger for  $PPO_8:NaClO_4$  than for  $PPO_8:NaSCN$ . This result is very similar to that observed in  $PEO_8:NaClO_4$  and  $PEO_8:NaSCN$  and thus the likelihood that this effect is due to phase equilibrium of a pure crystalline phase with the conducting phase is eliminated. These results, do not, of course rule out the possibility that other phases may be affecting the data.

Finally, the order of magnitude of the pressure dependence of the conductivity in PPO-alkali metal salt complexes is very similar to that for PEO-alkali metal salt complexes.(36) Consequently, these results have the same implication concerning the transport mechanism in PPO as in PEO. Specifically, the fact that the conductivity decreases with pressure argues against a "chain transfer" transport mechanism.(71) The reason is that the effect of pressure is to decrease the spacing between the chains and thus should make jumps between chains easier. Further, the magnitude of the decrease of conductivity with pressure is too large to be consistent with an intrahelical jumping process.(5) Specifically, the motion of the ions through the helical tunnels would not be expected to be greatly affected by pressure as the tunnels, themselves, should not be greatly affected. (Further evidence against this transport mechanism has recently been obtained by Dupon et al.(20)) This can be made quantitative via an approximate mode Gruneisen parameter defined by:

$$\gamma_a = -(\partial \ln \omega_a / \partial \ln V) \quad (6)$$

which can be calculated from:

$$v = 2\gamma_a g \chi \quad (7)$$

where  $g$  is the Gibb's energy and  $\chi$  is the compressibility. Approximate values of  $\chi$  and  $g$  yield  $\gamma_a = 2$ . This is much larger than mode

gammas for intrachain vibrations(72) which would govern the intrahelical jumping process. Consequently, it was concluded that interchain fluctuations govern the transport mechanism and are the origin of an "interstice-interstice" jumping process.(36) In that paper, it was postulated that the ions move through the spaces between the polymer chains. In support of this is the fact that fast ion transport has now been observed in a wide variety of polymers as mentioned above and thus fast ion transport does not seem to require a specific chain structure. One final comment is that it appears that fast ion motion usually occurs only above the glass transition. Consequently, it appears that chain mobility also contributes to the conductivity.(5,17,22) This factor is consistent with the "interstice-interstice" jumping process in that it adds chain translation to chain vibration as a factor responsible for fast ion motion. Of course, there may be still other contributions to the decrease of conductivity with pressure and, in fact, "association" of the ions with the chains or with each other may contribute. The extent to which this factor is important has yet to be determined.

#### Summary

While the NMR results for several ion conducting polymeric systems reveal qualitatively similar features such as "classic" motional narrowing behavior common to superionic solids, there exist some important differences between specific compositions. For example, changing the anion and/or the polymer/salt ratio has been observed to affect macroscopic properties such as the glass transition and microscopic structural arrangements such as the average cation coordination. Future  $T_1$  studies for a greater variety of complexes are expected to lead to a better understanding of local hopping processes which, ultimately, may

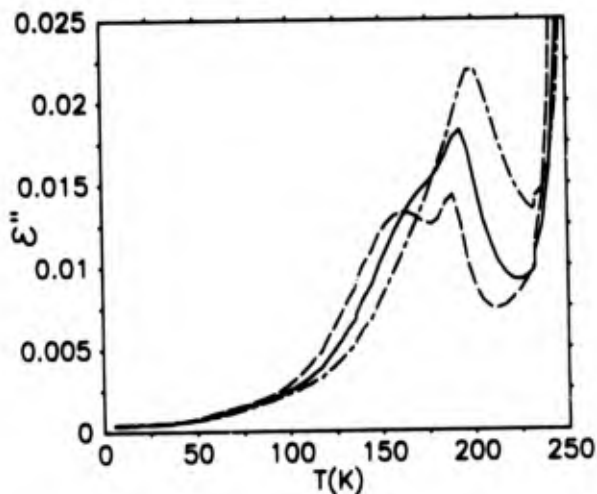


Fig. 11.  $\epsilon''$  vs.  $T(K)$  for  $PEO_{4.5}:NaI$ . The frequencies are: dash, 100 Hz; solid, 1,000 Hz; chain link, 10,000 Hz.

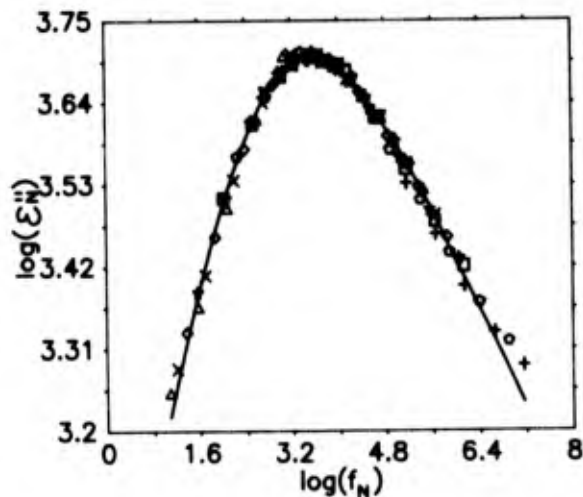


Fig. 12. "Universal" plot for the  $\gamma$  relaxation "pure" PEO.

provide insight into conduction mechanisms. Electrical relaxation is well established as a very useful tool in studying ion conducting polymers. Changes in chain structure can be detected in addition to multiphase behavior. Finally, the effects of high pressure on the electrical conductivity provide useful information concerning the transport mechanism. The best picture at the present time is that in both PEO and PPO, both anions and cations move via an "interstice-interstitial" jumping process. It is clear that more study is warranted, particularly with regard to systematic identification of compositional parameters which result in different kinds of structural or dynamic behavior.

#### Acknowledgments

The authors would like to thank Mary C. Wintersgill of U.S.N.A. for many helpful discussions and a critical reading of the manuscript. This work was supported in part by the Office of Naval Research. S.G.G. also acknowledges support from the Research Corporation.

1. A. Hooper and J. M. North, *Solid State Ionics* **9&10**, 1161 (1983).
2. D. E. Fenton, J. M. Parker, and P. V. Wright, *Polymer* **14**, 589 (1973).
3. P. V. Wright, *Br. Polym. J.* **7**, 319 (1975).
4. P. V. Wright, *J. Polymer Sci.: Polymer Phys.* **14**, 955 (1976).
5. M. B. Armand, J. M. Chabagno and M. J. Duclot, in *Fast Ion Transport in Solids*, J. N. Mundy and G. K. Shenoy, Eds., Pergamon Press, New York, 1979, p. 131.
6. C. C. Lee and P. V. Wright, *Polymer* **23**, 681 (1982).
7. D. R. Payne and P. V. Wright, *Polymer* **23**, 690 (1982).
8. J. M. Parker, P. V. Wright, and C. C. Lee,

- Polymer* **22**, 1305 (1981).
9. P. R. Sorensen and T. Jacobsen, *Electrochimica Acta* **27**, 1671 (1982).
10. P. R. Sorensen and T. Jacobsen, *Solid State Ionics* **9&10**, 1147 (1983).
11. P. R. Sorensen and T. Jacobsen, *Polymer Bulletin* **9**, 47 (1983).
12. J. E. Weston and B. C. H. Steele, *Solid State Ionics* **2**, 347 (1981).
13. J. E. Weston and B. C. H. Steele, *Solid State Ionics* **7**, 75 (1982); **81** (1982).
14. W. I. Archer and R. D. Armstrong, *Electrochimica Acta* **25**, 1689 (1980).
15. W. I. Archer and R. D. Armstrong, *Electrochimica Acta* **26**, 167 (1981).
16. B. L. Papke, R. Dupon, M. A. Ratner, and D. F. Shriver, *Solid State Ionics* **5**, 685 (1981).
17. B. L. Papke, M. A. Ratner, and D. F. Shriver, *J. Phys. Chem. Solids* **42**, 493 (1981).
18. R. Dupon, D. H. Whitmore, and D. F. Shriver, *J. Electrochem. Soc.* **128**, 715 (1981).
19. D. F. Shriver, B. L. Papke, M. A. Ratner, R. Dupon, T. Wong, and M. Brodwin, *Solid State Ionics* **5**, 83 (1981).
20. R. Dupon, B. L. Papke, M. A. Ratner, D. H. Whitmore, and D. F. Shriver, *J. Am. Chem. Soc.* **104**, 6247 (1982).
21. B. L. Papke, M. A. Ratner, and D. F. Shriver, *J. Electrochem. Soc.* **129**, 1434 (1982).
22. B. L. Papke, M. A. Ratner, and D. F. Shriver, *J. Electrochem. Soc.* **129**, 1694 (1982).
23. A. V. Chadwick, J. H. Strange, and M. R. Worboys, *Solid State Ionics* **9&10**, 1155 (1983).
24. C. K. Chiang, G. T. Davis, C. A. Harding, and J. Aarons, *Solid State Ionics* **9&10**, 1121 (1983).
25. C. Robitaille and J. Prud'homme, *Macromolecules* **16**, 665 (1983).
26. F. L. Tanzella, W. Bailey, D. Frydrych, G. C. Farrington and H. S. Story, *Solid State Ionics*, **5**, 681 (1981).
27. C. Berthier, W. Gorecki, M. Minier, M. B. Armand, J. M. Chabagno and P. Rigaud, *Solid State Ionics*, **11**, 91 (1983).

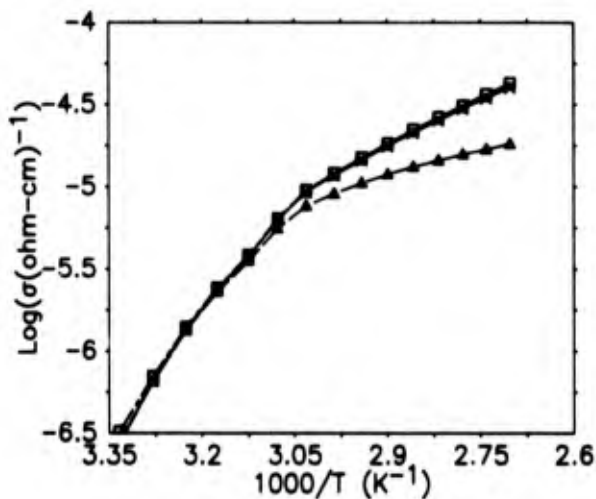


Fig. 13.  $\text{Log}_{10}(\sigma(\text{ohm-cm})^{-1})$  for  $\text{PEO}_{0.5}\text{NaI}$ . The frequencies are: triangles, 100 Hz; x, 1,000 Hz; squares, 10,000 Hz.

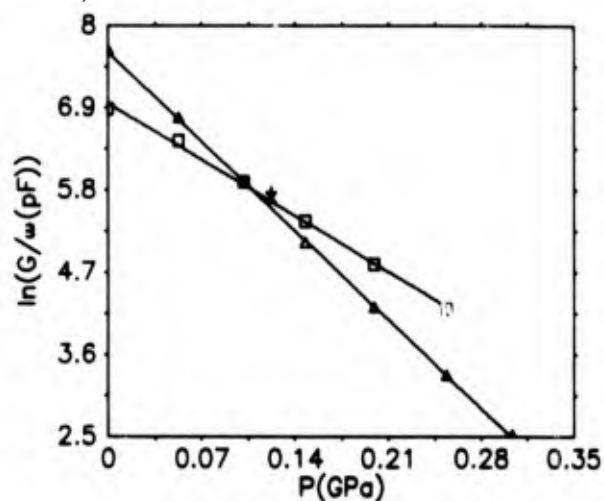


Fig. 14.  $\ln(G/\omega(\text{pF}))$  vs.  $P(\text{GPa})$  for  $\text{PPOg}:\text{NaSCN}$  (squares and plus) and  $\text{PPOg}:\text{NaClO}_4$  (triangles and x) at  $86.9^\circ\text{C}$ .

28. T. Hibma, *Solid State Ionics* **9&10**, 1101 (1983).
29. C. A. C. Sequeira and A. Hooper, *Solid State Ionics* **9&10**, 1131 (1983).
30. M. Minier, C. Berthier, and W. Gorecki, *Solid State Ionics* **9&10**, 1125 (1983).
31. C. R. A. Catlow, A. V. Chadwick, G. N. Greaves, L. M. Moroney, and M. R. Worboys, *Solid State Ionics* **9&10**, 1107 (1983).
32. A. Killis, J.-F. Le Nest, A. Gandini, H. Cheradame, and J.-P. Cohen-Addad, *Polymer Bulletin* **6**, 351 (1982).
33. A. Killis, J.-F. Le Nest, A. Gandini, and H. Cheradame, *Macromolecules* **17**, 63 (1984).
34. A. Killis, J.-F. Le Nest, and H. Cheradame, *Makromol. Chem., Rapid Commun.* **1**, 595 (1980).
35. E. Tsuchida, H. Ohno, K. Tsunemi, and N. Kobayashi, *Solid State Ionics* **11**, 227 (1983).
36. J. J. Fontanella, M. C. Wintersgill, J. P. Calame, F. P. Pursel, D. R. Figueroa, and C. G. Andeen, *Solid State Ionics*, **9&10**, 1139 (1983).
37. J. J. Fontanella, M. C. Wintersgill, J. P. Calame, and C. G. Andeen, *Solid State Ionics*, **8**, 333 (1983).
38. M. C. Wintersgill, J. J. Fontanella, J. P. Calame, D. R. Figueroa, and C. G. Andeen, *Solid State Ionics*, **11**, 151 (1983).
39. J. J. Fontanella, M. C. Wintersgill, J. P. Calame, and C. G. Andeen, *J. Polymer Sci.: Polymer Phys.*, submitted.
40. M. Watanabe, M. Kanba, H. Matsuda, K. Tsunemi, K. Mizoguchi, E. Tsuchida, and I. Shinohara, *Makromol. Chem., Rapid Commun.* **2**, 741 (1981).
41. M. Watanabe, K. Nagaoka, M. Kanba, and I. Shinohara, *Polymer Journal* **14**, 877 (1982).
42. R. Dupon, B. L. Papke, M. A. Ratner, and D. F. Shriver, submitted for publication.
43. M. C. Wintersgill, J. J. Fontanella, J. P. Calame, S. G. Greenbaum, and C. G. Andeen, *J. Electrochem. Soc.*, to be published.
44. K. L. Ngai, *Comments Solid State Phys.* **9**, 141 (1980).
45. K. L. Ngai, *Solid State Ionics* **5**, 27

- (1981).
46. N. G. McCrum, B. E. Read, and G. Williams, *Anelastic and Dielectric Effects in Polymeric Solids*, (John Wiley & Sons, New York, 1967).
47. P. Hedvig, *Dielectric Spectroscopy of Polymers*, (Adam Hilger Ltd., Bristol, 1977).
48. G. M. Bartenev and Yu. V. Zelenev, Editors, *Relaxation Phenomena in Polymers*, (John Wiley & Sons, New York, 1974).
49. N. Koizumi and T. Hanai, *J. Phys. Chem.* **60**, 1496 (1956).
50. T. M. Connor, B. E. Read and G. Williams, *J. Appl. Chem.* **14**, 74 (1964).
51. Y. Ishida, M. Matsuo, and M. Takayanagi, *J. Polym. Sci.* **B3**, 321 (1965).
52. K. Hikichi and J. Furuichi, *J. Polym. Sci.* **A3**, 3003 (1965).
53. K. Arisawa, K. Tsuge and Y. Wada, *Jap. J. of Appl. Phys.* **4**, 138 (1965).
54. C. H. Porter and R. H. Boyd, *Macromolecules* **4**, 589 (1971).
55. T. Suzuki and T. Kotaka, *Macromolecules* **13**, 1495 (1980).
56. K. Se, K. Adachi, and T. Kotaka, *Polymer Journal* **11**, 1009 (1981).
57. T. F. Schatzki, *J. Polymer Sci.*, **57**, 496 (1962).
58. R. F. Boyer, *Rubber Rev.*, **35**, 1303 (1963).
59. B. Valeur, J. Jarry, F. Geny, and L. Monnerie, *J. Polymer Sci.: Polymer Phys.*, **13**, 667 (1975).
60. B. Valeur, L. Monnerie, and J. Jarry, *J. Polymer Sci.: Polymer Phys.*, **13**, 675 (1974).
61. D. Brinkmann, *Solid State Ionics* **5**, 53 (1981).
62. J. L. Bjorkstam, M. Villa, *Magnetic Resonance Review* **6**, 1 (1980).
63. J. B. Boyce, S. A. Huberman, *Phys. Reports* **51**, 191 (1979).
64. C. Berthier, in *Fast Ion Transport in Solids*, P. Vashishta, J. N. Mundy, G. K. Shenoy, eds. (North Holland, Amsterdam, 1979), p. 171.
65. N. Bloembergen, E. M. Purcell, and R. V. Pound, *Phys. Rev.* **73**, 679 (1948).

66. A. Abragam, Principles of Nuclear Magnetism, (Oxford University Press, Oxford, 1978).
67. C. G. Andeen, J. J. Fontanella, M. C. Wintersgill, P. J. Welcher, R. J. Kimble, and G. E. Matthews, Jr., J. Phys. C: Solid State Phys., 14, 3557 (1981).
68. M. C. Wintersgill, J. J. Fontanella, J. P. Calame, and C. G. Andeen, unpublished work.
69. A. K. Jonscher, Nature 267, 673 (1977).
70. A. K. Jonscher, Phys. Stat. Sol. (b) 83, 585 (1977); 84, 159 (1977).
71. M. Armand, Solid State Ionics 9&10, 745 (1983).
72. C. K. Wu, G. Jura, and M. Shen, J. Appl. Phys. 43, 4348 (1972).

## Electrical Relaxation in Oxide Glasses

H. Jain  
Brookhaven National Laboratory  
Upton, NY 11973

and

K. L. Ngai  
Naval Research Laboratory  
Washington, D.C. 20375-5000

### Abstract

Electrical relaxations of mobile ions in ionic conductors are reviewed.

#### 1. INTRODUCTION

Due to its technological importance the electrical behavior of common oxide glasses has been studied extensively. A large number of these studies have been conducted to determine the compositional and structural dependence of electrical conductivity, but during this course basic knowledge of ionic conduction has also evolved [1-5]. In recent years the interest in electrical behavior of glasses has increased considerably because of their potential use as solid electrolytes [6]. The information concerning ionic motion is also useful in the development of high leach resistance nuclear waste glasses [7]. Because of such enhanced interest and improved experimental techniques, more accurate and extensive data on better characterized samples are available now, which in turn has helped in developing a microscopic picture of the electrical behavior of glasses.

The subject of electrical relaxation is a description of the time-dependent response of a given system (mobile ions in a glass in our case) under the application of an electric field. With emphasis on the latest developments, the present paper is an overview of this phenomenon as observed in oxide glasses. This paper is not meant to be an exhaustive review of all the available data; small quantitative differences among various glass systems are not discussed here in any detail.

#### 2. EXPERIMENTAL OBSERVATIONS

The usual method of studying electrical relaxation in glasses is to prepare a disc-shaped specimen with thin film metal electrodes deposited on its two parallel faces. An ac

bridge or similar arrangement is used to measure conductance (G) and capacitance (C) of the specimen assembly as a function of frequency ( $\omega=2\pi f$ ). At very low frequencies such information may be obtained from the charging and discharging current response under an electric field [5]. Generally, the procedure is repeated to collect data at a series of temperatures depending on the instrumentation limits. Note that the specimen is represented here as a parallel combination of a resistor and a capacitor. The applied ac signal is sufficiently small so that the values of G and C can be treated as field independent.

All the experimental information regarding electrical relaxation at a given temperature is contained in G( $\omega$ ) and C( $\omega$ ). For various reasons, these variables may be transformed into complex resistivity ( $\rho^*$ ), complex modulus ( $M^*$ ), complex permittivity ( $\epsilon^*$ ) or some other formalism. Considering the confusion generated by the frequent interchange of various formalisms in literature, it is important to remember that such transformations may emphasize and therefore, help resolve one particular aspect of the relaxation process, but no new information, which was not already included in G( $\omega$ ) and C( $\omega$ ), can be extracted. Details of these formalisms may be found in recent monographs [8,9]. For a specimen of unit thickness and unit area of cross section

$$\rho^* \equiv \rho' - i\rho'' = \frac{G}{G^2 + \omega^2 C^2} - i \frac{\omega C}{G^2 + \omega^2 C^2} \quad (1)$$

$$M^* \equiv M' + iM'' = \frac{\omega^2 C}{G^2 + \omega^2 C^2} + i \frac{\omega G}{G^2 + \omega^2 C^2} \quad (2)$$

and

$$\epsilon^* \equiv 1/M^* \quad (3)$$

Also, complex conductivity

$$\sigma^* \equiv 1/\rho^* \quad (4)$$

and loss tangent

$$\tan \delta \equiv \epsilon''/\epsilon' = G/\omega C \quad (5)$$

From Eqs. (1) and (2) it is clear that a plot of  $\rho''$  or  $M''$  vs  $\log \omega$  will be a Debye peak at  $\omega\tau=1$  where  $\tau=RC$  is the time constant ( $R=1/G$  is the resistance). The  $\rho'$  or  $M'$  vs  $\log \omega$  plot will give a sigmoidal curve with point of inflection at  $\omega\tau=1$ . On a complex plane  $\rho''$  vs  $\rho'$ , or  $M''$  vs  $M'$  will show a semicircle passing through origin. However, the experimental data for any system measured over sufficiently large frequency range rarely agrees with this description, thus suggesting that the specimen cannot be treated simply as a parallel combination of a resistive and a capacitive element. An obvious reason for this departure from the behavior of an ideal capacitor is that a real sample usually consists of a discontinuity at the electrode/glass interface which has different polarization properties than the bulk of the specimen. In many instances this configuration can be approximated to a series combination of two parallel R-C elements.

The electrode interface polarization is a highly capacitive phenomenon and, therefore, has much larger time constant than the bulk phenomena. Complex resistivity plots ( $\rho''$  vs  $\rho'$ ) are generally used to separate these two effects, each appearing as an arc of a semicircle [10-15]. A typical example of complex impedance data is shown in Fig. 1. The bulk conductivity (also referred as dc conductivity) is given by the intersection of the high frequency semicircle with the real axis, as shown by the arrows in the figure. Figure 1(b) shows that the bulk resistivity obtained in this fashion, as expected, varies according to the specimen thickness (which is proportional to volume for fixed cross section) and is independent of the electrode effects. Thus, we can separate the surface area dependent electrode phenomena from such plots. The arc in Fig. 1(a) or the high frequency segments in Fig. 1(b) primarily represent the behavior of the bulk of the glass and will therefore be the focus of the present discussion. In phase separated glasses the electrochemical discontinuity at interphase boundary, or at the hydrated surface of silicate glasses [13] can lead to an additional arc, but such complex phenomena are not to be included in the discussion.

A close examination of the bulk data such as shown in Fig. 1(a) indicates that it does not fall on a semicircle as expected from an ideal capacitor. Instead, the data can be better approximated to an arc of a semicircle whose center lies below the real axis. This departure from the ideal behavior can also be observed in

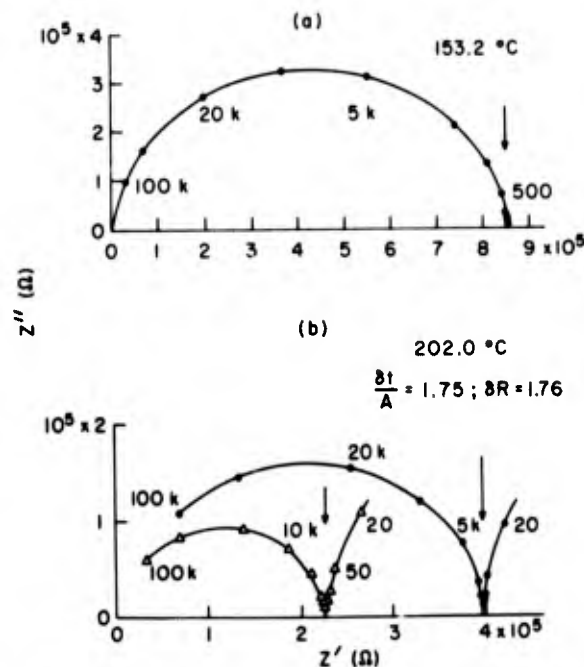


Fig. 1. Complex impedance plots for two borate glasses. (a) Sodium borate glasses at 153.2°C. (b) Lithium borate glass of two different thicknesses ( $t$ ), but the same electrode area ( $A$ ). The implicit parameter, frequency, is identified for some of the data points. The arrows indicate the value of bulk resistance [15].

$\rho''$  or  $M''$  vs  $\log \omega$  plot as shown in Fig. 2 for a lithium borate glass [16]. In this case we find that the peaks are asymmetric as well as wider than expected from a Debye peak which has the full width of 1.144 decades at half the maximum. Also note that the positions of  $M''$  and  $Z''$  ( $\rho''$ ) peaks do not coincide. Almond and West [17] have analytically treated this non-ideal frequency dispersion by adding a frequency dependent admittance element to the equivalent circuit of an ideal dielectric.

Macedo et al. [18] have proposed that since the conduction related phenomena in the present context may be considered due to the series processes of ionic motion and the highly capacitive phenomena are suppressed in  $M''$  vs  $\log \omega$  plots, the experimental data should be analyzed preferably in the modulus formalism. Figure 3 shows  $M''$  vs  $\log \omega$  plots at seven different temperatures for potassium trisilicate glass obtained by Boesch et al. [19] over the frequency range of eight orders of magnitude. From such data it is interesting to note that the peak frequency in these plots shows the same temperature dependence as dc conductivity [20]. For this reason the behavior of  $M''$  vs  $\log \omega$  has been often identified as conductivity relaxation.

Traditionally, complex permittivity formalism has been employed to describe the dielectric

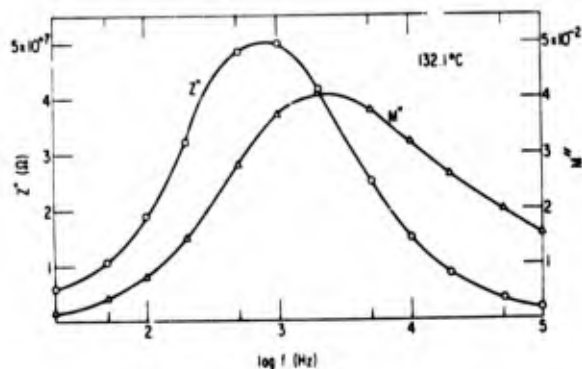


Fig. 2. Imaginary parts of complex impedance  $Z''$  and modulus  $M''$  vs log frequency ( $f$ ) at 132.1°C for lithium borate glass [16].

relaxation phenomena [21]. In this formalism

$$\epsilon^* \equiv \epsilon' - i\epsilon'' = C/C_0 - iG/\omega C_0 \quad (6)$$

where  $C_0$  is the equivalent capacitance of the free space. In the ideal case of frequency independent conductivity ( $G=G_0$ ) and dielectric constant,  $\epsilon''$  decreases monotonically as  $\omega$ . Therefore, to study frequency dependent or purely ac relaxation effects, it is often thought that it is better to subtract the dc contribution from the observed value i.e.

$$\epsilon''_{ac} = (G - G_{dc})/\omega C_0 \quad (7)$$

The usefulness of Eq. (7) is realized best where  $G_{dc}$  is negligible such as in the study of dipolar relaxation in a quartz crystal at low temperatures [22]. Here,  $\epsilon''$  vs log  $\omega$  at constant temperature, or  $\epsilon''$  vs  $T$  at a fixed frequency shows a Debye-like peak due to the reorientation of dipoles between two equivalent positions. It does not involve any long-range atom movement and usually has lower activation energy than does dc conductivity. This kind of local motion of alkali ions in alkali trisilicate glasses has been studied by Agarwal and Day [23] using thermally stimulated depolarization current technique below room temperature. However, as noted above nearly the same activation energy for dc conductivity and conductivity relaxation indicates that both of these phenomena are very closely related. It has been, therefore, argued that subtraction of dc conductivity (Eq. (7)) in the present context may be somewhat artificial [18]. Moreover, in many cases the determination of  $G_{dc}$  may not be trivial. Then, for a glass the use of an  $M''$  vs log  $\omega$  plot and study of its departure from Debye peak are preferred methods to understand conductivity relaxation.

To summarize the experimental observations, the electrical relaxation in glass is related to the long-range migration of charge carriers. It manifests itself as a departure from the ideal behavior of frequency independent conductance

and capacitance. It can be observed in the frequency and temperature region where the electrode, the surface layer, the interphase (in phase separated glasses) and the local ion jump phenomena are not dominant. Most commonly it is described as the peak in  $\epsilon''$  vs log  $\omega$  plot or non-Debye behavior of  $M''$  vs log  $\omega$  plot.

### 3. ANALYTICAL EMPIRICAL MODELS

When an externally applied electric field across a solid is turned off, an ideal system under thermal equilibrium will respond according to

$$E(t) = E(0) \exp(-\frac{t}{\tau}) \quad (8)$$

where  $E(t)$  is the field strength at time  $t$  and  $\tau$  is the relaxation time. However, in a real glass specimen  $\tau$  usually does not have a unique value and is usually represented by a "distribution function"  $g(\tau)$  i.e.

$$E(t) = E(0) \int_0^{\infty} g(\tau) \exp(-\frac{t}{\tau}) d\tau = E(0) \phi(t) \quad (9)$$

Clearly, the form of  $\phi(t)$  or equivalently  $g(\tau)$  is the key factor in describing the experimental observations. Moynihan, Macedo and co-workers [18-20, 24-25] have extensively analyzed their electrical modulus data on several glasses using this approach where

$$M^* = M_s \int_0^{\infty} dt g(\tau) [i\omega\tau / (1+i\omega\tau)] \quad (10)$$

where  $M_s$  is the inverse of static dielectric constant. They find that the data of alkali silicate glasses and a glass-forming 40%  $\text{Ca}(\text{NO}_3)_2$ -60%  $\text{KNO}_3$  fused salt mixture can be best described by the fractional exponential (Williams-Watts [26]) function

$$\phi(t) = \exp[-(t/\tau_p)^\beta] \quad 0 < \beta \leq 1 \quad (11)$$

where  $\tau_0$  and  $\beta$  are relaxation parameters. Williams and Watts [26] have proposed the empirical function [11] (previously used to describe mechanical relaxations by others [27]) for the primary dielectric relaxations of fixed dipoles in several viscous liquids and a few polymers. Its general applicability has been brought out by one of us by an exhaustive examination of available data of many more viscous liquids and glasses [28-30]. We have also extended the discovery of Moynihan and Macedo that ionic conductivity relaxation is also well-described by the same empirical function to other ionic conductors [29,31-34] including concentrated aqueous lithium chloride solutions, lithium borate glasses, an  $\text{Ag}_7\text{I}_4\text{AsO}_4$  glass and Na $\beta$ alumina; and to electronic conductors [35] such as lightly-doped polyacetylene. The discovery of Moynihan and Macedo is important for anyone who is making an attempt to construct a theoretical model to explain the empirical relaxation function given by Eq. (11). The theoretical model would not be any good unless it leads to Eq. (11) naturally

for both fixed dipoles and for mobile charged carriers.

As noted earlier, the electrical relaxation on complex impedance plane (Fig. 1(a)) is observed in terms of an arc of a semicircle with center below the real axis. Ravaine and Souquet [11] have found that for a given glass system the centers of such arcs obtained at different temperatures fall on a straight line which passes through origin making an angle  $-\alpha$  with the real axis. They analyze their data using the Cole-Cole function which gives

$$Z^* \propto \frac{1}{1+(i\omega\tau)^{1-\alpha}} \quad 0 < \alpha < 1 \quad (12)$$

although the data show small but systematic departure from theory. The commonly used expressions (11), (12), or  $[(1+i\omega\tau)^{-\beta}]$  due to Cole- Davidson [26] are described by a single distribution parameter ( $\alpha$ ,  $\beta$ , etc.).

#### 4. PHYSICAL MODELS

The analytical expressions as mentioned in the previous section are empirical forms to describe experimental data, and do not give any physical insight of the relaxation mechanisms. In this section we examine the development of various physical models with particular reference to electrical relaxation in glasses. Most of these models make use of the non-crystalline and random nature inherent to glasses. In the latter part of the section, recent approaches to the relaxation phenomena as being due to the very fundamental nature of condensed matter are discussed.

##### (a) Distribution of Activation Energies Model

Stevens [37] and Taylor [38] were the first to recognize that the lack of translational symmetry in a glass could contribute to electrical polarization as an ion moves. In their model an ion moving in a glass must overcome energy barriers which are of varying heights due to the lack of periodicity. As can be seen in Fig. 1 of Ref. 18, varying amounts of charges are accumulated against barriers of different heights. Thus, the system is polarized and electrical conductance and capacitance become frequency dependent. In comparison, in an ideal crystal all energy barriers are of the same height and the charge is uniformly shifted under the influence of an electric field. Macedo et al. [18] have extended this concept of distribution of activation energies to the data on aluminosilicate glasses using two log gaussian energy distribution functions. In this regard, it is interesting to note that the distribution of activation enthalpy in glasses appears to be rather narrow [19,39]. Boesch and Moynihan [19] from the temperature dependence of relaxation spectra of silicate glasses (Fig. 3) show that the distribution of electrical relaxation time

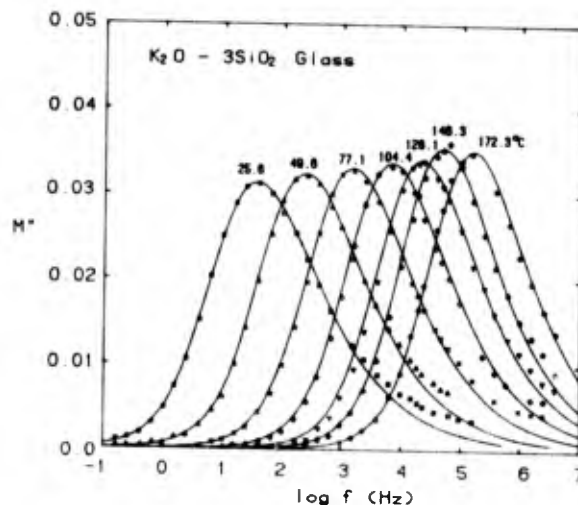


Fig. 3. A replot of the data of  $M''$  vs log frequency for potassium trisilicate glass at seven different temperatures [19].

arises primarily from the distribution in pre-exponential factor containing attempt frequency, entropy, and structure related factors, rather than in activation enthalpy.

##### (b) Random Orientation Model

In analogy to crystals, Charles [40] postulated electrical conduction in glasses due to the migration of point defects. For example, in a sodium silicate glass several equivalent sites for sodium are assumed around each non-bridging oxygen. A sodium ion may then move in an interstitial fashion by jumping between empty sites. Because of random distribution of non-bridging oxygen ions, a sodium ion changes its orientation randomly. Similar mechanisms have been proposed [41,42] assuming that there are only two stable sites for each moving ion. DC conductivity is then considered as the long range random walk of a charged ion and ac phenomena as due to the hopping of "bound" charges between nearest neighbor sites. This mechanism can be likened to dipolar relaxation except that an ion performs continuous reorientations causing dc conduction rather than only local jumps of a bound pair; the latter may also involve random orientations but at the local level and, is not considered in the model. The most useful consequence of the random orientation model is that it predicts the observed correlation [43]

$$\sigma_{dc} = p \Delta\epsilon' \omega_p \quad (13)$$

between dc conductivity ( $\sigma_{dc}$ ) and the peak frequency for dielectric relaxation ( $\omega_p$ ). Here,  $p$  is the correlation parameter of the order of unity and  $\Delta\epsilon'$  is the difference between the static and high frequency dielectric constant. Otherwise, in this model, no attempt is made to explain the shape or other details of the relaxation spectra.



### (c) Microheterogeneous Structure Model

It was mentioned earlier that interfacial polarization in phase separated glasses gives rise to dielectric relaxation. This Maxwell-Wagner type polarization arises due to the discontinuity in dielectric properties at the interface. Isard [44] proposed that similar heterogeneities, which exist in all the so-called homogeneous glasses although at a much finer microscopic scale, cause the observed electrical relaxation. He derived analytical expressions assuming a glass to consist of layers of two different dielectric materials primarily differing in their electrical conductivity. According to his estimates the layers of equal width but differing in conductivity by a factor of ten provide agreement between theory and experiment.

Recently, Ravaine and co-workers [11,45,46] have considered heterogeneity of a glass in terms of fluctuations in ionic concentration. Since conductivity of a glass system strongly depends on alkali concentration ( $c$ ), the mean square fluctuations in concentration,  $\langle(\Delta c)^2\rangle$  are directly related to those in conductivity. Thus, the alkali density fluctuations give rise to a distribution of local conductivity; the effect on local dielectric constant is assumed to be negligible. Their analysis leads to a Cole-Cole type distribution function given in Eq. (12). The parameter  $\alpha$ , which is the angle of depression of the arc on complex impedance plane, is a measure of  $\langle(\Delta c)^2\rangle$ . It is interesting to note [47] that the values of concentration fluctuation from the complex impedance plots of alkali silicate glasses are of the same order as obtained from small angle neutron scattering measurements. However, a close examination of the complex impedance data shows systematic departure from the fit to an arc of a semi-circle, which is also not symmetric [12,47]. Abelard and Boumard [48] have also analyzed the frequency dependence of electrical conductivity in terms of angle  $\alpha$  using continuous time random walk formalism for non-interacting ions which move by hopping. It is noted [49] that the trap sites for an ion have complex structure presumably involving clusters. The jump distance and the residence time of an ion on its site are distributed due to the random structure of glass and are, therefore, treated as stochastic variables. Essentially, the model assumes a distribution of jump frequency.

Tomandl [50] and Aitken and MacCrone [51] have proposed that the non-uniformity of conduction path for the charge carriers in glass leads to a distribution of conductivity relaxation times. In this mechanism an ion moves along open path lengths which have a distribution corresponding to the observed spectra. For example, Aitken and MacCrone assume a distribution of path lengths (chains) which is inversely proportional to the square of chain length. By adjusting the maximum chain length (a fitting

parameter) complicated dielectric loss spectra can be obtained. The basic jump step in these models is the same for all ions so that the activation energy for migration is unique.

Boksay and Lengyel [52] have treated the heterogeneity of conduction path assuming that the conducting species in a glass are "vacancies" which encounter "impasses" or obstructions while moving in an electric field; the distance between two impasses is not fixed but has a distribution. At present these models have been tested for a very limited number of glasses and, therefore, need further verification.

### (d) Debye-Huckel Atmosphere Relaxation Model

In contrast to the above-described models which depend on the structure of glass, the Debye Huckel atmosphere relaxation model emphasizes the Coulomb interaction forces among various ions. In this case a glass sample is treated as consisting of negatively charged centers (non-bridging oxygen ions) surrounded by a uniform distribution of positive (alkali) ions. In the absence of electric field the charge distribution around a negative ion is spherical. However, when an electric field is applied the charge distribution is polarized as the center of gravity of positive and negative charges are shifted with respect to each other. Falkenhagen [53] considered the relaxation of this polarization of Debye-Huckel atmosphere for the case of dilute electrolyte solutions. Following the suggestion by Owen [54], Tomozawa [5] has adapted the Debye-Falkenhagen theory for a glass arguing that it can be treated as a weak solid electrolyte. That is, even though the bulk concentration of positive charge carriers in a glass may be very high, only a small fraction of these is assumed to be free to move. This concept is similar to that in ionic crystals where electrical conduction occurs due to the migration of point defects (e.g. interstitials). Lesikar et al. [55] have examined the validity of Debye-Falkenhagen-Tomozawa (DF $\bar{T}$ ) model for a borosilicate glass containing 150 ppm sodium and silicate glasses with higher alkali concentrations. They find that the model can be fitted only for very dilute alkali glasses for which approximately 8% of the total alkali concentration is determined to be freely conducting at a given moment. However, in a typical glass, although Coulomb forces will contribute to the broadening of modulus spectra, the charge carrier concentration is too large for DFT theory to be applicable.

### (e) Unified Models

Intuitively an explanation of electrical relaxation in glasses based on its vitreous nature or presumably heterogeneous structure appears attractive, particularly when we note [47] that an  $M''$  vs  $\log \omega$  plot for a quartz crystal shows nearly ideal Debye peak (Fig. 4). However, a departure from this ideal behavior in many other crystalline materials is sufficient

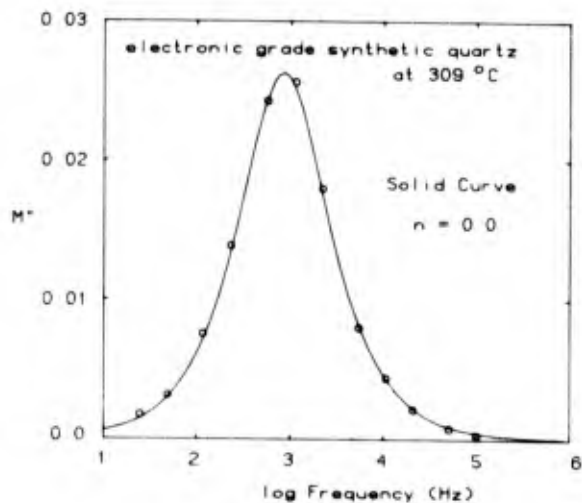


Fig. 4.  $M''$  vs log frequency plot for an electronic grade synthetic quartz crystal at 309°C, H. Jain, unpublished work (1979).

to suggest that non-crystallinity alone may not explain electrical relaxation in glasses. Similarly, if one finds a depressed arc of a semi-circle on  $Z^*$  plane for conduction in a single crystal, the concept of concentration fluctuations based on the heterogeneity of a glass becomes questionable. The basis of asking such questions, in fact, comes from the very similar experimental observations on a wide variety of materials which have structure and other properties as diverse as glasses, polymers, electrolytes, supercooled liquids, amorphous semiconductors, spin glasses, etc. [48]. In fact, Ngai in a recent review [29] shows that the "universal" behavior is not limited to dielectric relaxation only but is common to all kinds of relaxation phenomena including creep, internal friction, nuclear magnetic resonance, transient electronic transport, transient optical luminescence, volume and enthalpy relaxations, noise, spin relaxations, etc. The "universal" property of relaxations in condensed matter is predicted by a model which starts from a physical mechanism for time-dependent relaxation rate in condensed matter. A review of the model can be found in two review articles by Rajagopal and Ngai [50], and by Rendell and Ngai [27] in this Volume. Here we merely point out the general nature of the model and the additional predictions it makes (called "second universality" in Refs. 29, 27 and 56). For conductivity relaxations, the temperature dependence at temperatures sufficiently above the glass transition temperature [29,35,27], and the anomalous isotope mass dependence are beautiful examples of the relevance of the second universality relation. The latter has been verified in several other relaxation phenomena and in materials that have nothing to do with conductivity relaxation. A theoretical model is acceptable only if it predicts both Eq. (11), called the first universality, and the second universality relation. Also

it must be general enough that it is applicable to diverse classes of materials and relaxation phenomena.

#### References

1. W.A. Weyl and E.C. Marboe, The Constitution of Glasses, vol. 2 (John Wiley and Sons, New York, 1964).
2. Electrical Properties of Glass and Glass-Ceramics: A Bibliography for the period 1957-1968, Int. Comm. on Glass, Charleroi, Belgium.
3. R.H. Doremus, Glass Science, Ch. 9 (John Wiley & Sons, New York, 1973).
4. L.L. Hench and H.F. Schaake in Introduction to Glass Science, eds. L.D. Pye, H.J. Stevens and W.C. La Course (Plenum Press, New York, 1972), p. 583.
5. M. Tomozawa in Treatise on Materials Science and Technology, Vol. 12, ed. M. Tomozawa and R.H. Doremus (Academic Press, New York, 1977), p. 283.
6. H.L. Tuller, D.P. Button and D.R. Uhlman, J. Non-Cryst. Solids **40**, 93 (1980).
7. A. Baskett, J.H. Simmons and P.B. Macedo, Nuc. Chem. Waste Management **2**, 3 (1981).
8. C.J.F. Böttcher and P. Bordewijk, Theory of Electric Polarization, Vols. I, II, 2nd ed. (Elsevier, New York, 1978).
9. J. Wong and C.A. Angell, Glasses: Structure by Spectroscopy (M. Dekker, NY, 1976).
10. I.M. Hodge, M.D. Ingram and A.R. West, J. Electroanal. Chem. **74**, 125 (1976).
11. D. Ravaine and J.L. Souquet, J. Chim. Phys. **71**, 693 (1974).
12. R. Syed, D.L. Gavin, C.T. Moynihan and A.V. Lesikar, J. Am. Ceram. Soc. **64**, C118 (1981).
13. E.N. Boulos, A.V. Lesikar and C.T. Moynihan, J. Non-Cryst. Solids **45**, 419 (1981).
14. H. Jain, N.L. Peterson and H.L. Downing, J. Non-Cryst. Solids **55**, 283 (1983).
15. H. Jain, H.L. Downing and N.L. Peterson, J. Non-Cryst. Solids (1984) in press.
16. H.L. Downing, N.L. Peterson and H. Jain, J. Non-Cryst. Solids **50**, 203 (1982).
17. D.P. Almond and A.R. West, Solid State Ionics **11**, 57 (1983).
18. P.B. Macedo, C.T. Moynihan and R. Bose, Phys. Chem. Glasses **13**, 171 (1972).

19. L.P. Boesch and C.T. Moynihan, *J. Non-Cryst. Solids* 17, 44 (1975).
20. V. Provenzano, L.P. Boesch, V. Volterra, C.T. Moynihan and P.B. Macedo, *J. Am. Ceram. Soc.* 55i, 492 (1972).
21. K.S. Cole and R.H. Cole, *J. Chem. Phys.* 9, 341 (1941).
22. D.S. Park and A.S. Nowick, *Phys. Stat. Solidi* 26, 617 (1974).
23. A.K. Agarwal and D.E. Day, *J. Am. Ceram. Soc.* 65, 111 (1982).
24. C.T. Moynihan, L.P. Boesch and N.L. Laberge, *Phys. Chem. Glasses* 14, 122 (1973).
25. F.S. Howell, R.A. Bose, P.B. Macedo and C.T. Moynihan, *J. Phys. Chem.* 78, 639 (1974).
26. G. Williams and D.C. Watts, *Trans. Faraday Soc.* 66, 80 (1970).
27. For references, see the article by R.W. Rendell and K.L. Ngai, "A Fundamental Relation Between Microscopic and Macroscopic Relaxation Times: Evidence in Relaxation Data," in this Volume.
28. K.L. Ngai, *Comments Solid State Phys.* 9, 127 (1979); 9, 141 (1980).
29. K.L. Ngai, "Evidences for Universal Relaxation Properties of Condensed Matter," in Non-Debye Relaxations in Condensed Matter, ed. T.V. Ramakrishnan (World Press, Singapore, 1985).
30. K.L. Ngai, A.K. Rajagopal, and C.Y. Huang, *J. Appl. Phys.* 55, 1714 (1984).
31. K.L. Ngai, *Solid State Ionics* 5, 27 (1981).
32. K.L. Ngai and U. Strom, *Phys. Rev.* B27, 6031 (1983).
33. U. Strom and K.L. Ngai, *Solid State Ionics* 9 & 10, 283 (1983).
34. K.L. Ngai, R.W. Rendell and H. Jain, *Phys. Rev.* B30, 2305 (1984).
35. K.L. Ngai and R.W. Rendell in Handbook on Conjugated Polymeric Conductors, Vol. 1, ed. T. Skotheim (Marcel-Dekker, New York, 1985).
36. D.W. Davidson and R.H. Cole, *J. Chem. Phys.* 19, 1484 (1951).
37. J.M. Stevels in Handbuch der Physik 20, ed. S. Fluegge (SpringerVerlag, Berlin, 1957) p. 372.
38. H.E. Taylor, *J. Soc. Glass Tech.* 41, 350t (1957); 43, 124t (1959).
39. H. Jain, "Temperature Dependence of Electrical Conductivity of Glasses," *J. Non-Cryst. Solids*, (1984) in press.
40. R.J. Charles, *J. Appl. Phys.* 32, 1115 (1961).
41. T. Nakajima in Ann. Rept. Conf. Elec. Insulation Dielec. Phenomenon, Nat. Acad. Sci. (1971).
42. K. Shimakawa, *J. Non-Cryst. Solids* 43, 145 (1981).
43. H. Namikawa, *J. Non-Cryst. Solids* 18, 173 (1975).
44. J.O. Isard, Proc. Inst. Elec. Eng. Part B Suppl. 22, 440 (1982).
45. D. Ravaine and Wright, *J. Physique Colloq.* C9, 399 (1982).
46. D. Ravaine, *J. Non-Cryst. Solids* 49, 507 (1982).
47. C.T. Moynihan, N.S. Saad and A.V. Lesikar, *J. Am. Ceram. Soc.* 63, 458 (1980).
48. P. Abelard and J.F. Baumard, "Dielectric Relaxation in Alkali Silicate Glasses: A New Interpretation," Preprint of the paper presented at the Intl. Conf. Solid Electrolytes, Grenoble, France, July 1983.
49. V. Srivastava and M. Chaturvedi, *J. Non-Cryst. Solids* 6, 375 (1983).
50. G. Tomandl, *J. Non-Cryst. Solids* 14, 101 (1974).
51. J. Aitken and R.K. MacCrone in Mass Transport Phenomena in Ceramics, ed. A.R. Cooper and A.H. Hauer (Plenum Press, New York, 1975).
52. Z. Boksay and B. Lengyel, *J. Non-Cryst. Solids* 14, 79 (1974).
53. H. Falkenhagen, Electrolytes (Oxford University Press, 1934).
54. A.E. Owen, *Prog. Ceram. Sci.* 3, 77 (1963).
55. A.V. Lesikar, C.J. Simmons and C.T. Moynihan, *J. Non-Cryst. Solids* 40, 171 (1980).
56. A.K. Rajagopal and K.L. Ngai, this Volume.

## ELEMENTARY EXCITATIONS IN GLASSES

U. Strom  
Naval Research Laboratory  
Washington, D.C. 20375

### Abstract

A review of experimental and theoretical evidence is presented which provides support for the concept of elementary excitations in glasses. Specifically, the nature of dispersion and lifetimes are examined for transverse and longitudinal acoustic phonons, as well as optic phonons in glasses and other disordered solids. Disorder modes are defined as two-level tunneling states (TLS) as well as low energy "correlated states." The view of such modes as elementary excitations is less justified on the basis energy and lifetime arguments than on their universal existence and their usefulness in the modelling of much experimental data which cannot be understood in terms of Debye-like phonon excitations.

### Introduction

Elementary excitations have been a most important concept in the study of crystalline solids. Pines (1) has defined elementary excitations as states which have well-defined energies, are long-lived, and interact weakly with one another. Phonons, polarons, and quasiparticles are some well-known examples of excitations in crystals which meet these criteria. Crystalline periodicity is often used for the theoretical derivation of many of the elementary excitations. Lattice periodicity leads to the definition of a Brillouin zone (BZ) which in turn defines the properties of electronic and lattice quasiparticles. There is no general analogue of a BZ for glasses. However, there is a question whether lattice periodicity is required for the existence of phonons. Zwanzig (2) has provided strong theoretical arguments that longitudinal and transverse phonons are elementary excitations in liquids and glasses. Recent molecular dynamics calculations for a glass structure by Grest, Nagel and Rahman (3) as well as calculations by Hafner (4) and Heimendahl (5) have provided some support for the existence of longitudinal acoustic lattice excitations near "crystal" momenta which are appropriate for an "effective BZ." Such calculations represent an encouraging trend in modeling glassy elementary excitations. For the most part, however, the

approach for glasses has been to postulate the existence of excitations in order to explain certain experimental observations. For example, two-level tunneling states (TLS) were proposed by Anderson, Halperin and Varma (6), as well as Phillips (7), in order to account for the anomalous low temperature thermal properties of glasses. Small polarons have been invoked by Emin (8) in connection with the transport and optical properties of chalcogen (O, S, Se, Te) containing glasses. Anderson suggested that diamagnetic paired electronic states (9) (so-called "negative U centers") should be considered in order to understand the optical properties of glasses near their fundamental band gap. Other postulated glassy excitations include lattice modes with fractional dimension (fractals) (10) and extreme low frequency "correlated states" which are thought to be connected with a wide range of low frequency (much less than optical phonon frequency) fluctuation and dissipation phenomena (11). This paper will examine a few possible candidates for elementary excitations in insulating and semiconducting glasses as well as polymers. Two types of excitations will be considered: high frequency phonons and low frequency disorder modes. No attempt will be made to present an exhaustive summary but to highlight recent developments in each of these areas. For more detailed reviews of some of these topics the reader is referred to the articles on vibrational properties of glasses by Weaire and Taylor (12), on polarons by Emin (8), on TLS by Hunklinger and Schickfus (13) as well as other papers in the book edited by Phillips (13). The effects of disorder on the optical electronic and structural properties of the disordered ionic conductor Na $\beta$  Alumina have been recently reviewed by this author (14).

### Phonons

#### Acoustic Phonons

(1) Low frequency acoustic phonons ( $\omega/2\pi < 450$  GHz). Acoustic phonons in glasses (15) have been shown to be well-defined elementary excitations at low temperatures, provided that the phonon wavelengths are large compared to

microscopic structural variations. Generally, longitudinal and transverse excitations can be generated in the glass (15). For example, the sound velocities measured in glassy  $\text{SiO}_2$  by means of ultrasonic techniques ( $<1 \text{ GHz}$ ) are  $5.85 \times 10^5 \text{ cm/sec}$  for longitudinal and  $3.75 \times 10^5 \text{ cm/sec}$  for transverse phonons. Brillouin scattering measurements in  $\text{SiO}_2$  by Love (16) and more detailed measurements by Vacher and Pelous (17) demonstrated the existence of thermal phonons between 1.7 and 300K as well-defined elementary excitations in the 10-30 GHz frequency range. The phonon velocities determined by Love (16) in  $\text{SiO}_2$  were  $5.85 \times 10^5 \text{ cm/sec}$  at 23.5 GHz and  $3.68 \times 10^5 \text{ cm/sec}$  at 14.8 GHz for longitudinal and transverse excitations, respectively. These results are in good agreement with the lower frequency acoustic transport data. Very recently, Rothenfusser, Dietsche and Kinder (18) have performed transmission measurements of monochromatic phonons through a thin film of  $\text{SiO}_2$  which was grown on a Si crystal. The phonon source was a PbBi tunnel junction and the detector an Al tunnel junction. The authors utilized the phonon focusing properties of Si in order to enhance the propagation of LA phonons along the [111] and TA phonons along the [100] directions of the Si substrate, respectively. The results obtained by Rothenfusser et al. are reproduced in Fig. 1. The respective LA and TA sound velocities are  $5.84 \times 10^5 \text{ cm/sec}$  and  $3.7 \times 10^5 \text{ cm/sec}$ , which are

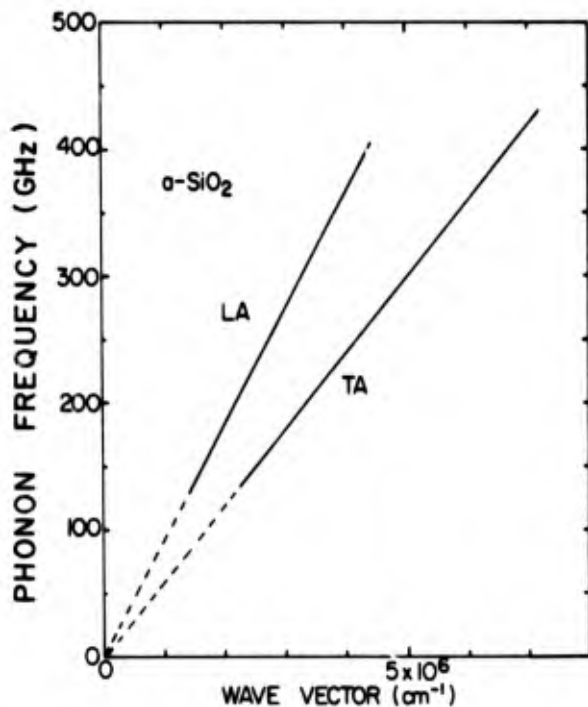


Fig. 1. Phonon dispersion relations for longitudinal and transverse acoustic modes in vitreous silica (from Ref. 18).

essentially identical to the Brillouin scattering and sound propagation measurements. The data demonstrate convincingly that acoustic phonons are well-defined elementary excitations in glassy  $\text{SiO}_2$  up to frequencies of  $\sim 450 \text{ GHz}$  with a linear dispersion  $\omega = kv_{L,T}$ , where  $k$  is phonon propagation constant and  $v_{L,T}$  the respective longitudinal or transverse sound velocity.

Additional information about phonon energies can be obtained from Raman scattering and infrared absorption. Both techniques yield experimental quantities which are proportional to the product of a coupling coefficient and a density of vibrational states  $g(\omega)$ . Thus the infrared absorption  $\alpha(\omega)$  is written in general as

$$\alpha(\omega) = M(\omega)g(\omega) \quad (1)$$

where  $M(\omega)$  is a coupling coefficient. For Raman scattering it is customary to define a reduced scattering function  $I^R(\omega) \equiv I(\omega)\omega / (1+n(\omega))$ , where  $I(\omega)$  is the Raman scattering function (all tensor indices are omitted here for clarity) and  $n(\omega) = 1/[\exp(\hbar\omega/kT) - 1]$ , such that

$$I^R(\omega) = c(\omega)g(\omega) \quad (2)$$

where  $c(\omega)$  is the Raman coupling coefficient. In order to determine  $g(\omega)$  it is necessary to determine  $c(\omega)$  and  $M(\omega)$ . It can be shown that for low frequencies, where the glass can be considered an elastic continuum (i.e.  $k = \omega/v$ ), the coupling coefficients become (19,20)

$$M(\omega) \propto c(\omega) \propto \omega^2 \quad (\text{low } \omega) \quad (3)$$

At sufficiently high frequencies, the excitation of vibrational states is spatially uncorrelated, and in that limit certain models predict that (19,20)

$$M(\omega) \propto c(\omega) \propto \text{constant} \quad (\text{high } \omega) \quad (4)$$

The critical angular frequency  $\omega_c$ , that separates the two regions described by eqs. 3 and 4, is determined by the condition for which the wavelength of the optically excited lattice modes is comparable to a physical correlation length  $\ell$  in the glass. This relation is generally written as (20)

$$\omega_c = v_D/\ell \quad (5)$$

where  $v_D$  is an averaged (Debye) sound velocity. From nuclear magnetic resonance and other studies one has inferred that there exist regions in the glass which reflect remnants of crystalline order (21). The average dimension of such regions has been estimated to be on the order of 10-20 Å. Substituting in eq. 5  $\ell = 10 \text{ Å}$  and  $v_D = 1 \times 10^5 \text{ cm/sec}$  it is found that  $f_c = \omega_c/2\pi \approx 150 \text{ GHz}$  (or  $5 \text{ cm}^{-1}$ ). Given the variations in  $v_D$  and  $\ell$  it can be expected that the transition region ranges from  $\sim 5$  to  $\sim 50 \text{ cm}^{-1}$ , depending on

the specific glass. This is actually borne out by experiments.

Nemanich has measured the low frequency Raman spectra for various chalcogenide glasses (22). The function  $I^R(\omega)$  is found to be proportional to  $\omega^4$  for  $\omega < 15 \text{ cm}^{-1}$ . Similar conclusions were reached by Lannin (23) on the basis of low frequency Raman measurements in a-Si and by Winterling (24) for Raman measurements in vitreous silica. Combining the Raman results with eq. (3), i.e.  $c(\omega) \sim \omega^2$ , these experimental results provide further evidence that  $g(\omega) \sim \omega^2$ , as expected for a Debye density of states, for  $\omega/2\pi < 450 \text{ GHz}$ .

Evidence that the absorption coupling constant  $M(\omega) \sim \omega^2$  in the correlated regime comes from infrared absorption measurements of the crystalline, but disordered, ionic conductor Na $\beta$  alumina. This solid exhibits all the anomalous low temperature thermal, dielectric and acoustic properties of glasses (14). Its optical properties are dominated by the crystalline host ( $\text{Al}_2\text{O}_3$ ) lattice except for the low

( $< 100 \text{ cm}^{-1}$ ) frequency region, where the vibrational modes of the cation-containing conduction planes are observed. The  $65 \text{ cm}^{-1}$  mode shown in the absorption spectrum in Fig. 2 is due to local cation ( $\text{Na}^+$ ) motion. It is expected that the conduction plane disorder leads to a breakdown of selection rules which in turn allows the optical excitation of acoustic phonons. The Debye modes in  $\beta$ -alumina reflect those of the crystalline host and thus  $g(\omega) \sim \omega^2$  with little dispersion below  $\sim 50 \text{ cm}^{-1}$ . The observed absorption in Fig. 2 is found to vary as  $\alpha(\omega) \sim \omega^{3.5}$  below  $\sim 60 \text{ cm}^{-1}$ . This suggests that  $M(\omega) \sim \omega^m$ , with  $m \sim 1.5$ . It is quite likely that  $m$  is effectively reduced due to tunneling mode contributions at the lowest frequencies. A value of  $m=2$  is expected on the basis of the calculated correlation length  $\ell$ . It is esti-

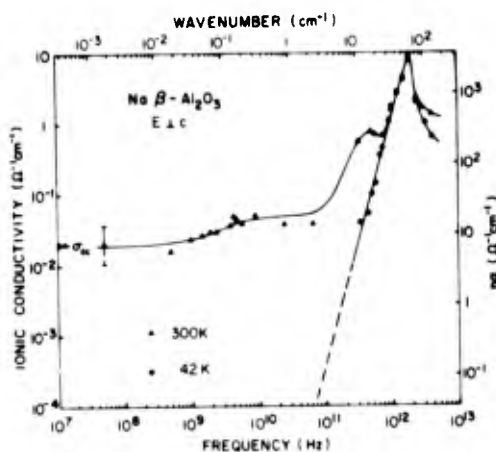


Fig. 2. Microwave and far infrared conductivity (or absorption) of nonstoichiometric Na $\beta$ -alumina (from Ref. 14).

mated that  $\ell \sim 5 \text{ \AA}$  for Na $\beta$  alumina (14) which implies that the critical frequency  $f_c$  below which  $M(\omega) \sim \omega^2$  is given by  $f_c = (1/2\pi) 5 \times 10^5 \text{ cm/sec} / 5 \times 10^{-8} \text{ cm} \cong 1.6 \times 10^{12} \text{ sec}^{-1}$  ( $\sim 50 \text{ cm}^{-1}$ ), which is in agreement with the experimental results shown in Fig. 2.

In Fig. 3 are shown absorption measurements (20) for a-As $_2$ S $_3$  and a-SiO $_2$ . The dashed curves at low frequencies approach a quadratic frequency dependence. For  $\omega/2\pi < 15 \text{ cm}^{-1}$  the absorption is temperature dependent. The data points at  $\sim 1 \text{ cm}^{-1}$  for temperatures of 10 and 25 K represent an upper bound for a temperature independent contribution to the absorption. Although the data are very limited, the results are nevertheless consistent with a quadratic coupling coefficient and a quadratic phonon density of states for frequencies below 450 GHz.

(2) High frequency "acoustic" phonons ( $\omega/2\pi > 450 \text{ GHz}$ ). With increasing frequency the definition of "acoustic" phonons in glasses becomes less clear. There is evidence that high frequency "acoustic" excitations are strongly damped and that the density of states deviates from the  $\omega^2$  Debye form. On the other hand, there is considerable experimental evidence (for metallic glasses) and theoretical argumentation that longitudinal acoustic phonons are well-defined elementary excitations in glasses, even for phonon wave vectors which are comparable in magnitude to Brillouin zone wave vectors in crystals. The following discussion will first examine the implications of far infrared optical absorption measurements in semiconducting and insulating glasses over the  $15\text{-}100 \text{ cm}^{-1}$  frequency range and then focus on neutron scattering measurements in metallic glasses.

For "high" frequencies ( $\omega/2\pi > 15 \text{ cm}^{-1}$ ) the optical absorption  $\alpha$  is essentially temperature independent but quadratically dependent on frequency (20). For a constant coupling coefficient ( $M(\omega) = \text{const.}$ ) this observation leads directly to an  $\omega^2$  phonon density of states. A

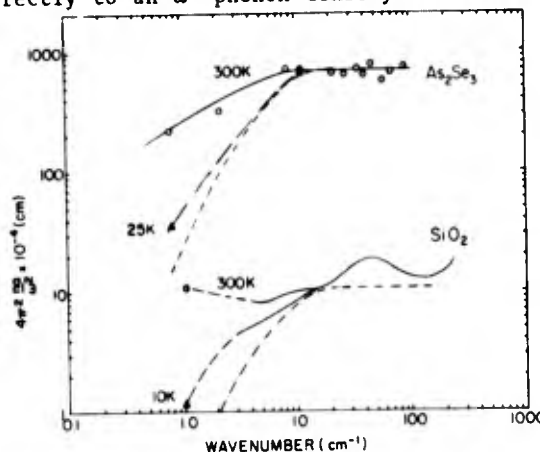


Fig. 3. Reduced far infrared absorption for vitreous As $_2$ Se $_3$  and SiO $_2$  (from Ref. 20).

simple model, in which disorder induced charge fluctuations couple the FIR radiation to acoustic phonons, leads to the following expression for the absorption coefficient (25):

$$\alpha(\omega) = \frac{K_0 (\hbar\omega)^2}{n} [1 - 1/(1 + \omega^2/\omega_c^2)] \quad (6)$$

where  $K_0$  is a constant,  $n$  is the index of refraction, and  $\omega_c$  is the critical angular frequency as defined in eq. (5). This form of  $\alpha(\omega)$  was first derived by Vinogradov (26) and Schlömann (27) for defect induced optical absorption in crystals. This model was later applied by Stolen (28) and subsequently Strom and Taylor (25) to the FIR absorption in glasses. An  $\omega^2$  phonon density of states follows from these results only if it is assumed that  $M(\omega) = \text{constant}$ . If  $M(\omega)$  is frequency dependent, then the FIR absorption measurement leads to the relation

$$M(\omega)g(\omega)/\omega^2 \sim \text{constant} \quad (7)$$

for  $\omega/2\pi c$  between  $\sim 15$  and  $100 \text{ cm}^{-1}$ , where  $g(\omega)$  may deviate from a Debye-like  $\omega^2$  density of states.

It has been recently suggested that the problem of high frequency lattice excitations in glasses should be examined in terms of "fractal" theory (29). Within such a framework the elementary lattice excitations are defined as "fractons" with a density of states given by

$N(\omega) \sim \omega^{\bar{d}-1}$ , where  $\bar{d}$  is the so-called "spectral dimension" as defined by Alexander et al. (10). Within their model, the FIR results can be interpreted as a coupling coefficient

$$M(\omega) \sim \omega^{3-\bar{d}} \quad (8)$$

and a density of states

$$g(\omega) \sim \omega^{\bar{d}-1} \quad (9)$$

where  $\bar{d} \leq 3$ . Further experimental and theoretical work is required in order to determine whether fractons, if they exist, can be considered elementary excitations in glasses.

Regardless of the physical interpretation of the modes observed near and above  $\sim 15 \text{ cm}^{-1}$ , there is circumstantial evidence that these modes are making the dominant contribution to the  $T^3$  term of the specific heat ( $c_3$ ). In Fig. 4 is shown a comparison between  $K_0$  and  $c_3$ . There is apparently a good correlation between  $K_0$  and  $c_3$  which suggests a common contribution of low energy excitations to these diverse physical quantities. It is of interest to speculate on the relationship of the FIR absorption to the peak near  $\sim 10 \text{ K}$  in the low temperature thermal conductivity observed in most glasses (30). It has been previously suggested that this peak was due to an increased

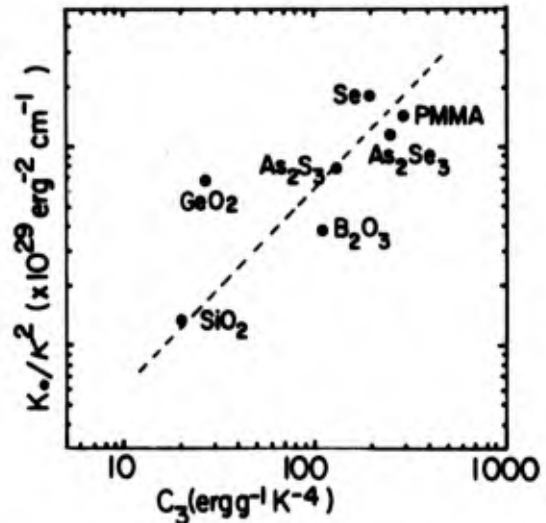


Fig. 4. Comparison between reduced far infrared optical absorption ( $K_0/K^2$ ) (where  $K \equiv 1/3(n^2+2)$ ) and coefficients of cubic term in specific heat ( $c_3$ ) for various disordered solids.

density of Debye phonons (31). However, such an increase in the density of acoustic modes would be reflected in a reduction of the sound velocity above  $\sim 300 \text{ GHz}$ , which is contrary to the observations of Rothenfusser et al. (18). Consequently, it has been suggested (18) that phonon scattering from non-Debye-like vibrational modes are responsible for the thermal conductivity near  $T \sim 10 \text{ K}$ .

Detailed fits to the thermal conductivity data, which are based on the scattering of thermal phonons by two-level tunneling systems (TLS), have been presented (30). The required density of TLS is found to be comparable to the number of charged defects that have been postulated to explain the FIR absorption. The magnitudes of  $K_0$  and  $c_3$  are also related to the magnitude of the glass transition temperature  $T_g$  as shown in Figs. 5 and 6. These correlations may reflect no more than a modified version of the Lindemann melting criterion for crystals, which states that a solid melts when the thermal motion of the atoms becomes a significant fraction of a lattice constant. For our purpose, Figs. 5 and 6 represent additional confirmation that  $K_0$  is proportional to  $c_3$ .

The above results point to interesting correlations between the thermal and optical properties of glasses. However, they provide only indirect information about the energy-momentum relations of the high frequency vibrational excitations in these materials. Hubbard and Beeby (32) presented a theory of collective motion in liquids. This theory was suggested to apply also to amorphous solids. Their conclusions were qualitatively similar to the later work of Takeno and Goda (33) who considered theoretically the problem of dispersion of elementary lattice excitations in disordered

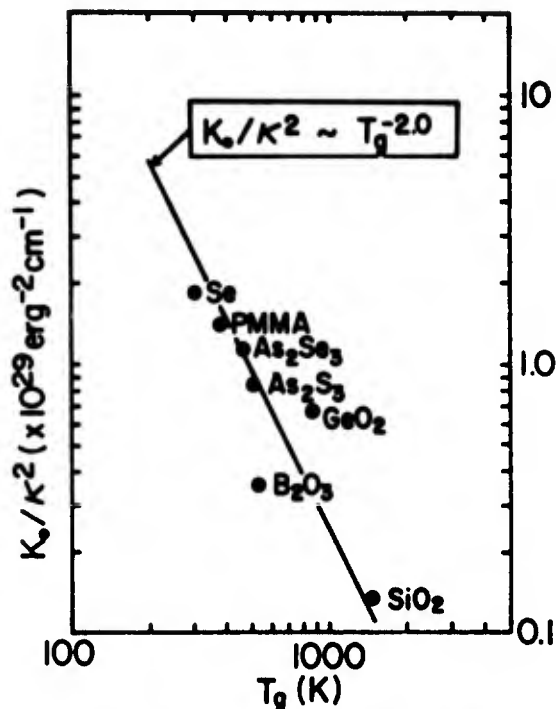


Fig. 5. Scaling of reduced far infrared optical absorption to glass transition temperature ( $T_g$ ) for various disordered solids.

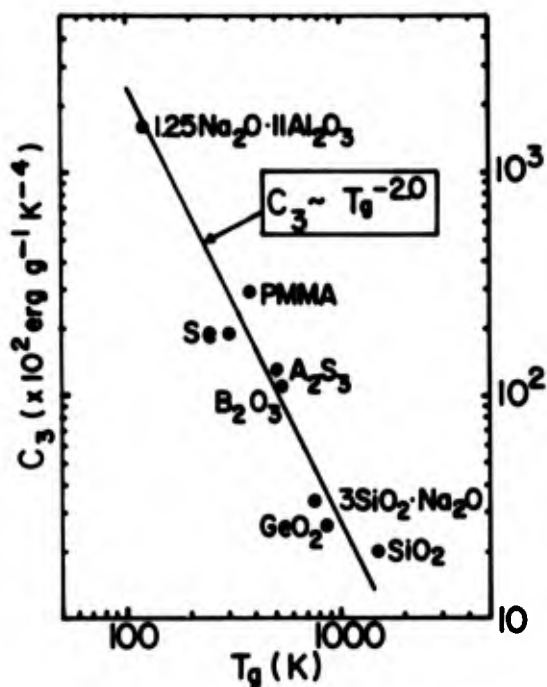


Fig. 6. Comparison between coefficient of cubic term in specific heat ( $c_3$ ) and glass transition temperature  $T_g$  for various disordered solids.

solids. Takeno and Goda applied their theory to calculate the phonon eigenfrequencies of a one-dimensional model system with local deviations from the lattice spacing as a disorder parameter. Their most significant finding for a disordered solid was a phonon-roton-like dispersion curve with a deep minimum near  $k=2\pi/a$ , where "a" was the average atomic spacing. A well defined peak appears near  $k=\pi/a$ , as would be expected for the BZ boundary of a crystal.

Later studies were aimed at understanding the vibrational properties of amorphous metals. Rehr and Alben (34) calculated the vibrational and electronic properties of a glass which was modelled as a 500 atom unit cell model, as had previously been used by Rahman et al. (35). They deduced a neutron scattering function  $S(Q, \omega)$  where  $Q$  and  $\omega$  are respectively proportional to the momentum transfer and energy loss of the neutrons, which exhibits the same roton-like behavior found by Takeno and Goda, but also includes additional lifetime information in the width of  $S(Q, \omega)$ .

Subsequently, von Heimendahl (5) used an improved "relaxed model structure" with periodic boundary conditions and realistic atomic pair potentials in order to calculate the dynamical structure factor  $S(k, \omega)$  for a two-component metallic glass. From  $S(k, \omega)$  he determined the dispersion relations for longitudinal and transverse waves, as shown in Fig. 7. These results clearly showed that longitudinal phonons have a well-defined  $k$  versus  $\omega$  relation extending to an effective BZ edge, whereas transverse waves are increasingly less well-defined with higher frequencies with no evidence for "repeated zone" behavior.

A further advance in this area is represented by the work of Hafner (4). His most recent

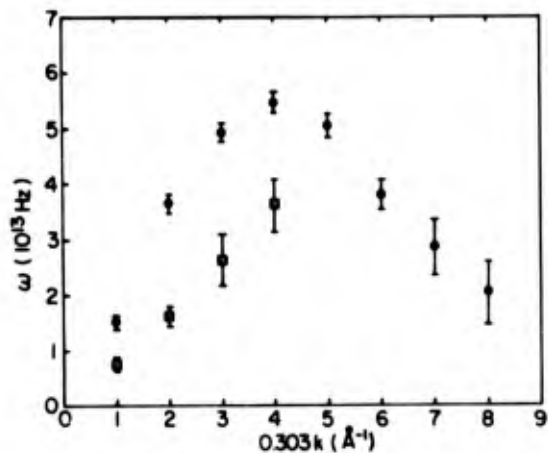


Fig. 7. Theoretical dispersion relation for a two-component metallic glass ( $Mg_{70}Zn_{30}$ ) (from Ref. 5). Circles - LA, squares - TA.



calculations of the vibrational properties of the metallic glass  $\text{Ca}_{70}\text{Mg}_{30}$  lead him to the following conclusions: (a) Longitudinal collective excitations are well-defined up to momenta  $k \sim 2Q_p$ , whose  $Q_p$  is the wavevector corresponding to the first peak in the structure factor. (b) The transverse excitations are well-defined for small  $k$  only--already for  $k \sim Q/2$ , the transverse phonon spectrum is identical with the total density of vibrational states (VDOS) (i.e. there are no more momentum conserving selection rules). The softening of the transverse modes is thought to be due to the effective relaxation of shear strains by internal displacements. Furthermore, long wavelength transverse modes are coupled to short wavelength collective excitations with  $k \sim Q_p$  via a "diffuse Unklapp" scattering mechanism (36). (c) Additional low and high energy modes appearing in the calculated total VDOS are possibly related to localized "defect" regions. It may be interesting to speculate on the relationship of some of these conclusions to the anomalous low temperature thermal, dielectric and acoustic properties of solids. In particular, there may be a close association between the softening of the transverse modes and the appearance of the postulated TLS.

Some of the conclusions contained in (a) and (b) of the above discussion were also obtained on the basis of the molecular dynamics calculations of Grest, Nagel and Rahman (3), who calculated the normal vibrational modes of a "Lennard-Jones glass." They found dispersion relations which were very much as those found earlier by Heimendahl. Most recently, these authors examined the effect of varying the degree of disorder on the calculated scattering functions (37).

The conclusions arrived by these various theoretical studies are well borne out by neutron scattering experiments on metallic glasses (38, 39). There have also been a limited number of experimental neutron scattering experiments performed on semiconducting and insulating glasses (40-42) which exhibit some of the same features which were observed for metallic glasses. This suggests that the various conclusions drawn for the nature of high frequency lattice excitations in metallic glasses are likely to be applicable to conventional glass systems.

(3) Phonon Lifetimes. In order for phonons to be defined as elementary excitations they must be sufficiently long-lived. In general, this requires that the inverse of the lifetime of a given state must be small compared to the energy of the state. This discussion will focus on the lifetimes of acoustic modes. Information about acoustic phonon lifetimes (in glasses) is derived primarily from coherent phonon transport (18,43), Brillouin scattering (16,17) and thermal conductivity measurements (44). In Fig. 8 is shown a compendium of

phonon lifetime measurements for vitreous silica obtained from several sources. The results are expressed as the phonon mean free path  $\Lambda$  versus phonon frequency. Also shown in Fig. 8 are the phonon wavelengths reproduced from Fig. 1. Details about how  $\Lambda$  is obtained from thermal conductivity have been discussed by Zaitlin and Anderson (44). The region where  $\Lambda \sim 1/\omega$  is ascribed to phonon scattering from TLS (44). A rapid drop in  $\Lambda$  is apparent above  $\sim 250$  GHz. If this drop is expressed as

$\Lambda(\omega) \sim \omega^{-m}$  then the best fits to the thermal conductivity are obtained for  $m \geq 4$ . On the other hand, the coherent phonon transport data by Dietsche and Kinder (43) suggest that  $m \sim 3$ , at least between 100 and 300 GHz. The curve drawn in Fig. 8 represents a compromise to accommodate these diverse predictions. A qualitatively similar curve for  $\Lambda(\omega)$  was obtained by Kelham and Rosenberg (45) in order to fit thermal conductivity data for epoxy resins. These data were used by Alexander et al. (10) as evidence for the validity of the fractal concept in the far infrared absorption of glasses and polymers.

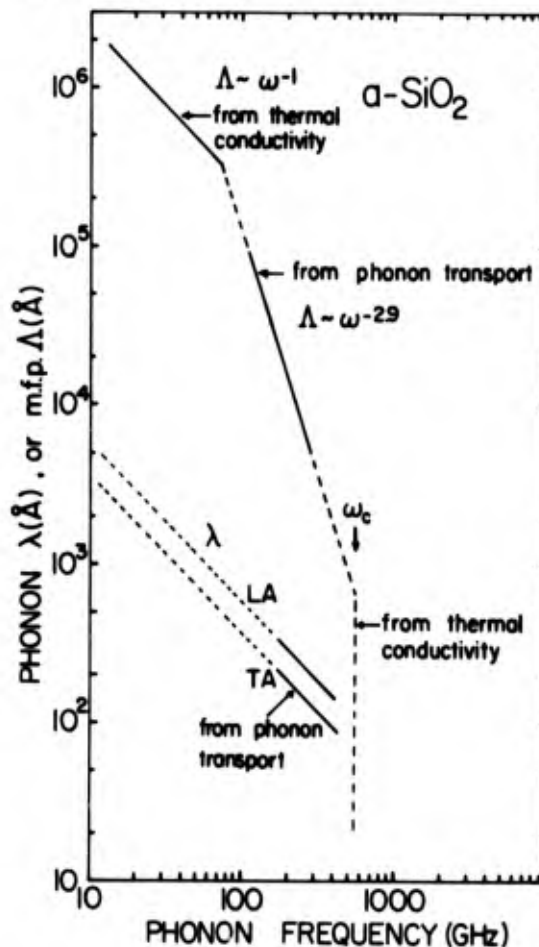


Fig. 8. Phonon mean free path  $\Lambda$  obtained from thermal conductivity (Ref. 44) and phonon transport (Ref. 43). Phonon wavelength  $\lambda$  obtained from phonon transport (Ref. 18), dotted lines extrapolate to low frequency sound velocities (Refs. 16, 17).

For  $f > 450$  GHz the phonon m.f.p. is estimated to be on the order of a few interatomic spacings (44). The inhibited phonon transport above  $f \sim 450$  GHz is contrasted by the far infrared absorption, which was interpreted in terms of the disorder induced absorption to acoustic modes (20). Strong phonon damping occurs for phonon wavelengths  $\sim 100$  Å. The reason for this phenomenon has been variously interpreted as due to phonon scattering from structural defects or from TLS. It is interesting that molecular dynamics calculations for a model glass yield an intermediate frequency range in which acoustic phonons are severely damped (3). At higher frequencies LA phonons are well-defined elementary excitations, whereas TA phonons are strongly damped (3-5). Thus, it is plausible that the far infrared absorption in glasses observed above  $\sim 450$  GHz is primarily due to the excitation of LA phonons which are sufficiently long lived to exist for several oscillatory periods, but which do not contribute significantly to long-range thermal transport.

### Optic Phonons

Optic phonons in glasses have been studied extensively by means of Raman and infrared spectroscopy. The interpretation of these spectra in terms of the microscopic glass structure is very much a topic of current interest. Only very recently has there been an attempt to understand to what extent crystal-line-like momentum conservation rules play a role in the interpretation of the spectra.

In their classic work concerning Raman scattering in glasses, Shuker and Gammon (46) proposed that the coherence length of the normal vibrational modes of the glass is very much shorter than the wavelength of light used in the Raman scattering experiment ( $\sim 5000$  Å). This assumption was shown to lead to a breakdown of momentum conservation so that nearly all the normal vibrational modes contribute to the Raman scattering lineshape. The Raman spectra, in fact, are expected to reflect closely the vibrational density of states. Recent in-depth comparisons of neutron scattering, Raman scattering and the infrared reflectivity of glasses and their crystalline modifications have verified the close relationship of the VDOS to the HH polarized Raman spectra (47). These IR and Raman spectra also supported previous reports of LO-TO mode splittings (48) which are thought to be due to the effects of long range coulombic forces.

However, there is some recent evidence that models based on a complete breakdown of crystalline selection rules are incomplete. Hyper Raman (2 photon) scattering measurements in fused quartz convincingly show that the spatial coherence length of optical vibrational modes can be as large as  $\sim 1$   $\mu$ m (49). This conclusion was based on the observation of polariton effects (i.e. sensitive dependence of the

coupled phonon-photon mode on Raman scattering angle) in fused quartz (49). From the angular dependence of the polariton frequency it is possible to derive an  $\omega(k)$  relation for the polariton. The measured polariton frequency approaches the TO phonon frequency for large  $k$  and the photon dispersion curve for low  $k$ . The values of measured  $k$  range from  $6 \times 10^3$   $\text{cm}^{-1}$  to  $20 \times 10^3$   $\text{cm}^{-1}$ , which translate into spatial coherence lengths of 1.6  $\mu$ m and 500 Å, respectively. The apparent contrasting information that is obtained from the Raman and hyper Raman scattering data has lead Denisov et al. (49) to propose a susceptibility which includes crystal-like (subject to selection rules) and disordered contributions. This model does not envision microcrystallinity but may be related to models which are based on "intermediate range order" in glasses. Clearly, any comprehensive model for the vibrational properties of glasses must address the two most important experimental findings: (1) The nearly identical VDOS obtained by neutron scattering for crystal and glass and, (2) the existence of polar modes with well-defined dispersion relations in glasses.

### Disorder Modes

#### Introduction

By "disorder modes" are loosely meant those lattice excitations which have energies that are lower than typical phonon energies and which cannot be described in terms of classical phonon excitations. These modes have not been derived in terms of structural models for glasses. Instead, their existence has been postulated. The associated mathematical models based on the disorder modes have shown to be extremely useful for the description of diverse low frequency properties of disordered solids.

The most celebrated disorder mode is the two-level tunneling system (TLS) proposed by Anderson, Halperin and Varma (6), and Phillips (7). As will be discussed in detail, such modes are generally strongly coupled to the lattice, but nevertheless have well defined energies and long lifetimes (at sufficiently low temperatures) to be considered as elementary excitations. However, TLS provide only a partial description of the wide range of anomalous (non-Debye-like) low frequency fluctuation-dissipation phenomena observed in glasses, polymers, amorphous metals, etc. In the following section are summarized the experimental results which have been interpreted in terms of TLS, and in the subsequent section are described those experimental observations which can be understood in terms of other postulated very low frequency excitations.

#### Two Level Systems

A listing of properties which have been interpreted in terms of TLS are presented in the

following set of figures. Wherever possible the disordered crystalline solid Na $\beta$  alumina has been used as a model to illustrate a particular phenomenon. This material was chosen in no small part because of personal bias, but also because Na $\beta$  alumina exhibits most of the low frequency and low temperature properties observed in glasses (14), and often in a more spectacular fashion. However, this does not imply that the structural basis for disorder modes in Na $\beta$  alumina is identical or even related to that in glasses such as vitreous quartz. Instead, the disorder induced anomalous properties of this solid can serve as a test case for the mathematical models which have been proposed to describe conventional glasses. The exhibited properties can be divided into thermal, dielectric, acoustic and resonance properties.

The low temperature thermal properties for Na $\beta$  alumina are shown in Figs. 9 and 10. The specific heat (50,51) (Fig. 9) is seen to vary approximately linear in temperature. This is typical for most glasses (52). The "linear" contribution to the specific can be expressed

as  $c_1 \cong aT^\alpha$ , where  $\alpha \cong 1.18$  for Na $\beta$  alumina. For vitreous silica, Lasjaunias et al. (53) found  $\alpha \cong 1.3$ . For a constant density of states of TLS the specific heat is expected to be exactly proportional to  $T$ , i.e.  $\alpha = 1$ . The observation of  $\alpha > 1$  has been interpreted as evidence for the existence of a low energy gap in the TLS density of states (53). Figure 9 also shows  $T^3$  contributions above  $\sim 1$  K which are significantly enhanced over what is expected on the basis of Debye theory (51). This anomalous observation is not well understood.

Interpretation of the  $T^3$  excess specific heat in terms of an increased phonon density of states is not borne out by the lack of phonon dispersion (18), as shown in Fig. 1. The added contribution of TLS or other localized excitations has been considered (18,44), but then a satisfactory agreement with time dependent specific heat studies (54) must be reached. Similar arguments can be applied to the plateau region (near 10 K) in the thermal conductivity as shown in Fig. 10. The solid lines are theoretical fits which assume that the low temperature thermal transport is dominated by phonon-TLS scattering (55).

The dielectric properties, which have been interpreted in terms of TLS, are shown in Figs. 11-14. The most striking feature of the loss data (56,14) in Fig. 11 is the minimum in the conductivity observed near 5 K and the subsequent increasing dielectric loss with decreasing temperature. A comparable observation of acoustic loss in  $\alpha$ -SiO<sub>2</sub> provided the first evidence for the existence of two-level excitations in glasses (57,58). The loss at the lowest temperatures is due to the resonant excitation of TLS, whereas the loss above  $\sim 5$  K is due to the so-called "relaxation" absorption in which the applied electric field couples via

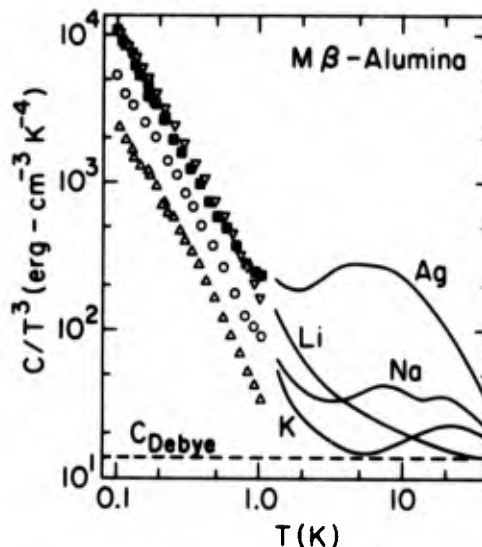


Fig. 9. Specific heat of  $\beta$ -alumina (from Ref. 50). Data above 1 K from Ref. 51.

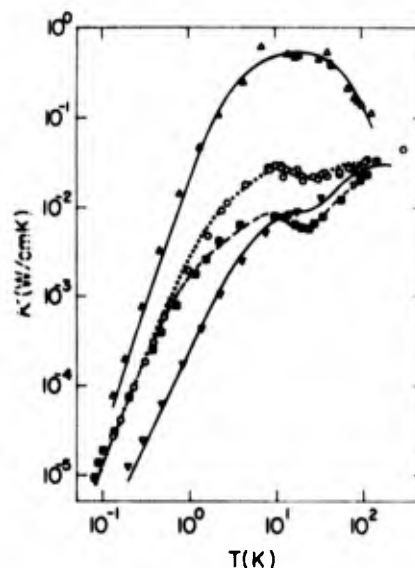


Fig. 10. Thermal conductivity of  $\beta$ -alumina (from Ref. 55). Symbols as in Fig. 9.

a strain field to perturb the level spacing of a TLS and the perturbed TLS return to thermal equilibrium via coupling to phonons (59). At  $T \gtrsim 50$  K in Fig. 11 dielectric loss mechanisms which are not related to TLS begin to dominate (14). The solid curve near the data points is a theoretical fit based on the tunneling model and an empirical expression for the highest temperature loss data:

$$\alpha(\omega, T) = \alpha(\text{TLS}) + BT^\beta \quad (10)$$

where  $\beta \sim 2.1$  and where  $\alpha(\text{TLS})$  is as given in Ref. 14. The relatively good fit to the data is indicative of the power of the TLS model description. In fact, the small deviations between theory and experiment near 5 and 20 K can be accounted for by higher order phonon-TLS relaxation processes (56,60). These higher

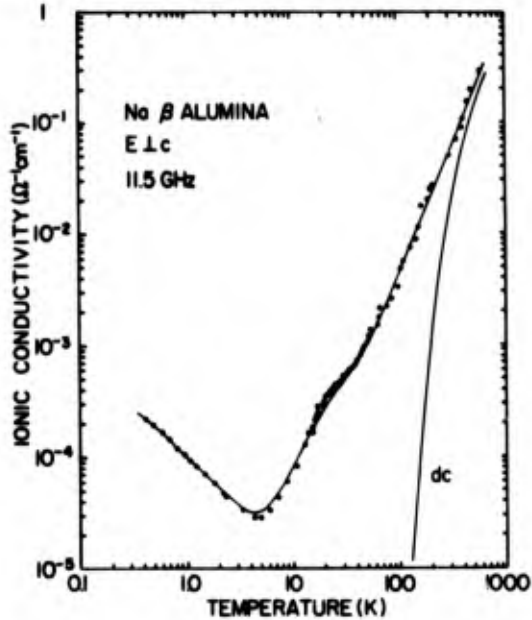


Fig. 11. Microwave dielectric loss of Na  $\beta$ -alumina (from Refs. 56 and 14).

order processes have a particularly strong effect on the occurrence of the minimum in the temperature variation of the real part of the dielectric constant as shown in Figs. 12 and 13. The best fit of the low frequency data (61) in Fig. 13 predicts a minimum in  $\Delta\epsilon/\epsilon$  at 11.5 GHz at a much higher temperature than is actually observed (56) in Fig. 12. This apparent discrepancy in the TLS model is qualitatively accounted for by a higher order one-phonon Raman process (56,60).

At sufficiently low temperatures the phase memory times of TLS become longer than the duration of an applied rf field pulse. As a consequence, coherent pulse echo phenomena can be observed. Coherent acoustic echo phenomena in glasses have been extensively investigated by Graebner and Golding (62) as well as Arnold et al. (63). Dielectric echoes have been observed for glasses (64) and Na $\beta$  alumina (65). The results in Fig. 14 exhibit the variation of the two-pulse echo magnitude as a function of time and temperature. The solid lines do not represent model fits. However, the data can be understood qualitatively in terms of the effects of spectral diffusion (65). For the present discussion, the observation of coherent echo phenomena underscores the validity of the TLS model with phase memory times ( $T_2$ ) on the order of  $\mu$ sec and longitudinal relaxation times ( $T_1$ ) on the order of msec at temperatures in the mK regime.

The low temperature acoustic properties exhibit generally temperature and frequency dependences which are analogous to the low temperature dielectric properties. The acoustic absorption measurements by Doussineau et al. (60) for Na $\beta$ -

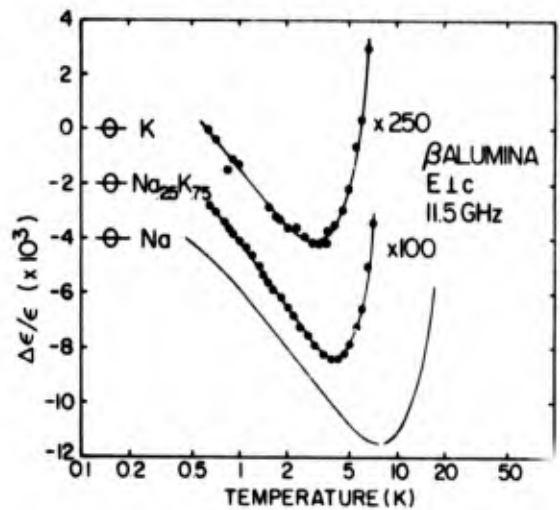


Fig. 12. Temperature dependence of variation of dielectric constant at 11.5 GHz (from Ref. 56).

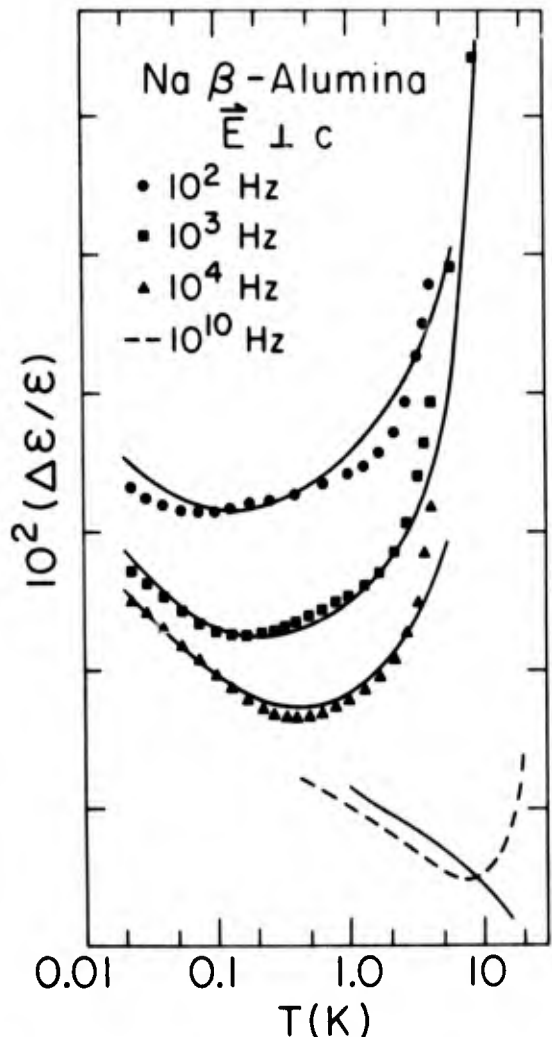


Fig. 13. Low frequency variation of dielectric constant of Na $\beta$ -alumina (from Ref. 61). Lower solid curve: extrapolation to  $10^{10}$  Hz; dashed curve: data from Fig. 12.

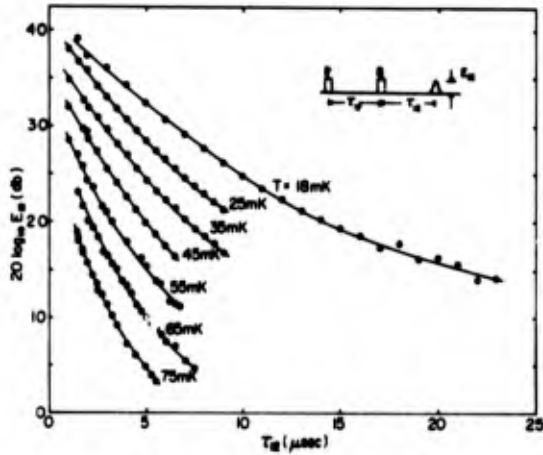


Fig. 14. Spontaneous echo amplitude as function of pulse separation  $T_{12}$  and temperature. Curves are displaced vertically for clarity (from Ref. 65).

alumina shown in Fig. 15 are particularly interesting since they display a broad temperature independent plateau which is predicted by the TLS model for the case of a broad distribution of TLS relaxation times. Such a distribution is expected on the basis of a wide variation of microscopic tunneling mode parameters. This distribution in turn is expected to lead to a time-dependent specific heat which has been observed for glasses (54) and for Na $\beta$ -alumina (66). Doussineau et al. have been able

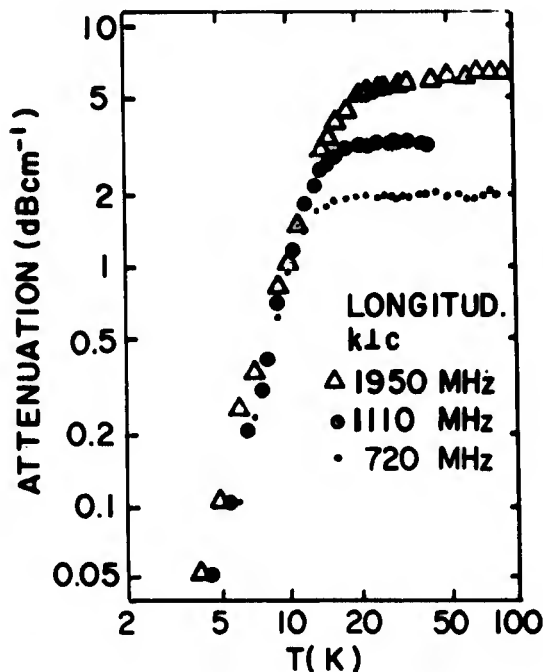


Fig. 15. Relaxation absorption of high frequency ultra sound of Na $\beta$ -alumina (from Ref. 60).

to fit the data in Fig. 15 accurately with the TLS model and the assumption of a higher order Raman-TLS relaxation process which becomes important for higher temperatures.

Nuclear or electronic spins can relax by transferring their energy to nearby TLS via one of various coupling mechanisms (67,68). The observation is that for many glasses the temperature dependence of the spin relaxation rate below  $T \sim 100$  K is given by  $T_1^{-1} \sim T^m$  where  $1 \leq m \leq 2$ . In Fig. 16 this behavior is illustrated in terms of the data for  $^{23}\text{Na}$  and  $^{27}\text{Al}$  NMR in the MHz regime for Na $\beta$ -alumina (69,70). The slope of the straight line is given by  $m \approx 1.2$ . Again, although a detailed theoretical understanding is lacking, it is generally agreed that TLS are responsible for the observed anomalous spin relaxation rates.

In summary, there exists a large body of low temperature thermal, dielectric, acoustic and resonance data for glasses which cannot be interpreted in terms of the vibrational elementary excitations of a Debye solid. These varied anomalous properties, illustrated for the disordered solid Na $\beta$ -alumina, can be understood if a new type of excitation is introduced. This excitation represents the ability of the glass to exist in various energetically nearly equivalent configurational states. These are chosen to be modelled according to the double well potential shown in Fig. 17. At low temperatures the solid can change from one configuration to another only by tunneling. Even for two equal symmetric wells ( $\Delta=0$ ) the degenerate energy levels are split by the wavefunction overlap energy  $\Delta_0$ . For harmonic oscillator wells separated by potential barrier  $V$  and distance  $d$  it is found that  $\Delta_0 = \hbar \omega e^{-\lambda}$  where  $\lambda = d(2mV/\hbar^2)^{1/2}$  with  $m$  the mass of the atom or group of atoms. For asymmetric wells ( $\Delta \neq 0$ ) the energy levels are further split such that energy splitting between the two normal modes of the system is given by

$$E = (\Delta^2 + \Delta_0^2)^{1/2} \quad (11)$$

Much of the experimental evidence points to the conclusion that the density of states  $n(E)$  is very slowly varying, in agreement with the initial proposition of the model. In fact, excellent agreement with experiment is obtained with the assumption that  $n(E) = \text{constant}$ . However, cutoffs have been suggested for both small and large  $E$ . A low energy limit has been related to the plausible existence of a maximum barrier height  $V$ . Typical proposals place a minimum energy  $E_{\text{min}}$  at  $\sim 10^{-3}$  K in equivalent temperature units. A high energy cutoff is proposed to be the glass transition temperature  $T_g$ . The coupling of these modes to the lattice is generally strong for glasses (deformation potential  $\sim 1-2$  eV) but is relatively weak for Na $\beta$ -alumina (deformation potential  $\sim 0.3$  eV). Nevertheless, at low temperatures there is

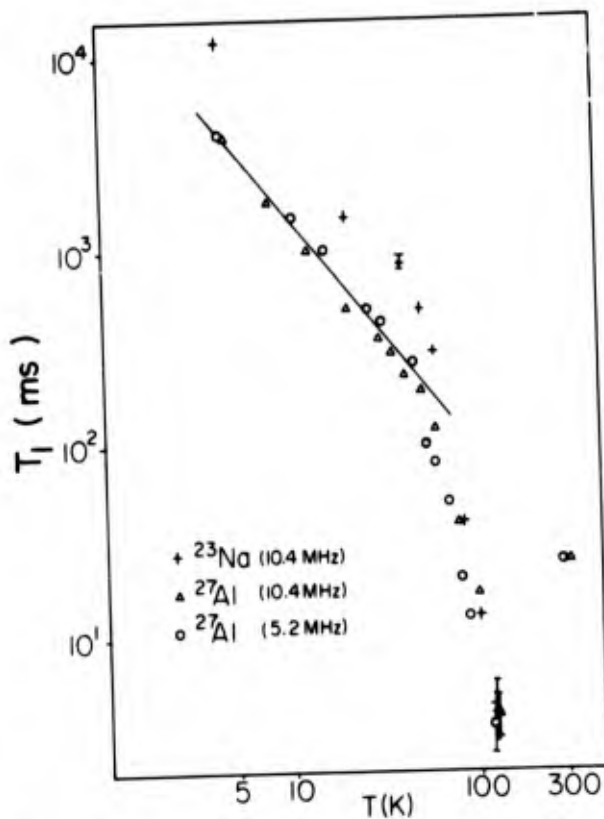


Fig. 16. Temperature dependence of  $T_1$  for  $^{23}\text{Na}$  in  $\text{Na}\beta$ -alumina. Straight line: best fit with  $T_1 \sim T^{-1.2}$  (from Ref. 69).

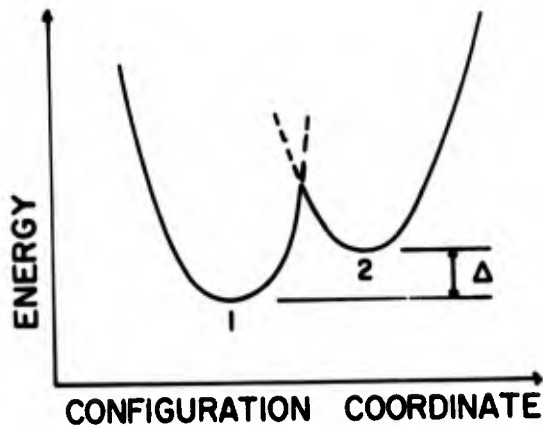


Fig. 17. Configuration diagram for tunneling mode (TLS).

generally a subset of modes which have energies  $E/\hbar$  which are large compared to relaxation rates  $T_1^{-1}$  and  $T_2^{-1}$  and hence can be defined as elementary excitations of the system.

The TLS excitations discussed in this section have characteristic energies in the range from  $\sim 10^{-3}\text{K}$  to  $T_0$  (i.e.  $\sim 100\text{-}1000\text{K}$ ). These thermal energies are large compared to  $\hbar\omega$  for  $\omega/2\pi <$

$10^8\text{sec}^{-1}$ . Can disorder modes exist with energies much less than  $10^{-3}\text{K}$ ? Such small splittings might be the consequence of the tunneling motion of configurational states which consist of large groups of atoms. It has been proposed that the existence of very low energy ( $<10^{-3}\text{K}$ ) modes is consistent with the observation of various low frequency ( $<10^9\text{sec}^{-1}$ ) relaxation phenomena. These will be discussed briefly in the next section.

#### Correlated States

There exist a number of experimental observations which are not explained in terms of the tunneling motion of "standard" TLS. These observations include: (i) A low temperature conductivity which is approximately linear in frequency. This type of conductivity is shown for  $\text{Na}\beta$ -alumina in Fig. 18 for  $T < 0.05\text{K}$ . Such a behavior is also observed in other dielectric solids. (ii) At "high" frequencies ( $\sim 10^{10}\text{sec}^{-1}$ ) the conductivity reaches a frequency independent plateau. This is shown for  $\text{Na}\beta$ -alumina in Fig. 19. (iii) At higher temperatures, many glasses exhibit dielectric and mechanical loss peaks which cannot be fitted by Debye theory with a single relaxation rate. Again for  $\text{Na}\beta$ -alumina, the dielectric loss peak (expressed as  $M'' = \text{Im}(1/\epsilon)$ ) is shown in Fig. 20, the mechanical loss is shown in Fig. 21, and the  $T_1$  minimum vs  $1/T$  for  $^{23}\text{Na}$  NMR is shown in Fig. 22. Qualitatively, these results reflect the thermally activated motion of Na ions over local potential barriers. For a single barrier height  $V$  and relaxation time  $\tau = \tau_0 \exp(V/kT)$ , the response to an oscillating electric field is described by the susceptibility  $\chi \sim 1/(1+i\omega\tau)$  which leads to a symmetric peak for  $\chi''$  at  $\omega = 1/\tau$ . The susceptibility can also be expressed as the Fourier transform of the response function  $f(t) = \exp(-\omega t)$ . It has been known for some time that few dielectric solids exhibit a dielectric response which can be described in terms of the  $\exp(-\omega t)$  response function (71). Instead an empirical function

$$f(t) = t^{-n} \quad (12)$$

which is known as the Curie-von Schweidler law (72,73), provides a better fit to the experimental results. Ngai and coworkers have made theoretical arguments which lead to the

derivation of the  $t^{-n}$  response function. Their proposal rests on the assumption that there exist certain low energy excitations which interact with the particular relaxing species (such as hopping ions) and thereby alter the measured dielectric response from the non-interacting Debye behavior. The proposed low energy excitations are thought to arise from the correlated motion of large numbers of atoms, hence the name correlated states. The parameter  $0 \leq n < 1$  appearing in eq. (12) determines the shape of the loss peak. The model is

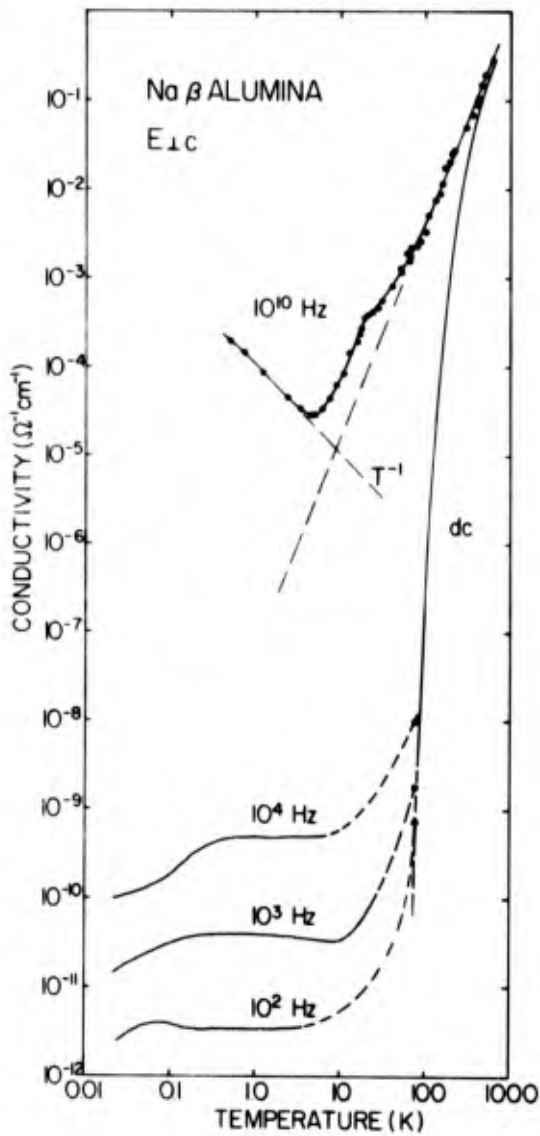


Fig. 18. Conduction plane conductivity of Na $\beta$ -alumina,  $10^{10}$  Hz data (actual frequency  $1.15 \times 10^{10}$  Hz) from Ref. 56. Low frequency data: solid lines from Ref. 61; symbols from Ref. 74.

based on the following points (11): (a) the density of energy level spacings of the correlated states is proportional to their energy, i.e.  $N(E) \sim E$ , as  $E \rightarrow 0$ ; (b) the interaction between correlated states and dipolar species (e.g. hopping ion) is "infrared divergent," i.e. the relation  $V^2 N(E) = nE$  holds, where  $V$  is a sudden potential associated with the relaxing species. These assumptions lead to a condition where the number of excitations diverges logarithmically as  $E \rightarrow 0$ , but that all observables are finite. The postulated correlated states are characterized by  $n$  and the energy  $E_c$ , which is the upper limit for which the relation  $n(E) \sim E$  holds. A best fit to the dielectric loss data for Na $\beta$ -alumina such as in Fig. 19 yields  $n \approx 0.6$  and  $E_c \sim 10^{-3}$  K (in thermal

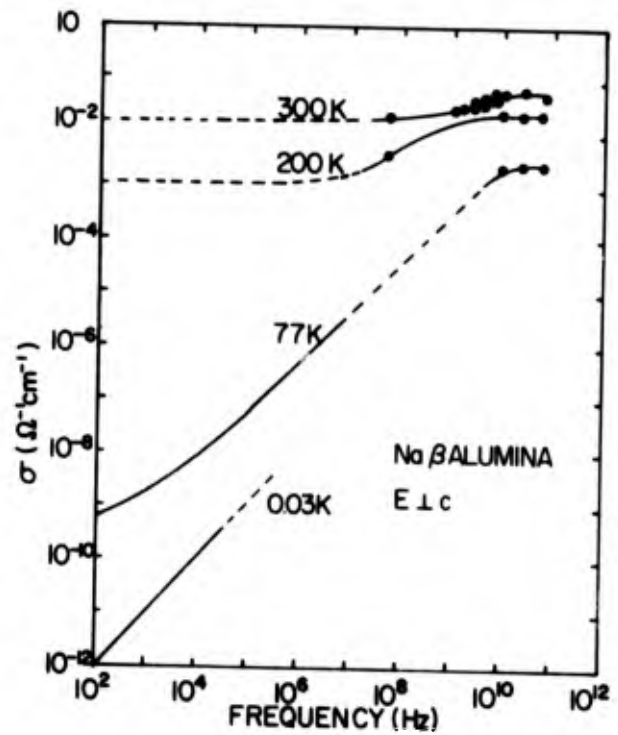


Fig. 19. Ionic conductivity of Na $\beta$ -alumina as a function of frequency and temperature. Data at 0.03K from Ref. 61. Data at 77K from Ref. 74. Data at 200 and 300K from Ref. 14.

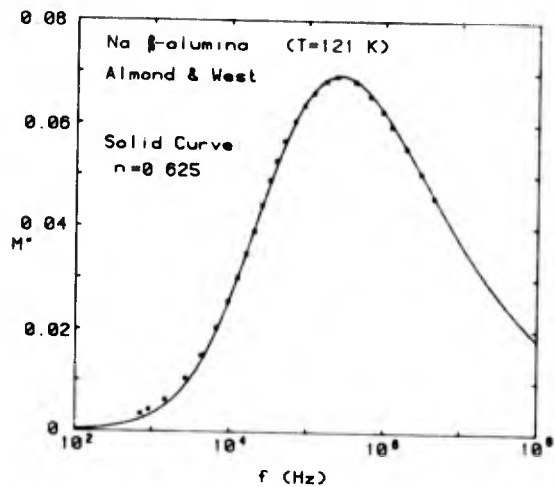


Fig. 20. Imaginary part of electric modulus  $M'' \equiv \text{Im}(\frac{1}{\epsilon^*})$  for Na $\beta$ -alumina as a function of frequency  $f$  for  $T=121$  K. Crosses - data (ref. 76). Solid curves - theoretical fit (see ref. 77).

units). This implies that the spectrum of correlated states can be considered as the low energy complement to the higher energy TLS spectrum. The power of the model is well illustrated by the model fits in Figs. 20-22 for three quite different relaxation experiments. Nearly identical values for  $n$  provide surprisingly good fits to the data. Further details concerning these fits are discussed in Ref. 14.

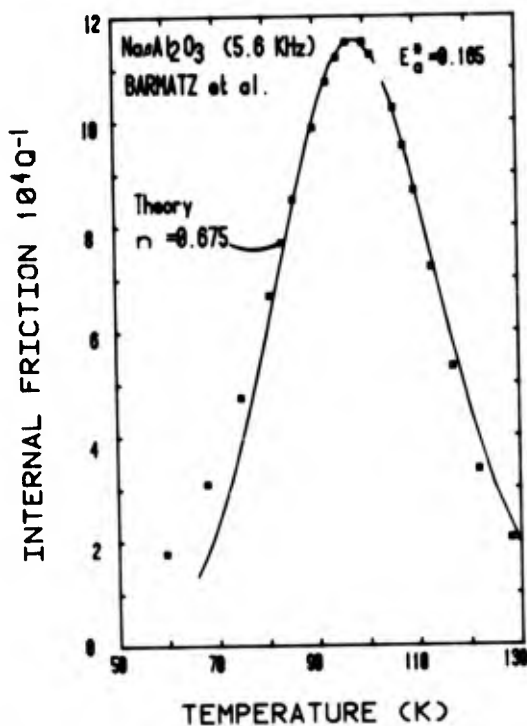


Fig. 21. Internal friction versus temperature for Na $\beta$ -alumina. Squares - data (ref. 78); solid curve - theory (ref. 79).

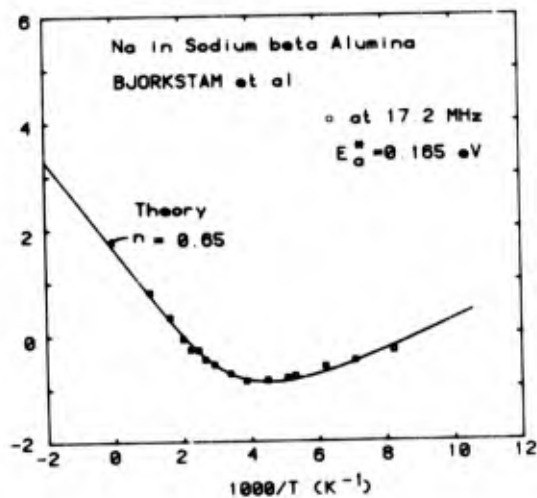


Fig. 22.  $\log T_1$  versus  $\frac{1000}{T}$  for  $^{23}\text{Na}$  NMR in Na $\beta$ -alumina. Solid line - theory (ref. 79)

Dissado and Hill (75) have also examined the problem of non-Debye-like relaxation behavior. They have proposed a similar physical model to that discussed above for correlated states which envisions thermal activation as well as tunneling processes. In contrast to the work of Ngai et al., their model proposed two exponents which characterize the relaxation response for times which are short and long, respectively, compared to the relaxation peak position  $t \sim \omega_p^{-1}$ .

Although the arguments for low energy correlated states are convincing, proof of their existence is difficult, particularly because their energies cannot be easily measured directly. Direct resonant excitation ( $\hbar\omega > kT$ ) is improbable because the highest estimated energy splittings ( $\sim 10^{-3}\text{K}$ ) are smaller than the typically lowest available experimental temperatures. In addition, the nature of the interaction between these states and the rapid dipolar transitions is not well understood. Finally, the correlated states are expected to involve the motion of large numbers of atoms. This requires considerable stretching of the concept of a single particle elementary excitation. The "proof" of the existence of correlated states must remain in their role in defining the apparent universal low frequency response of many diverse disordered materials.

### Conclusion

A considerable body of experimental and theoretical work points to the existence of well-defined phonon excitations in glasses. In particular, LA phonons appear to retain much of the characteristic dispersion expected for periodic structures, including the existence of a pseudo "Brillouin Zone." These conclusions support the interpretation of the  $\sim \omega^2$  far infrared absorption observed in glasses and polymers as due to disorder induced optical coupling to acoustic excitations. The sudden drop of the phonon mean free path above  $\sim 450\text{ GHz}$ , inferred from thermal conductivity, should then be interpreted in terms of structural units in the glass which have dimensions considerably larger than a single molecular unit. Longitudinal acoustic phonons with shorter wavelengths are possibly well-defined but would not contribute to heat transport. In contrast to LA phonons, TA phonons do not exhibit crystalline dispersion and are increasingly damped with decreasing wavelength.

The existence of disorder modes had been invoked in order to conceptualize well-documented mathematical descriptions of glass properties. The low temperature properties of glasses are extremely well-described by the pseudo-spin  $\frac{1}{2}$  formalism (see the paper by S. Hunklinger (81) for recent developments), whereas higher temperature fluctuation-dissipation phenomena are well-described in terms of the  $t^{-n}$  Curie von Schweidler law. However, the interpretation of tunneling and correlated states as elementary excitations of a glass is made difficult by the lack of structural models. A possible approach toward such models is to explore the connection between the inability of a glass to support high frequency TA shear waves and the existence of low energy disorder modes.



## References

- (1) D. Pines, Elementary Excitations in Solids (W.A. Benjamin, New York, 1964), p.1.
- (2) R. Zwanzig, Phys. Rev. **156**, 190 (1967).
- (3) G. S. Grest, S. R. Nagel and A. Rahman, Phys. Rev. Lett. **49**, 1271 (1982).
- (4) J. Hafner, Phys. Rev. **B27**, 678 (1983).
- (5) L. von Heimendahl, J. Phys. **F9**, 161 (1979).
- (6) P. W. Anderson, B. I. Halperin, and C. M. Varma, Phil. Mag. **25**, 1 (1972).
- (7) W. A. Phillips, J. Low Temp. Phys. **7**, 351 (1972).
- (8) D. Emin, Adv. Phys. **24**, 305 (1975); Phil. Mag. **35**, 1189 (1977a).
- (9) P. W. Anderson, Phys. Rev. Lett. **34**, 953 (1975).
- (10) A. Alexander, C. Laermans, R. Orbach, and H. M. Rosenberg, Phys. Rev. **B28**, 4615 (1983).
- (11) K. L. Ngai, Comments Solid State Phys. **9**, 127 (1979); **9**, 141 (1980).
- (12) D. Weaire and P. C. Taylor, Dynamical Properties of Solids, Vol. 4, ed. by G. K. Horton and A. A. Maradudin (North Holland, 1980), p. 1.
- (13) S. Hunklinger and M. V. Schickfus, Amorphous Solids, ed. by W. A. Phillips (Springer, 1981), p. 13.
- (14) U. Strom, Solid State Ionics **8**, 255 (1983).
- (15) S. Hunklinger and W. Arnold, Physical Acoustics, ed. by W. P. Mason and R. N. Thurston (Academic, New York, 1976), Vol. XII, pp. 155-215.
- (16) W. F. Love, Phys. Rev. Lett. **31**, 822 (1973).
- (17) R. Vacher and J. Pelous, Phys. Rev. **14**, 823 (1976).
- (18) M. Rothenfusser, W. Dietsche, and H. Kinder, Phys. Rev. **B27**, 5196 (1983); and in Phonon Scattering in Condensed Matter, eds. W. Eisenmenger, K. Lassmann, and S. Döttinger (Springer, 1984), p. 419.
- (19) J. Jäckle, Amorphous Solids, ed. by W. A. Phillips (Springer, 1981), p. 135.
- (20) U. Strom and P. C. Taylor, Phys. Rev. **B16**, 5512 (1977).
- (21) M. Rubinstein and P. C. Taylor, Phys. Rev. **B9**, 4258 (1974).
- (22) R. J. Nemanich, Phys. Rev. **B16**, 1655 (1977).
- (23) J. S. Launin, Solid State Commun. **12**, 947 (1973).
- (24) G. Winterling, Phys. Rev. **B12**, 2432 (1975).
- (25) U. Strom and P. C. Taylor, Phys. Rev. **B16**, 5512 (1977).
- (26) W. S. Vinogradov, Sov. Phys. Sol. State **2**, 2332 (1961).
- (27) E. Schlömann, Phys. Rev. **133**, A413 (1964).
- (28) R. H. Stolen, Phys. Chem. Glasses **11**, 83 (1970).
- (29) R. Rammal, Phys. Rev. **B28**, 4871 (1983).
- (30) M. Dutta and H. E. Jackson, Phys. Rev. **B24**, 2139 (1981).
- (31) D. P. Jones, J. Jäckle, and W. A. Phillips, in Phonon Scattering in Condensed Matter, ed. by H. J. Maris (Plenum, New York, 1980), p. 49.
- (32) J. Hubbard and L. L. Beeby, J. Phys. C (Solid St. Phys.) **2**, 556 (1969).
- (33) S. Takeno and M. Goda, Progr. Theor. Phys. **47**, 790 (1972).
- (34) J. J. Rehr and R. Alben, Phys. Rev. **B16**, 2400 (1977).
- (35) A. Rahman, M.J. Mandell, and J.P. McTague, J. Chem. Phys. **64**, 1564 (1976).
- (36) J. Hafner, J. Phys. C, **14**, L287 (1981).
- (37) G. S. Grest, S. R. Nagel, and A. Rahman, Phys. Rev. **B29**, 5968 (1984).
- (38) J. B. Suck, H. Rudin, H. J. Güntherodt, and H. Beck, J. Phys. C, **14**, 2305 (1981).
- (39) J. B. Suck and H. Rudin, in Glassy Metals II, Topics in Applied Physics, ed. by H. Beck and H. J. Güntherodt (Springer, Berlin, in press).
- (40) A. C. Wright and A. J. Leadbetter, Phys. Chem. Glasses **17**, 122 (1976).
- (41) A. J. Leadbetter and A. C. Wright, J. Non-cryst. Solids **3**, 239 (1970).
- (42) A. J. Leadbetter, J. Chem. Phys. **51**, 779 (1969).
- (43) W. Dietsche and H. Kinder, Phys. Rev. Lett. **43**, 1413 (1979).
- (44) M. P. Zaitlin and A. C. Anderson, Phys. Status Solidi **B71**, 323 (1975).
- (45) S. Kelham and H. M. Rosenberg, J. Phys. C **14**, 1737 (1981).
- (46) R. Shuker and R. W. Gammon, Phys. Rev. Lett. **25**, 222 (1970).
- (47) F. L. Galeener, A. J. Leadbetter, and M. W. Stringfellow, Phys. Rev. **B27**, 1052 (1983).
- (48) F. L. Galeener and G. Lucovsky, Phys. Rev. Lett. **37**, 1474 (1976).
- (49) V. N. Denisov, B. N. Mavrin, V. B. Podobednov, K. E. Sterin, and B. G. Varshal, J. Noncryst. Solids **64**, 195 (1984).
- (50) P. J. Anthony and A. C. Anderson, Phys. Rev. **B16**, 3827 (1977).
- (51) D. B. McWhan, S. M. Shapiro, J.P. Remeika, and G. Shirane, J. Phys. C8, L487 (1975).
- (52) R. O. Pohl, Amorphous Solids, ed. by W. A. Phillips (Springer, 1981), p. 27.
- (53) J. C. Lasjaunias, R. Maynard, and M. Vandorpe, J. de Physique, **C6**, 972 (1978).
- (54) M. T. Loaponen, R. C. Dynes, V. Narayana-murti, and J. P. Garno, Phys. Rev. Lett. **45**, 457 (1980).
- (55) P. J. Anthony and A. C. Anderson, Phys. Rev. **B14**, 5198 (1976).
- (56) U. Strom, M. v. Schickfus, and S. Hunklinger, Phys. Rev. **B25**, 2405 (1982).
- (57) S. Hunklinger, W. Arnold, S. Stein, R. Nava, and K. Dransfeld, Phys. Lett. **30**, 23 (1972).
- (58) B. Golding, J. E. Graebner, B. I. Halperin, and R. J. Schutz, Phys. Rev. Lett. **30**, 223 (1973).
- (59) J. Jäckle, Z. Phys. **257**, 212 (1972).
- (60) T. Doussineau, C. Frenois, R. G. Leisure, A. Levelut and J. Y. Prieur, J. Phys. (Paris) **41**, 1193 (1980).
- (61) P. J. Anthony and A. C. Anderson, Phys. Rev. **B19**, 5310 (1979).
- (62) J. E. Graebner and B. Golding, Phys. Rev. **B19**, 964 (1979).

- (63) W. Arnold, C. Martinon, and S. Hunklinger, *J. Phys. (Paris) Lett.* **39**, C6-961 (1978).
- (64) B. Golding, M. v. Schickfus, S. Hunklinger, and K. Dransfeld, *Phys. Rev. Lett.* **43**, 1817 (1979).
- (65) M. v. Schickfus and U. Strom, *Phys. Rev.* **B28**, 1068 (1983).
- (66) V. Narayanamurti (private communication).
- (67) J. Jofirin and A. Levelut, *J. Phys. (Paris)* **36**, 811 (1975).
- (68) S. R. Kurtz and H. J. Stapleton, *Phys. Rev. Lett.* **42**, 1773 (1979).
- (69) S. G. Greenbaum, U. Strom, and M. Rubinstein, *Phys. Rev.* **B26**, 5226 (1982).
- (70) S. G. Greenbaum and U. Strom, *Solid State Commun.* **46**, 437 (1983).
- (71) A.K. Jonscher, *Nature (London)* **256**, 566 (1975).
- (72) J. Curie, *Ann. Chim. Phys.* [6] **17**, 385 (1888); [6] **18**, 203 (1889);
- (73) E. von Schweidler, *Ann. Physik* **24**, 711 (1907).
- (74) R.J. Grant, I.M. Hodge, M.D. Ingram, and A.R. West, *Nature* **266**, 42 (1977).
- (75) L.A. Dissado and R.M. Hill, *Phil. Mag. B* **41**, 625 (1980).
- (76) D.P. Almond and A.R. West, *Solid State Ionics* **34**, 73 (1981).
- (77) K.L. Ngai and U. Strom, *Phys. Rev. B* **27**, 6031 (1983).
- (78) M. Barmatz and R. Farrow in *Proc. 1976 Ultrasonics Symposium*, eds. J. de Klerk and B. McAvoy (IEEE, New York, 1976).
- (79) K.L. Ngai, *Solid State Ionics* **5**, 27 (1981).
- (80) J.L. Bjorkstam, M. Villa, S. Aldravandi, M. Corti, and J.S. Frye, in *Nuclear and Electron Resonance Spectroscopies Applied to Materials Science*, eds. Kaufman and Shenoy (North Holland, 1981), p. 295.
- (81) S. Hunklinger, in *Phonon Scattering in Condensed Matter*, eds. W. Eisenmenger, K. Laßmann, and S. Döttinger (Springer, New York, 1984), p. 378.

# **THEORY AND MODELS**

# FIRST PRINCIPLES MICROSCOPIC UNDERSTANDING OF GLASSES AND GLASS TRANSITIONS

Siu-Tat Chui  
Bartol Research Foundation of The Franklin Institute  
University of Delaware  
Newark, Delaware 19716

## Abstract

This paper is an attempt at a first principles quantitative understanding of the physical properties of glasses and the glass transition. The basic philosophy is to describe glasses with respect to a reference system, the fluid before the quench. A specific example for a very simple case is worked out. Reasonable agreement with results on Lennard-Jones computer glasses is found. It is hoped that this example can be generalized to metallic glasses. In the example discussed, the effect of quench rate has not been treated quantitatively. These and many other open questions beg for further exploration.

## I. Introduction

The physics of glasses is one of the fundamental problems in condensed-matter physics which remain relatively unexplored. A major obstacle to a clear picture of glasses is the lack of an analytical formulation of the structure of the glassy state and the glass transition.

Glasses can be prepared in many different ways. A common view is to rapidly quench a fluid to below its melting temperature. As a fluid is quenched, it is generally thought that a kind of "jamming" takes place as a range of temperature, the glass transition temperature, is approached.

The particles in the glassy phase in general has not moved very far away from their original position in the fluid phase right before the quench. The philosophy of our approach is to regard the fluid phase as a reference system and to describe the glassy state with respect to this reference system. Since the displacements after the quench is small, the description in terms of the reference system should be simpler.

This philosophy is reminiscent to the Van der Waals idea of the fluid, which describes a general fluid with respect to a reference system, the hard core fluid. Recent perturbation theories of fluid exploiting this technique has

led to a simple and successful quantitative description of simple fluids.<sup>1</sup>

Glasses in general can be made from many different molecules. The program that we want to follow is quite complicated. In order to get some understanding of what is involved, we want to test it on the simplest possible system.

A more detailed understanding of the nature of glasses and the glass transition has motivated much recent computer work on those glasses obtained by quenching particles interacting through simple model potentials. This includes the works of Alder and Wainwright,<sup>2</sup> Rahman, Mandel, and McTague,<sup>3</sup> Stillinger and Weber,<sup>4</sup> Wendt and Abraham,<sup>5</sup> Angel, Clarke and Woodcock,<sup>6</sup> Raveche,<sup>7</sup> Hudson and Anderson,<sup>8</sup> Nagel, Rahman, and Grest,<sup>9</sup> and Steinhardt, Nelson, and Ronchetti.<sup>10</sup> It is generally observed that, within the time scale of the simulation, a metastable phase is obtained if the high temperature fluid phase is quenched sufficiently rapidly to a low enough temperature.

Many of the properties of this glassy state have now been computed, including the pair correlation function, the diffusion constant, and phonon structure factors. While experimental systems are in general more complicated than this, it is hoped that a detailed understanding of such simple systems will provide insight into the technologically more important real glasses.

There have been other attempts at understanding glasses.<sup>2-16</sup> Notable among these is the free volume theory of Turnbull and Cohen<sup>13</sup> and Cohen and Grest,<sup>14</sup> theories of topological defects due to Rivier and Duffy,<sup>15</sup> by Klamann, Sadoc and Mosseri,<sup>15</sup> and by Phillips,<sup>15</sup> and a theory by Vitek, Egami, and coworkers.<sup>16</sup> These approaches are complementary to ours.

In the next section, we will first recapitulate the essential idea of our approach. Next, possible avenues and methods of further research will be discussed.

## II. Basic ideas and possible avenues of further research

Most of our ideas are spelled out in two recent papers.<sup>11</sup> Atomic movements in fluids usually exhibit two time scales. There is a short time scale on the order of  $10^{-12}$  sec that describes motion on the scale of atomic distances, and there is the much longer time scale of a diffusive "collective" motion over much longer distances. After a fluid is quenched from a high temperature, there is an initial relaxation over atomic-scale distances. If a glass is formed, then no further motion would take place. It is the properties of this relaxed low-temperature "state" and not those of the high-temperature fluid phase which govern the nature of glass transitions and glassy states.

Our model differs from previous approaches in that it focuses on this low-temperature relaxed state. For simplicity, assume that the quenching is infinitely fast. Immediately after the quenching, each atom relaxes from an initial position  $r_i^0$  to a final position  $r_i$ , a point of the order of an atomic distance away from the initial position. These atoms are then momentarily stopped as they run against other particles. To relax further, an atom must move around another particle to seek a new saddle point in the potential energy barrier.<sup>17</sup>

In the fluid, this latter motion presumably involves many other particles, each moving by a small amount, so that a "channel" is opened up at essentially zero cost in free energy.<sup>18</sup> As this diffusive motion takes place, the directions of the vectors  $\delta r_i = r_i - r_i^0$  must rotate. If there is a cooperative interaction effect among the directions of these vectors such that they are "frozen" and are no longer free to rotate, the above motion will be impeded and we interpret this as a glassy state. The glass transition then corresponds to a kind of transition in which the orientations of these vectors are frozen. The probability for this relaxed state is then the same as that of the glassy state.

In principle, one must solve Newton's equation of motion to determine the relaxation and so determine the probability distribution. Just as is done in the formulation of statistical mechanics, we shall bypass this by proposing a probability measure for the relaxed state.

There are essentially three ingredients that enter into the formulation of statistical mechanics and thus determine the measure in probability space. In addition to the ergodic hypothesis that arbitrarily small neighborhoods of all points in phase space are visited, the necessary conditions for the determination of phase space measure are the existence of a conserved quantity and the validity of Liouville's theorem. For most statistical-mechanical problems, energy plays the role of the conserved quantity and the phase-space measure is an invariant of the motion. From this, one may derive the canonical distribution.

For a general dynamical system described by nonlinear differential equations, Kerner<sup>19</sup> has discussed a recipe by means of which the probability measure can be obtained, with the proviso that the dynamical system be ergodic. For glasses, the equation of motion remains Newton's equation, energy is a conserved quantity, and Liouville's equation is satisfied. We now make the additional restricted ergodic hypothesis that, within the region of phase space that a glass can sample immediately after the quench, all states are visited.

We thus propose that the probability  $P$  of finding a particle at site  $r$  is given by the probability of its being at some initial site  $r^0$  multiplied by the conditional probability of a particle relaxing from  $r^0$  to  $r$ . The conditional probability is determined from the restricted canonical distribution we have introduced above. The initial probability is determined by the liquid distribution function. Hence

$$P = \frac{1}{Z_i Z_f} \exp \left[ -\sum_{i,j} (\beta_i V(r_i^0, r_j^0) + \beta_f V(r_i, r_j)) \right] \prod_i \theta(|\delta r_i| < c) \quad (1)$$

Here  $\beta = 1/k_B T$  ( $k_B$  is the Boltzmann constant) and  $\theta(x)$  is a Heaviside unit step function.  $Z_f$  is the partition function for the final liquid distribution, taken over the restricted phase space. The  $\theta$  function embodies the restriction that immediately after the quench particles cannot relax by more than an atomic distance  $c$  from their positions prior to the quench. Using  $P$ , one can investigate a possible transition involving the orientations of the vectors  $\delta r_i$ .

$P$  can also be interpreted as the distribution of a liquid of fictitious diatomic molecules with atoms at  $r_i$  and  $r_i^0$  and an intramolecular interaction in the form of a hard-perimeter attractive potential. It is known that there can be long-range orientational positional order of such molecules. In fact, much effort has been devoted to understanding the nematic liquid crystals where such ordering occurs.

We have performed a self consistent calculation to investigate this orientational transition. The details of this are given in Appendix A. It employs the approximations used in the spin glass problem. Randomness and frustration<sup>20</sup> are generally thought to be key ingredients of the spin glass. The same features appear in the present problem. Randomness comes about because we have to do an ensemble average over the initial distribution before the quench. Frustration comes about because of the following. To lowest order in the displacement of the particles from their initial positions, the particles like to move in the same direction after the quench. This corresponds to a net motion of the center of mass and

hence is not of much interest. In the next order, the particles like to move perpendicular to each other; in the language of our fictitious molecules this corresponds to an "anti-nematic" interaction. For most arrangement of these "molecules", it is not possible to have all the nearest neighbor anti-nematic bonds satisfied. We have determined the short range order of the fluid<sup>21</sup> and find that it is f.c.c. like. Frustration effects certainly exist in that case. With  $\langle \delta r \rangle$  obtained directly from a computer simulation, we obtain transition temperatures comparable to those obtained by Monte-Carlo simulations. At a reduced density  $\rho^* = 0.95$ , simulations indicate that  $0.25 < T_g^* < 0.34$ ,<sup>5</sup> while our estimate indicates that  $T_g^* \approx 0.37$ . Since our calculation is mean-field like, we have not really addressed the question of the existence of a true thermodynamic singularity. Our calculation only suggests when relaxation rates become extremely long.

There has been some interest in whether the repulsive part of the interaction potential plays an important role in the glass transition. Our anti-nematic interaction is dominated by the repulsive part of the Lennard-Jones potential. Indeed, the attractive part of the potential provides a nematic rather than an anti-nematic contribution. It is interesting to note the dependence of  $T_g$  on the softness of a potential of the form  $V = \epsilon r^{-m}$ . Roughly speaking,  $T_g \rho^{-m/3}$  depends on the fourth derivative of the potential, and hence depends on  $m^4$ . On the other hand, according to Lindemann's criterion, the melting temperature  $T_m$  depends on the second derivative of the potential and hence  $m^2$ . If  $\langle \delta r^4 \rangle (\rho^2/2)^{2/3}$  does not change appreciably as  $m$  is changed, we then expect that as the potential becomes softer  $T_g/T_m$  will decrease; it would thus be more difficult to form a glass. This is consistent with the conjectures of Angell, et al.;<sup>2</sup> our reasoning, however, differs from theirs.

Based on the analogy to molecules<sup>22</sup> and using the "replica" approximation used in spin glasses, we have derived a set of integral equation for the pair correlation function in the glassy state. This equation corresponds to that of a molecular fluid of  $(m+1)$  atomic molecules in the limit  $m$  approaching zero. We have previously looked at the pair correlation function of glasses with a cruder approximation but the same general philosophy. We find that the first peak can be reasonably reproduced but fail to find a split second peak observed in computer simulations when the final quenching temperature is low enough. It would be interesting to see if the present approach provides for an improvement.

Finally, let us turn our attention to the diffusion coefficient. The diffusion coefficient  $D$  is related to the Fourier transform  $\tilde{\xi}(\omega)$  of the memory function  $\xi(t)$  by  $D = T/m\tilde{\xi}(0)$ .<sup>23</sup> It has been proposed that<sup>23</sup>

$$\xi(t) = \alpha_0^2 \exp(-\frac{1}{2} B_0 t^2) + A_0 t^4 \exp(-\alpha_0 t). \quad (2)$$

The first term in this expression arises from the short time effect,

$$\alpha_0^2 = \frac{\rho}{3m} \int dr g(r) \nabla^2 v(r). \quad (3)$$

The second term is a consequence of the caging effect of neighboring atoms and is chosen so that the first term will produce the correct time dependence to order  $t^2$ . In fact, due to these backscattering effects, the velocity autocorrelation function becomes negative at long times and high densities. With the physical interpretation of the second term given here, we expect  $\alpha_0$  to be inversely proportional to the relaxation time  $\tau$  of our quadrupolar system. Close to  $T_g$ , we expect  $\tau \propto (T-T_g)^{-z}$ , where  $z$  is the dynamic critical exponent. From equation (2) one obtains  $D^{-1} \propto (T-T_g)^{-5z}$  when  $\alpha_0$  is small ( $\tau$  large).<sup>15</sup> Even though this is not of the Doolittle form,  $\exp(-\text{const.}/(T-T_g))$ , it is rather difficult to distinguish between the two forms for  $z$  of the order of unity. In fact, Levesque and Verlet<sup>23</sup> have fitted their computer data for LJ particles for density  $\rho$  up to 0.85 and temperature  $T$  down to 0.76 by the form  $\alpha_0 = 4.12 - 2.61\rho = 2.61(\rho_0 - \rho)$ , where  $\rho_0 = 1.6$ . If we follow the common practice of replacing  $\rho - \rho_0$  with  $T - T_g$ , we then obtain a dynamic critical exponent  $z = 1$ . It is amusing to note that a mean field treatment of spin glasses provides the same exponent. We have also replotted the data of Woodcock and Angell<sup>6</sup> for the diffusivities of hard-sphere liquids and find that they can also be fitted with a dependence of the form  $(\rho - \rho_0)^x$  with  $x$  around four. Our argument that  $\alpha_0 \propto (T-T_g)^2$  should, however, apply only in the "critical region." It is not clear how wide this region is.

#### Appendix A

Our calculation is based on the similarity of the present problem to that in the spin glass transition. To bring this similarity into focus, let us write the logarithm of the partition function (the free energy) as

$$[\ln Z] = [\ln \int \prod_i dr_i \int \prod_i \theta(|\delta r_i| < c) \exp - \beta_f \sum_{i,j} V(r_{ij})] \quad (A1)$$

Here the square bracket indicates an average with respect to the initial distribution of the particle positions, viz.

$$[f(r^0)] \equiv \frac{1}{Z_i} \int \prod_i dr_i^0 f(r^0) \exp - \beta_f \sum_{i,j} V(r_{ij}^0) \quad (A2)$$

In the spin glass problem, disorder is introduced via a distribution in the exchange constants. In the calculation of the free energy, one has to do an average over such exchange constants. This averaging over the exchange constants is analogous to the averaging over the  $r_i^0$  indicated by the square bracket above.

An approximation known as the replica method has been extensively studied in the spin glass problem. In the simplest version without what is known as replica symmetry breaking<sup>25</sup>, this approximation leads to a reasonable estimate of when things begin slowing down. This approximation breaks down at very low temperatures. We shall apply this approximation to a calculation of the "transition" temperature and the pair correlation function in the glassy phase. Let us formulate our ideas more precisely.

First we derive a formula for the pair correlation function  $N(12)$ . We follow tradition by introducing external potentials  $\psi(i)$  acting on particle  $i$ . The partition function now looks like

$$Z = \int \prod_i dr_i \theta(\delta r_i < c) \exp(-\beta_f \sum_{i,j} V(ij) - \sum_i \beta_f \psi(i))$$

It is straightforward to show that

$$N(12) = \frac{1}{\beta_f^2} \frac{\delta^2}{\delta \psi(1) \delta \psi(2)} [\ln Z] |_{\psi=0} \quad (A3)$$

In general, the average  $[\ln Z]$  is very difficult to do. We now follow the spin glass idea<sup>24</sup> and rewrite  $\ln Z$  as

$$\ln Z = \lim_{m \rightarrow 0} (Z^m - 1)/m$$

and

$$N(12) = \frac{1}{\beta_f^2} \frac{\delta^2}{\delta \psi(1) \delta \psi(2)} [Z^m] / m |_{\psi=0} \quad (A4)$$

Note that  $[Z^m]$  corresponds to the partition function of a fluid of molecules each composing of  $m+1$  atoms, viz.

$$[Z^m] = \int \prod_{\alpha} \theta(|r_i^{\alpha} - r_i^0| < c) \prod_{\alpha=1}^m dr_i^{\alpha} dr_i^0 \exp(-\beta_f \sum_{\alpha, i, j} V(r_{ij}^{\alpha}) - \beta_f \sum_i V(r_i^0)) \quad (A5)$$

An approximate method to calculate the pair correlation function of molecular fluids have been discussed by Chandler<sup>22</sup> and collaborators. This can be generalized to the present problem to any integer  $m$ . One gets

$$\hat{h}_{\alpha\alpha} = \hat{C}_{\alpha\alpha} + W \hat{C}_0 \hat{W} + \sum_{\beta \neq \alpha, 0} \hat{W}_{\alpha\beta} \hat{C}_{\beta\beta} \hat{W}_{\beta\alpha} + \rho \hat{C}_{\alpha\alpha} \hat{h}_{\alpha\alpha} + \rho \hat{W} \hat{C}_0 \hat{h}_{0\alpha} + \sum_{\beta \neq \alpha, 0} \hat{W}_{\alpha\beta} \hat{C}_{\beta\beta} \hat{h}_{\beta\alpha}$$

$$\hat{h}_{\alpha 0} = \hat{W}_{0\alpha} \hat{C}_{\alpha\alpha} + \hat{C}_0 \hat{W}_{\alpha 0} + \sum_{\beta \neq \alpha, 0} \hat{W}_{0\beta} \hat{C}_{\beta\beta} \hat{W}_{\beta\alpha} + \rho \hat{W}_{0\alpha} \hat{C}_{\alpha\alpha} \hat{h}_{\alpha\alpha} + \rho \hat{C}_0 \hat{h}_{\alpha\alpha} + \rho \sum_{\beta \neq 0, \alpha} \hat{W}_{0\beta} \hat{C}_{\beta\beta} \hat{h}_{\beta\alpha}$$

$$\hat{h}_{\beta\alpha} = \hat{W}_{\beta\alpha} \hat{C}_{\alpha\alpha} + \hat{W}_{\beta 0} \hat{C}_0 \hat{W}_{0\alpha} + \hat{C}_{\beta\beta} \hat{W}_{\beta\alpha} + \rho \hat{W}_{\beta\alpha} \hat{C}_{\alpha\alpha} \hat{h}_{\alpha\alpha} + \rho \hat{C}_{\beta\beta} \hat{h}_{\beta\alpha} + \rho \hat{W}_{\beta 0} \hat{C}_0 \hat{h}_{0\alpha} + \rho \sum_{\alpha' \neq \beta, \alpha, 0} \hat{W}_{\beta\alpha'} \hat{C}_{\alpha'\alpha'} \hat{h}_{\alpha'\alpha}$$

Here  $h_{\alpha\beta} = g_{\alpha\beta} - 1$   
 $g_{\alpha\beta} = N_{\alpha\beta}/\rho^2$ ;  $\rho$  is the density of the fluid. The "hat's" indicate Fourier transforms.  $C_{\alpha\beta}$  are the direct correlation functions.  $W_{\alpha\beta}$  are the infra-molecular correlation function. We have used the notation of Chandler et al. We shall assume that the subscript  $\alpha$  is indistinguishable from each other, viz.

$$W_{0\alpha} = W \text{ for all } \alpha \\ W_{\beta\alpha} = \hat{W} \text{ for all } \alpha \neq \beta \\ C_{\alpha\alpha} = C_2 \text{ for all } \alpha \neq 0 \quad h_{\alpha\alpha} = h_2 \text{ for all } \alpha \neq 0$$

It is then straightforward to take the  $m \rightarrow 0$  limit and one obtains

$$\hat{h}_{\alpha\alpha} (1 - \rho \hat{C}_0) = \hat{W} \hat{C}_2 + \hat{C}_0 \hat{W} - \hat{W} \hat{C}_2 \hat{W} + \rho \hat{W} \hat{C}_2 \hat{h}_{22} - \rho \hat{W} \hat{C}_2 \hat{h}_{\beta\alpha} \\ \hat{h}_{\beta\alpha} = \hat{W} \hat{C}_2 + \hat{W} \hat{C}_0 \hat{W} + C_2 \hat{W} + \rho \hat{W} \hat{C}_2 \hat{h}_{\alpha\alpha} + \rho \hat{C}_2 \hat{h}_{\beta\alpha} + \rho \hat{W} \hat{C}_0 \hat{h}_{0\alpha} \quad (A6)$$

K. B. Ma and myself are attempting to solve these equations numerically at the moment and hopefully results will be forthcoming.

We now turn our attention to an estimate of the transition temperature.

The philosophy behind our approach is to express physical quantities in terms of its deviation from the reference system, the

fluid before the quench. We hence rewrite  $Z^m$  as

$$Z^m = \int \prod_{i,\alpha=0}^m dr_i^\alpha \exp - \beta_f \sum_{\alpha,ij} \Delta V_\alpha(ij) - \beta_i \sum V(r_{ij}^0) + m \beta_f \sum V(r_{ij}^0)$$

$$\text{where } \sum_{ij} \Delta V_\alpha(ij) = \sum_{ij} (V(r_{ij}^\alpha) - V(r_{ij}^0))$$

We now proceed to do the averaging with respect to  $r_i^0$  in a cumulant expansion with respect to  $\Delta V$ . This is the crucial approximation behind the present approach. If the particles have not moved far away from the original position before the quench  $\Delta V$  should be small in some sense.

We hence have

$$[Z^m] = \int \prod_{i,\alpha=1}^m dr_i^\alpha \exp - ([\beta_f \sum \Delta V]) + [\frac{1}{2}(\Delta V^2 - V^2)]$$

It is possible to write  $\Delta V$  in an angular momentum expansion as  $\Delta V(12) = \sum Y_{l_1 m_1}(\Omega_{\delta r 1}) Y_{l_2 m_2}(\Omega_{\delta r 2}) Y_{l_1 m_1}(\Omega_{ij}^0) Y_{l_2 m_2}(\Omega_{ij}^0) \langle l_1 l_2 l_1 m_1 m_2 | l_0 m_0 \rangle V_1$ .

The above form is dictated by rotation invariance. In general, it is unlikely that all angular momentum components become important at the same time. Hence we shall focus on only a single component  $l = l_1 = l_2$ . Note that

$$[\Delta V] = \sum Y_{l_1 m_1}(\Omega_i^0) Y_{l_1 m_1}^*(\Omega_j^0) \langle l_1 l_1 l_0 m_0 | 0 \rangle V_0$$

In general, this will induce a periodic order in the system. This is not what we are interested in and hence will be discarded.  $[\Delta V^2]$  is even in  $\delta r_{ij}$ . Hence the smallest  $l_0$  is 2. The self-consistent equation for the order parameter  $X_{ma,mb} = \langle Y_{2m_a}(\Omega_1^\alpha) Y_{2m_b}(\Omega_1^\beta) \rangle$

can be easily written down and one gets

$$X_{ma,mb} = \frac{n}{2} \sum_{l \neq 0} V_l^2 \langle l -m_a \quad 2 \quad l \quad m \rangle \langle l -m_b \quad 2 \quad l \quad m \rangle X_{m_2, m_4} / (4\pi)^3$$

Where  $n$  is the number of nearest neighbors. We have been able to find a solution given by

$$X_{ma,mb} = \delta_{ma,-mb} X \text{ with } X \text{ satisfying the equation}$$

$$X = \frac{n}{2} \sum_{l,m} V_l^2 ((2l+1)/5) X / (4\pi)^3 \quad (A7)$$

We have made use of some of the properties of the Clebsch Gordon coefficient in arriving at the above equation. For Lennard-Jones potentials, it is possible to obtain an estimate of  $V_2$  and  $V_4$ . Finally one obtains a transition

temperature  $T_g = 0.37$ .

## References

- (1) H. C. Andersen, D. Chandler, J. D. Weeks, *Advances in Chem. Phys.* **34** 105 (1976).
- (2) B. S. Alder and T. E. Wainwright, *J. Chem. Phys.* **33**, 1439 (1960).
- (3) A. Rahman, M. J. Mandell, and J. P. McTague, *J. Chem. Phys.* **64**, 1564 (1976).
- (4) F. H. Stillinger and T. A. Weber, *J. Chem. Phys.* **70**, 4879 (1979).
- (5) H. R. Wendt and F. F. Abraham, *Phys. Rev. Lett.* **41** 1244 (1978); F. F. Abraham, *J. Chem. Phys.* **72**, 359 (1980).
- (6) C. A. Angell, J. H. R. Clarke, and L. V. Woodcock, in *Advances in Chemical Physics*, edited by I. Prigogine and S. A. Rice (Wiley, New York 1981), Vol. 48, and references therein. Also C. A. Angell and L. V. Woodcock, *Phys. Rev. Lett.* **47**, 1129 (1982).
- (7) H. J. Raveche, *Ann. N.Y. Acad. Sci.* **279**, 36 (1976).
- (8) S. Hudson and H. C. Anderson, *J. Chem. Phys.* **69**, 2323 (1978).
- (9) S. R. Nagel, A. Rahman, and G. S. Grest, *Phys. Rev. Lett.* **47**, 1665 (1981), G. S. Grest, S. R. Nagel, and A. Rahman, *Phys. Rev. Lett.* **49**, 1271 (1982).
- (10) P. J. Steinhardt, D. R. Nelson, and M. Ronchetti, *Phys. Rev. Lett.* **47**, 1297 (1981).
- (11) S. T. Chui, G. O. Williams, and H. L. Frisch, *Phys. Rev.* **26** 171 (1982), S. T. Chui and G. O. Williams, "A new model of a glass transition" (unpublished).
- (12) S. F. Edwards and W. Warner, *Phil. Mag.* **A40**, 257 (1979), C. H. L. Goodman, *Nature* **257**, 370 (1975), *Ann. N.Y. Acad. Sci.* **279** (1976), *Ann. N. Y. Acad. Sci.* **371** (1981), and G. S. Cargill, in *Solid State Physics*, Vol. 30, edited by F. Seitz and D. Turnbull (Academic Press, New York, 1975).
- (13) M. H. Cohen and D. Turnbull, *J. Chem. Phys.* **31**, 1164 (1959), and D. Turnbull and M. H. Cohen, *J. Chem. Phys.* **52**, 3038 (1970).
- (14) G. S. Grest and M. H. Cohen, *Phys. Rev. B* **21**, 4113 (1980), and G. S. Grest and M. H. Cohen in *Advances in Chemical Physics*, edited by I. Prigogine and S. A. Rice (Wiley, New York, 1981) Vol. 48.



- (15) N. Rivier and D. M. Duffy, in Critical Phenomena, Vol. 9 of Springer Series in Synergetics, edited by J. Della Dora, J. Demongeot, and J. Lacolle (Springer, New York 1981); M. Kleman and J. F. Sadoc, J. Phys. (Paris) 40, L569 (1979); J. F. Sadoc and R. Mosseri, Phil. Mag. B45, 467 (1982); M. Kleman, J. de Phys. 43, 1389 (1982); J. C. Phillips in Solid State Physics, Vol. 37, p. 93, ed. F. Seitz and D. Turnbull, Academic Press).
- (16) D. Srolovitz, K. Maeda, V. Vitek, and T. Egami, Phil. Mag. A 44, 847 (1981), D. Srolovitz, K. Maeda, S. Takeuchi, T. Egami and V. Vitek, J. Phys. F (in press), T. Egami and D. Srolovitz, J. Phys. F. (in press), D. Srolovitz, T. Egami, and V. Vitek, Phys. Rev. B 24, 6936 (1981), and T. Egami (unpublished).
- (17) This roughly corresponds to the picture of a cade in the language of Cohen and Grest (Ref. 13).
- (18) This is consistent with the picture of L. V. Woodcock and C. A. Angell (Ref. 5) who pointed out that the probability of finding a particle-sized hole is negligible in a 512 hard-sphere particle sample around the freezing temperature, during the period in which the diffusion remains substantial.
- (19) E. H. Kerner in Advances in Chemical Physics, edited by I. Prigogine and S. A. Rice, Vol. 19 (Wiley, New York, 1971).
- (20) G. Toulouse, Commun. Phys. 2, 145 (1977). In the present context, this just means that there is no way for all the "anti-nematic" intermolecular bonds to be satisfied.
- (21) We select a coordinate system with the z-axis along the nearest-neighbor bond and the y-axis perpendicular to another nearest-neighbor bond and compute

$$g(\underline{r}) = \sum_{\ell, m} g_{\ell m}(\underline{r}) Y_{\ell m}(\hat{\underline{r}}). \quad ( )$$

The  $g_{4m}(\underline{r})$  and the  $g_{6m}(\underline{r})$  for both the liquid and quenched systems show remarkable similarity to those for a quantum LJ face-centered cubic crystal analyzed by P. A. Whitlock suggesting that the short range order in both systems is approximately face-centered cubic, as has been suggested by Abraham. (Full details of this analysis together with the results of our Monte Carlo simulation will be presented elsewhere.)

## BROKEN ERGODICITY IN GLASS

R.G. Palmer

Department of Physics, Duke University  
Durham, N. C. 27706

and

D.L. Stein

Department of Physics, Princeton University  
Princeton, N. J. 08540

### Abstract

The breakdown of conventional infinite-time-average statistical mechanics is discussed for glass and other examples. To obtain physical results the usual theory must be modified by the addition of constraints which limit the system to the part of phase space in which it becomes frozen. Some general thermodynamic consequences are considered, including a discussion of the residual entropy, and a conceptual theory of anomalous relaxation is presented.

### Introduction

We generally regard a firm grounding in equilibrium statistical mechanics as a prerequisite for the study of condensed matter physics. We come to think of computing a partition function as the central task in obtaining macroscopic predictions from microscopic descriptions. And yet in most cases of real interest, the canonical (partition function) prescription, if followed faithfully, does *not* yield acceptable macroscopic results. The trouble, of course, is that the canonical prescription involves summing over *all* accessible parts of phase (or configuration) space, whereas real systems tend to become stuck, or frozen, in some one sub-region thereof. A particularly familiar category of such behavior is the *broken symmetry* observed in most phase transitions, where the system picks one of two or more symmetry equivalent macrostates that have the symmetry of the Hamiltonian only when taken together, not individually. We generally define an order parameter  $\phi$  (not necessarily a 3-vector) whose norm  $\phi$  is a measure of the degree of frozenness and whose (generalized) direction  $\phi/\phi$  labels the possible alternative macrostates. The unmodified canonical prescription, using a symmetric Hamiltonian  $\mathcal{H}$ , automatically gives  $\langle\phi\rangle=0$ . We have learned, of course, to circumvent this problem in many ways, such as adding a conju-

gate field term  $-\mathbf{h}\cdot\phi$  to  $\mathcal{H}$  (thus breaking its symmetry), or using an approximate method (e.g. mean field theory) that allows us to insert a non-zero  $\langle\phi\rangle$ .

There are two possible mechanisms underlying broken symmetry. If the order parameter is a constant of the motion, then the dynamics never allows escape from a given macrostate; the system is not ergodic. The standard example is the Heisenberg ferromagnet, where  $[M,H]=0$ . On the other hand, many broken symmetry systems are described by an order parameter that is *not* a constant of the motion, but where a transition from one macrostate to another is overwhelmingly improbable. Here the system is *effectively* not ergodic, even though ergodic behaviour may reappear in the infinite time limit for a finite system. In most such broken symmetry cases the time to reach ergodic behaviour (and thus restore symmetry) diverges in the thermodynamic limit. A good example is an Ising ferromagnet below the critical temperature, where a transition from the predominantly *up* state to the predominantly *down* state requires the creation of a defect wall across the sample, costing a free energy of order  $N^{(d-1)/d}$  for  $N$  spins in  $d$  dimensions.

With glass in mind, it is important to realize that this failure of ergodicity can occur *without* the presence of a symmetry to be broken. The general case may be called *broken ergodicity* (1). Without symmetry the first mechanism (an additional constant of the motion) cannot be expected, but the second can. Of course, in the absence of symmetry, there is no reason for different macrostates to be degenerate, so one of them will have the absolute lowest free energy (defined with a restricted partition function) at any tempera-

ture, and the others will be only metastable. In practice, however, there can be such a high density of macrostates near the lowest one that the difference has little importance. If a high density of macrostates occurs away from an isolated lowest one, as is probably the case for most glasses with a low-lying crystalline state, the lowest one may actually be irrelevant in many circumstances. In either case the relevant macrostates must differ only sub-extensively (i.e. not in order  $N$ ) in their free energy if they are to be relevant in infinite-time equilibrium (2), but it is often not infinite time equilibrium that is of physical interest. Many systems display a succession of (quasi-) equilibria on increasingly long timescales. In each equilibrium domain some degrees of freedom have essentially come to equilibrium (with a heat bath) while others are still frozen. In such cases the physically relevant macrostates in a given context may have much higher free energy (e.g. order  $N$ ) than the lowest, even though they are thus effectively omitted from the unmodified canonical prescription.

Some examples will provide illustrations and raise further points. In Figure 1 are shown schematically relevant timescales for various systems, with a particular observation time  $\tau_{obs}$  picked out.

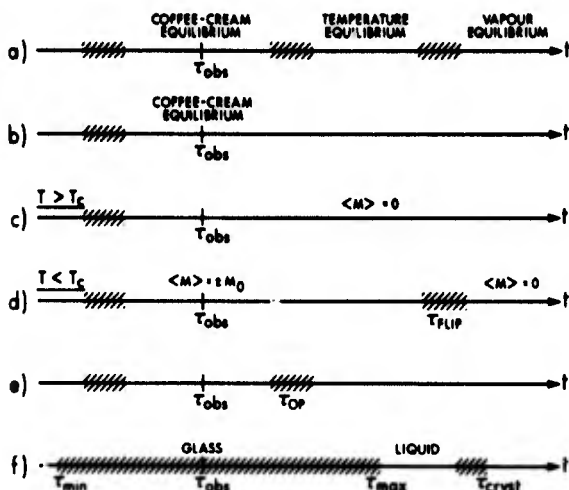


Fig. 1: Time-lines (logarithmic scale) for several systems. Shaded regions are characteristic system timescales.

**Coffee and cream:** Fig. 1a illustrates the process of adding cream (or milk) to an uncovered cup of hot coffee. There are relaxation timescales for mixing, cooling to room temperature, and evaporation, separating relatively wide domains of equilibrium. In each equilibrium domain "all the fast things have happened and all the slow things have not" (3) with the meaning of "fast" and "slow" dependent on the domain considered. Given a system whose microscopic description (Hamiltonian) includes the whole room, it is clearly not appropriate

to take  $\tau_{obs} \rightarrow \infty$  if one wishes to study hot coffee-cream mixtures. Instead, one must keep  $\tau_{obs}$  in the appropriate domain, as in Fig. 1a. It is however easy (and less perverse) to re-define the Hamiltonian to ignore the degrees of freedom for evaporation and to introduce a heat bath to inhibit cooling. Fig. 1a then becomes 1b and the usual methods of statistical mechanics ( $\tau_{obs} \rightarrow \infty$ ) may be used with impunity. The example is only trivial because we understand how to separate the fast and slow degrees of freedom, or how to define an appropriately idealized Hamiltonian. We have not reached that understanding for glass.

**Ising ferromagnet:** Figs. 1c and 1d illustrate this simple broken symmetry system, assuming free boundary conditions and a Glauber dynamic. For  $T > T_c$  (Fig. 1c) the time-averaged magnetization  $\langle M \rangle$  is zero (in order  $N$ ) beyond some short relaxation time, whatever the initial state. For  $T < T_c$  (Fig. 1d) there is a wide time domain in which there are two possible frozen states with  $\langle M \rangle = \pm M_0(T)$ . In a finite system there is a long relaxation time  $\tau_{flip}$  for crossing the barrier between these states, and for  $\tau_{obs} \gg \tau_{flip}$  one finds  $\langle M \rangle = 0$ , the true  $\tau_{obs} \rightarrow \infty$  result. However, the time  $\tau_{flip}$  diverges with  $N$  and is thus impossible in the thermodynamic limit  $N \rightarrow \infty$ . The limits  $\lim_{N \rightarrow \infty} \lim_{t \rightarrow \infty}$  and  $\lim_{t \rightarrow \infty} \lim_{N \rightarrow \infty}$  therefore lead to very different results. The first is the conventional (ergodic) order of limits in statistical mechanics, whereas the second is the order appropriate for the study of ferromagnetism. Since the broken ergodicity is understood here, it is relatively easy to modify the system to eliminate the equilibrium beyond  $\tau_{flip}$ , as in Fig. 1a  $\rightarrow$  1b. Application of an infinitesimal field ( $h \geq 1/N$ ) is the best-known method.

**Ortho/para hydrogen:** Fig. 1e applies to molecular hydrogen, with *ortho* and *para* species. The ortho/para conversion time  $\tau_{op}$  is of the order of years in the absence of a catalyst. The  $\tau_{obs} \rightarrow \infty$  result corresponds to ortho-para equilibrium, which disagrees totally with practical experiments. Even purely thermal quantities, such as the specific heat, are miscalculated if full equilibrium is used; the problems are *not* limited to quantities like order parameters which take different values in different components. Again, it is easy to rectify the problem, by imposing  $\Delta J = \text{even}$ , because we understand the nature of the frozen states. Note that this example displays broken ergodicity without broken symmetry.

**Glass:** Fig. 1f is a suggestion for glass, shown at a temperature somewhat below the

freezing temperature  $T_g$ . There is a quasi-continuum of relevant timescales, stretching over many decades of time. This is to be expected from the anomalous relaxation observed, with non-exponential decay of response and correlation functions also extending over many decades. The upper limit of the continuum,  $\tau_{max}$ , is strongly temperature dependent, obeying a Vogel-Fulcher law near  $T_g$ . Fig. 2 shows the domains in the  $T$ - $t$  plane.

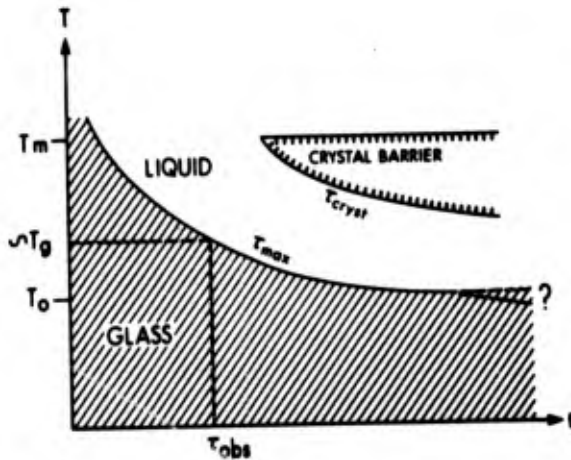


Fig. 2: Temperature dependence of system timescales for glass.

The system should be called a liquid if  $\tau_{obs} \gg \tau_{max}(T)$  and a glass if  $\tau_{obs} \leq \tau_{max}(T)$ , thus defining an approximate  $T_g(\tau_{obs})$ ; this criterion is essentially equivalent to one based on viscosity (e.g. glass if  $\eta > 10^{14}$  poise) since  $\eta(T)$  and  $\tau_{max}(T)$  behave similarly. If  $\tau_{max}(T)$  really diverges to infinity (or becomes order  $N^x$ ,  $x > 0$ , perhaps) at the Kauzmann temperature  $T_0$  then there is no liquid phase observable for  $T \leq T_0$ . However, most materials seem to show a crossover below  $T_g$  back to an Arrhenius law for  $\tau_{max}(T)$ , in which case a liquid would be seen in principle for long enough  $\tau_{obs}$ . There is of course also the possibility of a crystal phase for many materials below a melting temperature  $T_m$ . To reach the crystal one must wait a time longer than  $\tau_{max}(T)$ , as shown by  $\tau_{cryst}$  in Figs. 1f and 2. The crystal phase itself is an alternative, more stable, phase in the whole region of Fig. 2 below  $T_m$  (beyond crystal relaxation times of order phonon frequencies) but is only accessible from the liquid through the crystal barrier,  $\tau_{obs} > \tau_{cryst}$ . Sufficiently rapid cooling avoids the crystal altogether. Note that the

crystal is not accessible at all for  $T < T_0$  if  $\tau_{max}(T)$  really diverges at  $T_0$ . Note also that the unmodified canonical prescription is expected to give the crystal phase at  $T < T_m$ , or if that is somehow excluded, the liquid phase.

The most important feature that makes glass different from the other examples is the continuum of relevant system timescales. At a given  $\tau_{obs}$ , some degrees of freedom (with  $\tau < \tau_{obs}$ ) are active, or even in equilibrium ( $\tau \ll \tau_{obs}$ ) whereas others ( $\tau > \tau_{obs}$ ) are still frozen. Which are which depends critically and continuously on  $\tau_{obs}$ . Of course the classes are not sharp, but a sensible first approximation may be to define them sharply. To treat such a system with a modified canonical prescription we must clearly find some way of introducing  $\tau_{obs}$ -dependent constraints (or ordering fields, or boundary conditions, etc.) that ensures that the sum over accessible states includes only the fast ( $\tau \leq \tau_{obs}$ ) degrees of freedom, not the frozen ones. This has not yet been done satisfactorily. In general the crucial step in solving nontrivial condensed matter problems has been the characterization of the relevant macrostates (e.g. by definition of an order parameter) followed by a statistical mechanical calculation (e.g. mean field theory) that is somehow restricted to a part of phase or configuration space representing just one macrostate (e.g. fixed order parameter). The problem in glass is that we do not know how to characterize the macrostates, particularly as they are  $\tau_{obs}$ -dependent.

Without a detailed theory proceeding from microscopic to macroscopic there are at least two things we may do. We may attempt to find general properties of systems displaying broken ergodicity, and we may try to build models of possible sets of macrostates and their relations (as a function of time, temperature, etc.). Neither is very satisfying, but both may shed light on the problems surrounding the construction of a complete theory. The following two sections are devoted to these two tasks.

#### Component Averaging

The general properties of systems displaying broken ergodicity are discussed at length in ref. (4), which also contains applications to spin glasses; see also (5). The broken symmetry case involves many further symmetry-related phenomena; see (6). Ref. (4) begins, in effect, by making the ansatz that given  $\tau_{obs}$ , phase space  $\Gamma$  can be divided into disjoint components  $\Gamma^\alpha$  (with  $\Gamma = \bigcup_\alpha \Gamma^\alpha$ ) such that

A) the probability of escape from  $\Gamma^\alpha$  within

$\tau_{\text{obs}}$  (averaged over initial states within  $\Gamma^\alpha$ , and over possible evolutions) is negligible, and

B) within  $\Gamma^\alpha$  one may use the techniques of equilibrium statistical mechanics, restricted to  $\Gamma^\alpha$ .

B amounts to assuming that the components are effectively ergodic. The components defined here are the macrostates discussed in the introduction, and the net effect of the ansatz is to make an artificially sharp division into slow (frozen) and fast (active) degrees of freedom. In condition A it is essential that "negligible" be used in place of "zero", which would make any finite free energy barrier ineffective. One could demand  $\text{Prob}(\text{escape from } \Gamma^\alpha < p_0)$ , a small significance level, say

$10^{-3}$  (4). Given a firm-- though not operational -- definition of components, we are interested in comparing the properties of components with canonical predictions, which are (in principle) calculable without characterizing the broken ergodicity. We normally compare the canonical prediction  $Q_c$  for a quantity

$Q$  with a *component average*

$$\bar{Q} = \sum p^\alpha Q^\alpha \quad (1)$$

of its value  $Q^\alpha$  in each component  $\Gamma^\alpha$ . In principle component averaging is undesirable since the physical system remains stuck in a single component. It may nevertheless (a) prove practical where specification of a single component is impractical or unsolved, and (b) yield a *typical* result when the distribution of  $Q^\alpha$ 's is narrow, as frequently seems to occur. Indeed, the motivation for component averaging is analogous to that for using statistical mechanics rather than microscopic dynamics. The information required to specify a single component may be impossibly large (probably diverging with  $N$ ) in a glass, like that required to specify a particular microstate in any macroscopic system.

The canonical prediction  $Q_c$  can be computed as an expectation value

$$Q_c = \langle Q(x) \rangle = \text{Tr}[x \epsilon \Gamma] Q(x) \exp(-\beta \mathcal{H}(x)) / Z \quad (2)$$

if  $Q$  is an *observable* with a value  $Q(x)$  in each microstate  $x$ . In other cases (e.g., free energy, specific heat, compressibility),  $Q_c$  must be computed from the partition function  $Z$  or its derivatives. Similarly,  $Q^\alpha$  is computed from the *restricted* expectation value

$$Q^\alpha = \langle Q(x) \rangle^\alpha = \text{Tr}[x \epsilon \Gamma^\alpha] Q(x) \exp(-\beta \mathcal{H}(x)) / Z^\alpha, \quad (3)$$

where

$$Z^\alpha = \text{Tr}[x \epsilon \Gamma^\alpha] \exp(-\beta \mathcal{H}(x)), \quad (4)$$

for an observable, or from  $Z^\alpha$  otherwise.

The probability  $p^\alpha$  provides a weight for component  $\Gamma^\alpha$ . The real system is described by  $p^\alpha = 1$  for  $\alpha = \alpha_0$ ,  $p^\alpha = 0$  otherwise, but we are averaging in order to replace such specific knowledge of  $\alpha_0$  and its history and parameter dependence. A natural choice is the Gibbs weight

$$p^\alpha = \exp(\beta F^\alpha) / Z = Z^\alpha / Z, \quad (5)$$

which is correctly normalized because  $\sum Z^\alpha = Z$  from  $\Gamma = \cup \Gamma^\alpha$ . This is also the least biased choice in an information theoretic sense (4). It is certainly not always appropriate since, for example, history dependence is eliminated, but serves as a sensible first guess. An alternative, discussed by Jäckle (7), is to evaluate Eqn. (5) at a fixed temperature near  $T_g$

where the components first become isolated. This procedure has the advantage that  $p^\alpha$  is not  $T$  dependent, but does not easily account for components that only become defined well below  $T_g$ . Consistent with the continuum of timescales at fixed  $T$  (Fig. 2), we expect a sequence of divisions of  $\Gamma$  into more and more components  $\Gamma^\alpha$  as either  $\tau_{\text{obs}}$  or  $T$  is reduced.

We may think of the system being trapped in a "valley" of a complex free energy surface, as shown schematically in Fig. 3.

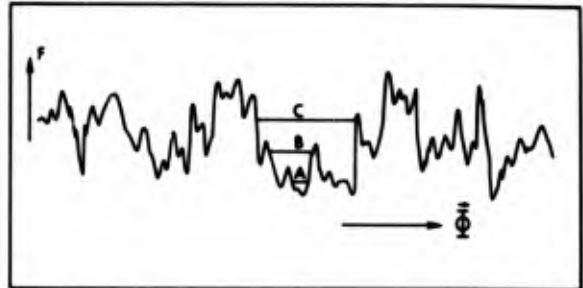


Fig. 3: A schematic free energy surface.

The horizontal axis represents (poorly) many appropriate configurational coordinates  $\phi_i$ ;  $F(\phi)$  is in reality a very high dimensional surface. For small  $\tau_{\text{obs}}$  or low  $T$  the system will be frozen in one of many local valleys such as A. With increased  $\tau_{\text{obs}}$  or  $T$  the lower free energy barriers become passable and the system is only confined in a larger region B, then C, and so on. Clearly there are more alternative A's than there are B's, etc.; ideally, of course, we would redefine the set of  $\phi_i$ 's by integrating out the fast degrees of freedom as  $\tau_{\text{obs}}$  or  $T$  is increased, proceeding from a full microscopic energy surface  $E(x)$  (i.e.,  $\phi \equiv x$ ) at very short  $\tau_{\text{obs}}$  to a free energy function of a few microscopic vari-

ables for  $\tau_{\text{obs}} > \tau_{\text{max}}(T)$ .

From Eqns. (1)-(5) it is easy to derive relations between  $Q_c$  and  $\bar{Q}$  for particular  $Q$ 's.

Some results are (4):

(i)  $\bar{Q} = Q_c$  if  $Q$  is an observable. This applies, for example, to the energy.

(ii)  $F = F_c + TI$  and  $S = S_c - I$  for the free energy and entropy, where

$$I = -k \sum_{\alpha} p^{\alpha} \ln p^{\alpha} \quad (6)$$

is the intercomponent entropy, or complexity. Note that  $\bar{S} \neq -\partial F/\partial T$  in general, because derivatives of  $I$  enter.  $K^* = \exp(I/k)$  is a useful measure of the effective number of components.  $K^*$  is less than or equal to the actual number of components, with equality only when the  $p^{\alpha}$ 's are identical.  $F$  and  $S$  are only modified appreciably (i.e. in order  $N$ ) if  $K^*$  is order  $c^N$ . The existence of frozen states *without* long range order implies that  $I$  grows with  $N$ , since otherwise a fixed amount of information would suffice to describe the frozen order everywhere, amounting to long range order.

(iii) The specific heat obeys

$$C_c = \bar{C} + \sigma^2 (E^{\alpha})/kT^2 \quad (7)$$

where  $\sigma^2$  means an intercomponent variance computed with the weight  $p^{\alpha}$ . The difference  $C_c - \bar{C}$  is necessarily positive, and can be of macroscopic significance (order  $N$ ) when the spread of  $E^{\alpha}$  is unobservable (order  $N^{\frac{1}{2}}$ ). The difference  $C_c - \bar{C}$  comes essentially from the fact that the canonical partition function includes all components weighted by  $p^{\alpha}$ , and the temperature derivatives in  $C_c$  involve derivatives of  $p^{\alpha}$ , whereas in the more physical component average  $p^{\alpha}$  is kept fixed during differentiation.

In applying these results to glass we assume that the component average quantities ( $F, S, C$ ) correspond to typical values for a real system.  $F$  and  $S$  are not directly measurable however, and we should not expect  $\bar{S}$  to equal the "experimental" entropy  $S_{\text{exp}}$ , defined by

$$S_{\text{exp}}(T) = S_{\text{exp}}(T_r) - \int_{T_r}^T C_p(T') d \ln T'. \quad (8)$$

$S_{\text{exp}}(T_r)$  at the reference temperature  $T_r$  ( $T_r > T_m$ ) is determined by calorimetry from the crystal phase. Although  $C_p = \bar{C}$  in eqn.

(8),  $S_{\text{exp}}$  differs from  $\bar{S}$  for two reasons.

Firstly  $S_{\text{exp}}(T_r)$  is the full canonical value,

$\bar{S}(T_r) + I(T_r)$ , not just  $\bar{S}$ . Secondly,  $\bar{C} \neq T \partial \bar{S} / \partial T$  in general. If only the first reason were present, as in Jäckle's approach (7) with  $T$ -independent  $p^{\alpha}$ , we would expect  $S_{\text{exp}}(T) = \bar{S}(T) + I(T_r)$ , and in particular  $S_{\text{exp}}(0) = I(T_r)$  for the residual entropy, since  $S(0)$  is surely zero.

Neither is  $S_{\text{exp}}(T)$  equal to the canonical value  $S_c(T)$  except at (and probably above)  $T_r$ . It is obvious from the relation  $C_c \geq \bar{C}$  that equation (8) with  $C_p = \bar{C}$  gives  $S_{\text{exp}} \geq S_c$ . Indeed, assuming  $S_c(0) = 0$ , the residual entropy  $S_{\text{exp}}(0)$  is just the integrated specific heat difference  $C_c - \bar{C}$ . This difference is, of course, observed experimentally when  $C_p (= \bar{C})$  drops below the extrapolated liquid value. This occurs at a temperature that decreases with increased  $\tau_{\text{obs}}$ , so the measured  $\bar{C}$  increases with  $\tau_{\text{obs}}$ , as would be expected from having fewer larger components.

A useful analogy is again ortho/para hydrogen. As is well known the measured specific heat ( $\bar{C}$  for equilibrium mixtures) is much less than the equilibrium value  $C_c$  (calculable, and measurable with a catalyst present) over a wide  $T$  range. This system also has a residual entropy  $S_{\text{exp}}(0)$  if computed with eqn. (8). This applies whether  $C_p(T)$  is taken as  $\bar{C}(T)$ , using mixtures in ortho-para equilibrium for each  $T$ , or as  $C_{3:1}(T)$ , using the high temperature 75% ortho mixture. It is also worth noting that at high temperature  $\bar{C} \approx C_{3:1} \approx C_c$ , but

$\bar{S} \approx S_{3:1} \approx S_c - \Delta$ , where  $\Delta = -Nk(0.75 \ln 0.75 + 0.25 \ln 0.25)$  is a high temperature mixing entropy that corresponds to  $I(T_r)$  for the glass.

Without a detailed model, or characterization of the components, this sort of discussion is all that can be hoped for. We can, for example, understand the residual entropy conceptually, but cannot predict its value. Other quantities (e.g., compressibility, Prigogine-DeFay ratio) can also be discussed at the same level (4,7). In the spin glass problem the approach succeeds in explaining the failure of linear response theory and the various observed susceptibilities (4,5). In any case, an understanding of the limitations and modifications of standard equilibrium theory seems an essential first step, especially when  $I$  is of order  $N$ .

## Anomalous Relaxation

Non-exponential relaxation of the approximate form

$$f(t) = f(0) \exp(-t/\tau)^\beta, \quad 0 < \beta < 1 \quad (9)$$

has been observed for many response and correlation functions (mechanical, thermal, and dielectric) of a wide variety of glassy liquids (8). In this section we present a simple theory of this effect for any system exhibiting broken ergodicity with a continuum of relevant timescales (Figs. 1f and 2). The theory is quite general, needing one scaling assumption in addition to the general principles espoused here. Generality is both an advantage--the phenomenon is suprising ubiquitous--and a disadvantage in that the theory is barely concrete enough to be falsifiable. A more specific model is under development (9).

Given a continuum of relevant timescales (Figs. 1f and 2, for  $\tau_{\text{obs}} < \tau_{\text{max}}(T)$ ) the system finds itself effectively stuck in some component (or "valley") in phase space for any given  $\tau_{\text{obs}}$ .

We may think of the system as moving on a multidimensional free energy surface (cf. Fig. 3) in which (given  $\tau_{\text{obs}}$ ) some barriers are easily crossed, and could even be integrated out, others are effectively impassible, and an intermediate class governs the current evolution. The dividing line  $\Delta F_{\text{max}}$  (not related to  $\tau_{\text{max}}$ ) is given by

$$\tau_{\text{obs}} = \tau_1 \exp(\Delta F_{\text{max}}/kT) \quad (10)$$

where  $\tau_1$  is a microscopic attempt frequency; the crossing rate for barriers appreciably larger than  $\Delta F_{\text{max}}$  is small compared to  $1/\tau_{\text{obs}}$ .  $\Delta F_{\text{max}}$  depends continuously on the observation time  $\tau_{\text{obs}}$  because the system escapes from inner components into larger and larger outer components as  $\tau_{\text{obs}}$  increases, as represented by  $A \rightarrow B \rightarrow C$  in Fig. 3. Correspondingly, the number of possible alternate components decreases as  $\tau_{\text{obs}}$  increases, and we may expect in general a hierarchical tree in which several components at level  $n$  are effectively combined into one at level  $n+1$  (4).

Now consider the relaxation of some chosen macroscopic quantity. The relaxing variable will in general depend only on *some* of the system's degrees of freedom, not all of those involved in the growth of the components with  $\tau_{\text{obs}}$ . To treat the problem in principle, we should freeze the slow degrees of freedom ( $\tau > \tau_{\text{obs}}$ ), integrate out the fastest one ( $\tau \ll \tau_{\text{obs}}$ ), and thus construct an effective free energy surface

$F(\phi)$  which is a function of the remaining degrees of freedom  $\phi$ . By definition the largest (containing) barriers of this surface will be of size  $\Delta F_{\text{max}}$ . The relaxation process will depend on other barriers within this surface, say  $\Delta F_{\text{relax}}$ . We may think of the relaxation as corresponding to "longitudinal" motion on this surface, in the presence of typically far more "transverse" motion. In principle the transverse degrees of freedom could also be integrated out as far as the relaxation process is concerned; they would then contribute to the entropy part of  $\Delta F_{\text{relax}}$ .

Our scaling assumption for glass is that the free energy surface  $F(\phi)$  has only one free energy scale, set by  $\Delta F_{\text{max}}$ . Then

$$\Delta F_{\text{relax}} = \alpha \Delta F_{\text{max}} \quad (11)$$

with  $0 \leq \alpha \leq 1$ . Loosely stated, the free energy surface is self similar (or "fractal"), but really it is a different surface, obtained by freezing/integrating different degrees of freedom, as  $\tau_{\text{obs}}$  is changed. Without a more concrete model the assumption can only be justified on the basis of its simplicity, its reasonableness, and its a posteriori predictions.

The relaxation process may be represented by

$$f(t) = f(0) \exp(-t/\tau_{\text{relax}}) \quad (12)$$

where  $1/\tau_{\text{relax}}$  is a current relaxation rate given by

$$\tau_{\text{relax}} = \tau_2 \exp(\Delta F_{\text{relax}}/kT) \quad (13)$$

with  $\tau_2$  another microscopic attempt frequency.

Equations (10) - (13) immediately give

$$f(t) = f(0) \exp(-t \tau_1^\alpha / \tau_2 \tau_{\text{obs}}^\alpha) \quad (14)$$

or

$$f(t) = f(0) \exp(-Ct^{1-\alpha}) \quad (15)$$

with  $C = \tau_1^\alpha / \tau_2$  on substituting the current time  $t$  for the observation time  $\tau_{\text{obs}}$ . This is the required eq. (9) with  $\beta = 1 - \alpha$ . The limit  $\alpha = 0$  ( $\beta = 1$ ) gives Debye relaxation when  $\tau_{\text{relax}}$  is independent of  $\tau_{\text{obs}}$ . The opposite limit  $\alpha = 1$  ( $\beta = 0$ ) gives logarithmic relaxation when all the relevant degrees of freedom are longitudinal,  $\Delta F_{\text{relax}} = \Delta F_{\text{max}}$ .

The derivation presented here is necessarily crude, but we believe it correctly emphasizes the central role of a succession of free energy

barriers that are surmounted *sequentially*. In contrast we reject the "distribution of free energy barriers" picture with many independent degrees of freedom relaxing in parallel. Our specific models (9) involve ordered classes of degrees of freedom such that a member of a given class is constrained not to change unless those in lower classes take particular values. This represents the real structural constraints on rearranging atoms, groups of atoms, groups of groups of atoms, and so on. We can obtain power-law or  $\exp(-t/\tau^\beta)$  relaxation depending on the detailed assumptions. We also find that  $\tau$  has Vogel-Fulcher behaviour in a limited temperature range, outside of which it crosses over to Arrhenius behaviour, as is often found experimentally.

#### Acknowledgements

We thank E. Abrahams, P.W. Anderson, and J. Jäckle for helpful discussions. Supported in part by NSF grant DMR 8011937.

#### References

- (1) F.T. Bantilan, Jr. and R.G. Palmer, J. Phys. F11, 261 (1981).
- (2) A.C.D. van Enter and J.L. van Hemmen, Phys. Rev. A29, 355 (1984).
- (3) R.P. Feynman, Statistical Mechanics (Benjamin: Reading 1972).
- (4) R.G. Palmer, Adv. Phys. 31, 669 (1982).
- (5) R.G. Palmer, in Heidelberg Colloquium on Spin Glasses, Ed. J.L. van Hemmen and I. Morgenstern (Springer: Berlin 1983).
- (6) P.W. Anderson, Basic Notions of Condensed Matter (Benjamin/Cummings: Reading 1984).
- (7) J. Jäckle, Phil. Mag. B44, 533 (1981).
- (8) For a review see S. Brawer, Relaxation in Viscous Liquids and Glasses, preprint.
- (9) R.G. Palmer, D. Stein, P.W. Anderson, and E. Abrahams, in preparation.



FRactal Time Defect Diffusion and the  
Williams-Watts Model of Dielectric Relaxation

John T. Bendler

Relaxation Workshop Participant  
Polymer Physics and Engineering Branch  
General Electric Corporate Research and Development  
Schenectady, New York 12301

and

Michael F. Shlesinger

Relaxation Workshop Speaker  
Physics Division  
Office of Naval Research  
800 North Quincy Street  
Arlington, Virginia 22217

ABSTRACT

Power-laws in transport properties of disordered glasses are interpreted as evidence for dynamical scaling, and modeled using momentless (Lévy stable) densities which exhibit hierarchical clustering on all time scales (fractal time structure). The Williams-Watts dielectric relaxation function is not stable, but is shown to be subordinated to a stable process, defect diffusion to a frozen dipole. This generalizes the Glarum model, in which the defects move with a constant renewal rate. Activation energy effects are discussed using a Kramers escape model with dispersion in the barrier heights. Dispersion in barrier heights results in a stable waiting-time density, with fractal (Hausdorff) dimension equal to the ratio of the thermal energy divided by magnitude of the dispersion. If the dispersion is small, normal non-fractal motion occurs. When the dispersion is greater than  $kT$ , event times occur in self-similar clusters and in an average sense form a Cantor set. Low-temperature backbone motions of a polymer molecule are suggested as defect candidates, whose motion to a large conformer defect leads to  $T_g$  relaxation. Megahertz motions of low-temperature  $\beta$  processes can generate dispersion in the saddle-point region of the  $T_g$  process.

Introduction

Dynamic modeling for complex disordered materials faces experimental and theoretical uncertainty. Simulation techniques including Monte Carlo, molecular dynamics,

etc. are applied to small-molecule systems, yet progress toward long-time/low temperature behavior is slow. Larger and faster computers are likely, but an investment in hardware and software is needed to cope with viscous polymers and glassy solids. New electronic,

optical and engineering applications of amorphous solids focuses experimental attention on time-dependent transport properties which control physical aging, fatigue and fracture. Though a coherent phenomenology has yet to emerge, it is clear that mechanical and thermal history influence bulk properties (1,2).

On theoretical grounds one anticipates that long-time behavior of complicated materials may be described by a diffusion equation obtained by averaging Liouville's equation over momenta. This reasonable expectation is difficult to test since a many-body problem in coordinate space still separates theory and experiment. Guided by intuition and available experimental data (eg., dielectric, NMR), a contracted model is often arrived at and the task of comparing its predictions with experiment remains. (In some cases this is nearly impossible because of computational problems, unknown model parameters, unavailable experimental data, etc.) When predictions and data are able to be compared, a successful fit does not prove the correctness of the model and lack of agreement can have many origins; velocity averaging, coordinate separation and/or identification, or systematic experimental error.

From the empirical side, interest in viscous polymeric and non-polymeric melts and glasses has resulted in renewed use of ad-hoc relaxation functions such as the one proposed by Williams and Watts (3) for the fitting of dielectric loss and dispersion;

$$\phi_{\alpha}(T) = e^{-\left(\frac{t}{\tau}\right)^{\alpha}} \quad 0 < \alpha \leq 1 \quad (1)$$

This two-parameter form has been

shown by Williams and co-workers (3,4) to provide an excellent description of the complex dielectric constant of many polymers in the vicinity of the glass transition temperature  $T_g$ . It is found for most polymers that  $0.3 \leq \alpha \leq 0.7$  near  $T_g$ . In addition  $\phi_{\alpha}(t)$  is useful for the analysis of dynamic light scattering (5), NMR (6,7), and mechanical relaxation data (1,8,9). Generalizations of the two-parameter form have been used to describe path dependencies for volume and enthalpy relaxation and recovery (10,11). One of the earliest appearances of  $\phi_{\alpha}(t)$  in the physical literature is Rudolf Kohlrausch's application to polarization decay in a Leyden jar (1854) (8,12,13). At about the same time (1853) Cauchy introduced it to discuss a generalized theory of errors, and it was later used by Rudolf's son Friedrich (1863) to describe mechanical relaxation of silk and glass fibers (12).

This article concerns a recent continuous time random-walk (CTRW) model for dielectric relaxation near  $T_g$  (14) which is a generalization of Giarun's defect-diffusion theory (15) and which leads to a fractional exponential form (equation 1). The novel aspect of this description of relaxation is the introduction and use of momentless waiting-time probability densities (WTD), in turn limiting cases of Levy stable densities equivalent to the Williams-Watts distribution of relaxation times (16). Empirically these are evident from the power-law spectral densities displayed by glass-forming materials around  $T_g$ . Theoretically such power-laws imply self-similarity and the absence of a time-scale beyond a shortest time. Mandelbrot emphasizes that scaling behavior is characteristic of fractal structures (17). Fractal sets are highly irregular and clustered and their component parts are

variants of the whole.

In the next section we discuss momentless-time processes by introducing a familiar example, the probability density (PD) for first passage times (FPT) in a homogeneous 1D lattice random walk. Some intuition about the resulting fractal set of passage times is gained by considering the collection of generating walks. A second, more direct example of a scaling WTD is then found by summing a series of Poisson PD's each of which contains longer and longer pauses, though with ever diminishing probabilities. The resulting PD may generate, on the average, a Cantor set of time events provided the coefficients and duration times fall below a critical ratio. A defect diffusion derivation of the Williams-Watts relaxation function is then given. Treatment of activation energy problems requires explicit introduction of temperature dependence and a WTD starting from Kramers barrier escape problem is given. Conformer defects associated with the glassy-state  $\beta$  process are identified possible sources of the  $\alpha$  relaxation. Self-similarity is possible if the barrier height for  $\beta$  defect motion is treated as a Poisson variable. A critical value of the barrier fluctuation causes the WTD to become fractal. Other possible sources of activation energy effects are discussed.

Momentless Waiting-Time Densities (WTD) and Fractal Time (18).

The prominent feature of fractal-time processes is a self-similar clustering of events on all scales beyond a smallest cutoff-time. To develop a concrete example and practical experience, it is

useful to consider events generated by a nearest-neighbor random walker on a periodic one-dimensional lattice (18).

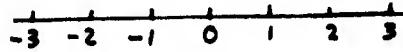


Figure 1. One dimensional lattice for homogeneous random walks.

Consider a walker on the lattice of Fig. 1 who steps to the right with a probability  $p$  and to the left with a probability  $q = 1-p$ . The probability that the walker is at  $s$  after  $n$  steps is

$$P_n(s) = \frac{1}{2\pi} \int_{-\pi}^{\pi} [pe^{i\theta} + qe^{-i\theta}]^n e^{-is\theta} d\theta \quad (2)$$

For an unbiased walk,  $p = q = 1/2$  and

$$P_n(s) = \frac{1}{2\pi} \int_{-\pi}^{\pi} [\cos\theta]^n e^{-is\theta} d\theta \quad (3)$$

Consider the behavior of  $P_n(s)$  for large  $n$ ;

$$\log(\cos x) = -\left[\frac{x^2}{2} + \frac{x^4}{12} + \frac{x^6}{45} + \dots\right] \quad (4)$$

therefore

$$(\cos x)^n \sim e^{\left[\frac{-nx^2}{2} - \dots\right]} \quad (5)$$

and so when  $n \gg 1$

$$P_n(s) \sim (2\pi n)^{-\frac{1}{2}} e^{-\frac{s^2}{2n}} \quad (6)$$

If  $a$  is the lattice spacing and  $\tau$  is the time between steps, then the continuum variables  $t = n\tau$  and  $x = sa$  are customary

$$(2\pi n)^{-\frac{1}{2}} e^{-\frac{s^2}{2n}} ds = (4\pi Dt)^{-\frac{1}{2}} e^{-\frac{x^2}{4Dt}} dx \quad (7)$$

so that

$$P(x,t) = (4\pi Dt)^{-\frac{1}{2}} e^{-\frac{x^2}{4Dt}} \quad (8)$$

where  $dx = a ds$  and  $D = \frac{a^2}{2\tau}$ . Eq 8 is the Gaussian transition probability for unbiased 1D diffusion away from the origin on an unbounded spatial domain. In this continuum limit, the first passage time (FPT) distribution  $W(y,T)$  for a transition from 0 to  $y$  in time  $T$  obeys the convolution equation

$$P(x_2 - x_1, t) = \int_0^t P(x_2 - x, t-T) W(x - x_1, T) dT \quad (9)$$

which states that every passage  $x_1 \rightarrow x_2$  in time  $t$  occurs by first proceeding to  $x - x_1$  in time  $T$  and then completing the remaining distance  $x_2 - x$  in the time left  $t - T$ . Solving the convolution by Laplace transforms and inverting

$$W(x - x_1, T) = L^{-1} \left[ \frac{P(x_2 - x_1, u)}{P(x_2 - x, u)} \right] \quad (10)$$

To apply eq 10 to the Gaussian transition probability of eq 8, the Laplace transform is needed;

$$P(x, u) = \int_0^\infty [(4\pi Dt)^{-\frac{1}{2}} e^{-\frac{x^2}{4Dt}}] dt = (4uD)^{-\frac{1}{2}} e^{-x(\frac{u}{D})^{\frac{1}{2}}} \quad (11)$$

so that  $W(y, u) = e^{-y(\frac{u}{D})^{\frac{1}{2}}}$  and inverting

$$W(y, t) = \frac{y}{(4\pi Dt^3)^{\frac{1}{2}}} e^{-[\frac{y^2}{4Dt}]} \quad (12)$$

with  $t > 0$ . ( $W(y, t) = 0$  for  $t < 0$ .) This is the FPT density for a transition  $0 \rightarrow y$  in time  $t$ . For large  $t$  it displays a long-time tail

$$W(y, t) \sim \frac{y}{(4\pi D)^{\frac{1}{2}}} t^{-1.5} \quad (13)$$

and the asymptotic distribution is hyperbolic, which Mandelbrot (17) stresses is the hallmark of a fractal process.  $W(y, t)$  itself has no moments. The mean FPT would be

$$\langle t \rangle = \int_0^\infty t W(y, t) dt = -\lim_{u \rightarrow 0} \frac{d}{du} \int_0^\infty e^{-ut} W(y, t) dt$$

$$-\lim_{u \rightarrow 0} \frac{d}{du} W(y, u)$$

$$= \lim_{u \rightarrow 0} \left[ \frac{y \left(\frac{u}{D}\right)^{\frac{1}{2}}}{\left(\frac{u}{D}\right)^{\frac{1}{2}}} \right] \quad (14)$$

Thus the mean FPT does not exist, though events do occur and each point is visited with probability 1 since

$$\int_0^T W(y, t) dt = 1 - \operatorname{erf} \left[ \frac{y}{(4DT)^{\frac{1}{2}}} \right] \quad (15)$$

where erf is the error function. The median time  $T_m$  for reaching any  $y$  is finite;

$$\int_0^{T_m} W(y, t) dt = \frac{1}{2} \quad (16)$$

$$= 1 - \operatorname{erf} \left[ \frac{y}{(4DT_m)^{\frac{1}{2}}} \right]$$

and given by the solution to

$$\operatorname{erf} \left[ \frac{y}{(4DT_m)^{\frac{1}{2}}} \right] = \frac{1}{2}$$

An interesting point is that the momentless FPT density  $W(y, t)$  results from a well-behaved random-walk with a Gaussian transition probability on a discrete (unbounded) 1D lattice. The median time  $T$  for a walker to reach  $y=1$  starting from the origin for a diffusion constant  $D=1/\text{sec}$  is 1.04 sec, but the average time is infinite! The reason is that walkers who head off in the wrong direction take a long time to return and the moments are heavily weighted

by late-comers.

The FPT density  $W(y, t)$  belongs to the class of PDs termed stable or Levy stable by Mandelbrot because they describe random processes which are invariant under addition (16,17,18). As with the most famous example, the Gaussian, they satisfy the chain equation;

$$P(y_2 - y_1, t) =$$

$$\int P(y_2 - y, t_1) P(y - y_1, t - t_1) dy \quad (17)$$

where translational invariance has been assumed. The stable densities are derived from

$$Q(x; \alpha, \beta) =$$

$$\frac{1}{\pi} \int_0^{\infty} e^{-u^\alpha} \cos[xu + \beta u^\alpha \omega(u, \alpha)] du \quad (18)$$

where

$$\omega(u, \alpha) = \tan\left(\frac{1}{2}\pi\alpha\right) \text{ for } \alpha \neq 1$$

$$\text{and } \frac{2}{\pi} \log u \text{ for } \alpha = 1$$

The solutions to eq 17 are then

$$P(y, t) = (bt)^{-\alpha} Q[y(bt)^{-\alpha}]$$

A special case of eq 18 is

$$Q(x; \frac{1}{2}, -1) =$$

$$\frac{1}{\sqrt{2\pi}} x^{-1.5} e^{-(2x)^{-1}} \quad (19)$$

and the FPT density of eq 11 corresponds to

$$x = \frac{2Dt}{y^2}$$

in eq 19. The stable densities (SD) of eq 18 were first studied by Cauchy for the symmetric case  $\beta = 0$ . The case  $\alpha = 2$  is the Gaussian and  $\alpha = 1$  is the Cauchy distribution. For small  $\alpha$ , if  $\log y \ll 1$ , the SD is mimicked by the lognormal (16). For  $0 < \alpha \leq 1$ , the SD display a long-time Pareto tail

$$\sim x^{-1-\alpha}$$

which results in interesting scaling behavior. Mandelbrot refers to the distribution  $x^{-\alpha}$  as hyperbolic, and an important property of this distribution is its non-uniformity and clustering behavior. For example, in the case of the FPT density, if it is known that two events have occurred and the second takes place at time  $\tau$ , then the conditional PD for the first event is

$$W(y,t;\tau) = \frac{W(\tau-t)W(t)}{\int_0^\tau W(\tau-t)W(t)dt} \quad (20)$$

and from the asymptotic form

$$\sim [t(\tau-t)]^{-1-\alpha}$$

the conditional probability is seen to peak at 0 and at  $\tau$ , with the least likely time being in the middle. The hyperbolic distribution is

the only one which scales under truncation. Consider again the FPT distribution of eq 12 for  $y=1$  and  $D=1/\text{sec}$ ;

$$W(1,t) = \frac{1}{\sqrt{4\pi t^3}} e^{-(4t)^{-1}} \quad (21)$$

At 60 seconds this is near to the hyperbolic form for

$$\frac{-1}{e^{240}} \sim 1.004$$

and

$$W(1,t) \sim \left(\frac{1}{4\pi}\right)^{3/4} t^{-1.5}$$

Consider the distribution times on the scale of hours instead of seconds;

$$\frac{W(1,3600h)}{W(1,3600)} = W(1,h) \quad (22)$$

so that on the scale of hours, or days or years the distribution has the same form. It has the same form on all scales greater than 1 minute or so. Qualitatively the bursts and gaps in the arrival time distribution  $W(y,t)$  may be thought of in terms of the number of walks of a fixed length. The shortest passage time in the model  $T_0 = n\tau$  results from that single walk which proceeds directly in  $n$  steps to the finish line at  $y=na$ . A number of walks have a single digression and a passage time  $T_1 = (n+2)\tau$ , and so forth. The arrival time clustering reflects the length distribution in the collection of all walks which start at the origin and end at  $y$ .

The importance of the stable densities of eq 18 for relaxation theory is that they are solutions of the chain equation 17 and therefore

candidates for constructing generalized diffusion models in systems with interruptions, bursts and gaps of events, and self-similarity on many time scales. To introduce such a model for dielectric relaxation, we follow Montroll and Weiss (19) and consider a continuous-time random walk (CTRW) in which random intervals of time occur between successive steps of the walker. The waiting-time density (WTD) of the walker is  $\psi(t)$  (independent of lattice site) so that the probability of a step taking place between  $t=0$  and  $t$  is

$$\int_0^t \psi(t) dt \quad (23)$$

If consecutive events occur without memory, then  $\psi(t)$  is a Poisson distribution  $\psi(t) = \lambda e^{-\lambda t}$  and the walker moves at regular intervals equal to the mean waiting time  $\lambda^{-1}$ . In the case of a momentless WTD all time scales appear beyond a shortest time and events are rare. Shlesinger and Hughes (20) presented a scaling WTD by beginning with a Poisson density and then proceeding to add longer and longer durations with smaller and smaller probabilities;

$$\psi(t) = p \lambda e^{-\lambda t} +$$

$$p^2 \lambda^2 e^{-\lambda^2 t} + p^3 \lambda^3 e^{-\lambda^3 t} + \dots \quad (24)$$

so that an order of magnitude longer duration  $\lambda^{n+1} t$  is an order of magnitude less probable  $p^{n+1}$ , where  $\lambda < p < 1$ . Summing eq 24 over all positive integer powers and normalizing;

$$\psi(t) = \left(\frac{1-p}{p}\right) \sum_{n=1}^{\infty} \lambda^n p^n e^{-\lambda^n t} \quad (25)$$

The spacings between events generated by  $\psi(t)$  are the same on average as those which occur in a Cantor set. Laplace transforming

$$\begin{aligned} \Psi(s) &= \left(\frac{1-p}{p}\right) \sum_{n=1}^{\infty} \frac{\lambda^n p^n}{\lambda^n + s} \\ &= p \Psi\left(\frac{s}{\lambda}\right) + \frac{1-p}{1 + \frac{s}{\lambda}} \end{aligned}$$

and

$$\Psi(s) = 1 + s^\alpha K(s) +$$

$$\left(\frac{1-p}{p}\right) \sum_{n=1}^{\infty} \frac{(-1)^n s^n p^n}{\lambda^n - p} \quad (26)$$

where  $\alpha = \frac{\log p}{\log \lambda}$  and  $\alpha < 1$ . Thus

$$\langle t \rangle = \left[ \frac{d\Psi(s)}{ds} \right]_{s=0} = - \quad (27)$$

where  $K(s)$  is an oscillatory function periodic in  $\log s$  with period  $\log \lambda$ .  $\Psi(t)$  behaves as  $t^{-1-\alpha}$  at long time and the appearance of self-similarity and the fractal dimension are clearly identifiable in this example.

#### Defect Diffusion and Dielectric Relaxation (14).

A CTRW generalization of Glarum's defect diffusion model (15) has been found from which one can derive the Williams-Watts form for dipole relaxation function in limiting cases (14). Ignoring parallel mechanisms for decay, one considers a frozen dipole at the origin of a regular lattice of  $V$  sites, which is only able to move when a mobile defect located on another site is

successful in diffusing to it for the first time. The  $N$  defects are distributed over the remaining lattice sites with a uniform probability  $c$ , so that  $c=N/V$ . Experimentally, the relaxation spectrum of polymer glasses exhibits scale invariance with fractal dimension  $\alpha$  to be identified with

$$\frac{\log p}{\log \lambda}$$

from the discussion of eq 25. The larger the probability of finding longer relaxation times, the smaller the exponent  $\alpha$ . As  $p \rightarrow 0$ ,  $\alpha \rightarrow 1$  for fixed  $\lambda$ . The consequences of configurational bottlenecks leading to scaling densities are contained in the WTD  $\Psi(t)$  for defect motion. Define  $F(l_0, t)$  as the FPT density for a walker who begins at  $l_0$  at time  $t=0$  to reach the origin for the first time at  $t$ . The probability that a walker starting at  $l_0$  does not reach the origin by time  $t$  is

$$1 - \int_0^t F(l_0, t) dt \quad (28)$$

and multiplying this by the probability  $V^{-1}$  that a single walker is found on site  $l_0$  and summing over all sites gives the dipole survival probability in the presence of a single defect;

$$\begin{aligned} \phi_1(t) &= \sum_{l_0=1}^V \frac{1}{V} \left[ 1 - \int_0^t F(l_0, t) dt \right] \\ &= \left[ 1 - V^{-1} \sum_{l_0=1}^V \int_0^t F(l_0, t) dt \right] \quad (29) \end{aligned}$$

For non-interacting defects, the dipole survival probability  $\phi_N(t)$  in the presence of  $N$  defects is

$$\phi_N(t) =$$

$$\left[ 1 - V^{-1} \sum_{l_0=1}^V \int_0^t F(l_0, t) dt \right]^N \quad (30)$$

Fixing the concentration of defects  $c=N/V$  while allowing  $N$  and  $V$  to become very large, gives

$$\phi(t) =$$

$$\begin{aligned} \lim_{N \rightarrow \infty} \left[ 1 - \frac{c}{N} \sum_{l_0=1}^V \int_0^t F(l_0, t) dt \right]^N \\ \sim e^{-c \int_0^t I(t) dt} \quad (31) \end{aligned}$$

where

$$I(t) = \sum_{l_0=1}^{\infty} F(l_0, t)$$

is the flux of defects into the origin. Montroll and Weiss determined the FPT density for a CRW. From their paper (19);

$$I(u) = \sum_{l_0=1}^{\infty} \sum_{n=0}^{\infty} F_n(l_0) [\Psi(u)]^n \quad (32)$$

where  $F_n(l_0)$  is the probability that a walker originally at site  $l_0$  arrives at the origin for the first time at the  $n$ th step and  $\Psi(u)$  is the Laplace transform of the WTD  $\Psi(t)$ . Letting  $F(l_0, t)$  be the generating function of the set  $\{F_n(l_0)\}$



$$F(l_0, z) = \sum_{n=1}^{\infty} F_n(l_0) z^n \quad (33)$$

and

$$I(u) = \sum_{l_0=1}^{\infty} F[l_0, \varphi(u)] \quad (34)$$

If  $P_n(l_0)$  is the probability that a walker originally at the origin is at  $l_0$  after  $n$  steps (not necessarily for the first time), then the generating function of the  $\{P_n(l_0)\}$

$$P(l_0, z) = \sum_{n=0}^{\infty} P_n(l_0) z^n \quad (35)$$

is related to the generating function  $F(l_0, z)$  by

$$F(l_0, z) = \frac{P(l_0, z) - \delta_{l_0, 0}}{P(0, z)} \quad (36)$$

but

$$\sum_{l_0=1}^{\infty} P_n(l_0) = 1$$

since after the  $n$ th step the walker is somewhere, and so

$$I(u) + 1 =$$

$$[(1 - \varphi(u))P(0, \varphi(u))]^{-1} \quad (37)$$

(The Kronecker delta in  $F(l_0, z)$  doesn't contribute since the sum in the flux excludes  $l_0=0$ ; the sum in the site-visitation generating function  $P(l_0, z)$  is over all sites, and the 1 corrects for this.) The generating function  $P(0, z)$  is known for a simple cubic 3D lattice and the

linear chain. For a Poisson waiting-time density

$$\varphi(u) = \frac{\lambda}{u+\lambda}$$

and the long-time behavior of the flux is readily found;

$$I(t) = 0.659\lambda \quad (3D)$$

and

$$I(t) = \left[\frac{2\lambda}{\pi t}\right]^{1/2} \quad (1D) \quad (38)$$

Integrating the flux from 0 to  $t$  and substituting into eq 31 gives

$$\varphi(t) = e^{-c_1 t} \quad (3D)$$

and

$$\varphi(t) = e^{-c_2 t^{1/2}} \quad (1D) \quad (39)$$

which is identical in form to Bordewijk's results (21). (The short-time behavior will be reported separately.) In the case of a momentless WID,  $\sim t^{-1-\alpha}$ , the long-time behavior of the survival probability is:

$$\varphi(t) = e^{-c_3 t^\alpha} \quad (3D)$$

and

$$e^{-c_4 t^{1/2}} \quad (1D) \quad (40)$$

so that the 3D behavior is Williams-Watts like while the 1D case has a maximum exponent of  $1/2$ .

**Activation Energy Effects.**

Relaxation kinetics near  $T_g$  are often non-Arrhenius (22,23) and one goal of modeling is to offer insight into molecular mechanisms. Since the WTDs discussed so far were introduced in an ad-hoc fashion so as to generate time-scale invariance, no discussion of temperature behavior is possible without a kinetic model for  $\Psi(t)$  itself. In this section we introduce a primitive model related to the Kramers barrier escape problem (24,25), guided now by the knowledge that we must introduce mechanisms to generate self-similar clusters of time scales. In fact, the reasoning employed to arrive at the Cantor function of eq 25 is now applied in reverse. Introducing the superposition expression;

$$\Psi(t) = \int_0^{\infty} \lambda e^{-\lambda t} \rho(\lambda) d\lambda \quad (41)$$

which describes  $\Psi(t)$  as being composed of Poisson WTDs with characteristic rates  $\lambda$  integrated over the density of rates. A quantitatively reliable rate constant can be calculated for the Kramers problem of particle escape from a potential well in the high-friction limit when the barrier height  $\epsilon$  exceeds the thermal energy  $kT$  (25). The activation energies and viscosities of polymer glass-formers at high temperatures above  $T_g$  appear large enough to satisfy these criteria. The difficult assumption to justify is treating the glass transition process as a single, thermally-activated local-mode transition, though for polymers this idea has the merit of both precedent and simplicity. From the steady-state flux assumption, the rate of barrier-jumping is (25)

$$\lambda_0 =$$

$$\left( \frac{\omega_0 \omega_b}{2\pi\beta} \right) e^{-\frac{\epsilon_0}{kT}} \quad (42)$$

where the potential in the well at A is approximated by  $U(x) \sim \frac{1}{2}\omega_0^2 x^2$ , the corresponding expression in the saddle region C is  $U(x) \sim \epsilon_0 - \frac{1}{2}\omega_b(x-x_0)^2$ , and  $\beta$  is the friction constant. Solid-state NMR, dielectric, and mechanical relaxation studies reveal that high-frequency main-chain motions persist to very low temperatures (also see discussion) in the glassy state, so we suggest that the saddle region parameters  $\omega_0$  and  $\epsilon_0$  are random variables whose dispersion is controlled by the rate and amplitude of the low-temperature motions. As the rate in eq 42 is more sensitive to  $\epsilon_0$  than to  $\omega_0$ , only a distribution of barriers  $f(\epsilon)$  is introduced;

$$f(\epsilon) = 0 \text{ for } \epsilon < \epsilon_0$$

and

$$q e^{-q(\epsilon-\epsilon_0)} \text{ for } \epsilon > \epsilon_0 \quad (43)$$

with  $\epsilon_0$  the minimum saddle-point barrier and  $q$  the inverse of the barrier fluctuation. The density of relaxation rates  $\rho(\lambda)$  due to  $f(\epsilon)$  is;

$$\rho(\lambda) = \frac{kTq}{\lambda} \left( \frac{\lambda}{\lambda_0} \right) kTq$$

for

$$0 \leq \lambda \leq \lambda_0 \quad (44)$$

Introducing  $\alpha = kTq$ , the long-time behavior of the WTD of eq 41 is

$$\psi(t) =$$

$$\alpha = kTq = \frac{kT}{\langle \epsilon - \epsilon_0 \rangle} \quad (50)$$

$$\frac{\alpha \Gamma(\alpha+1)}{\lambda_0^\alpha} t^{-\alpha-1} \quad (45)$$

where Watson's lemma is used for  $t \rightarrow \infty$ . The Tauberian theorem then gives the Laplace transform for small  $u$ ;

$$\varphi(u) \sim$$

$$1 - \frac{\pi \alpha}{\sin \pi(1+\alpha)} \lambda_0^{-\alpha} u^\alpha + \dots$$

$$\sim 1 - Au^\alpha + \dots \quad (46)$$

from

$$\Gamma(1+\alpha)\Gamma(-\alpha) = \frac{\pi}{\sin \pi(1+\alpha)}$$

With eq 46 in the flux expression, eq 37 gives

$$\Upsilon(u) \sim \frac{.659}{Au^\alpha} \quad (47)$$

for a simple cubic 3D lattice. Thus

$$\varphi(t) \sim e^{-cr(\lambda_0 t)^\alpha} \quad (48)$$

where

$$r = \frac{.659\pi}{\sin \pi(1+\alpha)[\alpha \Gamma(\alpha)]} \quad (49)$$

$c$  is the density of defects, and

Eqs 48-50 give the Williams-Watts parameters for the simple kinetic waiting-time model density of eq 45, and shows several explicit temperature effects. The original Kramers defect-hopping rate  $\lambda_0$  appears under the exponent  $\alpha$  so that its activation energy  $\epsilon_0$  appears in  $\tau$  of eq 1. The exponent

$$\alpha = kTq = \frac{kT}{\langle \epsilon - \epsilon_0 \rangle}$$

contains an explicit linear temperature dependence plus that of the barrier fluctuation  $q^{-1} = \langle \epsilon - \epsilon_0 \rangle$ .  $r$  in eq 50 is temperature dependent through  $\alpha$  and renormalizes the activation energy. If the defect density changes with temperature, this adds a further activation-energy contribution. Finally, the CRW model assumes that all dipole-defect "collisions" are successful in bringing about relaxation. If a threshold energy exists, this adds yet another term.

#### Discussion.

The primitive model scaling WTD of eq 45 suggests several mechanisms for temperature-dependent relaxation exponents  $\alpha$  and activation energies, and numerical comparisons will be reported separately. The significant fact is that the Williams-Watts function emerges rather directly from a defect-diffusion picture if the defect waiting times obey the stable hyperbolic form, which contains self-similar clusters of pausing times on all scales beyond a shortest time. Of course the Williams-Watts function itself is not scaling (except at early times)

since its moments exist. For problems such as creep, the early time behavior is important, and it is interesting that the Andrade-Weber creep expressions are self-similar (17). One has to subordinate the relaxation event ( dipole, or a  $T_g$  process ) to another process, here modeled as defect diffusion, to recover Williams-Watts.

Of course, it is useful to identify glass relaxation processes with scaling fractals, Cantor sets, and stable distributions, but in practice one needs to discover what the defects are and how the fractal dimension  $\alpha$  is calculated. The Kramers escape model with dispersion in the barrier height makes a step toward that goal. In the case of a polymer near its glass transition, a mechanism for mechanical or dielectric loss is monomer/dimer or trimer motions involving the backbone (26). In a crude sense, this thermally-activated conformer transition might be modeled by Kramers particle escape method, where the particle is the local-mode center-of-mass (24). In this instance, though, the co-existence of the low-temperature  $\beta$  motion in the backbone should be considered (7,26). Such backbone motions occur at megahertz frequencies near  $T_g$ , and persist to low temperatures in the solid. The conformational rearrangements which accompany the low-temperature process may themselves act as defects, and could cause barrier dispersion in the saddle region for the "high" temperature glass event.

The ratio of the thermal energy to the barrier dispersion, eq 50, corresponds to the Hausdorff dimension  $\alpha$  of the stable density of eq 45. The character of the random process changes drastically when this ratio falls below 1. When the dispersion is small and  $\alpha > 1$  the first moment exists and there is a

characteristic time, a relaxation time, in the problem. The motion is not fractal or transient, and the set of occurrence times is dense. When the dispersion gets larger than  $kT$ , no average time exists, the set of occurrence times is a Cantor set, on the average, and motions are rare and occur in self-similar bursts and gaps. Some model calculations to estimate barrier dispersion are underway.

#### Acknowledgments.

Professor Elliott W. Montroll (Deceased) was a major collaborator in this work. He took seriously the implications of dynamic scaling in disordered materials, and sought by patient and wise instruction and example to help us unravel them.

We wish to acknowledge the kindness and hospitality of Drs. Kia Ngai, T.K. Lee and the Physics Dept. Staff of VPI who made the Workshop so enjoyable and interesting.

#### References

1. L.C.E. Struik, Physical Aging In Amorphous Polymers and Other Materials, Elsevier Scientific Publishing Company, Amsterdam, 1978.
2. Proceedings of the 12 th North American Thermal Analysis Society, Williamsburg, VA., September 1983.
3. G. Williams and D.C. Watts, Trans. Faraday Soc. 66, 80 (1971).
4. G. Williams, D.C. Watts, S.B. Dev, and A.M. North, Trans. Faraday Soc. 67, 1323 (1971).

5. G.D. Patterson, *Adv. Polymer Science* 48, 127 (1983).
6. K.L. Ngai, *Comments Solid State Physics* 9, 127-147 (1979).
7. A.A. Jones, J.F. O'Gara, P.T. Inglefield, J.T. Bendler, A.F. Yee, and K.L. Ngai, *Macromolecules* 16, 658 (1983).
8. H. Leaderman, *Elastic Creep and Properties of Filamentous Materials and Other High Polymers*, The Textile Foundation, Washington, D.C., 1943.
9. K.L. Ngai and R.W. Rendell, *Polymer Preprints* 23, 2, 46 (1982).
10. C.T. Moynihan and A.V. Lesikar, *Ann. N.Y. Acad. Sci.* 371, 151 (1981) and references therein.
11. J.T. Bendler and K.L. Ngai, *General Electric Report No. 82CRD169*, 1982 and *Macromolecules*, In Press (1984).
12. J.T. Bendler, 3rd Conference on Fractals, Bethesda, MD, Nov. 1983, to appear in *J. Statistical Physics*.
13. An historical discussion of the fractional exponential may be found in L.C.E. Struik, *Abstracts of the 10th Europhysics Conference, Macromolecular Physics*, 135 (1980). Also (8,12).
14. M.F. Shlesinger and E.W. Montroll, *Proceedings National Academy Sci.*, In Press (1984).
15. S.H. Glarum, *J. Chem. Phys.* 33, 1371 (1960).
16. E.W. Montroll and J.T. Bendler, *J. Statistical Physics*. 34, 129 (1984).
17. B.B. Mandelbrot, *The Fractal Geometry of Nature*, W.H. Freeman and Co, San Francisco (1982).
18. E.W. Montroll and B.J. West, in *Fluctuation Phenomena*, p. 61, E.W. Montroll and J.L. Lebowitz, eds., North Holland, Amsterdam (1979).
19. E.W. Montroll and G.H. Weiss, *J. Math. Phys.* 6, 167 (1965).
20. M.F. Shlesinger and B.D. Hughes, *Physica* 109A, 597 (1981).
21. P. Bordewijk, *Chem. Phys. Lett.* 32, 592 (1975).
22. M.L. Williams, R.F. Landel, and J.D. Ferry, *J. Amer. Chem. Soc.* 77, 3701 (1955).
23. R.M. Hill and L.A. Dissado, *J. Phys. C Solid State* 15, 5171 (1982).
24. H.A. Kramers, *Physica* 7, 284 (1941).
25. S. Chandrasekhar, in *Selected Papers on Noise and Stochastic Processes*, N. Wax, ed., Dover, New York (1954).
26. N.G. McCrum, B.E. Read, and G. Williams, *Anelastic and Dielectric Effects in Polymeric Solids*, John Wiley and Sons, London (1967).

# Models of Temporal Stretched Exponential Relaxation in Condensed Matter Systems

A. K. Rajagopal  
Department of Physics and Astronomy  
Louisiana State University  
Baton Rouge, Louisiana 70803

and

K. L. Ngai  
Naval Research Laboratory  
Washington, D.C. 20375-5000

## Abstract

The purpose of this paper is to give a comprehensive review of the work on non-Debye relaxation which should serve as a useful account of the present understanding of the subject. We have reviewed several models of stretched exponential decay in time of many physical relaxation properties such as stress relaxation in polymers, dielectric relaxation, thermoremanent magnetization in spin glasses, etc. It is found experimentally that not only the time-dependence is a fractional exponential, but also the observed time scale of the fractional exponential is related to some fundamental time constant associated with an exponential decay via another universal relationship. Many of the models give the first relationship (we call these Type A theories) and they either do not or have not been sufficiently examined to give the second universality relation mentioned above. The models which give rise to both the features are called Type B. We have further classified Types A and B theories into subclasses: (Aa) Distribution of relaxation times, (Ab) Mathematical Analogy theories, (Ac) Stochastic processes, and (Ad) Other schemes, (Ba) Original Model of Ngai, and (Bb) Evolution of Entropy theory for correlated states. Three special cases: (i) spin glasses, (ii) polymers, and (iii) electron glasses are briefly discussed. We end the paper with a few concluding remarks. A commentary on four papers which appeared after the manuscript was essentially completed is also given at the end.

## 1. Introduction

It has been known for quite some time now that the long time relaxation of many properties of condensed matter systems is slower than exponential and is of the stretched exponential form

$$\phi(t) = \exp(-t/\tau_p)^{1-n}, \quad 0 < n < 1 \quad (1)$$

where  $n$  is an index of slowness and  $\tau_p$  is a characteristic time.<sup>1,2</sup> Here  $\phi$  stands for the normalized relaxation function appropriate to the physical property whose time dependence is being considered. It may stand for stress

relaxation function or dielectric relaxation function, or thermo-remanent magnetization in spin glasses and so on. Historically, this function, Eq. (1), gives a good fit to the experimental results on a wide variety of physical quantities in different contexts.<sup>2</sup> Ngai<sup>1</sup> has given a model which delivers Eq. (1) as well as a second relationship connecting  $\tau_p$  with the "fundamental" relaxation time  $\tau_0$  associated with the system:

$$\tau_p = [(1-n)\exp(n\gamma)\omega_c^n \tau_0]^{1/(1-n)} \quad (2)$$

$\tau_0$  here, in principle, can be measured also experimentally independent of the relationship (1).  $\omega_c$  is another characteristic of the system and  $\tau_0^{-1}$  is a measure of the lower cutoff in time,  $\omega_c^{-1}$ , below which Eq. (1) is not expected to hold.<sup>1</sup>  $\gamma$  is the Euler constant, 0.577 ... . Since  $\tau_p$  depends on a variety of physical properties of the system such as temperature, isotopic mass, molecular weight, etc., in different circumstances in a simple way, the characteristic time  $\tau_p$  that is required to fit the experimental time dependence via Eq. (1) is found to display an appropriately scaled dependence on these quantities as required by

Eq. (2). This observation<sup>1,2</sup> is so overwhelming that this has been called the "second universality relationship" whereas the stretched time-dependence in Eq. (1) is called the "first universality." These two observations, even apart from any physical model upon which its derivation is based, are indeed remarkable and that an understanding of basis of these expressions is expected from quite general, universal considerations.

In this paper, we shall present in more detail (some of which has not been published before) a variety of models proposed in the literature over the last few years, much of which is concerned with a derivation of Eq. (1) partly because this relation has historically been known for a long time.<sup>2</sup> Most of these models in their present form will be shown to be incapable of giving the second relation, Eq. (2) and hence they do not provide a complete explanation of the long time relaxation processes in condensed matter physics. In view of this, we have broadly classified the models into two large groups, A type, which give only Eq. (1) as far as the present interpretation of

them is concerned, and B type, which give both Eq. (1) and (2). These large groups of models furthermore fall into finer types. We will give here a brief description of these.

(Aa) Distribution of Relaxation Times:

There are several theories proposed by diverse groups which fall into this class. The basic idea here is that the expression (1) is fundamentally a superposition of a large number of exponentially decaying functions,  $\exp(-t/\tau_i)$ , where  $\tau_i$ 's are relaxation times associated with the constituents of the system. More explicitly one writes

$$\phi(t) = \int_0^{\infty} g(\tau) \exp(-t/\tau) d\tau \quad (3)$$

where  $g(\tau)$  is some distribution function of relaxation times. We may then try to invert this relationship by inverse Laplace transformation to obtain  $g(\tau)$  if we assume  $\phi(t)$  to be of the form given by Eq. (1). Only for  $n=1/2$  this inversion can be done analytically. However, one may use approximate methods to infer  $g(\tau)$ , such as the "method of steepest descents." For  $0 < n < 1$ , the result is

$$g(\tau) \cong \left[ \frac{(1-n)}{2\pi\tau^2 n} \right]^{1/2} \left[ \frac{(1-n)\tau}{\tau^p} \right]^{(1-n)/2n} \exp\left[-n \left( \frac{(1-n)\tau}{\tau^p} \right)^{1/n}\right] \quad (4)$$

It is not clear on physical grounds what  $g(\tau)$  really means. There are physical mechanisms that one may conceive of which essentially lead to forms of "effective"  $g(\tau)$ , such as Majumdar's diffusion model,<sup>3,4</sup> Grest and Cohen's free volume model,<sup>5</sup> and models based on Glauber's kinetic Ising model of Dhar,<sup>6,7</sup> Skinner,<sup>8</sup> and McMillan.

(Ab) Mathematical Analogy Theories:

In some circles it is fashionable to recognize the structure displayed by Eq. (1) with some known mathematical result. Invariably these observations are interesting in themselves but do not shed any light on the physics of the problem. Several such efforts will be mentioned and a few have no physical implication at all. Fractional Brownian motion studied by Mandelbrot and van Ness<sup>10</sup> and examined for the purpose of studying relaxation by Rajagopal and Rendell<sup>11</sup> is an example of this which could not be related to physics of condensed matter systems for which Eq. (1) is known to hold experimentally. Another mathematical result known for some time is the superposable, stable distributions due to Lévy. It was first realized by Tunaley<sup>12</sup> that if the frequency distributions in metallic films are superposable in the sense of Lévy, then the observed noise characteristics in them may be understood. Hughes, Shle-

singer, and Montroll<sup>13</sup> and Montroll and Shlesinger<sup>14</sup> examined random walks with self similar clusters leading to "Lévy flights" and "1/f noise."

(Ac) Stochastic Processes:

Under this class, we shall examine theories based on continuous time random walk<sup>15</sup> (CTRW) and the generalized master equation<sup>16</sup> (there is a recent review article on this subject by Weiss and Rubin<sup>17</sup>). Here the probability density function for the time between arrival of a walker at a given lattice point and the initiation of the next step to another site, denoted by  $\psi(t)$ , is the basic entity, upon whose structure the time-dependence of the relaxation function of interest depends. If we take for  $\psi(t)$  the negative of the time derivative of function of the form given by Eq. (1), then the CTRW framework can be applied to discuss the relaxation problems. But in Ref. 19, it was pointed out that when the moments  $\mu_m$  of  $\psi(t)$  are all finite, the Markovian master equation is an appropriate description for times which are

large compared to  $T^* = \text{Sup}(\mu_m/m!)^{1/m}$ . For  $\psi(t)$  given by minus the derivative of an expression of the form given by Eq. (1) it is found that  $T^*$  is finite for  $-1 < n < 0$  and infinite for  $0 < n < 1$ .<sup>19</sup> Thus a non-Markovian description is always needed for relaxation functions of the

form Eq. (1). In most CTRW applications,<sup>14-17</sup> the physical picture assumed is an inhomogeneous distribution of waiting times and in order to have a  $\psi(t)$  which is universal for all sites, one has to perform an average over all possible configurations of the walkers. In condensed matter one commonly has short-range order and this precludes such a picture of random walk with an inhomogeneous distribution of waiting times. For example, in a-SiO<sub>2</sub>, holes in the 2p lone pair orbitals of oxygen being small polarons hop from one oxygen to one of its nearest neighbor oxygens. In a-SiO<sub>2</sub>, the short range order is preserved and the nearest neighbor oxygen-oxygen distance remains invariant. It is difficult to see how an inhomogeneous distribution of waiting times will arise. Another classic model employed in statistical mechanics for describing exponential decay of time correlations in a chain of coupled harmonic oscillators serving as a heat bath to a

Brownian particle.<sup>21</sup> For arbitrary oscillator interactions, the Brownian particle obeys a generalized Langevin equation with time-dependent friction coefficient, and a Gaussian random force determined solely by the Hamiltonian of the coupled harmonic oscillators and the canonical distribution of the initial coordinates and momenta. In the original work,<sup>21</sup> the semiboundedness of the spectrum of the Hamiltonian of the bath oscillators was ignored in deriving the usual exponential decay. The Paley-Wiener theorem can be applied to this problem.<sup>19</sup> This then leads to a bound for

relaxation function of the form Eq. (1). It was also noted that the covariance of the random force of the same form is obtained in the long time limit from fractional Brownian motion.<sup>11</sup> But this connection is tenuous because the form of the noise does not uniquely specify the stochastic equation of motion.

(Ad) Other Schemes: In this subsection we shall discuss the incapacity of a direct application of the Kubo formula to obtain Eq. (1) for an important physical reason, missed by Young<sup>23</sup> who claimed to arrive at Eq. (1) by the use of the Kubo formula. He obtained something like Eq. (1) but the coefficients had the incorrect temperature and other dependences. Another approach is due to Palmer<sup>24</sup> using models of broken ergodicity. This seems as yet not definitive.

As pointed out earlier, none of these models are really satisfactory not only because they seem to lead to Eq. (1) for reasons which cannot be given a universal physical basis (since Eq. (1) is found to be applicable to a wide class of systems which do not fit the physical model that may be adduced to the specific mathematical program discussed here) but also because they do not give rise to the second universality, Eq. (2). There have been several attempts by our group (Ngai and coworkers) in the recent past to obtain such a general derivation, applicable under a wide set of assumptions, but relevant to the condensed matter systems of interest. We call these Type B models and we describe there here under two subclasses.

(Ba) Original Model of Ngai<sup>1</sup>: This model employed the Wigner random matrix Hamiltonian scheme to describe the complex condensed matter systems such as polymers, glasses, spin glasses etc., and considers the interaction of a relaxing species with such a complex background system. The original version has been re-examined recently<sup>25</sup> and we describe it here. It has also been shown recently<sup>26</sup> that a chaotic Hamiltonian may replace the Wigner scheme.

(Bb) Evolution of Entropy Theory for Correlated States: The original model<sup>1</sup> has been recently recast in another form.<sup>27</sup> This model involves time dependent transition rates which are obtained from time independent ones. The time dependence is due to an environment that provides a time dependent entropy contribution to the free energy which controls the transitions. We present this theory in a slightly different form so as to relax some mathematically simplifying assumptions made in the original version.

We also discuss three systems of current interest to condensed matter physicists: (1)

spin glasses, (ii) polymers, and (iii) electron glasses. In the last section of the paper, we give a summary of the results obtained thus far and also outline some of the open problems for future investigations. We also open the discussion of what stringent tests besides Eq. (1) and (2) for a proper relaxation theory in condensed matter system ought to obey. After this manuscript was completed, four articles of relevance to this review appeared. We have given a commentary on these works at the end.

## 2. Type A Theories

### (Aa) Distribution of Relaxation Times

Majumdar<sup>3,4</sup> is perhaps the first to try to give a physical basis of Eq. (1) which appeared in a description of stress relaxation in glasses. He proposed to understand the stress relaxation in glasses as microbrownian motion of its molecular constituents. This leads to a consideration of diffusion equation as the underlying equation for the stress relaxation phenomena. It is assumed that the stress field  $S(\vec{x}, t)$  at any given point in the glass is made up of "elementary stress relaxation modes" which are solutions of the diffusion equation

$$\frac{\partial u(\vec{x}, t)}{\partial t} = D \nabla^2 u(\vec{x}, t) . \quad (6)$$

Each mode decays exponentially with a relaxation time  $\tau$ , so that

$$u(\vec{x}, t) = \phi(\vec{x}) e^{-t/\tau} , \quad (7)$$

and

$$D \nabla^2 \phi(\vec{x}) + \frac{1}{\tau} \phi(\vec{x}) = 0 . \quad (8)$$

The elementary modes  $\{\phi_{\vec{k}}(\vec{x})\}$  associated with Eq. (8) have

$$\frac{1}{\tau} = D |\vec{k}|^2 \quad (9)$$

where  $\vec{k}$  is the usual wave-vector determined by suitable boundary conditions. The diffusion coefficient  $D$  for glasses is assumed to be inversely proportional to the viscosity,  $\eta$ , of the glass (Einstein relation). Thus, each relaxation time in (4) is proportional to  $\eta$ . It is important to stress that Eq. (6) is a postulate for the elastic stress field. This implies that for large viscosities, the Navier-Stokes equation contains the reciprocal of the viscosity whereas for small viscosities it contains the viscosity itself. In glasses, the viscosity is large and hence such a modification of the Navier-Stokes equation is suggestive in view of the Einstein relation. Thus, with the postulate as above, we may calculate the stress field  $S(\vec{x}, t)$  in terms of the complete set of functions given by Eq. (8):



$$S(\vec{x}, t) = \sum_{\vec{k}} a_{\vec{k}} \phi_{\vec{k}}(\vec{x}) e^{-D|\vec{k}|^2 t} \quad (10)$$

Following Majumdar,<sup>3</sup> by considering how each class of modes in different time regimes contributed to relaxation, one may derive Eq. (1) with some special values of  $n$ . Effectively this scheme is formally equivalent to distribution of relaxation times because Eq. (10) is rewritten in the form

$$S(\vec{x}, t) = \int e^{-D|\vec{k}|^2 t} \phi_{\vec{k}}(\vec{x}) P(\vec{k}) \frac{d^3 k}{(2\pi)^3} \quad (11)$$

where  $P(\vec{k})$  is the distribution in  $\vec{k}$ -space of the dominating specific mode  $\phi_{\vec{k}}(\vec{x})$  which is picked from physical considerations.  $P(\vec{k})$  is such that

$$\int P(\vec{k}) \frac{d^3 k}{(2\pi)^3} = 1 \quad (12)$$

In particular, Majumdar points out that one may take

$$P(\vec{k}) = A \exp[-(|\vec{k}|/\bar{k})^{-m}] \quad (13)$$

Here  $\bar{k}$  is a parameter and  $A$  is such that (12) is obeyed and

$m=1$  for short times  $t \ll \tau_s$  where a linear scale dominates the relaxation modes;

$m=2$  where surface dominated relaxation modes occur;

and

$m=3$  for volume dominated relaxation modes controlling  $S$ .

He obtains in these cases respectively

$$S_1(\vec{x}, t) \cong \exp(-t/\bar{\tau}_1)^{1/3} \quad (14a)$$

$$\bar{\tau}_1 = 4/27D\bar{k}^2$$

$$S_2(\vec{x}, t) \cong \exp(-t/\bar{\tau}_2)^{1/2} \quad (14b)$$

$$\bar{\tau}_2 = 1/2D\bar{k}^2$$

and

$$S_3(\vec{x}, t) \cong \exp(-t/\bar{\tau}_3)^{3/5} \quad (14c)$$

$$\bar{\tau}_3 = \frac{3}{2} \left(\frac{2}{5}\right)^{5/3} / D\bar{k}^2$$

At asymptotically large times, the largest mode dominates and then

$$P(\vec{k}) \sim \delta(|\vec{k}| - \bar{k}_{\max})$$

and

$$S_4(\vec{x}, t) \cong \exp(-t/\bar{\tau}_4) \quad (14d)$$

with

$$\bar{\tau}_4 = 1/D\bar{k}_{\max}^2$$

Observing that the various time scales  $\bar{\tau}_i$  differ from each other only by numerical pre-factors of order unity, he takes

$$\bar{\tau}_1 = \bar{\tau}_2 = \bar{\tau}_3 = \bar{\tau}_4 = \bar{\tau} = 1/4D\bar{k}^2$$

$$\cong \frac{6\pi\eta a}{4kT\bar{k}^2} \cong 10^5 \text{ sec} \quad (15)$$

for a typical glass and the experimental  $\bar{\tau}$  is  $4 \times 10^4$  sec, and so (15) is a fair estimate! Clearly there is no second universality in such a scheme.

Cohen and Grest<sup>5</sup> employ the free-volume theory to discuss the observed dispersion of relaxation times in dense liquids and glasses and show that it is simply related to the dispersion of the total surface-to-volume ratio of the liquid clusters. Without going into too many details of the free volume theory, we point out here that this is, like Majumdar's theory, an average over relaxation times scheme with a physical basis for the distribution function given via the free volume theory. In particular, they write for the relaxation function

$$\phi(t) = \int_0^\infty P(W) \exp(-Wt) dW \quad (16)$$

where  $P(W)$  is the probability distribution associated with the inverse relaxation time,  $W^{-1}$ . They then argue based on percolation theory that

$$W = W_0 \nu^{-x} \quad (17)$$

where  $\nu$  is the fragment size, and  $W_0$  is a parameter depending on temperature, molecular weight, etc.,  $x$  is an index. Changing variables from  $W$  to  $\nu$  and assuming that the new distribution function  $g(\nu)$ , which is now the probability of cluster sizes, to be of the form given by percolation theory,

$$g(\nu) = A \exp(-C\nu^y) \quad (18)$$

where  $C$  is a constant,  $A$  is slowly varying function of they perform the steepest descent calculation of the form in obtaining Eq. (4) and deduce for long times

$$\phi(t) \cong \exp(-C'(W_0 t)^z) \quad (19)$$

where

$$z = y/(x+y)$$

They then argue using percolation theory estimates that

$$2/3 < z < 1 \quad (20)$$

Here again there is no second universality and the percolation model and free volume schemes are of infrequent occurrence in condensed matter systems than even diffusion proc-

esses and inapplicable to spin glasses, electron glasses, secondary relaxations of amorphous polymers far below  $T_g$ , terminal relaxation of entangled polymer melts, for example. Moreover, the singular distribution functions for the cluster sizes themselves need a physical basis!

There is a third class of theories in this framework which attempts to arrive at Eq. (1) by kinetic Ising model approach. Dhar<sup>6,7</sup> proposes to explain this behavior in terms of Lifshitz states near the band edges in a disordered material. As an illustration of this scheme, he considered a one-dimensional kinetic Ising model with bond disorder. Skinner<sup>8</sup> also considers such a model to study cooperative dynamics of linear chain molecules, and basically the problem is recast in the form of Eq. (3). McMillan<sup>9</sup> considers a Monte Carlo simulation of the two-dimensional random ( $\pm J$ ) Ising model. He finds that the correlation function scales and the equilibration time obeys an Arrhenius law at low temperatures. He gives a simple cluster model as a means of understanding these Monte Carlo studies. We outline here briefly Dhar's scheme<sup>6,7</sup> as it is the earliest and perhaps the clearest of the descriptions based on the kinetic Ising model. Dhar shows that the kinetic Ising model equation may be written in the form

$$\frac{d}{dt} |S(t)\rangle = -\Lambda |S(t)\rangle \quad (21)$$

where  $\Lambda$  is a  $N \times N$  tridiagonal matrix, independent of time, but contains the random exchange constants of the random Ising model. The average magnetization  $M(t)$  is then expressed in the form (compare Eq. (3))

$$M(t) = \int_0^\infty d\lambda \exp(-\lambda t) D(\lambda) \quad (22)$$

with

$$D(\lambda) d\lambda = \langle \sum_{\lambda \geq \lambda'} \sum_{\lambda + d\lambda} \frac{1}{N} \langle S(0) | \lambda' \rangle \langle \lambda' | S(0) \rangle \rangle_c \quad (23)$$

where  $|\lambda'\rangle$  and  $\langle \lambda'|$  are the right- and left-eigenvectors of  $\Lambda$  with eigenvalues  $\lambda'$  and  $\langle \dots \rangle_c$  denotes the configuration average over the random exchange constants. Dhar then uses the arguments of Lifshitz to show that  $D(\lambda)$  is semibounded and behaves as  $\exp[-(\lambda - \lambda_0)^{-1/2} c]$  as  $\lambda \rightarrow \lambda_0$ , where  $c$  is a known constant and  $\lambda_0$  is given by  $(1 - \tanh(2\beta J_0))$ , with  $2\beta J_0$ , a typical exchange constant in the distribution of  $J$ 's, scaled by the temperature ( $\beta = 1/kT$ ). This leads to

$$M(t) \cong \exp(-\lambda_0 t - at^{1/3}), \quad t \rightarrow \infty \quad (24)$$

This model gives  $\exp(-at^{1/3})$  always with a temperature independent exponent  $n=2/3$  (in our notation). In higher dimensions, Dhar gives an argument based on percolation theory. In conclusion, Dhar tries to illustrate that the

existence of very large clusters determines the long time relaxation of magnetization in a kinetic Ising model. Further, he suggests that the Lifshitz states in the vicinity of the band edge as ideal candidates for producing  $\exp(-t^D)$  because this corresponds to  $D(\lambda) \sim \exp(-\lambda^{-D})$ . (cf-Majumdar<sup>3,4</sup>)

#### (Ab) Mathematical Analogy Theories:

In (Aa), we described one of the ways of arriving at Eq. (1) by consideration of diffusion. From stochastic processes point of view, diffusion is a manifestation of Brownian motion of a particle under the influence of random forces exerted on it by the environment. We will first, by way of introduction, show briefly this relationship as it will be a basis for discussion later on also. Explicitly stated, the ordinary Brownian motion is a real Gaussian process. Consider time  $t$ ,  $-\infty < t < \infty$ . The Brownian motion is described by a random variable  $B(t)$  with the following properties:

$$\langle B(t) \rangle = 0 \quad (25a)$$

$$\langle (B(t_1) - B(t_2))^2 \rangle = |t_1 - t_2| \quad (25b)$$

or equivalently, the autocorrelation

$$\begin{aligned} R_B(t_1, t_2) &\equiv \langle B(t_1) B(t_2) \rangle \\ &= \min(t_1, t_2) \end{aligned} \quad (25c)$$

and the derivative  $B'(t)$  is such that

$$R_{B'}(t_1, t_2) \equiv \langle B'(t_1) B'(t_2) \rangle = \delta(t_1 - t_2) \quad (25d)$$

The first order density of  $B(t)$  is obtained by using (25c) with  $t_1 = t_2 = t$ ,

$$R_B(t, t) = \langle B^2(t) \rangle = t, \quad (26)$$

and

$$\begin{aligned} f_{B(t)}(x) &= (2\pi \langle B^2(t) \rangle)^{-1/2} \exp(-x^2/2\langle B^2(t) \rangle) \\ &= (2\pi R_B(t, t))^{-1/2} \exp(-x^2/2R_B(t, t)) \end{aligned} \quad (27)$$

This is just the solution of traditional diffusion equation! The second order density of  $B(t)$  is a two-variable Gaussian density with auto-correlation function  $R_B(t_1, t_2)$ :

$$\begin{aligned} f_{B(t_1), B(t_2)}(x, y) &= \\ \exp - \frac{1}{2} \left\{ \frac{R_B(t_2, t_2)x^2 - 2R_B(t_1, t_2)xy + R_B(t_1, t_1)y^2}{R_B(t_1, t_1)R_B(t_2, t_2) - R_B^2(t_1, t_2)} \right\} \\ &\quad \frac{2\pi(R_B(t_1, t_1)R_B(t_2, t_2) - R_B^2(t_1, t_2))^{1/2}}{} \end{aligned}$$

and so on.

Mandelbrot and van Ness<sup>10</sup> considered a more general class of stochastic processes which they called fractional brownian motion (fbm) with parameter  $H$  and starting value  $b_0$  at

$t=0$ . They defined  $B_H(t)$  as the moving average of  $dB(t)$  weighted by a kernel,  $(t-s)^{H-\frac{1}{2}}$ :

$$B_H(t) = \frac{1}{\Gamma(H+\frac{1}{2})} \int_{-\infty}^t (t-s)^{H-\frac{1}{2}} dB(s), \quad (-\infty < t < \infty) \quad (29)$$

with

$$B_H(0) = \frac{1}{\Gamma(H+\frac{1}{2})} \int_{-\infty}^0 (-s)^{H-\frac{1}{2}} dB(s) \quad (30)$$

$\Gamma(H+\frac{1}{2})$  is the gamma function of argument  $(H+\frac{1}{2})$ . Here  $dB(s) = B'(s)ds$  where  $B'(s)$  is the derivative of the ordinary Brownian process with its associated correlation (25d). This fbm is also a Gaussian process determined by its autocorrelation function  $\langle B_H(t_1) B_H(t_2) \rangle$ . Note that for  $H=\frac{1}{2}$ , (29),  $B_{H=\frac{1}{2}}(t)=B(t)$ , the ordinary Brownian motion. Denote

$$b_H(t) \equiv B_H(t) - B_H(0) \quad (31)$$

Clearly

$$\langle b_H(t) \rangle = 0 \quad (32)$$

And, after some algebra, using (25d), for  $t_1 \neq t_2$

$$\begin{aligned} \langle b_H(t_1) b_H(t_2) \rangle = & \left\{ \frac{|t_1 - t_2|^{2H-t_1-2H-t_2}}{(\Gamma(H+\frac{1}{2}))^2} \right\} \\ & \left\{ \int_{-\infty}^0 (-s)^{H-\frac{1}{2}} [(1-s)^{H-\frac{1}{2}} - (-s)^{H-\frac{1}{2}}] ds \right\} \end{aligned}$$

Or, equivalently after some manipulation of the integral,

$$\begin{aligned} \langle b_H(t_1) b_H(t_2) \rangle = & \frac{[t_1^{2H+t_2-2H} - |t_1-t_2|^{2H}]}{2(\Gamma(H+\frac{1}{2}))^2} \\ & \left\{ \int_{-\infty}^0 ds [(-s)^{H-\frac{1}{2}} - (1-s)^{H-\frac{1}{2}}]^2 + \frac{1}{2H} \right\} \quad (33) \end{aligned}$$

This is valid for  $t_1=t_2$  also. This has an interesting self-similarity property:

$$\langle b_H(\lambda t_1) b_H(\lambda t_2) \rangle = \lambda^{2H} \langle b_H(t_1) b_H(t_2) \rangle, \quad (\lambda > 0) \quad (34)$$

Mandelbrot and van Ness<sup>10</sup> suggested many applications of this new process to several physical and other phenomena.

Maccone<sup>28</sup> suggested an alternative class of non-stationary Gaussian Stochastic processes which are a variant of the above fractional Brownian motion, which were originally suggested by Lévy, and mentioned in the work of Mandelbrot and van Ness.<sup>10</sup> This has the form

$$B_{LH}(t) = \int_0^t \frac{(t-s)^{H-\frac{1}{2}}}{\Gamma(H+\frac{1}{2})} B'(s) ds \quad (t \geq 0) \quad (35)$$

For  $H=\frac{1}{2}$ ,  $B_{L\frac{1}{2}}(t)=B(t)$ , the usual Brownian motion given by (25a-d). Maccone erred in his algebra

and Mandelbrot<sup>29</sup> pointed this out without giving details and Rajagopal and Rendell<sup>11</sup> had also noticed the error and had worked out details of this model with the hope of using it in relation to the relaxation process. They found<sup>11</sup> that

$$\begin{aligned} (t_1 \neq t_2) \langle B_{LH}(t_1) B_{LH}(t_2) \rangle = & \frac{(t_1 t_2)^{H-\frac{1}{2}}}{[\Gamma(H+\frac{1}{2})\Gamma(H+\frac{3}{2})]} \{ t_1 \eta(t_2 - t_1) {}_2F_1(-H+\frac{1}{2}, 1; \\ & H+\frac{3}{2}; \frac{t_1}{t_2}) + t_2 \eta(t_1 - t_2) {}_2F_1(-H+\frac{1}{2}, 1; \\ & H+\frac{3}{2}; \frac{t_2}{t_1}) \} \quad (36) \end{aligned}$$

$$\text{and for } t_1=t_2 \langle B_{LH}^2(t_1) \rangle = t_1^{2H}/2H[\Gamma(H+\frac{1}{2})]^2 \quad (37)$$

In (36),  $\eta(t)$  is positive unit step function,  $\eta(t) = 0$  if  $t < 0$ , and  $1$  if  $t > 0$ . From (36), if we take  $t_1 \rightarrow t_2$  or  $t_2 \rightarrow t_1$ , and use  ${}_2F_1(-H+\frac{1}{2}, 1;$

$H+3/2; 1) = \frac{H+\frac{1}{2}}{2H}$  we obtain (37). These relations were missed by Maccone<sup>28</sup> because of an error in the evaluation of  $\langle B_{LH}(t_1) B_{LH}(t_2) \rangle$  above where he missed the hypergeometric function appearing in (36) above. For  $H=\frac{1}{2}$ , this result goes over to (25c). It can be shown that  $B_{LH}(t)$  is a gaussian process by actual computation of say  $\langle B_{LH}(t_1) B_{LH}(t_2) B_{LH}(t_3) B_{LH}(t_4) \rangle$  etc. Now, consider the first order density associated with  $B_H(t)$  as in Eq. (27):

$$f_{B_{LH}}(x) = (2\pi \langle B_{LH}^2(t) \rangle)^{-\frac{1}{2}} \exp(-x^2/2\langle B_{LH}^2(t) \rangle) \quad (38)$$

which coincides with Maccone's result but his second order density is wrong because of his error in Eq. (36).

It is important to realize that the self-similarity property

$$B_{LH}(\lambda t) = \lambda^H B_{LH}(t), \quad \lambda > 0 \quad (39)$$

is preserved. Discussions based on one-variable distribution function are all correct in Maccone's work but others are wrong as well as his discussion of stochastic independence of the increments because the correlations are not as in the ordinary diffusion process.

Our interest in this process was exactly in Eq. (38) and (37). In explaining the experimentally observed dispersive diffusion in amorphous semiconductors, one finds Eq. (1) leading to a time-dependent diffusion coefficient. From (27) we see that  $\langle x^2(t) \rangle = \langle B^2(t) \rangle = t$  or had we introduced a diffusion coefficient  $D$

in the usual way  $D \equiv \frac{\langle x^2(t) \rangle}{t}$ , we would have  $D$  independent of  $t$  in the usual diffusion theory. Experimentally,  $D$  is found to be time-dependent<sup>23</sup> and depends on  $t$  for long times as  $t^{-n}$ , with  $0 < n < 1$ , as in Eq. (1). From (38), we note that the diffusion constant in this case is  $\int_0^t D_{LH}(s) ds = \langle x^2(t) \rangle \propto t^{2H}$ . For  $0 < H < \frac{1}{2}$ , we may identify  $n = (1-2H)$  so that  $0 < n < 1$  and in this case, the fractional Brownian motion as discussed by Lévy and Maccone serve as a model for anomalous dispersion in amorphous semiconductors. Under subsection (Ac) we shall return to this sort of model again when we discuss Langevin theory, which is a little more physical, but leads to results of this type also. Clearly, if we have to identify the physical process with the fractional Brownian motion defined by Eq. (35) and not by Eq. (29), the former is valid for  $0 < t < \infty$  whereas the latter for  $-\infty < t < \infty$ , nature must have a physical basis for this choice and we must understand this from some basic physical principle. Also, as pointed out earlier, not all physical entities which give rise to time-dependence of the form Eq. (1) can be described in terms of diffusion!

The theory of infinitely divisible processes have been known for some time. (See for example, Feller.<sup>30</sup>) The most general form of probability density which when convoluted any number of times preserves its form was derived by Lévy. The well-known cases of Gaussian and Cauchy distributions were thus extended and an immediate consequence of this generalization was that these functions had long tails unlike the Gaussian. Since in the physical observations one has the concept of energy or frequency distributions whose fourier transform gives the nature of time-dependence, it seems a form of time-dependence given by Eq. (1) requires low energy (or frequency) tails in its distribution. The question of superposable energy or frequency distribution is not hard to invoke because superposability in physics is a natural occurrence. The Gaussian distribution and the law of large numbers are central to many of our statistical mechanical thinking and a generalization of this to cover instances where the second energy or frequency moment may not exist is only a slight generalization. It

appears that Tunaley<sup>12</sup> was the first to invoke such notions to explain  $1/f$  noise in thin metallic films from such physical processes. Tunaley noted that if we restrict ourselves to very low frequencies, mean and variance may be infinite on some long time scale and on a local time scale the envelope of these processes may have a normal distribution with finite mean and variance. Furthermore, he considered the stable densities as attractive because of their scaling properties, which seem to be consistent with the idea of homogeneous fluctuation generation in a semiconductor. He stressed that the possibility of infinite mean and variance in

the traversal time should be given careful consideration in any stochastic model where it is likely to have profound effect on the predictions. Hughes et al.<sup>13</sup> considered random walks with self-similar clusters but with no apparent physical application. Montroll and Shlesinger<sup>14</sup> reported on examples of distribution functions with long tails. These same authors have recently written three articles<sup>31,32,33</sup> where many diverse physical phenomena are shown to display close analogy with systems having long tail distribution in their wave length and frequency properties. They do not offer any detailed physical processes that would derive these distributions in some plausible way. Also, there is no prediction made, after having made this analogy. We should point out that all these authors use a symmetric form of the distribution for mathematical convenience only and do not offer any physical reasoning for the parameters appearing in the Lévy distribution.

Tunaley,<sup>12</sup> Montroll and his coworkers<sup>13,14</sup> had noted that Lévy distributions lead to functions of the form (1) with  $-1 < n < 1$  for symmetric distributions (more general form is of no concern to us here), which were employed by these authors without explanation except to state that the choice is dictated by simplicity.  $n = -1$  corresponds to the Gaussian spectrum  $\rho(\epsilon)$ , and  $n = 0$  to the Cauchy  $\rho(\epsilon) = (a^2 + \epsilon^2)^{-1}$ , both of which are unbounded from below. This point was never realized by these authors. It was Rajagopal et al.<sup>19</sup> who imposed the boundedness from below condition via the Paley-Wiener theorem and restricted the  $n$  values to  $0 < n < 1$ . We stress again that the mathematical analogies while useful and point to the correct direction, they did not give all the required results without the careful use of general physical requirements which are model independent.

Rajagopal et al.<sup>19</sup> were groping for the full use of the general requirements of semiboundedness and superposability of the spectrum and they went for square integrability of the spectrum as an additional requirement so as to employ the PW theorem and hence they called their result as a bound and PW criterion.

#### (Ac) Stochastic Processes

An alternate scheme to the one given in § Ab is the stochastic process or master equation approach. Here again, the linear time proportional probabilities play a crucial role in setting up the equations. This framework goes under the name of continuous time random walk (CTRW)<sup>15</sup> and the associated master equation (GME)<sup>16</sup> for studying time-dependent problems (see also the review, Ref. 17). Montroll and coworkers popularized this model by their pioneering work in this area.<sup>31,32,33</sup> (See also Ref. 34.) The approach popularized by this school is the so-called generalized Glarum model which we shall describe here in

some detail, in which defects move with a constant renewal rate. This theory deduces Eq. (1) from such considerations. Implicit in this model are the concepts of a "site" and of a "defect." It is then assumed that the defects move through the system by a random walk process and at any site relaxation cannot occur until a defect arrives. The Montroll school suggests that the Lévy tails must be introduced with the waiting time probability densities,  $\psi_m(t) \propto t^{-2-n}$  so that Eq. (1) ensues. Ngai and Liu<sup>18</sup> have argued that the weighting time distribution in carrier hopping transport, the hopping time distribution is negative of the derivative of Eq. (1) and hence  $\psi_{NL}(t) \propto (1-n)at^{-n} \exp(-at^{1-n})$  which enters the CTRW equations. Thus there is a controversy as to the correct form of  $\psi(t)$  to be used in CTRW formalism. There are two points of interest to note with the choice of  $\psi_{NL}(t)$ . Another important outcome of the NL scheme is that in the final result the time dependence is always of the form  $\exp(-at^{1-n})$  where  $a$  depends on the physical dimension of the lattice in which the random walker is walking, whereas in the M scheme, besides depending on the physical dimension, the exponent  $(1-n)$  is halved as we go from 3-D to 1-D. When the moments  $\mu$  of the waiting time distributions function<sup>m</sup>  $\psi(t)$  are all finite, the Markovian master equation is an appropriate description for times which are large compared to  $t^* = \sup(\mu_m/m!)^{1/m}$ . For  $\psi_{NL}(t)$ , it is found that  $t^*$  is finite for  $-1 < n < 0$  and infinite for  $0 < n < 1$ . Thus, a non-Markovian description is always required for relaxation functions of the form given by Eq. (1). The second point is that the memory function of the GME is related to the  $\psi(t)$  of CTRW. If the GME is to describe a time-dependent statistical mechanical phenomenon, it must obey the H-theorem, which is a statement of the second law of thermodynamics. Only for  $\psi_{NL}(t)$  one can demonstrate the validity of the H-theorem. There are several other important differences between the outcomes of  $\psi_M(t)$  vs.  $\psi_{NL}(t)$ . The most important consequence of the NL theory is that the form of Eq. (1) for the relaxation function follows whereas the  $\psi_M$  scheme does give Eq. (1) for long times. The bimolecular reaction rates in  $\psi_{NL}$  scheme are very different from the  $\psi_M$  theory and experimental results seem to need a bimolecular setup with NL approach. The number of molecules at a long time  $t$  in the unimolecular reaction theory in the NL theory is  $N_A^{NL}(t) \cong \exp(-t^{1-n})$  whereas in the bimolecular case  $N_A^{NL}(t) \cong t^{-n+1}$ . This important difference is not given by the M theory. The most important criticism of CTRW is that not all physical properties giving rise

to Eq. (1) can be reasonably modelled as a random walk process, whereas (1) seems too ubiquitous!

There is another important approach to relaxation problems, via the Langevin equation. Here the relaxing entity moves in an effective medium and obeys a Langevin equation with a friction coefficient due to the medium and a random force also due to the medium. Ford, Kac, and Mazur (FKM) in their classic work<sup>21</sup> describe a Brownian particle imbedded in a heat bath of harmonic oscillators. The equation of motion for the Brownian particle velocity  $u(t)$  (we consider a one-dimensional case for simplicity) can be written as<sup>21,22</sup>

$$\frac{du(t)}{dt} + \gamma(t)u(t) = E(t) \quad (40)$$

If the velocity auto-correlation function of the oscillator bath system is

$$c(t) \equiv \langle u(0)u(t) \rangle = kT [\cos \underline{A}^{1/2}t]_{00} = kT \int_{-\infty}^{\infty} g(\omega) \exp(i\omega t) d\omega \quad (41)$$

where  $g(\omega)$  is the frequency distribution function associated with the eigenvalue spectrum of the interaction matrix  $A$  of the harmonic oscillators.  $T$  is the temperature of the bath system, etc. Then the friction sufficient  $\gamma(t)$  is given by

$$\gamma(t) = -\frac{d}{dt} \log c(t) \quad (42)$$

and  $E(t)$ , which represents the force due to all other oscillators making up the heat bath has a covariance written in the form<sup>22</sup>

$$\begin{aligned} \langle E(t)E(t+\tau) \rangle = & -\frac{d^2}{d\tau^2} c(\tau) + \gamma(t)\gamma(t+\tau)c(\tau) \\ & + [\gamma(t) - \gamma(t+\tau)] \frac{dc(\tau)}{d\tau} \quad (43) \end{aligned}$$

It is important to stress that this is an exact result for a bath of harmonic oscillators with which the relaxing harmonic oscillator is in contact.  $\langle \dots \rangle$  in the above denotes average over the initial coordinates and velocities of the harmonic oscillators as usual. Moreover the friction coefficient  $\gamma(t)$  and the covariance of the random force  $E(t)$  are related in this definite way. FKM<sup>21</sup> assumed  $c(t)$  in Eq. (41) to be exponentially decaying

$$c(t) = kT \exp(-\tilde{\gamma}|t|) \quad (44)$$

so that from (42), one obtains a time-dependent constant friction coefficient

$$\gamma(t) = \tilde{\gamma} \quad (45)$$

and from (43), we obtain white noise spectrum for the random force:

$$\langle E(t)E(t+\tau) \rangle = 2\tilde{\gamma}kT\delta(\tau) \quad (46)$$

Thus one obtains exponentially decaying solutions for the relaxing particle. From Doob's theorem, (44) ensures a Gaussian Markoff process as the underlying stochastic process and we can only get exponential decay in such a scheme. From (41), this implies that  $g(w)$  is Lorentzian,  $\sim (w^2 + \tilde{\gamma}^2)^{-1}$  which is unbounded from below, a physically unacceptable spectrum! If we employ a Paley-Wiener structure for  $c(t)$  or better still a Lévy structure, we may then work out the long time behavior quite easily, because then

$$c(\tau) = kT \exp[-\tilde{\gamma} a_n (1-n)^{-1} |\tau|^{1-n}] \quad (47)$$

with  $0 < n < 1$ . Then  $\gamma(t)$  is the long time limit is given by

$$\gamma(t) \cong \tilde{\gamma} a_n t^{-n} \quad (48)$$

The bath noise covariance (43) evaluated for long times, takes the form

$$\langle E(t)E(t') \rangle \cong 2kT\gamma(t)\delta(t-t') \quad (49)$$

At long times, the motion of the Brownian particle appears to be that of a classical white-noise Brownian motion if a clock is used which measures time  $\theta$ , given by

$$\theta(t) = a_n (1-n)^{-1} t^{1-n} \quad (50)$$

where  $a_n \rightarrow 1$  as  $n \rightarrow 0$ . In the  $\theta$ -frame, Eq. (40) becomes

$$\frac{d\tilde{u}(\theta)}{d\theta} + \tilde{\gamma} \tilde{u}(\theta) = \tilde{E}(\theta) \quad (51)$$

where

$$\tilde{u}(\theta) = u(t), \quad \tilde{\gamma} = \gamma(t) / \left(\frac{d\theta}{dt}\right), \quad \tilde{E}(\theta) = E(t) / \left(\frac{d\theta}{dt}\right) \quad (52)$$

Equation (51) can be solved in a standard way and the results may then be transformed back to  $t$ -clock. This again leads to Eqs. (40), (48), and (49). We note here in passing that the modified white noise of Eqs. (49) and (48) also results at long times from the covariance of the fractional Brownian motion<sup>10,11</sup> discussed in §Ab. However, the connection of the present results to this fractional Brownian motion is rather tenuous. The autocorrelation of the Lévy form, Eq. (47), uniquely specifies the low frequency eigenvalue spectrum and the equations of motion, whereas the form of the bath noise does not. Autocorrelations which are power laws in time,  $t^{-n}$ , also lead to noise covariance of the form  $t^{-n}\delta(t-t')$  at long times but result in rather different equations of motion. This is because, in the FKM framework, the specification of  $c(t)$  determines the covariance of  $E(t)$  and not vice versa. The device of using the  $\theta(t)$  clock at long times is a convenient way to carry out all the manipulations. For example, the conditional probability distribution for the occurrence of velocity  $u$  at time  $t$  given that  $u = u_0$  at  $t = 0$ ,  $W(u, t; u_0)$  can be found

by requiring that, by the  $\theta(t)$ -clock, a Maxwellian distribution is obtained at long times. This is a required result of the classical Langevin treatment<sup>35</sup> i.e.

$$W(\tilde{u}, \theta; \tilde{u}_0) \rightarrow (\tilde{\gamma}/2\pi\tilde{q})^{1/2} \exp[-\tilde{\gamma}|\tilde{u} - \tilde{u}_0|^2/2\tilde{q}]$$

as  $\theta \rightarrow \infty$ , where  $\tilde{q} = \tilde{\gamma}kT$ . But since  $\tilde{u}(\theta) = u(t)$ , a Maxwellian distribution is also found in the  $t$ -clock and equipartition holds for our modified Brownian motion. The approach to a Maxwellian however will be slower than in the Langevin case. On the other hand, the probability distribution for position  $W(\tilde{r}, t; \tilde{r}_0, u_0)$  is altered in form as  $t \rightarrow \infty$ . By the  $\theta(t)$ -clock,  $W(\tilde{r}, \theta; \tilde{r}_0, \tilde{u}_0) = (\tilde{\gamma}^2/4\pi\tilde{q}\theta)^{1/2} \exp[-\tilde{\gamma}^2|\tilde{r} - \tilde{r}_0|^2/4\tilde{q}\theta]$  as  $\theta \rightarrow \infty$ . This predicts the classical diffusion by means of the equation

$$\frac{\partial W}{\partial \theta} = D \frac{\partial^2 W}{\partial \tilde{r}^2} \quad (53)$$

with constant diffusion coefficient  $\tilde{D} = \tilde{q}/\tilde{\gamma}^2$ . Transforming (53) back to  $t$ -clock, we find a diffusion equation with a  $t$ -dependent diffusion coefficient  $D(t)$  given by

$$D(t) = \tilde{D} a_n t^{-n} \quad (54)$$

The form of  $W$  by the  $t$ -clock then becomes (because the use of  $\theta(t) = \int_0^t D(t') dt'$  will connect this diffusion equation in  $\theta$ -space to one with constant  $D$  as in Eq. (53))

$$W(\tilde{r}, t; \tilde{r}_0, u_0) = [4\pi \int_0^t D(t') dt']^{-1/2} \exp(-|\tilde{r} - \tilde{r}_0|^2 / 4 \int_0^t D(t') dt'), \quad (55)$$

as  $t \rightarrow \infty$ . Note that both the friction coefficient and the diffusion coefficient are decreasing functions of time, and for consistency this requires  $D(t) = q(t)/\gamma^2(t)$  where  $q(t) = \tilde{q}(d\theta/dt)^3$ . The result  $\tilde{q}/\tilde{\gamma} = kT$  is a consequence of the requirement that the velocity distribution function asymptotically approach the Maxwellian distribution function with a given temperature  $T$  of the bath. In the  $t$ -dependent case, this is found to be  $q(\cdot)/\gamma(t) = kT(d\theta/dt)^2$ . What is remarkable is the consequence that the result (54) is in conformity with the observed dispersive diffusion in amorphous semiconductors. The result  $D(t)$  obtained in this way coincides with the Ngai-Liu theory<sup>18</sup> who obtain  $D(t) = D_0 e^{-n\gamma t^{-n}}$  and their mobility is given by  $\mu_n(t) = \mu_0(1-n) e^{-n\gamma t^{-n}}$ . We should point out that in our model Langevin theory, non-stationary Gaussian processes cannot be fully implemented except for asymptotically long-times by the  $\theta$ -transformation.<sup>19,36</sup>

(Ad) Other Schemes

There is a traditional approach to relaxation functions in a general setting due to Kubo which is known as the linear response theory. At long times or equivalently for low frequencies, this formula simplifies because for frequencies less than  $10^{10}$  Hz which is a typical low frequency regime where Eq. (1) is observed experimentally, which corresponds to a temperature of  $\frac{1}{2}K$ , essentially the classical limit of the Kubo linear response suffices. Thus the frequency response may be written in the form

$$\chi_{\text{Kubo}} \sim \text{F.T. of } \frac{d}{dt} \exp\{-\phi(t)\} \quad (56)$$

where  $\phi(t)$  obeys a master equation in general, of the form

$$\frac{d}{dt}\phi(t) = -W(t)\phi(t) \quad (57)$$

where  $W(t)$  is the time dependent transition rate induced by the heat bath at such long times. If instead of (57), one employs the leading order perturbation expansion as in the Kubo formalism, one obtains

$$\phi(t) \cong \phi^{(2)}(t) \quad (58)$$

Young<sup>23</sup> has used this perturbation approach to a solvable model consisting of a charge hopping between sites and which is in contact with a heat bath of harmonic lattice vibrations. Then the computation of  $\phi^{(2)}(t)$  for this model gives also the exact answer in his case, and one gets

$$\phi^{(2)}(t) = \frac{1}{2} \sum_i \coth\left(\frac{w_i}{2kT}\right) \frac{\lambda^2(w_i)}{w_i^2} (1 - \cos w_i t) \quad (59)$$

where  $\lambda(w_i)$  is the coupling between the flipping dipole and the phonon field. Hence for low frequencies when  $w/kT \ll 1$  (for  $w=10^{10}$  Hz at room temperature 3000K, this ratio is  $10^{-3}$ !) one obtains

$$\phi^{(2)}(t) = kT \int_0^\infty dw \frac{\lambda^2(w)}{w^3} n(w) (1 - \cos wt) \quad (60)$$

where  $n(w)$  is the density of states of the bath system. Here a continuum of frequencies is assumed instead of a discrete set as in Eq. (59). Assuming  $\lambda(w)=\lambda_0$  a constant at low frequencies, and assuming  $n(w)$  may be expanded in a power series, Young<sup>23</sup> obtained  $n(w) = n_1 w + n_2 w^2 + \dots$ ,

$$\phi^{(2)}(t) \cong \alpha t + \beta \ln(w_0 t) + \gamma + O(1/t) \quad (61)$$

where

$$\alpha = \frac{\pi}{2} \lambda_0^2 n_1 T, \quad \beta = \lambda_0^2 n_2 T,$$

and

The final result obtained is then of the form which has a temperature dependence which makes the answer irrelevant unlike in the expression (1). The important ingredient missing in the above model is the absence of an appropriate heat bath. Observe that the first term in Eq. (61) gives the usual exponential decay and the heat bath correlations in this scheme gives the residual  $\phi_r(t)$ . Another way of stating this is that this theory would give a relaxing species the usual nominal exponential decay,  $e^{-\alpha t}$  and then the low frequency correlated bath excitations would modify this to  $e^{-\alpha t} e^{-\phi_r(t)}$ . In a proper theory, this is not what happens, but rather  $\exp[-\int_0^t W(t') dt']$ . For  $W(t')$  one makes a cumulant expansion and observes that the temperature factors such as appear in Young's calculation do not enter because at high temperatures all the states are all equally occupied etc. If we take  $W(t') = \alpha$ , the constant transition rate, we obtain the exponential decay but the low frequency excitations of the bath modify this constant rate in an entirely different way than a careless application of Kubo formula would suggest. This will be discussed in more detail in §Ba.

The derivation of Young<sup>23</sup> gives a form of Eq. (1) but with vanishing coefficients at such "high temperatures" and hence Young's calculation misses the point entirely and is irrelevant to a proper derivation of Eq. (1).

Palmer<sup>24</sup> has attributed the non-exponential decay to broken ergodicity on such large time scales. He tries to argue based on relevant time scales invoked in long time relaxation in condensed matter systems such as glasses, polymers etc., that there is a self-similar set of free energy surfaces at such long time scales and the system readjusts to this new situation by altering the time-independent transition rate,  $\tau^{-1}$  appearing in the traditional exponential decay  $\exp(-t/\tau)$ , to a time-dependent one in the form

$$\tau \sim c^*(t/\tau_0)^n, \quad 0 < n < 1$$

and hence

$$\exp(-t/\tau) \rightarrow \exp-A(t/\tau_0)^{1-n}$$

He then tries to connect this  $\tau$  with the entropy change induced for such situations in an argumentative way but not based on any theoretical model or scheme. See however the notes added at the end of the paper.

We now develop a language for discussing time-dependent transition rates (TDTR) that arise from time-independent transition rates (TITR) which seem to be so common in long time relaxation processes in condensed matter. In

this fashion, we give here a description of simple relaxation which is the ultimate approach to equilibrium, in a model-independent way which gives the result (1) of the Introduction. Also, we make contact with the language of stochastic processes which has been one of the phenomenological ways of discussing the relaxation phenomena.

From Refs. 1 and 2, it seems clear that the time-dependent transition rates that determine relaxation phenomena in condensed matter may be viewed as one with time-independent transition rates on a different time scale.<sup>36</sup> Then the original process in the experimentally measured time  $t$  with TDTR may be viewed as derivable from a process with TTR by means of a time-scale transformation. A time scale or development parameter is taken to be positive, cumulative function that increases from an origin monotonically. Consider two continuous time scales  $\theta$  and  $t$  where  $\theta$  may be expressed as a function of the experimentally measured time  $t$ . Without loss of generality, we may take  $\theta$  and  $t$  to be aligned such that their origins coincide:

$$\theta = \theta(t) \quad , \quad \theta(0) = 0 \quad . \quad (63)$$

Let us specify further that  $d\theta/dt$  is positive, and finite everywhere except possibly at isolated points. Such a  $\theta$ - $t$  relationship is thus nonlinear.

Suppose now that the transition rates on the  $\theta$  time scale,  $W(\theta)$  are stationary (constant). Then

$$W(\theta) = W_s \quad . \quad (64)$$

On the  $t$ -scale, the transition rates

$$W(t) = \frac{d\theta}{dt} W_s \quad (65)$$

are time-dependent since  $d\theta/dt$  is a nontrivial function of  $t$ . If  $W$  represents the matrix of transition rates, the matrix is time-independent on the  $\theta$ -scale and all components of the matrix are subjected to the same time-scale transformations.

Several features of such time scale transformations must be noted. Causality is maintained because the time scale does not alter the order of events. The mechanism of transitions are not affected by the time scale but only the way the transitions are counted. Thus a Markoff process remains a Markoff process and non-Markoff process retains its character under such time scale transformations.

To illustrate the effects of TDTR in stochastic processes, we consider for simplicity the most commonly discussed Gaussian Markoff process with only a single, scalar transition

rate. We start with a description of the process on a time scale for which the transition rate is a constant. Let  $\alpha$  be a random variable representing deviations from equilibrium. We discuss a Langevin type approach.

The fluctuation process may be represented by a linear regression or Langevin equation

$$\frac{d\alpha(\theta)}{d\theta} = -W_s \alpha(\theta) + \varepsilon(\theta) \quad (66)$$

where we have employed an effective linear decay interaction (i.e.,  $-W_s \alpha$ ) and  $\varepsilon(\theta)$  is assumed to be Gaussian with moments

$$\langle \varepsilon(\theta) \rangle = 0 \quad , \quad (67a)$$

$$\langle \varepsilon(\theta_1) \varepsilon(\theta_2) \rangle = 2\lambda \delta(\theta_1 - \theta_2) \quad . \quad (67b)$$

The angular brackets represent stochastic averaging. Although the introduction of the  $\delta$ -function (negligibly short correlations for the stochastic driving term) here is not formally correct,<sup>37</sup> its use in a straightforward way does lead to the same results as in a rigorous development.<sup>38</sup> This is a phenomenological equation since it describes a system already decoupled from its environment with both reactive forces and fluctuation sources represented as effective interactions within the system. It appears that on a phenomenological level, such an equation may provide a satisfactory description of a physical process, at least in some time regime where reference is made to an apparent origin. The success of the Langevin equation on the  $t$ -scale is indeed well known and hence the usefulness of the equation is borne out. We have here generalized this customary description, (66), to be valid on the  $\theta$  time scale. However, one would expect the  $\theta$  and  $t$  scales to coincide at the earliest times since the physical mechanisms that lead to TDTR must first be established before there is a difference between the two time scales. Similarly at very long times, when regression is completed, time differences must coincide so that  $d\theta/dt$  must become unity.

As usual, the equilibrium distribution is taken to be Gaussian and may be viewed as resulting from an expansion of the entropy with retention only of quadratic terms<sup>39</sup>

$$P(\alpha) = (g/\pi k)^{1/2} \exp(-g\alpha^2/k) \quad (68)$$

where  $k$  is a Boltzmann constant. Also, since the restoring force  $X = \frac{\partial S}{\partial \alpha} = -g\alpha$ ,  $g$  is a linear force coefficient expressed in entropy units. It can be converted into energy units by multiplication by the absolute temperature  $T$ . The usual results for equilibrium fluctuations follow, e.g., assuming  $\alpha(\theta=0) = \alpha(0)$ , we have



$$\alpha(\theta) = \alpha(0) \exp(-W_s \theta) + \int_0^\theta \exp(-W_s \theta') \exp(\theta' W_s) \varepsilon(\theta') d\theta' \quad (69)$$

$$\langle \alpha(\theta) \rangle = \alpha(0) \exp(-W_s \theta) \quad (70)$$

$$\{ \langle \alpha(\theta) \rangle \} = 0 \quad (71)$$

$$\langle \alpha(\theta_1) \alpha(\theta_2) \rangle = \frac{\lambda}{W_s} \exp(-|\theta_1 - \theta_2| W_s) + (\alpha^2(0) - W_s^{-1} \lambda) \exp(-(\theta_1 + \theta_2) W_s) \quad (72)$$

and

$$\{ \langle \alpha(\theta_1) \alpha(\theta_2) \rangle \} = \frac{\lambda}{W_s} \exp(-|\theta_1 - \theta_2| W_s) + (k(2g)^{-1} - W_s^{-1} \lambda) \exp(-(\theta_1 + \theta_2) W_s) \quad (73)$$

where the curly brackets {...} represent an average over the equilibrium distribution (68). In deriving (70) and (72), the equations (67a,b) were used along with the fact that  $\langle \alpha(0) \varepsilon(\theta) \rangle = 0$ . The requirement that the autocorrelation function (73) should be of the form

$$\{ \langle \alpha(\theta_1) \alpha(\theta_2) \rangle \} = \lambda W_s^{-1} \exp(-|\theta_1 - \theta_2| W_s) \quad (74)$$

so that Doob's theorem<sup>37</sup> would give us a Gaussian Markoff process for  $\alpha(\theta)$ , leads to the relationship

$$\lambda = k W_s (2g)^{-1} \quad (75)$$

Another way of stating this is that the equilibrium distribution is independent of  $\theta$  so that from (73), taking  $\theta_1 = \theta_2$ , we should have  $\{ \langle \alpha^2(\theta) \rangle \} = \{ \langle \alpha^2(0) \rangle \}$ . (Note a factor  $\frac{1}{2}$  in (75) is different from that given in Ref. 36, due to a misprint), and hence we would obtain (74) and Doob's theorem would lead us to conclude that  $\alpha(\theta)$  obeys a stationary Gaussian Markoff process. Thus TDTR introduced here leads to familiar results on a  $\theta$ -scale by virtue of general physical considerations only.

Consider now the dynamics of a macroscopic perturbation  $\bar{\alpha}$  caused by an external force  $\bar{X}$  to be represented on the  $\theta$  time scale by

$$\frac{d\bar{\alpha}}{d\theta} = L\bar{X} \quad (76)$$

Again a linear approximation is made for  $\bar{X}$  when  $\bar{\alpha}$  is undergoing decay and it is assumed that the path of decay is the same as that for a regression of a fluctuation  $\alpha$  in the stochastic process-Langevin theory discussion given above. In energy units,

$$\bar{X} = -gT\bar{\alpha} \quad (77)$$

where  $T$  is the absolute temperature. Then the following identity holds:

$$W_s = LgT \quad (78)$$

It follows that

$$\bar{\alpha}(\theta) = -(gT)^{-1} \exp(-\theta W_s) \bar{X}(0) \quad (79)$$

On the basis of (79), one may define a time-dependent response function  $Z(\theta)$  as

$$Z(\theta) = (2gT)^{-1} \exp(-\theta W_s) \quad (80)$$

Then from Eq. (74), it follows that

$$Z(\theta) = (kT)^{-1} \{ \langle \alpha(\theta) \alpha(0) \rangle \} \quad (81)$$

This formula for the relaxation function may be immediately recognized as being of the Kubo-Green type<sup>40</sup> in the classical regime.

We shall now apply this general framework to the relaxation problem. First we note that  $W_s^{-1}$  may be identified as a relaxation time  $\tau_s$  and the response function (80) is dependent only on the ratio  $\theta/\tau_s$ . In other words a natural unit of time in  $\theta$  space is  $\tau_s$ . Now define, in general, a proper relaxation process to be one for which the time dependence is controlled by a function only of the ratio of the time  $t$  to a relaxation time  $\tau$ . This relaxation property does not in general hold on the  $t$  time scale for arbitrary TDTR. However, suppose there is a time regime for which this relaxation property holds on the  $t$  scale and such that  $\theta$  and  $t$  scales are aligned at the apparent origin. Moreover, suppose there is a self-consistency in the definition of relaxation times so that they are related by the same time transformation that relates the two time scales, i.e.,

$$\theta(\tau) = \tau_s \equiv W_s^{-1} \quad (82)$$

The macroscopic relaxation equation (76) in this representation is

$$\frac{d\bar{\alpha}}{d\theta} = -\frac{1}{\tau_s} \bar{\alpha} \quad (83)$$

in the  $\theta$ -scale and in view of the definition of the proper relaxation process, we may express the same process in the  $t$ -scale in the form

$$\frac{d\bar{\alpha}}{dt} = -\frac{1}{\tau} f(t/\tau) \bar{\alpha} \quad (84)$$

where  $f$  is some function of the dimensionless ratio  $t/\tau$ . Comparing (84) with (83) we obtain

$$\frac{1}{\tau} f(t/\tau) = \frac{1}{\tau_s} \frac{d\theta}{dt} \quad (85)$$

in order to be able to describe the same phenomena. Using (82), we observe that

$$\frac{1}{\tau} f(t/\tau) = \frac{d}{dt} \left( \frac{\theta(t)}{\theta(\tau)} \right) \quad (86)$$

Upon integration of this equation, since at  $t=0$ ,  $\theta(0)=0$ , we get

$$\int_0^t \frac{1}{\tau} dt' f(t'/\tau) = \theta(t)/\theta(\tau) \quad ,$$

which may be recast in the form

$$\int_0^{t/\tau} dy f(y) = \theta(t)/\theta(\tau) \quad , \quad (87)$$

upon a change of variable,  $t'/\tau = y$ . The left hand side of (87) is a function of the ratio  $t/\tau$  and hence in order for  $\theta(t)/\theta(\tau)$  to be a function of  $t/\tau$ , it is necessary that  $\theta(t)$  be a monomial:

$$\theta(t) = at^b \quad (88)$$

where  $a$  has the dimensions of time to the  $(1-b)$ -th power and  $b > 0$  so that  $d\theta/dt$  is positive and  $\theta$  satisfies (63). Thus one obtains from such general phenomenological, model independent considerations, relaxation functions of the form of Eq. (1), on the  $t$ -scale.

We have thus reviewed a large class of models all of which try to derive Eq. (1) based on models for special physical events. No one theory has a generic character that Eq. (1) seems to have. Moreover, the second relation (2) does not appear in any of these theories. In the next section we shall give an account of a set of ideas that Ngai and his group have put forward in recent times which goes out of specificity of models as in Type A theories but based on general physical considerations only. Both universalities are deduced in this approach.

### 3. Type B Theories

#### (Ba) Original Model of Ngai

We will now describe the original model of Ngai<sup>1</sup> in a slightly different form,<sup>25</sup> as this may be pedagogically clearer than the original version. The evolution of a system is given by the Liouville operator once the initial state of the system is specified. The only thing known about the evolution is that the system evolves into an equilibrium state. No comment can be made as to the nature of time dependence, except that for long times the system approaches the equilibrium state. In the discussion of "relaxation" in a condensed matter system, this question is the same as the time dependence of a physical property such as electric or magnetic or thermodynamic or structural property. These properties may be thought of as being a reflection of the time evolution of a "species" such as dipoles for dielectric relaxation, spins for magnetic relaxation etc., whose evolution at long times ( $> 10^{-10}$  sec) is the regime of interest in condensed matter problems. For such times, one is probing energy levels of the systems of order  $\hbar/(10^{-10} \text{ sec})$  or  $10^{-1}$  eV. For shorter time

scales such as  $10^{-13}$  sec., the corresponding energy levels probed are of order  $300^\circ\text{K}$ ; these may correspond to excitations of the system such as phonons, etc. But at energies of order  $10^{-1}$  eV, no known excitations of the system can be invoked and a new low energy mechanism must be sought for understanding the relaxation process. Since the equilibrium thermal energies at which experiments are usually conducted are much larger than the  $10^{-1}$  eV, we must ask ourselves what these new excitations could be and how should these be described? Another feature that must be incorporated in any such theory is that the new long time regime must be incorporated smoothly over the higher energy processes such as phonons, magnons, etc., of the shorter time regime. In other words, a smooth modification of the processes must come about as one probes these new excitations as the system relaxes at longer and longer time scales. Thus the second universality relationship, Eq. (2), is a manifestation of this alteration in time scales. Thus, ordinary quantum statistical mechanical description must accommodate these low energy processes in such a way the time dependence of the form, Eq. (1) follows. From the thermodynamic stability consideration, the Hamiltonian of the system must be bounded from below and from many arguments we know that pure exponential decay has to be ruled out as this would violate the thermodynamic stability requirement.<sup>19</sup> The relaxation mechanism is a coupling of the relaxing "species" with the low energy excitations of the Heat Bath in which the given system is immersed. The heat bath is assumed to be a much larger system which is itself unaffected by the presence of the relaxing system under study. When the relaxing system ultimately relaxes to equilibrium, its temperature becomes the same as that of the heat bath. The interaction between the system and the bath is such that nothing happens to the heat bath itself. Conventional relaxation theory contains only the average of the heat bath hamiltonian which is needed to specify the temperature of the system and the energy spectrum of the bath hamiltonian is continuous with no apparent discrete energy scale. It is thus clear that the bath Hamiltonian cannot be specified in detail but yet in determining the long time relaxation phenomena, small energy-level spacings of the order of  $10^{-4}$  eV or lower (corresponding to  $\frac{1}{10}$  eV) of the spectrum of the heat bath seems essential.

Thus, the use of a non-specific large system whose average spectral properties are required in a proper theory of relaxation phenomena in condensed matter systems. Ngai<sup>1</sup> invoked for this reason, the use of the Wigner random matrix hamiltonian theory for this purpose. Only recently it is pointed out<sup>26</sup> that a chaotic hamiltonian also meets the same speci-

fications. We now proceed to outline this theory in some detail.<sup>25</sup> There are three basic steps in the theory each of which incorporates the various physical facts involved in the long time relaxation phenomena. They are: (i) derivation of the relaxation function; (ii) introduction of the jump rate of transition; and (iii) calculation of the jump rate. To facilitate understanding this scheme, an elementary model is pictured. The relaxation process pertains to some actors. They flip between equivalent energy states (energy degenerate  $\equiv$  equivalent) and are thought to be immersed in a heat bath which is described by the Wigner random matrix hamiltonian. We use the Gaussian Orthogonal Random Matrix Hamiltonian (GOE) because the heat bath is considered time-reversal invariant and also that it has a definite average energy so that one may employ a canonical picture to describe it with a fixed temperature  $T$ , associated with it. In equilibrium then, the actors acquire this same temperature,  $T$ .

Step (i): Let 1 and 2 represent the two equivalent system states with  $p_1(t)$  and  $p_2(t)$  as

their occupancies at an instant,  $t$ . For simplicity we have here considered a system of two-equivalent-states. The interaction of these system states with the heat bath induces transitions between these two states. We are interested in computing the relaxation of this system which is merely the correlation of  $P(t) \equiv p_1(t) - p_2(t)$  at two different times. Thus

$$\psi(t) \equiv -\langle\langle P(t_0)P(t-t_0) \rangle\rangle, \quad (89)$$

$\langle\langle \dots \rangle\rangle$  is the quantum statistical thermal average<sup>41</sup> over the entire bath plus system Hamiltonian. Here  $t_0$  is some initial time. We are interested here in the long time ( $t \rightarrow \infty$ ) behavior of this function. Thus, for frequencies less than  $10^{10}$  Hz which is equivalent to a temperature of  $1/10^\circ\text{K}$  and below, we may make the approximation  $kT \gg \hbar\omega$  and so only the classical limit of Eq. (89) suffices. In this limit, Eq. (89) becomes<sup>41</sup>

$$\psi(t) \equiv -\beta \langle P(t_0) \dot{P}(t-t_0) \rangle_0 \quad (90)$$

where  $\langle \dots \rangle_0$  is the classical average over the equilibrium<sup>0</sup> distribution function and  $\beta = 1/kT$ .  $\dot{P}$  here is the time derivative. It is important to stress here that in the long time limit, the classical limit of (89) suffices, because then  $kT \gg \hbar\omega$ .

Step (ii): In this limit, it suffices to consider rate equations for the populations  $p_1(t)$  and  $p_2(t)$  and deduce a form for the relaxation function, (90). Define  $W(t)$  as the general time-dependent jump transition rate for going from state 1 to 2 and vice versa. Then we have the rate equations

$$\begin{aligned} \dot{p}_1(t) &= -W(t) (p_1(t) - p_2(t)) \\ \dot{p}_2(t) &= -W(t) (p_2(t) - p_1(t)) \end{aligned} \quad (91)$$

where we have taken into account the fact that the flipping occurs between the two equivalent states only and that there is no loss of species in the process i.e.,  $p_1 + p_2 = 0$ . Thus, we obtain

$$\dot{P}(t) = -2W(t)P(t) \quad (92)$$

where  $P(t) = p_1(t) - p_2(t)$  introduced in step (i). Thus we obtain

$$P(t) = P_0 \exp(-2 \int_0^t W(t') dt') \quad (93)$$

where we have chosen  $t=0$  for convenience. The relaxation function (90) then takes the form

$$\psi(t) = 2\beta P_0^2 \int_0^t W(t') \exp(-2 \int_0^{t'} W(t'') dt'') dt' \quad (94)$$

It should be noted that if  $W(t)$  is taken as a constant, independent of time, say  $W_0$ , then we obtain the classical result of Debye:<sup>0</sup>

$$\psi_{\text{Debye}}(t) \cong 2\beta P_0^2 W_0 \exp(-2W_0 t) \quad (95)$$

and the relaxation time is  $\tau = 1/2 W_0$  (compare this with §(Ad)). In obtaining the rate (or master) equation, (91), one often goes through a detailed analysis of the density matrix with Markovian assumptions concerning the process and the constant  $W_0$  is the time-independent

transition rate (TITR) given by the Golden rule of Quantum Mechanics<sup>42</sup> (see also §Bb). It should therefore be stressed that the steps (i) and (ii) above are really stemming from more fundamental considerations even though we have presented them here in a simple, physical way. The question then is to consider the evaluation of  $W(t)$  in greater detail than was done before.

Step (iii): The mechanism that gives rise to  $W(t)$  is the interaction of the equivalent states introduced in step (i) with low lying many body states with energies less than  $10^{10}$  Hz, say, in order to determine the long time decay phenomena. This calculation is very similar to the phonon side band calculation except that here we work<sup>43</sup> with the Wigner system instead of the phonons. The result is

$$W(t) = W_0 \exp(-\phi(t)) \quad (96)$$

where  $\phi(t)$  is the time response of the heat bath, taking care to remember that the energies involved here,  $\hbar\omega$ , are all much less than  $kT$ , the thermal energy, so that the associated occupation probabilities for both emission and absorption of excitations are just constants, and here a factor of  $1/2$ . Also,  $\phi(t)$  is real with no threshold effects. To derive (96), we consider a relaxing system. The system is said to be in a relaxing state after a certain induction time,  $\tau$ . Given such a  $\tau$ , we define

destruction and creation operators  $R$  and  $R^\dagger$  associated with relaxing states such that

$$R| \rangle = 0 \text{ in the relaxing state} \quad (97)$$

where  $| \rangle$  refers to a pseudo "vacuum" of the relaxing state and the heat bath with which the system is in contact. The  $R^\dagger(o)| \rangle$  is the given relaxing state at an initial reference time (this is the time the system had begun to relax!) which we denote here as the zero of our reckoning of time. We now ask how this state evolves in time. This is given by the usual time evolution

$$R^\dagger(t)| \rangle = e^{iHt} R^\dagger(o)e^{-iHt}| \rangle \quad (98)$$

where  $H$  is the Hamiltonian describing the relaxing system, the heat bath with which it is in contact, and the interaction between them. This we denote by  $H_o+V$ . We are thus led to calculate

$$\begin{aligned} b(t) &= \langle R(t) R^\dagger(o)| \rangle \\ &= \langle e^{iHt} R(o) e^{-iHt} R^\dagger(o)| \rangle \end{aligned} \quad (99)$$

Since  $R^\dagger(o)| \rangle$  represents the given relaxing state,

$$e^{-iHt} R^\dagger(o)| \rangle = R^\dagger(o) \exp(-i(H_o+V)t)| \rangle$$

where  $(H_o+V)_R$  stands for that part of the Hamiltonian associated with the relaxing state under study. Since we are here considering only one relaxing state, for simplicity,  $R(o)R^\dagger(o) = 1$ , and moreover  $\langle e^{i(H_o+V)t} \rangle = \langle e^{iH_o t} \rangle$  because  $| \rangle$  by virtue of its definition contains no interaction between the relaxing state and the heat bath. Thus

$$b(t) = \langle \exp(iH_o t) \exp(-i(H_o+V)_R t) \rangle \quad (100)$$

The relaxing state  $R$  in the above does not contain any index because we will invoke the "randomness" of the heat bath Hamiltonian to eliminate reference to any special state. With this understanding, we drop the subscript  $R$  in Eq. (100) and compute

$$U(t) = \exp(iH_o t) \exp(-i(H_o+V)t) \quad (101)$$

by using standard cluster expression techniques. The result is

$$b(t) = \exp\{\phi(t)\} \quad (102)$$

where

$$\phi(t) = \sum_{n=1}^{\infty} \phi_n(t) \quad (103a)$$

with

$$\phi_1(t) = -i \int_0^t dt_1 \langle IV(t_1)I \rangle \quad (103b)$$

$$\begin{aligned} \phi_2(t) &= -\frac{1}{2} \int_0^t dt_1 \int_0^t dt_2 \{ \langle IV(t_1)V(t_2)I \rangle \\ &\quad - \langle IV(t_1)I \rangle \langle IV(t_2)I \rangle \} \text{ etc.} \end{aligned} \quad (103c)$$

We have thus reduced the problem to consideration of the bath states only. Remembering that the bath states are treated in a canonical ensemble framework, and since  $\phi_1(t)$  involves expectation value of the interaction between the system and the bath, it may be dropped from further consideration and consider  $\phi_2(t)$  only. The other higher order terms may be dropped, partly because of the weak coupling between the bath and the system and partly because they would involve the multiple energy level distributions which may be expected to be of smaller significance compared with the first nontrivial contribution,  $\phi_2$ . Thus,

$$\begin{aligned} \phi_2(t) &= -\frac{1}{2} \sum_{i \neq j} \frac{|V_{ij}|^2}{(E_i - E_j)^2} \{ \frac{1}{2}(1 - e^{it(E_i - E_j)}) \\ &\quad + \frac{1}{2}(1 - e^{-it(E_i - E_j)}) \} \end{aligned} \quad (104)$$

The factors  $\frac{1}{2}$  in  $\{ \dots \}$  appear from equal occupancies of states  $E_i, E_j$  of the bath. The sum over  $i, j$  can be written as

$$\phi_2(t) = -\frac{1}{\epsilon} \left( \sum_{E_i - E_j = \epsilon} \frac{1}{2} |V_{ij}|^2 \left( \frac{1 - \cos t\epsilon}{\epsilon^2} \right) \right) \quad (105)$$

We now argue that  $\sum_{E_i - E_j = \epsilon} |V_{ij}|^2$  is independent

of  $\epsilon$  because  $|V_{ij}|^2$  is a random quantity, uncorrelated with  $\epsilon$  except perhaps when there are strong correlations which may occur when the energies are high such that the modes are well localized. This is the basic strength of the approach presented here because the "randomness" now has been separated out of the main problem so that a universal result is obtained without the knowledge of the random distribution of  $|V_{ij}|^2$  with  $E_i - E_j = \epsilon$ . Thus, introducing

$$\sum_{\epsilon} \left( \frac{1}{2} \sum_{i \neq j} \frac{|V_{ij}|^2}{E_i - E_j = \epsilon} \right) \rightarrow \int_0^{\epsilon_c} d\epsilon |V|^2 N(\epsilon) \quad ,$$

we obtain

$$\phi_2(t) = \int_0^{\epsilon_c} d\epsilon N(\epsilon) |V|^2 \left( \frac{1 - \cos \epsilon t}{\epsilon^2} \right) \quad (106)$$

The cutoff  $\epsilon_c$  ( $\cong 10^{10}$  Hz) is introduced here such that

$$|V|^2 N(\epsilon) = \epsilon n \quad , \quad 0 < n < 1 \quad (107)$$

is violated beyond  $\epsilon = \epsilon_c$ . Here we have invoked the Wigner result concerning the level-spacings distribution of a GOE. This final result then

leads to the universal form<sup>1</sup> of relaxation form given in Eq. (1). The spacings distribution (107) also appears for chaotic Hamiltonians which have the same features that make them prime candidates for describing a heat bath in the same way a GOE random matrix hamiltonian fits the requirement.<sup>26</sup> Thus we obtain in this model, the TDTR of Eq. (96) in the form

$$W(t) = \frac{(1-n)}{\tau_p} \left( \frac{t}{\tau_p} \right)^{-n} \quad (108)$$

with  $\tau_p$  given by Eq. (2) where  $\tau_o = 1/W_o$ . This  $W(t)$  is substituted into Eq. (94) and finally one obtains Eq. (1).

At this point, we may compare this approach with Young's approach<sup>23</sup> described in §Ad. Young's expression for  $\chi$  is the same as ours except that  $\phi(t)$  in Eq. (56) was calculated using the linked cluster expansion for it using only the nominal coupling of the system to the nominal bath. In our picture, the nominal coupling leads to the basic relaxation time  $\tau_o (=W_o^{-1})$  and not to  $\tau_p$ . The relaxing species then interacts with the finer spectral characteristics of the heat bath which modifies  $W_o$  to  $W(t)$  for which one ought to consider Eq. (57). At this point, the level structure occupancies involve equally likely occupancy because of high temperature regime applicable to this system and hence in the linked cluster expansion, (103), the appropriate occupation factors are introduced. Thus the modification of  $W_o$ , the nominal time independent transition rate<sup>o</sup> to a time dependent transition rate  $W(t)$  due to coupling with the low frequency excitations of the system as the relaxation proceeds to longer and longer times is the central point of issue which is missed in a calculation such as that of Young's.<sup>23</sup> We are thus pointing out an essential difference in the use of the Kubo formula at low frequencies. In the next section, we shall give another derivation of  $W(t)$  which traces the three steps given above in a more basic framework of the density matrix theory of long time relaxation phenomena. This derivation makes explicit the appearance of the transition rates in the theory in a logical fashion whereas in the description given here, as was originally done in Ref. 1, these steps may appear to have been taken in a phenomenological fashion. Thus, a firm foundation is laid to this framework in the next section.

#### (Bb) Evolution of Entropy Theory for the Correlated States of the Heat Bath

The development to be given here is a generalization of the density matrix method to derive the long time decay equations with appropriate TDTR. We will give here a more complete account of the theory than was given

earlier by us.<sup>27</sup> The model of relaxation constructed in §Ba is consistent with the occurrence of low energy excitations of glasses and polymers revealed by experiment almost over a decade ago by Zeller and Pohl.<sup>44</sup> These low energy excitations are now known as two-level systems (TLS).<sup>45,46</sup> The exact identity of these TLS are not known but they seem to be invariably present in glasses, polymers, amorphous metals, and even spin glasses. These TLS seem to appear only in a limited energy range ( $E = \omega, \hbar = 1$ )  $10^9 < \omega < 10^{11}$  radians/sec by specific heat, thermal conductivity, and ultrasonic experiments. In the proposed model, it is considered that these are indeed part of an expanded low energy excitation scheme. The origin of this scheme according to the model, is in the distribution of eigenvalues of the very complex hamiltonians that describe glasses and polymers. Because the eigenvalues have an apparently statistical character, they were considered to be derived from a random matrix hamiltonian,<sup>1</sup> in particular, by a Gaussian Orthogonal Ensemble (GOE). The distribution of energy level spacings for this is linear from zero energy difference up to an upper cut-off energy  $E = \omega_c$ , level off to a plateau at intermediate energies, and vanish exponentially at high energies. The plateau region, which has approximately constant density, was identified in the model with the TLS that are responsible for the low temperature properties of glasses and polymers cited above. The relaxation of a given primary species (PS) was treated by a generalization of the usual models of relaxation that only involve a direct interaction of a PS with a heat bath (HB) by incorporating the coupling of the PS with the level spacing excitations whose spectrum is determined by that of the GOE. Coupling of the primary species to the level structure generates the LS excitations and modifies the interaction of the primary species with the heat bath. The dynamics of the displaced PS as controlled by the direct interaction with the HB is described in terms of a master equation, to be defined here. For a PS that itself consists of two levels, the master equation reduces to a simple rate equation with a constant transition rate,  $W_o$ . We emphasize that when the PS is itself a 2-state system, its 2-states' character is not related to, and is therefore distinct from the two-level description used to model the LS excitations. A more general multilevel scheme involves carrying many more indices etc., which do not alter the final conclusions in any significant way. The algebra involved in the two-level scheme described herein is simple enough to follow and the complications of multilevel schemes do not seem necessary at this stage.

After the PS is itself driven away from equilibrium by an external agent, its interaction with the LS drives the latter away from equilibrium. Since the energies involved in

the pertinent LS excitations are very small (corresponding to temperature less than  $\frac{1}{2}$  °K), in equilibrium the LS excitations are typically in the high temperature limit so that all the states are equally populated. The interaction of the displaced PS decreases the entropy of the LS excitations. Thus, in condensed matter that is endowed with a significant density in LS excitations and non-negligible coupling strength between the LS excitation and the relaxing PS, the relaxation rate is modified by operating in an environment with decreased entropy caused by the PS-LS interaction. At a fixed temperature, T, the decreased entropy in the environment i.e., of the LS excitations, is the only time-dependent contribution to the free energy controlling the behavior of the relaxation rate. In analogy with the reaction rate theory (Glasstone et al.<sup>47</sup> and Laidler<sup>48</sup>) we may write

$$W(t) = W_0 \exp[-\Delta S_{LS}(t)/k] \quad (109)$$

where  $\Delta S_{LS}(t)$  is the magnitude of the time-dependent decrease in the entropy of the LS excitations. From this viewpoint, the randomness of the environment as represented by the LS excitations leads to a time-dependent relaxation rate.

It is evident that the introduction of this environmental modification always serves to delay the relaxation process since the LS excitations have maximum entropy at equilibrium and can only lose entropy by its interaction with an already displaced PS. The overall entropy increases since it is dominated by the increase in the entropy of the PS as it relaxes to equilibrium. This increase in entropy is only slowed by the presence of the environment that can have its entropy decreased by its interaction with a displaced PS. The key ingredient in the second part of the present procedure is therefore the calculation of the entropy evolution of the LS excitations.

We first develop the theory of the dominant relaxation process for the perturbed primary species (PS) that is caused by the direct interaction of the PS with a heat bath (HB) in the absence of level spacing (LS). In general a relaxation process for some measurable quantity may be considered to be the trace average of an operator over a density matrix that is relaxing to equilibrium.<sup>42</sup> Thus this latter motion may be considered as a surrogate for the relaxation of the quantity of interest. The relaxation of the density matrix with only the direct PS-HB interaction taken into account is very often described by means of a master equation. This equation is a result of many approximations in which a von Neumann equation which is microscopically reversible is turned into an irreversible equation with only diagonal components (Blum,<sup>42</sup> Fano,<sup>49</sup> and Fain<sup>50</sup>). To provide a context for, and contrast with the

treatment of the effect of the LS described in the next few paragraphs, we find it helpful here to specify a typical set of approximations and to adduce the master equation.

The PS interacting with the HB is described by means of a duplex system density matrix  $\rho(t)$  whose dynamics is controlled by the duplex hamiltonian  $H = H_p + H_B + V$ . Here  $H_p$  and  $H_B$  are the hamiltonians for the uncoupled systems PS and HB respectively, and  $V$  represents their interaction. It is assumed that the HB has such a large thermal inertia that it retains its thermal equilibrium distribution at constant temperature at all times despite the interaction  $V$ . The duplex density matrix is then of the form

$$\rho(t) = \rho_p(t)\rho_B(0) \quad (110)$$

where

$$\rho_B(0) = \exp(-\beta H_B)/Z_B, \quad \beta = 1/kT. \quad (111)$$

While of course  $\rho_B(0)$  is an ensemble density matrix, we consider  $\rho_p(t)$  to be the density matrix of a member of an ensemble. This will be important later.

The equation for  $\rho_p(t)$  may be written in the interaction representation:<sup>42</sup>

$$\dot{\rho}_{pI}(t) = -i \text{tr}_B [V_I(t), \rho_p(0)\rho_B(0)] - \int_0^t dt' \text{tr}_B [V_I(t), [V_I(t'), \rho_{pI}(t')\rho_B(0)]] \quad (112)$$

Here  $\text{tr}_B$  represents the trace over the states of HB, and an operator  $O(t)$  in the interaction representation is

$$O_I(t) = \exp[i(H_p + H_B)t] O(t) \exp[-i(H_p + H_B)t] \quad (113)$$

so that  $O_I(t=0) = O(t=0)$ . We make the additional assumption that  $V_I(t)$  is non-diagonal in states belonging to  $H_B$ . This means that the first term on the right hand side of Eq. (112) vanishes. Another assumption to be made is the so-called Markoff assumption<sup>42</sup> which allows the replacement of  $\rho_{pI}(t')$  by  $\rho_{pI}(t)$  in the time integral in Eq. (112).

We now make explicit the phase factors that are associated with each matrix element of  $\rho_{pI}(t)$  because this part of the density matrix represents only a member of an ensemble. Thus we expect closure with states belonging to  $H_p$  to introduce member-dependent phases. In addition we expect distinct member dependent phase factors to arise in the matrix element projections of  $V$  for states,  $|s\rangle$ , belonging to  $H_p$ . On the other hand, we do not expect any phase

factors to be associated with matrix element projections of  $V$  with states,  $|b\rangle$ , belonging to  $H_B$  since  $\rho_B(0)$  already represents an ensemble. Thus, we write

$$\langle s | \dot{\rho}_{pI}(t) | s' \rangle = \exp(i(\phi_s - \phi_{s'})) \langle s | \dot{\rho}_{pZ}(t) | s' \rangle, \quad (114)$$

$$\langle s | V_I(t) | s' b \rangle = \exp(i(\phi_s - \phi_{s'})) \langle s | \bar{V}_I(t) | s' b \rangle, \quad (115)$$

where  $\phi_s, \phi_{s'}$  are respective member dependent phase factors, and the bar over an operator means that member dependent phase factors have been factored out.

Now an ensemble sum can be carried out by means of a double phase average over the two independent phase factors introduced in (114) and (115). We assume a principle of uncompensated phases; namely, for random phases, terms which have uncompensated phases vanish in the ensemble average. Then the resulting ensemble average of Eq. (112) (with  $V$  taken as non-diagonal in  $H_B$  states and for the Markoff assumption) yields, after several algebraic steps, the usual master equation:

$$\begin{aligned} \dot{\langle s | \dot{\rho}_{pI}(t) | s \rangle} &= \sum_{s_1} \{ \langle s_1 | \dot{\rho}_{pI}(t) | s_1 \rangle \\ W_{ss_1}(t) - \langle s | \dot{\rho}_{pI}(t) | s \rangle W_{s_1s}(t) \}. \end{aligned} \quad (116)$$

Here

$$W_{ss_1}(t) \equiv 2 \sum_{bb_1} \langle s | \bar{V} | s_1 b_1 \rangle^2 \frac{e^{-\beta E_{b_1}} \sin(E_s - E_{s_1} + E_b - E_{b_1})t}{Z_B (E_s - E_{s_1} + E_b - E_{b_1})} \quad (117)$$

is the usual rate of transition, which in the long time limit,  $(E_s - E_{s_1} + E_b - E_{b_1})t \gg 1$ , becomes

independent of time. The  $E_s, E_b$  are the respective energy eigenvalues of  $H_p$  and  $H_B$ . It should be pointed out that this rate of transition obeys the usual detailed balance condition and hence we have a H-theorem guaranteeing the approach to equilibrium. This scheme gives the usual exponential decay with the relaxation time related to the inverse of the time independent transition rate arising from (117) in the long time limit.

We now turn to the interaction of the perturbed primary species (PS) with the level spacing (LS) which serves to slow down the above relaxation process. Our basic interest is in the measured relaxation of PS. If the PS

did not interact with LS, the description of the relaxation given in the preceding paragraph, Eqs. (116,117) would suffice. We now quantify the nature of the time dependence in transition rates arising out of the PS-LS interaction. We assume that this time dependence arises from the entropy of the LS which provides a time dependent contribution of the free energy that modifies the transition rates in analogy to reaction rate theory, Eq. (109). We consider the PS-LS interaction that generates LS excitations to be expressible as a random external potential for the LS decoupled from the PS. The coupling loop is closed by means of the modification of the PS transition rates through the entropy of the LS excitations as just described. In the non-equilibrium situation, the LS is driven away from equilibrium by its interaction with the perturbed PS. We maintain focus on the relaxation of the PS so our interest is in a time regime during which the PS is relaxing, but during which the LS is driven away from equilibrium. Thus, we are assuming that the PS-LS interaction dominates the interaction of the LS with the heat bath which serves to equilibrate the LS after the PS has completed its relaxation.

The excitation arising from the PS-LS interaction are assumed to be describable in terms of a stochastic two-level system. (This two-level structure is for mathematical convenience only!) The stochasticity reflects the random nature of level structure arising from the complexity of the underlying system. The PS-LS interaction results in an assembly of such excitations. In carrying out our calculation of the entropy of the excitations, we start by considering the dynamics of a member density matrix of a two-level system. We then consider the ensemble average over the members, and afterwards the assembly of the ensemble-averaged two-level systems. We then calculate the entropy of the assembly. In the following, we shall deal with quantities that are member-dependent for members of an ensemble as well as assembly-dependent for ensemble constituents of the assembly.

We start then with a two-by-two Hamiltonian for an assembly of two-level systems which have level spacings corresponding to that of a random matrix Hamiltonian discussed earlier. Thus, the spectrum of the LS excitations will be expressed in terms of the energy difference of the two levels which correspond to the level spacing variable entering into the Gaussian Orthogonal Ensemble (GOE):

$$H_{a\lambda}^m = \begin{pmatrix} H_{11a} & \lambda H_{12a}^m \\ \lambda H_{21a}^m & H_{22a} \end{pmatrix}. \quad (118)$$

Here  $m$  stands for member of the ensemble and  $a$  for the assembly. The diagonal part is assembly-dependent only. The off-diagonal element  $\lambda H_{12a}^m$  in a random external potential that

provides the phenomenological driving force on the LS caused by the perturbed PS. Here  $\lambda$  is a dimensionless strength parameter whose value varies from 0 to 1, and is introduced here so that as one reaches the full strength of the LS-PS interaction for which  $\lambda = 1$ , the effects of the interactions are properly taken account of in an appropriate adiabatic perturbation theory which does not violate any of the requirements of the underlying GOE. In this manner, all  $\lambda H_{12a}^m$  will be small so that the LS still retain their relationship to a GOE random matrix for all pertinent level spacings. Further  $\lambda H_{12a}^m$  will be consistently small in the sense that they are not directly included in the PS Hamiltonian but only affect the transition rates of the PS by controlling the entropy in the surrounding environment. The use of the  $\lambda$ -trick here is reminiscent of the Pauli trick elsewhere in dealing with cumulative perturbations which at each stage is "small" but upon appropriate adiabatic superposition leads to nontrivial answers for the effect one is looking for at full strength of the perturbation. The member density matrix of this subcomplex depends on  $\lambda$ , which can be calculated exactly in terms of the initial states whose elements have phases in them. Also note that we may write

$$\lambda H_{12a}^m = \lambda H_{21a}^{m*} = \lambda |H_{12a}| \exp i \phi_{12a}^m \quad (119)$$

where  $\phi_{12a}^m$  is both a member and assembly dependent phase. The corresponding density matrix associated with (118) is

$$\sigma_{-a\lambda}^m(t) \equiv \begin{pmatrix} \sigma_{11a\lambda}^m(t) & \sigma_{12a\lambda}^m(t) \\ \sigma_{21a\lambda}^m(t) & \sigma_{22a\lambda}^m(t) \end{pmatrix} \quad (120)$$

with

$$\text{tr} \sigma_{-a\lambda}^m(t) = 1 = \sigma_{11a\lambda}^m(t) + \sigma_{22a\lambda}^m(t) \quad (120a)$$

This is obtained by solving the member states in the usual way:

$$i \frac{\partial}{\partial t} \begin{pmatrix} c_{1a\lambda}^m(t) \\ c_{2a\lambda}^m(t) \end{pmatrix} = \begin{pmatrix} H_{11a} & \lambda H_{12a}^m \\ \lambda H_{21a}^m & H_{22a} \end{pmatrix} \begin{pmatrix} c_{1a\lambda}^m(t) \\ c_{2a\lambda}^m(t) \end{pmatrix} \quad (121)$$

The initial states are given by

$$\begin{pmatrix} c_{1a\lambda}^m(0) \\ c_{2a\lambda}^m(0) \end{pmatrix} = \begin{pmatrix} c_{1a\lambda}(0) \exp i \phi_{1\lambda}^m \\ c_{2a\lambda}(0) \exp i \phi_{2\lambda}^m \end{pmatrix} \quad (122)$$

Since  $\phi_{i\lambda}^m$ 's ( $i=1,2$ ) are initial state phases, for convenience we have taken them to be only member dependent but may in general depend on  $\lambda$ . The associated density matrix  $\sigma_{-a\lambda}^m(t)$  given in (120) is expressed as

$$\sigma_{-a\lambda}^m(t) = \begin{pmatrix} |c_{1a\lambda}^m(t)|^2 & c_{1a\lambda}^{m*}(t) c_{2a\lambda}^m(t) \\ c_{1a\lambda}^m(t) c_{2a\lambda}^{m*}(t) & |c_{2a\lambda}^m(t)|^2 \end{pmatrix} \quad (123)$$

It is enough to provide only the expressions for  $\sigma_{11a\lambda}^m(t)$  and  $\sigma_{12a\lambda}^m(t)$  because  $\sigma_{22a\lambda}^m(t) = 1 - \sigma_{11a\lambda}^m(t)$  and  $\sigma_{21a\lambda}^m(t) = \sigma_{12a\lambda}^{m*}(t)$ .

$$\begin{aligned} & \Omega_{12a\lambda}^2 \sigma_{11a\lambda}^m(t) \\ &= P_{a\lambda} \sigma_{11a\lambda}^m(0) P_{a\lambda}^* + P_{a\lambda} \sigma_{12a\lambda}^m(0) Q_{a\lambda}^{m*} \\ & - P_{a\lambda}^* \sigma_{21a\lambda}^m(0) Q_{a\lambda}^m - Q_{a\lambda}^m \sigma_{22a\lambda}^m(0) Q_{a\lambda}^{m*}, \quad (124) \end{aligned}$$

$$\begin{aligned} \Omega_{12a\lambda}^2 \sigma_{12a\lambda}^m(t) &= P_{a\lambda} \sigma_{11a\lambda}^m(0) Q_{a\lambda}^m \\ & + P_{a\lambda} \sigma_{12a\lambda}^m(0) P_{a\lambda} - Q_{a\lambda}^m \sigma_{21a\lambda}^m(0) Q_{a\lambda}^m \\ & - Q_{a\lambda}^m \sigma_{22a\lambda}^m(0) P_{a\lambda} \quad (125) \end{aligned}$$

Here

$$\Omega_{12a\lambda}^2 = \Delta_{12a}^2 + 4\lambda^2 |H_{12a}|^2 \quad (126a)$$

$$\Delta_{12a} = H_{11a} - H_{22a} \quad (126b)$$

$$\begin{aligned} P_{a\lambda} &= \Omega_{12a\lambda} \cos(\Omega_{12a\lambda} t/2) \\ & - i \Delta_{12a} \sin(\Omega_{12a\lambda} t/2) \quad (126c) \end{aligned}$$

$$Q_{a\lambda} = -2i\lambda H_{12a}^m \sin(\Omega_{12a\lambda} t/2) \quad (126d)$$

We now want to obtain the ensemble average of  $\sigma_{-a\lambda}^m(t)$ . As before, we accomplish this by means of a phase average over members of the ensemble. We expect this random phase average to eliminate  $\sigma_{12a\lambda}^m$  (and  $\sigma_{21a\lambda}^m$ ) but also leave an assembly-dependent residue in  $\sigma_{11a\lambda}^m$  and  $\sigma_{22a\lambda}^m$  that may be attributed to the correlation among the ensembles of the assembly. We accomplish both purposes by assuming that the phase  $\phi_{12a\lambda}^m$  associated with  $\lambda H_{12a}^m$  as in Eq. (119) is equal to a sum of a member-dependent part and an assembly-dependent part such that the member-dependent phase is equal and opposite to the member-dependent phase of  $\sigma_{12a\lambda}^m$ . Thus

$$\phi_{12a\lambda}^m = \phi_{1\lambda}^m - \phi_{2\lambda}^m + \phi_{12a\lambda} \quad (127)$$

This assumption appears to provide a unique decomposition of the phases,  $\phi_{a\lambda}^m$ , modulo the convenient choices of phases of  $c_{ia\lambda}^m(t=0)$ .

Thus, we obtain the ensemble averaged diagonal



density matrix by application of the principle of uncompensated phases in a phase average over the member-dependent phases.

$$\bar{\sigma}_{11a\lambda}(t) = \bar{\sigma}_{11a}(0) - A_{a\lambda}(t) \quad (128)$$

and

$$\bar{\sigma}_{22a\lambda}(t) = \bar{\sigma}_{22a}(0) + A_{a\lambda}(t) \quad (129)$$

where

$$A_{a\lambda}(t) = 4\lambda^2 \frac{|H_{12a}|^2}{\Omega_{12a\lambda}^2} (\bar{\sigma}_{11a}(0) - \bar{\sigma}_{22a}(0)) \sin^2 \left( \frac{\Omega_{12a\lambda} t}{2} \right) - 4\lambda \frac{|H_{12a}|}{\Omega_{12a\lambda}} (\bar{\sigma}_{11a}(0) \bar{\sigma}_{22a}(0))^{1/2} \sin \left( \frac{\Omega_{12a\lambda} t}{2} \right) \left[ \Omega_{12a\lambda} \sin \phi_{12a\lambda} \cos \frac{\Omega_{12a\lambda} t}{2} + \Delta_{12a} \cos \phi_{12a\lambda} \sin \frac{\Omega_{12a\lambda} t}{2} \right] \quad (130)$$

The entropy of the LS ensemble for a fixed strength  $\lambda$  of the LS-PS interaction is

$$- \frac{S_{LSa\lambda}(t)}{k} = \{ (\bar{\sigma}_{11a}(0) - A_{a\lambda}(t)) \ln(\bar{\sigma}_{11a}(0) - A_{a\lambda}(t)) + (\bar{\sigma}_{22a}(0) + A_{a\lambda}(t)) \ln(\bar{\sigma}_{22a}(0) + A_{a\lambda}(t)) \} \quad (131)$$

The LS structure is initially in thermal equilibrium with the HB and hence is in a state of maximum entropy. The maximization of  $S_{LSa}(0)/k$  gives us the usual result for  $\bar{\sigma}_{11a}(0)$  and  $\bar{\sigma}_{22a}(0)$ :

$$\bar{\sigma}_{11a}(0) = (1 + \exp \beta \Delta_{12a})^{-1}, \quad \bar{\sigma}_{22a}(0) = (1 + \exp -\beta \Delta_{12a})^{-1} \quad (132)$$

It will turn out that the LS excitations of most pertinent interest will be those in which  $\beta^{-1} = kT \gg \Delta_{12a}$ . In that case we have from (132),

$$\bar{\sigma}_{11a}(0) \cong \bar{\sigma}_{22a}(0) \cong \frac{1}{2} \quad (133)$$

We can now compute for each value of  $\lambda$ , the total time-dependent entropy associated with the LS excitations. This entropy is obtained by summing the ensemble entropy given by Eq. (131) over the assembly for each  $\lambda$  with  $\lambda < 1$ , and then finally integrating over  $\lambda$  from 0 to 1. This sum is written as follows:

$$\int_0^1 d\lambda \sum_{\{a\}} \int_0^1 d\lambda \int_0^{2\pi} \frac{d\phi_{12a\lambda}}{2\pi} \int_0^\infty d|\Delta_{12a}| N_\lambda(|\Delta_{12a}|) \int_0^\infty d|H_{12a}| P(|H_{12a}|) \quad (134)$$

In this way, at each stage of the perturbation theory in  $\lambda |H_{12a}|$ , we can maintain the GOE structure as will be evident in the following computation. The  $\phi_{12a\lambda}$  integration provides an average over the assembly phases which are not random but are instead correlated.  $N_\lambda(|\Delta_{12a}|)$  is the energy level spacings distribution of the GOE random matrix. This is  $\lambda$ -dependent because even though  $|\Delta_{12a}|$ 's do not depend on the  $\lambda |H_{12a}|$ , the GOE structure of a general 2x2 matrix would involve  $|\Omega_{12a\lambda}|$ , the energy difference of the GOE 2x2 matrix itself. Since  $\lambda < 1$ ,  $|\Omega_{12a\lambda}| \cong |\Delta_{12a}| + O(\lambda^2)$  but the actual level spacings distribution  $N_\lambda(|\Delta_{12a}|)$  which is a measure of the number of level spacings for a given  $|\Omega_{12a\lambda}|$  could depend on  $\lambda$  more significantly than  $|\Omega_{12a\lambda}|$  on  $\lambda$ . For consistency in signs for expressions in which the first power of  $\Delta_{12a}$  arises, we specify the  $\Delta_{12a} = |\Delta_{12a}|$  i.e., that the energy of the levels labelled 1 is greater than or equal to those labelled 2.  $P(|H_{12a}|)$ , which is assumed to be independent of  $|\Delta_{12a}|$  is the probability distribution of the magnitude of the phenomenological random external potential representing the PS-LS interaction effect on the LS.

In applying (134) to (131), we note that  $\lambda |H_{12a}|$  are small. Or, we may specify that

$$\lambda |H_{12a}| \ll \omega_{L\lambda} \quad (135)$$

where  $|\Omega_{12a\lambda}| \cong |\Delta_{12a}|$  for  $\Delta_{12a} \geq \omega_{L\lambda}$ , and  $\omega_{L\lambda}^{-1}$  is a time much greater than the time of interest in the relaxation process so that

$$\omega_{L\lambda} t \ll 1 \quad (136)$$

Carrying out the phase integral and retaining only lowest order terms in  $\lambda |H_{12a}|$ , which is justified in view of the smallness of  $\lambda$  at any stage of  $\lambda$ -calculation, we obtain the LS entropy

$$(S_{LS}(t) - S_{LS}(0))/k \cong - 2 \int_0^1 d\lambda \lambda^2 \int_0^\infty d|H_{12a}| P(|H_{12a}|) |H_{12a}|^2 \int_{\omega_{L\lambda}}^\infty \frac{N_\lambda(|\Delta_{12a}|) (1 - \cos |\Delta_{12a}| t)}{|\Delta_{12a}|^2} d|\Delta_{12a}|, \quad \omega_{L\lambda}^{-1} \gg t \quad (137)$$

Now recall that  $N_\lambda(|\Delta_{12a}|)$  is linear up to a cut off frequency,  $\omega_c$ , for the GOE random matrix being modeled. We write

$$N_\lambda(|\Delta_{12a}|) = C(\lambda) |\Delta_{12a}|, \quad 0 \leq |\Delta_{12a}| \leq \omega_c \quad (138)$$

where  $C(\lambda)$ , the slope of the linear law will depend on  $\lambda$  in general. It is clear that the lower limit of the  $|\Delta_{12a}|$  integral can be

extended to zero, not only because there is a vanishing contribution for  $0 < |\Delta_{12}| < \omega_{L\lambda}$  but also because the  $\lambda$ -trick allows one to make  $\omega_{L\lambda}$  as small as we please. Then using formula 3.782-1 in Gradsteyn and Ryzhik<sup>51</sup> and the fact that for  $t \gg \omega_c^{-1}$  an integral with bounded integrand and a  $\cos|\Delta_{12}|t$  factor over the  $|\Delta_{12}|$  range  $(\omega_c, \infty)$  is negligibly small, we obtain

$$(S_{LS}(t) - S_{LS}(0))/k \cong n \ln(\omega_c t) - n\gamma - S_\gamma/k, \quad t \gg \omega_c^{-1}. \quad (139)$$

Here

$$n = \int_0^1 d\lambda \lambda^2 C(\lambda) \int_0^\infty |H_{12}|^2 P(|H_{12}|) d|H_{12}|, \quad (140)$$

$\gamma$  is the Euler constant (0.577), and  $S_\gamma/k$  is a time independent term.

$$S_\gamma/k = 2 \int_0^1 d\lambda \lambda^2 \int_0^\infty |H_{12}|^2 P(|H_{12}|) d|H_{12}| \int_{\omega_c}^\infty N_\lambda(|\Delta_{12}|) \frac{d|\Delta_{12}|}{|\Delta_{12}|^2}. \quad (141)$$

The time regime of relaxation described by the present model is specified by the upper cut off frequency  $\omega_c$  only.

Thus as a consequence of the PS-LS coupling, relaxation of the PS is accompanied by a decrease in the entropy of the LS, and that decrease is a logarithmic function of time. With this negative LS entropy contribution in hand, we use Eq. (119) to obtain the modification of the transition rates  $W_{ss}$ , of Eq. (116) to

$$W_{ss}(t) = W_{ss} \exp(-S_\gamma/k) \exp(-n\gamma) (\omega_c t)^{-n}, \quad t \gg \omega_c^{-1}. \quad (142)$$

The master equation (116) when modified to incorporate the  $W_{ss}(t)$  given in Eq. (142)

leads to a description of relaxation characterized by the coupled (they have the same key parameter  $n$ ) equation (1) and (2). In the latter case, the exact agreement is only modulo a factor  $\exp(S_\gamma/k)$ .

We note now that all  $W_{ss}(t)$  are modified by the same factor. Thus the master equation (116) can be restored to its original form if we define a new order parameter  $\theta$  such that

$$d\theta = \exp(-S_\gamma/k) \exp(-n\gamma) (\omega_c t)^{-n} dt, \quad t \gg \omega_c^{-1}. \quad (143)$$

We choose the origin of  $\theta$  to coincide with the origin of  $t$  so we may write,

$$\theta(t) = \omega_c^{-1} (1-n)^{-1} \exp(-S_\gamma/k) \exp(-n\gamma) (\omega_c t)^{1-n}, \quad t \gg \omega_c^{-1}. \quad (144)$$

If  $\theta$  is a good order parameter i.e.,  $\theta$  increases monotonically with increasing  $t$ , the arguments that lead to a Boltzmann H-theorem which ensure approach to equilibrium for phenomena described using an ordinary master equation apply equally as well when a master equation with transition rates given by Eq. (142) is appropriate. We require then that  $\theta$  be a good order parameter on the physical grounds that we are dealing with relaxation phenomena. It follows immediately from Eq. (144) that  $n < 1$ . But we have already established that  $n > 0$  by its definition, Eq. (140), where all the quantities entering are positive. We find then that

$$0 \leq n < 1. \quad (145)$$

For such a general  $n$ , it is clear from the definition of  $\theta$  that the effect of the PS-LS interaction on the ordinary master equation may be viewed as just a dilation of time for the PS relaxation. The approach of the PS to equilibrium still proceeds albeit at a slower pace than that of an approach characterized by the ordinary master equation.

This derivation differs that that in §Ba in several aspects as well as that given in Ref. 27. In §Ba, the new master equation was not derived from basic considerations such as that given here. The present derivation perhaps gives a theoretical basis for step (ii) of §Ba. In step (iii) of §Ba, the TDTR was derived by analogy with phonon side band calculation. Here a more physical, entropy based argument is given for its derivation. In the process, a new derivation of the parameter  $n$  is given, Eq. (140), in contrast to a simpler form given by Eq. (107). The extra factor  $\exp(-S_\gamma/k)$  in Eq. (142) is also a new feature which Ngai has exploited in interpreting experimental data elsewhere.<sup>2</sup> In contrast to Ref. 27, a cumulative perturbation theory is given which relaxes some of the simplifying assumptions made earlier in obtaining  $n$ .<sup>27</sup>

#### 4. Some New Applications

We will now briefly discuss specific problems of current interest in condensed matter physics in the new way of handling relaxation problems.

(i) Spin Glasses: Materials such as Cu:Mn, Pd:Mn metallic systems, metglasses, the Er Sr<sup>1-x</sup>S system and others are called spin-glass systems. A basic feature of these systems is that they are all complex alloy systems with magnetic ions in them which begin to

behave "cooperatively" at some point. Specifically, the existence of a cusp in the susceptibility vs. temperature curve is a common characteristic of spin glasses. The relaxation phenomena associated with this bear some degree of resemblance to those in ordinary glasses and polymers. In a recent paper,<sup>52</sup> we have examined to what extent these analogies and similarities exist and we present here some of that discussion. Also, we try here to relate the basic entities in spin glasses with the mathematical entities needed in our formalism outlined in earlier sections.

Relaxations in glasses remarkably conform to Eq. (1). The primary relaxation responsible for the glass transition conforms to Eq. (1) near, below, and above the glass transition temperature,  $T_g$ , although  $n$  can be a function of  $T_g$ . Far above  $T_g$ , generally for nonpolymeric glass, the exponent  $n$  is zero or approximately zero and the effective relaxation time,  $\tau_p$ , shifts with temperature  $T$  in an Arrhenius way:

$$\tau_p = \tau_\infty \exp(E_A/kT)$$

Here  $\tau_\infty$  and  $E_A$  are, respectively, the inverse of the attempt frequency and the activation energy for an activated process. As  $T \rightarrow T_g$ ,  $n$  increases and the "spectrum" broadens. By "spectrum" we mean that if we formally interpret a "spectrum of relaxation times/frequencies" through the identity

$$\int g(\tau) \exp(-t/\tau) d(\log \tau) \equiv \exp[-(t/\tau_p)^{1-n}] \quad (146)$$

larger  $n$  corresponds to a broader "spectrum." At the same time,  $\tau_p$  as well as the mean

$$\langle \tau \rangle \equiv \int \tau g(\tau) d(\log \tau) = \tau_p / (1-n) \Gamma(1/(1-n)) \quad (147)$$

depart from the Arrhenius behavior, increasing more rapidly for a glass. Such relaxation properties near  $T_g$  will be called type A behavior. They are generally observed for many glasses and polymers though not always. For example,  $\text{SiO}_2$  and  $\text{GeO}_2$  glasses have constant  $n$  and for which  $\tau_p$  shifts in an Arrhenius manner throughout the temperature range near  $T_g$  studied. These can be classified as Type B glasses. There is a third class which we call Type C, e.g., alcohols, which exhibit non-Arrhenius behavior near  $T_g$  with no significant  $T$  dependence of  $n$ . In Ref. 2, extensive data displaying these are given. In all these glasses, the second universality relation, Eq. (2), is obeyed. For type A glasses, at high  $T$ , we have  $n \rightarrow 0$  and from Eq. (2), we find  $\tau_p \rightarrow \tau_0$ . Hence  $\tau_0$  can be identified with  $\tau_\infty \exp(E_A/kT)$ , at all  $T$ .  $n$  increases as  $T$

approaches  $T_g$  above, then from Eq. (2) it follows that  $\tau_p$  becomes non-Arrhenius even though  $\tau_0$  is. For a smooth monotonic increase of  $n$ ,  $\tau_p$  will have qualitative features of the empirical WLF behavior,<sup>53</sup> and the viscosity  $\eta \equiv G_\infty \langle \tau \rangle$  may well be described by the empirical Vogel-Tamann-Fulcher (VTF) equation.<sup>53</sup> Very near  $T_g$ ,  $\eta$  deviates from VTF equation and reverts back to a steep Arrhenius behavior. In this regime, the relaxation time is often so long that data on the exponent  $n$  for the relaxation process responsible for viscous flow are not available. Below  $T_g$ ,  $n$  depends on thermal history.

The relaxation properties of glasses near  $T_g$  can be quite adequately parameterized by variations of  $n$  with  $T$  determined from experiments in the simple manner described above. This success motivated us to simulate the relaxation properties of spin glasses near spin freezing temperature,  $T_f$ , by the variations of  $n$  with  $T$  determined from experiment. From such analyses, we find Cu:Mn 5% and  $\text{Eu Sr}_{1-x}\text{S}$  spin glasses of Type A, holmium borate spin glass is of Type B, and we have not come across any spin glass which resembles Type C. Similar analysis of the data on spin glasses in the presence of a magnetic field  $H$  by simulating  $n$  as a function of  $H$  and  $T$ , shows that relaxation behavior of the spin glass  $\text{Fe}_{10}\text{Ni}_{70}\text{P}_{20}$  has also been made.<sup>54</sup>

It should be mentioned that Chamberlin et al.<sup>55</sup> have recently published data and their own analysis of time-decay of remanent magnetization in spin glasses using Eqs. (1) and (2) but making an unnecessary assumption  $\omega_c = 1/\tau \propto \omega$ , and concluded that the Ngai scheme<sup>5</sup> is not directly applicable to spin glasses. We have<sup>56</sup> shown that no relation between  $\omega_c$  and  $\tau_0$  exists nor has been suggested by the model and they are independent physical quantities. We have moreover shown<sup>56</sup> that no difficulty arises in interpreting their data if only the model is properly used and the controversy mentioned by Chamberlin et al.<sup>55,56</sup> does not exist.

From this discussion, several things emerge. First of all, the phenomenon is due to spins which are randomly oriented in a host medium and their relaxation properties are exhibited by measuring magnetization and spin susceptibility as a function of frequency at various temperatures. Quite often, in the literature, spin glass phenomenon is modelled by means of spin Hamiltonians such as Ising or Heisenberg form or even Ruderman-Kittel-Korringa-Yosida interaction with random exchange constants. These models have not been successfully developed to address the relaxation properties of these systems as yet.

We may therefore take the viewpoint that as models go, the only feature to take account of in our picture is the existence of interacting spins whose mutual interactions are random and may have long range also. The next main conclusion from our description in the paragraph above describing the phenomenon is that Eqs. (1) and (2) can be used to understand the observed data on spin glasses with the exponent  $n$  treated as a function of the temperature,  $T$ , and the external field,  $H$ . We will now try to make a case for employing our theoretical framework for justifying this last statement by drawing the correspondence between our physical process and the mathematical structure which gives Eqs. (1) and (2).

In our view, the interacting spins in the spin glass form the truly many particle relaxing system which is imbedded in the host material composed of the rest of the chemical environment that makes up the spin glass. In the "subdynamics" picture, one then examines the evolution of the spin structure in contact with the rest of the spin glass system acting as heat bath. The boundedness of the spectrum from below is then easy to accept. Since the index,  $n$ , may be interpreted as the new characteristic of the heat bath for describing the relaxation properties and the temperature as well as the external fields are equilibrium parameters of the heat bath, the index,  $n$ , can indeed reflect these parameters by being a function of these. In the original language of the random matrix picture of Ngai, one may think of this as arising from the random many-spin system, whose energy spacings distributions in a GOE scheme is linear for small energy separations. Our theory then makes it possible to arrive at Eqs. (1) and (2) with the picture of the spin glass relaxation phenomena as painted above. The mathematics suggests that using the parameters  $n$  and the  $\tau_p$  arising from general principles, one may understand these phenomena.

A basic feature of most theoretical approaches has been to recognize and incorporate in some measure the random spin interactions as well as incorporate the complicated nature of competing interactions ("frustration" or in RKKY, the alternating signs of exchange with long range). In our scheme, these appear as the spacings distribution of the level structure excitation spectra.

(ii) Electron Glass: The metal-insulator transition in systems such as Si:P is due to both the randomness and the long range Coulomb interactions.<sup>57,58</sup> The low frequency electronic relaxation properties of this system seem to resemble those of glasses and spin glasses.<sup>59</sup> Because of these features, the electron system on the localized (insulator) side near the transition is often called an "electron glass."<sup>60</sup> The analogy with the

glassy state arises from a competition between the long range Coulomb interactions and the randomness of site energies. Experimentally the slow relaxation behavior in the a.c. conductivity<sup>59</sup> bears a strong resemblance to magnetization relaxation in spin glasses and dielectric and mechanical relaxations in glasses.<sup>1,2,52</sup> In our view, if  $\hbar\omega \ll kT$ , as is the case in all low frequency measurements,<sup>59</sup> a relaxation description of the entire assembly is more appropriate, particularly in the critical region. Before leading to the mathematical scheme, let us first give a physical approach to this complex phenomena.<sup>61</sup> We first note that the random interactions and correlation among electrons give rise to an assembly of near degenerate levels. Relaxation of a single electron is necessarily followed by sequential relaxation of other electrons because of its correlation with the others.<sup>1,2</sup> An effective way of accounting for these complex multiparticle processes is to compute the evolution of entropy<sup>27</sup> of the level structure with time caused by the sequential transitions of the multiparticles. The spectrum of these excitations is determined by the level spacings distribution<sup>1,2</sup> of a Gaussian orthogonal ensemble of random matrix hamiltonian which mimics these interactions. Coupling of an electron to these level spacings generates the level spacing excitations and modifies the interaction of the electron with the nominal heat bath. This is best understood in terms of the environmental modification which serves to delay the relaxation process since the level structure excitations have maximum entropy and can lose entropy by its interaction with an already displaced electron. The overall entropy increases since it is dominated by the increase in entropy of the electron as it relaxes to equilibrium. This increase in entropy is only slowed by the presence of the environment that can have its entropy decreased by its interaction with displaced electrons. The calculation of the entropy evolution of the level structure excitations is the key to our procedure. The decrease of this entropy  $-\Delta s(t)$  is logarithmic in time  $\Delta s(t)/k_B = n \ln(\omega_c t)$ , where  $\omega_c$  is an upper cut-off frequency and  $n$  is a measure of the effective coupling to these low lying modes. In analogy with absolute reaction rate theory, the transition rate is

$$W(t) = W_0 \exp[-\Delta s(t)/k_B] = W_0 (\omega_c t)^{-n}$$

The master equation for relaxation with this transition rate leads to a description of relaxation characterized by the coupled (they have the same key parameter  $n$ ) equations, (1) and (2), where  $\tau_0 \equiv W_0^{-1}$ .

The relaxation function given by Eq. (1) when differentiated w.r.t  $t$  and then Fourier

transformed with frequency variable  $\omega$  gives us (to within a numerical factor) the frequency dependent susceptibility,<sup>1,2</sup>  $\chi(\omega) = \chi'(\omega) - i\chi''(\omega)$ . The conductance  $G(\omega)$  is proportional to  $\omega\chi''$  and the donor capacitance  $C(\omega)$  is related to  $\chi'(\omega)$ . It is interesting to note that a sample calculation with  $n=0.9$  of  $\chi'$  and  $\chi''$  and  $\sigma(\omega)$  are found to be in accord with experimental measurements obtained over three decades of frequency.<sup>59</sup> It is interesting also to note that the value of  $n \approx 0.9$  for the electron glass in the critical region at 13 mk is comparable with the  $n$  value for magnetic relaxations in spin glasses near  $T_c$ . It is between 0.7 and 0.9 for Cu:Mn<sup>62</sup> and for  $\text{Eu}_x\text{Sr}_{1-x}\text{S}$ .<sup>52</sup> The large value of  $n$  in the electron glass is a reflection of the importance of many electron correlation effects in the critical region. The results obtained so far are independent of the specific nature of the relaxation process. Although the relaxation function is predicted to have the form of Eq. (1), the value of  $n$  cannot be predicted or calculated exactly. In fact the complexity of the system is such that the actual experiment can be considered as the best analogue computer for the estimation of  $n$ . In many other relaxation phenomena, after taking  $n$  directly from experimental data, Eq. (2) permits another stringent test of the relation between the dependences of the observed  $\tau_p$  and the fundamental  $\tau_0$  on some parameters such as temperature, isotope mass, molecular weight, etc.

The cooperative relaxation model for an electron-glass leads to isoenergetic multi-particle collective relaxation with time-dependent relaxation rate, stretching the fundamental time scale  $\tau_0$  to a much longer effective time scale  $\tau_p$  as quantified by Eqs. (1) and (2). The Austin-Mott hopping conductivity has been rejected by experiment.<sup>59</sup> We do not find the ac conductivity calculated by Efros and Shklovskii<sup>63</sup> can explain the data either. Since  $\hbar\omega \ll k_B T$ , finite temperature formula (Eq. (4.1) of Ref. 63) has to be used which gives  $\sigma(\omega) \sim \omega^2$  in contrast to the experimental  $\omega^{0.9}$ . These latest developments indicate that the understanding of low frequency dielectric relaxation is still incomplete.

(iii) Polymers: In polymers one has molecules that are arranged along long chains and these chains form the constituents of the system. This conglomerate of long chain molecules exhibit very interesting properties quite similar to glassy state. The equilibrium statistical mechanics of the polymer system is best handled by the general methods developed by Khinchine and is explained in detail in a recent book by Weiner.<sup>64</sup> The problem involves

unusual geometrical constraints because of the long chain system will in general have many possible complicated conformations. One of the principle methods of handling this complicated system is to use the superposability principle with given mean square distance between the end to end distance of a polymer chain as a constraint, for example. This leads to the usual Gaussian distribution for the ensemble of such polymer chains. Several models of this sort are discussed in Weiner's book. The time-dependent properties of this system in its viscoelastic properties etc., has been shown by Ngai and co-workers (see Ref. 2 for example) to fit Eqs. (1) and (2). The complicated nature of interactions and the many-chain complex of molecules in a polymer lends itself to an analysis of the type we have been examining in other similar systems. For a detailed discussion of this topic, see the companion article by Rendell and Ngai,<sup>65</sup> in this volume.

In conclusion, the purpose of this review was to present a variety of different models of nonexponential decay in condensed matter physics. The basic requirement for any successful model is that it must satisfy the two empirically verified "universal" relationships that are found in the slow relaxation process. Most of the models are of type A, giving only the nonexponential decay so that they do not yield the second universal relation. Hence in our opinion they do not constitute a complete theory of the phenomena. It has been noted that Ngai's model, by incorporating general features of the systems in a random matrix hamiltonian scheme is of type B. It provides the observed non-Debye relaxation and leads to the second universality as a prediction. In the future there may be other models invoking some other general features that may lead to the empirical relationships as well. Also there may be newer aspects of slow relaxation not yet fully explored or even known at present which may call for different requirements for a successful model besides the two universalities which we used here. It is clear that the subject of slow relaxation in condensed matter is a new challenge to theoretical physicists. It is hoped that the present review gives the reader a flavor of this exciting area of research. A glance at the variety of mathematical tools used in the models discussed in this work clearly displays the challenging difficulties in arriving at a satisfactory model of the phenomena.

## Acknowledgements

AKR was supported in part by ONR contract number N00014-K-0477 and KLN in part by ONR under task NR 600-021. We both thank Drs. S. Teitler and R.W. Rendell for their continuous valuable discussions and collaborations on the subject.

## Notes Added on October 1, 1984

Since completing the work, four papers have appeared,<sup>66-69</sup> which are relevant to the present discussion. We give here an account of these along with our commentary on each in the spirit of this article. We may point out at the outset that all these works focus attention on deriving Eq. (1) and pay no attention to Eq. (2).

1. Palmer et al.<sup>66</sup> suggest a class of models, called "hierarchically constrained models" for relaxation in strongly interacting glassy materials. In the process of developing their model, these authors stress that theories based on "distribution of relaxation time" and variations thereof, are describing the relaxation function, Eq. (1), based on a picture of "parallel relaxation" which is not universal and microscopically arbitrary, in conformity with our view of such models as well, expressed in Sec. 2 of this review. They go on to suggest that any theory which tries to arrive at the universal law, Eq. (1), must be based on (a) dynamics, not just statistics, (b) with constraints, and, (c) involve a hierarchy of degrees of freedom so that a "series" interpretation is more appropriate. These authors then go on to discuss a variety of scenarios, some of which do give Eq. (1), but they do not yet have a clear physical model of relaxation. We should draw attention of the reader to the model described by us in Sec. 3 where it is clear from the development given there that the Ngai theory is a "series" model and that the

constrained dynamics is exhibited by the scheme of the special PS-LS phase averaging. (Palmer et al.<sup>66</sup> state that the Ngai model is not a hierarchically constrained model but as described in Sec. 3, it is clear it is.) More importantly, the second universality is a consequence of this "series scheme" which is not addressed by Palmer et al.<sup>66</sup> It is important to point out that this work for the first time sets down conditions that any model is likely to obtain the universal relaxation of the form given by Eq. (1). To this, we must add that Eq. (2) must also be obtained in such a scheme.

2. Brawer<sup>67</sup> presents a theory of relaxation of nonpolymeric viscous liquids and glasses. It is clearly a "distribution of relaxation times" type theory as his final answer is obtained in that form. It is therefore a "parallel relaxation" scheme in the sense of Palmer et al.<sup>66</sup> and does not possess any aspect of sequential processes. He describes the fluid by a set of quasi-equilibrium structures and sets up a master equation that gives transitions among these structures. In his subsequent manipulation of the master equation, he makes assumptions that lead to a "parallel relaxation" scheme in which each of the quasi-equilibrium structures relaxes independently with characteristic decay time of its own. To make a "series" scheme, he would require a more sophisticated scheme than what he has given in this paper. Brawer<sup>67</sup> also compares his theory with other existing theories and comes to the conclusion that his theory is similar to the free-volume model of Cohen and Grest,<sup>5</sup> which as we have pointed out in Sec. 2 is also a "parallel relaxation" model. In describing the Ngai theory in comparison with his own, he unfortunately does not fully comprehend the Ngai theory and goes on to present his own version of it. In so doing, he finds his version of the Ngai model gives only exponential decay! It is clear from his own work, that an attempt to understand a "series theory" such as Ngai's in terms of a "parallel model" is doomed to failure and his allegations of "improper averaging out the heat bath," etc. in his version of the Ngai model are inappropriate. A detailed rebuttal of Brawer's version of the Ngai scheme is given elsewhere.<sup>70</sup>

3. In an interesting paper, Shlesinger and Montroll<sup>68</sup> have proposed a derivation of Eq. (1) based on a model of diffusion of defects with a waiting time distribution function with long tail

$$\psi(t) \sim t^{-1-\alpha} \quad (148)$$

The model considers a frozen dipole at the origin of a periodic lattice and defects lie initially (at  $t=0$ ) with equal probability at any lattice point. Diffusion of the defects on

the periodic lattice are described by the continuous time random walk formation described in Sec. 2 with a waiting time distribution function given by Eq. (148). The relaxation of the dipole at the origin is supposed to take place whenever a defect reaches it. The defects are treated as independent and each has the same waiting time distribution function, (148), and may arrive at the origin independently. The problem thus reduces to a calculation of the statistics of first time arrival of the defects at the origin from all the lattice sites. It is clear from this Shlesinger-Montroll picture of the relaxation that it is also a "parallel model" with just a statistical basis. In terms of the Palmer et al.<sup>66</sup> description, this model cannot give the result, Eq. (1). But the Shlesinger-Montroll model does give Eq. (1)! It therefore appears that we have here a counter-example to the criterion setup by Palmer et al.<sup>66</sup> Upon more careful analysis of this model, it is found that it is hard to understand the origin of the long time tail in Eq. (148). First of all, it is essential for  $\psi(t)$  to be normalizable in  $t(0, \infty)$  and so (148) is really valid for  $t$  greater than some long time cutoff,  $t_e$ . The question then arises as to the nature of  $\psi(t)$  for  $0 < t < t_e$ . Shlesinger and Montroll note that the same long tail arises from a stable Lévy distribution that is defined for  $(0, \infty)$  and normalizable. If we take this Lévy distribution seriously in place of just the long tail in (148) one finds that Eq. (1) obtains truthfully for  $t > t_e$  whereas Eq. (1) is really found to hold for  $0 < t < \infty$ . The use of Lévy distribution for  $\psi(t)$  raises a question as to the microscopic origin of the independent random variables that should be superposed in order to lead to the Lévy stable distribution.<sup>30</sup> By examining the Lévy distribution for some special cases, it is found that the tail region really occurs for times when a significant fraction of the dipoles would have already relaxed!

4. In another paper, Montroll and Bendler<sup>69</sup> observe that the form Eq. (1) is mathematically the same as the Laplace transform of a one-sided stable Lévy distribution of the "relaxation times." This leads to the conclusion, using Feller,<sup>30</sup> that the relaxation times ought to be independent random variables of a special type such that

$$\lim_{N \rightarrow \infty} \frac{\tau_1^{-1} + \dots + \tau_N^{-1}}{N^{1/\alpha}} \rightarrow \tau^{-1} \quad (149)$$

Note that the limit of the sum of  $N$   $\tau_i$ 's for large  $N$  has to be defined in a definite way, unlike the usual mean value of  $\tau$ 's, because the one-sided Lévy distribution has no moments!

The normalization  $N^{-1/\alpha}$  needs to be explained on plausible physical terms in order to provide

an insight to the universality of Eq. (1). These authors themselves realized the lack of physical content of this observation (see p. 151 of their paper<sup>69</sup>). From this description, it is clear that the use of Lévy distribution in this way is indeed a "parallel mechanism" with as yet unknown physical meaning. In closing, the parallel mechanisms that lead to Eq. (1) seem to have physically hard to understand basic processes underlying them which are difficult to test experimentally. It should again be pointed out that none of these schemes have obtained the Second Universality, Eq. (2).

#### References

1. K.L. Ngai, *Comments Solid State Physics* **9**, 127 (1979), and **9**, 141 (1980).
2. K.L. Ngai in *Non-Debye Relaxation in Condensed Matter*, ed. T.V. Ramakrishnan (World Scientific, Singapore, 1985). To appear.
3. C.K. Majumdar, *Solid State Comm.* **9**, 1087 (1971).
4. C.K. Majumdar, in *Non-Debye Relaxation in Condensed Matter*, ed. T.V. Ramakrishnan (World Scientific, Singapore, 1985). To appear.
5. M.H. Cohen and G.S. Grest, *Phys. Rev.* **B24**, 4091 (1981).
6. D. Dhar and M. Barma, *J. Stat. Phys.* **22**, 259 (1980).
7. D. Dhar, in *Non-Debye Relaxation in Condensed Matter*, ed. T.V. Ramakrishnan (World Scientific, Singapore, 1985). To appear.
8. J.L. Skinner, *J. Chem. Phys.* **79**, 1955 (1985).
9. W.L. McMillan, *Phys. Rev.* **B28**, 5216 (1983).
10. B.B. Mandelbrot and J.W. van Ness, *SIAM Review* **10**, 422 (1968).
11. A.K. Rajagopal and R.W. Rendell Unpublished Notes (1982).
12. J.K.E. Tunaley, *J. Appl. Phys.* **43**, 3851 (1972) and *ibid.* **43**, 4777 (1972).
13. B. D. Hughes, M. F. Shlesinger, and E.W. Montroll, *Proc. Natl. Acad. Sci. (USA)* **78**, 3287 (1981).
14. E. W. Montroll and M. F. Shlesinger, *J. Stat. Phys.* **32**, 209 (1983).
15. E.W. Montroll and G.H. Weiss, *J. Math. Phys.* **6**, 167 (1965).
16. V.M. Kenkre, E.W. Montroll, and M. Shlesinger, *J. Stat. Phys.* **9**, 45 (1973).
17. Review article by G. H. Weiss and R. J. Rubin, in *Adv. in Chem. Phys.* **52**, 363 (1983), ed. I. Prigogine and S.A. Rice.
18. K.L. Ngai and F.H. Liu, *Phys. Rev.* **B24**, 1049 (1981).
19. A.K. Rajagopal, K.L. Ngai, R.W. Rendell, and S. Teitler, *J. Stat. Phys.* **30**, 285 (1983).
20. A.K. Rajagopal, K.L. Ngai, R.W. Rendell, and S. Teitler, Unpublished notes (1982) quoted in Ref. 19.

21. G.W. Ford, M. Kac, and P. Mazur, *J. Math. Phys.* **6**, 504 (1965).
22. R.W. Rendell, A.K. Rajagopal and K.L. Ngai, Unpublished notes (1982), quoted in Ref. 19.
23. K. Young, *Phys. Rev.* **B25**, 2899 (1982).
24. R.G. Palmer, lecture at Blacksburg Symposium (1983), this volume.
25. K.L. Ngai and A.K. Rajagopal, in *Non-Debye Relaxation in Condensed Matter*, ed. T.V. Ramakrishnan (World Scientific, Singapore, 1985), to appear.
26. A.K. Rajagopal and F.W. Wiegel, *Physica* (to appear) (1984). See also in the Blacksburg Symposium Proceedings (1984), this volume.
27. A.K. Rajagopal, S. Teitler, and K.L. Ngai, *J. Phys. C*, to appear (1984).
28. C. Maccone, *Il Nuovo Cim.* **61B**, 229 (1981) and *ibid.* **65B**, 259 (1981).
29. B.B. Mandelbrot, *Letter al Nuovo Cim.* **33**, 549 (1982).
30. W. Feller, *An Introduction to Probability Theory and its Applications*, Vol. 2 (Wiley, New York, 1966).
31. M.F. Shlesinger and E.W. Montroll, "Fractal Stochastic Processes: Clusters and Intermittencies," Preprint (1983).
32. E.W. Montroll and M.F. Shlesinger, "On the Wedding of Certain Dynamical Processes in the Disordered Complex Materials to the Theory of Stable (Lévy) Distribution Functions," Preprint (1983).
33. E.W. Montroll and M.F. Shlesinger, "A Wonderful World of Random Walks," Preprint (1983).
34. J.T. Bendler and M.F. Shlesinger, in the Proceedings of the Blacksburg Symposium held during July 1983, (1984), this volume.
35. S. Chandrasekhar, *Rev. Mod. Phys.* **15**, 1 (1943).
36. S. Teitler, A.K. Rajagopal, and K.L. Ngai, *Phys. Rev.* **A26**, 2906 (1982).
37. J.L. Doob, *Ann. Math.* **43**, 351 (1942).
38. R.F. Fox, *Phys. Rep.* **48**, 179 (1978).
39. L. Onsager and S. Machlup, *Phys. Rev.* **91**, 1505 (1953).
40. R. Zwanzig, *Annual Rev. Phys. Chem.* **16**, 67 (1955).
41. D.N. Zubarev, *Nonequilibrium Statistical Thermodynamics*, Sec. Ch. III (Consultant Bureau, NY, 1974).
42. K. Blum, *Density Matrix Theory and Applications*, Ch. 7 (Plenum, NY, 1981), p. 161.
43. G.D. Mahan in *Advances in Solid State Physics*, ed. F. Seitz, D. Turnbull, and H. Ehrenreich, **29**, 98 (1974).
44. R.C. Zeller and R.O. Pohl, *Phys. Rev.* **B4**, 2029 (1971).
45. P. W. Anderson, B. T. Halperin, and C.M. Varma, *Phil. Mag.* **25**, 1 (1972).
46. W.A. Phillips, *J. Low Temp. Phys.* **7**, 351 (1972).
47. S. Glasstone, K.J. Laidler, and H. Eyring, *The Theory of Rate Processes* (McGraw-Hill), New York, 1942).
48. K.J. Laidler, *Theory of Chemical Reaction Rates* (McGraw-Hill, New York, 1969).
49. U. Fano, *Rev. Mod. Phys.*, **29**, 74 (1957).
50. B. Fain, *Theory of Rate Processes* **20**, Lecture Notes in Chemistry (Springer-Verlag, Berlin, 1980).
51. I.S. Gradshteyn and I.M. Ryzik, *Table of Integrals, Series, and Products* (Academic Press, New York, 1980).
52. K.L. Ngai, A.K. Rajagopal, and C.Y. Hung, *J. Appl. Phys.* **55**, 1714 (1984).
53. J.D. Ferry, *Viscoelastic Properties of Polymers*, 3rd ed. (Wiley, New York, 1980).
54. M.B. Salamon and J.L. Tholance, *J. Mag. Mag. Mater.* **31-34**, 1375 (1983).
55. R.V. Chamberlin, G. Mozurkevich, and R. Orbach, *Phys. Rev. Lett.* **52**, 867 (1984).
56. K.L. Ngai and A.K. Rajagopal, *Phys. Rev. Lett.* **53**, 1024 (1984). See also R.V. Chamberlin et al., *Phys. Rev. Lett.* **53**, 1025 (1984). See also a correction to this Chamberlin et al. article in *Phys. Rev. Lett.* **53**, 1510 (1984).
57. M. Pollak, *Disc. Faraday Soc.* **50**, 13 (1970).
58. A. Efros and B. Shklovskii, *J. Phys. C* **8**, L49 (1975).
59. M.A. Paalanen, T.F. Rosenbaum, G.A. Thomas, and R.N. Bhatt, *Phys. Rev. Lett.* **51**, 1896 (1983).
60. J.H. Davis, P.A. Lee, and T.M. Rice, *Phys. Rev. Lett.* **49**, 758 (1980); also *Phys. Rev. B* **29**, 4260 (1984).
61. K.L. Ngai and A.K. Rajagopal, *Proc. Int. Conf. Physics of Semiconductors*, San Francisco, California (1984).
62. T.F. Rosenbaum, R.F. Milligan, M.A. Paalanen, G.A. Thomas, R.N. Bhatt, and W. Lin, *Phys. Rev. B* **27**, 7509 (1983).
63. B.I. Shklovskii and A.L. Efros, *Soviet Phys. JETP* **54**, 218 (1981).
64. J.H. Weiner, *Statistical Mechanics of Elasticity* (John Wiley and Sons, New York, 1983).
65. R.W. Rendell and K.L. Ngai, article in these proceedings (1984).
66. R.G. Palmer, D.L. Stein, E. Abrahams, and P.W. Anderson, *Phys. Rev. Lett.* **53**, 958 (1984).
67. S.A. Brawer, *J. Chem. Phys.* **81**, 954 (1984).
68. M.F. Shlesinger and E.W. Montroll, *Proc. Natl. Acad. Sci. U.S.A.* **81**, 1280 (1984).
69. E.W. Montroll and J.T. Bendler, *J. Stat. Phys.* **34**, 129 (1984).
70. K.L. Ngai, A.K. Rajagopal, R.W. Rendell, and S. Teitler, submitted to *J. Chem. Phys.* (1984).



# NONEXPONENTIAL DECAY IN RELAXATION PHENOMENA AND THE SPECTRAL CHARACTERISTICS OF THE HEAT BATH<sup>†</sup>

A. K. Rajagopal and F. W. Wiegel\*  
 Department of Physics and Astronomy  
 Louisiana State University  
 Baton Rouge, Louisiana 70803  
 U.S.A

## ABSTRACT

After a brief survey of the characteristics of a heat bath and its role in relaxation phenomena leading to the familiar exponential decay, it is argued that the nonexponential form found commonly in many condensed matter systems indicates that the energy spectrum of the heat bath plays a crucial part in these phenomena. In equilibrium statistical mechanics, the mean energy of a heat bath determines the temperature of a system placed in contact with it. We show that the relaxation of a system placed in contact with this heat bath is determined by the distribution of the energy level spacings for level spacings small as compared to the mean spacing. After presenting arguments in favor of a linear behavior of this distribution, we show, in a somewhat heuristic way, that the resulting relaxation function has a nonexponential form.

## I. INTRODUCTION

Experimental data on relaxation phenomena in diverse areas of condensed matter physics are quite generally found to exhibit slower than exponential decay for long times in the form (see ref. 1. and references therein)<sup>1-6</sup>

$$\exp[-(t/\tau_p)^{1-n}], \quad 0 < n < 1 \quad (1)$$

where  $\tau$  is a characteristic time in the system. <sup>p</sup> This is called the first universality relationship by Ngai. References 4,5,6 are representative set selected at random out of a large number of papers on this subject. See ref. 1 for more citations. Traditionally,<sup>2,3</sup> the residual part of relaxing quantities are discussed in terms of a pure exponential decay

$$\exp[-t/\tau] \quad (2)$$

where  $\tau$  is the "relaxation time" which is related to the time-independent transition rate given by the Golden Rule. The physical

picture of relaxation here is that the system which is relaxing and which is described by a Hamiltonian,  $H_S$ , is in contact with a heat bath which is a much larger system described by a Hamiltonian,  $H_B$ , and which is not affected by the interaction ( $H_{BS}$ ) with the relaxing system. This interaction is supposed to be "weak" and leads to relaxation. The equilibrium properties of the given system in contact with the heat bath are determined by the temperature of the bath, which in turn is just the mean energy associated with the bath.<sup>7,8</sup> An alternative scheme to derive (2) is the master equation approach (see for example Ref. 8). Here again the time-independent transition rate is employed in setting up the master equation. The physical model for relaxation is however still the same - system, heat bath, and their mutual (weak) interaction. An elementary discussion of the exponential decay in stochastic processes and in quantum mechanics may be found in Merzbacher's book,<sup>9</sup> and an extensive discussion of the role of time independent transition rates is found in Tolman.<sup>7</sup> Now, since exponential decay is not observed, and the decay law given by (1) is more a rule than an exception, it is natural to seek an explanation for this behavior by examining in more detail the origin of the time-independent transition rate. (Historically<sup>1</sup> one sought to obtain Equ. (1) by a superposition of Equ. (2) with a distribution of  $\tau$ .) This shift of emphasis from time independent transition rate (TITR) to time dependent transition rate (TDTR) in order to arrive at (1) has been emphasized recently by Teitler et.al.<sup>10</sup> from phenomenological considerations of rate equations, and from general considerations based on the Paley-Wiener theorem by Ngai et.al.<sup>11</sup> It was found that  $\tau_p$  in Equ. (1) and  $\tau$  in Equ. (2) are not independent and a definite relationship between them exists:

$$\tau_p = [(1-n) \exp(n\gamma) \omega_c^n \tau]^{1/(1-n)} \quad (3)$$

where  $\gamma \approx 0.577$  is the Euler constant and  $\omega_c$  is an upper cut off frequency to be specified presently. If  $W_0$  is the time-independent transition rate, then  $2W_0 = \tau^{-1}$  and the behaviour given by Equ. (1) is governed by a time-dependent transition rate

$$Q(t) = W_0 \exp(-n\gamma) (\omega_c t)^{-n},$$

$$0 < n < 1, \quad \omega_c t \gg 1. \quad (4)$$

The relationship (3) is called the second universality<sup>1</sup> by Ngai which is not derivable from the superposition of  $\tau$ 's by means of a distribution of relaxation times. The relations (1) and (3) are called universal because they are found to be obeyed by a very large number of systems undergoing relaxations. We may think of  $Q(t)$  as a modification of the background TTR induced by the heat bath due to interaction of the system with the finer levels of the heat bath at larger times,  $\omega_c t \gg 1$ .  $\omega_c$  then is a characteristic frequency (or energy) scale when the time-dependence sets in or equivalently, when the low-energy excitations of the "heat bath" begin to play an important role. The purpose of the present paper is to suggest that the heat bath be described by a chaotic quantum system. The reasons for this suggestion are given in Sec. II. In Sec. III, we set up the calculational scheme for computing TDR and obtain the required time-dependence in terms of the slope and cut off of the level spacings distribution at "small spacings" of this heat bath. In Sec. IV a direct summary of the results obtained is given.

## II. SPECTRAL CHARACTERISTICS OF THE HEAT BATH

We are primarily interested in the long time relaxation of any physical property of a system, for example a dielectric or a mechanical property. In general terms, the system that is undergoing relaxation is described by a Hamiltonian  $H_S$ , and it is supposed to be in contact with a much larger system described by a bath (or reservoir) hamiltonian  $H_B$ . The interaction between the two, whose hamiltonian is  $H_{BS}$ , is assumed to be weak and is supposed to induce the process of relaxation in the physical quantity of interest in the system. It is important to realize that the bath system is large compared to the system that is under investigation so that while the bath is not affected by the interaction with the system, its effect on the system is paramount. The precise nature of the heat bath is left unspecified except for stating that the system in contact with it acquires its temperature after thermal equilibrium has been established. In the conventional approach, the details of the bath hamiltonian are not important even though it is

recognized to have an almost continuous energy spectrum, by virtue of its enormous size.<sup>7</sup> Also, in the final analysis, the bath variables do not occur in the description of the system so that one averages over these variables in computing properties of the system. Since only the temperature of the bath enters the picture the only relevant entity appearing in this picture is the mean energy of the bath system, which is kept fixed, thus determining the temperature. It is clear from this description of the heat bath that a detailed knowledge of  $H_B$  is not required, except for its temperature and the obvious observation that  $H_B$  has an almost continuous spectrum bounded from below with a finite mean. One of the approaches to the theory of relaxation is to construct the density matrix associated with the system plus bath in the presence of  $H_{BS}$  and integrate out the bath variables by tracing over all the states of the bath, leaving behind a residual density matrix for the system, which can be used to compute any property,  $P(t)$ , of the system, by calculating the appropriate average of the operator representing  $P(t)$  over the residual density matrix. Feynman and Vernon<sup>12</sup> have given a formal path integral representation for this density matrix and Fano<sup>13,14</sup> has given an expression in the interaction representation. It may not be out of place here to point out that there are circumstances when the nature of the heat bath is known purely from the physical consideration of the energy or time domain one is examining. For certain electronic properties, phonons (the motion of the crystal lattice) are the relevant heat bath system and so for excitations, involving frequencies of the order of  $10^{13}$  Hz and above, the phonon excitations determine the relaxation properties upto times of order  $10^{-13}$  sec and here the relaxation rate is essentially exponential. When one waits for longer times, say  $10^{-10}$  sec, the phonon excitations provide only a background rate of transition and the relevant bath system which leads to slower than exponential rate must be something else. It must be pointed out however, that the phonon system is itself imbedded in the new bath system which we are proposing so that there is a common temperature for all the entities making up the system. Thus we may picture a hierarchy of heat baths, each imbedded in the other, so that they all have a common temperature and each contributes to the relaxation in the appropriate time regime. What we are interested in for the present work is the relatively long time domain such as  $10^{-10}$  sec and longer, where the usual known excitations must be replaced by new, low-energy excitations. In the present paper we are concerned only with this regime. It must be stressed that the theoretical formalism given by Fano<sup>13,14</sup> is applicable quite generally to all these situations. In the traditional

description<sup>7</sup> no mention of the nature of the heat bath energy spectrum is made except for it being continuous. Thus we describe the system undergoing relaxation by means of the Hamiltonian

$$H = H_S + H_B + H_{BS} \quad (5)$$

It is assumed here that the background time-independent transition rate,  $W_0$ , is also induced by  $H_{BS}$  which in the long time regime is modified by interaction with the finer level spacings of the heat bath. One may then compute the density matrix of the entire system, given that at time  $t=0$  the system and the bath are not interacting, and have been prepared such that the system is in some preassigned state and the bath is in thermal equilibrium. As a model for the heat bath we shall adopt any large quantum system whose classical motion is irregular. For such systems Berry has shown in a series of elegant papers<sup>15-19</sup> that the quantum levels are fairly regularly distributed and that the probability density  $P(S)$  for the spacings between neighboring levels has the asymptotic form

$$P(S) = \alpha \delta \quad (6)$$

$$(0 < S \ll \delta)$$

provided  $S$  is small as compared to the average spacing  $\delta$ . For larger values of  $S$  the spacings distribution  $P(S)$  goes through a maximum to decay to zero at large values of  $S$ . These details depend on the precise choice of the quantum system, but the linear behavior of the spacings distribution appears to be universal, i.e. it holds for a "generic" chaotic quantum system. It is remarkable that the same linear behavior (6) of the spacings distribution is found if the heat bath is described by means of a random matrix hamiltonian. The hamiltonian for the heat bath is very complex so that we may replace it by a statistical description. For the determination of equilibrium properties of a system in contact with the heat bath, only the average of the bath hamiltonian is needed. Hence one can try to use a "Gaussian Orthogonal Ensemble" (GOE) for the random matrix for describing the heat bath because we take the bath system as being time reversal invariant. Since only the mean value of the bath Hamiltonian is required for equilibrium properties, we use a "canonical ensemble" in setting up its density matrix. We now observe that the GOE has known average spectral properties, which we employ in our analysis of the Golden Rule in determining the TDTR induced by the bath in the system. For a description of the philosophy and the theory of random matrix hamiltonians one may refer to Porter's collection of papers and his clear introductory summary<sup>20</sup>, Mehta's book<sup>21</sup>, and a more recent review by Brody et. al.<sup>22</sup>. It is remarkable that both models for

the heat bath which we have considered in this section, (a) an irregular quantum system and (b) a random matrix hamiltonian, lead to the same linear behavior of the spacings distribution. We feel that (a) is the physically correct model for a heat bath and that the random matrix is just a convenient way to simulate an irregular quantum system. It may not be out of place here to conjecture that the random matrix hamiltonian may indeed be a very accurate model for a generic irregular quantum system if one coarse grains the energy spectrum. A hint of this equivalence may be found when one compares the average density of states for the quantum version of Sinai's billiard<sup>18</sup> with the middle part of the semi-circular law appropriate for the density of states of a random matrix.<sup>20-22</sup> It seems that the possibility of a connection between the statistical theory of spectra and nonintegrable quantum systems was first clearly noticed by Casati, Valz-Gris and Guarneri<sup>23</sup> only three years ago. This paper does two things: (1) It clearly states the problem; (2) For a quantum particle in a "stadium" the authors calculate the first 170 eigenvalues with a numerical, finite element method and represent  $P(S)$  by an expression of the form

$$P(S) = A S^\nu \exp(-\mu S^2) \quad (7)$$

where  $A$ ,  $\nu$  and  $\mu$  are positive constants. They found that

$$0.2 \leq \nu \leq 0.5 \quad (8)$$

This is not consistent with a linear take-off, but as the statistics is guessed from only 170 levels the estimate (8) is very inaccurate. It is noteworthy that the Gaussian tail  $\exp(-\mu S^2)$  in (7) is of the same form as the tail of the level distribution of a random matrix. Quite recently, Bohigas et.al.<sup>24</sup> have found that the level fluctuations of the quantum Sinai's billiard are consistent with the predictions of the Gaussian orthogonal ensemble of random matrices. This is an attempt to put in close contact the random matrix theory and the study of chaotic motion. These authors suggest that the methods developed in random matrix theory<sup>22</sup> to study fluctuations provide a way of characterising chaotic spectra and that the generality of GOE fluctuations is found in properties of chaotic systems.

### III. CALCULATION OF THE TIME DEPENDENT TRANSITION RATE

The calculation proceeds in three steps: (i) set up a rate equation for the physical quantity that is undergoing relaxation in terms of a TDTR; (ii) compute the TDTR; and (iii) solve the rate equation once the TDTR is determined. Our goal is to examine the

long time limit of the time dependence and so there is much simplification that can be made right from the start. A formal justification of step (i) is given elsewhere<sup>25</sup>. We are concerned here mainly with step (ii) and calculate the transition rate using the Golden Rule with proper attention paid to the types of interactions that could be suggested for H<sub>BS</sub>. Having done this, we then invoke the cumulant expansion technique<sup>13</sup> or equivalently the linked cluster scheme to calculate the TDTR essentially to all orders in H<sub>BS</sub>. This is in the same spirit as in the binary correlation approximation.<sup>22</sup> We are thus led to consider the survival probability of a state of the system when it interacts with the bath. Let the heat bath have states |b> and the relaxing system two representative states |1> and |2>. At t=0, the combined system (S + B) is in a state |s,b> where |b> is some state with its energy in the range E - Δ < E < E + Δ. For a "good" heat bath, in general, one does not know the state |b> apart from the fact that it has an energy E<sub>b</sub> in some energy region (E - Δ, E + Δ). The standard Golden Rule result<sup>6</sup> for the probability that the total system is in the state |s'b'> at time t given the initial state is |sb> is

$$|C_{s'b'}(t)|^2 = \frac{2}{M^2} |V_{sb,s'b'}|^2 (1 - \cos \omega_{sb,s'b'} t) \omega_{sb,s'b'}^{-2} \quad (9)$$

where  $M \omega_{sb,s'b'} = E_{s'} + E_{b'} - E_s - E_b$ , with E<sub>s</sub> the system energy. The matrix element of the system-bath coupling Hamiltonian H<sub>BS</sub> between the states |sb> and |s'b'> is denoted by V<sub>sb,s'b'</sub>. In order to obtain the total transition probability Q<sub>s,s'</sub><sup>(0)</sup>(t) within the Golden Rule for the system to go from state |s> to state |s'> irrespective of the state of the heat bath we sum over |b> and average over |b>, noting that the bath states are all equally likely to be occupied with probability,  $\frac{1}{B}$ , because they are in a state of maximum entropy. This gives for the probability to find the system in state |s'> at time t

$$Q_{s,s'}^{(0)}(t) = \frac{2}{M^2 B} \sum_{b,b'} |V_{sb,s'b'}|^2 (1 - \cos \omega_{sb,s'b'} t) \omega_{sb,s'b'}^{-2} \quad (10)$$

where B denotes the number of heat bath states in (E-Δ, E+Δ). In order to express the relaxation function Q<sub>s,s'</sub><sup>(0)</sup>(t) in terms of the spectral characteristics of the heat bath one now proceeds, in a somewhat heuristic fashion, as follows. Firstly, as the system-bath coupling will depend only on the global properties of the heat bath the matrix element V<sub>sb,s'b'</sub> will be practically independent of the choice of |b> and |b'> in the energy range (E-Δ, E+Δ). This enables us to put

$$V_{sb,s'b'} \approx V_{s,s'} \quad (11)$$

and to bring the constant V<sub>s,s'</sub> outside the summation sign in (10). Secondly, we note that the resulting sum over b' will be independent of the choice of b. Hence the average over b is trivial and (10) can be written as the sum

$$Q_{s,s'}^{(0)}(t) = \frac{2}{M^2} |V_{s,s'}|^2 \sum_{b'} (1 - \cos \omega_{sb,s'b'} t) \omega_{sb,s'b'}^{-2} \quad (12)$$

In a relaxation process, the transition occurs from a state of the system to another state of the system which is essentially degenerate with it and so  $M \omega_{sb,s'b'} = E_{b'} - E_b$ . The sum (7) can now be written as an integral

$$Q_{s,s'}^{(0)}(t) = 2 |V_{s,s'}|^2 \int_0^\infty (1 - \cos \epsilon t / M) \epsilon^{-2} \rho(\epsilon) d\epsilon, \quad (13)$$

where  $\rho(\epsilon) d\epsilon$  denotes the average number of heat-bath quantum states with energies in (E<sub>b</sub> + ε, E<sub>b</sub> + ε + dε) given a heat-bath level at E<sub>b</sub>. For ε large as compared to the average level spacing δ one has  $\rho(\epsilon) \approx \delta^{-1}$ . On the other hand, for ε ≤ δ we can use the result (5) for the distribution of level spacings of an irregular quantum system and put  $\rho(\epsilon) \approx \alpha \epsilon$ . Thirdly, we use the following qualitative form for ρ suggested by the preceding remarks

$$\rho(\epsilon) = \alpha \epsilon \quad 0 < \epsilon < M \omega_c \quad (14a)$$

$$\rho(\epsilon) = \delta^{-1} \quad M \omega_c < \epsilon < \infty, \quad (14b)$$

with  $M \omega_c = (\alpha \delta)^{-1}. \quad (14c)$

The calculation of the integral (13) is now straightforward, and leads to the asymptotic behavior

$$Q_{s,s'}^{(0)}(t) \approx 2 \alpha |V_{s,s'}|^2 \ln(\omega_c t e^\gamma) + \dots, \quad (\omega_c t \gg 1), \quad (15)$$

The dots in (15) denote terms that vanish for t → ∞, and the constant γ = 0.577 is Euler's constant. Of course, for small values of t the quantity Q<sub>s,s'</sub><sup>(0)</sup>(t) will be proportional to t<sup>2</sup>. The calculation outlined above amounts to lowest order perturbation theory. It was shown by Fano<sup>13</sup> that when one proceeds in a rigorous fashion one obtains a cumulant expansion for the transition probability, which essentially leads to an exponentiation of the Golden Rule result (15)

$$Q_{s,s'}(t) \approx W_0 \exp(-n\gamma) (\omega_c t)^{-n} \quad 0 < n < 1, \quad \omega_c t \gg 1, \quad (16a)$$

$$n = 2 \alpha |V_{s,s'}|^2. \quad (16b)$$

Here W<sub>0</sub> is the residual transition

probability which would normally lead to exponential decay, Eq. (2). With a time dependent transition rate of this form the solution of a rate equation will lead to terms of the form (1), with  $0 < n < 1$ , for otherwise, with  $n > 1$ , one has faster than exponential decay.

#### IV. CONCLUDING REMARKS

We have shown, in a somewhat heuristic way, how the fine-grained spectral characteristics of the heat bath determine the form of the relaxation function. It is remarkable that the only quantities which enter are the average spacing  $\delta$ , or equivalently the cut off frequency  $\omega_c$ , the average system-bath matrix element  $V_{cs}$ , and the slope  $\alpha$  of the spacing distribution at small spacings. The linear behavior of this distribution at small spacings is a generic feature of irregular quantum systems<sup>15-19</sup>, hence an irregular (chaotic) quantum system is a universal model for a heat bath. Our considerations also show that one can use the Gaussian orthogonal ensemble of random matrices to simulate a chaotic quantum system, and hence to model a heat bath. This might also explain the success of random matrix theory in nuclear physics and other branches of physics. The main motivation of the work reported in this paper was to make the concept of the heat bath, which up till now inhabited the literature on statistical physics as an almost featureless entity, more specific and to determine which of its properties enter into the physics of relaxation.

#### ACKNOWLEDGMENTS

We thank Dr. K. L. Ngai and Professor J. B. French for reading the manuscript and making valuable comments on it.

† Supported in part by Office of Naval Research, contract Number N00014-82-K-0477.

\* Permanent address: Department of Applied Physics, Twente University of Technology, 7500 AE Enschede, The Netherlands

#### REFERENCES

- (1) K. L. Ngai, *Comments Solid State Physics* **9**, 127 (1979); **9**, 141 (1980). See also K. L. Ngai in *Recent Developments in Condensed Matter Physics, Vol I, Invited Papers*, ed. J. T. Devreese, (Plenum, N. Y.) (1981) p 527. See also the proceedings of the conference on "Non-Debye Relaxation in Condensed Matter" held at the Indian Institute of Science, Bangalore, September 14-17, 1982, to appear (1984).
- (2) J. C. Maxwell, *Phil. Trans. Roy. Soc. (London)* **157**, 49(1867)

- (3) P. Debye, *Polar Molecules*, Dover Reprint, New York (1929)
- (4) R. Kohlrausch, *Pogg. Ann.* **5**, 430 (1847)
- (5) K. S. Cole and R. H. Cole, *J. Chem. Phys.* **9**, 341 (1941)
- (6) G. Williams and D. C. Watts, *Trans. Faraday Soc.* **66**, 80(1970)
- (7) R. C. Tolman, *The Principles of Statistical Mechanics*, (Oxford University Press, London) (1938) Chapters XI and XII, pp 395-523.
- (8) I. Oppenheim, K. E. Shuler, and G. H. Weiss, *Stochastic Processes in Chemical Physics: The Master Equation* (The MIT Press, Cambridge, Mass) (1977).
- (9) E. Merzbacher, *Quantum Mechanics* (John Wiley & Sons, Inc., N. Y.) (1961) pp 471-475.
- (10) S. Teitler, A. K. Rajagopal, and K. L. Ngai, *Phys. Rev.* **A26**, 2906 (1982).
- (11) K. L. Ngai, A. K. Rajagopal, R. W. Rendell and S. Teitler, *Phys. Rev.* **B28**, 6073 (1983).
- (12) R. P. Feynman and F. L. Vernon, Jr., *Ann. Phys. (NY)* **24**, 118 (1963)
- (13) U. Fano, *Rev. Mod. Phys.* **29**, 74 (1957) in particular Sec. 10, 11(b), and 11(c).
- (14) U. Fano in *Lectures on the Many-Body Problem* (ed. E. R. Caianiello) (Academic Press, N.Y.) (1964) pp 217-239.
- (15) M. V. Berry, *Aspects of semiclassical mechanics*, to appear.
- (16) M. V. Berry and M. Tabor, *Proc. Roy. Soc.* **A356**, 375 (1977).
- (17) M. V. Berry, *J. Phys.* **A10**, L 193 (1977).
- (18) M. V. Berry, *Ann. Phys.* **131**, 163 (1981).
- (19) P. J. Richens and M. V. Berry, *Pseudointegrable systems in classical and quantum mechanics*, *Physica D*, in press.
- (20) C. E. Porter, *Statistical Theories of Spectra: Fluctuations*, (Academic Press, N.Y.) (1965). This book has reprinted many of the important papers on the subject.

- (21) M. L. Mehta, Random Matrices and the Statistical Theory of Energy Levels, (Academic Press, N.Y.) (1967)
  
- (22) T. A. Brody, J. Flores, J. B. French, P. A. Mello, A. Pandey, and S. S. M. Wong, *Rev. Mod. Phys.* 53, 385 (1981)
  
- (23) G. Casati, F. Valz-Gris and I. Guarnieri, *Lett. Nuov. Cim.* 28, 279-282 (1980).
  
- (24) O. Bohigas, M. J. Giannoni, and C. Schmit, *Phys. Rev. Letts.* 52, 1 (1984).
  
- (25) K. L. Ngai and A. K. Rajagopal, Proceedings of the conference on "Non-Debye Relaxation in Condensed Matter" held at the Indian Institute of Science, Bangalore, September 14-17, 1982 to appear (1984).

A Fundamental Relation Between Microscopic and Macroscopic  
Relaxation Times: Evidence in Relaxation Data

R. W. Rendell\* and K. L. Ngai  
Naval Research Laboratory  
Washington, D.C. 20375-5000

Abstract

In recent years it has become clear from empirical results that the time dependence of various relaxations in a wide range of condensed matter has a fractional exponential form. For mechanical relaxations the fractional exponential can be traced back to Kohlrausch and Pierce; for dipolar primary dielectric relaxations, to Williams-Watts; for ionic conductivity relaxations, to Moynihan and Macedo. But for other relaxations including spin-lattice, luminescence, electronic hopping, magnetization, dipolar secondary, entangled polymer melt terminal, nonlinear viscoelastic recombinations or reactions, etc., the connections between the fractional exponential form and observed phenomena were first made by our group at NRL. Even in mechanical and dielectric relaxations, we have enhanced the credibility of the fractional exponential form by an exhaustive examination of available data. The widespread adherence of relaxation data to the fractional exponential is referred to as the first universality. We have also developed a model which provides a basis for the fractional exponential form and also predicts a relationship between the measured macroscopic effective relaxation time and an underlying microscopic fundamental relaxation time. This relationship between relaxation times is quite new but it is widely observed and it is referred to as the second universality. The second universality involves the same fractional exponent as in the fractional exponential function and leads to renormalization relations that have been repeatedly verified. In several cases they provide an explanation for previously puzzling phenomena. This article gives an overview of the first universality and the realm of its validity, the physical meaning of relaxation in complex systems, and the second universality and examples of its predictions in several fields of relaxation.

\*Sachs/Freeman Associates.  
Supported in part by ONR-NRL Contract No. N00014-84-WR2-4054.

Contents

Introduction  
First Universality  
Physics of Slow Relaxation  
Second Universality  
Perspective on Relaxation

Introduction

There has been a recent dramatic increase in the general recognition that relaxation data exhibit similar regularities across many different relaxation processes and materials. This can be seen by the appearance of more and more papers presented in polymer, glass, and physics meetings which refer to fractional exponential decaying processes. These are relaxation processes which are well-described by the empirical fractional exponential function:

$$\phi(t) = \phi_0 \exp[-(t/\tau_p)^{1-n}] \quad (1.1)$$

Experimentally, the values of  $n$  cover nearly the entire range between 0 and 1 depending on the particular relaxation process and material.

Most of these recent papers only address the functional form of (1.1), either by its use for fitting some particular data or by considering possible mathematical formalisms which might include these functions. The specific form (1.1) has by no means been shown to be a unique description of the time dependence of relaxation. Aside from convenience, does (1.1) have further physical significance? In order to answer this question, deeper problems concerning the nature of relaxation in disordered systems must be investigated and solved. These problems are not currently being generally addressed and the full significance of the relaxation problem is usually not appreciated. The observation that (1.1) is consistent with a large amount of relaxation data is significant, but does not in itself lead to insight into any underlying, more fundamental physics. However, there does exist a second class of empirical observations which is able to relate the observed time scale (i.e.  $\tau_p$  in (1.1)) of the relaxation process to the microscopic time scale. The relation between these two time scales involves the fractional exponent  $n$  in (1.1). This second class of

observations is not nearly as well known as the first class (i.e. applicability of (1.1)) but there is clear evidence of its widespread appearance. The existence of both types of observation has far-reaching implications. We believe this second class of observations begins to cut to the real heart of the relaxation problem.

The purpose of this paper is to illustrate these aspects of relaxation. It is not at all meant to be a complete review of the data or a detailed treatment of relaxation models which describe the data. Rather, it will be a more informal discussion of the physical questions that must be addressed in order to resolve the relaxation problem. This discussion will be supported by presenting a sufficient amount of experimental data so that the reader can get a feeling for the quantitative relationships which are exhibited by the relaxation data. Further details will be found in the references. We feel that this type of presentation is useful because the relaxation problem cuts across a large number of different disciplines and because a physical understanding of the relaxation data requires some new approaches to the problem. It is useful to have an informal discussion which presents a broad view of the situation.

The first class of empirical relaxation observations mentioned above, namely that the fractional exponential (1.1) - a nearly universal description of the time decay across the entire range of relaxation phenomena, will be referred as the "first universality." The extent of even this first universality was not appreciated until a recent exhaustive examination of the data was carried out.<sup>1,2</sup> The first universality will be discussed in the next section. The physical issues that must be confronted if the first universality is taken seriously will be discussed in the section after that. One of these issues is the question of how the relaxation time scale is affected by the interaction of a relaxation mode with its environment. A second class of empirical observations indicates that the relaxation time  $\tau_c$  on the microscopic level is "stretched" by this interaction up to the macroscopically observed time scale  $\tau_p$ . All relaxation experiments to date are consistent with the following expression for this stretching:

$$\tau_p = [(1-n)\omega_c^n \tau_c]^{1/(1-n)} \quad (1.2)$$

Here,  $n$  and  $\tau_p$  are the same parameters that appear in (1.1). The frequency  $\omega_c$  is required at least for dimensional reasons, but it must be related to some new physics in the problem which determines this characteristic stretching. Most current models of relaxation do not even attempt to address this question of the relaxation time, but we shall briefly describe a model, and its accompanying physics, in the third section which predicts both (1.1) and (1.2). The data indi-

cate that (1.2) is as widespread as (1.1) and we shall refer to (1.2) as the "second universality." The second universality is not as well-known as the first, but it is clearly exhibited by the data. The fourth section describes the second universality for a variety of relaxation processes and how it can often resolve long standing problems. We then close with a perspective summary of the present situation.

### First Universality

The fractional exponential function (1.1) has appeared from time to time over the past century as an empirical description of data from mechanical, dielectric and other relaxation experiments on glasses, polymers and other materials. This includes the work of Kohlrausch<sup>3</sup> in 1847 who used the inverse of (1.1) to describe the creep of glass, and Pierce<sup>4</sup> in 1923 who used (1.1) to describe the stress relaxation of fibrous materials. In 1925, Stotts<sup>5</sup> and later Jones<sup>6</sup> found their data for creep in glasses to be consistent with (1.1) for  $n=0.5$ . De Bast and coworkers,<sup>7</sup> and also Kruithof and Zijlstra<sup>8</sup> in 1954 used (1.1) for stress relaxation. In 1963 Hopkins<sup>9</sup> and Kurkjian,<sup>10</sup> and DeBast and Gilard<sup>7</sup> again confirmed that stress relaxation is fractional exponential, this time in inorganic glasses. In 1970 Williams and Watts<sup>11</sup> found the fractional exponential decay function also applicable to the dipolar dielectric relaxation of a number of polymers and supercooled liquids. In the 1970's, Moynihan and Macedo<sup>12,13</sup> found it to be applicable to describe ionic conductivity relaxations in glasses and viscous liquids. It was shown applicable to photon correlation spectroscopy of glasses by Bucaro, Dardy and Corsaro,<sup>14</sup> and also Lai, Macedo and Montrose<sup>15</sup> in 1975 and later in polymers just above the glass transition by Patterson, Lindsey and Stevens<sup>16</sup> and also Lee, Jamieson and Simha<sup>17</sup> in 1979. In 1984 Chamberlin, Mozurkewich, and Orbach<sup>18</sup> found that the thermoremanent magnetization of Cu:Mn and Ag:Mn spin glasses obeys the fractional exponential. Many other historical examples could be given<sup>2</sup> and some of these will be mentioned below. However these uses of the fractional exponential are either isolated cases or at least restricted to one field of relaxation phenomena. In addition, the specific form of (1.1) is not taken seriously but only as a convenient two parameter representation which can be fit to time dependent data well. After all, (1.1) is a very versatile and flexible function and its widespread utility may have no more significance than this. Alternative forms can certainly be devised which, while perhaps not being as succinct in form, will fit the time or frequency dependence of relaxation as well.



In order to determine whether the fractional exponential has any real physical significance, additional questions must be addressed. These will be discussed in the next section. However, the consistency of (1.1) with relaxation data is significant and it is truly widespread and covers nearly the entire scope of relaxation processes. The extent of this similarity was not known to most workers because of the traditional separation of research fields. Appreciating this requires becoming familiar with the experimental measurements and the physical mechanisms of relaxation in phenomena as dissimilar as physical aging in glasses, electronic transport in semiconductors, polymer melt rheology, and thermoremanent magnetization in spin glasses. That the fractional exponential has a large degree of universality in relaxation was first demonstrated in a program carried out by one of us (K.L.N.) beginning in 1978.<sup>1,2</sup> This involved an exhaustive search and analysis of dielectric, mechanical, and conductivity relaxation data and the demonstration of the general applicability of (1.1) to an even wider class of materials than previously thought. In addition, its application was extended to include fluctuation phenomena including NMR spin-lattice relaxations and noise, and to electronic and optical relaxation processes. This program has since been continued and extended, along with various collaborators, to include systems as diverse as amorphous polymers, conducting polymers, polymer melts, spin glasses, electron glasses, ionic conductors and very large scale integrated circuits (VLSI).<sup>19-53</sup> Furthermore, it has been shown that (1.1) can continue to be valid when the material structure is modified and the fractional exponent  $n$  is structure dependent.<sup>43,46,49,50</sup>

As mentioned in the introduction, the conformation of relaxation data from diverse relaxation processes and materials to the fractional exponential (1.1) will be referred to as the first universality. The evidence at present is overwhelming and involves analyzed data on thousands of condensed matter samples and tens of different relaxation phenomena.<sup>2</sup> Relaxation phenomena which exhibit the first universality include dielectric relaxation, AC conductivity, creep, stress relaxation, internal friction, relaxations observed through photon correlation spectroscopy, nuclear magnetic resonance (NMR) relaxations, spin-echo measurements, transient capacitance, transient (i.e. time-resolved) electrical transport, transient optical luminescence, volume and enthalpy recovery, differential scanning calorimetry (DSC), steady flow viscosity, stress-strain relationship and its dependence on strain-rate, ultrasonic attenuation, noise, diffusion, diffusion controlled chemical reactions, electronic recombinations, magnetic relaxation, etc. Materials involved include liquids, supercooled liquids, liquid crystals, inorganic glasses, electrolytes, ionic conductors, insulators, dielectrics, gate insu-

lators of electronic devices, electrets, semiconductors, amorphous semiconductors, xerographic materials, polymer melts and solutions, amorphous polymers, rubbers, plastics, epoxies, metals, amorphous metals, metallic glasses, lubricants, ceramics, piezoelectrics, pyroelectrics, ferroelectrics, biopolymers, coal, oil shales, spin glasses, electron glasses, very large scale integrated circuits (VLSI), etc.

These applications represent an enormous diversity of physical phenomena and material composition. The materials vary from rather small molecules quenched into glasses to long chains of molecules forming entangled polymer melts to the dilute concentrations of magnetic impurities in insulating, semiconducting, or metallic hosts which are spin glasses. The physical entity which takes part in the relaxation can be as different as charge carriers (i.e. electrons, ions) hopping through a semiconductor or glass, the motion of long flexible polymer chains, or the magnetization of a quenched spin glass. The first universality result is that in spite of the enormous differences in the physical properties of these systems and the experimental techniques used in the relaxation measurements, the time dependences are all consistent with the fractional exponential form (1.1). Equation (1.1) has a very characteristic shape and skewness for a given value of  $n$  and it is possible that the data would not have had these features. The first universality is thus significant and interesting.

A decay described by (1.1) can be transformed into different representations corresponding to the variety of displays of data from different measurement techniques. For instance in a dipolar dielectric experiment, an electric field is applied to polarize the dipoles and the decay of the polarization or dielectric displacement is observed. The dielectric displacement decays according to (1.1) and the corresponding complex dielectric function is:

$$\epsilon^*(\omega) = \int_0^{\infty} dt \exp(-i\omega t) (-d\phi/dt) \quad (2.1)$$

The imaginary part of this,  $\epsilon''(\omega)$ , exhibits the familiar low frequency dielectric loss peaks as measured by low frequency techniques. By contrast, for ionic conduction in a glass, it is the electric field that decays according to (1.1). For this situation, a complex electric modulus is given by:<sup>12,13</sup>

$$M^*(\omega) = M_{\infty} [1 - \int_0^{\infty} dt \exp(-i\omega t) (-d\phi/dt)] \quad (2.2)$$

which is related to the dielectric function by:

$$\epsilon^*(\omega) = 1/M^*(\omega) \quad (2.3)$$

and the corresponding conductivity is:

$$\sigma^*(\omega) = i\omega \epsilon_0 \epsilon^*(\omega)$$

The electric modulus for the conductivity of lithium ions in a lithium borate glass is shown

in Figs. 1 and 2. For viscoelastic relaxation in polymers, the response to a constant applied strain is a relaxation modulus described by (1.1) (e.g. shear modulus  $G(t)$  or Young's modulus  $E(t)$ ). An example is shown in Fig. 3 for the long time relaxation of high molecular weight polymer melts. A corresponding complex modulus is related to this by:

$$G^*(\omega) = \int_0^\infty dt \exp(-i\omega t) (-d\phi/dt) \quad (2.4)$$

In the complementary viscoelastic experiment, a constant applied stress gives rise to a time

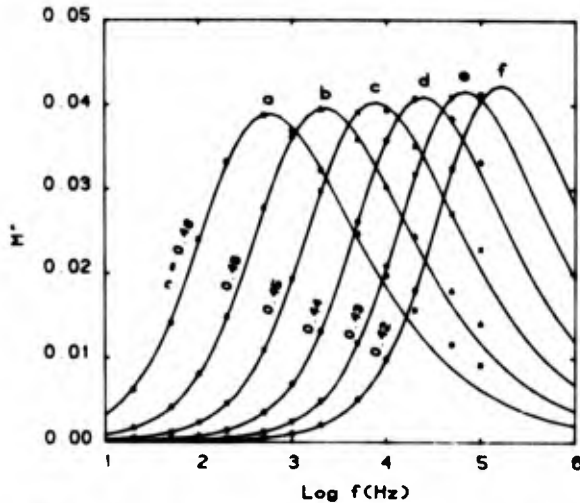


Fig. 1. Imaginary part of the electric modulus vs. frequency at a range of temperatures for a  $\text{Li}_0.3\text{B}_2\text{O}_3$  glass containing predominantly  $^6\text{Li}$  alkali species. Solid curves are theoretical fits from (1.1) and (2.1) with  $n$  values indicated. (a)  $T=108.9^\circ\text{C}$ ; (b)  $T=131.0^\circ\text{C}$ ; (c)  $T=153.8^\circ\text{C}$ ; (d)  $T=177.5^\circ\text{C}$ ; (e)  $T=200.5^\circ\text{C}$ ; (f)  $T=222.2^\circ\text{C}$  (data of H. Jain et al., replotted. See Refs. 127, 45).

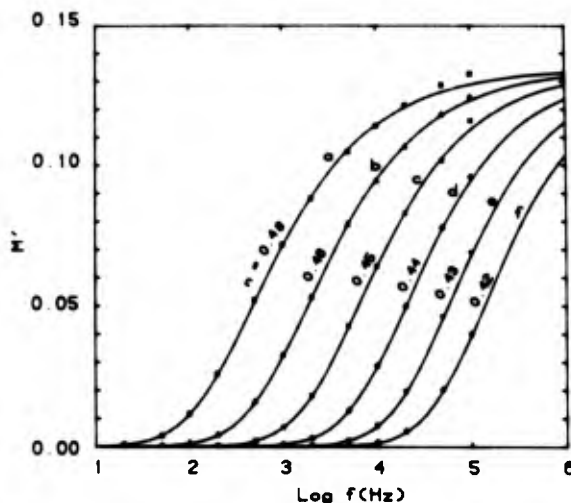


Fig. 2. Real part of the electric modulus corresponding to Fig. 1.

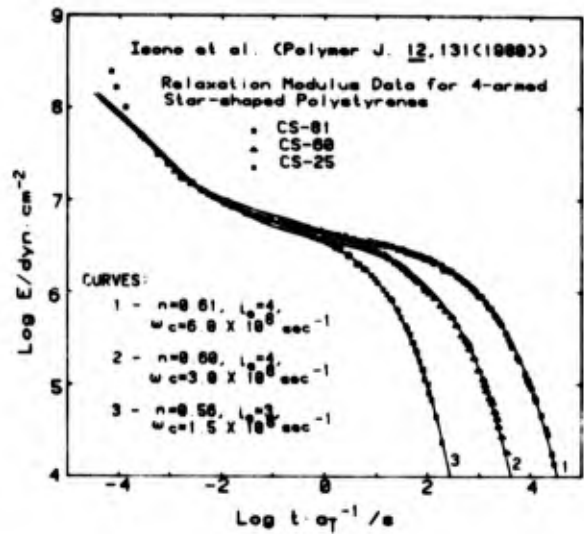


Fig. 3. Relaxation modulus data for 4-armed star-shaped polystyrenes (data of Isono et al., replotted).

response called the creep compliance,  $J(t)$ . For linear viscoelasticity, the compliance is related to the relaxation modulus by a convolution expression:<sup>54</sup>

$$\int_0^t d\tau G(t-\tau)J(\tau) = t \quad (2.5)$$

This can be solved numerically for  $J(t)$  given the form (1.1) for  $G(t)$ . An example of this is shown in Fig. 4 for a glassy polystyrene at different periods of annealing. This is only a small sample of relaxing quantities and their representations. Figures 1-4 will not be discussed in detail here, although some of them will be mentioned again in the section on the second universality. They are shown here as representative examples of the first universality in various representations. More detailed discussions can be found in a recent review of the data.<sup>2</sup> Note that the values of  $n$  in Figs. 1-4 are significantly different from zero. The case  $n=0$  corresponds to Debye relaxation and exponential decay with a single power of time. Values of  $n$  near zero are definitely measured in some systems, such as in liquids at high temperatures, but it is important to realize that for the majority of systems of central interest to researchers such as glasses, polymers and semiconductors, the value of  $n$  is much larger than zero. It is important to bear in mind that a different representation of the data may emphasize certain features of the relaxation process and may facilitate the resolution of some physical problem, but no new information can be extracted by changing representations.

These and other first universality fits are all consistent with the data within the experimental error except for a few cases where there are some small deviations from (1.1). Such

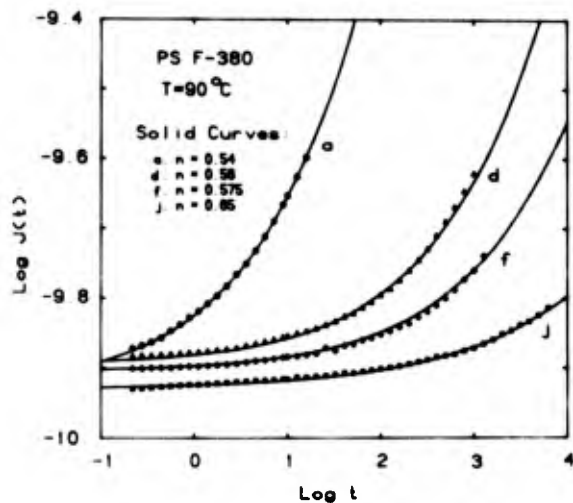


Fig. 4. Creep compliance data for a polystyrene (mol. wt. =  $3.8 \times 10^6$ ) at  $90^\circ\text{C}$  during annealing. Solid curves are predicted  $J(t)$  according to (1.1) and (2.5) with  $n$  values indicated (data of D.J. Plazek, see Ref. 47).

deviations, when they occur, are well understood in terms of competing relaxation processes in the vicinity of the relaxation mode under study. For instance, Fig. 1 shows the  $M''(\omega)$  peaks for diffusion of lithium ions in borate glasses. The solid lines are fits based on (1.1) and (2.2) at different temperatures.<sup>45</sup> The fits are excellent up to some 1.5 decades beyond the  $M''$  maximum where some deterioration in the fit begins to appear and the data lie above the theoretical curves. This has been observed in similar fits of electric modulus data from many glasses and ionic conductors,<sup>12,13,37</sup> and is consistent with the existence of an excess contribution to the electric modulus which can be considered physically distinct from the ion hopping mechanism. This is best illustrated by replotting the data as  $\epsilon''(\omega) = M''(\omega) / [M'(\omega) + M''(\omega)]$  from (2.3) and this is shown in Fig. 5(a). The value of  $\epsilon''(\omega)$  is seen to drop about 3-4 decades and the deviations are noticeable only when  $\epsilon''$  is below about 0.15. In fact, if a constant background contribution of magnitude  $\Delta\epsilon'' = 0.15$  is added to all the theoretical curves, the resulting fits are excellent over the entire frequency range at all temperatures and this is shown in Fig. 5(b). Several workers have suggested specific physical mechanisms for the excess background contribution in some systems.<sup>12,37</sup>

Another example of nearby relaxing processes is in the primary and secondary relaxation of glassy polymers.<sup>54</sup> Relaxation modes respond in particular temperature regimes and as the temperature is lowered below the glass transition temperature,  $T_g$ , a polymer can exhibit a

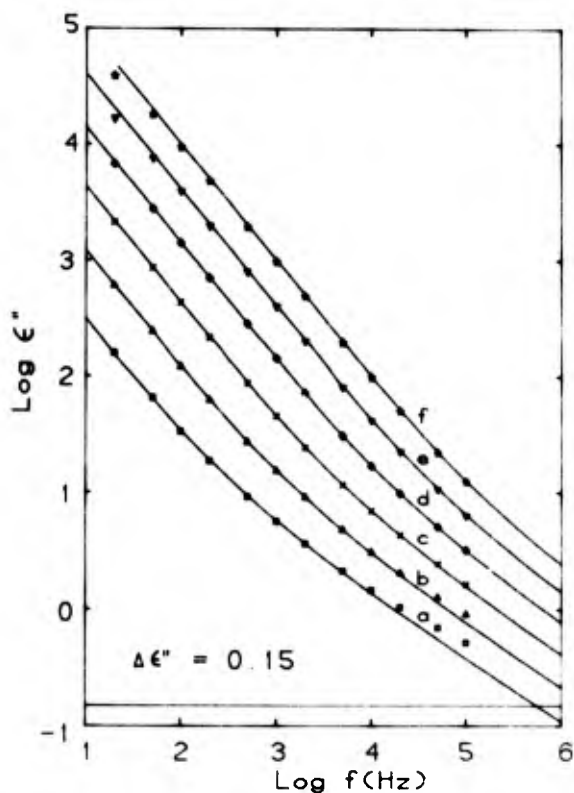


Fig. 5(a). Data and theoretical curves of Figs. 1 and 2 replotted as  $\epsilon''(\omega)$  according to (2.3). Straight line at bottom indicates approximate magnitude of excess background contribution.

series of distinct modes. The first one encountered on going through  $T_g$  is called the  $\alpha$  relaxation and the next one is called the  $\beta$ . The  $\alpha$  and  $\beta$  modes are sometimes well separated and in these cases, they each are found to follow the first universality. For some polymers, the  $\alpha$  and  $\beta$  are found to partially overlap and this can obscure the first universality which is followed by each of the modes separately. The combined overlap mode then may not be well fit by (1.1), but this does not invalidate the first universality which applies only to distinct relaxation processes.

Since it is important to recognize whether or not the first universality is being followed, we will mention yet another example which can have several distinct relaxation modes, that of polydispersity in polymers. This will help clarify the type of situations in which the first universality can be expected to be distinguished in relaxation data. The example will also be useful in the section on the second universality. Consider a large collection of molecules linked together into a long chain to form a polymer. For instance,  $\text{CH}_2$  molecules or "monomer units" are linked by molecular bonds to form the polymer chain called polyethylene. For simplicity, let us suppress all the molecular details and view the polymer as a succession of

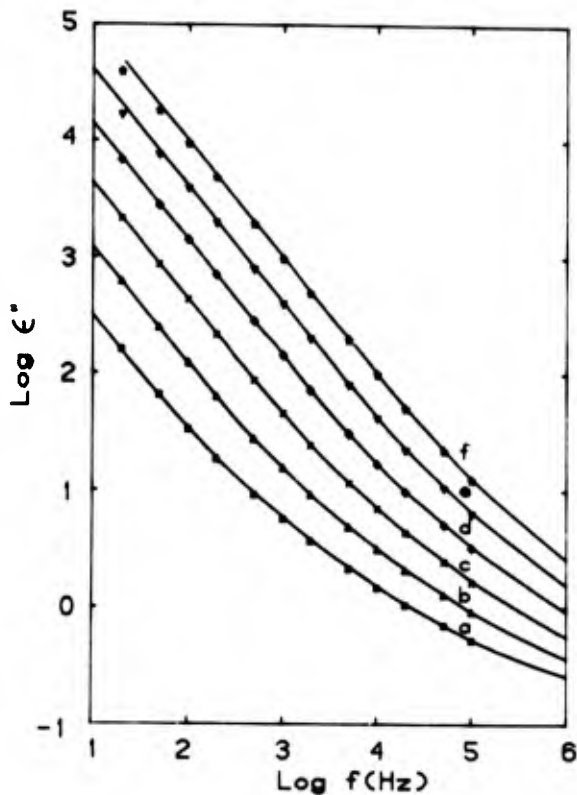


Fig. 5(b). Theoretical curves including background contribution, corresponding to Fig. 5(a).

beads at positions  $r_1, r_2, \dots, r_N$  linked by "springs" of average length  $a$ . Phenomenological models such as this can be very useful for describing the large scale motion of polymer chains. Actually, it is not necessary to identify each monomer unit with a bead but several monomers can be lumped into a single bead. The chain is damped by the monomeric friction coefficient  $\zeta$ . A model like this was first worked out by Rouse in 1953 and it exhibits normal modes typical of a damped chain.<sup>55</sup> In particular, the relaxation times of the Rouse modes scale as the square of the chain length  $N$ . This is a general characteristic of a large class of diffusion systems and, indeed, in the continuum limit the chain obeys a diffusion equation:

$$\frac{\partial r_n}{\partial t} = \frac{6kT}{a^2\zeta} \frac{\partial^2 r_n}{\partial n^2} \quad (2.6)$$

Here  $6kT/a^2$  plays the role of the spring constant. The normal modes for this simple chain must look like:

$$r_{n_i}(t) \sim \cos(n\pi i/N) \exp(-t/\tau_i) \quad , \quad (2.7)$$

and with chain end boundary conditions  $\partial r/\partial n=0$  at  $n=0$  and  $n=N$ , (2.6) yields the dependence of  $\tau_i$  on the chain length  $N$  as claimed:

$$\tau_i = \frac{a^2\zeta}{6\pi^2} \frac{N^2}{i^2} \quad (2.8)$$

These details of the chain will be useful for us in a later section, but the point here is that we have a situation where the relaxation times depend on the length of the chain,  $N$ . Suppose we focus on the longest time mode  $\tau_1$ , which is called the terminal time. If we have a large collection of chains with different lengths  $N_a, N_b, N_c, \dots$ , then there will be a number of different relaxation times  $\tau_1(N_a), \tau_1(N_b), \dots$ , in our system. This is referred to as a polydisperse polymer system. This is another situation which can obscure identification of the first universality. Fortunately, polymer chemists can make monodisperse polymer systems in which the lengths are all nearly the same. Indeed, when a monodisperse collection of sufficiently long chains are brought together to form a concentrated solution or a bulk polymer melt, the observed terminal relaxation from all available data on such monodisperse systems is no longer given by a single exponential as in (2.7) but instead is modified to the first universality form (1.1). We will look into the physical reasons for this in the following section. However, a polymer which is very polydisperse does not fit (1.1) very well. The reason is that there are several relaxation modes each described by a term of the form (1.1) with relaxation times  $\tau(N)$  which vary with the distribution in chain length. A polydisperse polymer is therefore not a good system in which to test the first universality.

The first universality is still not expected to apply to every form of condensed matter without exception, even if the relaxation is not overlapping with a distribution of nearby modes. It may not occur if the material is sufficiently disordered so that even the short range order found in many amorphous systems around atomic sites was destroyed. We will discuss why this may be so in the next section, but it is important to try to find and understand the limitations of the first universality. It is significant that if a polymer rheologist is given some spin glass data with the axis labels covered, he might mistake it for some of his own measurements. However, in order that the first universality be useful and not just an empty generalization, certain questions concerning the physics of slow relaxation must be asked.

#### Physics of Slow Relaxation

As mentioned in the introduction, there is now a great deal of discussion about the first universality among workers in glass, polymers, electronics, and various other types of condensed matter physics. Although the degree of universality was not appreciated before the exhaustive treatment of data recently carried out and discussed in the previous section, it is now generally accepted by long-time workers in relaxation as well as newcomers to the field. However, most of the recent discussions have amounted to no more than a restatement of the first universality along with, in some cases,

suggestions of a formal framework within which functions of the form (1.1) might be discussed.

Since the first universality, though significant, is of limited use by itself, let us instead ask for the physical meaning of (1.1). What is the meaning of the timescale  $\tau_p$ ? Can it be identified with or related to a timescale of the relaxing quantity of interest, say the normal mode time to move a segment of a polymer? Does it instead characterize the material system in which the relaxing quantity resides, say an energy barrier which a hopping charge carrier confronts in a glass? Or is it characteristic of both the relaxing quantity and material, or yet some other effects? What is the meaning of the exponent  $n$ ? What determines its magnitude from material to material and between different relaxation processes? Can the values of  $n$  and  $\tau_p$  be tailored by changing experimental variables? Is  $\tau_p$  independent of  $n$ ? If these and other questions are not asked, the relaxation problem has not been fully addressed.

When the large program of data analysis which demonstrated the first universality was first undertaken in 1978, one of us (K.L.N.) also addressed these questions and suggested a physical interpretation. This will be described briefly below, but before going into the details of this let us simply ask ourselves what we would expect to happen. Consider a relaxing quantity with a characteristic timescale  $\tau_p$ . For instance, this could be one of the long polymer chains considered in the previous section with a timescale given by (2.8), say the terminal  $i=1$  mode. Experimental data on dilute solutions of such chains or on chains which are short enough to move essentially independently are consistent with single exponential relaxation as in (2.7). When the concentration of the solution is increased sufficiently or when the length of the chains is long enough so that they cannot avoid touching, then the relaxation ought to be slowed down since the motion of the chain is now hindered by the surrounding ones. A model might be worked out for a group of chains which are allowed to entangle with one another, perhaps by modifying the chain diffusion equation (2.6) by including some types of constraints. Well perhaps, but the modification of the chain relaxation must not be tied too closely to the fact that the relaxation mode in this case happens to be a long polymer chain because the first universality is not at all restricted to this situation. Experiments on nearly monodisperse entangled linear polymer melts do in fact find that the terminal relaxation obeys (1.1) with  $n$  between 0.40 and 0.47, depending on the type of polymer and sample preparation.<sup>35</sup> The measured relaxation time  $\tau_p$  is not found to be equal to the timescale  $\tau_p$  for an isolated chain but is much larger. How can a relaxation of the form  $\exp(-t/\tau_p)$  become modified by the entangling of other chains to the form (1.1) and with a much longer relaxation time  $\tau_p$ ?

Suppose instead that the relaxing quantity is a mobile charge carrier, with a characteristic hopping time  $\tau_0$ , hopping through a material. The electric field inside the material decays due to the migration of the mobile carriers. For materials with long range order such as metals, the electric field is found to decay as a single exponential  $\exp(-t/\tau_0)$ . What happens if instead the carriers migrate in a material without long range order such as a glass? In the metallic case, as the charge carrier jumps to a region of lower potential energy, it interacts with the surrounding atoms in the crystal and causes them to vibrate. These effects can all be incorporated by means of a simple activated rate form for  $\tau_0$  (i.e.  $\tau_0 \sim \exp(-\Delta F/kT)$ , where  $\Delta F$  is the change in free energy needed to move the carrier).<sup>56,57</sup> In the case of a glass, the carrier ought to have more complicated interactions with its surroundings due to the lack of long range order and the migration should be hindered. The standard theory for charge migration might be modified to incorporate the lack of long range order in a glass, perhaps by way of a random array of activated barriers. Well perhaps, but as we commented in the polymer chain case, the way in which the relaxation is modified had better not rely on details which are too specific to the system. Experiments on the motion of ions in glasses have repeatedly verified that the electric field follows the first universality (1.1).<sup>12,13,45</sup> The measured value of  $\tau_p$  is found to be larger than timescales which would typify  $\tau_0$ . How can a relaxation of the form  $\exp(-t/\tau_0)$  become modified by the lack of long range order to the form (1.1) and with a much longer relaxation time  $\tau_p$ ?

The timescale  $\tau_p$  for the slow relaxation processes can be very large indeed. For polymer relaxation, practical limits for direct measurement lie around seven decades in time (i.e. a year). The relaxation times  $\tau_p$  for high molecular weight melts are commonly on the order of 10<sup>7</sup> seconds or more. Data for very long relaxations are often obtained by accelerating the process with increased temperature and then using a technique of shifting the data taken at different temperatures onto one master curve representative of a particular reference temperature.<sup>54</sup> At very low temperatures (i.e. below the glass transition), the relaxation times can easily approach the estimated age of the universe. These are certainly much larger than any relaxation times that can be associated with the individual polymer chains or monomer molecular units. The relaxation times for the decay of electric fields in a glass due to the migration of charge carriers range from hundredths of seconds to seconds depending on the temperature. This is much longer than the time scale associated with ionic hopping.<sup>13</sup> Of course, motion of a chain in a bulk polymer or an ion in a bulk glass requires some cooperativity so it is not surprising that the relaxation times are long

compared to molecular time scales. Most attempts to describe transport and response in amorphous materials have tried to include cooperativity in some way. Concepts used in the past have included enhanced friction due to the dragging of entangled polymers, availability of free volume for motion within liquids and glasses, distributions of traps, energy barriers, and bond lengths for the motion of charge carriers in semiconductors and glasses, and long-range random interactions between spins in spin glasses. Similar concepts and elements have been used in other fields of relaxation.

The manner in which these and other concepts may play a role in the magnitude of the relaxation time and also in producing the form of the first universality (1.1) is, however, severely restricted by the way in which the observed relaxation time  $\tau$  is quantitatively related to the microscopic time scale  $\tau_0$ . This is the relationship referred to in the introduction as the second universality. The amount by which  $\tau_0$  is stretched to the value  $\tau_p$  in (1.2) depends on the exponent  $n$  which appears in (1.1). Thus (1.1) and (1.2) are coupled relations, the same value of  $n$  appearing in each. Relaxation data exhibit a very specific correlation between the timescale of the relaxation and the shape of the time decay function. This will be discussed and demonstrated using several examples in the next section. One of its consequences is that it can be used to relate the dependence of the microscopic relaxation time  $\tau_0$  on various physical quantities, such as temperature or molecular weight, to the dependence of  $\tau_p$  on these same quantities for the bulk relaxation. Therefore, if  $\tau_0$  has a certain dependence:

$$\tau_0 = \tau_0(T, M, \dots) \quad (3.1)$$

then (1.1) requires:

$$\tau_p(T, M, \dots) \propto [\tau_0(T, M, \dots)]^{1/(1-n)} \quad (3.2)$$

For instance, if  $\tau_0$  described the physics of the motion of some mode over an energy barrier with activation energy  $E_A$ :

$$\tau_0 = \tau_\infty \exp(E_A/RT) \quad (3.3)$$

then (3.2) describes a macroscopic effective relaxation time given by:

$$\tau_p = \tau_\infty^* \exp(E_A^*/RT) \quad (3.4)$$

where:

$$E_A^* = \frac{E_A}{1-n} \quad (3.5)$$

When the value of  $n$  is found by fitting the time dependence of the relaxation according to (1.1) or one of its other representations, then (3.5) can be used to relate the microscopic and macroscopic activation energies. As shown in the

following section, (3.5) is repeatedly verified quantitatively in relaxation processes which are temperature activated. These include relating secondary relaxations in glassy polymers to the motion of molecular groups,<sup>39</sup> relating the flow activation energy in polymer melts to molecular rotational isomerism barriers,<sup>53</sup> relating the observed temperature dependence in dispersive transport in amorphous semiconductors and insulators to that of small polaron transport,<sup>1,28,29</sup> and many other examples.<sup>2</sup> Equation (3.5) is only a special case of the full second universality (1.2) and the presence of an energy barrier is not required. Whenever data are available to test any part of the predicted relation (1.2) between  $\tau_0$  and  $\tau_p$  it has been found to hold quantitatively in any system which also follows the first universality (1.1). Data are not available in every single case for a complete test of both (1.1) and (1.2) but the evidence to date is nevertheless widespread and quite persuasive.<sup>2</sup> In some cases, the data are sufficiently detailed to test the complete relation (1.2), including an identification for the physical meaning of the frequency  $\omega_c$ .<sup>36</sup>

Compliance of relaxation data with the second universality implies that there is in fact a single physically identifiable relaxation time  $\tau_0$  which is dominant on the molecular level. At first sight, this may seem at odds with repeated suggestions in the literature that glasses and amorphous materials should be interpreted as random configurations of atoms and molecules. Such structural randomness would almost certainly give rise to a random distribution of  $\tau_0$ 's instead of a well-defined single  $\tau_0$ . For instance, consider borate glasses containing lithium ions. Diffusion of the lithium ions in this system is consistent with both first and second universalities. In 1932, Zachariasen<sup>58</sup> proposed his random network model for the structure of glasses. If some form of the random network model were appropriate for the lithium borate glass, the lithium ions would be expected to occupy a spectrum of sites, each slightly different from the other. This would produce a spectrum of activation energies for lithium ion conductivity resulting in a non-Arrhenius temperature dependence. However, the lithium borate conductivity data indicate (essentially) a single well-defined activation energy just as is commonly found for cubic crystalline solids.<sup>59</sup> Although glasses do not have the long-range order present in crystals, they do retain some short range order so the presence of a single  $\tau_0$  for glasses in fact is not surprising. For instance, extended X-ray absorption fine structure studies of silicate glasses have shown that the structure is dominated by the invariance of the  $\text{SiO}_4$  pyramid unit from site to site.<sup>60</sup> The Si-O bond length and the O-Si-O bond angle are preserved, although long-range order is lost due to random variations in the Si-O-Si bond angle. If the molecular relax-

ation time  $\tau_0$  is determined locally, the presence of short-range order in glasses, polymers, and amorphous semiconductors allows one  $\tau_0$  to dominate throughout the material.

This does not mean that several different  $\tau_0$ 's cannot be present in some situations. Examples where relaxations from different  $\tau_0$ 's can overlap were mentioned in the previous section. Also, it may be possible to deliberately disorder a sample so severely that even much of the short-range order is destroyed. However, as shown by the examples in the next section, many problems of great interest to researchers are consistent with the first and second universalities. For these situations, a single dominant  $\tau_0$  at the molecular level does exist.

How can the first and second universalities be physically understood? These two observed phenomena are essential features which must be contained in any physical description of relaxation and in any accompanying theory used to quantify the description. Most recent work has focussed only on the functional form of (1.1) and not on explaining the nearly universal appearance of (1.1) or on the associated second universality. The most common suggestion is for interpreting (1.1) as a distribution of either parallel or sequential relaxation processes:

$$\phi(t) = \sum_n W_n e^{-t/\tau_n} \quad (3.6)$$

For the case of parallel processes, this view suggests that a statistical distribution of relaxation processes relax independently (e.g. random network) and contribute additively to  $\phi(t)$ , each being weighted from the distribution of relaxation times:  $W_n = g(\tau_n)$ . For the case of

sequential processes,<sup>61</sup> the faster degrees of freedom successively constrain the slower ones and this is accomplished in (3.6) by choosing functions  $\alpha$  and  $\beta$  to relate the successive  $W_n$ 's and  $\tau_n$ 's:

$$W_{n+1} = \alpha(W_n) \quad (3.7)$$

$$\tau_{n+1} = \beta(\tau_n) \quad (3.8)$$

In either of these cases, the form (1.1) is obtained only if the distributions (i.e.  $g(\tau)$  for parallel or  $\alpha(W)$  and  $\beta(\tau)$  for sequential) are chosen in just the right way. The physical interpretation of (1.1) then rests on the physical interpretation of  $g$  or  $\alpha$  and  $\beta$ . Not only must a physical interpretation be provided, but an explanation is needed as to why the distributions are the same for glasses, polymers, semiconductors, spin glasses and the large number of other systems which follow the first universality. Finally, the second universality must also be obtained. None of this has yet been accomplished. For instance, the suggestion has been made that  $g(\tau)$  is determined by the way clusters of free volume cells are distributed according to percolation theory.<sup>62</sup> However, these con-

cepts are almost certainly not appropriate in systems such as spin glasses or covalently-bonded solids, and thus it is not general enough for the first universality. In addition, there is not even a hint of second universality.

Over the years, there have been different variations of relaxation models that rely on the diffusion of some sort of defect.<sup>63</sup> In addition to the defects there are relaxing entities (e.g. dipoles). The dipoles are pictured as being frozen and they can relax only when the diffusing defects reach them. Specialized versions of this have obtained the form (1.1) in certain time regimes with a particular value of the exponent  $n$  (e.g. 1/2).<sup>64,65</sup> Such particular exponents can be traced back to the assumption of specific mechanisms, for example the diffusion properties of classical Brownian motion (i.e. root mean square position  $\sim t^{1/2}$ ). The defect diffusion approach has most recently been generalized within the framework of continuous time random walk (CTRW).<sup>66</sup> In CTRW, the diffusing defect has a waiting time probability density  $\psi(t)$  which allows the defects to wait between hops. It has been suggested that the waiting distribution should be chosen as a power law in time at long times,  $\psi(t) \sim t^{-1-\alpha}$ , because then the defect diffusion boundary value problem can be arranged to result in a relaxation of the form (1.1) with  $\alpha=1-n$ . This allows more general values for the exponent  $n$ , but the problem of the power law of time in  $\phi(t)$  has simply been replaced by the problem of a power law in  $\psi(t)$ . No justification for this form of  $\psi(t)$  and its universality across many different processes and materials has been given. Choosing  $\psi(t)$  arbitrarily is on a similar level to choosing  $W_n$  in (3.6) arbitrarily. No physical insight or predictions result. In addition, the second universality does not fit into such a picture. The reliance on a diffusing defect is not in itself satisfactory because such diffusing defects are not present in some systems which follow the first and second universalities (e.g. spin glasses). Therefore the mechanism would not be general enough even if the physics was satisfactory. Also, there exist systems such as migrating ions in glasses in which there are only diffusing particles and no second relaxing entity (i.e. dipoles). In these cases, the observed diffusion of the ions through conductivity relaxation is easily shown to be totally inconsistent with the form  $\psi(t) \sim t^{-1-\alpha}$ . The decay of the electric field due to the migration of the ions would be predicted by the defect diffusion model to be simply  $t^{-1-\alpha}$ , but as mentioned earlier the experiments find<sup>12,13,2</sup> that the electric field decays according to the fractional exponential (1.1). The fractional exponential is observed in the migration relaxation of the charged carrier.

There are still other proposals for dealing with the fractional exponential form (1.1) but which do not address the first and second uni-

versalities. Let us instead discuss the current physical understanding of how a dynamical system relaxes and how this might be modified by the properties of the actual material systems of interest (i.e. polymers, glasses, spin glasses, etc.) to give rise to the observed behavior (i.e. eqs. (1.1) and (1.2)). As mentioned at the beginning of this section, experimental measurements indicate that there are still vestiges of a single underlying relaxation process in the observed macroscopic behavior. This was consistent with the intuitive idea that a relaxing mode would be slowed down by coupling to its surroundings. The amorphous materials of current research interest have well-defined short range order and provide an appropriate setting for a well defined relaxation mode interacting with a complex environment. Then what is the physics of relaxation and what is the physics of complex environments?

The dynamics of a physical system is described on a fundamental level by Hamilton's equations of motion for classical mechanical systems or by Schrödinger's equation for quantum systems. These equations are totally reversible and do not describe dissipative behavior. The effort to understand the irreversible macroscopic behavior of a system which is governed by reversible microscopic equations of motion has a long history. Although questions still remain, a certain degree of understanding<sup>67</sup> has been achieved. In the 1870's, Boltzmann obtained an irreversible kinetic equation for a classical dilute gas by supplementing the dynamical laws with a stochastic mechanism: the "Stosszahlansatz." This is the assumption that correlations in the motions of the molecules of the gas are lost between each collision. This is similar to the repeated random phase assumption used by Pauli<sup>68</sup> in 1928 to derive an irreversible equation for a quantum mechanical system. The repeated randomness assumptions work roughly as follows.<sup>69</sup> For a classical system with N particles, the microscopic state of the system is described by the coordinates  $q_i$  and momenta  $p_i$ , where  $i=1, \dots, 3N$  in three dimensions. Using Hamilton's equations for the  $q_i$ 's and  $p_i$ 's, the rate of change of a macroscopic quantity  $\phi(q_1, \dots, p_{3N})$  can be found from:

$$\dot{\phi} = \sum_i \left( \frac{\partial \phi}{\partial q_i} \dot{q}_i + \frac{\partial \phi}{\partial p_i} \dot{p}_i \right) \quad (3.9)$$

The right hand side of (3.9) is a function of the  $6N$  coordinates and momenta and if two of these are eliminated in place of  $\phi$  and the energy (which is a constant of the motion), we may write

$$\dot{\phi} = f(\phi; x_i) \quad , \quad (3.10)$$

where the  $x_i$  represent the remaining variables. Since  $\phi$  is a macroscopic variable, it varies much more slowly than any of the  $x_i$ , and during some time interval  $\Delta t$  it may be possible for the  $x_i(t)$  to run through practically all their pos-

sible values while  $\phi(t)$  remains almost constant. In this case, the time integral in the solution of (3.10) can be replaced by an average over that part of phase space consistent with the given values of  $\phi(t)$  and the energy:

$$\phi(t+\Delta t) - \phi(t) = \Delta t \langle f(\phi(t); x) \rangle_{\phi} = \Delta t F(\phi(t)) \quad (3.11)$$

The use of the phase space average requires that the  $x_i$  vary sufficiently randomly at each time  $t$  and is the same as a repeated randomness assumption. If  $F$  is now a linear function of  $\phi$  (e.g.  $F(\phi) = -\phi/\tau_0$ ), then a simple exponential decay will result. These arguments can also be formulated in terms of a transition probability  $W(\phi'|\phi)$  which gives the probability of  $\phi$  changing its value to  $\phi'$  during the time interval  $\Delta t$ . The probability distribution  $P(\phi, t)$  for the value  $\phi$  at time  $t$  then obeys:

$$\frac{\partial P(\phi, t)}{\partial t} = \int d\phi' [W(\phi|\phi')P(\phi', t) - W(\phi'|\phi)P(\phi, t)] \quad (3.12)$$

This is referred to as a master equation. The decay law for  $\phi$  can be obtained by averaging over  $P(\phi, t)$ .

Repeated randomness assumptions have been criticized on physical grounds and in fact it has been demonstrated that the repeated randomness assumption can hold at all times only if the system is in equilibrium.<sup>70</sup> Repeated randomness was an attempt to quantify the behavior expected to give rise to dissipation when a macroscopic variable  $\phi$  interacts with the rest of the degrees of freedom of the system,  $x_i$ . The rest of the system is usually referred to as a heat bath and the physical situation is expected to be governed by two factors: (i)  $\phi$  changes on a time scale which is longer than any associated with the heat bath; (ii) the high number of degrees of freedom of the heat bath allow us to assume that its statistical properties are not affected by the interaction with  $\phi$ . The repeated randomness assumption was not a completely satisfactory way of including those elements. In 1955 and subsequent years, van Hove<sup>70,71</sup> developed a more refined way to implement the ideas in (i) and (ii). He considered a Hamiltonian  $H_0$  coupled to a potential  $V$  so that the total system is:

$$H = H_0 + \lambda V \quad (3.13)$$

Instead of assuming repeated randomness, van Hove assumes randomness only at the initial time and in addition uses two limiting procedures: (i) the weak-coupling limit  $\lambda \rightarrow 0$  in which the time is rescaled in such a manner that  $\tau = \lambda^2 t$  remains finite (this takes care of physical expectation (i) above) and (ii) the infinite volume limit in which the spectrum of  $H_0$  becomes continuous (this takes care of physical expectation (ii) above). We can see how this works by looking at one of the simplest possible classical systems, that of a one-dimensional line of



2N+1 particles interacting by harmonic forces<sup>72</sup> as in Fig. 6(a). The Hamiltonian is given by

$$H = \sum_i \frac{1}{2} \frac{p_i^2}{M_i} + \frac{1}{2} \sum_{i,j} q_j A_{ji} q_i \quad (3.14)$$

where  $M_i$ ,  $p_i$ , and  $q_i$  are the mass, momentum, and displacement of oscillator  $i$  and  $A_{ij}$  is the "spring constant" connecting oscillator  $i$  and  $j$ . Let us make the oscillator at the origin heavier than the others and choose:

$$\begin{aligned} M_i &= 1, & i \neq 0 \\ M_0 &= M \end{aligned} \quad (3.15)$$

We will look at the decay of the momentum correlations of the heavy particle as it interacts with the heat bath consisting of the large number of other rapid, light oscillators. The relaxing variable in this example is the momentum autocorrelation of the heavy particle:

$$\phi(t) = \langle p_0(0) p_0(t) \rangle \quad (3.16)$$

where  $\langle \rangle$  indicates an average over the canonical distribution  $\exp(H/kT)$ . This corresponds to van Hove's initial randomness assumption. Well, our system (3.14) is nothing but a bunch of harmonic oscillators, so we can easily solve for (3.16) exactly in terms of oscillatory functions. The solution is:

$$\phi(t) = \phi_0 (\cos \sqrt{B}t)_{00} \quad (3.17)$$

which is the 0-0 element of the matrix  $\cos \sqrt{B}t$ , where  $B_{jk} = (M_j M_k)^{-1/2} A_{jk}$  and  $\phi_0 = M/kT$ .

It is certainly reasonable that the response of the heavy particle to the other oscillators is periodic, but how can this system ever show dissipative effects? This will happen on the proper time scale when the light oscillators are made to form a proper heat bath. This is accomplished by carrying out van Hove's

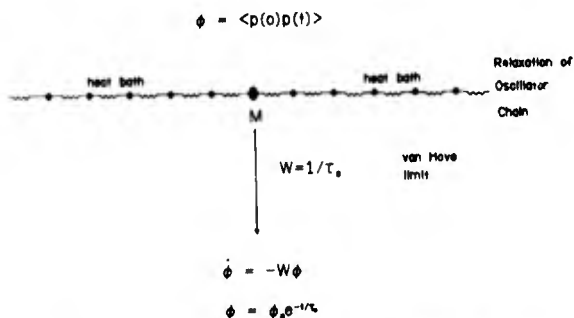


Fig. 6(a). Illustration of a simple relaxing system: a heavy particle of mass  $M$  in a heat bath of harmonic oscillators. The momentum autocorrelation of the heavy particle  $\phi$  relaxes as a single exponential as the number of heat bath particles becomes large and the mass  $M$  increases (i.e. van Hove's limits).

limiting procedures. First, the weak coupling limit corresponds to making the mass of the heavy particle arbitrarily large. Then we can introduce a time scale  $\tau = t/M$  which is to remain finite as  $t \rightarrow \infty$ ,  $M \rightarrow \infty$  (i.e. here  $\lambda$  in van Hove's problem corresponds to  $M^{-1/2}$ ). On the original time scale, an infinitely heavy particle would not react at all to interaction with the other oscillators. Second, the infinite volume limit corresponds to making the number of particles on the chain (i.e. in the heat bath) arbitrarily large. As  $N \rightarrow \infty$ , the period of the cycles in (3.17) become enormously large and the oscillator spectrum becomes continuous allowing  $\phi$  to approach zero as  $\tau \rightarrow \infty$ . The van Hove limits are easily implemented and give:

$$\begin{aligned} \phi &= \lim_{\substack{M \rightarrow \infty \\ t \rightarrow \infty \\ t/M = \tau}} \phi_0 (\cos \sqrt{B}t)_{00} = \lim_{M \rightarrow \infty} \phi_0 (\cos M \sqrt{B}t)_{00} \\ &= \phi_0 \exp(-\tau/\tau_0) \end{aligned} \quad (3.18)$$

$\phi$  then obeys:

$$\dot{\phi} = -\frac{1}{\tau_0} \phi \quad (3.19)$$

Here, the relaxation time  $\tau_0$  can be related explicitly to the frequency spectrum of the matrix of spring constants  $A_{ij}$ . In fact, the  $A_{ij}$  can be arbitrary (i.e. nearest-neighbor, long-range, etc.) except insofar as the resulting  $\tau_0$  should be non-zero and finite. In the general case of the van Hove problem (3.13),  $\tau_0$  would be given by a "Golden Rule" type of formula.

This is the way in which relaxation is currently understood. Of course there continues to be a great deal of work on alternative ways to understand relaxation. The van Hove limits specify at least one way of how a model system can be arranged so that a macroscopic variable decays with a well-defined relaxation time by way of a heat bath. This picture of relaxation apparently does not quite correspond to many materials of interest because we do not yet see how the observed relations (1.1) and (1.2) fit in except for the case when  $n=0$ . However, at least part of the situation must involve a heat bath in the sense of van Hove because the experiments indicate via (1.2) the existence of a well defined relaxation time  $\tau_0$ . In fact, the value of  $n$  can be altered by modifying the structure of the sample. For example,<sup>2,73-75</sup> the value of  $n$  from ultrasonic and hypersonic data on the molten salt  $0.6\text{KNO}_3 - 0.4\text{Ca}(\text{NO}_3)_2$  is observed to decrease from 0.65 to 0 as the temperature is increased between 105°C and 200°C. The value of  $n$  remains zero at still higher temperatures and the  $\tau_0$  can be described by a single temperature activated form,  $\tau_0 = \tau_\infty \exp(E_A/kT)$ , where an infinite temperature extrapolation gives a value for  $\tau_\infty$  which can be

identified with an infrared absorption band. Below 200°C, the temperature dependence is non-Arrhenius and can be described by a large effective temperature dependent activation energy.

$E_A(T) > E_A$ . Thus, this material changes from a sluggish dispersive regime at low temperatures to a high fluidity regime at high temperatures as  $n$  decreases from 0.65 to 0. This example is described further in the next section. In addition, values of  $n$  indistinguishable from zero are measured in materials such as simple liquids (e.g. water). This is an indication that the new elements in the relaxation picture which produce the non-zero  $n$ 's in (1.1) and (1.2) are related to the material structure containing the relaxing mode. As we discussed qualitatively before, the relaxing mode is affected by its coupling to the environment.

The physics of relaxation must then be discussed in conjunction with the physics of complex environments. How do we go about including the complex environments? The situation demands that we have more than just a macroscopic variable and a van Hove heat bath. Perhaps the heat bath in many of these materials is actually more complicated than demanded by van Hove. Many workers, including van Hove, have examined what happens in more general situations when the van Hove limit assumptions are not strictly enforced.<sup>76-80</sup> This work had led to the generalized master equations which are of the form (3.12) but with a memory kernel factor  $K(t-t')$  and an extra integral over  $t'$  on the right hand side. However, none of this type of work has led to any hint of first and second universalities.

As mentioned before, the real experimental situation does seem to at least partly involve a real van Hove limit. We should let the properties of the complex environments in these materials dictate to us how the relaxation picture should be altered. However, this appears to be difficult. How do we properly include disorder to form a complex environment for the relaxation mode? Instead of conductivity in a crystalline solid, we want to consider conductivity in a glassy solid. Instead of oscillations of a single polymer chain, we want to consider oscillations of a chain in an entangled network of polymer chains. How do we modify this problem to form the proper analog of the glassy conductor or the entanglement network? Above, we considered the relaxation of a heavy particle in a chain of oscillators. How do we quantify a "glass" of oscillator chains? Can we replace (3.14) with a Hamiltonian which properly includes the disorder so that when the macroscopic variable, the heat bath and the disorder are all sorted out and a van Hove limit taken, the first and second universalities result? This approach seems harrowing indeed. The Hamiltonian describing a glassy conductor would be quite different in detail from the Hamiltonian describing the entangled polymer network,

yet the macroscopic variable in both are described by the same equations (1.1) and (1.2). The direct Hamiltonian approach must involve an enormous amount of superfluous information for the relaxation behavior. The Hamiltonian approach may be at the limits of its usefulness in the present situation.

However, all is not lost. Indeed, the answer here is not to write down a Hamiltonian at all for the situation of complex environments. There does in fact exist a property of complex systems, independent of structural details within limits to be described below, which contains precisely the modification of relaxation necessary to obtain the first and second universalities. In this approach, the enormous amount of superfluous information mentioned above for the direct Hamiltonian approach is effectively buried in the material dependent parameters  $n$  and  $\omega$  which appear in (1.1) and (1.2). It doesn't matter whether we had tried to write down the Hamiltonian for a glassy conductor, a polymer entanglement network, or indeed a "glass" of oscillator chains. The modifications to the van Hove relaxation picture will be the same except for the values of  $n$  and  $\omega$ . The relevant property of complex systems which is active in modifying the van Hove picture of relaxation to the first and second universalities is the character of their low energy excitations. Excitations of any kind respond only over some particular energy or frequency range. For instance, a simple harmonic oscillator responds only near its resonance frequency. A very large class of complex systems have excitations which respond at very low frequency and these excitations are distributed in a particular way which can be characterized as follows. Define  $P(\omega)d\omega$  as the probability of the complex system responding at frequencies between  $\omega$  and  $\omega+d\omega$ . The low energy excitations of the complex systems have the property that:

$$P(\omega) \propto \omega, \text{ as } \omega \rightarrow 0 \quad (3.20)$$

As we will discuss below, the existence of the excitations with the property (3.20) is sufficient to modify the van Hove relaxation picture to that of the first and second universalities. The existence of these excitations is due to the complexity and disorder present in the materials obeying (1.1) and (1.2). This approach is successful in short-circuiting the enormous difficulties of the direct Hamiltonian method because the complexity and disorder are now controllable. As mentioned earlier, most of the systems of interest do not have long range order but do retain some short range order. Outside the short range order, the part of the disorder which controls the form of the first and second universalities is the frequency response of the set of low frequency excitations. All other aspects of the disorder will end up in the parameters  $n$  and  $\omega$ . To get more of a feeling for what  $P(\omega)$  means, consider first a simple system such as an L-C oscillator circuit. This can be excited near its resonant

frequency which is determined by the values of its inductance  $L$  and capacitance  $C$ . Suppose now we hook several such circuits together, perhaps with different  $L$ - $C$  values. The system will now have several resonance frequencies and these can be computed in terms of the eigenvalues of a matrix representing the circuit as constructed from Kirchoff's laws. The values of the resonance frequencies for the combined circuit will be different from the resonance frequencies of the individual circuits. These values depend on the manner in which the circuits are coupled together (e.g. series with capacitance shunt, mutual inductance coupling, etc.). Next, more and more circuits are added so that the number of resonance frequencies of the system increases. These frequencies begin to become rather difficult to compute directly as the size of the circuit matrix becomes unmanageable. At this point we may be tempted to set this problem up on a computer. However, as the complexity of the circuit continues to increase we reach a stage where even a direct computer solution is not attractive. With increase in complexity, we may not even have full control over the precise values of  $L$  and  $C$  which are added to new portions of the circuit system. The circuit network can now be considered as a large-scale many-body system. The number of resonance frequencies is so large that it is now more important to know the distribution of this frequency spectrum rather than the individual values. A probability distribution can be defined which contains statistical information about the system response frequencies. This is just the  $P(\omega)$  we defined above and this approach will be just as useful for materials such as glasses as it is for actual complicated circuits. The usefulness of this approach lies not only in the replacement of the explicit frequencies of response with a probability distribution, but also in the fact that the low frequency behavior of these distributions, Eq. (3.20), is nearly system independent. As we will see, this is a reflection of the existence of short-range order and the lack of special symmetries in the system.

The property (3.20) is important because if we drive the system with strength  $V$ , the average number of excitations which respond is:

$$\bar{N} = \mathcal{N} \int_0^{\omega_c} P(\omega) \left| \frac{V}{\omega} \right|^2 d\omega, \quad (3.21)$$

where  $\mathcal{N}$  is the total number of modes and the upper cutoff  $\omega_c$  is imposed by the physical system. Condition (3.20) means that the number of modes which respond diverges logarithmically. This is sometimes called infrared divergence. This rather unusual behavior means that large numbers of low frequency modes can be easily excited. The effect of this on relaxation is profound.

As we will discuss below, low frequency modes obeying (3.20) exist in an enormous class of complex systems. This generality is the root of the universal properties of relaxation. They

simply cannot be avoided unless the system is arranged in a special way. Suppose a primary species such as a polymer chain or an ion or the heavy particle in our oscillator chain example of Fig. 6(a) is part of a complex system. Initially the low frequency modes will be in equilibrium because ordinarily the experimental temperatures used will be such that  $kT$  is much greater than any excitation energy of these modes. The primary species is thrown out of equilibrium and as relaxation begins it starts to make transitions on the time scale of  $\tau_0$ . These sudden transitions create a potential  $\phi$  for the low frequency modes and they become excited and deexcited. The low frequency modes thus move out of equilibrium. The process of relaxation corresponds to an increase in entropy for the entire system. However, before coupling to the primary species, the entropy associated with just the low frequency modes was at its maximum because they were initially in equilibrium. As they are excited and deexcited by the coupling, the entropy of the low frequency mode can therefore only decrease with time. The result of this is that the increase of entropy of the primary species is slowed down as the relaxation proceeds. This is a slowing of the relaxation process and it occurs because now the relaxation is not complete until both the primary species and the low frequency modes return to equilibrium. The property (3.20) ensures the divergent response of the low frequency modes and they continue to be excited and deexcited throughout the relaxation. This guarantees that they will never become part of the heat bath and in this sense they are immune to the van Hove limit.

The constant relaxation rate  $W \equiv 1/\tau_0$  (e.g. see (3.19)) becomes modified to a time dependent relaxation rate  $W(t)$ . This takes the form

$$W(t) = (1/\tau_0) \exp(-\Delta S(t)), \quad (3.22)$$

where  $\Delta S(t)$  is the magnitude of the entropy change of the low energy modes. This can be considered as similar to an activated rate form (i.e.  $\tau_0 = \tau_\infty \exp(\Delta F/kT) = \tau_\infty \exp[(\Delta E/kT) - (\Delta S/k)]$ ).

A calculation<sup>1,81</sup> of the response gives the expression

$$\Delta S(t)/k = \left| V \right|_{av}^2 \mathcal{N} \int_0^{\omega_c} P(\omega) \frac{(1 - \cos \omega t)}{\omega^2} d\omega \quad (3.23)$$

The  $\cos \omega t$  factor accounts for the excitation and deexcitation of the modes. In this expression the crucial assumption has been made that the coupling potential  $V$  is independent of the mode excitation frequency. This is physically reasonable for a complex system containing randomness and the advantages gained are enormous. If  $V$  is independent of  $\omega$ , it can be taken outside the integral and  $V_{av}$  is the average of the potential over all sites. This immediately factors the problem into a structural part  $V_{av}^2$  and a time dependent part. As we shall see this

allows all the structural information to be lumped into a single parameter. If this had not been possible, the actual details of the material structure would have to be confronted in the calculation of the relaxation rate. The cutoff  $\omega_c$  in (3.23) is the maximum frequency for which the modes have the property (3.20). This cutoff frequency is then definitely system dependent and in fact we will discuss how it is determined in more detail below. The modes above  $\omega_c$  will not have the divergent response which keeps the low frequency modes out of equilibrium and thus they do not contribute to the time dependence of the relaxation rate. The factoring of the structural and time dependences in the problem allows us to exploit the low frequency property (3.20) and define:<sup>1</sup>

$$|V|_{av}^2 \mathcal{P}(\omega) \equiv n\omega \quad (3.24)$$

Here we see the first appearance of the exponent  $n$  which plays such a prominent role in the first and second universalities (1.1) and (1.2). From (3.24), the quantity  $n$  sets the coefficient for the response probability (3.20) in a manner that depends on the coupling strength to the low frequency modes  $|V|_{av}^2$  and the density of the low frequency modes. As claimed above, all the information for the structure averaged interaction potential and the density of the low energy modes are buried in a single parameter  $n$ . The value of  $n$  is determined both by how many modes there are and how strongly we couple to them. The cutoff frequency  $\omega_c$  is also determined by structural details. Circumstances in this set of very difficult problems have allowed us to write down (3.24) and the result is a remarkable simplification of the problem. The payoffs are enormous and we will now complete the steps leading to the first and second universalities. With (3.24), then (3.23) becomes

$$\Delta S(t) = n \int_0^{\omega_c} d\omega \frac{(1 - \cos \omega t)}{\omega} \quad (3.25)$$

At long times such that  $\omega t \gg 1$ , we can evaluate (3.25) using formula 3.782-1 in Gradshteyn and Ryzhik's book of integral tables.<sup>82</sup> The result is

$$\Delta S(t) = n \ln(\omega_c t) + \gamma \quad (3.26)$$

where  $\gamma \cong 0.577$  is Euler's constant. For  $\omega t \gg 1$ , the time dependent relaxation rate (3.22) in the presence of coupling to the low frequency modes then takes the explicit form:

$$W(t) = (1/\tau_0) (\omega_c t)^{-n} \quad (3.27)$$

For ease of notation we have absorbed the factor  $e^\gamma$  into the cutoff frequency  $\omega_c$ :  $\omega_c \rightarrow \omega_c e^\gamma$ . The modes with frequencies  $\omega > \omega_c$  can in general contribute an additional time independent factor. This factor can be identified as the shift in entropy  $\Delta S_\gamma$  of the TLS (and higher modes) and

will modify  $W(t)$  by a constant factor  $\exp(-\Delta S_\gamma/R)$ . Also for ease of notation, we will usually absorb this factor into  $\tau_0$ . We see in (3.27) that the relaxation rate slows down as the relaxation proceeds by an amount determined by  $n$ . The rate equation for the macroscopic variable is still determined by the heat bath and we can take the van Hove limits as before, but now the rate equation is modified from (3.19) to

$$\dot{\phi} = -1/\tau_0 (\omega_c t)^{-n} \phi \quad (3.28)$$

This can be immediately integrated as:

$$\phi(t) = \phi_0 \exp[-\int_0^t dt' (\omega_c t')^{-n}/\tau_0] \quad (3.29)$$

For situations in which the material dependent parameters  $n$  and  $\omega_c$  do not change on the time scale of the relaxation experiment, (3.29) is simply integrated to give:

$$\phi(t) = \phi_0 \exp[-(t/\tau_p)^{1-n}] \quad (3.30)$$

where the parameters  $n$ ,  $\omega_c$  and  $\tau_0$  determine the timescale  $\tau_p$  of the relaxation as:

$$\tau_p = [(1-n)\omega_c^n \tau_0]^{1/(1-n)} \quad (3.31)$$

These are of course the first and second universalities (i.e. see (1.1) and (1.2)). We see that they have emerged simultaneously from the time dependent rate (3.27) which was determined by coupling to low energy modes. This is illustrated schematically in Fig. 6(b) for a "glass" comprised of the heavy particle oscillator chains from our earlier example of Fig. 6(a). These are coupled expressions in that the same value of  $n$  appears in both. They predict a specific type of correlation between the timescale of the relaxation and the shape of the decay function. Both of these features are governed by the value of  $n$ . Although an accurate value of  $n$  cannot be determined on the basis of (3.24), the value of  $n$  can be measured by fitting data to (3.30) and then used to make predictions about the relaxation time (3.31) and its dependences. We discussed this briefly in the previous section, but the real power of the first and second universalities for coming to grips with real structural and dynamical problems is only appreciated by looking at examples of relaxation data in some detail. This will be done in the following section. The above relaxation model leading to the first and second universalities was developed<sup>1</sup> by one of us (K.L.N.) in 1978. It is interesting to note that the second universality was predicted by this model before any of the experimental confirmations. More recently, this same model has been described using the language of entropy decrease.<sup>81</sup>

Since the low energy modes with the property (3.20) play a crucial role we must ask what these modes really are and what is the evidence for their existence. In complex material systems, there is experimental evidence for the

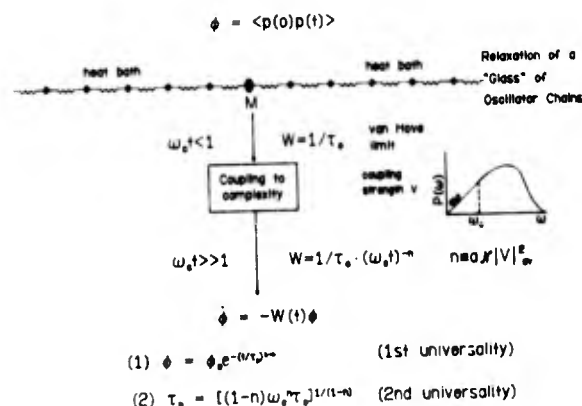


Fig. 6(b). Illustration of how the relaxation of Fig. 6(a) is modified to the first and second universalities when it is coupled to low frequency modes generic to complex systems. The probability distribution of the modes  $P(\omega)$  is nearly universal in shape, whereas the parameter  $n$  is system dependent and contains information about coupling strength and number of modes.

existence of excitations which respond at frequencies lower than typical phonon frequencies. These are the celebrated two level systems (TLS) proposed in 1972 by Anderson, Halperin and Varma<sup>83</sup> and independently by Phillips.<sup>84</sup> The TLS were required to explain anomalies in the low temperature thermodynamic properties of glasses, polymers, amorphous metals, semiconductors and most recently spin glasses, and they are now commonly believed to be an intrinsic property of disordered systems.<sup>85,86</sup> The evidence from experiments beginning with Zeller and Pohl<sup>87</sup> in 1971 and continuing to the present on specific heat, thermal conductivity and ultrasonic properties point overwhelmingly to the existence of low frequency modes (TLS) which are described by a response probability which is roughly independent of excitation frequency,  $P(\omega) \cong \text{constant}$ . This differs from the property (3.20) of the modes which give rise to the first and second universalities. However, the TLS thermodynamic experiments directly excite (i.e.  $\hbar\omega > kT$ ) the low frequency modes and not indirectly (i.e.  $\hbar\omega < kT$ ) via the coupling potential as in our relaxation picture. Due to experimental limitations, this direct excitation can only be performed down to temperatures of  $\sim 10^{-3}K$  and, more typically they are done in the range  $10^{-2}-1K$ . This corresponds roughly to excitation frequencies in the range  $10^8-10^{10} \text{ sec}^{-1}$ . Relaxation experiments typically involve much lower frequencies. Also, relaxation experiments are often done at higher temperatures. The TLS experiments probe only a limited portion and possibly a subset of the  $P(\omega)$  spectrum.

It is pertinent to ask what is the shape of  $P(\omega)$  if we continue to probe at lower frequencies. Although direct resonant excitation is

not presently possible at frequencies lower than about  $10^8 \text{ sec}^{-1}$ , there is a large body of indirect evidence that  $P(\omega)$  actually turns over and becomes linear in  $\omega$  as  $\omega \rightarrow 0$ . This comes from the actual examination of  $P(\omega)$  for complex model systems. Several distinct types of studies have been carried out and they all point to  $P(\omega) \propto \omega$  as  $\omega \rightarrow 0$ .

The first type of study was carried out by Wigner,<sup>88</sup> Dyson<sup>89</sup> and others,<sup>90,91</sup> beginning in the 1950's. They were concerned with the complex systems represented by large nuclei. A general framework was worked out to describe the excitation spectrum in statistical terms of a system which is completely random except for constraints imposed by certain general symmetries (e.g. time reversal invariance, etc.). Such a system is referred in their jargon as a Gaussian Orthogonal Ensemble (GOE) and this program of study is called Random Matrix Theory. The excitation distribution  $P(\omega)$  corresponding to GOE can be approximately described by:

$$P(\omega) = 2\pi(\omega/\Omega^2) \exp[-\pi(\omega/\Omega)^2] \quad (3.32)$$

This indeed has the property (3.20). One way to view an object such as (3.32) is as the classical limit of a distribution of spacings between a complex set of quantum energy levels. The limit  $\omega \rightarrow 0$  corresponds to examining quantum energy levels which are very closely spaced. That the probability  $P(\omega)$  vanishes as the levels approach implies that there exists a level repulsion and the levels do not want to become degenerate. This property can be understood in real complex materials as reflecting the existence of short range order. Level repulsion requires at least some correlation and this would not be present in a completely random system. This is analogous to the splitting of resonance frequencies observed when two or more L-C circuits are hooked together as in the complex circuit example mentioned earlier. However, we emphasize that  $P(\omega)$  is a completely classical object and no quantum effects are involved in the relaxation phenomena of concern here. Ensembles other than GOE result if some of the symmetries are relaxed (e.g. breaking of time reversal invariance) and these have different  $P(\omega)$ . However, GOE is appropriate for most condensed matter physics except, for example, perhaps at high magnetic fields.

The second line of studies of complex systems involve general arguments developed by Berry and by Pechukas. Berry<sup>92-95</sup> has utilized a 1929 theorem due to von Neumann and Wigner<sup>96</sup> which specifies the conditions for the occurrence of accidental degeneracies in excitations. He was able to show that, in the absence of special symmetries imposed on the complex system, the response probability obeys  $P(\omega) \propto \omega$  as  $\omega \rightarrow 0$ . Pechukas<sup>97</sup> has used general properties of the spatial distributions of the wave functions cor-

responding to quantum systems whose classical behavior is sufficiently complex. He is able to use these properties along with the Schrödinger equation to demonstrate that  $P(\omega)$  in the classical limit is identical to that found by GOE random matrix theory. In particular,  $P(\omega) \propto \omega$  as  $\omega \rightarrow 0$ . "Sufficiently complex" classical systems are essentially those which are not constrained by special symmetries.

The third line of work on complex systems involves direct calculations of  $P(\omega)$  on models which are simple enough to solve (analytically or numerically) but which exhibit very complex classical behavior. Many such systems have now been studied and the recent literature is full of these examples.<sup>92-95,98-101,52</sup> These include billiard systems contained within destabilizing boundaries, models of molecules with nonlinear couplings, and many others. All these direct calculations are in agreement with GOE random matrix theory. This agreement holds not only for  $\omega > 0$  but over the whole range (3.32).

The GOE form (3.32) for  $P(\omega)$  suggests a very appealing physical correspondence. This  $P(\omega)$  is linear in  $\omega$  at the lowest frequencies corresponding to the low frequency relaxation modes. It then turns over and is approximately constant for some range of frequencies corresponding to the flat spectrum measured by TLS experiments. The location of the flat regime is determined by the average excitation frequency  $\Omega$ . Finally, it falls off exponentially as we go up to phonon frequencies and beyond. This suggests that the TLS are merely the tip of the iceberg and all the low frequency relaxation modes with property (3.20) lie below this. The upper cutoff frequency  $\omega_c$  of the low frequency modes can then be identified with the lower end of the TLS spectrum. This suggests that  $\omega_c \sim 10^8 - 10^9$  sec<sup>-1</sup> and this is consistent with fits to the first and second universalities as we discuss in the following section.

The structural identification of the low frequency modes is another matter. This has been a difficulty for the TLS for over a decade now.<sup>85,86</sup> They are presumably composed of a large number of atoms, molecules, bonds, etc., which have configurations of two nearly equivalent local minima accessible to them. The movement from one local minimum to the other involves small rearrangements of large numbers of bonds, molecules, etc., so that the change between configurations is a slow process.

It is well accepted that a detailed quantitative description of the structure in glasses, polymers, and amorphous materials is a difficult problem, and this includes the structural realization of the low frequency modes as well. However, the relaxation model described above is able to actually take advantage of the presence of disorder to circumvent this problem. The properties of the randomness outside the short range order allowed the relaxation problem to be

factored into a structural part which is sensitive to the details of the system and a time-dependent part which is not sensitive to the details of the system. The observed macroscopic relaxation laws (1.1) and (1.2) give a succinct description of the relaxation data and the interrelated behavior of the decay function and the relaxation timescale. The data suggest that there is a fundamental significance to this way of parameterizing the relaxation data. The forms of (1.1) and (1.2) have a large degree of universality but the specific values and functional dependences of  $n$ ,  $\omega_c$  and  $\tau_0$  depend on the relaxation process and material.<sup>o</sup> The physical reasons for the simultaneous emergence of the particular parameterizations given by (1.1) and (1.2) can be understood within the above model of relaxation. However, it is to be emphasized that the first and second universalities impose stringent criterion for any model of relaxation. The degree to which (1.1) and (1.2) are embedded in the relaxation data is only appreciated by looking at specific examples of the second universality and the predictions which follow from its application.

### Second Universality

As mentioned in the section on the first universality, the use of the fractional exponential (1.1) has a long history even though the universal nature of this function was not appreciated until recently. However, the second universality (1.2) does not have a long history and was first predicted by one of us (K.L.N.) in 1979.<sup>1</sup> The universal aspects of (1.2) were subsequently verified within relaxation data. The second universality gives a physical meaning to the measured effective relaxation time  $\tau_p$  by relating it to the microscopic fundamental relaxation time  $\tau_0$  in a well-defined and quantitative manner.<sup>o</sup> The quantitative relation between  $\tau_p$  and  $\tau_0$  involves the same structure dependent parameter  $n$  that appears in the first universality. For convenience, we reproduce the first and second universality relations here.

$$\phi(t) = \phi_0 \exp[-(t/\tau_p)^{1-n}] \quad (4.1)$$

$$\tau_p = [(1-n)\omega_c^n \tau_0]^{1/(1-n)} \quad (4.2)$$

where  $\omega_c t \gg 1$  and  $0 < n < 1$ . Equations (4.1) and (4.2) are coupled relations and the same value of  $n$  appears in each equation. They describe a very specific correlation between the timescale of the relaxation and the shape of the time decay function. Such correlations will also show up in the dependences of the relaxation time on physical variables (see e.g. (3.2)).

An example of the second universality was mentioned briefly at Eqs. (3.3)-(3.5). This was the situation where  $\tau$  was temperature activated with an energy barrier  $E_A$  as in (3.3). The second universality then predicts that interaction with the complexity of the system will result in an observed effective relaxation time  $\tau_p$  described by (3.4). If the experimentally

observed values of  $n$  obtained by fitting (4.1) to data are found to be independent of temperature, then the second universality predicts an effective activation energy  $E_A^* = E_A / (1-n)$  (see (3.5)). Note that there is really no physical energy barrier with activation energy  $E_A^*$  that can be identified within the material structure. The real physical energy barrier has activation energy  $E_A$  and the experimentally observed energy  $E_A^*$  in the Arrhenius factor arises from  $E_A$  and the effects of its coupling with the complexity of the system as represented by  $n$ . As the relaxation proceeds to cross the energy barrier  $E_A$ , it is hindered by coupling to the low frequency modes of the system and the result is that this can be described as if the relaxation process had to cross a larger effective energy barrier of magnitude  $E_A^* = E_A / (1-n)$ .

The most detailed documentation of this phenomenon is in the case of dispersive hole transport in  $a\text{-SiO}_2$ , where there is general agreement on the physics of the hole transport mechanism which determines the properties of  $\tau_0$  for this situation. The hole in the non-bonding 2p orbital of an oxygen forms a small polaron and hole transport is via small polaron hopping. The dispersive hole transport in  $a\text{-SiO}_2$  was first observed by McLean et al. at times longer than  $10^{-4}$  sec. Hughes later performed high precision time resolution hole-transport. He has shown that after an initial very short time interval following the X-ray pulse, the hole relaxes to form a small polaron (self-trapped) in the non-bonding 2p orbital of an oxygen. Transport at times shorter than  $10^{-6}$  sec takes place by the hopping of the small polaron from one oxygen to another. Its mobility has magnitude, temperature dependence and electric field dependence all in agreement with the prediction of small polaron theory. In particular, the mobility is low, thermally activated (with activation energy  $E_A \approx 0.14$  eV, see Fig. 7) at temperatures above one third the Debye temperature and breaking to a non-activated behavior at lower temperatures. For times greater than about  $10^{-5}$  sec, dispersive transient current is observed with:

$$I(t) \sim t^{-n} \text{ for } t < t_T \quad (4.3)$$

and

$$I(t) \sim t^{-(2-n)} \text{ for } t > t_T \quad (4.4)$$

where  $0 < n < 1$  and  $t_T$  is the "transit time." The dependence of  $t_T$  on electric field  $E$  and sample thickness  $L$  through  $t_T \propto (E/L)^{-1/(1-n)}$  is also observed. The temperature dependence of  $t_T$  (Fig. 7) is thermally activated above 200 K and can be fit to a simple Arrhenius plot with activation energy  $E_A^* = 0.37$  eV. The large difference between  $E_A^*$  and  $E_A$  would seem to indicate that the transient transport mechanism is different from the earlier transport mechanism of small polaron hopping and in fact some workers have invoked the presence of structural defect traps

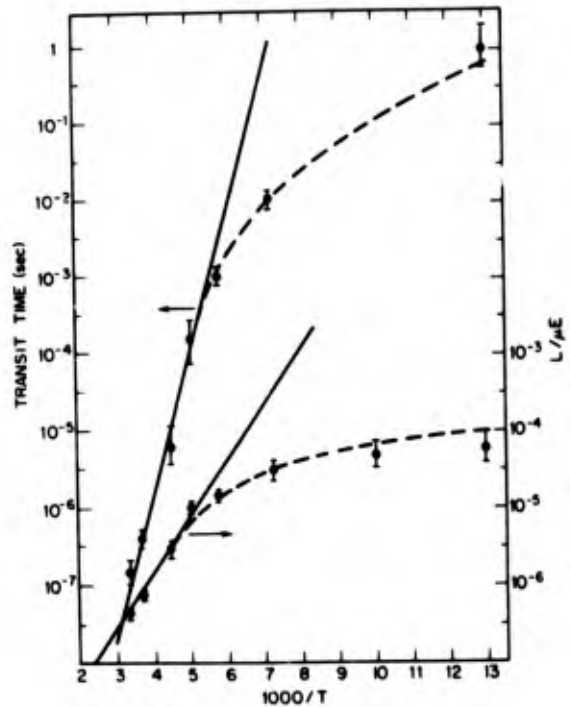


Fig. 7. Transit time  $t_T$  and  $L/\mu E$  of  $a\text{-SiO}_2$ .

The solid lines indicate Arrhenius behavior for  $T > 200$  K with activation energies 0.37 eV and 0.14 eV. At every  $T$ , the ratio of the local slope of the lower dashed curve to that of the upper dashed curve is  $(1-n) = 0.3$  (data of Hughes, replotted. See Ref. 103).

for this reason.<sup>104,105</sup> However, the hole transport dispersion in  $a\text{-SiO}_2$  is remarkably stable with temperature. The dispersion parameter was found by Hughes to have a constant value of  $n = 0.7$  for  $140\text{K} < T < 298\text{K}$ . This property rules out the mechanism of a distribution of trap depths for dispersive transport.

However, all of this data can be described by the first and second universalities.<sup>1,2,22,28,29</sup> If the carrier charge decays according to the first universality (4.1), the corresponding transient current can be calculated and it is found to have the form (4.3) and (4.4) in agreement with experiment. The observed value,  $n = 0.7$ , can then be used in the second universality to predict the relation between  $E_A$  and  $E_A^*$ , as well as the observed electric field and sample thickness dependence. The quantity  $E_A = (1-n)E_A^* = 0.3 \times 0.37 = 0.11$  eV is in good agreement with the directly measured small-polaron hopping activation energy of 0.14 eV. Such correlations are not expected from the tunneling/hopping among traps type of models for dispersive transport. Most remarkably, the second universality continues to hold for  $T < 200\text{K}$  where both the small polaron and dispersive transport become markedly non-Arrhenius with a decrease in the "local activation energy" as  $T$  decreases as given by  $\partial(\log t_T) / \partial(1/T)$ . In the

non-Arrhenius region, the local activation energies for the small polaron and dispersive transport as given by the local slopes in Fig. 7 are still quantitatively related by the factor of  $(1-n)=0.3$ . Thus even as the temperature dependence  $\tau_1(T)$  of the primary relaxation species (small polaron) changes its character, the predicted correlation between the shape of the decay function and the relaxation time scale remains. A true activated process is not required for the second universality. In addition to electronic transport in  $\alpha$ - $\text{SiO}_2$ , the first and second universalities quantitatively describe transport in chalcogenide glasses<sup>1,24,28,48</sup> including  $\alpha$ - $\text{As}_2\text{Se}_3$ ,  $\alpha$ - $\text{Se}$ ,  $\alpha$ - $\text{As}_2\text{S}_3$ , and  $\alpha$ - $\text{As}_2\text{Te}_3$ .

A quite similar correlation between activation energies is found in amorphous polymers below the glass transition temperature  $T_g$ . The most detailed study has been done on the  $\gamma$ -relaxation of chloral-polycarbonate which is a derivative of bisphenol-A-polycarbonate (BPA).<sup>39</sup> The physics of the relaxation is of course quite different from the small polaron hopping found in the electronic transport case. The primary relaxation species involved in the polycarbonate  $\gamma$ -relaxation has been identified by NMR techniques to involve phenylene ring rotation about the chain axis. Both NMR<sup>39</sup> and dynamic mechanical<sup>106</sup> relaxation measurements have been made on bulk polycarbonate. The dynamical mechanical data gave a  $G''(\omega)$  which can be described on the basis of (4.1) with  $n=0.8$ . The relaxation peak shifted with temperature in an Arrhenius manner with an activation energy  $E_A^* \approx 50$  kJ/mol. The  $T_g$  and  $T_g$  NMR data were also consistent with these values<sup>10</sup> of  $n$  and  $E_A^*$  and in addition gave a value for the Arrhenius prefactor of  $\tau_\infty^* = 2.29 \times 10^{-16}$  sec (see (3.4)).

On the basis of these data, the second universality would predict an activation energy for the fundamental phenylene ring motion of  $E_A = (1-n)E_A^* = 0.2 \times 50$  kJ/mol = 10 kJ/mol. This would be the activation energy in the absence of interaction with the bulk glassy polymer medium (e.g.  $n=0$ ). Available information on the isolated phenylene ring motion does in fact indicate an activation energy of about 10 kJ/mol.<sup>39</sup> This comes from spin relaxation studies on dilute solutions of polycarbonates. Measurements were made on 10 wt% solutions of four structural variations. In dilute solution, the low frequency excitations would be different from that in the solid and they are expected to have a weaker effect on the transition rate (see (3.27)) in dilute solution. The value of  $n$ , which is a measure of the density and coupling strength of the low frequency modes (see (3.24)), should be much decreased. Indeed, the measured activation energies were found to be 13 kJ/mol. in BPA solution and 15 kJ/mol. in chloral solution. This is consistent with values of  $n$  in these solutions of between 0.2

and 0.3, which indicates much reduced coupling compared to  $n=0.8$  in the bulk. Exact confirmation must wait for measurement of the value of  $n$  in these dilute solutions. If the coupling could be completely eliminated, the activation energy would be expected to be reduced to 10 kJ/mol. Hartree-Fock calculations of the various kinds of phenylene ring motion consistent with information derived from proton relaxation data also indicate an activation energy near 10 kJ/mol.<sup>107</sup>

These tests of the second universality have involved only predicted modifications by (4.2) of the exponent in an activated form for  $\tau_1$ . The prefactor will also be modified by the coupling to complexity and by comparing (3.3) and (3.4) with (4.2), we see that the prefactors are related by

$$\tau_\infty^* = [(1-n)\omega_c^n \tau_\infty]^{1/(1-n)} \quad (4.5)$$

The value of the frequency  $\omega_c$  was identified physically at end of the previous section with the lower end of the TLS spectrum or  $\omega_c \approx 10^7$  sec<sup>-1</sup>. Using this along with the measured values for  $n(=0.8)$  and  $\tau_\infty^*(=2.29 \times 10^{-16}$  sec), (4.5) predicts  $\tau_\infty = 2.3 \times 10^{-10}$  sec. This is a reasonable value for the preexponential for phenylene ring motion. Although the precise value of  $\omega_c$  was not independently measured for the present polycarbonate example, the TLS have been observed in a wide range of glassy and amorphous systems including amorphous polymers. An example where the value of  $\omega_c$  can be checked by other measurements is in dielectric data on the fast ionic conductor  $\text{Na}\beta$ -alumina. In this case, all the second universality parameters can be checked and the relation is quantitatively verified.<sup>30</sup> The second universality is quite successful in relating bulk dynamic behavior to molecular motions in terms of the low frequency modes of amorphous systems.

Below  $T_g$ , large scale polymer motions are frozen in and the temperature dependence of  $\tau_1$  is dominated by an activated term as in the above polycarbonate example. Sufficiently far above  $T_g$ , activated barrier terms can again dominate.<sup>8</sup> In the vicinity of  $T_g$ , the temperature dependence is more complicated and these deviations from Arrhenius behavior are often discussed using concepts such as free volume variation. For very flexible chain polymers which have low  $T_g$ 's, such as polyethylene and poly(dimethyl siloxane), the viscosity  $\eta$  is proportional to  $\exp(E_A^*/RT)$  throughout almost the entire temperature range in which viscosity measurements have been made. For less flexible polymers such as polystyrene and polycarbonate, the viscosity approaches or tends to approach the Arrhenius form only at the highest temperatures reached. Above  $T_g$ , the fast relaxation processes associated with more local motion, such as the  $\alpha$ ,  $\beta$ , and  $\gamma$  relaxations, quickly die



out. The remaining relaxation modes are associated with large scale flexing of polymer chains. The modes of such a flexible chain were discussed in the section on the first universality in terms of the Rouse bead and spring model as in Eqs. (2.6)-(2.8). There we demonstrated that the relaxation times of the Rouse modes depend on the product of the monomeric friction coefficient  $\zeta$  and the square of the number of monomers  $N$  in the chain (e.g. see (2.8)). The friction coefficient controls the major temperature dependence and the monomer number is proportional to the molecular weight  $M$  of the chain. Therefore the terminal relaxation time (i.e.  $i=1$  Rouse mode) can be written as the product of a temperature dependent factor and a molecular weight dependent factor:<sup>108</sup>

$$\tau_1 = F(M)\zeta(T) \quad (4.6)$$

where  $F(M) \propto M^2$  and  $\zeta(T) \propto \exp(E_A/RT)$  at temperatures sufficiently far above  $T_g$ . The Rouse model gives a description of polymer relaxation modes which have specific dependences on molecular weight and temperature (e.g. see (3.1)). For molecular weights below a characterizing critical molecular weight  $M_c$ , the Rouse model in fact gives a good quantitative description of the relaxation modulus, terminal relaxation time and viscosity including values for the prefactors.<sup>109</sup> The value of  $M_c$  depends on the particular polymer sample and indicates how long the polymer chains must be before entanglement with neighboring chains is important. A calculation of the relaxation modulus on the basis of (2.7) gives

$$G(t) = G_N^0 \sum_{i=1}^{\infty} \exp[-t/\tau_i] \quad (4.7)$$

where the plateau modulus  $G_N^0$  depends on molecular weight as  $M^{-1}$  for  $M < M_c$  in agreement with experiment. The steady-state flow viscosity is given by:

$$\eta = \int_0^{\infty} dt' G(t') = G_N^0 \sum_{i=1}^{\infty} \tau_i \approx G_N^0 \tau_1 \quad (4.8)$$

where the terminal relaxation time dominates the viscosity. The molecular weight dependence of the viscosity is then  $\eta \propto M^{-1} \times M^2 = M$ , or linear in the molecular weight for  $M < M_c$  in agreement with experiment.<sup>108,109</sup> At sufficiently long times (i.e. on the timescale of the flow viscosity), only the terminal relaxation survives and the modulus becomes:

$$G(t) \approx G_N^0 \exp[-t/\tau_1] \quad (4.9)$$

However when the polymer chains are sufficiently long,  $M > M_c$ , they no longer move independently but can strongly entangle with one another. A complex entanglement network is built up and the relaxation of the chains is dramatically changed. The interaction of a chain with its neighbors can be thought of roughly as occurring at "entanglement points"

where the chains cross. The critical entanglement molecular weight  $M_c$  is approximately equal to  $2M_e$ , where  $M_e$  is the average molecular weight between entanglement points.<sup>109</sup> The effects of chain entanglements on both the temperature and molecular weight dependence can be described<sup>35</sup> quantitatively using the first and second universalities which include the coupling to complexity by the parameter  $n$ . Note that the complexity of the entanglement network and its coupling to the Rouse mode is quite different from the complexity of the glass and its coupling to the  $\gamma$ -relaxation mode described above, although these are both examples of coupling to complexity in amorphous polymers. The values of  $n$  are not expected to be the same in these two situations. In fact, the degree of coupling may differ even between Rouse modes. The  $i=1$  terminal Rouse mode has the longest wavelength and it will intersect more entanglement points than the shorter wavelength (i.e.  $i>1$ ) Rouse modes. The  $i=1$  mode will then have stronger coupling to the complexity of the entanglement network and it should have a larger value of  $n$  than the other Rouse modes. The degree of cooperativity of the Rouse modes decreases with increasing  $i$ . Then (4.7) will be modified by entanglements to:

$$G(t) = G_N^0 \sum_{i=1}^{\infty} \exp[-(t/\tau_{p_i})^{1-n_i}] \quad (4.10)$$

$$\tau_{p_i} = \left\{ (1-n_i) \omega_c^{n_i} \tau_i \right\}^{1/(1-n_i)} \quad (4.11)$$

and

$$n_1 > n_2 > n_3 > \dots \quad (4.12)$$

This implies that  $\tau_{p_1} > \tau_{p_2} > \tau_{p_3} \dots$ . The viscosity

will again be dominated by the terminal relaxation time:

$$\eta \approx G_N^0 \frac{1}{1-n_1} \Gamma\left(\frac{1}{1-n_1}\right) \tau_{p_1} \quad (4.13)$$

At sufficiently long times, only the terminal relaxation contributes to the relaxation modulus:

$$G(t) = G_N^0 \exp[-(t/\tau_{p_1})^{1-n_1}] \quad (4.14)$$

The value of  $n_1$  is found by fitting (4.14) to terminal relaxation data. Figure 8 shows  $G''(\omega)$  data for a linear hydrogenated polybutadiene (HPB) entangled melt at 130°C and 190°C. The solid curve is a fit<sup>53</sup> on the basis of (4.14) and the fit is very good to the terminal regime with  $n_1=0.4$ . Examination<sup>35</sup> of all available data on nearly monodisperse linear polymer melts shows that (4.14) fits the terminal regime very

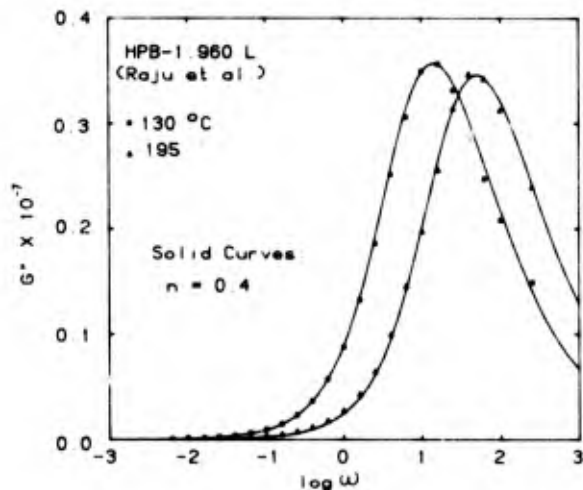


Fig. 8. Dynamic loss modulus of a linear hydrogenated polybutadiene at 130°C and 195°C (mol. wt. =  $1.8 \times 10^5$ ). The solid curves are fits to the data by the predictions of  $G''(\omega)$  that follow from (4.14) for a choice of  $n_1 = 0.4$  (data of Raju et al., replotted., J. Polym. Sci.: Polym. Phys. Ed. 17, 1223 (1979)). After Ref. 53.

well with  $n_1$  in the range 0.4-0.47. The value of  $n_1$  can then be used in the second universality to predict the temperature and molecular weight dependence of the terminal relaxation time  $\tau_{p1}$  or the viscosity (4.13).<sup>35</sup> Experimentally,  $G_N^0$  is independent of molecular weight for samples with  $M > M_c$  and thus does not contribute to the molecular weight of the viscosity in (4.13). Hence  $\eta$  and  $\tau_{p1}$  will have the same molecular weight dependence. The fundamental terminal relaxation time  $\tau_1$  of the underlying Rouse chain (4.6) can be related to  $\tau_{p1}$  by the second universality (i.e. substitute (4.6) into (4.11)):

$$\tau_{p1} \propto M^{1-n_1} \exp(E_A^*/RT) \quad (4.15)$$

where  $E_A^* = E_A/(1-n_1)$ .

Polyethylene is sufficiently flexible so that the high temperature Arrhenius region can be reached experimentally. In addition, polyethylene data are available from a large number of studies and thus it is a good choice for a test of the second universality in polymer melts. The flow activation energies can be measured from the viscosity while the value of  $n_1$  can be found from  $G''(\omega)$ . For instance,<sup>53</sup> three different linear polyethylene samples<sup>110,111</sup> have yielded  $E_A^* = 6.35$  kcal/mol with  $n_1 = 0.43$ ,  $E_A^* = 6.40$  kcal/mol with  $n_1 = 0.45$ , and  $E_A^* = 6.64$  kcal/mol with  $n_1 = 0.47$ . For each of these cases we

can deduce the underlying molecular activation energy using  $E_A = (1-n_1)E_A^*$ . Using the above numbers we find  $E_A = 3.62$ , 3.52, and 3.52 kcal/mol respectively.<sup>53</sup> All three bulk polymer melt measurements reduce by way of the second universality to the same fundamental  $E_A$  within experimental error. Remarkably, the predicted value for  $E_A$  agrees with the value of the internal rotational isomerism barrier<sup>53</sup> as measured directly by spectroscopic techniques on polyethylene analog molecules such as n-butane, and on long chain polyethylene oxide in dilute solution. As we had found in the  $\alpha$ -SiO<sub>2</sub> transport and the polycarbonate  $\gamma$ -relaxation examples, there is again a quantitative relation between the activation energies on the macroscopic and microscopic levels. In Fig. 9, we plot measured activation energies in polyethylene against molecular weight. Near  $M_c$ , the activation energies increase dramatically as entanglement sets in and coupling increases. The high and low molecular weight regimes can be related by the second universality using the coupling parameter  $n_1$ .

The molecular weight dependence of the terminal time or viscosity can be predicted simultaneously with activation energies using (4.15). This predicts a  $M^{\mu}$  dependence with  $\mu = 2/(1-n_1)$ . For the three linear polyethylene samples mentioned above, we have  $n_1 = 0.43$ , 0.45, and 0.47 respectively. The corresponding molecular weight dependences are then predicted to be  $\mu = 3.51$ , 3.63, and 3.77 respectively.<sup>53</sup> These predicted values agree with the experimentally quoted values of 3.52 for the first sample, and 3.60 for the second sample, although no value is quoted for the third sample. Predicted values of  $\mu$  for all available nearly monodisperse linear polymer melt data lie in the range  $\mu = 3.4$ -3.8 and is consistent with the measured value on a case by case basis.<sup>35</sup>

An alternative measure of the terminal dispersion for polymer melts is the product of the recoverable compliance  $J_e^0$  and the plateau modulus  $G_N^0$  given by:

$$J_e^0 G_N^0 = (G_N^0/\eta^2) \int_0^{\infty} dt' t' G(t') = \frac{(1-n_1)\Gamma(2/(1-n_1))}{\Gamma^2(1/(1-n_1))} \quad (4.16)$$

The measured values of  $J_e^0 G_N^0$  for linear polymer melts lie between 2.0 and 3.0 and agrees with the calculated value from (4.16) in each case as expected.<sup>35</sup>

The simultaneous testing of multiple predictions of terminal dispersion, temperature dependence and molecular weight dependence puts severe constraints on the second universality and yet it continues to hold up quantitatively. This is illustrated schematically in Fig. 10.

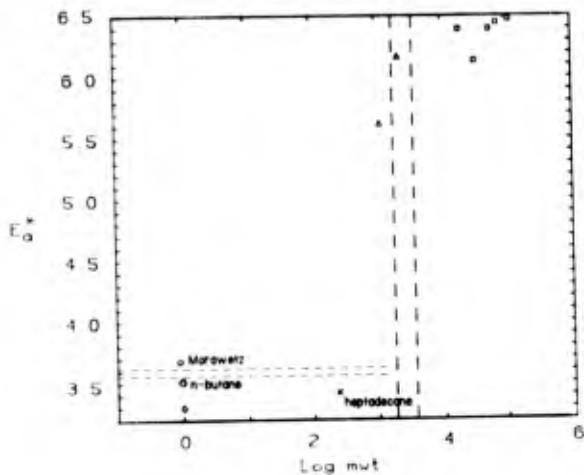


Fig. 9. Measured activation energies in polyethylene vs. molecular weight. The vertical dashed lines are  $M_c$  and  $M_e$ . The polymer melt data (i.e.  $M > M_c$ ) and spectroscopic data (i.e.  $M < M_c$ ) are related by the second universality (4.15). After Ref. 53.

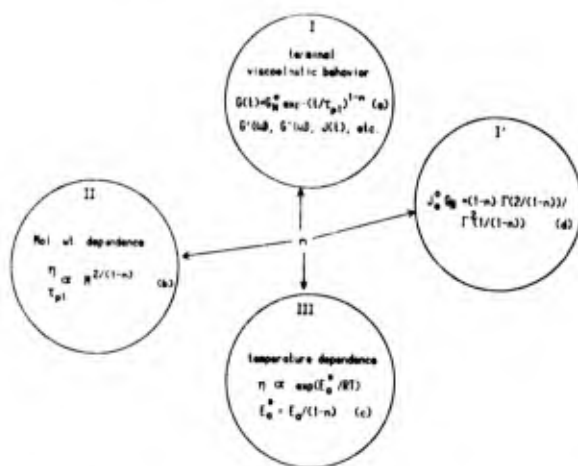


Fig. 10. A network of interconnections between the viscoelastic dispersion of the terminal zone (I, I'), the molecular weight dependence of the terminal relaxation time  $\tau_{p1}$  or the zero-shear flow viscosity  $\eta$ (II), and the temperature dependence of  $\tau_{p1}$ , or  $\eta$  in the high temperature Arrhenius region (III). Note that the same value of  $n$  appears in all the functional dependences (a)-(d) provided we are dealing with the same polymer which is monodisperse and has a fixed architecture. After Ref. 53.

For linear polymers, the value of  $n_1$  increased from nearly zero below  $M_c$  up to around 0.4 above  $M_c$ . This variation of  $n$  with the entanglement structure can be explored further by modifying the polymer architecture. One way to do this is by using polymers which contain several branches. The relaxation modes for branched polymers can be calculated in a manner analogous to the Rouse model and it is found that the  $M^2$  dependence of  $\tau_1$  is retained although the coef-

ficients are different from the linear case. Therefore (4.15) can be applied to branched polymer melt data as well.<sup>35</sup> The first universality was illustrated earlier for 4-armed star shaped polystyrene samples in Fig. 3 and the value of  $n_1$  is higher than that for a typical linear melt. Measurements on a branched polyethylene<sup>110</sup> are consistent with  $n_1=0.70$ . The presence of multiple branches is expected to increase the entanglement coupling as compared to linear samples and this is consistent with the physical interpretation of  $n_1$  as a measure of the coupling strength to the complexity in the system. The flow activation energy of branched polyethylene is measured to be 11.66 kcal/mol, also larger than the linear-polyethylene case. However, the second universality again reduces this to  $E_a=(1-0.70) \times 11.66$  kcal/mol=3.50 kcal/mol in agreement with the rotational isomerism barrier data.<sup>53</sup> The relation of the flow activation energies and rotational isomerism barriers in linear and branched polyethylene predicted by the second universality is summarized in Table I (taken from Ref. 53). Furthermore, the value  $n_1=0.70$  predicts a molecular weight dependence with exponent  $\mu=6.67$  in agreement with the measured value of 6.56.

TABLE I

Table I. Estimation of coupling constants  $n$  and primitive activation energies of polyethylene

Material	$n$	$E_a$ used to deduce $n$	$\alpha$	$E_a^*$ kcal/mole	$E_a$ kcal/mole
Linear Polyethylene					
$10^4 < M_w < 10^5$	0.43	11 (3.52)	(6.35) <sup>†</sup>	3.62	
SPNA-5, $M_w$	0.47	$G''(\omega)$ via 12	3.77	(6.64)	3.52
$1.93 \times 10^4$ $M_w$ , $35.2 \times 10^5$	0.45	11 (3.60)	(6.40) <sup>†</sup>	3.52	
$C_{17}H_{36}$				(3.42)	
n-butane					(3.4) <sup>*</sup>
Branched Polyethylene					
$10^4 < M_w < 2 \times 10^5$	0.70	11 (6.56)	(11.66)	3.50	

<sup>†</sup>mean flow activation energy \* ultrasonic absorption measurement  
Quantities in parentheses are measured. After Ref. 53.

The presence of long branches in the polymer sample caused strong entanglement coupling with the result that flow of the melt is delayed to very long times as compared to linear samples. This is reflected in the large value of  $n$  (e.g.  $\approx 0.7$  and larger) which shifts the terminal mode by way of (4.11). A modification in polymer architecture which will further increase the coupling is to permanently cross-link the sample. This can be thought of roughly as a situation with permanent entanglement points. The polymer network can still be deformed but there will be no real flow so the relaxation modulus does not decay to zero as in (4.14). Instead, there will be an equilibrium modulus  $E_{\infty}$  and the long-time behavior can be described by  $E(t)=E_{\infty}+(E_0-E_{\infty})\exp[-(t/\tau_p)^{1-n}]$ . The value of  $n$

for a cross-linked polymer is typically quite large (e.g.  $n$  close to the upper bound of 1.0). For  $n$  close to unity, the approach to the equilibrium modulus in the large  $t/\tau$  limit can be approximated by a term which is a power law with a small negative exponent. From this we can understand the origin of various empirical descriptions of the long-time behavior of cross-linked polymers, such as the Chasset-Thirion equation:  $E(t) = E_\infty [1 + (t/\tau)^{-m}]$ , where  $m$  is typically  $\sim 0.1$ .

At times earlier than the terminal time  $\tau_{p1}$ , the shorter wavelength Rouse modes also contribute as in Eqs. (4.10)-(4.12). Although the value of  $n_1$  can be obtained from the terminal spectrum, independent measurements of the values of  $n_2, n_3, \dots$  are more difficult to obtain. However, the full polymer melt spectrum can be described very well for linear samples by using the measured value of  $n_1$  (e.g. 0.4), an intermediate value for  $n_2$  (e.g. 0.2), and zero for  $n_i, i \geq 3$ . In principle, the value of  $w_c$  could also be different for each Rouse mode but we will keep it a constant here. An example is shown in Fig. 11 for a high molecular weight polystyrene as measured by creep.  $J(t)$  is calculated numerically from  $G(t)$  in (4.10) by using the convolution relation (2.5). The expression (4.11) for  $\tau_{p1}$  results in a nonuniform shifting of the different Rouse modes. This results in a plateau in the creep curve over several decades called the rubbery plateau. This is another manifestation of the second universality.<sup>35,50</sup>

There is no known way to quantitatively understand this large mass of polymer melt data other than by using the first and second univer-

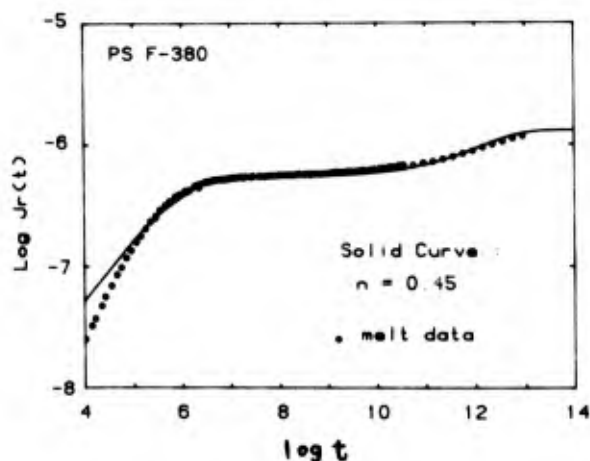


Fig. 11. Recoverable creep compliance for a polystyrene (mol. wt.  $= 3.8 \times 10^6$ ) showing the plateau and terminal dispersions. Solid curve is a fit from (4.10)-(4.12) and (2.5) as described in the text (data by D.J. Plazek, see Ref. 47).

salities. De Gennes,<sup>112</sup> and Doi and Edwards<sup>113</sup> have devised a model in which the diffusing chain is constrained to move within a fixed tube which represents the effect of the surrounding chains. The resulting curvilinear motion is referred to as reptation. For linear polymers, the predicted molecular weight dependence of the terminal time is  $M^3$ ,  $J_e^0 G_N^0 = 1.2$ , and the terminal relaxation is nearly a single exponential decay. No prediction is made concerning the temperature dependence and the reptation model is not easily adapted to branched samples. Furthermore, the method of including coupling to the surroundings used by the reptation model certainly cannot be applied to glassy polymer relaxation or amorphous semiconductor transport. It is now clear to most polymer melt workers that the reptation model must be modified in several ways if it is to have a chance of serious application to data. The predictions of the first and second universalities are superior to those of reptation in all respects and are far more general. Even within polymer melts, the reptation mechanism is too specialized. Recently, measurements on melts of ring shaped polystyrene molecules have been carried out. Viscosity measurements by McKenna, Hadziioannou, Kovacs and the Strasbourg group<sup>114</sup> and creep measurements by McKenna, Fetters, Plazek and Plazek<sup>115</sup> are found to be in quantitative agreement with the first and second universalities.<sup>116</sup> However, it is not presently clear how to even consider the ring melts using the reptation ideas.<sup>117</sup>

The high temperature Arrhenius region of the polymer melts was examined because it is relatively unambiguous to interpret a single temperature independent activation energy  $E_A^*$ . At lower temperatures, the viscosity becomes non-Arrhenius. Within a range of  $100^\circ$  or so above  $T_g$ , the temperature dependence of the viscosity  $\eta$  or the friction coefficient  $\zeta$  is often well described by the empirical Vogel-Fulcher-Tammann-Hesse (VFTH) equation:

$$\ln \zeta = \ln \zeta_0 + \frac{C}{T - T_\infty} \quad (4.17)$$

which is equivalent to the well known Williams-Landel-Ferry (WLF) equation. Although the justification for the form of (4.17) is often discussed in terms of the relative free volume for molecular mobility, there is no complete understanding of (4.17) or the deviations from it. Caution has to be exercised when applying the second universality to  $\zeta(T)$  near  $T_g$  and it is not clear at this time how it would be affected by other factors in this region. However, the second universality can be applied tentatively in polymers near  $T_g$  by including the information available from experiments and examining the results.<sup>25</sup> Such a tentative application is illustrated below for the case of a non-

polymeric material, a molten salt. Recall that in the case of electronic transport in  $\alpha\text{-SiO}_2$ , the physics of the  $\tau_0$  was understood in detail, even in the non-Arrhenius regime. Then the second universality could be applied unambiguously and quantitative agreement was found in all temperature regimes. In the future we shall return to the problems of viscosity and shift factors of viscoelastic functions near  $T_g$ .

Application of the second universality to the molten salt  $0.6\text{KNO}_3\text{-}0.4\text{Ca(NO}_3)_2$  is shown in Fig. 12 where the experimental relaxation times are plotted as a function of temperature.<sup>2</sup> The highest temperature data in the range  $175^\circ\text{C}$ - $382^\circ\text{C}$  are from hypersonic measurements of Torell,<sup>73</sup> and Angell and Torell.<sup>74</sup> These data show approximately single exponential relaxation behavior (i.e.  $n \approx 0$ ) with Arrhenius temperature dependence. The preexponential,  $\tau_\infty$ , obtained by

extrapolation of the high temperature Arrhenius behavior to infinite temperatures turns out to fall in between  $10^{-13}$  to  $10^{-14}$  sec which corresponds to the frequency region where a far infrared absorption band has been observed from a thin film of nitrate glass. This band is thought to come from the coupled transverse vibrational modes of the quasilattice. Thus, the far infrared absorption data gives us a physical identification for the underlying molecular relaxation time  $\tau_0$ . At  $177^\circ\text{C}$ , the lowest temperature studied by Angell and Torell, their data indicate the onset of non-Arrhenius behavior. The loss spectrum has now broadened sufficiently from the single exponential relaxation (i.e.  $n=0$ ) spectrum that we can assign the value  $n=0.15$  at  $177^\circ\text{C}$ . At lower temperatures, in the range of  $90$ - $130^\circ\text{C}$ , the ultrasonic relaxation data of Weiler et al.<sup>75</sup> have been fit to the first universality. The fits to the limited amount of data are good and the values of  $n$  can be seen to increase from  $0.4$  at  $126^\circ\text{C}$  to  $0.65$  at  $105^\circ\text{C}$ .

Using these values of  $n(T)$ , we can then attempt to apply the second universality. The second universality (4.2) is a prediction between the microscopic relaxation time  $\tau_0$  (and its dependences on physical variables) and the experimentally observed macroscopic time  $\tau_p$ . In situations where  $\tau_0$  is understood in detail experimentally and theoretically, such as in  $\alpha\text{-SiO}_2$  or in polymer melts at high temperature, the second universality can be tested unambiguously. The unambiguous applications have all quantitatively supported the second universality. However, in situations where the detailed properties of  $\tau_0$  are not known, applications of the second universality must be more tentative. One procedure is to apply it by making assumptions about the behavior of  $\tau_0$  based on the

limited available information. The consequences of the second universality prediction can then be examined. In fact, the confidence gained from the success of the second universality in other applications can be used to reverse the situation and the second universality can be used as a tool to help learn more about the properties of  $\tau_0$ . In the present case of the molten salt, the high temperature behavior can be understood in terms of a single activation barrier. However, a detailed theory for  $\tau_0$  is not available and possible modifications to this at lower temperatures cannot presently be described in detail. We can proceed tentatively by representing  $\tau_0$  by a single activation barrier,  $\tau_0 = \tau_\infty \exp(E_A/RT)$ , at all temperatures and examine the consequences of the second universality using the measured values of  $n(T)$ . The values of  $\tau_\infty$  and  $E_A$  are taken from the high temperature data. Using the available data, a least squares fit of (4.2) was performed to obtain a continuous curve. In the process, the value of  $\omega_c$  is obtained where for simplicity we have assumed it is constant. The best fit is

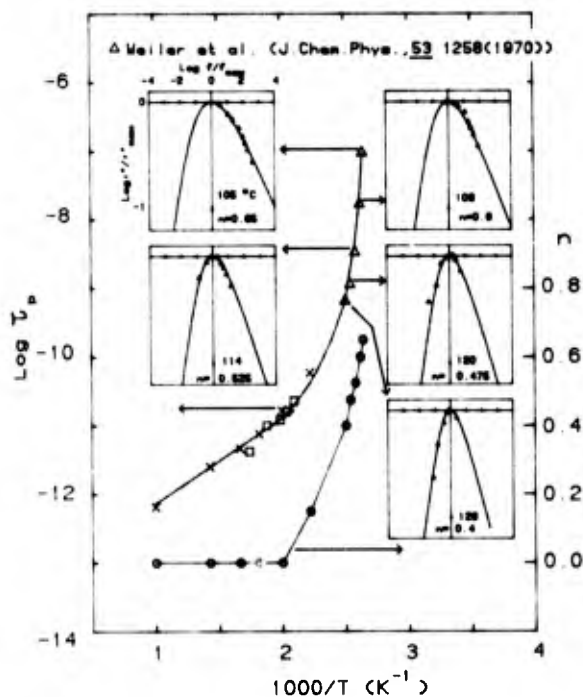


Fig. 12. Relaxation map for the molten salt of  $0.6\text{K(NO}_3)\text{-}0.4\text{Ca(NO}_3)_2$ . The insets depict the imaginary part of the longitudinal mechanical modulus as a function of frequency normalized to  $f_{\text{max}}$ , where  $f_{\text{max}}$  is the frequency of the modulus peak. At each temperature, the modulus is well fitted on the basis of the first universality (4.1) and the temperature variation of  $n$  is plotted.  $f_{\text{max}}$  is plotted as  $\tau_p \approx 1/2\pi f_{\text{max}}$  vs. inverse temperature and this agrees well with the second universality prediction based on the observed values of  $n$  (data by Weiler et al. Ref. 75) and Angell and Torrel (Refs. 73,74), replotted).

shown as the solid line in Fig. 12. It can be seen from the quality of the fit that it provides a satisfactory simultaneous account of both dispersion and relaxation time over the entire temperature range. A possible interpretation of this result is that deviations from the single activation barrier form for  $\tau_0$  are not important within the measured temperature range. It would be expected that free volume variation or other contributions to  $\tau_0$  will enter at temperatures sufficiently close to  $T_g$

and we emphasize that the above analysis is a tentative application of the second universality based on incomplete information. The non-Arrhenius region of Fig. 12 can be described empirically by a VFTH form as in (4.17). In many cases, though not all, part of the reason for this non-Arrhenius form can be traced to the change of the coupling parameter  $n$  with temperature. The complete picture of this situation will not emerge until a detailed theory of the glass transition is available. It is interesting to note that Litovitz and McDuffie<sup>118</sup> suggested in 1963 that the mechanism responsible for non-Arrhenius temperature dependence might also be responsible for the broadening of the spectrum of relaxation times in liquids. Such a mechanism may in fact be provided by the two universalities.

A similar application of the second universality to the conductivity relaxation data of the ionic conductor Na $\beta$ -alumina not only gives a satisfactory description of data, but the second universality parameters can be independently checked.<sup>36,37</sup> Nonstoichiometric Na $\beta$ -alumina exhibits glass-like dielectric, thermal and acoustic properties at low temperatures ( $\leq 50$  K).

At elevated temperatures ( $> 300$  K) the ionic conductivity is comparable to that of ionic liquids. The transition from the liquid-like to the glass-like phase is of fundamental interest. Dielectric loss data for Na $\beta$ -alumina in the MHz frequency range has been measured<sup>119</sup> at temperatures between 90 and 140 K. At such temperatures and frequencies, the dielectric loss is dominated by the thermally activated hopping motion of ions over local potential barriers, e.g.  $\tau_0 = \tau_\infty \exp(E_A/kT)$ . As discussed in the section on the first universality, the dynamic aspects of ion motion in vitreous ionic conductors can be characterized by the electric modulus,  $M^*(\omega)$ , which describes the relaxation of the applied electric field. This can be related to the first universality by (2.2) and the fit to the electric modulus data at various temperatures is shown in Fig. 13. The  $M''(\omega)$  frequency curves will peak at  $f_{\max} \cong 1/2\pi\tau_p$  where  $\tau_p$  is given by (4.2) whereas the shape of the  $M''(\omega)$  versus  $\omega$  curves is determined predominantly by the value of  $n$ . The deviations at high frequencies in electric modulus data are easily explained and this has been discussed in the section on the first universality using

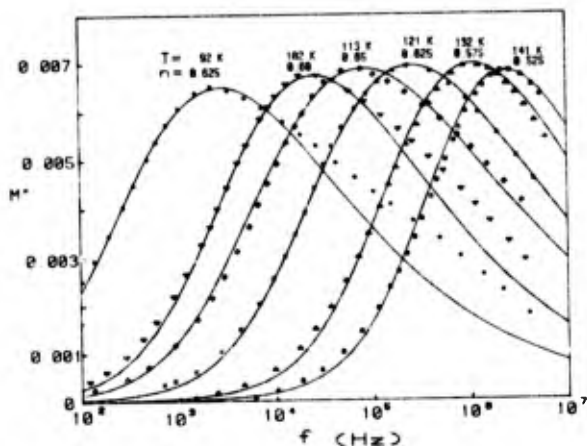


Fig. 13. Electric modulus data for nonstoichiometric Na $\beta$ -alumina as a function of temperature and frequency. Solid curves are fits based on (1.1) and (2.2) (data by Almond and West, replotted. See Ref. 119).

Figs. 5(a) and 5(b). Each curve of  $M''$  vs.  $\omega$  was least square fitted to determine the optimum value of  $n$  at each temperature.<sup>36,37</sup> With  $n(T)$  known for six temperatures, a least square fit of the second universality is made to the experimentally determined peak frequencies  $f_{\max}(T)$  by varying the parameters  $E_A$ ,  $\omega_c$  and  $\tau_\infty$ . The fit<sup>36,37</sup> is shown by the solid lines drawn between the  $f_{\max}(T)$  data points in Fig. 14. The good agreement with experiment justifies the assumed temperature independence of  $\omega_c$  and  $\tau_\infty$ .

The values of the parameters obtained from the fit were  $E_A = 0.059$  eV,  $\omega_c = 1.2 \times 10^8$  sec<sup>-1</sup> and  $\tau_\infty = 2.7 \times 10^{-10}$  sec. These parameters can be checked by directly relating them to other experiments.<sup>36</sup> The value of  $E_A = 0.059$  eV is in close agreement with the value of 0.058 eV which was determined from internal friction and NMR spin-lattice relaxation. Although there have been suggestions, there is at present no clear identification of the microscopic process which corresponds to this energy. This microscopic activation energy predicts  $E_A^* = 0.16$  eV by using the value  $n(92 \text{ K}) = 0.625$  in the second universality. Microwave conductivity data between 50 K and 680 K points to three distinct temperature regimes. Above  $T \sim 320$  K, the conductivity is thermally activated with activation energy  $E_A^* = 0.16$  eV, between 320 and 120 K a thermal activation energy of  $E_A = 0.05$  eV approximates the data, whereas a non-Arrhenius process dominates below 100 K which falls in the "glassy" regime of Na $\beta$ -alumina. This is consistent with NMR data and the second universality.

The value of  $\omega_c$  can be related to established microwave and dielectric loss ( $\epsilon''$ ) measurements. According to the physical interpretation of the previous section, the first and second universalities should be observed for

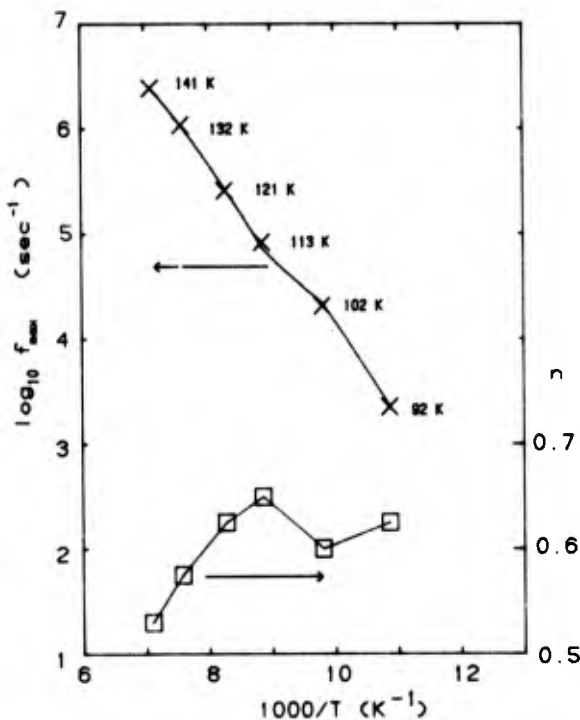


Fig. 14. Variation of  $n$  and  $f_{\max}$  (peak of  $M''(\omega)$ ) with temperature corresponding to Fig. 13. The upper curve shows  $f_{\max}$ , where the crosses are experimental data and the solid line is the second universality prediction based on the observed values of  $n$ .

$\omega t > 1$  or  $\omega < \omega_c$ . Only at frequencies below  $\omega_c$  do the modes have the property (3.20) and become excited in large numbers. At higher frequencies than  $\omega_c$ , deviations from the first universality are expected. An analysis<sup>36</sup> of AC conductivity data on Na $\beta$ -alumina is able to distinguish a low frequency region described by modes with  $P(\omega) \propto \omega$  (i.e. see (3.20)) and a high frequency region described by  $P(\omega) \approx \text{constant}$  (i.e. TLS). The transition between the two regions occurs near  $10^7$ - $10^8 \text{ sec}^{-1}$  and this is consistent with the value  $\omega = 1.2 \times 10^8 \text{ sec}^{-1}$  obtained from the second universality above.

The value  $\tau_0 = 2.7 \times 10^{-10} \text{ sec}$  obtained from the fit described above, however, seems too large for the preexponential factor of Na $\beta$ -alumina. This is instead expected to correspond to a typical phonon frequency in  $\beta$ -alumina,  $\tau_{\text{ph}} \sim 10^{-12} \text{ sec}$ . The reason for this apparent discrepancy lies in the contribution of the modes with  $\omega > \omega_c$ . As discussed after (3.27), these modes contribute a constant factor  $\exp(\Delta S_g/R)$  which, for ease of notation, we have usually absorbed into  $\tau_0$ .

Physically,  $\Delta S_g$  represents the entropy shift from the TLS (and higher modes). Thus both  $\tau_{\text{ph}}$  and  $\exp(\Delta S_g/R)$  should give rise to the preexponential factor,  $\tau_0 = \tau_{\text{ph}} \exp(\Delta S_g/R)$ . A reasonable approximation is<sup>36</sup>  $\Delta S_g/R \sim E_A/kT_g$ . Using  $E_A =$

$0.059 \text{ eV}$  and  $T_g \approx 120 \text{ K}$  for Na $\beta$ -alumina, we find  $E_A/kT_g \sim 6$  and therefore  $\tau_0 \approx 10^{-9.4} \text{ sec}$ . This is consistent with the value of  $\tau_0$  obtained from the second universality. The first and second universalities and their physical interpretation as described in the previous section are found to hold quantitatively when tested against the available data. As more detailed data become available, more refined tests of the second universality can be carried out.

The value of  $n$  is observed to change near  $T_g$  for many other glass-forming materials,<sup>2,25</sup> although there are many important exceptions.<sup>2</sup> Analogous situations are found in other strongly cooperative systems such as spin glasses. Spin glasses are metal, insulator, or semiconducting hosts containing magnetic "impurity" concentrations of about 0.1-10%. Concentrations higher than about 30% result in the more traditional forms of magnetic phases such as ferro or antiferromagnetism. When the concentrations are too dilute, however, the local magnetic moments are only weakly interacting and the spin glass state does not result. Examples of spin glasses are Cu:Mn,  $\text{Eu}_x\text{Sr}_{1-x}\text{S}$ ,  $\text{Cd}_x\text{Mn}_{1-x}\text{Te}$ , and many other systems.<sup>120-123</sup>

The magnetic impurities are placed substitutionally at normal atomic sites in the host but entirely randomly. The randomly distributed interacting spins respond cooperatively to experimental probes at low temperatures. At sufficiently high temperatures, the local moments respond paramagnetically to an applied magnetic field. The AC magnetic susceptibility  $\chi''(\omega)$  which is the ratio of the resulting magnetization to the applied magnetic field, follows a Curie law and is inversely proportional to the temperature. As the temperature is lowered,  $\chi''(\omega)$  (for a given  $\omega$ ) reaches a maximum and then decreases down to the lowest temperatures studied (e.g. 1°K). The temperature of the peak in  $\chi''$  is identified as the spin glass transition temperature  $T_g$ . The value of  $T_g$  decreases as  $\omega$  is lowered. For spin glasses such as the metallic system<sup>122</sup> Cu:Mn or the insulating system<sup>120</sup>  $\text{Eu}_x\text{Sr}_{1-x}\text{S}$ , the  $\chi''(\omega)$  peak broadens markedly as  $T$  is lowered corresponding to increasing values of  $n$ . This is qualitatively similar to the molten salt and the Na $\beta$ -alumina examples described above. These spin glasses can also be described by the first and second universalities (4.1) and (4.2) by using a single activated  $\tau_0$  and the temperature dependent values of  $n$ .<sup>42,44</sup>  $n$  increases to a value in the neighborhood of 0.9 near  $T_g$ . Other types of spin glasses, such as the insulator<sup>121</sup>  $(\text{Ho}_2\text{O}_3)_x(\text{B}_2\text{O}_3)_{1-x}$ , also follow the first and second universalities but with  $n$  remaining constant with temperature ( $n \approx 0.7$ ).

There are phenomena in addition to the peak at  $T_g$  which characterize the spin glass state.

If the system is cooled below  $T_g$  while in a static magnetic field  $H$ , the resulting magnetization consists of a piece due to the paramagnetic response and a second piece due to a developed magnetic remanence. If the field  $H$  is turned off at temperatures below  $T_g$ , the spin system remains partly oriented and this is called thermoremanent magnetization (TRM). Chamberlin, Mozurkewich, and Orbach<sup>18</sup> have recently shown that the time dependence of the TRM in Cu:Mn and Ag:Mn spin glasses follows the first universality. This is shown in Fig. 15. In fact, the data are consistent with both the first and second universalities.<sup>44,124</sup> There is currently no other way to understand relaxation in spin glasses than by the first and second universalities. The validity of the analyses given in terms of these two universalities is independent of whether there is a real phase transition or not in spin glasses, a question which remains unsettled.

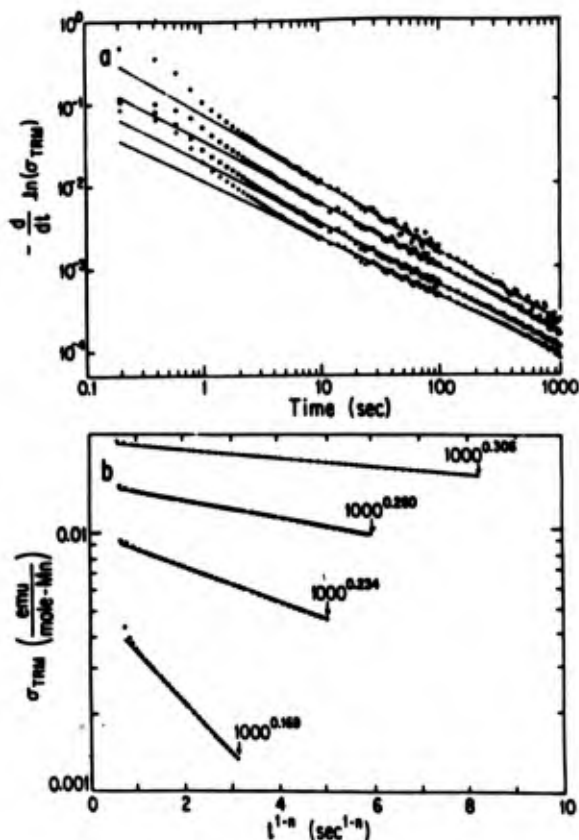


Fig. 15. Time decay of the thermoremanent magnetization,  $\sigma_{TRM}$ , of a metallic spin glass. The solid lines are the best fits to the data based on the first universality (4.1) (data by Chamberlin et al., reproduced with permission. See Refs. 18, 124, 44).

We have seen examples where  $n$  changes as temperature is lowered near  $T_g$  in polymers, liquids and spin-glasses. The values of  $n$  also changed as the molecular architecture was modified in polymer melt samples. These changes in  $n$  reflected the modified cooperativity in the system as the structure is altered. Throughout all these modifications, the first and second universalities (4.1) and (4.2) were still found to track with one another. There are many other examples of variations in  $n$ . At the beginning of this section, we considered  $\alpha$ -SiO<sub>2</sub> in different temperature regimes for a given value of  $n$ . There, we considered a situation where the temperature dependence of  $\tau_0$  changed but  $n$  remained constant. However, it is possible to vary the amount of water during the growth process to produce  $\alpha$ -SiO<sub>2</sub> samples with different  $n$  values. The value of  $n$  for wet oxide,  $n_{wet}$ , will be different from that for dry oxide,  $n_{dry}$ . The water does not affect the temperature dependence of the primary relaxation process, e.g.  $\tau_0 = \tau_0 \exp(E_A/kT)$  at high temperatures for small polaron hopping. The second universality then predicts that  $(1-n_{dry}) E_A^*$  and  $(1-n_{wet})$

$E_{A_{wet}}^*$  should both have the same value  $E_A$ . The measured values were  $E_{A_{dry}}^* = 0.6$  eV and  $n_{dry} = 0.8$ , and  $E_{A_{wet}}^* = 0.37$  eV and  $n_{wet} = 0.7$ . They yield

nearly identical predictions,<sup>1</sup> 0.12 eV and 0.11 eV, for  $E_A$ . A similar situation was observed for the absorption of water in polymers. Dielectric measurements<sup>125</sup> on the  $\beta$  relaxation in Nylon 66 showed that both the value of  $n$  and the value of  $E_A^*$  depend on the water content of the polymer. However, the second universality was obeyed once again,<sup>2</sup> reflecting a single underlying fundamental activation energy  $E_A$ .

The first and second universalities have predicted the temperature dependence of different systems under many different conditions. The polymer melts allowed a second simultaneous prediction, that of the molecular weight dependence  $M^{2/(1-n)}$ . Examples of modifications of mass dependence also occur in other systems. An example is the isotope mass dependence for ionic conductivity in alkali glasses.<sup>45</sup> The diffusion of interstitial solute atoms or defects in solids has usually been analyzed using absolute reaction-rate theory. These theories are based on the application of saddle-point methods to the decay of classical metastable states in crystalline solids.<sup>56,57</sup> In general the individual defect jump rates  $W_0 = \tau_0^{-1}$  are given by

$$W_0 = \tilde{\nu} \exp(-\Delta F/kT) \quad (4.18)$$

where  $\Delta F$  is the free energy needed to carry the defect from an initial equilibrium position to a saddle point and  $\tilde{\nu}$  is an effective frequency



associated with vibration of the defect in the direction of the saddle point. Although the validity of such models has often been challenged on several points, many experiments have been aimed at testing them. In particular, experiments on the diffusion of isotopes in solids have tested predictions of the isotope mass dependence of  $W_0$ . The simplest interpretation of (4.18) leads  $W_0 \propto m^{-1/2}$  where  $m$  is the mass of the diffusing atom and this results from a harmonic treatment of the lattice vibrations. Recall that the simple harmonic oscillator frequency has the same mass dependence. Even if such models are accepted as being valid, it has not been clear how to extend them to apply to noncrystalline systems.

Jain and coworkers<sup>121,127</sup> measured the electrical conductivity,  $\sigma$ , as a function of the  ${}^6\text{Li}/{}^7\text{Li}$  ratio in a series of  $({}^6\text{Li}/{}^7\text{Li})_2\text{O} \cdot 2.88\text{B}_2\text{O}_3$  glasses. If the simple relation  $W_0 \propto m^{-1/2}$  were to hold then we would expect  $\sigma^6/\sigma^7 = \sqrt{7/6} \cong 1.08$ , where  $\sigma^6$  and  $\sigma^7$  represent the conductivity of  ${}^6\text{Li}$  and  ${}^7\text{Li}$  in  ${}^6\text{Li}$ -borate and  ${}^7\text{Li}$ -borate glasses respectively. In fact, the data deviated considerably from this result and showed a temperature dependence which did not seem consistent with any interpretation of (4.18). These data are shown in Fig. 16.

In the case of light interstitial atoms, quantum corrections may be expected and some workers<sup>128,129,127</sup> have incorporated quantum partitions functions into the activated rate

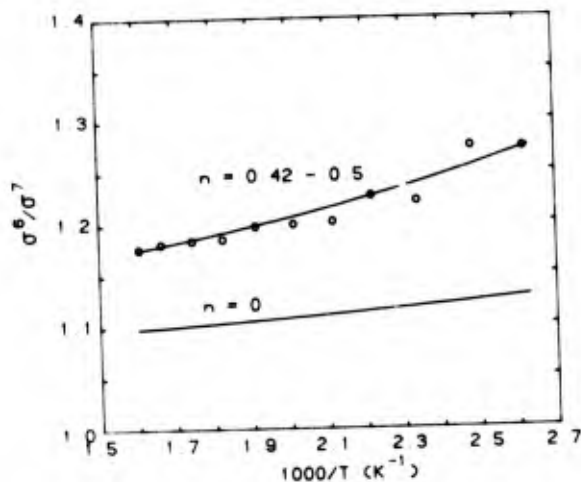


Fig. 16. Isotope mass data for conductivity in a lithium borate glass. Upper solid curve is theoretical fit based on (4.19) using  $n$  values of Fig. 1 and phonon frequencies  $h\nu/k=600$  K and  $h\nu'/k=250$  K. Lower solid curve corresponds to  $n=0$  (data by H. Jain et al., replotted. See Refs. 127, 45).

models so that the simple prediction  $\sigma^\alpha/\sigma^\beta = (m_\beta/m_\alpha)^{1/2}$  is modified to:

$$\sigma^\alpha/\sigma^\beta = (m_\beta/m_\alpha)^{1/2} F[(m_\beta/m_\alpha)^{1/2}, h\nu/kT, h\nu'/kT] \quad (4.19)$$

where  $\nu$  and  $\nu'$  are the vibration frequencies of particle  $\beta$  at its equilibrium and saddle point respectively, and  $F$  is a simple function involving quantum partition functions. Equation (4.19) has been used to describe the diffusion of hydrogen isotopes in single-crystal hosts.<sup>128,129</sup> Jain and Peterson<sup>127</sup> applied (4.19) to the lithium-borate glass data and they were able to find a wide range of combinations of  $\nu$  and  $\nu'$  which fit the data within the experimental uncertainty. However, in all cases, they find  $h\nu/k \geq 2280$  K and this is much higher than the equilibrium vibrational frequencies obtained from measurements of the far-infrared spectra by Exarhos and Risen.<sup>130</sup> These measurements on lithium borate glass systems indicate  $h\nu/kT \cong 600$  K. As we will see, such a value is in accord with the isotope mass data of Fig. 16, if we use the first and second universalities.<sup>45</sup>

In addition to the isotope mass data, the frequency dependence of the conductivity was measured.<sup>126</sup> This is plotted in terms of the imaginary and real parts of the electric modulus in Figs. 1 and 2. The electric modulus was discussed briefly in the section on the first universality. Migration of the ions leads to a decay of the electric field within the material. If this decay follows the first universality, the electric modulus can be calculated by (2.2). The first universality does indeed fit the data and this is shown as the solid curves in Figs. 1 and 2. The slight deviations at high frequencies were also discussed in the section on the first universality and they were explained using Figs. 5(a) and 5(b). The value of  $n$  was about 0.48 for both the  ${}^6\text{Li}$  and  ${}^7\text{Li}$  isotope, although a small dependence on  $n$  with temperature improved the fit somewhat. These values of  $n$  can now be used in the second universality to predict the isotope mass dependences. Equation (4.19) gives the mass dependences in the absence of coupling to the glassy system (i.e. gives information about  $\tau_0$  for each isotope, since  $\sigma \sim \tau_0^{-1}$ ). In the presence of coupling, the second universality will modify (4.19) to:<sup>45</sup>

$$\sigma^\alpha/\sigma^\beta = [(m_\beta/m_\alpha)^{1/2} F]^{1/(1-n)} \quad (4.20)$$

For  $h\nu/k = 600$  K, we find a best fit of (4.20) to the data with  $h\nu'/k = 250$  K and this is shown as the upper solid curve in Fig. 16. This used the same values of  $n$  that were found from the first universality in Figs. 1 and 2. The lower solid curve in Fig. 16 shows the calculation with the same  $\nu$  and  $\nu'$  but with  $n=0$  (i.e. no coupling to the glassy system). With a vibrational frequency near the observed value, the first and second universalities describe the isotope mass dependence within the experimental error over

the entire range of observed temperature. The first and second universalities not only allow us to quantitatively describe the data but they also make direct contact with the physics of the glassy system as measured by far-infrared spectra. Ionic conductivity is found to obey the first universality in many other systems and this was first pointed out in the pioneering work of Moynihan and coworkers.<sup>12,13</sup>

Besides modified dependences on mass, temperature, and other variables, the second universality (4.2) predicts a shift of the entire magnitude of the relaxation time. In the polymer melt discussion above, it was pointed out that the rubbery plateau illustrated in Fig. 11 is a manifestation of the relative shifting of Rouse modes from the second universality. The long wavelength terminal Rouse mode had a stronger coupling to the entanglement network than the more localized Rouse modes. Therefore the terminal mode had the largest  $n$  value, although independent measurements of the lower Rouse modes are difficult to obtain. Relative shifting of the relaxation time due to changes in  $n$  also are observed for other relaxation processes. An example is in the  $\alpha$  relaxation of glassy polymers where physical aging can cause  $n$  to increase.<sup>47</sup> When a liquid is rapidly cooled, the viscosity becomes enormous and it is thrown out of equilibrium. The result is a glass and its structural conformations are frozen in on timescales set by the viscosity. However, on longer timescales the glassy state does tend to return to the equilibrium liquid state. After quenching the liquid into a glass at a certain temperature, the glass can be annealed or aged. This means that it is allowed to recover towards equilibrium at that temperature. One manifestation of aging is a spontaneous increase of the density of the glass. This has attracted much interest and has a significant influence in determining the brittleness or toughness of glassy polymers. As the density of the glass increases with aging, we would expect the coupling of a relaxation process with the glassy system to become stronger. Aging of glasses may then be an appropriate place to test first and second universalities.

Figure 4 shows creep data taken by Plazek<sup>47</sup> on polystyrene for several values of annealing time. As the aging time  $t_a$  increases, the creep curve is seen to shift to longer times. The creep curves  $J(t)$  corresponding to a relaxation modulus  $G(t)$  of the first universality form (4.1) can be calculated using the convolution relation (2.5), which is valid for linear viscoelasticity. For a given value of  $n$ ,  $G(t)$  given by (4.1) can be converted to  $J(t)$  by solving (2.5). At sufficiently small times, the creep is given approximately by the inverse of (4.1):  $J_n(t) \approx J_0 \exp[+(t/\tau_p)^{1-n}]$ . This is a form used empirically by Kohlrausch<sup>3</sup> and Struik.<sup>131</sup> However, this form is not accurate at longer times and a complete solution for the creep function

can only be obtained by numerically solving (2.5). The solid curves in Fig. 4 show these first universality fits for the shapes of the creep curves at different aging times. The fits<sup>47</sup> are very good and the value of  $n$  required to fit the data is seen to increase as the aging proceeds. This is consistent with the expected increase in coupling as the density of the glass increases with aging. The value of  $n$  increased from an initial value of 0.54 to about 0.66 at the longest aging time examined. The aging time required to reach  $n=0.66$  depended on the temperature and at 10 degrees below  $T_g$  it took about three times as long as at 5 degrees below  $T_g$ .

The values  $n(t_a)$  can be used to test the second universality (4.2). There is no detailed theory available for the  $\alpha$  relaxation in polystyrene and the behavior of its  $\tau_0$  as the density increases with aging. We encountered similar situations in previous examples, and once again we can proceed tentatively in the absence of complete information about  $\tau_0$ . The simplest assumption is to let  $\tau_0$  and  $w_0$  be constant and just use the  $n(t_a)$  values in (4.2) to predict the relative shift in  $\tau_0$  with aging.<sup>47</sup> These second universality predictions are quite good, although we cannot rule out a small additional shift from changes in  $\tau_0$  or  $w_0$  with aging. The relative positions of the curves from the second universality are shown in Fig. 14. The aging data exhibit a simultaneous flattening in shape and shifting to longer times in a manner consistent with the first and second universality.

Several of the examples described above involved a series of samples in which each member of the series differed in polymer architecture, temperature, doping, or aging time, etc. The result was that each sample in the series had a different value of  $n$  and the universality laws could be tested. However, the value of  $n$  remained constant throughout the experiments performed on any given sample. This was an important feature to reduce the general prediction of the model (3.29) to the first and second universalities (3.30) and (3.31). The general prediction for the decay function allows the possibility that the material dependent parameters  $n$ ,  $w_0$ , or  $\tau_0$  could change on the timescale of the relaxation experiment. These situations actually involve following the dynamics of structural recovery and rearrangement. Equation (3.29) is a generalized version of the first and second universalities in which the correlated changing of the decay function and the relaxation time can take place continuously. Examples of its application include the volume or enthalpy recovery of a glass for a specific quenching history, stress relaxation at high strain levels, and hysteresis effects in spin glasses and charge density wave systems.

Several phenomenological models of the kinetics of recovery in glasses have been developed in recent years. These include the models

of Kovacs et al. and Moynihan et al. These models incorporate characteristic features which have been observed in a great variety of experimental studies since the pioneering work of Tool. These characteristic features are: non-linearity with respect to the magnitude of departure from equilibrium, asymmetry with respect to its sign, and memory effects observed after multiple perturbations. In the models of both Kovacs et al.<sup>132</sup> and Moynihan et al.,<sup>133</sup> the nonlinearity and asymmetry features are included by allowing the relaxation times to depend on the structural state of the glass in a phenomenological manner. Memory effects are produced if, in addition, there is effectively a distribution of relaxation times. The model of Kovacs et al. accomplishes this by using an actual distribution of relaxation times where each relaxation time depends on the structural state. The model of Moynihan et al. uses a particular generalization of the fractional exponential decay function:

$$\phi(t) = \phi_0 \exp[-(\int_0^t dt' \tau^{-1})^{1-n}] \quad (4.21)$$

where the single relaxation time  $\tau$  depends on the structural state.

These models have been successful in reproducing the major features of a large number of experiments. They are, however, phenomenological and are not based on a microscopic picture of relaxation. In addition, it has recently been pointed out that these models, although they contain many features of the glass-transition kinetics, may have to be modified to describe some experimental situations or to quantitatively agree with extensive sets of data.<sup>134,135</sup> The generalized first and second universality decay function (3.29) also contains the essential features of nonlinearity, asymmetry, and memory and has the advantage of a microscopic basis which allows us to make connections to structural details of the glass. The similarities and differences between the microscopically derived (3.29) and the phenomenological form (4.21) allow insight into the reasons for the success of the earlier phenomenological models.

For convenience, we will use the standard notation of fictive temperature,  $T_f$ , which describes the structural state in units of temperature. For a continuous series of perturbations (e.g. steps in temperature, strain, etc.) at times  $t'$ , we can make the assumption of a Boltzmann superposition principle so that:

$$T_f = T_{f_\infty} - \int_0^t dt' \frac{dT_{f_\infty}}{dt'} \exp[-\int_{t'}^t dt'' \tau_0^{-1} \{\omega_c(t''-t')\}^{-n}] \quad (4.22)$$

where  $T_{f_\infty}$  is the equilibrium value of  $T_f$  and in general the structural dependent parameters  $n$ ,  $\omega_c$  and  $\tau_0$  may depend on  $T_f(t'')$ . The recovery

back to equilibrium depends on the relaxation rate  $\tau_0^{-1} \{\omega_c(t''-t')\}^{-n}$  and how it changes with time. In this more general situation,  $n$ ,  $\omega_c$  and  $\tau_0$  may also contribute to the time dependence. For example in the situation where the deviation in fictive temperature represents the deviation of volume, we can consider the experiments of Kovacs.<sup>136</sup> In these experiments, single temperature jumps were made and the volume deviation  $\delta(t)$  measured. A single temperature jump corresponds to just a single term in the integral over  $t'$  in (4.22) and this becomes:<sup>43</sup>

$$\delta(t) = \delta_0 \exp[-\int_0^t dt' \tau_0^{-1} \{\omega_c t'\}^{-n} \delta(t')] \quad (4.23)$$

The dependence of  $n$  on  $\delta$  was emphasized in (4.23), but it is possible that  $\omega_c$  or  $\tau_0$  also depends on  $\delta$ . This is similar to situations described earlier where the details of  $\tau_0$  were not known near  $T_g$  or during physical aging. Information on the dependences of  $n$ ,  $\omega_c$ , or  $\tau_0$  is necessary before (4.23) can be tested in detail. However, it can be seen from the form of (4.23) that it is nonlinear in  $\delta$ , it is asymmetric in the sign of  $\delta$  as long as  $n$ ,  $\omega_c$ , and  $\tau_0$  are not completely symmetric, and it contains memory. The aspects of memory can be seen because the solution of (4.23) must be self-consistent in  $\delta$  on both the right and left hand sides and therefore the entire resulting function  $\delta(t)$  will be sensitive to the initial value  $\delta_0$ . Small changes in  $\delta_0$  can result in very different solutions  $\delta(t)$ .

These qualitative features can be demonstrated by solving (4.23) for a simple example where  $n[\delta] = a - b\delta$  and the other parameters are constant. This choice for  $n$  with  $a$  and  $b$  positive allows  $n$  to increase with the density as was demonstrated by the physical aging data. The constants  $a$  and  $b$  can be chosen so that the total change in  $n$  is about 0.1, also as suggested by the aging data. A solution<sup>137</sup> of this case by numerical iteration of (4.23) is shown as the solid lines in Fig. 17 where it has been fit to volume recovery data of Kovacs for poly-(vinyl-acetate) (PVAc). Here  $\tau_{eff}^{-1} \equiv \delta^{-1} d\delta/dt$  is a measure of the rate of change of  $\delta$ . These two curves correspond to single temperature jumps from 30°C to 35°C and from 32.5°C to 35°C. Despite the small difference in initial temperature, the corresponding  $\tau_{eff}$ 's differ by about half a decade near equilibrium as  $\delta$  approaches zero. The experimental data is sufficiently accurate to demonstrate this memory effect in PVAc. Equation (4.23) is able to reproduce this effect by way of the generalized first and second universalities which is built into it. The initial temperature of 30°C corresponds to a  $\delta_0$  which is negative but larger in magnitude than for 32.5°C. The initial  $n[\delta_0]$  will then be larger for 30°C than for 32.5°C. The initial rate in (4.23) which is determined by  $n$ , as well

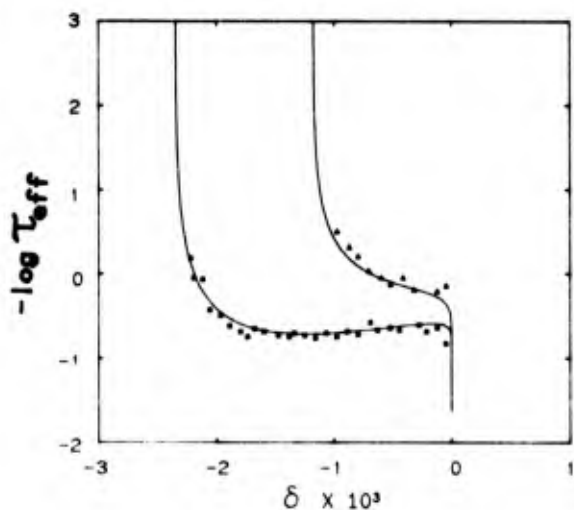


Fig. 17. Illustrative simulation of volume recovery after a temperature jump to illustrate how first and second universalities can reproduce large difference in  $\tau_{eff}$  near equilibrium

for a small difference in initial temperature. Preliminary result of Rendell, Aklonis, and Ngai. See Ref. 137. (Data by Kovacs, replotted. See Ref. 136.)

as  $\omega_c$  and  $\tau_o$ , will be slower for 30°C than for 32.5°C. The initial value of the rate determines the initial time decay of  $\delta$  which in turn subsequently determines the change in the rate parameter  $n$ . This self-consistent interplay between changes in  $\delta$  and changes in the rate determining coupling parameter  $n[\delta]$  leads to the large difference in  $\tau_{eff}$  near equilibrium. This is the same interplay between the shape of the decay function and the relaxation time demonstrated in the earlier examples of first and second universalities.

It must be emphasized that the above example is only a simulation to demonstrate some of the features built into (4.23). We do not yet have detailed information on the dependences of  $n$ ,  $\omega_c$ , and  $\tau_o$  on  $\delta$ . However, if these dependences can be measured by subsidiary experiments, then a strict test can be made of the first and second universalities in their generalized form. Dependence of  $\omega_c$  and  $\tau_o$  on  $\delta$  may be required in addition to  $n[\delta]$  to describe large sets of volume recovery data. Also note that for simplicity we have assumed that  $n$  can be specified by the single physical variable  $\delta$ . It may turn out that in actual materials, the dependence of  $n$  on structure is more complicated. These more complicated situations are easily incorporated but of course we always examine the simplest possibilities first.

Perturbing the glass with a single temperature jump pulled a single term out of the Boltzmann superposition (4.22). More general treatments of the sample can be considered, including any sort of thermal, annealing, strain or other

history of sample treatment. An example is the cooling of a liquid at constant rate, physical aging in the glassy state for a time  $t_g$ , and then heating back above  $T_g$  at another constant rate. This corresponds to a typical enthalpy recovery experiment as measured by differential scanning calorimetry (DSC). A simulation<sup>46</sup> of a DSC run based on (4.22) is shown in Fig. 18. Here a normalized, dimensionless heat capacity,  $C_p = dT_f/dT$ , for the heating leg of the cycle has been plotted. The three curves correspond to different aging times in the glassy state and the differences arise from the effect of self-consistent changes in  $n$  during aging on the rates in (4.22). This simulation includes, besides a linear dependence of  $n$  on  $T_f$ , a dependence of  $\tau_o$  on  $T_f$  of the form:

$$\tau_o [T_f] = \tau_{\infty} \exp[x(E_A/RT) + (1-x)(E_A/RT_f)] \quad (4.24)$$

where  $0 < x < 1$  is a parameter. Phenomenological generalizations of temperature activated forms to include structural dependence, such as the Narayanaswamy expression (4.24), have been used in the approaches of Kovacs et al. and Moynihan et al. Detailed calculations of enthalpy recovery including physical aging have been carried

out by Hodge<sup>138-140</sup> using (4.24) in the Moynihan phenomenological form of the decay function (4.21). Although this was able to reproduce the data (except for systematic deviations over large sets of data), anomalously small values of  $\tau_{\infty}$  and large values of  $E_A$  had to be used. Depending on the type of material, they were in

the range  $\tau_{\infty} \sim 10^{-75} - 10^{-650}$  sec and  $E_A = 80-430$  kcal/mol. The present microscopically derived formulation not only can attempt to describe the data but it can use physically meaningful values because of the second universality (4.2). The

exponent of  $1/(1-n)$  allowed us to use  $\tau_{\infty} \sim 10^{-15}$  sec and  $E_A \sim 17$  kcal/mol in the simulation of Fig. 18, which are more reasonable values for a polymer  $\alpha$  relaxation process. Better information about the dependences of  $n$ ,  $\omega_c$ , and  $\tau_o$  on the structure can be obtained by carrying out simulations such as these in conjunction with subsidiary relaxation experiments designed to take "snapshots" of the structural recovery under specific temperature, aging, strain or other conditions.

A series of such subsidiary experiments have been begun by Yee and Bankert.<sup>49</sup> Step-strain measurements on polycarbonate under uniaxial tension have been able to characterize the dependence of  $n$  and  $\tau_p$  on strain level. The

strain is ramped up within a few milliseconds to a given level (e.g. 1%, 2%, 3%, ...) and the stress relaxation is measured. It was found empirically that, although at early times after the strain ramp the stress is consistent with a form such as (3.29) where  $n$  changes during the relaxation, at times longer than about  $10^5$  sec (i.e. about 24 hrs) the stress is accurately

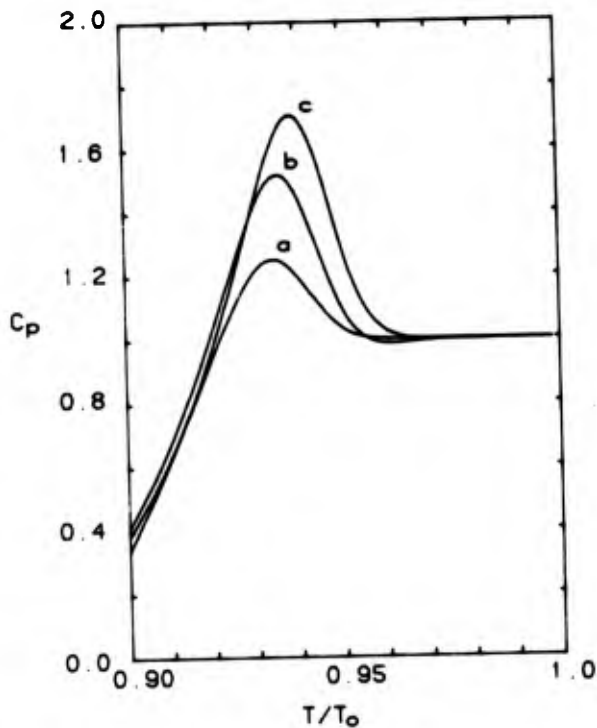


Fig. 18. Illustrative simulation of specific heat during heating after a history of cooling at a constant rate, annealing for (a) 18 s, (b) 180 s, and (c) 1800 s, and then heating at a constant rate. The calculation is based on (4.22). (See Ref. 46.)

described by a fractional exponential (4.1) with a single well defined  $n$  and  $\tau$ . The shape of the stress decay at long times<sup>p</sup> was obtained by adding an additional small strain increment, a "tickle" (e.g.  $\Delta\epsilon \sim 0.1\%$ ). This situation is consistent with a picture where the structure dependent parameters  $n[T_f]$  and  $\tau_p[T_f]$  settle down to nearly constant values as the structure settles down to a near equilibrium conformation  $T_{f\infty}$  (on the time scale of the tickle run) at

long times. Furthermore, the specific values of  $n$  and  $\tau_p$  depended on the strain level. The measured values of  $n$  are shown in Fig. 19 for an experiment performed at 35°C. The long-time value of  $n$  decreases from about 0.9 at 0% strain to about 0.6 at 5% strain. In a constant strain rate experiment, polycarbonate at 35°C yields near 5% strain. Near yielding, structural conformations are liquid-like allowing flow of the material to begin. These structural conformations determine a relaxation spectrum described by  $n \approx 0.6$ . However, structural conformations generated at 0% strain but at the actual glass transition temperature of polycarbonate,  $T_g \approx 147^\circ\text{C}$ , also determine a relaxation spectrum described by  $n \approx 0.6$ . This was borne out by repeating the step-strain tickle experiments at higher temperatures and also by earlier dielectric measurements on the  $\alpha$  relaxation of polycarbonate. This is consistent with a strain-

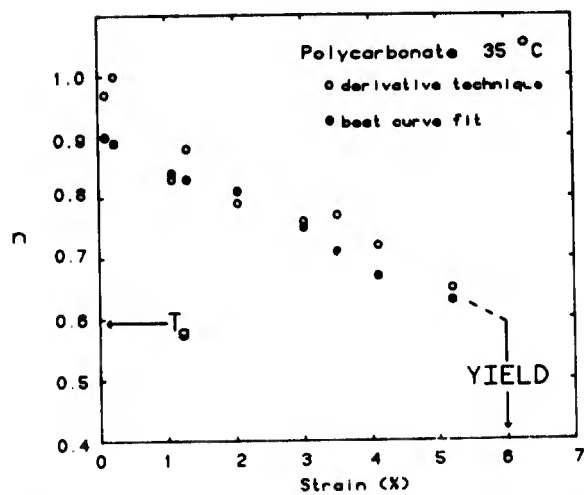


Fig. 19. Value of  $n$  as a function of strain level measured on polycarbonate by step-strain technique (data by Yee and Bankert. See Ref. 49).

temperature equivalence picture where the structural conformations, whether generated at low temperature and high strain or low strain and high temperature, determine the time decay of the stress. A strain-temperature equivalence was also found for  $\tau$ . These experiments are an important beginning<sup>p</sup> towards characterizing the structural dependent parameters. This information can be used in a constitutive equation for the stress:

$$\sigma(t) = E_0 \int_0^t dt' \frac{d\epsilon}{dt'} \exp\left[-\int_{t'}^t dt'' \tau_0^{-1} [w_c(t''-t')]^{-n} [T_f(t'')] \right], \quad (4.25)$$

to predict the results of different strain histories such as yielding, cycling, and fatigue as well as other experiments such as nonlinear creep.

These examples of the second universality are not intended as an exhaustive summary of the data, but only as representative of how it works in several fields. More extensive discussions can be found in the references and in a recent review of the data.<sup>2</sup>

#### Perspective on Relaxation

The current trend in condensed matter research is the study of strongly coupled systems involving complex interacting parts. Physicists are studying conducting polymers such as  $\text{CH}_x$ , spin glasses such as  $\text{Cu:Mn}$  and  $\text{Er}_x\text{Sr}_{1-x}\text{S}$ , electron glasses such as insulating  $\text{Si:P}$ , and charge density wave systems such as  $\text{TaS}_2$  and  $\text{K}_2\text{MoO}_6$ . Polymer workers are studying entangled networks of polymer melts and glassy polymers near the glass transition. Glass workers are studying charge transport in conducting glasses. Physicists, rheologists, metallurgists, engi-

neers, chemists and others are all drifting toward a set of problems with similar characteristics. These problems are of interest both technologically and for basic understanding. Technological applications which depend on this type of research include nuclear waste containment, new types of batteries, electronic circuit devices and materials, polymeric structural parts in spacecraft, aircraft, automobiles, and other machinery, industrial processing and characterization of materials, and many other examples.

Complex interacting systems involve cooperativity between the different components. The physicists speak of complicated interactions which cannot all be satisfied simultaneously (i.e. frustration in spin glasses) resulting in many local minima in the free energy surface of the system. Polymer rheologists speak of entanglement networks in which the dynamics of entanglement points must be followed in addition to the motion of individual chains. Glass transition researchers speak of free volume fluctuations allowing the mobility of atoms. Computer scientists speak of content-addressable memories where particular memories are stored non-locally in many circuit interconnections. These and many other concepts in different fields are all attempts to include the effects of the complicated structure on the dynamics of some physical process. This is certainly a difficult problem. It is advantageous for attempts to incorporate as much information from the experimental data as possible. This article has emphasized two coupled relations, the first and second universalities, which are supported by the experimental relaxation data. It is expected that these relations can be used to obtain a better understanding of these complicated problems.

It is very significant that as soon as the first universality is accompanied by the second universality, the discussion is able to become far more specific to the details of the material structure, short range order, relaxation mechanisms and dependences on physical variables, and coupling of the relaxation process to the rest of the system. The discussion is no longer limited to descriptions of the shape of the time decay or frequency dependence. The first and second universalities together address many physical questions concerning the meaning of relaxation and its relation to the material structure. A model and physical picture of relaxation in complex systems proposed earlier by one of us (K.L.N.) was also described on a physical level in this article. This model leads to the first and second universalities and gives physical interpretations for the parameters  $n$ ,  $\omega_c$ , and  $\tau_0$ . For instance,  $n$  is a measure of the coupling strength of the relaxation mode to its complex surroundings. This interpretation holds up qualitatively in that strongly coupled systems such as spin glasses, electron glasses, and polymer secondary relaxations have values of  $n$  in the range 0.7-0.9, while less strongly coupled systems such as

linear polymer melt entanglement networks and ionically conducting glass have values of  $n$  in the range 0.4-0.5, and weakly coupled systems such as simple liquids and crystals have  $n$  values near zero. However, when values of  $n$  are taken from experimental measurements, the first and second universality predictions are quantitatively obeyed. The physical model described in the article allows insight into how the structural details of these complex materials can be handled in a controllable way to quantitatively describe relaxation in these situations.

From the success of the first and second universalities, it is possible to understand the usefulness of several long-used empirical laws such as the Andrade and Kohlrausch-Struik creep laws, the Chasset-Thirion equation for stress relaxation in elastomers, the Curie-von Schweidler discharge law in dielectrics, the KAHR and Moynihan formulations of volume and enthalpy recovery, the BKZ, Shapery, and Green-Rivlin representations of nonlinear viscoelasticity, and many others. The appearance of the second universality furthermore allows the prediction of new relations and the explanation of many puzzling phenomena such as anomalous molecular weight and temperature dependences in polymer melts, anomalous isotope mass effect in glasses, unusual transport properties in semiconductors, and many other examples described above and in the references. Furthermore, the first and second universalities can be turned around and used as a probe to learn about phenomena that are not completely understood in microscopic detail such as the glass transition and nonlinear viscoelasticity. Further progress on relaxation in complex systems, by whatever approach, must take into account the existence of the first and second universalities.

Definite progress by applying the first and second universalities has been made in understanding aspects of amorphous polymers, polymer melts, electronic and ionic transport, spin glasses, and other fields of relaxation as described in this article and in the references. Work is continuing on these fields and further progress is expected, especially as data become available from experiments which have been explicitly designed to elucidate the first and second universalities. An area of relaxation which has great promise and which we are beginning to develop is that of electronic materials and devices. We have already examined electronic transport in materials, but here we refer to a much wider area of electronic materials phenomena which includes oxidation, electromigration, material flow, VLSI operation, and many others. These areas are important in regards to fabrication of integrated circuits and other devices as well as their operating properties.

Numerical simulations<sup>141</sup> and theoretical studies of transport in very small devices (i.e. submicron channel lengths) have found strong

size-related effects due to coupling of an individual device to its environment which includes contacts, interfaces, interconnects and other devices. The possibility of synergetic effects from device-device interactions has been noted. Indeed as the feature size decreases and complexity increases in VLSI, the individual devices must interact with each other. This coupling should have a randomness that is analogous to naturally occurring complex systems such as glasses, spin glasses and polymers which are made up of coupled component building blocks. A result of complexity and randomness in the latter is the slowing down of rate processes (i.e. first and second universalities) and this can also be studied in VLSI. For example, charge state relaxations in memory devices involved in read and write operations that have high speed (or short relaxation time  $\tau$ ) before high density integration, may be drastically slowed down (or have longer effective relaxation time) after scaling down in VLSI. It would be desirable to know how the time scale is shifted to longer times and the form of the modified time dependence of the relaxation process. These properties are very important for designing optimal devices characteristics, and the first and second universalities play a central role in these studies.<sup>142</sup>

Besides the operation of the device itself, the properties of the material from which the device is built are also important. One of the requirements in integrated circuit fabrication is the ability of conducting lines to cross over abrupt steps and to enter contacts without thinning or breaking. These are necessary to maintain reliability standards and prevent open circuit failures. A phosphorus doped oxide (phosphosilicate glass or PSG) has often been used as the dielectric between metal and polysilicon to round out the step profiles and produce better metal step coverage. For this technology, it is necessary to know the flow properties of PSG as a function of temperature, doping, ion implantation and other treatments.<sup>143,144</sup> A similar class of problems has been considered earlier in the context of glassy polymers. Yielding and flow, volume recovery, physical aging, polymer doping, and temperature dependences were studied in glassy polymers using the first and second universalities. Similar studies in the context of device fabrication materials and processes are also expected to allow an understanding of this phenomenon in relation to the microscopic material structure.

As a final example of relaxation in electronic materials, we consider the actual material growth and processing. Manufacture of materials for use in device fabrication involves many processes. An important one is the thermal oxidation of silicon. This involves both the transport of oxygen through the oxide film and the  $O_2$ -Si oxidation reaction at the Si/SiO<sub>2</sub> interface.<sup>145</sup> Our earlier work showed that various types of transport in glasses and amor-

phous semiconductors as well as diffusion controlled reactions can be described by the first and second universalities. The situation of oxide growth may have even more interesting features in that the rate controlling the transport and the rate controlling the reaction process may not be independent. The first and second universalities are powerful tools to analyze interdependent relaxation processes such as these.

#### References

1. K.L. Ngai, *Comments Solid State Phys.* 9, 127 (1979); *Comments Solid State Phys.* 9, 141 (1980).
2. K.L. Ngai, "Evidences for Universal Relaxation Properties of Condensed Matter," in *Proc. of the Conference on Non-Debye Relaxations in Condensed Matter*, Bangalore, India, Sept. 1982, ed. T.V. Ramakrishnan (World Press, Singapore, 1985).
3. R. Kohlrausch, *Pogg. Ann.* (3) 12, 393 (1847).
4. F.T. Pierce, *J. Textile Inst.* 14, T390 (1923).
5. V.H. Stott, *J. Soc. Glass Tech.* 9, 207 (1925).
6. G.O. Jones, *J. Soc. Glass Tech.* 28, 432 (1944).
7. H. Vandecappelle, P. Migeote and J.R. De Bast, XXVIII Congrès International de Chimie Industrielle, Bruxelles, p. 11, Sept. 1954; J. De Bast and P. Gilard, *Phys. Chem. Glasses* 4, 117 (1963).
8. A.M. Kriuthof and A.L. Zijlstra, *Verres et Réfr.* 8, 3 (1954).
9. I.L. Hopkins, *Phys. Chem. Glasses* 4, 137 and 139 (1963); *Physical Acoustics Vol. 2, Part B*, pp. 91-163, ed. W.P. Mason (Academic Press, New York, 1965).
10. C.R. Kurkjian, *Phys. Chem. Glasses* 4, 128 (1963).
11. G. Williams and D.C. Watts, *Trans. Faraday Soc.* 66, 80 (1970).
12. C.T. Moynihan, L.P. Boesch and N.L. Laberge, *Phys. Chem. Glasses* 14, 122 (1973).
13. F.S. Howell, R.A. Bose, P.B. Macedo, and C.T. Moynihan, *J. Phys. Chem.* 78, 639 (1974).
14. J.A. Bucaro, H.D. Dardy, and R.D. Corsaro, *J. Appl. Phys.* 46, 741 (1975).

15. C.C. Lai, P.B. Macedo and C.J. Montrose, *J. Amer. Ceramic Soc.* **58**, 120 (1975).
16. G.D. Patterson, C.P. Lindsey and J.R. Stevens, *J. Chem. Phys.* **70**, 643 (1979); G.D. Patterson, J.R. Stevens and C.P. Lindsey, *J. Macromol. Sci.-Phys.* **B18**, 641 (1980); G.D. Patterson, *Advances in Polymer Science* **48**, 125 (1983).
17. H. Lee, A.M. Jamieson and R. Simha, *Macromolecules* **12**, 329 (1979).
18. R.V. Chamberlin, G. Mozurkewich, and R. Orbach, *Phys. Rev. Lett.* **52**, 867 (1984).
19. K.L. Ngai, "Unified Theory of  $1/f$  Noise and Dielectric Response in Condensed Matter," *Phys. Rev.* **B22**, 2066 (1980).
20. S.T. Liu, K.L. Ngai and S. Teitler, "Voltage Noise in Pyroelectric Materials," *Ferroelectrics* **28**, 369 (1980).
21. K.L. Ngai, "The Universal Low Frequency Responses of Ionic Conductors: A Review of Data and a Unified Model Interpretation," International Conference on Fast Ionic Conductivity in Solids, Gatlinburg, May 1981; *Solid State Ionics* **5**, 27 (1981).
22. K.L. Ngai, "Diffusion Limited Electron-hole Recombination in  $\alpha$ -Si," in *Tetrahedrally Bonded Amorphous Semiconductors*, AIP Conf. Proceeding No. 73, p. 293 (1981).
23. K.L. Ngai and F.S. Liu, "Dispersive Diffusion Transport and Noise, Time-dependent Diffusion Coefficient, Generalized Einstein-Nernst Relation, and Dispersive Diffusion-controlled Unimolecular and Bimolecular Reactions," *Phys. Rev. B* **24**, 1049 (1981).
24. P.C. Taylor and K.L. Ngai, "Transient Electrical Transport in Pure and Doped Chalcogenide Glasses," *Solid State Commun.* **40**, 525 (1981).
25. K.L. Ngai, "Molecular Relaxations Near Glass Transition," *Polymer Preprints* **22**, 287 (1981).
26. K.L. Ngai and F.S. Liu, " $1/f$  Diffusion Noise," *Proc. Sixth Intl. Conf. on Noise in Physical Systems*, ed. Soules and Mountain, NBS Special Publication **614**, p. 161 (1981).
27. K.L. Ngai, "Temperature Dependence of Excess Noise in Metal Films," *ibid*, p. 164.
28. K.L. Ngai, "Progress in Low Frequency Dynamic Responses of Condensed Matter," in *Recent Developments in Condensed Matter Physics, Vol. I Invited Papers*, ed. J.T. Devreese, Plenum, NY (1981), p. 527.
29. K.L. Ngai, X. Huang and F.S. Liu, "Small Polaron Hopping Without Trap Participation in Dispersive Transport in  $\text{SiO}_2$  MOS Structures," in *Physics of MOS Insulators*, ed. G. Lucovsky (Pergamon, 1981), p. 44.
30. S. Teitler and K.L. Ngai, "A Diagnostic for the Condition of Dielectrics," *IEEE Transactions on Electrical Insulation EI-16*, No. 5, 414 (1981).
31. K.L. Ngai, "Transient Luminescence, Transport and Photoconductivity in Chalcogenide Glasses," to appear in *Proceedings of NATO Advanced Study Institute on "Polarons and Excitons"*, Corsendonk, Belgium, July 1982.
32. K.L. Ngai and I. Manning, *J. de Physique* **43**, C9-607 (1982).
33. K.L. Ngai and A.K. Rajagopal, "Conductivity Relaxation in the Electron Glass," to appear in *Proc. 17th Intl. Conf. Physics of Semiconductors*, San Francisco (1984).
34. K.L. Ngai and S.T. Liu, "Interface States of Silicon MOS Devices by Noise Measurements," *Thin Solid Films* **93**, 32 (1982).
35. K.L. Ngai and R.W. Rendell, "Stress Relaxation and Loss Moduli Measurements in Linear and Branched Polymer Systems Correlated with Steady State Viscosity: Molecular Weight Dependences," *ACS Polymer Preprints* **23**, No. 2, 46 (1982).
36. U. Strom and K.L. Ngai, "A Model for the Dielectric Response of  $\text{Na}\beta$ -Alumina at Intermediate Temperatures," *Solid State Ionics* **9 & 10**, 283 (1983).
37. K.L. Ngai and U. Strom, "Dielectric Response of  $\text{Na}\beta\text{-Al}_2\text{O}_3$  - Evidence for 'Glass Transition,'" *Phys. Rev.* **B27**, 6031 (1983).
38. K.L. Ngai and K. Murayama, "Luminescence, Transient Transport and Photoconductivity in Chalcogenide Glasses," to appear in *Proceedings of International Conference on Physics of Semiconductors*, Montpellier, France, 1982, *Physica* **117B** and **118B**, 920 (1983).
39. A.A. Jones, J.F. O'Gara, P.T. Ingelfeld, J.T. Bendler, A.F. Yee and K.L. Ngai, "Proton Spin Relaxation and Molecular Motion in a Bulk Polycarbonate," *Macromolecules* **16**, 658 (1983).
40. D. Emin and K.L. Ngai, "Hopping Conduction in Lightly-Doped Polyacetylene," *J. Phys. (Paris) Colloq.* **44**, C3-471 (1983).
41. A.K. Rajagopal, K.L. Ngai, R.W. Rendell, and S. Teitler, "Nonexponential Decay in Relaxation Phenomena," *J. Stat. Phys.* **30**, 285 (1983).



42. K.L. Ngai, A.K. Rajagopal and C.Y. Huang, "Relaxations in Spin Glasses: Similarities and Differences from Ordinary Glasses," *J. Appl. Phys.* 55, 1714 (1984).
43. J.T. Bendler and K.L. Ngai, "A Microscopic Approach to Volume Recovery of Polymers," *Macromolecules* 17, 1174 (1984).
44. K.L. Ngai and A.K. Rajagopal, "Comments on 'Time Decay of Remanent Magnetization in Spin-Glasses,'" *Phys. Rev. Lett.* 53, 1024 (1984).
45. K.L. Ngai, R.W. Rendell and H. Jain, "Anomalous Isotope Mass Effect in Conductivity of Lithium Borate Glasses," *Phys. Rev.* B30, 2133 (1984).
46. R.W. Rendell, T.K. Lee, and K.L. Ngai, "New Model of Physical Aging Effects in Enthalpy Recovery," *Polymer Engineering and Science* 24 (10), 1104 (1984).
47. D.J. Plazek, K.L. Ngai, and R.W. Rendell, "An Application of a Unified Relaxation Model to the Aging of Polystyrene Below Its Glass Temperature," *Polymer Engineering and Science* 24 (10), 1111 (1984).
48. K.L. Ngai, "Transient Luminescence, Transport and Photoconductivity in Chalcogenide Glasses," in "Polarons and Excitons in Polar Semiconductors and Ionic Crystals," ed. J.T. Devreese and F. Peeters (Plenum Publishing Corporation, 1984), p. 383.
49. A.F. Yee, R. Bankert, R.W. Rendell and K.L. Ngai, "Nonlinear Viscoelasticity Behavior of Glassy Polymers: Experimental Results and Theoretical Model," in Proceedings of the 9th International Congress of Rheology, Acapulco, Mexico, ed. B. Meno, A. Garcia-Rejon, and C. Rangel-Nafaile 3, 231 (1984).
50. K.L. Ngai, D.J. Plazek and R.W. Rendell, "Unified Model of Amorphous Polymer Relaxation: From the Plateau and Terminal Regimes Through the Softening Transition to the Glassy Region," *Ibid.* 3, 67 (1984).
51. K.L. Ngai and A.K. Rajagopal, "Conductivity Relaxation in the Electron Glass," to appear in *Proc. 17th International Conf. on Physics of Semiconductors*, San Francisco (1984).
52. K.L. Ngai and R.W. Rendell, "Dielectric and Conductivity Relaxations in Conjugated Polymeric Conductors," to appear as a chapter in *Handbook of Conjugated Polymeric Conductors*, ed. T. Skotheim (Marcel-Dekker, 1985) (in press).
53. K.L. Ngai and D.J. Plazek, "Relation of Internal Isomerism Barriers to the Flow Activation Energy of Entangled Polymer Melts in the High Temperature Arrhenius Region," *J. Polymer Sci.: Polymer Physics Edition* (submitted).
54. J.D. Ferry, *Viscoelastic Properties of Polymers*, 3rd ed. (Wiley, New York, 1980).
55. P.E. Rouse, *J. Chem. Phys.* 21, 1272 (1953).
56. G.H. Vineyard, *J. Phys. Chem. Solids* 3, 121 (1957).
57. J.S. Langer, *Ann. Phys.* 54, 258 (1969).
58. W.H. Zachariassen, *J. Am. Chem. Soc.* 54, 3841 (1932).
59. H.L. Downing, N.L. Peterson, and H. Jain, *J. Non-Cryst. Solids* 50, 203 (1982).
60. G.N. Greaves, A. Fontaine, P. Lagarde, D. Raoux, and S.J. Gurman, *Nature* 293, 611 (1981).
61. R.G. Palmer, D.L. Stein, E. Abrahams, and P.W. Anderson, *Phys. Rev. Lett.* 53, 958 (1984).
62. M.H. Cohen and G.S. Grest, *Phys. Rev.* B24, 4091 (1981).
63. S.H. Glarum, *J. Chem. Phys.* 33, 639 (1960); 33, 1371 (1960).
64. P. Bordewijk, *Chem. Phys. Letters* 32, 592 (1975).
65. J.L. Skinner and P.G. Wolynes, *J. Chem. Phys.* 73, 4022 (1980).
66. M.F. Shlesinger and E.W. Montroll, *Proc. Natl. Acad. Sci. U.S.A.* 81, 1280 (1984).
67. L. Boltzmann, *S.B. Akad. Wiss. Wien. (II)* 66, 275 (1872).
68. W. Pauli, *Festschrift zum 60. Geburtstage A. Sommerfelds (Hirzel, Leipzig (1928))*, p. 30.
69. N.G. van Kampen, in *Fundamental Problems in Statistical Mechanics*, ed. E.G.D. Cohen (North-Holland, Amsterdam, 1962), p. 173.
70. L. van Hove, in *Fundamental Problems in Statistical Mechanics*, ed. E.G.D. Cohen (North-Holland, Amsterdam, 1962), p. 157.
71. L. van Hove, *Physica* 21, 517 and 901 (1955); *Physica* 22, 343 (1956); *Physica* 23, 441 (1957); *Physica* 25, 268 (1959).
72. P. Mazur and E. Braun, *Physica* 30, 1973 (1964).

73. L.M. Torell, *J. Chem. Phys.* 76, 3467 (1982).
74. C.A. Angell and L.M. Torell, *J. Chem. Phys.* 78, 937 (1983).
75. R. Weiler, R. Bose, and P.B. Macedo, *J. Chem. Phys.* 53, 1258 (1970).
76. A. Janner, L. van Hove, and E. Verboven, *Physica* 28, 1341 (1962); A. Janner, *Helv. Phys. Acta* 35, 47 (1962).
77. R.J. Swenson, *J. Math. Phys.* 3, 1017 (1962).
78. I. Prigogine and P. Résibois, *Physica* 24, 795 (1958); *Physica* 27, 629 (1961).
79. S. Nakajima, *Prog. Theor. Phys.* 20, 948 (1958).
80. R.W. Zwanzig, *J. Chem. Phys.* 33, 1338 (1960); in *Lectures in Theoretical Physics*, ed. W. Downs and J. Downs (Boulder, CO, 1961), Vol. III.
81. A.K. Rajagopal, S. Teitler, and K.L. Ngai, *J. Phys. C* (in press) (1984).
82. I.S. Gradshteyn and I.M. Ryzhik, *Table of Integrals, Series, and Products* (Academic Press, New York, 1980).
83. P.W. Anderson, B.I. Halperin, and C.M. Varma, *Phil. Mag.* 25, 1 (1972).
84. W.A. Phillips, *J. Low Temp. Phys.* 7, 351 (1972).
85. *Amorphous Solids: Low Temperature Properties*, ed. W.A. Phillips (Springer-Verlag, New York, 1981).
86. H. v. Lohneysen, *Phys. Rep.* 79, 161 (1981).
87. R.C. Zeller and R.O. Pohl, *Phys. Rev.* B4, 2029 (1971).
88. E.P. Wigner, *Conference on Neutron Physics by Time-of-Flight*, Gatlinburg, Tennessee, November, 1956, Oak Ridge Natl. Lab. Rept. ORNL-2309, 1957, p. 59.
89. F.J. Dyson, *J. Math. Phys.* 3, 140, 157, and 166 (1962).
90. C.E. Porter, *Statistical Theory of Spectra: Fluctuations* (Academic Press, New York, 1965).
91. T.A. Brody, J. Flores, J.B. French, P.A. Mello, A. Pandez and S.S.M. Wong, *Rev. Mod. Phys.* 53, 385 (1981).
92. M. V. Berry, *Ann. Phys.* 131, 163 (1981).
93. M. V. Berry in *The Wave-Particle Dualism*, ed. S. Diner, D. Fargue, G. Lochak and F. Selleri (D. Reidel, Boston, 1984).
94. M. V. Berry in *Chaotic Behavior in Deterministic Systems*, *Les Houches Lectures XXXVI*, ed. R.H.G. Helleman and G. Iooss (North-Holland, Amsterdam, 1984).
95. M.V. Berry in *Proc. Como Conf. on Quantum Chaos*, ed. G. Casati (1984).
96. J. von Neumann and E. Wigner, *Physik Z.* 30, 467 (1929) [translated in R.S. Knox and A. Gold, *Symmetry in the Solid State* (Benjamin, New York, 1964)].
97. P. Pechukas, *Phys. Rev. Lett.* 51, 943 (1983).
98. S.W. McDonald and A.N. Kaufman, *Phys. Rev. Lett.* 42, 1189 (1979).
99. G. Casati, F. Valz-Gris and I. Guarneri, *Lett. Nuovo Cimento* 28, 279 (1980).
100. O. Bohigas, M.J. Giannoni and C. Schmidt, *Phys. Rev. Lett.* 52, 1 (1984).
101. E. Haller, H. Köppel, and L.S. Cederbaum, *Phys. Rev. Lett.* 52, 1665 (1984).
102. F.B. McLean, H.E. Boesch and J.M. McGarity, *IEEE Trans. Nuc. Sci.* NS-23, 1506 (1976).
103. R.C. Hughes, *Phys. Rev.* B15, 2012 (1977).
104. H. Scher and E.W. Montroll, *Phys. Rev.* B12, 2455 (1975).
105. G. Pfister and H. Scher, *Adv. Phys.* 27, 747 (1978).
106. A.F. Yee and S.A. Smith, *Macromolecules* 14, 54 (1981).
107. A.E. Tonelli, *Macromolecules* 5, 558 (1972); J.T. Bendler, *Annals N.Y. Acad. Sci.* 371, 299 (1981).
108. G.C. Berry and T.G. Fox, *Adv. Polymer Sci.* 5, 261 (1968).
109. W.W. Graessley, *Adv. Polym. Sci.* 16, 1 (1974).
110. R.A. Mendelsohn, W.A. Bowles, and F.L. Finger, *J. Polym. Sci.: Part A-2*, 8, 105 (1970).
111. V.R. Raju, G.G. Smith, G. Marin, J.R. Knox, and W.W. Graessley, *J. Polym. Sci.: Polym. Phys. Ed.* 17, 1183 (1979).
112. P.G. de Gennes, *J. Chem. Phys.* 55, 572 (1971).

113. M. Doi and S.F. Edwards, J.C.S., Faraday Trans. II 74, 1789, 1802, and 1818 (1978).
114. G. McKenna, G. Hadziioannou and A.J. Kovacs, to be published.
115. G. McKenna, L.J. Fetters, Daniel Plazek, and D.J. Plazek, to be published.
116. K.L. Ngai and R.W. Rendell, to be published.
117. Statement by S.F. Edwards during question period in 1st SPSJ International Polymer Conference, Kyoto, Japan, August 1984.
118. T.A. Litovitz and G. McDuffie, J. Chem. Phys. 39, 729 (1963).
119. D.P. Almond and C.R. West, Solid State Ionics 4, 73 (1981); Phys. Rev. Lett. 47, 431 (1981).
120. D. Hüser, L.E. Wenger, A.J. van Duynveldt and J. Mydosh, Phys. Rev. B27, 3100 (1983).
121. L.E. Wenger, in Heidelberg Colloquium on Spin Glasses, ed. J.L. van Hemmen and I. Morgenstern (Springer, Heidelberg, 1983).
122. F. Mezei and A.P. Murani, J. Magn. Magn. Mater. 14, 211 (1979).
123. L.E. Wenger and J.A. Mydosh, J. Magn. Magn. Mater. 55, 1717 and 1850 (1984).
124. R.V. Chamberlin, G. Mozurkewich, and R. Orbach, Phys. Rev. Lett. 53, 1025 (1984); also see the correction to this in Phys. Rev. Lett. 53, 1510 (1984).
125. H.W. Starkweather, Jr. and J.R. Barkley, J. Polymer Sci.: Polymer Physics Edition 19, 1211 (1981).
126. H.L. Downing, N.L. Peterson, and H. Jain, J. Non. Cryst. Solids 50, 203 (1982).
127. H. Jain and N.L. Peterson, Philos. Mag. A46, 351 (1982).
128. Y. Ebisuzaki, W.J. Kass, and M. O'Keefe, J. Chem. Phys. 46, 1373 (1967); J. Chem. Phys. 48, 1867 (1968).
129. H.D. LeClaire, Philos. Mag. 14, 1271 (1966).
130. G.J. Exarhos and W.M. Risen, Jr., Solid State Commun. 11, 755 (1972).
131. L.E.E. Struik, Physical Aging in Amorphous Polymers and Other Materials (Elsevier, Amsterdam, 1978).
132. A.J. Kovacs, J.J. Aklonis, J.M. Hutchinson, and A.R. Ramos, J. Polym. Sci.: Polym. Phys. Ed. 17, 1097 (1979).
133. M.A. De Bolt, A.J. Easteal, P.B. Macedo, and C.T. Moynihan, J. Am. Ceram. Soc. 59, 16 (1976).
134. J.M. O'Reilly, Proc. of the Twelfth North American Thermal Analysis Society Conference, Williamsburg, VA, Sept. 1983, p. 118.
135. W.M. Prest, Jr., F.J. Roberts, Jr., and I. Hodge, Proc. of the Twelfth North American Thermal Analysis Society Conference, Williamsburg, VA, Sept. 1983, p. 119.
136. A.J. Kovacs, Fortschr. Hochpolym. Forsch. 3, 394 (1963).
137. Preliminary result, R. W. Rendell, J.J. Aklonis, and K.L. Ngai, to be published.
138. I.M. Hodge and A.R. Berens, Macromolecules 15, 762 (1982).
139. I.M. Hodge and G.S. Huvard, Macromolecules 16, 371 (1983).
140. I.M. Hodge, Macromolecules 16, 898 (1983).
141. H.L. Grubin, D.K. Ferry, G.J. Infrate, and J.R. Barker in VLSI Electronics, ed. N.G. Einspruch (Academic Press, 1982), p. 197.
142. F. Buot, R.W. Rendell, and K.L. Ngai, to be published.
143. W. Kern and G.L. Schnable, RCA Review, 43 (3), 423 (1982).
144. D.C. Chen, R.T. Szeto and H. Fu, IEDM Technical Digest, International Electron Devices Meeting, Washington, D.C., Dec. 1983.
145. A.G. Revesz and H.L. Hughes, Electrochem. Soc. Meeting, New Orleans, LA, Oct. 1984.